ELECTRON IMPACT EXCITATION

OF

LIGHT ATOMS IN DISTORTED WAVE APPROXIMATIONS

A thesis submitted for the degree of

Doctor of Philosophy

in

the University of London

by

Timothy Scott, B.Sc. (London)

August 1976

CONTENTS

		PAGE
ABSTRACT		1
ACKNOWLEDGEMENTS		2
CHAPTER 1 : REVIEW OF RECENT THEORETICAL MODELS		
§1.1	Introduction	3
§1.2	Formal Scattering Theory	5
§1.3	The Born Approximation	7
§1.4	Eigenfunction Expansion Techniques	10
§1.5	Eikonal Methods	12
§1.6	Distorted Wave Theory	16
§1.7	Many-Body Theory	19
CHAPTER 2 : THE DISTORTED WAVE POLARIZED ORBITAL METHOD		
§2.1	The Polarized Orbital Method	22
§2.2	Derivation of the Scattering Equation	27
§2.3	Formulation of the T-Matrix Element	33
CHAPTER 3 : EXCITATION OF HELIUM		
§3.1	Preliminary Remarks	42
§3.2	The Radial Scattering Equation	46
§3.3	Cross Sections for the S-Levels	49
§3.4	Cross Sections for the P-Levels	57
§3.5	The Orientation and Alignment Parameters	72
CHAPTER 4 : EXCHANGE-POLARIZATION EFFECTS		
§4.1	Introduction	80
§4.2	The Radial Scattering Equation	81
§4.3	$1s \rightarrow n\ell$ Transitions in Hydrogen	83
§4.4	$1^1S \rightarrow n^{1,3}S$ Transitions in Helium	88

Continued.....

PAGE

CHAPTER 5 : COMPUTATION AND NUMERICAL METHODS

§5.1 Solution of the Scattering Equation 95
§5.2 Numerical Procedure for the Scattering Equation 103
§5.3 Numerical Methods for the Cross Sections 111
§5.4 The Born and Born-Oppenheimer Approximations 115

CHAPTER 6 : RESULTS

§6.1 Excitation of $H(1s \rightarrow 2s, 2p, 2s + 2p)$ 120
§6.2 Excitation of $He(1^1S \rightarrow n^1S)$ 125
§6.3 Excitation of $He(1^1S \rightarrow 2^3S)$ 138
§6.4 Excitation of $He(1^1S \rightarrow n^1P)$ 145
§6.5 Excitation of $He(1^1S \rightarrow 2^3P)$ 164
§6.6 Conclusions 168

APPENDIX A 171
APPENDIX B 175
APPENDIX C 176
APPENDIX D 182

REFERENCES 190

TABLES 197

FIGURES 272

ABSTRACT

This thesis is concerned with a study of inelastic electron-atom collisions with the incident energy ranging from just above the first ionization threshold to some energy where the First Born approximation becomes valid. The main physical effects which need to be included in the theoretical treatment of such collisions are electron exchange and distortion of both the atomic system and the wave describing the external electron. A method which takes account of these effects, to be referred to as the Distorted Wave Polarized Orbital (DWPO) approximation, is described. Three models based on this approximation are developed and applied to electron collisions with the light atoms hydrogen and helium.

In particular the models are applied to the following collision processes:

$$e + H(1s) \rightarrow e + H(2s,\ 2p,\ 2s + 2p);$$

$$e + He(1^1S) \rightarrow e + He(n^{1,3}L),\ n = 2,3,4,5,\ \ L = S,P.$$

Results are presented for the total (integral) and differential cross sections and also, where appropriate, for the parameters describing the orientation and alignment properties of the excited atom. The results are compared with those of other theoretical methods and with experimental measurements.

ACKNOWLEDGEMENTS

I should like to express my thanks and appreciation to Professor M.R.C. McDowell for his continued interest and advice throughout the course of this work. I am also grateful to Dr. L.A. Morgan for her helpful comments on the computational aspects.

I should also like to thank those who have in anyway assisted in the compilation of this thesis, particularly my father, Mr. T.R. Scott, for his preparation of figures and Mrs. B.A.F. Rutherford for typing the manuscript.

The use of the facilities provided by the University of London Computing Centre is gratefully acknowledged. Finally, I am indebted to the Science Research Council for the award of a research studentship.

T.S.

August, 1976.

CHAPTER 1

REVIEW OF RECENT THEORETICAL MODELS

§1.1 Introduction

During the last few years, there has been considerable progress in the understanding of electron impact excitation of atoms. Experimentally, an increasing volume of absolute differential cross section data is available for such collisions with the light atoms hydrogen and helium, particularly the latter. It is with these two atoms, theoretically the simplest to treat, with which this thesis will be mainly concerned. When dealing with electron impact excitation of these light atoms, it is convenient to divide the range of impact energy possessed by the incoming electron into three regions.

Firstly, there is the high energy region, defined essentially as that region where the First Born Approximation and its related methods are believed to be valid. Hence, this region may be accounted for theoretically; the papers of Truhlar et al. (1970) and Rice et al. (1972) provide a comprehensive review of the various Born models when applied to excitation of the 2^1P and 2^1S levels of helium respectively. At the other extreme, there is the low energy region, basically lying below the first ionization threshold. Here the close-coupling methods, developed by Burke, Smith, Seaton and others, have been used with considerable success to study low energy resonances. Applications to electron-hydrogen collisions have been made by Burke and Taylor (1966), Geltman and Burke (1970), Burke and Webb (1970) and more recently by Callaway and Wooten (1974, 1975).

For helium, reference may be made to the work of Smith et al. (1973), Ormonde and Golden (1973), Oberoi and Nesbet (1973). A more recent approach, based on the R-matrix method (Burke et al. 1971), has been applied to the elastic scattering of electrons from hydrogen and helium atoms by Burke and Robb (1972). The method has been further applied by Berrington et al. (1975) to a study of low energy electron scattering by helium atoms: where a comparison

is possible with experimental results, the agreement is satisfactory. Generally, it may therefore be said that methods are available for dealing with this impact energy region.

However, it is the intermediate energy region, lying between the two described above, which attracts much current interest. Here there is no longer a finite number of open channels as in the low energy case, rather an infinite number may now be open. A recent sophisticated model for electron-hydrogen collisions has been developed by Callaway and coworkers (see Callaway et al. (1976) and references quoted therein). Their method involves a close-coupling pseudo-state approach for the lower order partial waves and a distorted wave polarized orbital treatment of the higher partial waves. For energies below 4 Rydbergs the method is successful in predicting the $n = 2$ differential cross sections for hydrogen excitation compared with experiment, while above this energy, quite good agreement with experiment is obtained by a similarly sophisticated method due to Kingston et al. (1976). Here, the close-coupling approximation is employed for the lower order partial waves and the unitarized Born approximation for the higher partial waves.

Theoretical treatments, however, of the electron impact excitation of helium in the intermediate energy region are not quite so advanced, especially for transitions due to spin-exchange alone. Broadly speaking, theories may be classified into one of the following categories:

1. Plane wave models
2. Eigenfunction expansion techniques whereby the wave function for the whole system is expanded in a complete set of suitable eigenfunctions
3. Various semi-classical (eikonal) approaches
4. Distorted wave treatments
5. The many-body approach which in fact has recently been found to be connected to the fourth category (Rescigno et al. 1974).

In the following a brief and formal account of scattering theory will be presented, and in the remainder of the chapter, a short description of the above five categories of theoretical treatments to the problem.

§1.2 Formal Scattering Theory

Under this heading the elements of formal scattering theory will be presented; for a thorough and detailed account see, for example, Goldberger and Watson (1964). Let Ψ_i^+ be the wave function belonging to the initial channel for the complete physical system under consideration. Then Ψ_i^+ satisfies the Schrödinger equation

$$(H - E)\,\Psi_i^+ = 0 \tag{1.2.1}$$

where H is the Hamiltonian for the total system and E the corresponding energy. H is divided into two parts:

$$H = H_a + V_a \tag{1.2.2}$$

where H_a is the unperturbed Hamiltonian and V_a is a perturbation, due, for example, to the presence of the scattering electron. The subscript a denotes quantities in either the initial channel $(a = i)$ or the final channel $(a = f)$. The eigenfunctions of H_a will be denoted by ψ_a with energy eigenvalue E_a such that

$$H_a\psi_a = E_a\psi_a \,. \tag{1.2.3}$$

The Green's function operator for the unperturbed system in the initial channel is written formally as

$$G_i^+ = \frac{1}{E_i - H_i + i\varepsilon} \tag{1.2.4}$$

with ε a small positive number such that, when all manipulations have been completed, the limit as $\varepsilon \to 0_+$ is finally taken. With this definition of G_i^+ the Schrödinger equation (1.2.1) may be rewritten in the form

$$\Psi_i^+ = \psi_i + G_i^+ V_i \Psi_i^+ \tag{1.2.5}$$

which is often referred to as the Lippmann-Schwinger equation.

The Green's function operator for the full perturbed system may be similarly expressed as

$$G^{+} = \frac{1}{E-H+i\varepsilon} \quad . \tag{1.2.6}$$

The superscript (+) denotes here and elsewhere that the function satisfies outgoing wave boundary conditions. Hence equation (1.2.5) may be manipulated symbolically to give the formal solution

$$\begin{aligned} \Psi_i^{+} &= \psi_i + G^{+} V_i \psi_i \\ &= (1 + G^{+} V_i)\psi_i \quad . \end{aligned} \tag{1.2.7}$$

However this solution is no nearer to obtaining Ψ_i^{+} than (1.2.1) since the operator expression on the right hand side involves a knowledge of Ψ_i^{+}. Premultiplying (1.2.7) by V_i one obtains

$$T \psi_i = V_i \Psi_i^{+} \tag{1.2.8}$$

where the transition operator T acting on the initial unperturbed wavefuncion of the system is given by

$$T = V_i(1 + G^{+} V_i) \, . \tag{1.2.9}$$

The T-matrix element, T_{if}, for a transition from state i to state f is then

$$T_{if} = \langle \psi_f V \Psi_i^{+} \rangle \, . \tag{1.2.10}$$

The subscript on V has been deliberately omitted for the following reason: for rearrangement collisions there is no reason for preferring V_i to V_f in (1.2.10). In fact, instead of premultiplying (1.2.7) by V_i, the same operation and definition could have been derived from using V_f. The difference which may arise from calculations using either V_f or V_i in (1.2.10) is generally referred to as the post-prior discrepancy.

Working with atomic units, the differential cross section for electron impact excitation scattering processes is defined to be

$$\frac{d\sigma}{d\Omega} = \frac{1}{4\pi^2} \frac{k_f}{k_i} |T_{if}|^2 \, a_o^{\,2} \, sr^{-1} \quad . \tag{1.2.11}$$

Here, $\underline{k}_i$ denotes the momentum vector of the incoming electron and $\underline{k}_f$ that of the outgoing electron;(1.2.11) may essentially be interpreted as a measure of the probability of scattering into particular solid angles.

The probability of scattering at all is obtained by integrating (1.2.11) over all solid angle to obtain the total cross section in the form

$$Q_{if}(k_i^2) = \frac{1}{2\pi^2} \frac{k_f}{k_i} \int_{-1}^{1} |T_{if}|^2 \, d(\cos\theta) \; \pi a_o^2 \; . \qquad (1.2.12)$$

Comparison of experimental and theoretical total cross sections provides probably the simplest test of any theoretical model whereas that between differential cross sections provides a more stringent test.

A quantity closely related to the total cross section (1.2.12) is the generalized oscillator strength, $f_{if}(\underline{K})$, defined by

$$f_{if}(\underline{K}) = \frac{2}{K^2} (E_f - E_i) \, |\varepsilon_{if}(K)|^2 \qquad (1.2.13)$$

where

$$\varepsilon_{if}(K) = \sum_s \langle \psi_f | e^{i\underline{K}\cdot\underline{r}_s} | \psi_i \rangle \; . \qquad (1.2.14)$$

$\underline{K}$ is the momentum transferred by the scattered electron to the atom, that is $\underline{K} = \underline{k}_i - \underline{k}_f$, and the sum is over the number of atomic electrons. The generalized oscillator strength is related to the total cross section by

$$Q_{if}(k_i^2) = \frac{2}{E(E_f - E_i)} \int_{K_{min}}^{K_{max}} \frac{f_{if}(K)}{K} \, dK \; \pi a_o^2 \qquad (1.2.15)$$

with the limits of integration being given as $K_{min} = k_i - k_f$ and $K_{max} = k_i + k_f$.

§1.3 The Born Approximation

This section will be concerned with a brief outline of the Born approximation and comments on its application to electron-atom collisions. To begin with, equations (1.2.4) and (1.2.6) are combined so that symbolically one has

$$G^+ = G_i^+ + G_i^+ V_i G^+ \; . \qquad (1.3.1)$$

The Born Series for G^+ is then obtained by successive iteration of this equation

$$G^+ = G_i^+ + G_i^+ V_i G_i^+ + G_i^+ V_i G_i^+ V_i G_i^+ + \ldots \qquad (1.3.2)$$

Substituting this expression into the formal solution (1.2.7) for Ψ_i^+ and then considering the Transition matrix element (1.2.10) yields the Born Series for T_{if}

$$T_{if} = T_{if}^{FBA} + \langle\psi_f | V G_i^+ V_i | \psi_i\rangle + \langle\psi_f | V G_i^+ V_i G_i^+ V_i | \psi_i\rangle + \ldots \qquad (1.3.3)$$

where for convenience the first term has been denoted by

$$T_{if}^{FBA} = \langle\psi_f | V | \psi_i\rangle \quad . \qquad (1.3.4)$$

Retaining only this term in (1.3.3) results in the First Born Approximation (FBA) to T_{if}; retaining also the second term gives the Second Born Approximation (SBA):

$$T_{if}^{SBA} = \langle\psi_f | V(1 + G_i^+ V_i) | \psi_i\rangle \quad . \qquad (1.3.5)$$

Further terms may be included but the labour becomes prohibitively complicated; even in evaluating the second-order term, further simplification is required.

The FBA may be applied in a straightforward manner to electron-hydrogen collisions for which closed expressions are obtainable for the cross sections (Mott and Massey, 1965). For the case of helium this is no longer possible since exact atomic wave functions are not known and resort must therefore be made to approximate functions. Bell et al. (1969) have employed many-parameter correlated wave functions for both the initial and final states of helium to study excitation from the ground state to the n^1S, n^1P and n^1D states and obtained accurate values for the generalized oscillator strengths (see equation (1.2.13)) and for the total cross sections, equation (1.2.15).

SBA calculations have also been made by a number of authors for electron impact on hydrogen and helium atoms; see for example Woollings and McDowell (1973) and references quoted therein. More recently, Buckley and Walters (1974) have used a modified form of the Second Born Approximation to make detailed studies concerning elastic scattering of electrons by ground state helium atoms and in a further publication (Buckley and Walters, 1975) concerning excitation to

the 2^1S level. Both calculations allow for exchange, the inelastic case adopting the Ochkur approximation. Further details may be obtained from the respective papers.

For a description of those transitions which occur via spin-exchange, the First Born Approximation (1.3.4) is often referred to as the Born-Oppenheimer or Born-Exchange Approximation. In such processes, the interaction V no longer depends on the same coordinates before and after the collision, a result which gives rise to the post-prior discrepancy as remarked earlier. Born-Oppenheimer calculations have been carried out by Bell et al. (1966) to obtain total cross sections for excitation of the 2^3S and 2^3P levels of helium by electron impact over a wide range of incident energies. Differential cross sections have been calculated by Steelhammer and Lipsky (1970). When compared with experiment the Born-Oppenheimer Approximation is found to fail drastically, particularly at lower impact energies.

A serious drawback of plane wave theories, such as the Born-Oppenheimer approximation, is their treatment of the incoming and outgoing electron as a free particle. Provided the perturbation V is small, or equivalently the passage time of the incoming particle through the neighbourhood of the target atom is relatively small, this may be justifiable. If however, the electron is in the vicinity of the atom for a longer period, the incident wave distorts and may no longer be considered that of a free particle. Moreover, exchange-effects will become more prominent. It is precisely in this important region that the Born Approximation ignores the presence of the atom. Hence the Born Approximation can probably be assumed reliable for describing high energy electron impact excitation of atomic transitions which occur principally via direct processes as opposed to exchange processes. It is well known that large-angle differential cross sections calculated in the Born Approximation become rapidly poorer as the impact energy is decreased. The method also fails at small angles for elastic scattering and for transitions from one s-state to another, this being attributed to the neglect of polarization (see, for example, the review article by Bransden and McDowell (1976) on electron-atom collisions

at intermediate energies). At such energies, one is therefore forced to consider alternative methods and it is with these various methods that the remainder of this chapter is concerned.

§1.4 Eigenfunction Expansion Techniques

When the incident energy of the incoming electron lies below the first ionization potential of the target atom, close-coupling approximations have had considerable success. Essentially the wave function Ψ_i^+ for the total system is expressed as a sum over a set of eigenfunctions:

$$\Psi_i(\underline{r},\underline{x}) = \sum_{n=1}^{N} \psi_{in}(\underline{r})\, F_n(\underline{x}) + \chi(\underline{r},\underline{x}) \,. \qquad (1.4.1)$$

Here, and elsewhere, $\underline{r}$ represents collectively the coordinates of the orbital electrons and $\underline{x}$ the coordinatesof the external electron; the centre of mass is taken to coincide with the atomic nucleus. The $\psi_{in}(\underline{r})$ belong to a complete set, usually infinite, which must necessarily be truncated at some convenient point N for computation; $\chi(\underline{r},\underline{x})$ is a correction function which seeks to take account of those terms omitted by the truncation. Using such a method, Burke and Webb (1970) studied excitation of the $2s$ and $2p$ levels of atomic hydrogen by electron impact. In their calculations they chose as a basis the $1s$, $2s$ and $2p$ states ($N = 3$) of the target and substituted for χ modified $\bar{3}s$ and $\bar{3}p$ pseudo-states.

However, when the impact energy lies above the first ionization threshold, an infinite number of channels become open and close-coupling methods impractical. An alternative approach has been given by Bransden and Coleman (1972), referred to as the Second-Order Optical Potential method. Essentially, a second-order potential matrix is constructed in order to account for the terms omitted by truncating the eigenfunction expansion of Ψ_i^+. Referring to Bransden and Coleman (1972), a set of strongly coupled states can appear explicitly in the sum and representation also given to the omitted states. Briefly Bransden and Coleman write the eigenfunction expansion as

$$\Psi^{+}(\underline{r},\underline{x}) = \sum_{n} \psi_n(\underline{r})\, F_n(\underline{x}) \qquad (1.4.2)$$

where, for convenience the (i) subscript has been dropped and the $\psi_n(\underline{r})$ are eigenstates of the target atom with corresponding eigenenergies E_n. If those states to be retained in the sum are labelled $n = 0...N$, the Schrödinger equation for the system is shown to be

$$\left[\nabla^2 + k_n^2\right]F_n(\underline{x}) = 2 \sum_{m=0}^{N} V_{nm}(\underline{x})\, F_m(\underline{x}) + 4 \sum_{m=0}^{N} \int d\underline{x}'\, K_{nm}(\underline{x},\underline{x}')F_m(\underline{x}')$$

$$n = 0...N \qquad (1.4.3)$$

where $k_n^2 = 2(E - E_n)$, E the energy of the total system. $K_{nm}(\underline{x},\underline{x}')$ is the second-order non-local potential given in terms of the free particle Green's function $G(k_n^2;\underline{x},x')$ by the expression

$$K_{nm}(\underline{x},\underline{x}') = \sum_{p=N+1}^{\infty} G(k_p^2;\underline{x},\underline{x}')\, V_{np}(\underline{x})\, V_{pm}(\underline{x}') \,. \qquad (1.4.4)$$

The matrix elements of the interaction potential $V(\underline{r},\underline{x})$ appearing in this line are defined by

$$V_{nm}(\underline{x}) = \int \psi_n^{*}(\underline{r})\, V(\underline{r},\underline{x})\, \psi_m(\underline{r})\, d\underline{r} \,. \qquad (1.4.5)$$

Bransden and Coleman continue by using closure to simplify (1.4.4) which as it stands is too complicated to evaluate exactly. The problem therefore reduces to evaluation of (1.4.4) and subsequent calculation of the $F_n(\underline{x})$ using (1.4.3).

The model has had wide application, the results of which have been published in a series of papers. Initially, an impact parameter treatment was formulated and applied by Bransden et al. (1972) to electron and proton scattering off hydrogen atoms. A more sophisticated approach, but still in the impact parameter formalism, was later applied to the same problem by Sullivan et al. (1972), the chief difference being that former calculations were limited to the one- and two-channel versions of the theory whereas the latter was a four-channel approach. Berrington et al. (1973) extended the model to a study of elastic and inelastic scattering of electrons by helium atoms; in particular they studied excitation of the 2^1S and 2^1P levels. Excitation of the $n = 3$ levels

has been considered by Bransden and Issa (1975) who used two-, seven- and nine- state approximations in their calculations. Electron energies ranged from 100 to 1000 eV. However the validity of such semi-classical methods is restricted to applications where the incident energy lies in the higher region.

Developments have, therefore, been made to treat the same problem without the impact parameter assumption and allowing for exchange, hence enabling the model to be more realistically applied to the intermediate energy region. The results of a partial wave formalism applied to the elastic scattering of electrons by hydrogen and helium atoms have been summarized in a paper by Winters et al. (1974). Bransden and Winters (1975) later extended this distorted wave formalism to excitation of the 2s level of hydrogen and of the 2^1S and 2^3S levels of helium over the impact energy range 50-200 eV. In their work, Bransden and Winters allowed for polarization effects in the initial channel when calculating the distorted wave and in the final channel allowed only for the field of the final target state. This is in contrast to the many-body approach of Taylor and coworkers, which will be considered in §1.7.

§1.5 Eikonal Methods

For relatively high impact energies and particular transitions, namely those which can occur via direct interactions as opposed to exchange interactions, contributions arising from exchange effects may be considered small. In such cases methods can therefore be developed which are specifically applicable only to those processes considered to be dominated by the direct part of the transition amplitude. The eikonal approach is one such method and has been used extensively in many forms by a number of authors (the Glauber approximation is one such form and has recently been reviewed by Gerjuoy and Thomas, 1974). For a general review on the eikonal theory of electron-atom collisions, see the article by Joachain (1974).

In order to emphasise the main idea, the problem is first treated by direct analogy with potential scattering. The wave function Ψ_i^+ assumes the form

$$\Psi_i^+ = A\, e^{iS} \qquad (1.5.1)$$

with A and S real, A a slowly varying function of the incident wave number k_i. Essentially the idea is to treat the scattering semi-classically in which case scattering will be confined to small angles and the particle trajectory will be treated as a nearly straight line parallel to the direction of incidence.

Substituting (1.5.1) into the time independent Schrödinger Equation and making the fundamental eikonal approximation, which assumes that $\nabla^2 A \ll k^2 A$, $k^2 = 2E$, one finds

$$(\nabla S)^2 = 2(E - V). \qquad (1.5.2)$$

Equation (1.5.2) is the Eikonal Equation, whose solution S is now substituted into (1.5.1) which then becomes the eikonal wave function and forms the basis of the eikonal theory.

A recent development of eikonal methods has been the multichannel eikonal treatment, formulated and applied in a series of papers by Flannery and McCann. Briefly, equation (1.5.1) is replaced by a truncated sum over unperturbed target eigenstates $\phi_n(\underline{r})$:

$$\Psi_i^+(\underline{r},\underline{x}) = \sum_{n=1}^{N} \psi_n(\underline{r},\underline{x})\, a_n(\underline{x})\, e^{iS_n(\underline{x})}, \qquad (1.5.3)$$

$$\psi_n(\underline{r},\underline{x}) = \phi_n(\underline{r})\, e^{i\underline{k}_n \cdot \underline{x}},$$

which therefore allows for different trajectories in each channel represented in the sum. The coordinate $\underline{x}$ is expressed in terms of the impact parameter ρ and the distance z measured from the centre of mass along a line parallel to the incident direction, $\underline{x} = \underline{\rho} + z\hat{\underline{z}}$. Substituting (1.5.3) into the time-dependent Schrödinger Equation and noting that, classically $t = z/v_i$, it is found that the $a_n(\underline{\rho},z)$ satisfy the set of first-order coupled differential equations

$$\left[k_m^2 - 2\langle\psi_m|V|\psi_m\rangle\right]^{\frac{1}{2}} \frac{\partial a_m}{\partial z} = -i \sum_{n\neq m}^{N} a_n \langle\psi_m|V|\psi_n\rangle\, e^{i(S_n - S_m)} \qquad (1.5.4)$$

which is basically equation (9) of Flannery and McCann (1974). These equations are solved subject to the boundary conditions $a_n(\rho,-\infty) = \delta_{in}$. V is as usual the interaction potential.

The multichannel form of the T-matrix is then obtained by substituting for Ψ_i^+ in the expression

$$T_{if} = \langle \psi_f(k_f;\underline{r},\underline{x}) | V(\underline{r},\underline{x}) | \Psi_i^+(k_i;\underline{r},\underline{x}) \rangle \quad . \tag{1.5.5}$$

Further simplifications are made according to the process under consideration, details of which are outlined in the respective papers by Flannery and McCann.

A point to be made is that (1.5.3) allows for exchange only implicitly; no explicit account of exchange is included in the model. It is possible to include pseudo-states in an effort to make allowance for those states omitted by truncating the sum. Calculations have been carried out by Flannery and McCann (1974) with and without pseudo-states in a four-state and seven-state treatment for elastic and inelastic scattering of electrons from atomic hydrogen. Small-angle (less than 40°) differential cross sections for excitation of the 2p level are in very good agreement with experiment. Agreement for the 2s level is not so good, this being put down to the fact that exchange and polarization effects are neglected. The results of a ten-state calculation for inelastic electron-helium scattering have also been published (Flannery and McCann, 1975); as should be expected the method is generally successful for forward-angle scattering but fails appreciably in the backward direction where exchange is considered to dominate. Total cross sections are in good agreement with experiment for impact energies above 100 eV.

Another eikonal based method has been formulated by Byron and Joachain (1973a). The solution of (1.5.2) may be written

$$S = \text{const.} + \int \left[2(E - V)\right]^{\frac{1}{2}} dz \tag{1.5.6}$$

where the trajectory of a straight line along the z-axis parallel to $\underline{k}_i$ has been used.

As $z \to -\infty$, S is required to yield a plane wave, whence

$$S = k_i z - \int_{-\infty}^{z} \left[2(E - V)\right]^{\frac{1}{2}} dz' . \qquad (1.5.7)$$

For high impact energies the integral may be approximated to χ:

$$\chi = -\frac{1}{k_i} \int_{-\infty}^{\infty} V dz \qquad (1.5.8)$$

which is the well known Glauber approximation to S. Substituting into (1.5.5), one obtains the Glauber T-matrix element

$$T_{if}^{G} = \langle \psi_f | V | e^{-i\chi/k_i} \psi_i \rangle . \qquad (1.5.9)$$

Byron and Joachain (1973a) go on to show that this reduces to the form

$$T_{if}^{G} = -ik_i \int d\underline{\rho} e^{i\underline{K}.\underline{\rho}} \langle \psi_f | e^{i\chi} - 1 | \psi_i \rangle \quad . \qquad (1.5.10)$$

Here, ρ is again the impact parameter defining the straight line trajectory with respect to the target atom and $\underline{K}$ the momentum transfer. The eikonal factor is expanded and (1.5.10) rewritten in the form of the Glauber Series

$$T_{if}^{G} = -ik_i \sum_{n=1}^{\infty} \frac{i^n}{n!} T_n^{G} \qquad (1.5.11)$$

with

$$T_n^{G} = \langle \psi_f | \chi^n | \psi_i \rangle . \qquad (1.5.12)$$

This is in close analogy with the Born Series (1.3.3) for T_{if}. Byron and Joachain then take for the Eikonal Born Series

$$T_{if}^{EBS} = T_{if}^{FBA} + T_{if}^{SBA} + T_3^{G} \qquad (1.5.13)$$

where T_3^{G} is treated as a correction term to the Second Born element T_{if}^{SBA}. The model has been further developed by using the Ochkur approximation to account for exchange effects; details may be obtained from the paper by Byron and Joachain (1973a). The method has been successfully applied to the elastic scattering of fast electrons from helium (Byron and Joachain, 1973b)

and to the elastic scattering of electrons from atomic hydrogen at intermediate and higher energies (Byron and Joachain 1974). More recently, Byron and Latour (1976) applied the same method to electron impact excitation of the $n = 2$ states of hydrogen above 100 eV and obtained good agreement with experiment for scattering angles less than 100°. Byron and Joachain (1975) have also considered electron impact excitation of the 2^1S level of helium at intermediate and high energies. However, in this case a slightly modified version of T_{if}^{EBS} was adopted,

$$T_{if}^{EBS} = T^{G} - T_{2}^{G} + T^{SBA} \quad . \tag{1.5.14}$$

Their differential cross section results are seen to be in good agreement with experiment over the whole angular range.

§1.6 Distorted Wave Theory

It has already been remarked in §1.3 that, when the interaction between the incident electron and target atom causes only a small perturbation to the system, the external electron is considered to be adequately represented by a plane wave. This, it will be recalled, is basically the Born approximation which is expected to be valid at high impact energies. However, as was pointed out earlier, when the perturbation is no longer weak, distortion becomes important and plane wave theories break down. Essentially, the distorted wave technique recognises that the wave describing the incoming and outgoing particle will be distorted due to the presence of the target and consequently attempts to incorporate distortion effects into the equations defining the cross sections.

Denoting quantities in the initial channel by the subscript i and those in the final channel by f, the interaction potential V is divided into two parts

$$V = U_i + W_i \tag{1.6.1}$$

$$= U_f + W_f$$

such that the U's depend only upon $\underline{x}$, the coordinate of the free electron. Similarly the total Hamiltonian H is divided into two parts:

$$H = \bar{H}_i + W_i \qquad (1.6.2)$$

$$= \bar{H}_f + W_f$$

with

$$\bar{H}_i = H_i + U_i \qquad (1.6.3)$$

$$= H_f + U_f$$

and H_i, H_f the unperturbed Hamiltonians.

The Lippmann-Schwinger equations satisfied by the total wave functions for the system, Ψ_i^+ and Ψ_f^- (the time reversed Ψ_i^+), are written

$$\Psi_i^+ = \psi_i + \frac{1}{E_i - H_i + i\varepsilon} V \Psi_i^+$$

$$\Psi_f^- = \psi_f + \frac{1}{E_i - H_f - i\varepsilon} V \Psi_f^- \qquad (1.6.4)$$

where notation follows that of §1.2. Similarly the state functions of $\bar{H}_i$ and $\bar{H}_f$ satisfy the equations

$$\phi_i^+ = \psi_i + \frac{1}{E_i - H_i + i\varepsilon} U_i \phi_i^+$$

$$\phi_f^- = \psi_f + \frac{1}{E_i - H_f - i\varepsilon} U_f \phi_f^- \quad . \qquad (1.6.5)$$

Formally equations (1.6.4) and (1.6.5) have solutions in direct analogy with (1.2.7).

The T-matrix element is given by

$$T_{if} = \langle \psi_f V \Psi_i^+ \rangle = \langle \Psi_f^- V \psi_i \rangle \qquad (1.6.6)$$

so that from the above equations, after appropriate formal manipulations, the well known two-potential formulae may be obtained (see for example Messiah, 1970):

$$T_{if} = \langle\phi_f^-|V-W_f|\psi_i\rangle + \langle\phi_f^-|W_f|\Psi_i^+\rangle$$

$$= \langle\psi_f|V-W_i|\phi_i^+\rangle + \langle\Psi_f^-|W_i|\phi_i^+\rangle \quad . \tag{1.6.7}$$

Provided the initial and final target states are different, the first term may be shown to vanish in each case. The Distorted Wave Born Approximation (DWBA) to T_{if} is then derived by approximating Ψ_i^+ by ϕ_i^+ and similarly Ψ_f^- by ϕ_f^- so that (1.6.7) reduces to

$$T_{if}^{DWBA} = \langle\phi_f^-|W|\phi_i^+\rangle \quad . \tag{1.6.8}$$

It is instructive to compare thisexpression with the First Born Approximation to T_{if}:

$$T_{if}^{FBA} = \langle\psi_f|V|\psi_i\rangle \quad . \tag{1.3.4}$$

Physically, the potential U may be said to distort the waves subsequently seen by the second potential W. Equation (1.6.8) is interpreted as the Born Approximation for scattering by W in the presence of the distorting potential U. There is clearly a close analogy between (1.6.8) and (1.3.4), the latter describing the scattering of undistorted or plane waves by the potential V.

Joachain and Vanderpoorten (1973) have combined the DWBA with the Eikonal approach. Basically they choose U by using the Glauber approximation and then compute the distorted wave functions ϕ_i^+ and ϕ_f^- as eikonal wave functions (equation (2.4.2) of their paper). However, the method neglects the effects of exchange between the incoming electron and those of the target and hence is only suitable for describing direct excitation processes at higher impact energies. Coupled with the additional eikonal restrictions, the theory can only be expected to hold for small-angle scattering at intermediate and high impact energies. This is indeed found to be the case. Joachain and Vanderpoorten (1973) employed the model to study inelastic scattering of electrons and protons by atomic hydrogen at intermediate impact energies.

Similarly excitation of the 2^1S and 2^1P levels of helium has been discussed in later publications (Joachain and Vanderpoorten, 1974a and 1974b).

Distorted Wave results for excitation of the 2^1P level of helium by electron impact have also been published by Madison and Shelton (1973). In their calculation, the distorted waves are computed, without exchange considerations, on the potential

$$-\frac{2Z}{x} + V^S(\underline{x})$$

in the initial and final elastic scattering channels. Z is the nuclear charge and $V^S(\underline{x})$ is defined to be the spherical average of the interaction of the free electron with the atomic electrons in the respective channel. The calculation does not allow for target distortion which for intermediate energies is considered important. Nevertheless their results are surprisingly good.

§1.7 Many-Body Theory

The Many-Body Green's function techniques of Martin and Schwinger (1959) have been used by Schneider et al. (1970) to formulate an approximation scheme for the elastic scattering of electrons from atoms and molecules. Using this first-order approach, namely the Random Phase Approximation (henceforth abbreviated to RPA), Yarlagadda et al. (1973) studied elastic scattering of electrons from helium at impact energies below the first ionization threshold. Thomas et al. (1974) extended the method to treat inelastic scattering of electrons from helium over the intermediate energy region and obtained particularly good agreement with experimental results for excitation of the 2^1P level. In their paper the direct and exchange transition matrix elements are given in the RPA as

$$T^D = \int f^{(+)}_{k_i}(\underline{x})\, f^{(-)}_{k_f}(\underline{x})\, \frac{1}{|\underline{x}-\underline{y}|}\, X^{RPA}(\underline{y},\underline{y})\, d\underline{x}d\underline{y} \qquad (1.7.1a)$$

$$T^E = \int f^{(+)}_{k_i}(\underline{x})\, f^{(-)}_{k_f}(\underline{y})\, \frac{1}{|\underline{x}-\underline{y}|}\, X^{RPA}(\underline{y},\underline{x})\, d\underline{x}d\underline{y}. \quad (1.7.1b)$$

$f^{(+)}_{k_i}(\underline{r})$ and $f^{(-)}_{k_f}(\underline{r})$ are the Hartree-Fock continuum orbitals (distorted waves) with outgoing and incoming wave boundary conditions respectively. X^{RPA} is the transition density matrix element computed between the final and initial target states, calculated in the RPA. The theory allows for exchange in determining the distorted waves but omits polarization.

An interesting feature of the model is that the continuum orbitals are both calculated in the field of the initial state of the target. Or, in other words, the outgoing electron sees the initial state of the atom so that scattering occurs before the atom makes the transition to its final state. Such a description is referred to as the two-time model. More recently, many-body theory has been extended further by Yarlagadda and Taylor (1975) to describe electron impact ionization and has been applied in first-order form to the coincident ionization of helium by Baluja and Taylor (1976). The good agreement obtained with experiment lends further support to the two-time model.

The many-body approach has also proved useful by offering insight into other physical aspects of electron-atom collisions. For example, terms arise in the formalism which may be interpreted physically as arising from polarization effects, screening effects due to the atomic electrons, final-state interactions and each with corresponding exchange counterpart. A full description of these interaction terms and others is to be found in the papers by Csanak et al. (1973) and by Csanak and Taylor (1973). A detailed review of the many-body theory approach to atomic collisions is given in the article by Csanak et al. (1971).

It is interesting to note that in the distorted wave calculation by Madison and Shelton (1973), the best results were obtained when the final channel distorted wave was computed in the field of the target ground state, in agreement with the two-time model. Rescigno et al. (1974) have since shown that in lowest-order, the many-body field theory method can be

expressed as a distorted-wave model whereby the distorted wave in both the initial and final channels is a Hartree-Fock continuum orbital calculated in the field of the target ground state. Essentially, Rescigno et al. derive, by using second quantization techniques and the RPA, the expression given by Csanak et al. (1971) for T_{if}. Then, using the distorted wave approximation coupled with the RPA, they obtain the same expression for T_{if}, thus demonstrating the equivalence of the two methods.

CHAPTER 2

THE DISTORTED WAVE POLARIZED ORBITAL METHOD

§2.1 The Polarized Orbital Method

The method of Polarized Orbitals is particularly suited to the study of electron-atom collisions over the intermediate energy range referred to in Chapter 1. It is a method based on physical reasonableness rather than a mathematical derivation from first principles, and as such is an attempt to account for the distortion induced in the target system by the presence of the free electron. This distortion will, of course, also apply to the wave function for the scattering electron. Another dominant effect in this impact energy region arises from the exchange interactions between the scattering electron and the bound electrons. The Distorted Wave Polarized Orbital (abbreviated to DWPO) approach, applied by McDowell et al. (1973) to electron impact excitation of the $1s \rightarrow ns$ transitions in atomic hydrogen and singly ionized helium is designed to allow for these two effects of polarization and electron exchange. Earlier Bell and Kingston (1967a,b,c) used a polarized orbital approach to calculate photoionization cross sections of helium, singly ionized lithium and negative hydrogen ions respectively, and obtained accurate results. Motivated by this work, Lloyd and McDowell (1969) applied the polarized orbital approximation to calculate total cross sections for electron impact excitation of the $2s$ and $2p$ levels of atomic hydrogen for electron energies up to 9 Rydbergs. Subsequently, the DWPO method has been developed by McDowell and coworkers to study differential scattering.

Originally, in a study of polarization and exchange effects on the scattering of electrons from atoms, in particular, oxygen, Temkin (1957) introduced the method of polarized orbitals. The technique was later used by Temkin and Lamkin (1961) and by Sloan (1964) to calculate the lower order phase shifts for electron-hydrogen collisions.

Modifications to the polarized orbital method have been made by a number of authors. In particular, modified versions have been applied to the elastic scattering of electrons from helium by LaBahn and Callaway (1964) and from hydrogen and helium by Callaway et al. (1968). For a comprehensive review of Polarized Orbital Approximations, see the review by Drachman and Temkin (1972). In the following, a brief outline of the original polarized orbital approach will be presented with a view to emphasising the main ideas as summarized by Duxler et al. (1971) describing their application of the theory to scattering of electrons by helium. Hence to be specific, scattering of electrons by a general two-electron atom or ion possessing nuclear charge Z will be considered.

Here, and elsewhere, the centre of mass for the complete scattering system is assumed fixed at the target nucleus. The initially bound electrons will have position vectors $\underline{r}_1$ and $\underline{r}_2$ with respect to this point and that of the incident electron will be $\underline{r}_3$. Atomic units will be adopted here and elsewhere throughout the thesis, unless otherwise stated.

The method essentially offers a prescription to Ψ_i^+, the wave function for the whole system in the initial channel, which, it will be recalled, satisfies the Schrödinger Equation (1.2.1)

$$(H - E)\Psi_i^+ = 0 \quad . \tag{1.2.1}$$

H consists of the kinetic energy operators and Coulombic interactions between the particles comprising the system but omits spin-dependent terms. It is convenient to separate H into two parts

$$H = H' + \delta V \tag{2.1.1}$$

where H' is defined to be

$$H' = -\tfrac{1}{2}\nabla_1^2 - \tfrac{1}{2}\nabla_2^2 - \frac{Z}{r_1} - \frac{Z}{r_2} + \frac{1}{r_{12}} - \frac{(Z-2)}{r_3} \tag{2.1.2}$$

and δV given by

$$\delta V = -\tfrac{1}{2}\nabla_3^2 - \frac{2}{r_3} + \frac{1}{r_{13}} + \frac{1}{r_{23}} \quad . \qquad (2.1.3)$$

The abbreviation $r_{ij} = |\underline{r}_i - \underline{r}_j|$ has been used. Following Duxler et al. (1971), the polarized orbital method has three basic features which for ease of recognition will be labelled A,B,C.

Distortion of the target is recognised at the outset of the theory and is hence incorporated into the form of the atomic wave function as a perturbation correction. Thus, Ψ_i^+ assumes the form

(A) $$\Psi_i^+ = \mathcal{A}\{ \Phi_i(12) + \Phi^{pol}(12;3)\, F(3) \} \qquad (2.1.4)$$

where the following notation has been employed:

$\Phi_i(12)$ = unperturbed ground state atomic wave function;

$\Phi^{pol}(12,3)$ = correction function to $\Phi_i(12)$ due to the polarization of the atomic orbitals by the presence of the incident electron labelled 3;

$F(3)$ = electron wave function describing the scattering:

$\mathcal{A}$ is an antisymmetrising operator acting on all three electron labels.

The incoming electron will induce in the atom electric multipole moments so that a polarization potential is set up which in turn attracts the electron and produces further distortion. The adiabatic approximation is made that the interaction potential between the free electron and target is varying so slowly that the orbital electrons can smoothly adjust; semi-classically this amounts to saying that the speed of the incoming electron is considerably less than that of the bound electrons in their orbits. Mathematically it may be said that the free electron can be assumed stationary and its kinetic energy operator neglected in δV. However, it should be pointed out that for sufficiently polarizable targets, the incoming electron may attain a velocity of similar magnitude to the orbital electrons and hence

invalidate this assumption.

It is further reasoned that the dominant polarization effects come from that region where the incident electron is "outside" the atomic cloud of electrons, that is $r_i < r_3$ $(i = 1,2)$. Hence equation (2.1.3) is approximated to

$$\delta V = -\frac{2}{r_3} + \frac{\varepsilon(r_1,r_3)}{r_{13}} + \frac{\varepsilon(r_2,r_3)}{r_{23}} \qquad (2.1.5)$$

where $\varepsilon(x,y)$ is the unit step function defined by

$$\varepsilon(x,y) = 0 \qquad x > y$$

$$= 1 \qquad x < y \ .$$

Its effect is to "switch off" the perturbation when the incident electron is "inside" the target atom. Replacing the latter two terms in (2.1.5) by their multipole expansions and retaining only the first two terms of each, it is found that

(B)
$$\delta V = \frac{1}{r_3^2} \sum_{j=1}^{2} r_j \cos\theta_{j3}\, \varepsilon(r_j,r_3) \qquad (2.1.6)$$

with θ_{j3} the angle between the radius vectors $\underline{r}_j$ and $\underline{r}_3$. This is the dipole approximation to δV; physically it says that δV is due to a "stationary" external electron and that it is assumed to vanish when the incident electron penetrates the atom.

It remains to find an equation satisfied by the wave function $F(3)$ for the scattering electron. In the method of polarized orbitals this is obtained by projecting the Schrödinger Equation (1.2.1) onto the unperturbed ground state $\Phi_i(12)$ and integrating over the atomic coordinates:

(C)
$$\int \Phi_i^*(12)\,[H-E]\,\Psi_i^+(12;3)\,d\underline{r}_1 d\underline{r}_2 = 0 \ . \qquad (2.1.7)$$

$\Psi_i^+(12;3)$ takes the form given by (2.1.4). Equation (2.1.7) is a necessary condition for Ψ_i^+ to satisfy (1.2.1) but it is clearly not a sufficient condition. Ψ_i^+ would only be an exact solution of the Schrödinger Equation if the projection of $[H-E]\Psi_i^+$ onto all states of the target vanished.

Equation (2.1.7) is the scattering ansatz of the theory and will be further discussed in the next section (§2.2).

So far no mention has been made of how to determine the perturbation $\Phi^{pol}(12;3)$ of equation (2.1.4). Essentially, the unperturbed ground state may be taken to be represented by a separable wave function

$$\Phi_i(12) = \phi_{1s}(1)\phi_{1s}(2) \ . \qquad (2.1.8)$$

When the perturbation δV is introduced, the orbitals $\phi_{1s}(i)$ become polarized and $\Phi_i(12)$ goes over into the perturbed wave function $\Phi_I(12;3)$ obtained by replacing $\phi_{1s}(i)$ in (2.1.8) by $\phi_{1s}(i) + \phi_{pol}(i,3)$, $i = 1,2$. ϕ_{pol} is the dipole component of the perturbed atomic orbital due to the external electron; the problem hence centres on the determination of ϕ_{pol}.

Writing δV_D for the dipole approximation (2.1.6) to δV, the total Hamiltonian H of equation (2.1.1) is approximated to H_D:

$$H_D = H' + \delta V_D \ . \qquad (2.1.9)$$

The functions $\phi_{pol}(i,3)$, $i = 1,2$, may now be determined by using a variational principle, imposing the condition that

$$\delta \int \Phi_I^* \, H_D \, \Phi_I = 0 \ . \qquad (2.1.10)$$

The resulting equation is approximated to first-order in the perturbation (ϕ_{pol}) and subsequently reduced to a second-order differential equation satisfied by ϕ_{pol}. For further details reference should be made to the original paper by Temkin (1957).

To summarize, it is emphasised again that the principal features of the polarized orbital method lie in;(A) the choice of wave function for the complete system,(B) the adiabatic and dipole approximations to the interaction between the scattering and atomic electrons and (C) the scattering ansatz.

The Distorted Wave Polarized Orbital method of McDowell et al. (1973) allows only for dipole distortion implicitly in the initial channel, and calculates the distorted wave in the adiabatic-exchange approximation, to be

discussed in the next section. Explicit target distortion does not appear in the T-matrix element, T_{if}. This relatively simple method is referred to as the DWPO I model. A more sophisticated method (McDowell et al., 1974) allows for target distortion to appear explicitly through the direct part of T_{if} and is referred to as the DWPO II model. Both models have since been used to study excitation of the p-levels of atomic hydrogen and singly ionized helium by electron impact (McDowell et al., 1975a, 1975b; Morgan and McDowell 1975) with energy lying in the intermediate range. Good agreement in the DWPO II model is obtained with experiment for the total $n = 2$ differential cross sections at scattering angles below 60°. Syms et al. (1975) have recently generalized the DWPO II model and examined electron impact excitation of the $n = 3$ levels of atomic hydrogen.

The rest of the chapter will, however, be devoted to application of the DWPO model, in its different forms, to the excitation of helium by electrons with incident energy within the intermediate region. The two essential items are the scattering equation (§2.2) and the form taken by the T-matrix (§2.3).

§2.2 Derivation of the Scattering Equation

In the previous section, the scattering ansatz of the polarized orbital method was stated, equation (2.1.7). The purpose of this section will be to further examine this equation in the context of the Distorted Wave Polarized Orbital method when applied to scattering by helium and to hence derive the equation of motion satisfied by the distorted wave in the adiabatic-exchange approximation. The approximation accounts for distortion of the incident wave through a direct polarization potential and omits those terms arising from exchange-polarization. Moreover, if this direct polarization potential is also omitted, the approximation reduces to the static-exchange model of Morse and Allis (1933). Hence it is convenient to obtain the adiabatic-exchange equation from a derivation of the static-exchange equation coupled with a modification to the static potential to introduce the polarization term.

With this in mind, rather than use (2.1.4) for Ψ_i^+ in (2.1.7), the unperturbed function is adopted instead, that is:

$$\Psi_i^+(12;3) = \mathcal{A}\, \phi_i(12)F(3)\, S^+(12,3) \quad . \tag{2.2.1}$$

Here $\phi_i(12)$ is the spatial part of the helium ground state wave function and $S^+(12,3)$ a singlet spin function; other notation follows that of the previous section (§2.1).

$$\Phi_i(12) = \phi_i(12)\, S^+(12) \tag{2.2.2}$$

represents the unperturbed ground state wave function. The spin functions are defined to be (Mott and Massey, 1965)

$$S^+(12) = \frac{1}{\sqrt{2}} (\alpha_1\beta_2 - \beta_1\alpha_2) \ ,$$

$$S^+(12,3) = S^+(12)\alpha_3 \ ,$$

and the scattering ansatz is written

$$\int \Phi_i^*(12)\, [H-E]\, \Psi_i^+(12,3)\, d\underline{r}_1 d\underline{r}_2 d\zeta = 0 \tag{2.2.3}$$

where the spin integration has been specifically denoted by $d\zeta$. H is given by (2.1.1) with the substitutions (2.1.2) and (2.1.3). Substituting for $\Psi_i^+(12,3)$ by (2.2.1) and $\Phi_i(12)$ by (2.2.2) into (2.2.3) and noting that $\phi_i(12)$ and H are symmetric in 1 and 2, integration over spin yields

$$\int \phi_i^*(12)\, [H-E]\, \{\phi_i(12)F(3) - \phi_i(23)F(1)\}\, d\underline{r}_1 d\underline{r}_2 = 0 \quad . \tag{2.2.4}$$

For convenience, this will be written as

$$I - J = 0 \tag{2.2.5}$$

where I is the direct integral

$$I = \int \phi_i^*(12)[H-E]\, \phi_i(12)F(3) d\underline{r}_1 d\underline{r}_2 \tag{2.2.6}$$

and J the exchange integral

$$J = \int \phi_i^*(12)[H-E]\,\phi_i(23)F(1)d\underline{r}_1 d\underline{r}_2 \quad . \qquad (2.2.7)$$

It is now assumed that $\phi_i(\underline{r},\underline{t})$ is separable and, since the ground state has configuration $(1s)^2$, the Hartree-Fock function becomes a simple product function of the form

$$\phi_i(\underline{r},\underline{t}) = \phi_{1s}(\underline{r})\,\phi_{1s}(\underline{t}) \qquad (2.2.8)$$

where $\phi_{1s}(\underline{r})$ satisfies the Hartree-Fock equation (or equivalently, in this case, the Hartree Equation)

$$\left[\nabla^2 + \frac{2Z}{r} - V_o(r) + \varepsilon_{1s}\right]\phi_{1s}(\underline{r}) = 0 \,. \qquad (2.2.9)$$

Throughout this section, energies will be expressed in Rydberg units; here ε_{1s} is the single ionization energy of the atom. $V_o(r)$ is the potential energy of the electron at position vector $\underline{r}$ (with respect to the centre of mass at the nucleus) due to the field of the other electron:

$$V_o(r) = 2\int \frac{|\phi_{1s}(\underline{t})|^2}{|\underline{r}-\underline{t}|}\, d\underline{t} \quad . \qquad (2.2.10)$$

The ground state energy, E_i, of the atom is expressed then in the form

$$E_i = 2\,\varepsilon_{1s} - \int |\phi_{1s}(\underline{r})|^2\, V_o(r)\, d\underline{r} \qquad (2.2.11)$$

and the total energy, E, of the scattering system is given by

$$E = E_i + k_i^2 \qquad (2.2.12)$$

with $\underline{k}_i$ the incident nomentum.

Having established the form which $\phi_i(12)$ is to take, equations (2.2.6) and (2.2.7) are recalled and simplified in turn under the headings (a) and (b).

(a) $$I = \int \phi_i^*(12)[H-E]\,\phi_i(12)F(3)\, d\underline{r}_1 d\underline{r}_2 \qquad (2.2.6)$$

Substituting for $\phi_i(12)$ from (2.2.8) and also H, referred to after (2.2.3), one has

$$I = \int \phi_{1s}^{*}(1)\,\phi_{1s}^{*}(2)\left[-\nabla_1^2 - \frac{2Z}{r_1} + \frac{2}{r_{12}} \right]\phi_{1s}(1)\,\phi_{1s}(2)\,F(3)\,d\underline{r}_1 d\underline{r}_2$$

$$+ \int \phi_{1s}^{*}(1)\,\phi_{1s}^{*}(2)\left[-\nabla_2^2 - \frac{2Z}{r_2} + \frac{2}{r_{12}} \right]\phi_{1s}(1)\,\phi_{1s}(2)\,F(3)\,d\underline{r}_1 d\underline{r}_2$$

$$+ \int \phi_{1s}^{*}(1)\,\phi_{1s}^{*}(2)\left[-\nabla_3^2 - \frac{2Z}{r_3} - \frac{2}{r_{12}} + \frac{2}{r_{13}} + \frac{2}{r_{23}} - E \right]\phi_{1s}(1)\,\phi_{1s}(2)F(3)d\underline{r}_1 d\underline{r} \qquad (2.2.13)$$

The term $\frac{2}{r_{12}}$ has been added and subtracted for convenience and the nuclear charge number Z retained. With the aid of equations (2.2.10) and (2.2.11) this expression reduces to give

$$I = (2\varepsilon_{1s}-E)F(3) + \int \phi_{1s}^{*}(1)\phi_{1s}^{*}(2)\left[-\nabla_3^2 - \frac{2Z}{r_3} - \frac{2}{r_{12}} + \frac{2}{r_{13}} + \frac{2}{r_{23}}\right]\phi_{1s}(1)$$

$$\phi_{1s}(2)F(3)d\underline{r}_1 d\underline{r}_2 .$$

Then, employing the expression (2.2.12) for E and equation (2.2.11), the above becomes

$$I = \int \phi_{1s}^{*}(1)\phi_{1s}^{*}(2)\left[-\nabla_3^2 - \frac{2Z}{r_3} + \frac{2}{r_{13}} + \frac{2}{r_{23}}\right]\phi_{1s}(1)\phi_{1s}(2)F(3)d\underline{r}_1 d\underline{r}_2 - k_i^2 F(3)$$

which is symmetric in 1 and 2. Hence writing

$$2V_{oo}(r) = -\frac{2Z}{r} + 4\int \frac{|\phi_{1s}(\underline{t})|^2}{|\underline{r}-\underline{t}|}\,d\underline{t} \qquad (2.2.14)$$

the direct integral I may finally be written

$$I = -\left[\nabla_3^2 + k_i^2 - 2V_{oo}(r_3)\right]F(3) \quad . \qquad (2.2.15)$$

(b) $$J = \int \phi_i^{*}(12)[H-E]\,\phi_i(23)F(1)d\underline{r}_1 d\underline{r}_2 \qquad (2.2.7)$$

By hermiticity, or equivalently using Green's Theorem, $\phi_i^{*}(12)$ and $\phi_i(23)F(1)$ may be interchanged so that, writing H in full as in (a) above

$$J = \int \phi_{1s}(2)\phi_{1s}(3)F(1)\left[-\nabla_1^2 + \frac{2}{r_{12}} - \frac{2Z}{r_1}\right]\phi^*_{1s}(1)\phi^*_{1s}(2)d\underline{r}_1 d\underline{r}_2$$

$$+ \int \phi_{1s}(2)\phi_{1s}(3)F(1)\left[-\nabla_2^2 - \frac{2Z}{r_2}\right]\phi^*_{1s}(1)\phi^*_{1s}(2)\, d\underline{r}_1 d\underline{r}_2$$

$$+ \int \phi_{1s}(2)\phi_{1s}(3)F(1)\left[-\nabla_3^2 - \frac{2Z}{r_3} + \frac{2}{r_{13}} + \frac{2}{r_{23}} - E\right]\phi^*_{1s}(1)\phi^*_{1s}(2)\, d\underline{r}_1 d\underline{r}_2 . \tag{2.2.16}$$

With the help of equation (2.2.9) and (2.2.10), the first two terms are simplified so that

$$J = \phi_{1s}(3)\varepsilon_{1s}\int \phi^*_{1s}(1)F(1)d\underline{r}_1 + \int \phi_{1s}(2)\phi_{1s}(3)F(1)\left[-V_o(r_2) + \varepsilon_{1s}\right]$$

$$\phi^*_{1s}(1)\phi^*_{1s}(2)\, d\underline{r}_1 d\underline{r}_2$$

$$+ \int \phi_{1s}(2)\phi_{1s}(3)F(1)\left[-\nabla_3^2 - \frac{2Z}{r_3} + \frac{2}{r_{13}} + \frac{2}{r_{23}} - E\right]\phi^*_{1s}(1)\phi^*_{1s}(2)d\underline{r}_1 d\underline{r}_2 .$$

At this point, it is convenient to denote by G the integral

$$G = \int \phi^*_{1s}(\underline{r})\, F(\underline{r})\, d\underline{r} . \tag{2.2.17}$$

Using (2.2.10) and (2.2.11) J becomes, with suitable rearrangement:

$$J = \varepsilon_{1s}G\phi_{1s}(3) + [E_i - E]\, G\phi_{1s}(3)$$

$$+ 2\phi_{1s}(3)\int \phi^*_{1s}(1)\frac{1}{r_{13}}F(1)d\underline{r}_1 - G\left[\nabla_3^2 + \frac{2Z}{r_3} - V_o(r_3) + \varepsilon_{1s}\right]\phi_{1s}(3)$$

The final bracketed term vanishes by (2.2.9). Finally with the aid of equation (2.2.12), the exchange integral J may be written

$$J = \left[(\varepsilon_{1s} - k_i^2)G + 2\int \phi^*_{1s}(1)\frac{1}{r_{13}}F(1)\, d\underline{r}_1\right]\phi_{1s}(3) \tag{2.2.18}$$

Replacing G by its definition (2.2.17) and combining (2.2.15) and (2.2.18) into (2.2.5) yields the scattering equation for $F(\underline{r})$ in the static-exchange approximation:

$$\left[\nabla^2 + k_i^2 - 2V_{oo}(r)\right]F(\underline{r}) =$$

$$= -\left[(\varepsilon_{1s} - k_i^2) \int \phi_{1s}^*(\underline{t})F(\underline{t})d\underline{t} + 2 \int \frac{\phi_{1s}(\underline{t})F(\underline{t})}{|\underline{r}-\underline{t}|} \, d\underline{t}\right]\phi_{1s}(\underline{r}) \qquad (2.2.19)$$

The adiabatic-exchange approximation is now derived by recalling the definition of $V_{oo}(r)$, equation (2.2.14), and replacing $\phi_{1s}(\underline{t})$ by $\phi_{1s}(\underline{t}) + \phi_{pol}(\underline{t},\underline{r})$ where, it will be recalled, ϕ_{pol} is the dipole component of the perturbed atomic wave function. One then has that

$$2V_{oo}(r) = 2V_{1s,1s}(r) + 2V_{pol}(r) \qquad (2.2.20)$$

with

$$V_{1s,1s}(r) = -\frac{Z}{r} + 2 \int \frac{|\phi_{1s}(\underline{t})|^2}{|\underline{r}-\underline{t}|} \, d\underline{t} \, , \qquad (2.2.21)$$

$$V_{pol}(r) = 2 \int \frac{\phi_{1s}(\underline{t}) \, \phi_{pol}(\underline{t},\underline{r})}{|\underline{r}-\underline{t}|} \, d\underline{t} \, . \qquad (2.2.22)$$

$V_{1s,1s}(r)$ is the direct static potential, that is, the interaction of the free electron with the bound electronic cloud; $V_{pol}(r)$ is the direct polarization potential, due to the distortion of the target by the incident electron.

Inserting (2.2.20) into (2.2.19) the final result is obtained whereby $F(\underline{r})$ satisfies the integro-differential equation,

$$\left[\nabla^2 + k_i^2 - 2V_{1s,1s}(r) - 2V_{pol}(r)\right]F(\underline{r})$$

$$= -\left[(\varepsilon_{1s} - k_i^2) \int \phi_{1s}^*(\underline{t})F(\underline{t})d\underline{t} - 2 \int \frac{\phi_{1s}^*(t)F(t)}{|\underline{r}-\underline{t}|} \, dt\right]\phi_{1s}(r) \, . \qquad (2.2.23)$$

Equation (2.2.23) is the Adiabatic-Exchange approximation to the scattering ansatz (2.1.7) and is the central equation of the DWPO I and DWPO II models. Attention is drawn to the fact that only static-exchange terms have been retained, exchange-polarization having been omitted (see, however, Chapter 4). Essentially this equation may be viewed as an augmentation of the basic static-exchange approximation by the addition of a direct polarization potential. Historically, this is in fact how the approximation was first introduced (Bates and Massey, 1943)

§2.3 Formulation of the T-Matrix Element

This section will be concerned with the formulation of the T-Matrix element in the various DWPO models. Expressions will be obtained to represent transitions from the ground state to either a singlet or triplet spin state of the target. The use of the letter Z to denote the nuclear charge will be continued from the previous section (§2.2), so that the analysis will in fact be applicable to any two-electron atomic system.

To begin with, equation (1.2.10) for T_{if} is recalled and its constituent components defined in the context of the DWPO approximation,

$$T_{if} = \langle \psi_f \, V_f \, \Psi_i^+ \rangle \tag{1.2.10}$$

Here the final channel interaction potential is chosen for V and defined in the direct channel to be

$$V_f = -\frac{2}{r_3} + \frac{1}{r_{13}} + \frac{1}{r_{23}} \tag{2.3.1}$$

so that electrons 1 and 2 are bound and electron 3 is the scattered electron. Ψ_i^+ is defined by equation (2.2.1)

$$\Psi_i^+(12,3) = \phi_i(12)F(3)\, S^+(12,3) \tag{2.2.1}$$

The unperturbed function , ψ_f, for the system in the final channel is defined to be

$$\psi_f(12,3) = \phi_f^{\pm}(12)\chi_{k_f}(z,3)\, S^{\pm}(12,3) \tag{2.3.2}$$

where the plus and minus signs differentiate between either a singlet or a triplet final state respectively. This convention will also be adhered to elsewhere. ϕ_f denotes the spatial part of the atomic wave function and $\chi_{k_f}(z,3)$ is taken to be an outgoing Coulomb wave in the field of the residual charge, $z = Z - 2$, satisfying (McDowell and Coleman, 1970, equation (5.4.1))

$$(\nabla^2 + k_f^2 + \frac{2z}{r})\, \chi_{k_f} = 0 \tag{2.3.13}$$

The doublet spin functions for the system, $S^{\pm}(12,3)$ are given as (Mott and Massey, 1965)

$$S^{+}(12,3) = \frac{1}{\sqrt{2}} (\alpha_1\beta_2 - \beta_1\alpha_2)\,\alpha_3 \ , \qquad (2.3.3a)$$

$$S^{-}(12,3) = \frac{1}{\sqrt{6}} \left[2\beta_3\alpha_1\alpha_2 - \alpha_3(\alpha_1\beta_2 + \beta_1\alpha_2) \right] \ . \qquad (2.3.3b)$$

Substituting these expressions, together with the defining equations (2.2.1) and (2.3.2), into (1.2.10) and effecting the spin integration yields for both singlet (+) and triplet (-) excited states

$$T_{if}^{+} = T_{if}^{D} - T_{if}^{E+} \qquad (2.3.4a)$$

(I)

$$T_{if}^{-} = \sqrt{3}\, T_{if}^{E-} \ . \qquad (2.3.4b)$$

The terms on the right hand side are the matrix elements

$$T_{if}^{D} = \langle \phi_f^{+}(12) \chi_{k_f}(z,3) V_f \phi_i(12) F(3) \rangle \qquad (2.3.5)$$

$$T_{if}^{E\pm} = \langle \phi_f^{\pm}(12) \chi_{k_f}(z,3) V_f \phi_i(23) F(1) \rangle \qquad (2.3.6)$$

denoting the direct and exchange parts respectively. It is noted that for a transition to a triplet spin state, T_{if}^{-} consists of only an exchange term (equations (2.3.4b) and (2.3.6)), coinciding with the fact that such transitions from the ground state can only occur via charge exchange; there are no spin-dependent terms retained in the Hamiltonian of the system.

In §2.1, reference was made to including target distortion explicitly in T_{if}; in the above, this is only allowed for implicitly through calculation of the distorted wave, $F(\underline{r})$.

Such an account of distortion is incorporated by remembering that $\phi_i(\underline{r},\underline{t})$ is separable

$$\phi_i(\underline{r},\underline{t}) = \phi_{ls}(\underline{r})\, \phi_{ls}(\underline{t}) \qquad (2.2.8)$$

and replacing each of the orbitals by the polarized form

$$\phi_{ls}(\underline{r}) \rightarrow \phi_{ls}(\underline{r}) + \phi_{pol}(\underline{r},\underline{t}) \qquad (2.3.7)$$

just as in the derivation of the polarization potential V_{pol} (see equation (2.2.22)). Making this substitution into the direct term (2.3.5), equations (2.3.4) are modified to

$$T_{if}^{+} = (T_{if}^{D} + T_{if}^{P}) - T_{if}^{E+} \qquad (2.3.8a)$$

(II)

$$T_{if}^{-} = \sqrt{3}\, T_{if}^{E-} \qquad (2.3.8b)$$

where

$$T_{if}^{P} = 2\langle\phi_f^{+}(12)\, \chi_{k_f}(z,3)\, V_f\, \phi_{ls}(1)\, \phi_{pol}(2,3)\, F(3)\rangle \quad . \qquad (2.3.9)$$

The exchange matrix element remains unaltered. These approximations to $T_{if}^{\pm}$ are consistent with the adiabatic-exchange approximation (2.2.23) to $F(\underline{r})$; both allow for polarization in the direct terms but neglect entirely the effects of exchange-polarization contributions. If now, the modification (2.3.7) is inserted in the exchange term (2.3.6), equations (2.3.8) become

$$T_{if}^{+} = (T_{if}^{D} + T_{if}^{P}) - (T_{if}^{E+} + T_{if}^{E1+} + T_{if}^{E2+}) \qquad (2.3.10a)$$

(III)

$$T_{if}^{-} = \sqrt{3}\left[T_{if}^{E-} + T_{if}^{E1-} + T_{if}^{E2-}\right] \qquad (2.3.10b)$$

where the additional exchange terms are given by

$$T_{if}^{E1\pm} = \langle\phi_f^{\pm}(12)\, \chi_{k_f}(z,3)\, V_f\, \phi_{ls}(2)\, \phi_{pol}(3,1)\, F(1)\rangle \quad , \qquad (2.3.11)$$

$$T_{if}^{E2\pm} = \langle\phi_f^{\pm}(12)\, \chi_{k_f}(z,3)\, V_f\, \phi_{ls}(3)\, \phi_{pol}(2,1)\, F(1)\rangle \quad . \qquad (2.3.12)$$

This approximation to $T_{if}^{\pm}$ allows for both direct and exchange effects in the atomic wave function arising from dipole distortion of the target. However, the adiabatic-exchange approximation to $F(\underline{r})$ is inconsistent with this treatment. The scattering equation must be modified to include the additional terms which arise when account is taken of exchange on the polarization parts. This will

be discussed in Chapter 4.

The significance of the Roman numerals (I-III) is to indicate the various DWPO approximations to T_{if}. Hence equation (2.3.4) is the DWPO I approximation to T_{if}; equation (2.3.8) is the DWPO II approximation, and equation (2.3.10) is the DWPO III approximation. Physically these models may be summarized by saying that: DWPO I allows for target distortion only implicitly through the calculation of the distorted wave in the adiabatic-exchange approximation; DWPO II calculates the distorted wave also in the adiabatic-exchange approximation but, in addition, allows for target distortion explicitly in the direct term of the T-matrix; DWPO III takes account of distortion in both the direct and exchange terms of the T-matrix but no longer calculates the distorted wave in the adiabatic-exchange approximation. It is to be noted that for excitation to a triplet spin state, DWPO II reduces to the simpler DWPO I model.

The remainder of this section will centre upon a study of the constituent parts of the T-matrix namely equations (2.3.5), (2.3.6), (2.3.9), (2.3.11) and (2.3.12), in preparation for a partial wave analysis in the following chapters.

The final unperturbed target wave function, $\phi_f(12)$, is written

$$\phi_f^{\pm}(12) = \frac{1}{\sqrt{2}}\left[u_{1s}(1)\, v_{n\ell}^{\pm}(2) \pm v_{n\ell}^{\pm}(1)\, u_{1s}(2)\right] \qquad (2.3.14)$$

where $u_{1s}(\underline{r})$ is the core orbital and $v_{n\ell}^{\pm}(\underline{r})$ the valence orbital of the atom. The various direct and exchange contributions to $T_{if}^{\pm}$, when the substitutions indicated by equation (2.3.1) for V_f and (2.3.14) for $\phi_f^{\pm}$ are made, will now be considered in turn.

$\underline{T_{if}^{D}}$:

$$T_{if}^{D} = \frac{1}{\sqrt{2}} \int\left[u_{1s}^{*}(1)\, v_{n\ell}^{*+}(2) + v_{n\ell}^{*+}(1) u_{1s}^{*}(2)\right]\chi_{k_f}^{*}(z,3)\left(\frac{1}{r_{13}} + \frac{1}{r_{23}} - \frac{2}{r_3}\right)$$

$$\phi_{1s}(1)\phi_{1s}(2)F(3)\, d\underline{r}_{123}$$

where $d\underline{r}_{i\ldots j}$ indicates integration over the space variables $\underline{r}_i \ldots \underline{r}_j$, both here and elsewhere.

This expression is symmetric in 1 and 2 and may hence be written

$$T_{if}^{D} = \frac{2}{\sqrt{2}}\left[I_1 + I_2 - I_3 - I_4\right] \qquad (2.3.15)$$

with:

$$I_1 = \int u_{1s}^{*}(2)\, v_{n\ell}^{*+}(1)\, \chi_{k_f}^{*}(z,3)\, \frac{1}{r_{13}}\, \phi_{1s}(1)\phi_{1s}(2)\, F(3)\, d\underline{r}_{123} \qquad (2.3.16a)$$

$$I_2 = \int u_{1s}^{*}(1)\, v_{n\ell}^{*+}(2)\, \chi_{k_f}^{*}(z,3)\, \frac{1}{r_{13}}\, \phi_{1s}(1)\phi_{1s}(2)\, F(3)\, d\underline{r}_{123} \qquad (2.3.16b)$$

$$I_3 = \int u_{1s}^{*}(2)\, v_{n\ell}^{*+}(1)\, \chi_{k_f}^{*}(z,3)\, \frac{1}{r_{3}}\, \phi_{1s}(1)\, \phi_{1s}(2)\, F(3)\, d\underline{r}_{123} \qquad (2.3.16c)$$

$$I_4 = \int u_{1s}^{*}(1)\, v_{n\ell}^{*+}(2)\, \chi_{k_f}^{*}(z,3)\, \frac{1}{r_{3}}\, \phi_{1s}(1)\, \phi_{1s}(2)\, F(3)\, d\underline{r}_{123} \qquad (2.3.16d)$$

$\phi_{1s}(\underline{r})$ and $v_{n\ell}^{+}(\underline{r})$ are required to be orthogonal in which case

$$I_2 = I_3 = I_4 = 0 \quad .$$

The integral I_1 is separable so that one may define

$$B = \int u_{1s}^{*}(\underline{r})\, \phi_{1s}(\underline{r})\, d\underline{r} \quad , \qquad (2.3.17)$$

$$I_A = \int v_{n\ell}^{*+}(1)\, \chi_{k_f}^{*}(z,3)\, \frac{1}{r_{13}}\, \phi_{1s}(1)\, F(3)\, d\underline{r}_{13}; \qquad (2.3.18)$$

note that B should approximately be unity. T_{if}^{D} can hence be written as

$$T_{if}^{D} = B\, \sqrt{2}\, I_A \quad . \qquad (2.3.19)$$

$\underline{T_{if}^{P}}$:

$$T_{if}^{P} = \frac{2}{\sqrt{2}} \int \left[u_{1s}^{*}(1)\, v_{n\ell}^{*+}(2) + v_{n\ell}^{*+}(1)\, u_{1s}^{*}(2) \right] \chi_{k_f}^{*}(z,3)\, \left(\frac{1}{r_{13}} + \frac{1}{r_{23}} - \frac{2}{r_3} \right)$$

$$\phi_{1s}(1)\, \phi_{pol}(23)\, F(3)\, d\underline{r}_{123} \quad .$$

This is written more compactly as

$$T_{if}^{P} = \sqrt{2} \left[K_1 + K_2 - 2K_3 + K_4 + K_5 - 2K_6 \right] \qquad (2.3.20)$$

with:

$$K_1 = \int u^*_{1s}(1)\, v^{*+}_{n\ell}(2)\, \chi^*_{k_f}(z,3)\, \frac{1}{r_{23}}\, \phi_{1s}(1)\, \phi_{pol}(23)\, F(3)\, d\underline{r}_{123} \qquad (2.3.21a)$$

$$K_2 = \int u^*_{1s}(1)\, v^{*+}_{n\ell}(2)\, \chi^*_{k_f}(z,3)\, \frac{1}{r_{13}}\, \phi_{1s}(1)\, \phi_{pol}(23)\, F(3)\, d\underline{r}_{123} \qquad (2.3.21b)$$

$$K_3 = \int u^*_{1s}(1)\, v^{*+}_{n\ell}(2)\, \chi^*_{k_f}(z,3)\, \frac{1}{r_{3}}\, \phi_{1s}(1)\, \phi_{pol}(23)\, F(3)\, d\underline{r}_{123} \qquad (2.3.21c)$$

$$K_4 = \int u^*_{1s}(2)\, v^{*+}_{n\ell}(1)\, \chi^*_{k_f}(z,3)\, \frac{1}{r_{13}}\, \phi_{1s}(1)\, \phi_{pol}(23)\, F(3)\, d\underline{r}_{123} \qquad (2.3.21d)$$

$$K_5 = \int u^*_{1s}(2)\, v^{*+}_{n\ell}(1)\, \chi^*_{k_f}(z,3)\, \frac{1}{r_{23}}\, \phi_{1s}(1)\, \phi_{pol}(23)\, F(3)\, d\underline{r}_{123} \qquad (2.3.21e)$$

$$K_6 = \int u^*_{1s}(2)\, v^{*+}_{n\ell}(1)\, \chi^*_{k_f}(z,3)\, \frac{1}{r_{3}}\, \phi_{1s}(1)\, \phi_{pol}(23)\, F(3)\, d\underline{r}_{123} \qquad (2.3.21f)$$

From the orthogonality of $\phi_{1s}(\underline{r})$ and $v_{n\ell}(\underline{r})$

$$K_5 = K_6 = 0$$

so that T_{if}^{P} simplifies to

$$T_{if}^{P} = \sqrt{2}\left[K_1 + K_2 - 2K_3 + K_4\right] \quad . \qquad (2.3.22)$$

$\underline{T_{if}^{E\pm}}$:

$$T_{if}^{E\pm} = \frac{1}{\sqrt{2}} \int \left[u^*_{1s}(1)\, v^{*\pm}_{n\ell}(2) \pm v^{*\pm}_{n\ell}(1)\, u^*_{1s}(2) \right] \chi^*_{k_f}(z,3) \left(\frac{1}{r_{13}} + \frac{1}{r_{23}} - \frac{2}{r_3}\right)$$

$$\phi_{1s}(2)\, \phi_{1s}(3)\, F(1)\, d\underline{r}_{123}$$

In a more condensed form this is written

$$T_{if}^{E\pm} = \frac{1}{\sqrt{2}} \left[\pm J_1 + J_2 \pm J_3 \mp 2J_4 + J_5 - 2J_6 \right] \qquad (2.3.23)$$

with:

$$J_1 = \int u^*_{ls}(2)\, v^{*\pm}_{n\ell}(1)\, \chi^*_{k_f}(z,3)\, \frac{1}{r_{13}}\, \phi_{ls}(2)\, \phi_{ls}(3)\, F(1)\, d\underline{r}_{123} \qquad (2.3.24a)$$

$$J_2 = \int u^*_{ls}(1)\, v^{*\pm}_{n\ell}(2)\, \chi^*_{k_f}(z,3)\, \frac{1}{r_{23}}\, \phi_{ls}(2)\, \phi_{ls}(3)\, F(1)\, d\underline{r}_{123} \qquad (2.3.24b)$$

$$J_3 = \int u^*_{ls}(2)\, v^{*\pm}_{n\ell}(1)\, \chi^*_{k_f}(z,3)\, \frac{1}{r_{23}}\, \phi_{ls}(2)\, \phi_{ls}(3)\, F(1)\, d\underline{r}_{123} \qquad (2.3.24c)$$

$$J_4 = \int u^*_{ls}(2)\, v^{*\pm}_{n\ell}(1)\, \chi^*_{k_f}(z,3)\, \frac{1}{r_3}\, \phi_{ls}(2)\, \phi_{ls}(3)\, F(1)\, d\underline{r}_{123} \qquad (2.3.24d)$$

$$J_5 = \int u^*_{ls}(1)\, v^{*\pm}_{n\ell}(2)\, \chi^*_{k_f}(z,3)\, \frac{1}{r_{13}}\, \phi_{ls}(2)\, \phi_{ls}(3)\, F(1)\, d\underline{r}_{123} \qquad (2.3.24e)$$

$$J_6 = \int u^*_{ls}(1)\, v^{*\pm}_{n\ell}(2)\, \chi^*_{k_f}(z,3)\, \frac{1}{r_3}\, \phi_{ls}(2)\, \phi_{ls}(3)\, F(1)\, d\underline{r}_{123} \qquad (2.3.24f)$$

From orthogonality between bound states

$$J_5 = J_6 = 0.$$

$T_{if}^{E\pm}$ therefore reduces to

$$T_{if}^{E\pm} = \pm \frac{1}{\sqrt{2}} \left[J_1 \pm J_2 + J_3 - 2J_4 \right] . \qquad (2.3.25)$$

$\underline{T_{if}^{El\pm}}$:

$$T_{if}^{El\pm} = \frac{1}{\sqrt{2}} \int \left[u^*_{ls}(1)\, v^{*\pm}_{n\ell}(2) \pm v^{*\pm}_{n\ell}(1)\, u^*_{ls}(2) \right] \chi^*_{k_f}(z,3) \left(\frac{1}{r_{13}} + \frac{1}{r_{23}} - \frac{2}{r_3} \right)$$

$$\phi_{ls}(2)\, \phi_{pol}(31)\, F(1)\, d\underline{r}_{123}$$

which is written

$$T_{if}^{El\pm} = \frac{1}{\sqrt{2}} \left[\pm K_1^{El} \mp K_2^{El} + K_3^{El} \pm K_4^{El} + K_5^{El} - 2K_6^{El} \right] \qquad (2.3.26)$$

with :

$$K_1^{El} = \int u_{ls}^*(2)\, v_{n\ell}^{*\pm}(1)\, \chi_{k_f}^*(z,3)\left(\frac{1}{r_{13}} - \frac{1}{r_3}\right) \phi_{ls}(2)\, \phi_{pol}(31)\, F(1)\, d\underline{r}_{123} \quad (2.3.27a)$$

$$K_2^{El} = \int u_{ls}^*(2)\, v_{n\ell}^{*\pm}(1)\, \chi_{k_f}^*(z,3)\frac{1}{r_3}\, \phi_{ls}(2)\, \phi_{pol}(31)\, F(1)\, d\underline{r}_{123} \quad (2.3.27b)$$

$$K_3^{El} = \int u_{ls}^*(1)\, v_{n\ell}^{*\pm}(2)\, \chi_{k_f}^*(z,3)\frac{1}{r_{23}}\, \phi_{ls}(2)\, \phi_{pol}(31)\, F(1)\, d\underline{r}_{123} \quad (2.3.27c)$$

$$K_4^{El} = \int u_{ls}^*(2)\, v_{n\ell}^{*\pm}(1)\, \chi_{k_f}^*(z,3)\frac{1}{r_{23}}\, \phi_{ls}(2)\, \phi_{pol}(31)\, F(1)\, d\underline{r}_{123} \quad (2.3.27d)$$

$$K_5^{El} = \int u_{ls}^*(1)\, v_{n\ell}^{*\pm}(2)\, \chi_{k_f}^*(z,3)\frac{1}{r_{13}}\, \phi_{ls}(2)\, \phi_{pol}(31)\, F(1)\, d\underline{r}_{123} \quad (2.3.27e)$$

$$K_6^{El} = \int u_{ls}^*(1)\, v_{n\ell}^{*\pm}(2)\, \chi_{k_f}^*(z,3)\frac{1}{r_3}\, \phi_{ls}(2)\, \phi_{pol}(31)\, F(1)\, d\underline{r}_{123} \quad (2.3.27f)$$

By the usual orthogonality requirements one has

$$K_5^{El} = K_6^{El} = 0 \quad .$$

$T_{if}^{El\pm}$ hence becomes

$$T_{if}^{El\pm} = \pm \frac{1}{\sqrt{2}} \left[K_1^{El} - K_2^{El} \pm K_3^{El} + K_4^{El} \right] \quad . \qquad (2.3.28)$$

$\underline{T_{if}^{E2\pm}}$:

$$T_{if}^{E2\pm} = \frac{1}{\sqrt{2}} \int \left[u_{ls}^*(1)\, v_{n\ell}^{*\pm}(2) \pm v_{n\ell}^{*\pm}(1)\, u_{ls}^*(2) \right] \chi_{k_f}^*(z,3) \left(\frac{1}{r_{13}} + \frac{1}{r_{23}} - \frac{2}{r_3}\right)$$

$$\phi_{ls}(3)\, \phi_{pol}(21)\, F(1)\, d\underline{r}_{123}$$

This integral is rearranged so that defining

$$K_1^{E2} = \int u_{1s}^*(1)\, v_{n\ell}^{*\pm}(2)\, \chi_{k_f}^*(z,3)\, \frac{1}{r_{23}}\, \phi_{1s}(3)\, \phi_{pol}(21)\, F(1)\, d\underline{r}_{123} \qquad (2.3.29a)$$

$$K_2^{E2} = \int u_{1s}^*(2)\, v_{n\ell}^{*\pm}(1)\, \chi_{k_f}^*(z,3)\, \frac{1}{r_{23}}\, \phi_{1s}(3)\, \phi_{pol}(21)\, F(1)\, d\underline{r}_{123} \qquad (2.3.29b)$$

$$K_3^{E2} = \int u_{1s}^*(1)\, v_{n\ell}^{*\pm}(2)\, \chi_{k_f}^*(z,3)\, \frac{1}{r_{13}}\, \phi_{1s}(3)\, \phi_{pol}(21)\, F(1)\, d\underline{r}_{123} \qquad (2.3.29c)$$

$$K_4^{E2} = \int u_{1s}^*(1)\, v_{n\ell}^{*\pm}(2)\, \chi_{k_f}^*(z,3)\, \frac{1}{r_3}\, \phi_{1s}(3)\, \phi_{pol}(21)\, F(1)\, d\underline{r}_{123} \qquad (2.3.29d)$$

$$K_5^{E2} = \int u_{1s}^*(2)\, v_{n\ell}^{*\pm}(1)\, \chi_{k_f}^*(z,3)\, \frac{1}{r_{13}}\, \phi_{1s}(3)\, \phi_{pol}(21)\, F(1)\, d\underline{r}_{123} \qquad (2.3.29e)$$

$$K_6^{E2} = \int u_{1s}^*(2)\, v_{n\ell}^{*\pm}(1)\, \chi_{k_f}^*(z,3)\, \frac{1}{r_3}\, \phi_{1s}(3)\, \phi_{pol}(21)\, F(1)\, d\underline{r}_{123} \qquad (2.3.29f)$$

$T_{if}^{E2\pm}$ becomes

$$T_{if}^{E2\pm} = \frac{1}{\sqrt{2}} \left[K_1^{E2} \pm K_2^{E2} + K_3^{E2} - 2K_4^{E2} \pm K_5^{E2} \mp 2K_6^{E2} \right]. \qquad (2.3.30)$$

In connection with the exchange integrals, it is worth emphasing that, apart from the choice of $v_{n\ell}^{\pm}(\underline{r})$, the integrals are the same for excitation to either a singlet or triplet final spin state.

CHAPTER 3

EXCITATION OF HELIUM

§3.1 Preliminary Remarks

This chapter will be concerned with a partial wave treatment of the Adiabatic-Exchange Equation derived in §2.2, equation (2.2.23), and a partial wave analysis of the integrals obtained in §2.3 which constitute the T-matrix. These integrals will be dealt with according to the excited state under consideration (§3.3 for S-states, §3.4 for P-states) and expressions formulated for the differential and total cross sections. The chapter will conclude with a discussion of the (λ,χ) orientation and alignment parameters with application to $1^1S \rightarrow n^1P$ transitions.

In this first section, some basic definitions and notation for the wave functions employed will be established and various partial wave expansions summarised.

Previously, the approximate Hartree-Fock ground state wave function $\phi_i(12)$ of equation (2.2.8) was expressed as a product of two orbitals. Each of these orbitals is now written as

$$\phi_{1s}(\underline{r}) = R_{1s}(r)\, Y_{oo}(\hat{r}) \qquad (3.1.1)$$

where $R_{1s}(r)$ is the radial part of the function and has the form

$$R_{1s}(r) = N_1(e^{-ar} + c_1\, e^{-br}); \qquad (3.1.2)$$

N_1, a,b and c_1 are constants.

$Y_{\ell m}(\hat{r})$ is a spherical harmonic function satisfying the convention

$$Y^*_{\ell m}(\hat{r}) = (-1)^m\, Y_{\ell -m}(\hat{r}) ; \qquad (3.1.3)$$

$\hat{x}$ denotes the angular components of $\underline{x}$ in spherical polar coordinates, $\hat{x} = (\theta,\phi)$; $\hat{\underline{x}}$ will denote a unit vector in the direction of $\underline{x}$.

The excited state wave function $\phi_f(12)$, written as

$$\phi_f(12) = \frac{1}{\sqrt{2}} \left[u_{1s}(1)\, v^{\pm}_{n\ell}(12) \pm v^{\pm}_{n\ell}(1)\, u_{1s}(2) \right], \quad (2.3.14)$$

has the core orbital $u_{1s}(\underline{r})$ expressed in the form

$$u_{1s}(\underline{r}) = w(r)\, Y_{oo}(\hat{r}) \quad (3.1.4)$$

and the valence orbital $v^{\pm}_{n\ell}(\underline{r})$ as

$$v^{\pm}_{n\ell}(\underline{r}) = R^{\pm}_{n\ell}(r)\, Y_{\ell m}(\hat{r}). \quad (3.1.5)$$

The choice of the radial parts $R_{1s}(r)$, $w(r)$ and $R_{n\ell}(r)$ is discussed in Appendix A. In order to avoid unnecessarily complicating the notation, it should cause no ambiguity if the '$\pm$' superscript convention is not strictly adhered to in the analysis to follow.

Concerning the polarized orbital correction; the first-order perturbation term $\phi_{pol}(\underline{r},\underline{t})$ to the orbital $\phi_{1s}(\underline{r})$ is given in the following form by Temkin (1959), modified by Temkin and Lamkin (1961), as

$$\phi_{pol}(\underline{r},\underline{t}) = -\frac{\varepsilon(r,t)}{t^2} \cdot \frac{u_{1s\to p}(r)}{r} \cdot \frac{P_1(\cos\theta_{rt})}{\sqrt{\pi}} \; ; \quad (3.1.6)$$

$\varepsilon(r,t)$ is the unit step function introduced in equation (2.1.5) which causes the perturbation to vanish when the incident particle penetrates the atomic cloud. $P_1(x)$ is a first-order Legendre polynomial and the radial function $u_{1s\to p}(r)$ satisfies the Sternheimer Equation

$$-\left[\frac{d^2}{dr^2} - \frac{P_{1s}''(r)}{P_{1s}(r)} - \frac{2}{r^2} \right] u_{1s\to p}(r) = P_{1s}(r) \; . \quad (3.1.7)$$

Here $P_{1s}(r)$ is the r-multiplied radial component of the ground state orbital; primes denote differentiation with respect to r. This equation is obtained following the discussion after equation (2.1.10)—for a complete account see §6.3 of the article by Drachman and Temkin (1972). Usually Sternheimer's equation must be solved numerically. However, by a slight modification to $P_{1s}(r)$, a closed expression may be obtained for $u_{1s\to p}(r)$ as follows.

A function $f(r)$ is defined such that

$$u_{1s\to p}(r) = f(r)\, P_{1s}(r) \tag{3.1.8}$$

and can easily be shown to satisfy the equation

$$\left[-\frac{d^2}{dr^2} - \frac{2P'_{1s}(r)}{P_{1s}(r)} \frac{d}{dr} + \frac{2}{r^2} \right] f(r) = r \tag{3.1.9}$$

by substituting (3.1.8) directly into equation (3.1.7). The modification is to let $P_{1s}(r)$ have the hydrogenic form

$$P_{1s}(r) = 2Z_o^{3/2}\, r\, e^{-Z_o r} \tag{3.1.10}$$

with Z_o a screening parameter, to be determined in the next section (§3.2) in connection with the direct polarization potential. Upon insertion into (3.1.9) the subsequent equation is solved to yield

$$f(r) = \frac{1}{2Z_o^3} (Z_o r + \tfrac{1}{2} Z_o^2 r^2). \tag{3.1.11}$$

Hence $u_{1s\to p}(r)$ can now be written in closed form as

$$u_{1s\to p}(r) = Z_o^{-3/2}\, r\, e^{-Z_o r} (Z_o r + \tfrac{1}{2} Z_o^2 r^2). \tag{3.1.12}$$

Because $P_{1s}(r)$ has assumed a hydrogenic form, which for hydrogen is exact with $Z_o = 1$, this approximation to $u_{1s\to p}(r)$ will be referred to as the Self Consistent Field Hydrogenic Approximation.

Having dealt with the atomic wave functions, attention will now be drawn to the various partial wave expansions in spherical harmonics to be used in succeeding sections. The spherical harmonic addition theorem states that (Messiah, 197.0)

$$P_\ell(\cos\theta_{12}) = \frac{4\pi}{2\ell+1} \sum_{m=-\ell}^{\ell} Y^*_{\ell m}(\hat{r}_1)\, Y_{\ell m}(\hat{r}_2) \tag{3.1.13}$$

where θ_{12} is the angle between the directions specified by $\hat{r}_1$ and $\hat{r}_2$ and $P_\ell(x)$ denotes, of course, a Legendre polynomial.

The inverse of $|\underline{r} - \underline{t}|$ is expanded in the well known multipole formula

$$\frac{1}{|\underline{r}-\underline{t}|} = \sum_{\lambda=0}^{\infty} \sum_{\mu=\lambda}^{\lambda} \frac{4\pi}{2\lambda+1} \gamma_\lambda(r,t)\, Y^*_{\lambda\mu}(\hat{r})\, Y_{\lambda\mu}(\hat{t}) \qquad (3.1.14)$$

where

$$\gamma_\lambda(r,t) = \frac{r_<^{\lambda}}{r_>^{\lambda+1}} \qquad (3.1.15)$$

$$r_< = \min(r,t); \quad r_> = \max(r,t).$$

The incoming wave $F(\underline{r})$ is decomposed into a series of partial waves as

$$F(\underline{r}) = \sum_{\ell=0}^{\infty} A(\ell,k_i) \frac{u_\ell(k_i,r)}{r} P_\ell(\cos\theta) \qquad (3.1.16)$$

where $A(\ell,k_i)$ is a coefficient depending only upon ℓ and k_i. The $u_\ell(k_i,r)$ satisfy the boundary conditions

$$u_\ell(k_i,0) = 0 \; ; \; u_\ell(k_i,r) \underset{r\to\infty}{\sim} k_i^{-\frac{1}{2}} \sin(\phi(r) + \delta_\ell) \qquad (3.1.17)$$

with δ_ℓ the elastic scattering phase shift and

$$\phi(r) \underset{r\to\infty}{\sim} k_i r - \frac{\ell\pi}{2} + \frac{z}{k_i} \log(2k_i r) + \eta_\ell(k_i) \; ; \qquad (3.1.18)$$

$\eta_\ell(k)$ is the Coulomb phase shift given by

$$\eta_\ell(k) = \arg \Gamma(\ell + 1 - \frac{iz}{k}) . \qquad (3.1.19)$$

Specifically, $A(\ell,k_i)$ has the form

$$A(\ell,k_i) = (2\ell+1)\, i^\ell\, k_i^{-\frac{1}{2}} \exp[i\{\delta_\ell(k_i) + \eta_\ell(k_i)\}]. \qquad (3.1.20)$$

Using also the relation between spherical harmonics and associated Legendre polynomials

$$Y_{\ell m}(\theta,\phi) = (-1)^m \left[\frac{2\ell+1}{4\pi} \cdot \frac{(\ell-m)!}{(\ell+m)!}\right]^{\frac{1}{2}} P_\ell^{\,m}(\cos\theta)\, e^{im\phi}, \quad m \geq 0 \qquad (3.1.21)$$

(if $m < 0$, use is first made of relation (3.1.3))

with $m = 0$ in this case, it is convenient to rewrite (3.1.16) as

$$F(\underline{r}) = \sqrt{\frac{4\pi}{k_i}} \sum_{\ell=0}^{\infty} (2\ell+1)^{\frac{1}{2}}\, i^\ell \frac{u_\ell(k_i r)}{r} Y_{\ell 0}(\hat{r}) \exp[i\{\delta_\ell(k_i) + \eta_\ell(k_i)\}] \qquad (3.1.22)$$

The outgoing Coulomb wave $\chi_{k_f}(z,r)$ is expressed in a similar manner as

$$\chi_{k_f}(z,\underline{r}) = 4\pi \sum_{\lambda=0}^{\infty} \sum_{\mu=-\lambda}^{\lambda} i^{\lambda} H_{\lambda}(k_f r)\, Y_{\lambda\mu}(\hat{r})\, Y^{*}_{\lambda\mu}(\theta,0)\, \exp[i\eta_{\lambda}(k_f)] \qquad (3.1.23)$$

where it will be remembered that since the origin of coordinates is at the nucleus, the angle beween $\underline{r}$ and $\underline{k}_f$ in (3.1.23) is $\theta - \theta$ with θ the scattering angle defined by

$$\hat{\underline{k}}_i . \hat{\underline{k}}_f = \cos\theta . \qquad (3.1.24)$$

The function $H_{\lambda}(kr)$ is given by

$$krH_{\lambda}(kr) = G_{\lambda}(kr) \qquad (3.1.25)$$

where $G_{\lambda}(kr)$ is the regular Coulomb function satisfying (McDowell and Coleman, 1970, equation (5.4.18))

$$\left[\frac{d^2}{dr^2} + k^2 - \frac{\lambda(\lambda+1)}{r^2} + \frac{2z}{r} \right] G_{\lambda}(kr) = 0 \qquad (3.1.26)$$

subject to:

$$G_{\lambda}(k,0) = 0 \; ; \; G_{\lambda}(k,r) \underset{r\to\infty}{\sim} \sin(kr - \frac{\lambda\pi}{2} + \frac{z}{k}\log(2kr) + \eta_{\lambda}(k)). \qquad (3.1.27)$$

For helium, $z = 0$ (viz. $z = Z - 2$) so that $\chi_{k_f}(z,\underline{r})$ becomes a plane wave and $H_{\lambda}(kr)$ reduces to a spherical Bessel function.

Having established the above definitions and expressions, particularly the partial wave expansions, one can now proceed to look further at the scattering equation (2.2.23) and integrals of §2.3.

§3.2 The Radial Scattering Equation

The radial scattering equation satisfied by the $u_{\ell}(k_i,r)$ appearing in the partial wave expansion (3.1.22) is obtained by inserting (3.1.22) into the adiabtic-exchange equation (2.2.23). Use is made of the substitution (3.1.1) and of the expansion (3.1.14) so that after straightforward partial wave analysis, one obtains:

$$\left[\frac{d^2}{dr^2} + k_i^2 - \frac{\ell(\ell+1)}{r^2} - 2V_{ls,ls}(r) - 2V_{pol}(r)\right] u_\ell(k_i,r) = -\left[(\varepsilon_{ls} - k_i^2)\delta_{\ell 0}\right.$$

$$\left.\int_0^\infty R_{ls}(t)u_\ell(k_i,t)tdt + \frac{2}{2\ell+1}\int_0^\infty R_{ls}(t)u_\ell(k_i,t)\gamma_\ell(r,t)tdt\right] rR_{ls}(r). \quad (3.2.1)$$

Closed expressions, to be given below, may be derived for the direct potential terms $V_{ls,ls}(r)$ and $V_{pol}(r)$. Hence this equation is now amenable to integration by numerical methods. Discussion of such techniques for solving this type of equation is postponed until Chapter 5 on computation and numerical analysis.

Attention will now focus on the direct potentials. Recalling equation (2.2.21) for $V_{ls,ls}(r)$ and equation (3.1.1) for $\phi_{ls}(\underline{r})$, one finds with the aid of (3.1.14) and effecting the angular integration:

$$2V_{ls,ls}(r) = -\frac{2Z}{r} + 4\int_0^\infty R_{ls}^2(t)\,\gamma_o(r,t)\,t^2\,dt. \quad (3.2.2)$$

Replacing $R_{ls}(t)$ by the expression (3.1.2), the radial integration is carried out so that (3.2.2) reduces to

$$2V_{ls,ls}(r) = -\frac{2Z}{r} + \frac{4}{r}\left[1 - N_1^2\left\{(1+\frac{2}{2a})\,\frac{e^{-2ar}}{(2a)^2}\right.\right.$$

$$\left.\left. + 2c_1(1+\frac{2}{(a+b)})\,\frac{e^{-(a+b)r}}{(a+b)^2} + c_1^2\,(1+\frac{2}{2b})\,\frac{e^{-2br}}{(2b)^2}\right\}\right]. \quad (3.2.3)$$

It is noted that asymptotically

$$2V_{ls,ls}(r) \underset{r\to\infty}{\sim} \frac{-2(Z-2)}{r}$$

as expected since the scattering electron moves in the field of a nucleus screened by two electrons.

The polarization potential $V_{pol}(r)$ is treated similarly. In this case the wave functions appearing in equation (2.2.22) are replaced according to (3.1.1) and (3.1.6) so that one has

$$2V_{pol}(r) = -\frac{4}{r^2\sqrt{\pi}}\int_0^r R_{ls}(t)\,u_{ls\to p}(t)\left\{\int_\Omega \frac{Y_{oo}(\hat{t})P_1(\cos\theta_{rt})}{|\underline{r}-\underline{t}|}\,d\hat{t}\right\}tdt$$

where the radial and angular integrations have been indicated separately.

Using the addition theorem (3.1.13) on $P_1(\cos\theta_{rt})$ and inserting the expansion (3.1.14), the angular integration is carried out to give

$$2V_{pol}(r) = -\frac{8}{3r^4}\int_0^r R_{ls}(t)\, u_{ls\to p}(t)\, t^2\, dt\,. \qquad (3.2.4)$$

Inserting (3.1.2) and (3.1.12) for the functions $R_{ls}(t)$ and $u_{ls\to p}(t)$ and integrating finally gives

$$2V_{pol}(r) = -\frac{4}{3r^4}\cdot\frac{N_1}{\sqrt{Z_o}}\sum_{i=1}^{2}\alpha_i\left[\frac{24p_i}{Z_i^5} - \left\{\left(\frac{24}{Z_i^5}+\frac{24r}{Z_i^4}+\frac{12r^2}{Z_i^3}+\frac{4r^3}{Z_i^2}+\frac{r^4}{Z_i}\right)p_i + \frac{Z_o r^5}{Z_i}\right\}e^{-Z_i r}\right] \qquad (3.2.5)$$

where

$$\alpha_1 = 1, \quad \alpha_2 = c_1; \quad Z_1 = a + Z_o, \quad Z_2 = b + Z_o$$

and

$$p_i = 2 + \frac{5Z_o}{Z_i}\,, \quad i = 1,2.$$

As expected, equation (3.2.5) agrees exactly with equation (13) of McDowell et al. (1973) for the case of hydrogen, obtainable by writing $N_1 = 2$, $c_1 = 0$, $a = 1$ and $Z_o = 1$.

For numerical purposes, it is desirable to have power series expansions in r of $V_{ls,ls}(r)$ and $V_{pol}(r)$, suitable for evaluation at small r. Such expansions are derived by replacing the exponential terms in (3.2.3) and (3.2.5) by their respective power series sums and retaining terms up to a specified order in r. Explicit expressions for both potentials are given in Appendix B.

The remainder of this section will be occupied with finding a value for the screening parameter Z_o appearing in equation (3.1.12) for $u_{ls\to p}(r)$. $V_{pol}(r)$ is defined to behave asymptotically as

$$2V_{pol}(r) \underset{r\to\infty}{\to} -\frac{\alpha}{r^4} \qquad (3.2.6)$$

where α is the dipole polarizability, taken for helium to be 1.395 a.u. in accordance with the experimental value provided by Johnston et al. (1960). Equation (3.2.5) behaves asymptotically as

$$2V_{pol}(r) \underset{r\to\infty}{\to} -\frac{32}{r^4}\cdot\frac{N_1}{\sqrt{Z_o}}\left[\frac{p_1}{Z_1^5}+\frac{c_1 p_2}{Z_2^5}\right]. \qquad (3.2.7)$$

An equation satisfied by Z_o is now obtained by matching the above asymptotic expressions. Thus, making the relevant substitutions for p_i and Z_i $(i = 1,2)$, one has

$$\frac{\alpha}{32} = \frac{N_1}{\sqrt{Z_o}}\left[\frac{(7Z_o+2a)}{(Z_o+a)^6}+c_1\frac{(7Z_o+2b)}{(Z_o+b)^6}\right]. \qquad (3.2.8)$$

This line is then rearranged to give a polynomial equation of degree 25 in Z_o and solved numerically by the Newton-Raphson method, details of which follow in Chapter 5.

§3.3 Cross Sections for the S-Levels

The purpose of this section and the one to follow (§3.4) is to derive, via a partial wave analysis, suitable expressions from which the differential and total cross sections may be computed. Essentially one is concerned with substituting the various partial wave formulae of §3.1 into the basic integrals obtained for the T-matrix element in §2.3. The atomic wave functions $\phi_{ls}(\underline{r})$, $u_{ls}(\underline{r})$ and $v^{\pm}_{n\ell}(\underline{r})$ will take the form indicated by lines (3.1.1), (3.1.4) and (3.1.5) respectively. The resulting expressions are then simplified by integrating over the angular variables and employing properties of the spherical harmonics, particularly orthogonality. The order in which the direct and exchange parts of T_{if} were considered in §2.3 will also be adopted here. However, analysis of the exchange parts $T_{if}^{El\pm}$ and $T_{if}^{E2\pm}$, which arise only in the DWPO III model, will be deferred until the following chapter (Chapter 4) where exchange-polarization effects are dealt with more fully. Thus the first T-matrix component to be considered is T_{if}^{D}.

T_{if}^{D}:

$$T_{if}^{D} = B\sqrt{2}\, I_A \qquad (2.3.19)$$

where it will be recalled I_A is defined by (2.3.18):

$$I_A = \int v^{*+}_{n\ell}(1)\, \chi^{*}_{k_f}(z,3)\, \frac{1}{r_{13}}\, \phi_{1s}(1)\, F(3)\, d\underline{r}_{13}\,. \qquad (2.3.18)$$

With the choice of atomic wave functions adopted (see Appendix A for details) the integral represented by B, equation (2.3.17), is obtainable in closed form. The full expression is given in Appendix C. Regarding I_A, by substituting (3.1.14), (3.1.22) and (3.1.23) for r_{13}^{-1}, F(3) and $\chi_{k_f}(z,\underline{r}_3)$ respectively, one obtains using orthogonality of the spherical harmonics, that

$$I_A = \frac{4\pi}{\sqrt{k_i}} \sum_{\ell=0}^{\infty} (2\ell+1)\, I^{(A)}(\ell,k_i,k_f)\, e^{i\Delta_\ell}\, P_\ell(\cos\theta) \qquad (3.3.1)$$

where the following notation has been employed:

$$I^{(A)}(\ell,k_i,k_f) = \int_0^\infty u_\ell(k_i,r)\, H_\ell(k_f r)\, f_{1s,ns}(r)\, dr\,, \qquad (3.3.2)$$

$$f_{1s,ns}(r) = r \int_0^\infty R_{1s}(t)\, R_{ns}(t)\, \gamma_o(r,t)\, t^2\, dt\,, \qquad (3.3.3)$$

$$\Delta_\ell = \delta_\ell(k_i) + \eta_\ell(k_i) - \eta_\ell(k_f)\,. \qquad (3.3.4)$$

Provided $R_{ns}(t)$ is of a simple form, the integral $f_{1s,ns}(r)$ may be evaluated analytically (see Appendix C). Otherwise numerical methods are required. It is noted that with $R_{1s}(t)$ and $R_{ns}(t)$ orthogonal, $f_{1s,ns}(r) \to 0$ for increasing r, which effectively reduces the infinite range of the integral $I^{(A)}(\ell,k_i,k_f)$.

$T_{if}^{\ D}$ may now be summarized as

$$T_{if}^{\ D} = \frac{1}{\sqrt{2}} \cdot \frac{8\pi B}{\sqrt{k_i}} \sum_{\ell=0}^{\infty} (2\ell+1)\, I^{(A)}(\ell,k_i,k_f)\, e^{i\Delta_\ell} P_\ell(\cos\theta)\,. \qquad (3.3.5)$$

$\underline{T_{if}^{\ P}}$:

$$T_{if}^{\ P} = \sqrt{2}\left[K_1 + K_2 - 2K_3 + K_4\right] \qquad (2.3.22)$$

Each of the K_i integrals, defined by (2.3.21a,b,c,d) contains the function $\phi_{pol}(\underline{r},\underline{t})$. This function has been given explicitly in (3.1.6), whereby, with the aid of the addition theorem (3.1.13), the Legendre polynomial $P_1(\cos\theta_{rt})$ is expressed in terms of a sum over spherical harmonics.

Since this section is concerned with excitation to an S-level, one observes that integrating over $\hat{r}_2$, orthogonality of the spherical harmonics causes three of the integrals to vanish

$$K_2 = K_3 = K_4 = 0 .$$

T_{if}^{P} therefore in this case, requires only a closer study of K_1;

$$K_1 = \int u_{1s}^{*}(1) v_{n\ell}^{+*}(2)\, \chi_{k_f}^{*}(z,3)\, \frac{1}{r_{23}}\, \phi_{1s}(1)\, \phi_{pol}(23)\, F(3)\, d\underline{r}_{123} \qquad (2.3.21a)$$

Inserting repectively (3.1.14), (3.1.22) and (3.1.23) for r_{23}^{-1}, F(3) and $\chi_{k_f}(z,\underline{r}_3)$ as for T_{if}^{D} above and integrating over the angular variables with the aid of (3.1.13) and the familiar orthogonality property possessed by the spherical harmonics, one derives

$$K_1 = \frac{8\pi B}{3\sqrt{k_i}} \sum_{\ell=0}^{\infty} (2\ell+1)\, I^{(P)}(\ell,k_i,k_f)\, e^{i\Delta_\ell}\, P_\ell(\cos\theta) . \qquad (3.3.6)$$

B is defined as above by (2.3.17), Δ_ℓ by (3.3.4) and

$$I^{(P)} = \int_0^{\infty} u_\ell(k_i,r)\, H_\ell(k_f r)\, k_{ls,ns}(r)\, dr , \qquad (3.3.7)$$

$$k_{ls,ns}(r) = -\frac{1}{r^3} \int_0^{r} u_{ls\to p}(t)\, R_{ns}(t)\, t^2\, dt . \qquad (3.3.8)$$

Equation (3.3.8) may be compared with equation (9) of McDowell et al. (1974) who consider excitation of hydrogen atoms and singly ionized helium to the 2s level. Provided $R_{ns}(r)$ assumes a simple form (see Appendex A), $k_{ns,ns}(r)$ is obtainable analytically as in Appendix C. With (3.3.6) T_{if}^{P} reduces to

$$T_{if}^{P} = \frac{1}{\sqrt{2}} \cdot \frac{4}{3} \cdot \frac{4\pi B}{\sqrt{k_i}} \sum_{\ell=0}^{\infty} (2\ell+1)\, I^{(P)}(\ell,k_i,k_f)\, e^{i\Delta_\ell} P_\ell(\cos\theta). \qquad (3.3.9)$$

$\underline{T_{if}^{E\pm}}$:

$$T_{if}^{E\pm} \quad \pm \frac{1}{\sqrt{2}} \left[J_1 \pm J_2 + J_3 - 2J_4 \right] \qquad (2.3.25)$$

Rather than refer explicitly to the partial wave expansions used for r_{ij}^{-1},

$F(\underline{r})$ and $\chi_{k_f}(z,\underline{r})$ as was done under T_{if}^{D} and T_{if}^{P} above, their use will be assumed in the following without further mention. Each J integral is taken in turn and the corresponding result summarized.

J_1:

$$J_1 = \int u_{1s}^{*}(2)\, v_{n\ell}^{*\pm}(1)\, \chi_{k_f}^{*}(z,3)\, \frac{1}{r_{13}}\, \phi_{1s}(2)\phi_{1s}(3)\, F(1)\, d\underline{r}_{123} \qquad (2.3.24a)$$

The integration over $\underline{r}_2$ may be separated from that over $\underline{r}_2$ and $\underline{r}_3$ to give

$$J_1 = B\, J_A \qquad (3.3.10)$$

where J_A represents the integral

$$J_A = \int v_{ns}^{\pm}(1)\, \chi_{k_f}^{*}(z,3)\, \frac{1}{r_{13}}\, \phi_{1s}(3)\, F(1)\, d\underline{r}_{13}\,.$$

A straightforward partial wave analysis reduces this to the form

$$J_A = \frac{4\pi}{\sqrt{k_i}} \sum_{\ell=0}^{\infty} J^{(A)}(\ell,k_i,k_f) e^{i\Delta_\ell} P_\ell(\cos\theta) \qquad (3.3.11)$$

with:

$$J^{(A)}(\ell,k_i,k_f) = \int_0^\infty R_{ns}(r)\, u_\ell(k_i,r)\, g_{1s,\ell}(r)\, dr, \qquad (3.3.12)$$

$$g_{1s,\ell}(r) = r \int_0^\infty R_{1s}(t)\, H_\ell(k_f t)\, \gamma_\ell(r,t)\, t^2\, dt \qquad (3.3.13$$

$$= g_{1s,\ell}^{(1)}(r) + g_{1s,\ell}^{(2)}(r)\,,$$

where

$$g_{1s,\ell}^{(1)}(r) = \frac{1}{r^\ell} \int_0^r R_{1s}(t)\, H_\ell(k_f t)\, t^{\ell+2}\, dt\,,$$

$$g_{1s,\ell}^{(2)}(r) = r^{\ell+2} \int_r^\infty R_{1s}(t)\, H_\ell(k_f t)\, t^{-(\ell-1)} dt\,.$$

For small r it is desirable to make a series expansion in r of $g_{1s,\ell}^{(1)}(r)$. The expression is summarized in Appendix C. Returning to J_1, this integral is finally written as

$$J_1 = \frac{4\pi B}{\sqrt{k_i}} \sum_{\ell=0}^{\infty} J^{(A)}(\ell,k_i,k_f)\, e^{i\Delta_\ell} P_\ell(\cos\theta). \qquad (3.3.14)$$

J_2:

$$J_2 = \int u^*_{1s}(1)\, v^{*\pm}_{n\ell}(2)\, \chi^*_{k_f}(z,3)\, \frac{1}{r_{23}}\, \phi_{1s}(2)\phi_{1s}(3)\, F(1)\, d\underline{r}_{123} \tag{2.3.24b}$$

This integral is separable so that the integrations over $\underline{r}_1$ and $\underline{r}_{23}$ may be considered individually.

$$\int u^*_{1s}(1)\, F(1)\, d\underline{r}_1 = \sqrt{\frac{4\pi}{k_i}}\, c_1(k_i)\exp[i\{\delta_o(k_i)+\eta_o(k_f)\}],$$

$$\int v^{\pm}_{ns}(2)\chi^*_{k_f}(z,3)\, \frac{1}{r_{23}}\, \phi_{1s}(2)\phi_{1s}(3)\, d\underline{r}_{23} = \sqrt{4\pi}\, d_1^s(k_f)\, \exp[-i\eta_o(k_f)],$$

where

$$c_1(k_i) = \int_0^\infty w(r)\, u_o(k_i,r)\, rdr, \tag{3.3.15}$$

$$d_1^s(k_f) = \int_0^\infty R_{1s}(r)\, H_o(k_f r)\, f_{1s,ns}(r)\, rdr \tag{3.3.16}$$

and $f_{1s,ns}(r)$ is given by (3.3.3). Consequently J_2 is rewritten as

$$J_2 = \frac{4\pi}{\sqrt{k_i}}\, c_1(k_i)\, d_1^s(k_f)\, e^{i\Delta_o}. \tag{3.3.17}$$

J_3:

$$J_3 = \int u^*_{1s}(2)\, v^{*\pm}_{n\ell}(1)\, \chi^*_{k_f}(z,3)\, \frac{1}{r_{23}}\, \phi_{1s}(2)\phi_{1s}(3)\, F(1)\, d\underline{r}_{123} \tag{2.3.24c}$$

For excitation to an S-level with which this section is concerned, J_3 is observed to have similar structure to J_2; that is, J_3 only differs from J_2 in that $u_{1s}(r)$ and $v^{\pm}_{n\ell}(r)$ have been interchanged. The following integrals are hence defined:

$$c_2^s(k_i) = \int_0^\infty R_{ns}(r)\, u_o(k_i,r)\, rdr, \tag{3.3.18}$$

$$d_2(k_f) = \int_0^\infty R_{1s}(r)\, H_o(k_f r)\, f_{1s,w}(r)\, rdr \tag{3.3.19}$$

where

$$f_{1s,w}(r) = r\int_0^\infty w(t)\, R_{1s}(t)\, \gamma_o(r,t)\, t^2 dt. \tag{3.3.20}$$

Closed expressions are obtainable for $f_{ls,w}(r)$ and $d_2(k_f)$ with the choice made of atomic wavefunctions — see Appendix C. J_3 becomes

$$J_3 = \frac{4\pi}{\sqrt{k_i}} \; c_2^s(k_i) \; d_2(k_f) \; e^{i\Delta_o} . \qquad (3.3.21)$$

J_4:

$$J_4 = \int u_{ls}^*(2) \; v_{n\ell}^{\pm}(1) \; \chi_{k_f}^*(z,3) \; \frac{1}{r_3} \; \phi_{ls}(2)\phi_{ls}(3) \; F(1) \; d\underline{r}_{123} \qquad (2.3.24d)$$

This can be written as a product of three separate integrals:

$$J_4 = B \int v_{ns}^{\pm}(1) \; F(1) \; d\underline{r}_1 \int \chi_{k_f}^*(z,\underline{r}_3) \; \frac{1}{r_3} \; \phi_{ls}(3) \; d\underline{r}_3 \; .$$

The latter two integrals are simplified to yield

$$\int v_{ns}^{\pm}(1) \; F(1) \; d\underline{r}_1 = \sqrt{\frac{4\pi}{k_i}} \, c_2^s(k_i) \; \exp[i\{\delta_o(k_i) + \eta_o(k_i)\}] ,$$

$$\int \chi_{k_f}^*(z,\underline{r}_3) \; \frac{1}{r_3} \; \phi_{ls}(3) \; d\underline{r}_3 = \sqrt{4\pi} \; d_3^s(k_f) \; \exp[-i\eta_o(k_f)] .$$

$c^s(k_i)$ is defined by (3.3.18) and $d_3(k_f)$ by

$$d_3(k_f) = \int_0^\infty R_{ls}(r) \; H_o(k_f r) \; r dr \qquad (3.3.22)$$

which is obtainable in closed form and given in Appendix C. J_4 assumes the form

$$J_4 = \frac{4\pi}{\sqrt{k_i}} \; . \; B \; c_2^s(k_i) \; d_3(k_f) \; e^{i\Delta_o} . \qquad (3.3.23)$$

Expressions (3.3.14), (3.3.17), (3.3.21) and (3.3.23) are now collected together and inserted into line (2.3.25) for $T_{if}^{E\pm}$:

$$T_{if}^{E\pm} = \pm \frac{1}{\sqrt{2}} \; \frac{4\pi}{\sqrt{k_i}} \; \sum_{\ell=0}^{\infty} \Big[BJ^{(A)}(\ell,k_i,k_f) + \{c_2^s(k_i)[\, d_2(k_f) - 2Bd_3(k_f)]$$

$$\pm c_1(k_i) \; d_1^s(k_f) \} \; \delta_{\ell o} \Big] e^{i\Delta_\ell} P_\ell(\cos\theta) \; . \qquad (3.3.24)$$

The remainder of this section will now concentrate on obtaining explicit expressions for the differential and total cross sections in the DWPO I and DWPO II models (the DWPO III model is dealt with in Chapter 4). The

key expressions derived so far are: (3.3.5) for T_{if}^{D}, (3.3.9) for T_{if}^{P} and (3.3.24) for $T_{if}^{E\pm}$. Bearing these expressions in mind, the transition matrix element $T_{if}^{\pm}$ for the process under consideration (excitation from the ground (1^1S) state to either an n^1S or n^3S state of the atom) is written

$$T_{if}^{\pm} = \sum_{\ell=0}^{\infty} B_{\ell}^{\pm} e^{i\Delta_{\ell}} P_{\ell}(\cos\Theta). \qquad (3.3.25)$$

The $B_{\ell}^{\pm}$ are determined according to the spin state of the excited atom and to the DWPO model being employed. Thus to determine the $B_{\ell}^{\pm}$ in the DWPO I model, the expressions for T_{if}^{D} and $T_{if}^{E\pm}$ derived in this section are incorporated into equation (2.3.4) for $T_{if}^{\pm}$. In the DWPO II model, the same expressions together with the corresponding one for T_{if}^{P} are incorporated into equations (2.3.8) for $T_{if}^{\pm}$. Explicit expressions for the $B_{\ell}^{\pm}$ in terms of the integral expressions derived in this section are presented below:

DWPO I:

$$B_{\ell}^{+} = \frac{1}{\sqrt{2}} \cdot \frac{4\pi B}{\sqrt{k_i}} \Big[2(2\ell+1)\, I^{(A)}(\ell,k_i,k_f) - J^{(A)}(\ell,k_i,k_f) - \Big\{ \big[c_2^S(k_i)\, d_2(k_f) + c_1(k_i)\, d_1^S(k_f)\big] B^{-1} - 2c_2^S(k_i)\, d_3(k_f) \Big\} \delta_{\ell o} \Big] \qquad (3.3.26a)$$

$$B_{\ell}^{-} = -\sqrt{\frac{3}{2}} \cdot \frac{4\pi B}{\sqrt{k_i}} \Big[J^{(A)}(\ell,k_i,k_f) + \Big\{ \big[c_2^S(k_i) d_2(k_f) - c_1(k_i) d_1^S(k_f)\big] B^{-1} - 2c_2^S(k_i) d_3(k_f) \Big\} \delta_{\ell o} \Big] \qquad (3.3.26b)$$

DWPO II:

$$B_{\ell}^{+} = \frac{1}{\sqrt{2}} \cdot \frac{4\pi B}{\sqrt{k_i}} \Big[2(2\ell+1)\big[I^{(A)}(\ell,k_i,k_f) + \frac{2}{3} I^{(P)}(\ell,k_i,k_f)\big] - J^{(A)}(\ell,k_i,k_f) - \Big\{ \big[c_2^S(k_i)\, d_2(k_f) + c_1(k_i)\, d_1^S(k_f)\big] B^{-1} - 2c_2^S(k_i)\, d_3(k_f) \Big\} \delta_{\ell o} \Big] \qquad (3.3.27)$$

Since DWPO II only modifies the direct terms of T_{if} (and hence the B_{ℓ}^{+}) and leaves the exchange terms unaltered (compare (3.3.26a) and (3.3.27) above), B_{ℓ}^{-} assumes the same form as in (3.3.26b).

In fact the DWPO II approximation is easily obtained from the DWPO I

approximation by making the following transformation on $f_{ls,ns}(r)$ (cf. (3.3.3)) appearing in the $I^{(A)}(\ell,k_i,k_f)$ integral (3.3.2):

$$f_{ls,ns}(r) \rightarrow f_{ls,ns}(r) + \frac{2}{3} k_{ls,ns}(r) \qquad (3.3.28)$$

with $k_{ls,ns}(r)$ given by (3.3.8).

Recalling equation (1.2.11) for the differential cross section and inserting (3.3.25) for T_{if}, one has in a straightforward manner that

$$\frac{d\sigma}{d\Omega} = \frac{1}{4\pi^2} \cdot \frac{k_f}{k_i} \sum_{\ell=0}^{\infty} \sum_{\lambda=0}^{\infty} B_\ell B_\lambda \cos(\Delta_\ell - \Delta_\lambda) P_\ell(\cos\theta) P_\lambda(\cos\theta) \; a_o^2/sr . \qquad (3.3.29)$$

The superscript on the B_ℓ serves no further purpose and has been omitted. When computing cross sections, the appropriate expression is, of course, selected from either equation (3.3.26) or (3.3.27). For computational purposes, in order to economise on machine time, it is advantageous to rewrite the differential cross section in the form

$$\frac{d\sigma}{d\Omega} = \frac{1}{4\pi^2} \cdot \frac{k_f}{k_i} (R^2 + I^2) \qquad a_o^2/sr$$

where:

$$R = \sum_{\ell=0}^{\infty} B_\ell \cos\Delta_\ell P_\ell(\cos\theta),$$

$$I = \sum_{\ell=0}^{\infty} B_\ell \sin\Delta_\ell P_\ell(\cos\theta). \qquad (3.3.30)$$

Hence only two single summations are required as opposed to the double summation of equation (3.3.29). In practice the series may be adequately summed term by term up to some value of ℓ, say ℓ_{max}, at which point terms for $\ell > \ell_{max}$ have no significant effect on the cross sections. In order to determine an expression for the total (integrated) cross section, it is however mathematically easier to use (3.3.29). Hence, integrating over all solid angle and employing the property of orthogonality possessed by the Legendre polynomials the total cross section is given by

$$Q_{if}(k_i^2) = \frac{1}{4\pi^2} \cdot \frac{k_f}{k_i} 4 \sum_{\ell=0}^{\infty} \frac{B_\ell^2}{2\ell+1} \pi a_o^2 \,. \qquad (3.3.31)$$

§3.4 Cross Sections for the P-Levels

The comments made at the beginning of the previous section (§3.3) will apply here also. The form of the wave function will remain unchanged and the same partial wave expansions will be employed. However, the partial wave analysis becomes more involved, caused essentially by the valence orbital of the excited state now having an angle-dependent component:

$$v^{\pm}_{n\ell}(\underline{r}) = R^{\pm}_{np}(r)\, Y_{1m}(\hat{r}) \,. \qquad (3.4.1.)$$

Further complications arise due to the long-range dipole character of the interaction for optically allowed S - P transitions. This effects the direct part of the T-matrix element whereby the integrals extend over a considerably greater range than previously for the S - S transitions. Correspondingly, the direct partial wave sum converges much more slowly, since many more partial waves make a significant contribution. A method for overcoming this convergence problem is discussed but a technique for computing the long-range integrals themselves is deferred until Chapter 5. Here, the aim will be, as in the previous section, to derive manageable expressions for the differential and total cross sections in the DWPO I and DWPO II models. These will necessarily be more complex than for §3.3, since the cross sections not only have $m = 0$ contributions (m is the magnetic quantum number of the excited state as in equation (3.4.1.) above) but also $m = \pm 1$ contributions. However, due to the axial symmetry about $\underline{k}_i$ of the system, or mathematically,

$$Y_{\ell m}(\theta,0) = (-1)^m Y_{\ell,-m}(\theta,0) \qquad (3.4.2)$$

with the z-axis along $\underline{k}_i$, one sees that consequently it will be necessary to consider only the $m = 0$ and $m = 1$ contributions, $m = -1$ being the same as $m = 1$ to within a negative sign.

Discussion will begin with the direct component T_{if}^{D} of the T-matrix element.

$\underline{T_{if}^{D}}$:

$$T_{if}^{D} = B\sqrt{2}\, I_A \qquad (2.3.19)$$

with B defined by (2.3.17) and I_A by

$$I_A = \int v_{n\ell}^{*+}(1)\, \chi_{k_f}^{*}(z,3)\, \frac{1}{r_{13}}\, \phi_{1s}(1)\, F(3)\, d\underline{r}_{13} . \qquad (2.3.18)$$

Making the by now familiar substitutions and partial wave decompositions presented in §3.1, one finds, on carrying out the angular integration, that I_A becomes

$$I_A = \frac{4\pi}{\sqrt{k_i}} \cdot \frac{1}{\sqrt{3}} \sum_{\ell=0}^{\infty} \sum_{\mu=-\lambda}^{\lambda} \sum_{\ell=0}^{\infty} i^{\ell-\lambda}(2\ell+1)(2\lambda+1)^{\frac{1}{2}} \int_0^{\infty} u_\ell(k_i,r) H_\lambda(k_f r) f_{1s,np}(r)\, dr$$

$$\begin{pmatrix} \lambda & 1 & \ell \\ 0 & 0 & 0 \end{pmatrix} \begin{pmatrix} \lambda & 1 & \ell \\ -\mu & -m & 0 \end{pmatrix} Y_{\lambda\mu}(\Theta,0) \exp[i\{\delta_\ell(k_i) + \eta_\ell(k_i) - \eta_\lambda(k_f)\}] . \qquad (3.4.3)$$

The Wigner 3 - j symbols have been introduced through the relation given, for example, by Edmonds (1974, equation (4.6.3))

$$\int Y_{\ell_1 m_1}(\hat{r})\, Y_{\ell_2 m_2}(\hat{r})\, Y_{\ell_3 m_3}(\hat{r})\, d\hat{r} = \left[\frac{(2\ell_1+1)(2\ell_2+1)(2\ell_3+1)}{4\pi}\right]^{\frac{1}{2}} \begin{pmatrix} \ell_1 & \ell_2 & \ell_3 \\ 0 & 0 & 0 \end{pmatrix} \begin{pmatrix} \ell_1 & \ell_2 & \ell_3 \\ m_1 & m_2 & m_3 \end{pmatrix} \qquad (3.4.4)$$

This relation will be utilized throughout this section. The integral $f_{1s,np}(r)$ is defined in analogy with $f_{1s,ns}(r)$ (cf (3.3.3)) to be

$$f_{1s,np}(r) = r \int_0^{\infty} R_{1s}(t)\, R_{np}(t)\, \gamma_1(r,t)\, t^2\, dt \qquad (3.4.5)$$

which asymptotically does not tend to zero so rapidly as $f_{1s,ns}(r)$ but rather as

$$f_{1s,np}(r) \underset{r\to\infty}{\sim} \frac{1}{r} \qquad (3.4.6)$$

(see Appendix C for an evaluation of $f_{1s,np}(r)$ in closed form). It is precisely this behaviour which gives rise to the long-range nature of the radial integral appearing in (3.4.3) and mentioned earlier in this section.

Returning to the 3 - j symbols, one is able, with the aid of certain symmetry properties, to simplify further the integral I_A. In particular, the arguments appearing in the upper row satsify the triangle inequality so that in this case;

$$\ell = \lambda \pm 1 \qquad \lambda > 0 ,$$

$$= 1 \qquad \lambda = 0 .$$

Also, the sum of the arguments belonging to the lower row is zero so that here $\mu = -m$. These two properties will be used throughout this section but will not always be explicitly specified as above. For a thorough account of the properties and relations satisfied by the Wigner symbols, reference should be made to the book by Edmonds (1974).

At this point it is convenient to define by $I(\ell,\lambda)$ the radial integral

$$I(\ell,\lambda) = \int_0^\infty H_\ell(k_f r)\, u_\lambda(k_i,r)\, f_{ls,np}(r)\, dr \qquad (3.4.7)$$

and to let

$$\gamma^D = \frac{4\pi B}{\sqrt{k_i}} \sqrt{\frac{2}{3}} , \qquad (3.4.8)$$

$$\Delta_{\ell,\lambda} = \delta_\lambda(k_i) + \eta_\lambda(k_i) - \eta_\ell(k_f) . \qquad (3.4.9)$$

With the above results derived from the 3 - j symbols, (3.4.3) reduces essentially to a single summation where it is now appropriate to write

$$A_{\ell o} = i\gamma^D \{(\ell+1)\, I(\ell,\ell+1)\, e^{i\Delta_{\ell,\ell+1}} - \ell I(\ell,\ell-1)\, e^{i\Delta_{\ell,\ell-1}}\}, \qquad (3.4.10a)$$

$$A_{\ell 1} = i \frac{\gamma^D}{\sqrt{2}} \{I(\ell,\ell+1)\, e^{i\Delta_{\ell,\ell+1}} + I(\ell,\ell-1)\, e^{i\Delta_{\ell,\ell-1}}\}. \qquad (3.4.10b)$$

By employing (3.1.21) to express the remaining spherical harmonic of (3.4.3) in terms of a Legendre function, one can write down the $m = 0$ and $m = 1$ expressions for T_{if}^D, on evaluating the respective 3 - j symbols, in the compact form

$m = 0,1$ $$T_{if}^{D}(m) = \sum_{\ell=m}^{\infty} A_{\ell m} P_{\ell}^{m}(\cos\theta) . \qquad (3.4.11)$$

$\underline{T_{if}^{P}}$:

$$T_{if}^{P} = \sqrt{2}\left[K_1 + K_2 - 2K_3 + K_4\right] \qquad (2.3.22)$$

As before the addition theorem (3.1.13) is used to write the angular part of the function $\phi_{pol}(\underline{r},\underline{t})$ appearing in each $K_i (i = 1,\ldots 4)$ in terms of spherical harmonics. Each K_i is taken in turn.

K_1:

$$K_1 = \int u_{ls}^{*}(1)\, v_{n\ell}^{*+}(2)\, \chi_{k_f}^{*}(z,3)\, \frac{1}{r_{23}}\, \phi_{ls}(1)\phi_{pol}(23)\, F(3)\, d\underline{r}_{123} \qquad (2.3.21a)$$

The usual substitutions and angular momentum expansions are made and yield

$$K_1 = -\frac{2}{3}\,\frac{(4\pi)^3}{\sqrt{k_i}}\, B \sum_{\lambda'=0}^{\infty} \sum_{\mu'=-\lambda'}^{\lambda'} \sum_{\lambda=0}^{\infty} \sum_{\mu=-\lambda}^{\lambda} \sum_{\nu=-1}^{1} \sum_{\ell=0}^{\infty} i^{\ell-\lambda'} (2\ell+1)^{\frac{1}{2}}(2\lambda+1)^{-1} e^{i\Delta_{\lambda';\ell}}$$
$$\int_0^{\infty} H_{\lambda'}(k_f r)\, u_{\ell}(k_i,r) \left\{ \frac{1}{r} \int_0^{r} u_{ls\to p}(t) R_{np}(t) \left(\frac{t}{r}\right)^{\lambda+1} dt \right\} dr \int_{\Omega_r} Y_{lm}^{*}(\hat{r}) Y_{\lambda\mu}^{*}(\hat{r}) Y_{l\nu}^{*}(\hat{r}) d\hat{r} \qquad (3.4.12)$$
$$\int_{\Omega_t} Y_{\lambda'\mu'}^{*}(\hat{t})\, Y_{\lambda\mu}(\hat{t})\, Y_{l\nu}(\hat{t})\, Y_{\ell o}(\hat{t}) d\hat{t} \quad Y_{\lambda'\mu'}(\theta,0).$$

Use has been made of (2.3.17) for B and (3.4.9) for $\Delta_{\lambda';\ell}$. For notational purposes in evaluating the angular integrals, let $I(\Omega_{r\ldots t})$ denote the angular integration over $\hat{r}\ldots\hat{t}$. Then using (3.4.4) the angular integration over $\hat{r}$ becomes

$$I(\Omega_r) = 3\sqrt{\frac{2\lambda+1}{4\pi}} \begin{pmatrix} l & \lambda & l \\ 0 & 0 & 0 \end{pmatrix} \begin{pmatrix} l & \lambda & l \\ m & \mu & \nu \end{pmatrix}.$$

The integral over $\hat{t}$ consists of four spherical harmonics and is hence a little more involved. However, by using the result from, for example, Edmonds (1974, equation (4.6.5)) that

$$Y_{\ell_1 m_1}(\hat{r}) Y_{\ell_2 m_2}(\hat{r}) = \sum_{\ell=0}^{\infty} \sum_{m=-\ell}^{\ell} \left[\frac{(2\ell_1+1)(2\ell_2+1)(2\ell+1)}{4\pi}\right]^{\frac{1}{2}} \begin{pmatrix} \ell_1 & \ell_2 & \ell \\ 0 & 0 & 0 \end{pmatrix} \begin{pmatrix} \ell_1 & \ell_2 & \ell \\ m_1 & m_2 & m \end{pmatrix} Y_{\ell m}^{*}(\hat{r}), \qquad (3.4.13)$$

$I(\Omega_t)$ is reduced to an integral over three spherical harmonics. Hence, using also (3.4.4), $I(\Omega_t)$ can be performed. Having done this, the total angular integration is expressed as

$$I(\Omega_{rt}) = \frac{3(2\lambda+1)}{4\pi} \sum_{\mu=-\lambda}^{\lambda} \sum_{\nu=-1}^{1} \sum_{\ell'=0}^{\infty} \sum_{m'=-\ell'}^{\ell'} (2\ell'+1) \left[\frac{3(2\lambda'+1)(2\ell+1)}{4\pi}\right]^{\frac{1}{2}} \begin{pmatrix} 1 & \lambda & 1 \\ 0 & 0 & 0 \end{pmatrix}$$

$$\begin{pmatrix} 1 & \lambda & 1 \\ m & \mu & \nu \end{pmatrix} \begin{pmatrix} \lambda & 1 & \ell' \\ 0 & 0 & 0 \end{pmatrix} \begin{pmatrix} \lambda & 1 & \ell' \\ \mu & \nu & m' \end{pmatrix} \begin{pmatrix} \lambda' & \ell' & \ell \\ 0 & 0 & 0 \end{pmatrix} \begin{pmatrix} \lambda' & \ell' & \ell \\ m' & -m' & 0 \end{pmatrix}$$

where the summations over μ and ν come from the main integral expression (3.4.12). This can now be simplifed by use of the orthogonality property (Edmonds, 1974, equation (3.7.8))

$$\sum_{\mu=-\lambda}^{\lambda} \sum_{\nu=-1}^{1} \begin{pmatrix} \lambda & 1 & 1 \\ \mu & \nu & m \end{pmatrix} \begin{pmatrix} \lambda & 1 & \ell' \\ \mu & \nu & m' \end{pmatrix} = \frac{1}{3} \delta_{\ell' 1} \delta_{mm'} . \qquad (3.4.14)$$

The resulting expression for $I(\Omega_{rt})$ is then inserted back into (3.4.12) for K_1 to give

$$K_1 = -\frac{16\pi B}{\sqrt{k_i}} \cdot \sqrt{\pi} \sum_{\lambda'=0}^{\infty} \sum_{\lambda=0}^{\infty} \sum_{\ell=0}^{\infty} i^{\ell-\lambda'} (2\ell+1) \left[3(2\lambda'+1)\right]^{\frac{1}{2}} e^{i\Delta_{\lambda'\ell}}$$

$$\int_0^\infty H_{\lambda'}(k_f r) u_\ell(k_i, r) \left\{\frac{1}{r} \int_0^r u_{1s\to p}(t) R_{np}(t) \left(\frac{t}{r}\right)^{\lambda+1} dt\right\} dr \begin{pmatrix} \lambda & 1 & 1 \\ 0 & 0 & 0 \end{pmatrix}^2 \begin{pmatrix} \lambda' & \ell & 1 \\ 0 & 0 & 0 \end{pmatrix}$$

$$\begin{pmatrix} \lambda' & \ell & 1 \\ m & 0 & -m \end{pmatrix} Y_{\lambda', -m}(\theta, 0) . \qquad (3.4.15)$$

From the triangle inequality satisfied by the arguments appearing in the upper rows of the 3-j symbols, one has that (a) $\lambda = 0,2$ and (b) $\ell = \lambda' \pm 1$ for $\lambda > 0$, $\ell = 1$ for $\lambda' = 0$. The radial integral is consequently written as

$$P(\ell,\lambda) = \int_0^\infty H_\ell(k_f r)\, u_\lambda(k_i, r)\, h_{1s,np}(r) dr \qquad (3.4.16)$$

with

$$h_{1s,np}(r) = -\frac{1}{r} \int_0^r u_{1s\to p}(t) R_{np}(t) \left[\frac{t}{r} + \frac{2}{5} \cdot \frac{t^3}{r^3}\right] dt . \qquad (3.4.17)$$

Hence, with the aid of (3.1.21) to transform $Y_{\ell',-m}(\theta,0)$ into a Legendre function and the notation (3.4.8) for γ^D, the $m = 0$ and $m = 1$ expressions for K_1 are obtained respectively, on evaluating the corresponding 3 - j symbols, to be

$$m = 0 \quad K_1 = i\,\gamma^D \sqrt{2} \sum_{\ell=0}^{\infty} \left[(\ell+1)P(\ell,\ell+1)e^{i\Delta_{\ell,\ell+1}} - \ell P(\ell,\ell-1)e^{i\Delta_{\ell,\ell-1}}\right] P_\ell(\cos\theta), \tag{3.4.18a}$$

$$m = 1 \quad K_1 = i\,\gamma^D \sum_{\ell=1}^{\infty} \left[P(\ell,\ell+1)e^{i\Delta_{\ell,\ell+1}} + P(\ell,\ell-1)e^{i\Delta_{\ell,\ell-1}}\right] P_\ell^1(\cos\theta). \tag{3.4.18b}$$

K_2:

$$K_2 = \int u_{ls}^*(1)\, v_n^{*+}(2)\, \chi_{k_f}^*(z,3)\, \frac{1}{r_{13}}\, \phi_{ls}(1)\, \phi_{pol}(23)\, F(3)\, d\underline{r}_{123} \tag{2.3.21b}$$

Inserting the usual radial and angular parts of the atomic wave functions and making the various angular momentum expansions, the angular integration is carried out with the aid of (3.4.4) to give

$$K_2 = \frac{8\pi}{\sqrt{3}} \sqrt{\frac{4\pi}{k_i}} \sum_{\lambda=0}^{\infty} \sum_{\ell=0}^{\infty} i^{\lambda-\ell}(2\lambda+1)(2\ell+1)^{\frac{1}{2}}\, e^{i\Delta_{\ell,\lambda}} \int_0^\infty H_\ell(k_f r) u_\lambda(k_i,r)$$

$$f_{ls,w}(r)\, k_{ls,np}(r) dr \begin{pmatrix} \ell & 1 & \lambda \\ 0 & 0 & 0 \end{pmatrix} \begin{pmatrix} \ell & 1 & \lambda \\ m & -m & 0 \end{pmatrix} Y_{\ell,-m}(\theta,0)\,. \tag{3.4.19}$$

$\Delta_{\ell,\lambda}$ is given by the familiar expression (3.4.9) and $f_{ls,w}(r)$ by (3.3.20). $k_{ls,np}(r)$ is defined in analogy with $k_{ls,ns}(r)$ of (3.3.8) to be

$$k_{ls,np}(r) = -\frac{1}{r^2} \int_0^r u_{ls\to p}(t)\, R_{np}(t) t\, dt\,. \tag{3.4.20}$$

Let

$$Q(\ell,\lambda) = B^{-1} \int_0^\infty H_\ell(k_f r)\, u_\lambda(k_i r)\, f_{ls,w}(r)\, k_{ls,np}(r) dr\,. \tag{3.4.21}$$

Then, noting the relation between ℓ and λ obtained from the 3 - j symbols, the $m = 0$ and $m = 1$ expressions for K_2 take, after some manipulation, the respective forms

$$m = 0 \quad K_2 = i\gamma^D \sqrt{2} \sum_{\ell=0}^{\infty} \left[(\ell+1)Q(\ell,\ell+1)e^{i\Delta_{\ell,\ell+1}} - \ell Q(\ell,\ell-1)e^{i\Delta_{\ell,\ell-1}}\right] P_\ell(\cos\theta), \tag{3.4.22a}$$

$$m = 1 \qquad K_2 = i\gamma^D \sum_{\ell=1}^{\infty} \left[Q(\ell,\ell+1) e^{i\Delta_{\ell,\ell+1}} + Q(\ell,\ell-1) e^{i\Delta_{\ell,\ell-1}} \right] P_\ell^1(\cos\theta) \quad (3.4.22b)$$

K_3:

$$K_3 = \int u_{1s}^*(1)\, v_{n\ell}^{*+}(2)\, \chi_{k_f}^*(z,3)\, \frac{1}{r_3}\, \phi_{1s}(1)\phi_{pol}(23)\, F(3)\, d\underline{r}_{123} \quad (2.3.21c)$$

This is separable and making the usual substitutions and effecting the angular integration with the aid of (3.4.4), becomes

$$K_3 = \frac{4\pi B}{\sqrt{k_i}} \cdot \frac{4\sqrt{\pi}}{\sqrt{3}} \sum_{\lambda=0}^{\infty} \sum_{\ell=0}^{\infty} i^{\lambda-\ell} (2\lambda+1)(2\ell+1)^{\frac{1}{2}} e^{i\Delta_{\ell,\lambda}} \int_0^\infty H_\ell(k_f r) u_\lambda(k_i,r)$$

$$k_{1s,np}(r)dr \begin{pmatrix} \ell & \lambda & 1 \\ 0 & 0 & 0 \end{pmatrix} \begin{pmatrix} \ell & \lambda & 1 \\ m & 0 & -m \end{pmatrix} Y_{\ell,-m}(\theta,0) . \quad (3.4.23)$$

$k_{1s,np}(r)$ is given by (3.4.20) and $\Delta_{\ell,\lambda}$ by (3.4.9). Writing

$$R(\ell,\lambda) = \int_0^\infty H_\ell(k_f r) u_\lambda(k_i,r)\, k_{1s,np}(r)\, dr \quad (3.4.24)$$

and using similar analysis as in previous cases, the $m = 0$ and $m = 1$ expressions for K_3 assume the form

$$m = 0 \qquad K_3 = i\,\gamma^D \sqrt{2} \sum_{\ell=0}^{\infty} \left[(\ell+1) R(\ell,\ell+1) e^{i\Delta_{\ell,\ell+1}} - \ell R(\ell,\ell-1) e^{i\Delta_{\ell,\ell-1}} \right] P_\ell(\cos\theta), \quad (3.4.25a)$$

$$m = 1 \qquad K_3 = i\,\gamma^D \sum_{\ell=1}^{\infty} \left[R(\ell,\ell+1) e^{i\Delta_{\ell,\ell+1}} + R(\ell,\ell-1) e^{i\Delta_{\ell,\ell-1}} \right] P_\ell^1(\cos\theta) . \quad (3.4.25b)$$

K_4:

This is given by (2.3.21d). Substituting for $\phi_{pol}(\underline{r},\underline{t})$ by equation (3.1.6) and replacing the Legendre polynomial by the expansion (3.1.13), the angular integration over $\hat{r}_2$ causes the integral to vanish:

$$K_4 = 0 . \quad (3.4.26)$$

At this point the results (3.4.18), (3.4.22), (3.4.25) and (3.4.26) are collected together into (2.3.22) to formulate a general expression depending only upon m for T_{if}^P. For compactness, let

$$S(\ell,\ell\pm1) = 2\{P(\ell,\ell\pm1) + Q(\ell,\ell\pm1) - 2R(\ell,\ell\pm1)\} \quad (3.4.27)$$

and write

$$B_{\ell o} = i\gamma^D\{(\ell+1)\ S(\ell,\ell+1)e^{i\Delta_{\ell,\ell+1}} - \ell\ S(\ell,\ell-1)e^{i\Delta_{\ell,\ell-1}}\}, \qquad (3.4.28a)$$

$$B_{\ell 1} = i\frac{\gamma^D}{\sqrt{2}}\ \{S(\ell,\ell+1)e^{i\Delta_{\ell,\ell+1}} + S(\ell,\ell-1)e^{i\Delta_{\ell,\ell-1}}\}. \qquad (3.4.28b)$$

Then the required expression may be written (with $m = 0,1$) as

$$m = 0,1 \qquad T_{if}^{P}(m) = \sum_{\ell=m}^{\infty} B_{\ell m}\ P_\ell^m(\cos\theta)\ . \qquad (3.4.29)$$

$\underline{T_{if}^{E\pm}}$:

$$T_{if}^{E\pm} = \pm\frac{1}{\sqrt{2}}\left[J_1 \pm J_2 + J_3 - 2J_4\right] \qquad (2.3.25)$$

Each integral is treated in turn.

J_1:

$$J_1 = \int u_{1s}^*(2)\ v_{n\ell}^{*\pm}(1)\ \chi_{k_f}^*(z,3)\ \frac{1}{r_{13}}\ \phi_{1s}(2)\phi_{1s}(3)\ F(1)\ d\underline{r}_{123} \qquad (2.3.24a)$$

A straightforward partial wave analysis gives

$$J_1 = \frac{12\pi B}{\sqrt{k_i}}\ \sqrt{4\pi}\ \sum_{\lambda=0}^{\infty}\ \sum_{\ell=0}^{\infty}\ i^{\lambda-\ell}\ (2\lambda+1)(2\ell+1)^{-\frac{1}{2}}\ e^{i\Delta_{\ell,\lambda}} \int_0^\infty u_\lambda(k_i,r)R_{np}(r)g_{1s,\ell}(r)dr$$

$$\begin{pmatrix}\ell & \lambda & 1\\ 0 & 0 & 0\end{pmatrix}\begin{pmatrix}\ell & \lambda & 1\\ -m & 0 & m\end{pmatrix} Y_{\ell,-m}(\theta,0). \qquad (3.4.30)$$

The function $g_{1s,\ell}(r)$ is given by (3.3.13). Then, letting

$$J(\ell,\lambda) = \int_0^\infty u_\lambda(k_i,r)R_{np}(r)g_{1s,\ell}(r)dr \qquad (3.4.31)$$

and $\gamma^E = \frac{1}{2}\gamma^D$, the $m = 0$ and $m = 1$ expressions for J_1 become respectively

$$m = 0 \quad J_1 = i\ \gamma^E\sqrt{2}\ \sum_{\ell=0}^{\infty}\left[\frac{\ell+1}{2\ell+1}\ J(\ell,\ell+1)e^{i\Delta_{\ell,\ell+1}} - \frac{\ell}{2\ell+1}\ J(\ell,\ell-1)e^{i\Delta_{\ell,\ell-1}}\right]P_\ell(\cos\theta), \qquad (3.4.33a)$$

$$m = 1 \quad J_1 = i\ \gamma^E\ \sum_{\ell=1}^{\infty}\ \frac{1}{2\ell+1}\left[J(\ell,\ell+1)e^{i\Delta_{\ell,\ell+1}} + J(\ell,\ell-1)e^{i\Delta_{\ell,\ell-1}}\right]P_\ell^1(\cos\theta). \qquad (3.4.33b)$$

J_2:

$$J_2 = \int u_{1s}^*(1)\ v_{n\ell}^{*\pm}(2)\ \chi_{k_f}^*(z,3)\ \frac{1}{r_{23}}\ \phi_{1s}(2)\phi_{1s}(3)\ F(1)\ d\underline{r}_{123} \qquad (2.3.24b)$$

The angular integration may be evaluated using only the property of orthogonality

between the spherical harmonics. Concerning the radial integration, it is convenient to define $d_1^P(k_f)$, by analogy with $d_1^S(k_f)$ (c.f. equation(3.3.16)), to be

$$d_1^P(k_f) = \int_0^\infty R_{1s}(r)\, H_1(k_f r)\, f_{1s,np}(r)\, r\, dr \qquad (3.4.34)$$

with $f_{1s,np}(r)$ given earlier by (3.4.5) and to recall the integral $c_1(k_i)$ given by (3.3.15). The $m = 0$ and $m = 1$ expressions for J_2 can then be written as

$$m = 0 \quad J_2 = -i\,\gamma^E \frac{\sqrt{2}}{3B}\, c_1(k_i)\, d_1^P(k_f)\, e^{i\Delta_{1,0}}\, P_1(\cos\theta), \qquad (3.4.35a)$$

$$m = 1 \quad J_2 = i\,\gamma^E \frac{1}{3B}\, c_1(k_i)\, d_1^P(k_f)\, e^{i\Delta_{1,0}}\, P_1^1(\cos\theta). \qquad (3.4.35b)$$

J_3:

$$J_3 = \int u_{1s}^*(2)\, v_{n\ell}^{*\pm}(1)\, \chi_{k_f}^*(z,3)\, \frac{1}{r_{23}}\, \phi_{1s}(2)\, \phi_{1s}(3)\, F(1)\, d\underline{r}_{123} \qquad (2.3.24c)$$

Again the integration over the angular variables may be handled using only orthogonality of the spherical harmonics. It is found that the integral only exists for $m = 0$. By analogy with $c_2^S(k_i)$, defined in (3.3.18), it is convenient to write

$$c_2^P(k_i) = \int_0^\infty R_{np}(r)\, u_\ell(k_i,r)\, r\, dr \qquad (3.4.36)$$

and to recall $d_2(k_f)$, given by (3.3.19), in order to express the radial integral compactly. Hence, J_3 reduces eventually to

$$m = 0 \text{ only} \quad J_3 = i\,\frac{\gamma^E\sqrt{2}}{B}\, c_2^P(k_i)\, d_2(k_f)\, e^{i\Delta_{0,1}}\, \delta_{m0}\,. \qquad (3.4.37)$$

J_4:

$$J_4 = \int u_{1s}^*(2)\, v_{n\ell}^{*\pm}(1)\, \chi_{k_f}^*(z,3)\, \frac{1}{r_3}\, \phi_{1s}(2)\phi_{1s}(3)\, F(1)\, d\underline{r}_{123} \qquad (2.3.24d)$$

This integral is separated into three distinct integrals over $\underline{r}_1$, $\underline{r}_2$ and $\underline{r}_3$. That over $\underline{r}_2$ is just the integral represented by B, equation (2.3.17). Those over $\underline{r}_1$ and $\underline{r}_3$ are reduced respectively to:

$$\int v_{np}^{*\pm}(\underline{r})\, F(\underline{r})\, d\underline{r} = i\sqrt{\frac{4\pi}{k_i}} \cdot \frac{1}{\sqrt{3}}\, c_2^{P}(k_i)\, \exp[i\{\delta_1(k_i) + \eta_1(k_i)\}]\delta_{mo},$$

$$\int \chi_{k_f}^{*}(z,\underline{r})\, \frac{1}{r}\, \phi_{1s}(\underline{r})\, d\underline{r} = (4\pi)^{1/2}\, d_3(k_f)\, \exp[-i\eta_o(k_f)]$$

where $c_2^{P}(k_i)$ is given above by (3.4.36) and $d_3(k_f)$ by (3.3.22). It is observed that J_4 only exists for $m = 0$. Combining the above results, the required expression for J_4 is

$$m = 0 \text{ only} \qquad J_4 = i\,\gamma^{E}\sqrt{2}\, c_2^{P}(k_i)\, d_3(k_f)\, e^{i\Delta_{0,1}}\, \delta_{mo}. \tag{3.4.38}$$

Having now obtained the results (3.4.33), (3.4.35), (3.4.37) and (3.4.38), a general expression for $T_{if}^{E\pm}$ depending only upon m is derived. Inserting the above results into (2.3.25), and writing

$$C_{\ell 0}^{\pm} = \pm i\gamma^{E}\Big\{ \frac{\ell+1}{2\ell+1}\Big[J(\ell,\ell+1) + c_2^{P}(k_i)\,[B^{-1}d_2(k_f) - 2d_3(k_f)]\delta_{\ell 0}\Big] e^{i\Delta_{\ell,\ell+1}}$$

$$- \frac{\ell}{2\ell+1}\Big[J(\ell,\ell-1) \pm B^{-1}c_1(k_i)\, d_1^{P}(k_f)\delta_{\ell 1}\Big]\, e^{i\Delta_{\ell,\ell-1}}\Big\}, \tag{3.4.39a}$$

$$C_{\ell 1}^{\pm} = \pm \frac{i\gamma^{E}}{\sqrt{2}}\Big\{ \frac{1}{2\ell+1}\, J(\ell,\ell+1)\, e^{i\Delta_{\ell,\ell+1}} + \frac{1}{2\ell+1}\Big[J(\ell,\ell-1) \pm B^{-1}\, c_1(k_i)\, d_1^{P}(k_f)\delta_{\ell 1}\Big]$$

$$e^{i\Delta_{\ell,\ell-1}}\Big\}, \tag{3.4.39b}$$

the final expression for $T_{if}^{E\pm}$ $(m = 0,1)$ is written in the compact form

$$m = 0,1 \qquad T_{if}^{E\pm}(m) = \sum_{\ell=m}^{\infty} C_{\ell m}^{\pm}\, P_{\ell}^{m}(\cos\Theta). \tag{3.4.40}$$

This completes the partial wave analysis of the basic integrals contributing to the T-matrix element T_{if}. As in the case for S - S transitions in §3.3, the key expressions derived so far are: (3.4.11) for $T_{if}^{D}(m)$, (3.4.24) for $T_{if}^{P}(m)$ and (3.4.40) for $T_{if}^{E\pm}(m)$. One is now in a position to formulate expressions in the DWPO I and DWPO II models for computing the differential and integral cross sections describing excitation processes from the ground (1^1S) state of the target to either an n^1P or n^3P state. However, before embarking upon such a formulation, attention is drawn to the remark at the beginning of this section which concerns the slow convergence

of the series appearing in (3.4.11) and (3.4.29). This does not arise in the exchange case (3.4.40) since basically in each of the exchange integrals a partial wave function is integrated against a bound state function rather than another partial wave as in the direct case; partial waves (incoming and outgoing) have an oscillatory nature at large distances from the scattering centre whereas bound state wave functions decrease exponentially in magnitude. When computing total integrated cross sections this problem of convergence is not too serious a difficulty since only a relatively small number of partial waves contribute significantly, especially at lower impact energies. Hence for such energies, provided one is only interested in total (and therefore integral) cross sections, the series may be adequately summed term by term. On the other hand, for differential cross sections the difficulty takes on more significance, particularly from a computational point of view, since many more terms in the sum must now be included. In the following, an artifice is described to overcome this difficulty.

Essentially, it is the lower order partial waves which suffer most distortion, becoming progressively less distorted for higher order ℓ until they merge at some value of ℓ, say ℓ_o, into plane wave contributions. In practice, ℓ_o is set to the current value of ℓ when the elastic scattering phase shift δ_ℓ of (3.1.17) is typically less than 0.005. The idea then is, following McDowell et al. (1975b), to sum the series for the T-matrix element up to this value ℓ_o, to subtract the corresponding terms calculated in the Born Approximation and finally to add the complete T-matrix element calculated in the Born Approximation. Denoting Born terms by a B (not to be confused with the integral definition (2.3.17)), this is expressed mathematically in each case as (viz. m = 0,1):

$$T_{if}^{D}(m) = \sum_{\ell=m}^{\ell_o} [A_{\ell m} - A_{\ell m}^{B}] P_\ell^m(\cos\theta) + T_{if}^{B}(m), \qquad (3.4.41)$$

m = 0,1

$$T_{if}^{P}(m) = \sum_{\ell=m}^{\ell_o} [B_{\ell m} - B_{\ell m}^{B}] P_\ell^m(\cos\theta) + T_{if}^{PB}(m). \qquad (3.4.42)$$

The Born terms $A_{\ell m}^{B}$ and $B_{\ell m}^{B}$ are derived from the expressions for $A_{\ell m}$ and $B_{\ell m}$ respectively with $u_{\ell}(k_i,r)$ replaced by $\sqrt{k_i r}H_{\ell}(k_i r)$, viz. (3.4.10) and (3.4.28). Using previous notation the Born T-matrix element $T_{if}^{B}(m)$ is defined as

$$m = 0,1 \qquad T_{if}^{B}(m) = \langle \phi_f(12)\, e^{i\underline{k}_f\cdot\underline{r}_3}\, V_f\, \phi_i(12)\, e^{i\underline{k}_i\cdot\underline{r}_3} \rangle \qquad (3.4.43)$$

and the "Polarized-Born" T-matrix element $T_{if}^{PB}(m)$ as

$$m = 0,1 \qquad T_{if}^{PB}(m) = 2\langle \phi_f(12)\, e^{i\underline{k}_f\cdot\underline{r}_3}\, V_f\, \phi_{1s}(1)\phi_{pol}(23)\, e^{i\underline{k}_i\cdot\underline{r}_3} \rangle \qquad (3.4.44)$$

with $m = 0,1$ and $\phi_f(12)$ the corresponding final state target wave function. It is essential that closed expressions be obtainable for $T_{if}^{B}(m)$ and $T_{if}^{PB}(m)$. In order to make the integrals concerned tractable, simple Hartree-Fock functions were employed (Morse et al., 1935, for the 2^1P state; Goldberg and Clogston, 1939, for the 3^1P state) and to preserve consistency the same functions were adopted throughout the entire calculation of the cross sections. For the case of $T_{if}^{PB}(m)$, a slight modification is introduced to ease computation. It is seen that for large r

$$f_{1s,w}(r) \underset{r\to\infty}{\to} B \,. \qquad (3.4.45)$$

The modification is then to approximate $f_{1s,w}(r)$ by B for all r; physically this means that the core electron is assumed to be passive throughout the scattering process. The full expressions are derived in Appendix D.

In order to formulate both differential and total cross sections, the modified expressions (3.4.41) and (3.4.42) for T_{if}^{D} and T_{if}^{P} will now be used throughout the remainder of this section and the one to follow (§3.5), rather than (3.4.11) and (3.4.29). Of course, such modifications are unnecessary for singlet-triplet level transitions which only involve the exchange term (3.4.40). The general expression for the total differential cross section for excitation to a P state is obtained by averaging over the (single) initial state and summing over the (three) final states and hence written

$$\frac{d\sigma}{d\Omega} = \frac{d\sigma_o}{d\Omega} + \frac{d\sigma_1}{d\Omega} + \frac{d\sigma_{-1}}{d\Omega} \tag{3.4.46a}$$

where the subscripts $(0,\pm1)$ denote the magnetic substate quantum numbers. Due to axial symmetry of the system, the latter two terms are identical so that

$$\frac{d\sigma}{d\Omega} = \frac{d\sigma_o}{d\Omega} + \frac{2d\sigma_1}{d\Omega} \tag{3.4.46b}$$

with

$$\frac{d\sigma_m}{d\Omega} = \frac{1}{4\pi^2} \cdot \frac{k_f}{k_i} \left|T_{if}^{\pm}(m)\right|^2, \; m = 0,1 \; . \tag{3.4.47}$$

The "+" and "-" superscripts have been introduced to distinguish between excitation to either a singlet or a triplet spin state respectively.

In the DWPO I model (viz. (2.3.4)) one has that

$$T_{if}^{+}(m) = \sum_{\ell=m}^{\ell_o} [(A_{\ell m} - C_{\ell m}^{+}) - A_{\ell m}^{B}] P_\ell^m(\cos\theta) + T_{if}^{B}(m) \; , \tag{3.4.48a}$$

(I)

$$T_{if}^{-}(m) = \sum_{\ell=m}^{\ell_{max}} C_{\ell m}^{-} \, P_\ell^m(\cos\theta) \; . \tag{3.4.48b}$$

ℓ_{max} appearing in (3.4.48b) is defined by the assumption that all contributions for $\ell > \ell_{max}$ may be neglected.

In the DWPO II model (viz. (2.3.8)) one has that

$$\text{(II)} \quad T_{if}^{+}(m) = \sum_{\ell=m}^{\ell_o} [(D_{\ell m} - C_{\ell m}^{+}) - D_{\ell m}^{B}] P_\ell^m(\cos\theta) + T_{if}^{B}(m) + T_{if}^{PB}(m) \; . \tag{3.4.49}$$

$T_{if}^{-}(m)$ remains unchanged and has the form given by (3.4.48b) above. $D_{\ell m}$ is simply $A_{\ell m}$ modified by the addition of $B_{\ell m}$ in both the DWPO and Born terms:

$$D_{\ell m} = A_{\ell m} + B_{\ell m} \; , \qquad D_{\ell m}^{B} = A_{\ell m}^{B} + B_{\ell m}^{B} \; . \tag{3.4.50}$$

In fact the $D_{\ell m}$ are easily obtained from the $A_{\ell m}$ by making the following transformation on $f_{ls,np}(r)$ (c.f. (3.4.5)) appearing in the $I(\ell,\lambda)$ integral (3.4.7):

$$f_{ls,np}(r) \rightarrow f_{ls,np}(r) + 2\{[B^{-1}f_{ls,w}(r) - 2\,]k_{ls,np}(r) + h_{ls,np}(r)\}. \tag{3.4.51a}$$

$f_{ls,w}(r)$ is given by (3.3.20), $h_{ls,np}(r)$ by (3.4.17) and $k_{ls,np}(r)$ by (3.4.20). In line with the approximation described following (3.4.45), one finds that (3.4.51a) is in fact modified according to

$$f_{ls,np}(r) \rightarrow f_{ls,np}(r) + t_{ls,np}(r) \tag{3.4.51b}$$

with

$$t_{ls,np}(r) = -\frac{4}{5r^4}\int_0^r u_{ls\rightarrow p}(t)\, R_{np}(t)\, t^3\, dt \tag{3.4.52}$$

in agreement with equation (28) of McDowell et al. (1975a). $t_{ls,np}(r)$ is evaluated in Appendix C for the cases $n = 2,3$ when $R_{np}(t)$ is a simple Hartree-Fock Function. Note that asymptotically $t_{ls,np}(r)$ behaves according to

$$t_{ls,np}(r) \underset{r\rightarrow\infty}{\sim} \frac{1}{r^4} \tag{3.4.53}$$

which gives rise to the slow convergence previously mentioned for the series in (3.4.29).

It will be observed that in (3.4.48a) and (3.4.49), contributions from exchange have been omitted for $\ell > \ell_o$, it being tacitly assumed that exchange terms are negligible when compared to the direct terms for the $(\ell_o + 1)^{th}$ partial wave and beyond. In practice this assumption may not be true and due account of exchange terms required up to some other value of ℓ, say ℓ_{max} (indeed ℓ_{max} may be either greater or less than ℓ_o). However, in order to avoid unnecessary complications in the following theory, it will continue to be assumed that ℓ_o and ℓ_{max} coincide, the above amendment, if appropriate, being implicit.

The total integrated cross section, $Q_{if}(k_i^2)$, is obtained by integrating (3.4.46) over all solid angle Ω. Thus, taking account of axial symmetry,

$$Q_{if}(k_i^2) = Q_o + 2Q_1 \tag{3.4.54}$$

where the integral cross section $Q_m(m = 0,1)$ is defined to be

$$Q_m = \int \frac{d\sigma_m}{d\Omega} \, d\Omega \, . \tag{3.4.55}$$

Let $Q_m(\ell_o)$ denote the integral cross section computed from the first ℓ_o partial waves alone:

$$m = 0 \quad Q_o^{\pm}(\ell_o) = \frac{1}{4\pi^2} \cdot \frac{k_f}{k_i} 4 \sum_{\ell=0}^{\ell_o} \frac{|Q_{\ell o}|^2}{2\ell+1} \pi a_o^2 , \tag{3.4.56a}$$

$$m = 1 \quad Q_1^{\pm}(\ell_o) = \frac{1}{4\pi^2} \cdot \frac{k_f}{k_i} 4 \sum_{\ell=1}^{\ell_o} \frac{\ell(\ell+1)}{2\ell+1} |Q_{\ell 1}|^2 \pi a_o^2 \, . \tag{3.4.56b}$$

Here and in the following the final spin state of the target atom is denoted explicitly. $Q_{\ell m}^{\pm}$ $(m = 0,1)$ is defined below. The analogous Born expression $Q_m^B(\ell_o)$ is defined by inserting $A_{\ell m}^B$ in place of $Q_{\ell m}^+$ and the "Born plus Polarized-Born" expression $Q_m^{B+PB}(\ell_o)$ is defined by inserting $D_{\ell m}^B$. The integral cross section calculated in the Born Approximation is denoted by $\delta Q_m(B)$ and in the "Born plus Polarized-Born" Approximation by $\delta Q_m(B + PB)$. Evaluation of these latter two quantities which requires $T_{if}^B(m)$ (viz. (3.4.43)) and $T_{if}^{PB}(m)$ (viz. (3.4.44)), is discussed in Appendix D.

The DWPO I approximation to the integral cross section $Q_m^{\pm}$ is then obtained by setting

$$Q_m^+ = Q_m^+(\ell_o) - Q_m^B(\ell_o) + \delta Q_m(B) \, , \tag{3.4.57a}$$

(I)

$$Q_m^- = Q_m^-(\ell_{max}) \tag{3.4.57b}$$

with $Q_{\ell m}^+ = A_{\ell m} - C_{\ell m}^+$ and $Q_{\ell m}^- = C_{\ell m}^-$ in (3.4.55).

The DWPO II approximation to the integral cross section $Q_m^{\pm}$ is obtained by setting

(II)
$$Q_m^+ = Q_m^+(\ell_o) - Q_m^{B+PB}(\ell_o) + \delta Q_m(B+PB) \tag{3.4.58}$$

with this time $Q_{\ell m}^+ = D_{\ell m} - C_{\ell m}^+$; Q_m^- remains unchanged from (3.4.57b). The total integrated cross section for the process under consideration is then derived in the respective DWPO model by substituting either (3.4.57) or

(3.4.58) into (3.4.54).

§3.5 The Orientation and Alignment Parameters

So far this chapter has been occupied with the determination of inelastic differential and total (integrated) cross sections. However, in addition to the cross sections, information may also be obtained on the orientation and alignment of the final state of the target atom. After the collision, the state of the atom is taken to be a coherent superposition of the relevant magnetic substates. Eventually the atom undergoes a transition with the subsequent emission of light (photon); by analysing the angular distribution and polarization of this light, it is possible to gain information about the anisotropy of the atomic state. Experimentally, the orientation may be obtained by measuring the circular polarization of the emitted photon. The alignment may be determined by using a delayed coincidence technique to measure the angular correlations between the inelastically scattered electrons and photons emitted in the scattering plane. Such coincidence techniques have been developed by Eminyan and coworkers and used initially by Eminyan et al. (1973) to obtain the angular correlations between electrons with an incident energy of either 77.7 or 80 eV scattered inelastically from helium and the photons emitted from the decay of the 2^1P and 3^1P states. A succinct account of the theory is provided in the paper by Macek and Jaecks (1971). This, together with the related article by Eminyan et al. (1976), will form the basis for the brief theoretical description outlined below for the particular case of excitation of the n^1P levels of helium. Reference may also be made to the paper by Wykes (1972).

From a practical point of view, the collision time is always considered short compared to the radiation time. Hence, denoting the state vector of the n^1P level by $|\psi(t)\rangle$ one has that at time $t = 0$

$$|\psi(0)\rangle = b_1|1,1\rangle + b_0|1,0\rangle + b_{-1}|1,-1\rangle. \qquad (3.5.1)$$

$|LM\rangle$ is the state vector describing the particular atomic state with total orbital angular momentum $L(= P$ here) and magnetic sublevel quantum number $M(= 0,\pm 1$ here); spin-dependent interactions are assumed negligible. b_M is the amplitude for producing the respective excited state. $|\psi\rangle$ possesses mirrorsymmetry in the scattering plane so that $b_1 = -b_{-1}$. Further, $|\psi\rangle$ can be normalized so that the excitation amplitudes are related to their respective differential cross sections by

$$\sigma_o = |b_o|^2 , \tag{3.5.2a}$$

$$\sigma_1 = \sigma_{-1} = |b_1|^2 , \tag{3.5.2b}$$

$$\sigma = \sigma_o + 2\sigma_1 . \tag{3.5.2c}$$

Throughout this section σ will be used to denote the total differential cross section for exciting the n^1P state and σ_M to denote the differential cross section for exciting the magnetic substate labelled M. In general the b_M are complex so that writing χ_M for the phase,

$$b_M = |b_M| \, e^{i\chi_M} . \tag{3.5.3}$$

The dimensionless orientation and alignment parameters (λ,χ) are then defined as follows

$$\lambda = \sigma_o/\sigma \qquad (0 \leq \lambda \leq 1) \tag{3.5.4a}$$

$$\chi = \chi_1 - \chi_o \qquad (-\pi < \chi \leq \pi) \tag{3.5.4b}$$

and may be determined both experimentally and theoretically. Thus the accurate determination of λ and χ imposes a more stringent test on theory than that provided by determination of the differential and integral cross sections. From an experimental point of view, λ and χ are measured as functions of energy and electron scattering angle and are free from the problems of absolute calibration and normalization upon which the determination of differential cross sections must rely. It remains to see how these parameters may be used to obtain information about the state of the excited atom.

It is assumed that contributions from cascade are negligible and that LS coupling holds, which for a light atom such as helium may be taken as correct. Returning to the state vector (3.5.1), this is not an eigenstate of the atomic Hamiltonian and is written at time $t > 0$, with $\hbar = 1$,

$$|\psi(t)\rangle = \sum_M b_M |1,M\rangle\, e^{-(\gamma/2 + iE)t}. \qquad (3.5.5)$$

E is the energy of the excited n^1P state and $1/\gamma$ the mean lifetime of this state. Almost all lines observed in atomic (and molecular) spectra originate from the electric dipole nature of the transition. Hence, the probability dN_c of observing a photon with polarization vector $\hat{t}$ in a time Δt after the atom has made the transition to the excited state $|\psi\rangle$ is proportional to the square of the electric dipole matrix element integrated over Δt

$$dN_c = C \int_o^{\Delta t} |\langle 0|\, \hat{\underline{\varepsilon}}.\underline{X}\, |\psi(t)\rangle|^2\, dt. \qquad (3.5.6)$$

C is a proportionality factor and $\underline{X}$ is the electric dipole moment operator. $|0\rangle$ is the state vector for the lower (1^1S) level reached in the decay. The angles specifying the direction Ω_ν of the photon will be denoted by (θ_ν, ϕ_ν), and the polarization vector $\hat{\underline{\varepsilon}}$ written

$$\hat{\underline{\varepsilon}} = \hat{\underline{\varepsilon}}^{(1)} \cos\beta + \hat{\underline{\varepsilon}}^{(2)} \sin\beta \qquad (3.5.7)$$

where $\hat{\underline{\varepsilon}}^{(1)}$ and $\hat{\underline{\varepsilon}}^{(2)}$ are orthogonal unit vectors at right angles to the direction Ω_ν and β is the direction of polarization. The aim is to derive an expression for dN_c which depends on the minimum number of parameters. Substituting for $|\psi(t)\rangle$ by (3.5.5) into (3.5.6) yields

$$dN_c = C \Big| \sum_M \langle 0|\, \hat{\underline{\varepsilon}}.\underline{X}\, |1,M\rangle\, b_M \Big|^2 \int_o^{\Delta t} e^{-\gamma t}\, dt\,. \qquad (3.5.8)$$

By expressing $\hat{\underline{\varepsilon}}^{(1)}$ and $\hat{\underline{\varepsilon}}^{(2)}$ in terms of spherical tensor components, namely

$$\hat{\varepsilon}^{(1)}_{\pm 1} = \frac{\pm 1}{\sqrt{2}} \cos\theta_\nu\, e^{\pm i\phi_\nu}, \qquad \hat{\varepsilon}^{(1)}_o = -\sin\theta_\nu\,;$$

$$\hat{\varepsilon}^{(2)}_{\pm 1} = \frac{\mp 1}{\sqrt{2}} \, e^{\pm i\phi_\nu} , \qquad \hat{\varepsilon}^{(2)}_{o} = 0 \ ;$$

and using the Wigner-Eckart theorem to factor out the matrix elements, Eminyan et al. (1976) find that

$$dN_c = \frac{C}{3} \, |\langle 0 \| X \| 1 \rangle|^2 \sum_{MM'} b_M b^*_{M'} \, \varepsilon^{(\alpha)}_M \, \varepsilon^{(\alpha)*}_{M'} \int_o^{\Delta t} e^{-\gamma t} \, dt \qquad (3.5.9)$$

with $\alpha = 1,2$. In practice $\Delta t \gg 1/\gamma$ so that following the references cited above, the integration over time is carried out and, since the photon detector is insensitive to polarization, the result is summed over two independent polarization directions, say β and $\beta + \frac{\pi}{2}$. This gives, after much labour

$$\frac{d^2 N_c}{d\Omega_e d\Omega_\nu} = \frac{\sigma}{\Sigma} \, \frac{dN_c}{d\Omega_\nu} \qquad (3.5.10)$$

with

$$\frac{dN_c}{d\Omega_\nu} = \frac{3\gamma}{8\pi} \left[A_{oo} + A_{11} + (A_{11} - A_{oo}) \cos^2\theta_\nu + \sqrt{2} \, \mathrm{Re} A_{o1} \sin 2\theta_\nu \cos(\phi_e - \phi_\nu) \right.$$

$$\left. + A_{1-1} \sin^2\theta_\nu \cos 2(\phi_e - \phi_\nu) \right]. \qquad (3.5.11)$$

$d^2N_c/d\Omega_e d\Omega_\nu$ is the joint probability for electron scattering in the direction Ω_e specified by the angles (θ_e, ϕ_e) and photon scattering in the direction Ω_ν specified analogously just above line (3.5.7). $dN_c/d\Omega_\nu$ is the probability density for the emission of a photon in the direction Ω_ν after electron scattering. Σ, in the notation of Eminyan et al. (1976), is the total (integrated) cross section. σ is defined previously in (3.5.2). The A_{pq} are defined by Macek and Jaecks (1971) who find for helium that

$$A_{oo} = \frac{\sigma_o}{\gamma} , \quad A_{11} = - A_{1-1} = \frac{\sigma_1}{\gamma} , \quad A_{o1} = \frac{\langle b_o b_1 \rangle}{\gamma} . \qquad (3.5.12a)$$

With the aid of definitions (3.5.2) to (3.5.4) the above A_{pq} can be expressed as:

$$A_{oo} = \frac{\sigma\lambda}{\gamma} , \quad A_{11} = - A_{1-1} = \frac{\sigma}{2\gamma} (1-\lambda), \quad A_{o1} = \frac{\sigma}{\gamma} \sqrt{\frac{\lambda(1-\lambda)}{2}} \, e^{i\chi} . \qquad (3.5.12b)$$

Hence by substituting into (3.5.11) one finds

$$\frac{dN_c}{d\Omega_\nu} = \frac{3N}{8\pi} \qquad (3.5.13a)$$

where N is the angular correlation function defined by

$$N = [\lambda\sin^2\theta_\nu + \tfrac{1}{2}(1-\lambda)(\cos^2\theta_\nu+1) - \tfrac{1}{2}(1-\lambda)\sin^2\theta_\nu\cos^2(\phi_\nu-\phi_e)$$

$$+ [\lambda(1-\lambda)]^{\frac{1}{2}} \cos\chi \sin2\theta_\nu \cos(\phi_\nu-\phi_e)] \; . \qquad (3.5.13b)$$

Equation (3.5.13) corresponds to equation (17) of Eminyan et al. (1976). In practice, Eminyan and coworkers set the electron detector at $\phi_e = 0$ and the photon detector at $\phi_\nu = \pi$ so that

$$N = \lambda\sin^2\theta_\nu + (1-\lambda)\cos^2\theta_\nu - [\lambda(1-\lambda)]^{\frac{1}{2}} \cos\chi \sin2\theta_\nu \; . \qquad (3.5.14)$$

Since N depends on $\cos\chi$, the experiment will only determine χ up to a sign. Eminyan et al. (1974) have used the delayed coincidence technique to obtain values for λ and $|\chi|$ by observing emission from the 2^1P level of helium over the angular range $16^\circ \leq \theta_e \leq 40^\circ$ and for electron impact energies ranging from 40 eV to 200 eV. In a later publication (Eminyan et al., 1975) λ and $|\chi|$ have been similarly determined for excitation of the 3^1P level for $10^\circ \leq \theta_e \leq 30^\circ$ and electron energies lying between 50 eV and 150 eV.

Moreover, Fano and Macek (1973) have made a theoretical study of impact excitation and polarization of the emitted photon. Essentially, they show that the average intensity of emission over all directions Ω_ν depends on dynamical factors such as the line strength whereas the anisotropy and polarization of the light (photon) depends on the alignment and orientation of the excited atom. The intensity of the emitted light is formulated in terms of the components of an orientation vector $\underline{O}^{col}$ and the components of an alignment tensor $\underline{A}^{col}$, determined in the 'collision frame' (x,y,z) which has been used above as opposed to the 'detector frame' defined by the photon detector in the notation of Fano and Macek (1973). These components

are independent of one another in the sense that a change of excitation process may alter any one of them and leave the others fixed.

Using spherical tensor notation, the non-vanishing components of $\underline{O}^{col}$ and $\underline{A}^{col}$ are defined by Fano and Macek (1973) in terms of the mean values of expressions involving the components of the orbital angular momentum vector $\underline{L}$ and by Eminyan et al. (1976) in terms of λ and χ so that

$$O_{1-}^{col} = \langle L_y \rangle [L(L+1)]^{-1} = -[\lambda(1-\lambda)]^{\frac{1}{2}} \sin\chi \qquad (3.5.15a)$$

$$A_{o}^{col} = \tfrac{1}{2}\langle 3L_z^2 - \underline{L}^2 \rangle [L(L+1)]^{-1} = \tfrac{1}{2}(1-3\lambda) \qquad (3.5.15b)$$

$$A_{1+}^{col} = \tfrac{1}{2}\langle L_x L_z + L_z L_x \rangle [L(L+1)]^{-1} = [\lambda(1-\lambda)]^{\frac{1}{2}} \cos\chi \qquad (3.5.15c)$$

$$A_{2+}^{col} = \tfrac{1}{2}\langle L_x^2 - L_y^2 \rangle [L(L+1)]^{-1} = \tfrac{1}{2}(\lambda-1) \qquad (3.5.15d)$$

The mean values are of course taken with respect to the excited state. Hence one sees how the parameters λ and χ may be used to obtain information about the orientation and alignment of the excited state.

Physically λ represents a relative measurement of σ_o which, according to the definition (3.5.4a), can be made absolute when σ is known from an absolute measurement. Together with (3.5.2c), a knowledge of the individual differential cross sections σ_o and σ_1 may then be derived. For a comparison between such cross sections for excitation of the n^1P level in helium, see the papers by Chutjian and Srivastava (1975, n = 2) and Chutjian (1976, n = 3).

χ on the other hand may be physically interpreted as the phase difference between the excitation amplitude of the respective magnetic substates (see equation (3.5.4b)). However, it has recently been shown (Kleinpoppen, 1976) that a measurement of χ for the excitation/de-excitation process $^1S \rightarrow {}^1P \rightarrow {}^1S$ in helium coincides with the phase difference between two electric field vectors of the radiated photon emitted from the second transition. In other words, one has the remarkable conclusion that a quantum mechanical phase difference appears as a directly measurable

(macroscopic) phase between two observable light vectors.

The angular correlation function N of equation (3.5.13b) may be expressed in terms of the components of $\underline{A}^{col}$ as

$$N = \frac{2}{3} + A_{2+}^{col} \sin^2\theta_\nu \cos 2(\phi_\nu - \phi_e) + A_{1+}^{col} \sin 2\theta_\nu \cos(\phi_\nu - \phi_e) + \frac{1}{3} A_o^{col} (3\cos^2\theta_\nu - 1). \tag{3.5.16}$$

Hence, an experimental determination of N contains no information about the orientation $\underline{O}^{col}$. In other words the angular correlation depends only upon the alignment of the atom as remarked at the beginning of this section.

However, O_{1-}^{col} may be determined by examining the degree of circular polarization, P, of the correlated photons. P is defined in terms of integral cross sections as

$$P = \frac{Q_o - Q_1}{Q_o + Q_1} \tag{3.5.17}$$

when $\theta_\nu = \pi/2$. For coincident photons emitted perpendicular to the plane of scattering, that is $\theta_\nu = \phi_\nu = \pi/2$ and $\phi_e = 0$, Eminyan et al. (1976) show that

$$P = 2[\lambda(1-\lambda)]^{\frac{1}{2}} \sin\chi . \tag{3.5.18}$$

Therefore, with the aid of (3.5.15a), a measurement of P determines O_{1-}^{col} and also fixes the sign of χ. Experimentally, determination of P is difficult due to the short wavelength of the light.

Physically one sees from (3.5.15a) that O_{1-}^{col} is a measure of the expectation value of the orbital angular momentum received by the atom perpendicular to the plane of scattering and is hence an indication of the extent to which the atom is oriented. Moreover, it can be shown that $\langle L_x \rangle = \langle L_z \rangle = 0$ so that the net orbital angular momentum transferred to the atom is restricted to a component along $\hat{y}$.

In order to compute the orientation and alignment parameters (λ,χ) using the DWPO models, some results from §3.4 must be recalled.

λ is quite simply computed from (3.5.4a) with the aid of (3.4.46) and (3.4.47) with the appropriate insertions for $T_{if}(m)$ depending on whether one chooses DWPO I or DWPO II.

χ is computed by considering $T_{if}(m)$ as given by (3.4.48a) or (3.4.49) depending again on the choice of model. For convenience the superscript has been omitted from $T_{if}(m)$, since it serves no purpose in the following discussion. $T_{if}(m)$ is divided into its real and imaginary parts, denoted respectively by $R_m(\theta_e)$ and $I_m(\theta_e)$ where the dependence upon scattering angle (written in this section as θ_e rather than θ) has been made explicit.

$$T_{if}(m) = R_m(\theta_e) + i\, I_m(\theta_e), \quad m = 0,1. \tag{3.5.19}$$

The phase χ_m referred to in equation (3.5.3) is then given by

$$\chi_m = \tan^{-1}\left(I_m(\theta_e)/R_m(\theta_e)\right), \quad m = 0,1\ . \tag{3.5.20}$$

so that the relative phase χ may be obtained by substituting for χ_o and χ_1 in (3.5.4b). It is noted that when $\theta_e = 0$ or π, the $m = 1$ component of T_{if} vanishes so that χ_1 and hence χ remain undefined at these angles.

Finally, the excitation amplitudes, when calculated in the First Born Approximation, are always either purely real or purely imaginary. Hence this approximation predicts that $\chi = 0$ or $\pm\pi$, in clear disagreement with experiment. One therefore sees that in this respect the First Born Approximation is inadequate, particularly for predicting the orientation of the excited atom. Hence, a measurement of χ may consequently be used to define further the region of validity of the First Born Approximation.

CHAPTER 4

EXCHANGE-POLARIZATION EFFECTS

§4.1 Introduction

This chapter will be concerned with a treatment of the effects arising from a consideration of the Pauli exclusion principle upon the polarization terms which occur in calculating cross sections for inelastic electron-atom scattering. In general, the inclusion of such effects in scattering theory adds considerable complexity to the calculations. Taylor and coworkers have introduced terms due to exchange-polarization interactions into their many-body formalism via a second-order transition potential (see, for example, Csanak et al. (1973) and Csanak and Taylor (1973)). Close-coupling methods also allow for the effects of exchange-polarization, though only implicitly through the very nature of the close-coupling expansion. However, in the following discussion, an attempt is made to develop a theory which takes explicit account of exchange-polarization interactions in electron-atom collisions.

For two-electron target systems, such as helium, the treatment of these extra interactions has already been briefly mentioned in Chapter 2 in connection with the Distorted Wave Polarized Orbital approximation. It was remarked there that the scattering equation satisfied by the distorted wave $F(\underline{r})$ (c.f. §2.2) could no longer be considered in the adiabatic-exchange approximation but rather should be supplemented by further terms arising from a full analysis of the polarized orbital ansatz (2.1.7). Moreover, the T-matrix element, formulated in §2.3, should also be modified as in (2.3.10) to allow explicitly for exchange effects on the polarized wave function representing the ground state of the target atom. In the context of the DWPO approximation, the DWPO III model endeavours to allow for these effects of exchange-polarization via the initial channel; final channel distortion is omitted altogether. The purpose of this chapter then is to develop the DWPO III model and in particular to enable an account of exchange-polarization

to be incorporated into the formalism concerning (a) excitation from the ground (1s) state to any excited (nℓ) state in atomic hydrogen (§4.3) and (b) excitation from the ground (1^1S) state to another S-state ($n^{1,3}S$) in helium (§4.4). Essentially, therefore, one is concerned with the new form of the scattering equation and with the corresponding modifications to the T-matrix element.

§4.2 The Radial Scattering Equation

The scattering equation is obtained from the polarized orbital ansatz (2.1.7) for both hydrogen and helium by making the relevant choice of wave functions. Such an analysis has been performed for hydrogen by Sloan (1964) and for helium by Duxler et al. (1971). Following these authors, the radial scattering equation for the $u_\ell(k_i,r)$ appearing in the expansion (3.1.16) for $F(\underline{r})$ is written, adopting previous notation, as

$$\left[\frac{d^2}{dr^2} + k_i^2 - \frac{\ell(\ell+1)}{r^2} - NV_{1s,1s}(r) - NV_{pol}(r)\right] u_\ell(k_i,r)$$

$$= -\tau\left[rR_{1s}(r)\left[(\varepsilon_{1s}-k_i^2)\delta_{\ell o}\int_o^\infty R_{1s}(t)u_\ell(k_i,t)tdt + \frac{2}{2\ell+1}\int_o^\infty R_{1s}(t)u_\ell(k_i,r)\gamma_\ell(r,t)tdt\right]\right.$$

$$- u_{1s\to p}(r)\left\{4\left[\frac{\ell}{(2\ell+1)(2\ell-1)}\, r^{\ell-1}\int_r^\infty \frac{R_{1s}(t)u_\ell(k_i,t)dt}{t^{\ell+1}} + \frac{\ell+1}{(2\ell+1)(2\ell+3)}\, r^{\ell+1}\right.\right.$$

$$\left.\left.\int_r^\infty \frac{R_{1s}(t)u_\ell(k_i,t)}{t^{\ell+3}}\, dt\right]\right.$$

$$\left.- \frac{2}{3}(-\varepsilon_{1s} + k_i^2)\delta_{\ell 1}\int_r^\infty \frac{R_{1s}(t)u_\ell(k_i,t)}{t}\, dt\right\} - \frac{2}{3}\delta_{\ell 1}\left\{u_{1s\to p}(r)\frac{d}{dr}\left(\frac{R_{1s}(r)}{r}\right)\right.$$

$$\left.\left. + 2\,\frac{R_{1s}(r)}{r}\,\frac{d}{dr}\left(u_{1s\to p}(r)\right) + u_{1s\to p}(r)\,\frac{R_{1s}(r)}{r}\,\frac{d}{dr}\right\}u_\ell(k_i,r)\right]. \qquad (4.2.1)$$

The factors N and τ have been introduced merely for convenience; they depend upon the target atom under consideration.

For hydrogen; $N = 1$, $\tau = +1$ for a singlet spin state

$\tau = -1$ for a triplet spin state.

For helium; $N = 2$, $\tau = 1$.

ε_{1s} is defined to be the single ionization energy, as in equation (2.2.9). The terms in the latter pair of curly brackets arise from the operation of the Laplacian operator ∇^2 on the step function $\varepsilon(r,t)$ contained in $\phi_{pol}(\underline{r},\underline{t})$. Such terms were first derived by Sloan (1964) in a study of the method of polarized orbitals for the elastic scattering of slow electrons by atomic hydrogen and singly ionized helium. It is to be noted that these terms contain a derivative of $u_\ell(k_i,r)$, that is, a velocity-dependent term, which consequently constitutes a non-adiabatic effect. Moreover, their inclusion in (4.2.1) improves the phase shifts in the p-wave, the only case for which they arise. Equation (4.2.1) will now be discussed briefly in connection with hydrogen and helium.

In the case of hydrogen, (4.2.1) should be compared with the equivalent equation in the adiabatic-exchange approximation given by McDowell et al. (1973, equations (11) and (14)). The radial function $R_{1s}(r)$ is replaced by the exact (hydrogenic) function $R^H_{1s}(r)$ where

$$R^H_{1s}(r) = 2Z^{3/2}\, e^{-Zr}, \quad Z = 1 \text{ for hydrogen} . \tag{4.2.2}$$

The direct potentials $V_{1s,1s}(r)$ and $V_{pol}(r)$ may be obtained from equations (3.2.3) and (3.2.5) respectively, making, of course, the appropriate choice of parameters. The resulting expressions agree with equations (12) and (13) of McDowell et al. (1973) as previously remarked in §3.2. Temkin and Lamkin (1961) also derived (4.2.1) in their application of the method of polarized orbitals to the scattering of electrons from hydrogen, but omitted the final set of terms first included by Sloan (1964).

In the case of helium, (4.2.1) should be compared with the equivalent equation in the adiabatic-exchange approximation given earlier by equation (3.2.1). The direct potentials $V_{1s,1s}(r)$ and $V_{pol}(r)$ remain of course

unaltered and are given as before by (3.2.3) and (3.2.5) respectively. However, compared with hydrogen, two additional integral terms should now be included in (4.2.1) for helium as in equation (3.1) of Duxler et al. (1971). In the present treatment, these two terms (which effect only the s- and p-waves, respectively) have been omitted in order to simplify the method of solution for (4.2.1). Comparison between calculated s and p phase shifts with those published by Duxler et al. (1971) showed very close agreement despite this omission.

Having presented the radial scattering equation in a form suitable for electron scattering by either hydrogen or helium, discussion will now focus on the modification to the T-matrix element.

§4.3 1s → nℓ Transitions in Hydrogen

Differential cross sections, describing excitation of 1s → nℓ transitions in atomic hydrogen by electron impact, have been published in the DWPO I and DWPO II models in a series of papers by McDowell and coworkers. Briefly, 1s → ns transitions have been considered in the DWPO I model by McDowell et al. (1973) and in the DWPO II model by McDowell et al. (1974). Subsequently, work on the 1s → np transitions has been published in both models by McDowell et al. (1975a). Excitation of the n = 2 level has been discussed in a further paper, in the DWPO I and DWPO II models, by McDowell et al. (1975b) and similarly excitation of the n = 3 level by Syms et al. (1975). The idea then of the present section (§4.3) is to extend the DWPO model used in the above papers to include an account of exchange-polarization (DWPO III). The scattering equation has already been considered in the previous section (§4.2) so that here one will be occupied with including the effects of exchange-polarization explicitly in the T-matrix element.

The starting point, therefore, of this section will be equation (2) of McDowell et al. (1975b) which, to conform with notation of this thesis, is written

$$T_{if}^{\pm} = \langle \phi_f(1)\ \chi_{k_f}(z,2)\ V_f\ \mathcal{A}[(\phi_{ls}(1) + \phi_{pol}(12))\ F^{\pm}(2)]\rangle. \qquad (4.3.1)$$

$\mathcal{A}$ is an antisymmetrising operator on electrons 1 and 2; the plus and minus signs refer respectively to singlet and triplet spin states of the complete system (projectile and target). The interaction potential in this section (§4.3) is given by

$$V_f = -\frac{1}{r_2} + \frac{1}{r_{12}} \qquad (4.3.2)$$

and must not be confused with that for helium given by equation (2.3.1). The final unperturbed atomic wave function $\phi_f(\underline{r})$ is written in the exact form

$$\phi_f(\underline{r}) = R^H_{n\ell}(r)\ Y_{\ell m}(\hat{r}) \qquad (4.3.3)$$

with $R^H_{n\ell}(r)$ the radial (hydrogenic) wave function. Similarly, the unperturbed ground state wave function $\phi_{ls}(\underline{r})$ is written

$$\phi_{ls}(\underline{r}) = R^H_{ls}(r)\ Y_{oo}(\hat{r}) \qquad (4.3.4)$$

with $R^H_{ls}(r)$ defined in (4.2.2). The 'H' superscript only serves to distinguish between atomic wave functions for hydrogen and helium and in fact will be dropped where there is no possibility of ambiguity. $\phi_{pol}(\underline{r},\underline{t})$ is defined by equation (3.1.6) with $Z_o = 1$. $F(\underline{r})$ and $\chi_{k_f}(z,\underline{r})$ are expressed as in (3.1.22) and (3.1.23) respectively; note however, that in the present case, the residual charge z is taken rather to be defined as $z = Z - 1$ where Z denotes as before the nuclear charge.

Equation (4.3.1) is expanded to give;

$$T_{if}^{\pm} = (T_{if}^{D} + T_{if}^{PD}) \pm (T_{if}^{E} + T_{if}^{PE}) \qquad (4.3.5)$$

where:

$$T_{if}^{D} = \langle \phi_f(1)\ \chi_{k_f}(z,2)\ \ V_f\ \phi_i(1)\ F^{\pm}(2) \rangle \tag{4.3.6a}$$

$$T_{if}^{PD} = \langle \phi_f(1)\ \chi_{k_f}(z,2)\ \ V_f\ \phi_{pol}(1,2)\ F^{\pm}(2) \rangle \tag{4.3.6b}$$

$$T_{if}^{E} = \langle \phi_f(1)\ \chi_{k_f}(z,2)\ \ V_f\ \phi_i(2)\ F^{\pm}(1) \rangle \tag{4.3.6c}$$

$$T_{if}^{PE} = \langle \phi_f(1)\ \chi_{k_f}(z,2)\ \ V_f\ \phi_{pol}(2,1)\ F^{\pm}(1) \rangle \tag{4.3.6d}$$

Retaining T_{if}^{D} and T_{if}^{E} in (4.3.5) gives the DWPO I model (c.f. equation (19) of McDowell et al. (1973) or equation (1) of McDowell et al. (1974)). Retaining also T_{if}^{PD} gives the DWPO II model (c.f. equation (2) of McDowell et al. (1974) or equation (25) of McDowell et al. (1975a)). Both these models have been fully developed elsewhere. Emphasis is consequently now placed upon a partial wave analysis of T_{if}^{PE} in (4.3.6d). Notation will follow that of §3.1.

Hence, in T_{if}^{PE}, the atomic wave functions $\phi_f(\underline{r})$ and $\phi_{pol}(\underline{r},\underline{t})$ are replaced by their respective forms outlined earlier in this section. The Legendre polynomial $P_l(\cos\theta_{rt})$ appearing in the expression for $\phi_{pol}(\underline{r},\underline{t})$ is expanded in spherical harmonics according to the addition theorem given by (3.1.13). $F(\underline{r})$ and $\chi_{k_f}(z,\underline{r})$ are expressed as mentioned above just after equation (4.3.4) and r_{12}^{-1} appearing in V_f of (4.3.2) is replaced by its multipole expansion (3.1.14). One therefore finds that

$$T_{if}^{PE} = -\frac{2(4\pi)^3}{3\sqrt{k_i}} \sum_{\lambda=0}^{\infty} \sum_{\lambda'=0}^{\infty} \sum_{\ell'=0}^{\infty} i^{\ell'-\lambda} \frac{(2\ell'+1)^{\frac{1}{2}}}{2\lambda'+1} e^{i\Delta_{\lambda,\ell'}} Y_{\lambda\mu}(\Theta,0) \tag{4.3.7}$$

$$\int_0^{\infty} R_{n\ell}(r)\ u_{\ell'}^{\pm}(k_i,r) \left\{ \frac{1}{r} \int_0^{r} u_{ls\to p}(t)\ H_{\lambda}(k_f t)\ \tilde{\gamma}_{\lambda'}(r,t)dt \right\} dr\ I_{\lambda\lambda'\lambda'}(\Omega_{rt})$$

where

$$\Delta_{\lambda,\ell} = \delta_{\ell}(k_i) + \eta_{\ell}(k_i) - \eta_{\lambda}(k_f)\ , \tag{3.4.9}$$

$$\tilde{\gamma}_{\lambda}(r,t) = \frac{t^{\lambda}}{r^{\lambda+1}} - \frac{1}{t}\delta_{\lambda o}\ . \tag{4.3.8}$$

$I_{\lambda\lambda'\ell'}(\Omega_{rt})$ denotes the total angular integration and is given by

$$I_{\lambda\lambda'\ell'}(\Omega_{rt}) = \sum_{\mu'=-\lambda'}^{\lambda'} \sum_{\mu=-\lambda}^{\lambda} \sum_{\nu=-1}^{1} \int_{\Omega_r} Y^*_{\ell m}(\hat{r})\, Y^*_{\lambda'\mu'}(\hat{r})\, Y^*_{1\nu}(\hat{r})\, Y_{\ell' o}(\hat{r})\, d\hat{r}$$

$$\int_{\Omega_t} Y^*_{\lambda\mu}(\hat{t})\, Y_{\lambda'\mu'}(\hat{t}) Y_{1\nu}(\hat{t}) d\hat{t} \,. \qquad (4.3.9)$$

In order to perform the integral over $\hat{r}$, use is first made of relation (3.4.13) to express the product $Y^*_{\lambda'\mu'}(\hat{r})\, Y^*_{1\nu}(\hat{r})$ in terms of a single spherical harmonic, say $Y_{pq}(\hat{r})$. The integral may then be evaluated with the aid of (3.4.4) to yield

$$I(\Omega_r) = (-1)^m \sum_{p=o}^{\infty} \sum_{q=-p}^{p} \left[\frac{3(2\lambda'+1)(2p+1)}{4\pi}\right]^{\frac{1}{2}} \left[\frac{(2p+1)(2\ell'+1)(2\ell+1)}{4\pi}\right]^{\frac{1}{2}}$$

$$\cdot \begin{pmatrix} 1 & \lambda' & p \\ 0 & 0 & 0 \end{pmatrix} \begin{pmatrix} p & \ell' & \ell \\ 0 & 0 & 0 \end{pmatrix} \begin{pmatrix} 1 & \lambda' & p \\ \nu & \mu' & q \end{pmatrix} \begin{pmatrix} p & \ell' & \ell \\ q & 0 & -m \end{pmatrix} .$$

Note that from the last Wigner 3-j symbol one has that $q = +m$. The integral over $\hat{t}$ is straightforward using (3.4.4) and gives

$$I(\Omega_t) = (-1)^{\mu} \left[\frac{3(2\lambda+1)(2\lambda'+1)}{4\pi}\right]^{\frac{1}{2}} \begin{pmatrix} 1 & \lambda & \lambda' \\ 0 & 0 & 0 \end{pmatrix} \begin{pmatrix} 1 & \lambda & \lambda' \\ \nu & -\mu & \mu' \end{pmatrix} .$$

These two results for $I(\Omega_r)$ and $I(\Omega_t)$ are subsequently inserted into (4.3.9) and advantage taken of the orthogonality property possessed by the Wigner 3-j symbols which is given by Edmonds (1974, equation (3.7.8)). One finds that

$$I_{\lambda\lambda'\ell'}(\Omega_{rt}) = \frac{3(2\lambda'+1)}{4\pi} \left[\frac{(2\ell+1)(2\ell'+1)(2\lambda+1)}{4\pi}\right]^{\frac{1}{2}} \begin{pmatrix} \ell & \ell' & \lambda \\ 0 & 0 & 0 \end{pmatrix} \begin{pmatrix} \lambda & \lambda' & 1 \\ 0 & 0 & 0 \end{pmatrix}^2$$

$$\begin{pmatrix} \ell & \ell' & \lambda \\ m & 0 & -m \end{pmatrix} \delta_{\mu,-m} \,. \qquad (4.3.10)$$

From the 3-j symbols appearing in (4.3.10) one observes that $\lambda' = \lambda \pm 1$ if $\lambda > 0$; $\lambda' = 1$ if $\lambda = 0$. It is convenient to define by $t^{\ell,\lambda}_{ls\to p}(r)$ the following radial integral:

$$t^{\ell,\lambda}_{ls\to p}(r) = \int_o^r u_{ls\to p}(t)\, H_\ell(k_f t) t^{\lambda+1}\, dt \,. \tag{4.3.11}$$

Let $g^{(p)}_{ls,\lambda}(r)$ be defined by

$$g^{(p)}_{ls,\lambda}(r) = -\frac{2(\lambda+1)}{2\lambda+3} \cdot \frac{1}{r^{\lambda+3}}\, t^{\lambda,\lambda+1}_{ls\to p}(r) - \frac{2\lambda}{2\lambda-1} \cdot \frac{1}{r^{\lambda+1}}\, t^{\lambda,\lambda-1}_{ls\to p}(r) + \frac{2}{r}\, t^{1,-1}_{ls\to p}(r)\delta_{\lambda 1} \,. \tag{4.3.12}$$

For small r, it is desirable to make a series expansion in r of $g^{(p)}_{ls,\lambda}(r)$. This is readily obtained if $t^{\ell,\lambda}_{ls\to p}(r)$ defined in (4.3.11) is expressed as a series expansion in r. Such an expansion is derived in Appendix C.

Recalling (4.3.7) for T_{if}^{PE} and substituting for $I_{\lambda\lambda'\ell'}(\Omega_{rt})$ with the aid of (4.3.10), it is consequently seen that

$$T_{if}^{PE} = \frac{(4\pi)^{3/2}}{\sqrt{k_i}} \sum_{\lambda=0}^{\infty} \sum_{\ell'=0}^{\infty} i^{\ell'-\lambda}(2\ell'+1) \sqrt{\frac{2\ell+1}{2\lambda+1}} \int_o^\infty R_{n\ell}(r) u^{\pm}_{\ell'}(k_i,r)\, g^{(p)}_{ls,\lambda}(r)\, dr$$

$$\begin{pmatrix} \ell & \ell' & \lambda \\ 0 & 0 & 0 \end{pmatrix} \begin{pmatrix} \ell & \ell' & \lambda \\ m & 0 & -m \end{pmatrix} e^{i\Delta_{\lambda,\ell'}}\, Y_{\lambda,-m}(\Theta,0) \tag{4.3.13}$$

The expression (4.3.6c) for T_{if}^{E} may be evaluated in a similar way. The angular integrations are relatively straightforward and are performed by making use of orthogonality between the spherical harmonics together with (3.4.4). The result is summarized as

$$T_{if}^{E} = \frac{(4\pi)^{3/2}}{\sqrt{k_i}} \sum_{\lambda=0}^{\infty} \sum_{\ell'=0}^{\infty} i^{\ell'-\lambda}\,(2\ell'+1) \sqrt{\frac{2\ell+1}{2\lambda+1}} \left[\int_o^\infty R_{n\ell}(r)\, u^{\pm}_{\ell'}(k_i,r)\, g_{ls,\lambda}(r)\, dr \right.$$

$$\left. - \delta_{\lambda o} \int_o^\infty R_{n\ell}(r) u^{\pm}_{\ell'}(k_i,r) r dr \int_o^\infty R_{ls}(r)\, H_\lambda(k_f r) r dr \right] \begin{pmatrix} \ell & \ell' & \lambda \\ 0 & 0 & 0 \end{pmatrix} \begin{pmatrix} \ell & \ell' & \lambda \\ m & 0 & -m \end{pmatrix}$$

$$e^{i\Delta_{\lambda,\ell'}}\, Y_{\lambda,-m}(\Theta,0) \,. \tag{4.3.14}$$

This is the exchange term adopted by McDowell and coworkers in the DWPO I and DWPO II models. The function $g_{1s,\lambda}(r)$ is defined by McDowell et al. (1973, equation (32)) and is observed to coincide with the definition of $g_{1s,\ell}(r)$ in this thesis (equation (3.3.13)), given the appropriate choice of $R_{1s}(r)$ and $H_{\ell}(k_f r)$.

The total exchange T-matrix element in the DWPO III model is defined as the sum of T_{if}^{E} and T_{if}^{PE}, that is

$$T_{if}^{E} + T_{if}^{PE}.$$

By comparing (4.3.13) and (4.3.14), one sees that this is most easily obtained by making the following transformation on $g_{1s,\lambda}(r)$ appearing in equation (4.3.14) for T_{if}^{E}:

$$g_{1s,\lambda}(r) \rightarrow g_{1s,\lambda}(r) + g_{1s,\lambda}^{(p)}(r) \qquad (4.3.15)$$

where $g_{1s,\lambda}^{(p)}(r)$ is defined by (4.3.12). Note that $g_{1s,\lambda}(r)$ and $g_{1s,\lambda}^{(p)}(r)$ are both independent of ℓ, the orbital angular momentum quantum number of the excited state. It is consequently emphasised that (4.3.15) is the only modification required to include exchange-polarization effects explicitly in the T-matrix element for excitation from the ground $(1s)$ state to any other $(n\ell)$ state.

To summarize: the DWPO III model for describing excitation of $1s \rightarrow n\ell$ transitions in atomic hydrogen is obtained by solving for $u_{\ell}(k_i,r)$ in the appropriate version of (4.2.1) and incorporating the modification (4.3.15) into the exchange T-matrix element of the DWPO II model.

§4.4 $1^1S \rightarrow n^{1,3}S$ Transitions in Helium

As in the previous section (§4.3) the object here will be to investigate the result of explicitly including the effects of exchange-polarization in the T-matrix element. For helium (or indeed any two-electron atomic system) such effects have already been noted to give rise to two additional terms;

$T_{if}^{El\pm}$ given by (2.3.28) and $T_{if}^{E2\pm}$ given by (2.3.30). In the following, a partial wave analysis will be performed on each of these terms. When considering excitation of atomic hydrogen, a general result (4.3.15) was derived which was suitable for any transition. However, such a result is not possible in the case of helium, due essentially to the further exchange interactions arising through the presence of the core electron. Hence, the analysis will be restricted to S - S transitions. Notation follows exactly that adopted in Chapter 3. The correction term $\phi_{pol}(\underline{r},\underline{t})$ is expressed by (3.1.6) coupled with (3.1.13) to expand the Legendre polynomial and $|\underline{r}-\underline{t}|^{-1}$ is replaced by the multipole expansion (3.1.14). $F(\underline{r})$ and $\chi_{k_f}(z,\underline{r})$ are decomposed into partial wave sums according to (3.1.22) and (3.1.23) respectively. Consideration will first be given to $T_{if}^{El\pm}$.

$\underline{T_{if}^{El\pm}}$:

$$T_{if}^{El\pm} = \pm \frac{1}{\sqrt{2}} \left[K_1^{El} - K_2^{El} \pm K_3^{El} + K_4^{El} \right] \qquad (2.3.28)$$

The $K_i^{El}(i = 1,\ldots 4)$ are evaluated in turn with the aid of the above mentioned partial wave expansions, remembering that $v_{n\ell}^{\pm}(\underline{r})$ represents an s-state $(\ell = s)$.

K_1^{El}:

$$K_1^{El} = \int u_{1s}^{*}(2)\, v_{n\ell}^{*\pm}(1)\, \chi_{k_f}^{*}(z,3)\left(\frac{1}{r_{13}} - \frac{1}{r_3}\right) \phi_{1s}(2)\phi_{pol}(31)F(1)d\underline{r}_{123} \qquad (2.3.27a)$$

It is noted that the integration over $\underline{r}_2$ may be separated completely from that over $\underline{r}_{13}$ and denoted by the usual expression B of (2.3.17). The remaining integral over $\underline{r}_{13}$ is then observed to closely resemble that for T_{if}^{PE} in the case of hydrogen, equation (4.3.6d). Consequently, one may utilise the final expression (4.3.13) given for T_{if}^{PE}, with of course the appropriate choice of wave functions applicable to helium.

Since one is only concerned with S-S transitions so that putting $\ell = 0$ in (4.3.13), the two Wigner 3-j symbols reduce to give

$$\begin{pmatrix} 0 & \ell' & \lambda \\ 0 & 0 & 0 \end{pmatrix}^2 = \frac{\delta_{\ell'\lambda}}{2\ell'+1} \quad . \tag{4.4.1}$$

Let

$$\mathcal{J}^{(P)}(\ell,k_i,k_f) = \int_0^\infty R_{ns}(r)\, u_\ell(k_i,r)\, g^{(p)}_{ls,\ell}(r)\, dr \tag{4.4.2}$$

where $g^{(p)}_{ls,\ell}(r)$, with helium wave functions, is defined by (4.3.12). For small r, a series expansion in r is readily obtained from Appendix C. Then, expressing the remaining spherical harmonic $Y_{\ell o}(\theta,0)$ as a Legendre polynomial with the help of (3.1.21) and employing the notation of (3.3.4) for the phases, one sees that K_1^{El} may be written as

$$K_1^{El} = \frac{4\pi B}{\sqrt{k_i}} \sum_{\ell=0}^{\infty} \mathcal{J}^{(P)}(\ell,k_i,k_f)\, e^{i\Delta_\ell}\, P_\ell(\cos\theta) \quad . \tag{4.4.3}$$

K_2^{El}:

$$K_2^{El} = \int u^*_{ls}(2)\, v^{*\pm}_{n\ell}(1)\, \chi^*_{k_f}(z,3)\, \frac{1}{r_3}\, \phi_{ls}(2)\, \phi_{pol}(31)\, F(1)\, d\underline{r}_{123} \tag{2.3.27b}$$

The integration over $\underline{r}_2$ is separable as above in K_1^{El} and is denoted by B (equation (2.3.17)). Inserting the various partial wave expansions, the integration over $\underline{r}_{13}$ is straightforward. The angular integrals are performed using only orthogonality of the spherical harmonics. The radial integral is denoted by $p_1^{El}(k_i,k_f)$ where

$$p_1^{El}(k_i,k_f) = -\int_0^\infty R_{ns}(r)\, u_1(k_i,r)\left(\frac{1}{r}\int_0^r u_{ls\to p}(t)\, H_1(k_f t)\,dt\right)dr \quad . \tag{4.4.4}$$

Hence, writing Δ_1 for the phases (see equation (3.3.4)) and employing (3.1.21), K_2^{El} is reduced to

$$K_2^{El} = \frac{8\pi B}{\sqrt{k_i}}\, p_1^{El}(k_i,k_f)\, e^{i\Delta_1}\, P_1(\cos\theta) \quad . \tag{4.4.5}$$

K_3^{El}:

$$K_3^{El} = \int u^*_{ls}(1)\, v^{*\pm}_{n\ell}(2)\, \chi^*_{k_f}(z,3)\, \frac{1}{r_{23}}\, \phi_{ls}(2)\, \phi_{pol}(31) F(1) d\underline{r}_{123} \tag{2.3.27c}$$

After substituting the appropriate partial wave expansions, the angular

integral is seen to present no complications and requires only the property of orthogonality between the spherical harmonics. Concerning the radial integral, this is denoted by $q^{El}(k_i,k_f)$:

$$q^{El}(k_i,k_f) = -\int_o^\infty w(r)\, u_l(k_i,r)\left(\frac{1}{r}\int_o^r u_{ls\to p}(t)\, H_l(k_f t) f_{ls,ns}(t)dt\right)dr \quad (4.4.6)$$

where $f_{ls,ns}(r)$ is defined by equation (3.3.3). K_3^{El} is consequently summarized as

$$K_3^{El} = \frac{8\pi}{\sqrt{k_i}}\, q^{El}(k_i,k_f)\, e^{i\Delta_l}\, P_l(\cos\theta). \quad (4.4.7)$$

K_4^{El}:

$$K_4^{El} = \int u_{ls}^*(2)\, v_{n\ell}^{*\pm}(1)\, \chi_{k_f}^*(z,3)\, \frac{1}{r_{23}}\, \phi_{ls}(2)\, \phi_{pol}(31)\, F(1)\, d\underline{r}_{123} \quad (2.3.27d)$$

It is observed that (2.3.27c) and (2.3.27d) differ only by the interchange of the electron labels in the first two functions under the integral. Hence, since this section is only concerned with S-S transitions, the angular integrals are identical in (2.3.27c) and (2.3.27d). Also, the radial integral of the latter is easily determined from that of the former by interchanging $w(r)$ and $R_{ns}(r)$ (which appears in $f_{ls,ns}(r)$), and is consequently given by

$$p_2^{El}(k_i,k_f) = -\int_o^\infty R_{ns}(r) u_l(k_i,r)\left(\frac{1}{r}\int_o^r u_{ls\to p}(t) H_l(k_f t) f_{ls,w}(t)dt\right)dr \quad (4.4.8)$$

where $f_{ls,w}(r)$ is defined by equation (3.3.20). K_4^{El} is finally written as

$$K_4^{El} = \frac{8\pi}{\sqrt{k_i}}\, p_2^{El}(k_i,k_f)\, e^{i\Delta_l}\, P_l(\cos\theta). \quad (4.4.9)$$

Returning to equation (2.3.28) for $T_{if}^{El\pm}$, this can now be summarized by collecting together the results (4.4.3), (4.4.5), (4.4.7) and (4.4.9) for the K_i^{El} $(i = 1,\ldots 4)$ to give

$$T_{if}^{El\pm} = \pm \frac{1}{\sqrt{2}} \frac{4\pi}{\sqrt{k_i}} \sum_{\ell=0}^{\infty} \Big[B\, J^{(P)}(\ell,k_i,k_f) + 2\{ (p_2^{El}(k_i,k_f) - B p_1^{El}(k_i,k_f)) \pm q^{El}(k_i,k_f) \} \delta_{\ell 1} \Big] e^{i\Delta_\ell} P_\ell(\cos\theta) . \quad (4.4.10)$$

$\underline{T_{if}^{E2\pm}}$:

$$T_{if}^{E2\pm} = \frac{1}{\sqrt{2}} \left[K_1^{E2} \pm K_2^{E2} + K_3^{E2} - 2K_4^{E2} \pm K_5^{E2} \mp 2K_6^{E2} \right] \quad (2.3.30)$$

The K_i^{E2} $(i = 1,\ldots 6)$ are defined in (2.3.29). It is noted that each K_i^{E2} depends on the function $\phi_{pol}(\underline{r},\underline{t})$ given explicitly by equation (3.1.6). The Legendre polynomial $P_1(\cos\theta_{r\,t})$ appearing in $\phi_{pol}(\underline{r},\underline{t})$ is subsequently expressed as a sum over spherical harmonics by the addition theorem (3.1.13). Performing the integration over the angular variable $\hat{r}_2$ and remembering that only S-S transitions are under consideration, it is then easily seen that

$$K_3^{E2} = K_4^{E2} = K_5^{E2} = K_6^{E2} = 0 . \quad (4.4.11)$$

T_{if}^{E2} hence reduces to a further analysis of only K_1^{E2} and K_2^{E2}. K_1^{E2} is considered first.

K_1^{E2}:

$$K_1^{E2} = \int u_{1s}^{*}(1)\, v_{n\ell}^{*\pm}(2)\, \chi_{k_f}^{*}(z,3)\, \frac{1}{r_{23}}\, \phi_{1s}(3)\, \phi_{pol}(21)\, F(1)\, d\underline{r}_{123} \quad (2.3.29a)$$

Making the usual partial wave expansions, the angular integration is readily performed using only orthogonality between the spherical harmonics. The radial integral is subsequently denoted by $q^{E2}(k_i,k_f)$ where

$$q^{E2}(k_i,k_f) = \frac{-1}{3} \int_o^\infty w(r)\, u_1(k_i,r) \left(\frac{1}{r} \int_o^r R_{ns}(t)\, u_{1s\to p}(t)\, g_{1s,1}(t)dt \right) dr. \quad (4.4.12)$$

$g_{1s,1}(r)$ is defined by equation (3.3.13). K_1^{E2} is finally written as

$$K_1^{E2} = \frac{8\pi}{\sqrt{k_i}}\, q^{E2}(k_i,k_f)\, e^{i\Delta_1}\, P_1(\cos\theta) . \quad (4.4.13)$$

K_2^{E2}:

$$K_2^{E2} = \int u_{ls}^{*}(2)\, v_{n\ell}^{*\pm}(1)\, \chi_{k_f}^{*}(z,3)\, \frac{1}{r_{23}}\, \phi_{ls}(3)\, \phi_{pol}(21) F(1)\, d\underline{r}_{123} \quad (2.3.29b)$$

One sees by comparing (2.3.29a) and (2.3.29b) that the same argument which was used to evaluate K_4^{E1} from the expression for K_3^{E1} may also be applied here. Hence, interchanging $w(r)$ and $R_{ns}(r)$ in (4.4.12) and writing

$$p^{E2}(k_i,k_f) = \frac{-1}{3} \int_o^\infty R_{ns}(r)\, u_1(k_i,r) \left(\frac{1}{r} \int_o^r w(t) u_{ls\to p}(t) g_{ls,1}(t)\, dt\right) dr \quad (4.4.14)$$

with $g_{ls,1}(r)$ given as above by equation (3.3.13), K_2^{E2} reduces to

$$K_2^{E2} = \frac{8\pi}{\sqrt{k_i}}\, p^{E2}(k_i,k_f)\, e^{i\Delta_1}\, P_1(\cos\theta) \,. \quad (4.4.15)$$

Collecting together (4.4.13) and (4.4.15) for K_1^{E2} and K_2^{E2} respectively and substituting these expressions into (2.3.30), together with the trivial result (4.4.11), $T_{if}^{E2\pm}$ is summarized by writing

$$T_{if}^{E2\pm} = \pm \frac{1}{\sqrt{2}}\, \frac{8\pi}{\sqrt{k_i}} \left[p^{E2}(k_i,k_f) \pm q^{E2}(k_i,k_f) \right] e^{i\Delta_1}\, P_1(\cos\theta) \,. \quad (4.4.16)$$

The total exchange T-matrix element in the DWPO III model for helium, given by(2.3.10), may then be derived by combining expressions (3.3.24), (4.4.10) and (4.4.16) for $T_{if}^{E\pm}$, $T_{if}^{El\pm}$ and $T_{if}^{E2\pm}$ respectively. One has that

$$T_{if}^{E\pm} + T_{if}^{El\pm} + T_{if}^{E2\pm} = \pm \frac{1}{\sqrt{2}} \cdot \frac{4\pi}{\sqrt{k_i}} \sum_{\ell=0}^{\infty} \Big[B\{ \mathcal{J}^{(A)}(\ell,k_i,k_f) + \mathcal{J}^{(P)}(\ell,k_i,k_f) \}$$

$$+ \{ c_2^{\,s}(k_i) \left[d_2(k_f) - 2B d_3(k_f) \right] \pm c_1(k_i) d_1^{\,s}(k_f) \}\, \delta_{\ell o} + 2\{ [p_2^{El}(k_i,k_f) + p^{E2}(k_i,k_f)$$

$$- B p_1^{El}(k_i,k_f)] \pm [q^{El}(k_i,k_f) + q^{E2}(k_i,k_f)] \}\delta_{\ell 1} \Big]\, e^{i\Delta_\ell}\, P_\ell(\cos\theta) \,. \quad (4.4.17)$$

The sum $\mathcal{J}^{(A)}(\ell,k_i,k_f) + \mathcal{J}^{(P)}(\ell,k_i,k_f)$ is most easily obtained by making the following transformation on $g_{ls,\ell}(r)$ appearing in $\mathcal{J}^{(A)}(\ell,k_i,k_f)$:

$$g_{ls,\ell}(r) \to g_{ls,\ell}(r) + g_{ls,\ell}^{(p)}(r) \quad (4.4.18)$$

where $g^{(p)}_{ls,\ell}(r)$ is given as is appropriate by (4.3.12). This is in exact analogy with the case for hydrogen (c.f. equation (4.3.15)).

To summarize: for treating $1^1S \rightarrow n^{1,3}S$ transitions in helium with the DWPO III model, the appropriate version of equation (4.2.1) is solved for the $u_\ell(k_i,r)$ and the exchange T-matrix element, $T_{if}^{E\pm}$, appearing in the DWPO II model, modified according to equation (4.4.17) above.

CHAPTER 5

COMPUTATION AND NUMERICAL METHODS

§5.1 Solution of the Scattering Equation

The present section will be concerned with the method of solution employed to solve the radial scattering equation which embodies one of the principal features of the Distorted Wave Polarized Orbital approximation. In the DWPO I and DWPO II models, the scattering function is computed in the adiabatic-exchange approximation summarized by equation (3.2.1). When allowance is also made for exchange-polarization effects, resulting in the DWPO III model, the scattering equation is correspondingly modified and summarized by equation (4.2.1). It will be noted that the adiabatic-exchange equation is incorporated into the full polarized orbital equation. Further, the equation for scattering by a one-electron atomic system (in the present case hydrogen) and for scattering by a two-electron atomic system (in the present case helium) are, apart from detail differences, very similar. The adiabatic-exchange equation for one-electron systems has been summarized by McDowell et al. (1973, equation (11)).

In practice a general program (RADIAL) was developed to compute in the adiabatic-exchange approximation the $u_\ell(k_i,r)$ for scattering by either one-electron or two-electron systems. Such a program also contained switches to neglect the exchange (integral) terms and the direct polarization potential $V_{pol}(r)$. Later, RADIAL was subsequently modified to solve equation (4.2.1), but a switch retained to output in the adiabatic-exchange approximation. Hence, by reading in various switches, results are produced in a number of approximations:

1. the static approximation (Taylor, 1972, §9d).
2. the static-exchange approximation (introduced by Morse and Allis, 1933, and summarized by Bransden 1970).
3. the adiabatic-exchange approximation (equation (3.2.1) and McDowell et al. 1973).

4. the polarized orbital approximation (equation (4.2.1)).

Since results in each of the above approximations may be deduced from the polarized orbital equation by setting the relevant switches to zero, discussion will be restricted to solving equation (4.2.1). In particular, it should be observed that the solution of (4.2.1) for the p-wave ($u_1(k_i,r)$) involves not only a second derivative of $u_1(k_i,r)$ but also a first derivative and consequently provides the most complicated version of (4.2.1). Hence, in the following, consideration will be given to the method of solving (4.2.1) for $\ell = 1$, and therefore simultaneously including the method for any of the other cases by setting the appropriate switches accordingly. The method of solution will follow closely that employed by McDowell et al. (1974) and by Sloan (1964); it should be clear which terms are to be retained in any other approximation so that it will be unnecessary to explicitly denote the omission of such terms when considering a particular approximation. In order to simplify equation (4.2.1), some preliminary remarks and definitions are first made.

The second integral term on the right hand side is denoted by $Y_\ell(k_i,r)$:

$$Y_\ell(k_i,r) = r \int_o^\infty R_{ls}(t)\, u_\ell(k_i,t)\, \gamma_\ell(r,t)\, t\, dt. \qquad (5.1.1)$$

This defines the Hartree-function which satisfies the following second-order linear differential equation given by Hartree (1957):

$$\frac{d^2}{dr^2} Y_\ell(k_i,r) = \frac{\ell(\ell+1)}{r^2}\, Y_\ell(k_i,r) - (2\ell+1)\, R_{ls}(r)\, u_\ell(k_i,r) \qquad (5.1.2)$$

subject to the boundary conditions

$$Y_\ell(k_i,r) \underset{r\to 0}{\sim} r^{\ell+1}, \quad Y_\ell(k_i,r) \underset{r\to\infty}{\sim} r^{-\ell}.$$

The remaining integrals have a similar structure whereby it is convenient to write

$$W_\ell(a,b;n) = \int_a^b \frac{R_{ls}(r)\, u_\ell(k_i,r)\, dr}{r^{(\ell+1)+n}} \quad . \tag{5.1.3}$$

Further, it is convenient to let

$$f_\ell(k_i,r) = k_i^2 - \frac{\ell(\ell+1)}{r^2} - NV_{ls,ls}(r) - NV_{pol}(r) \tag{5.1.4}$$

$$g_\ell(r) = \frac{2\tau}{2\ell+1}\ R_{ls}(r) \tag{5.1.5}$$

$$h(r) = -\ r\ R_{ls}(r)(-\ \varepsilon_{ls} + k_i^2)\tau \tag{5.1.6}$$

$$p_\ell(r) = -\ 4\tau\ u_{ls\to p}(r)\ \frac{\ell r^{\ell-1}}{(2\ell+1)(2\ell-1)} \tag{5.1.7}$$

$$q_\ell(r) = -\ 4\tau\ u_{ls\to p}(r)\ \ \frac{(\ell+1)r^{\ell+1}}{(2\ell+1)(2\ell+3)} \tag{5.1.8}$$

$$s_1(r) = -\ \frac{2\tau}{3}\left[u_{ls\to p}(r)\ \frac{d}{dr}\left(\frac{R_{ls}(r)}{r}\right) + \frac{2R_{ls}(r)}{r}\ \ \frac{d}{dr}\left(u_{ls\to p}(r)\right)\right] \tag{5.1.9}$$

$$s_2(r) = -\ \frac{2\tau}{3}\ \ u_{ls\to p}(r)\ \frac{R_{ls}(r)}{r} \tag{5.1.10}$$

$$t(r) = -\ \frac{2\tau}{3}\left[\ r^2\ R_{ls}(r) - u_{ls\to p}(r)(-\ \varepsilon_{ls} + k_i^2)\ \right] \tag{5.1.11}$$

ε_{ls} is taken to be the experimental value for the single ionization energy. The integrals from r to infinity are manipulated using the result that

$$\int_r^\infty = \int_\varepsilon^\infty - \int_\varepsilon^r$$

where ε is usually chosen to be zero. Then, by writing D as a linear differential and integral operator involving integration only up to r, defined by

$$Du_\ell(k_i,r) = \left[\frac{d^2}{dr^2} + f_\ell(k_i,r) - \delta_{\ell 1}\left\{s_1(r) + s_2(r)\,\frac{d}{dr}\right\}\right] u_\ell(k_i,r) - g_\ell(r)\, Y_\ell(k_i,r)$$

$$+ p_\ell(r)\, W_\ell(0,r;0) + q_\ell(r)\, W_\ell(\varepsilon,r;2) + \delta_{\ell 1}\, t(r)\, W_\ell(0,r;-1), \qquad (5.1.12)$$

it is possible to rewrite equation (4.2.1) in the following simplified form:

$$Du_\ell(k_i,r) = p_\ell(r)\, W_\ell(0,\infty;0) + q_\ell(r)\, W_\ell(\varepsilon,\infty;2) + \delta_{\ell 1} t(r)\, W_\ell(0,\infty;-1)$$

$$+ \delta_{\ell 0} h(r)\, W_\ell(0,\infty;-2). \qquad (5.1.13)$$

At this stage it is worthwhile to point out that the integral $W_\ell(a,b;2)$ multiplying $q_\ell(r)$ in equations (5.1.12) and (5.1.13) diverges according to $1/r$ as $r \to 0$, since the integrand behaves as $1/r^2$. Thus it is expedient to choose $\varepsilon > 0$ which has been indicated explicitly by writing in ε rather than 0. However, the multiplying factor $q_\ell(r)$ behaves as $r^{\ell+3}$ for small r and effectively reduces the product to zero in the limit as $r \to 0$.

Essentially, equation (4.2.1) has been reduced to a system of two coupled linear differential and integro-differential equations, namely equations (5.1.2) and (5.1.13). Consideration will now be given to the method adopted for solving simultaneously these two equations. The method is a non-iterative one devised originally by Percival and subsequently applied by Marriott (1958) in a study of 1s - 2s electron impact excitation cross sections of atomic hydrogen.

One defines the following corresponding homogeneous and inhomogeneous solutions of equations (5.1.2) and (5.1.13):

homogeneous solutions: $u_\ell^{H1}, Y_\ell^{H1}; u_\ell^{H2}, Y_\ell^{H2}$

inhomogeneous solutions: $u_\ell^{I1}, Y_\ell^{I1}; u_\ell^{I2}, Y_\ell^{I2}; u_\ell^{I3}, Y_\ell^{I3}$.

The homogeneous solutions u_ℓ^H satisfy the homogeneous equation

$$D\, u_\ell^H = 0 \tag{5.1.14}$$

where the operator D is defined in (5.1.12). The inhomogeneous solutions u_ℓ^{I1}, u_ℓ^{I2} and u_ℓ^{I3} satisfy respectively the inhomogeneous equations

$$\begin{aligned} D\, u_\ell^{I1} &= h(r) \qquad \ell = 0 \\ &= p_\ell(r) \qquad \ell > 0 \\ D\, u_\ell^{I2} &= q_\ell(r) \\ D\, u_\ell^{I3} &= t(r)\,. \end{aligned} \tag{5.1.15}$$

Each of the Y_ℓ satisfies the differential equation (5.1.2). At this stage, it is remarked that if one is interested in either the static-exchange or adiabatic-exchange approximation, it is only necessary to solve for u_o^{I1} in (5.1.15) since the other equations only arise in the full polarized orbital treatment.

General solutions of (5.1.2) and (5.1.13) may now be written as

$$u_\ell(k_i,r) = c_1\, u_\ell^{H1} + c_2\, u_\ell^{H2} + c_3\, u_\ell^{I1} + c_4\, u_\ell^{I2} + c_5\, u_\ell^{I3} \tag{5.1.16a}$$

$$Y_\ell(k_i,r) = c_1\, Y_\ell^{H1} + c_2\, Y_\ell^{H2} + c_3\, Y_\ell^{I1} + c_4\, Y_\ell^{I2} + c_5\, Y_\ell^{I3} \tag{5.1.16b}$$

where the c_i ($i = 1,\ldots 5$) are mixing coefficients. It can easily be checked that these solutions satisfy (5.1.2). In order that they satisfy (5.1.13), one finds by substituting into (5.1.13) that the mixing coefficients must satisfy the relation

$$c_3 p_\ell(r) + c_4 q_\ell(r) + c_5\, t(r) = p_\ell(r) \sum_{i=1}^{5} c_i P_i + q_\ell(r) \sum_{i=1}^{5} c_i Q_i + t(r) \sum_{i=1}^{5} c_i T_i, \tag{5.1.17}$$

where, writing $\alpha_1 = H1$, $\alpha_2 = H2$, $\alpha_3 = I1$, $\alpha_4 = I2$ and $\alpha_5 = I3$, one has in an obvious notation from definition (5.1.3)

$$P_i = W_\ell^{\alpha_i}(0,\infty;-2) \qquad \ell = 0$$

$$= W_\ell^{\alpha_i}(0,\infty;0) \qquad \ell > 0$$

$$Q_i = W_\ell^{\alpha_i}(\varepsilon,\infty;2) \qquad \text{all } \ell$$

$$T_i = W_\ell^{\alpha_i}(0,\infty;-1) \qquad \text{all } \ell .$$

Since according to the definition (5.1.7), $p_o(r)$ is zero, it is convenient for notational purposes only in (5.1.17) to let $p_o(r)$ denote the expression $h(r)$ given by (5.1.6). The functions $p_\ell(r)$, $q_\ell(r)$ and $t(r)$ are linearly independent so that equating the respective coefficients, the mixing parameters are found to satisfy the system of linear equations given below:

$$\begin{aligned} c_3(1 - P_3) - c_4 P_4 - c_5 P_5 &= (c_1 P_1 + c_2 P_2) \\ - c_3 Q_3 + c_4(1-Q_4) - c_5 Q_5 &= (c_1 Q_1 + c_2 Q_2) \\ - c_3 T_3 - c_4 T_4 + c_5(1-T_5) &= (c_1 T_1 + c_2 T_2) . \end{aligned} \qquad (5.1.18)$$

In practice, since the overall normalization of the solution $u_\ell(k_i,r)$ given by (5.1.16a) is to be fixed later, one is at liberty to set $c_1 = 1$. The system (5.1.18) is consistent and subsequently solved for c_3, c_4 and c_5 in terms of c_2. It is subsequently necessary to find a further relation in order to determine c_2.

The differential equations (5.1.2) and (5.1.13) are solved numerically up to some sufficiently large r, say $r = R$, such that $Y_\ell^{(\alpha_i)}(k_i,r)$ may be written as the asymptotic expression

$$Y_\ell^{(\alpha_i)}(k_i,R) = R^{-\ell}\, I_\ell^{(\alpha_i)}(k_i,R) \qquad (5.1.19)$$

with

$$I_\ell^{(\alpha_i)}(k_i,R) = \int_o^R R_{ls}(r)\, u_\ell^{(\alpha_i)}(k_i,r)\, r^{\ell+1}\, dr. \qquad (5.1.20)$$

This should be compared with the asymptotic behaviour of $Y_\ell(k_i,r)$ given in connection with equation (5.1.2). The α_i are defined immediately below equation (5.1.17). Hence with $Y_\ell^{(\alpha_i)}(k_i,R)$ computed from (5.1.2) and $I_\ell^{(\alpha_i)}(k_i,R)$ computed from (5.1.20), one writes

$$\sum_{i=1}^{5} c_i\, Y_\ell^{(\alpha_i)}(k_i,r) = R^{-\ell} \sum_{i=1}^{5} c_i\, I_\ell^{(\alpha_i)}(k_i,R)\,. \qquad (5.1.21)$$

Substituting for c_3, c_4, c_5 and recalling that c_1 has been set to unity, equation (5.1.21) furnishes an expression from which one can determine c_2.

Finally, it remains to normalize $u_\ell(k_i,r)$ as given in (5.1.16a) so that asymptotically

$$u_\ell(k_i,r) \underset{r\to\infty}{\sim} k_i^{-\frac{1}{2}} \sin(\phi(r) + \delta_\ell). \qquad (3.1.17)$$

This is carried out following McDowell et al. (1974) who use the JWKB method formulated by Burgess (1963). The idea is to match the numerical solution of $u_\ell(k_i,r)$ with the corresponding JWKB solution at some convenient point r_N such that $\bar{R} < r_N < R$. $\bar{R}$ is defined to be the smallest value of r such that

$$|f_\ell(k_i,r) - w| \;<\; |w|\,\varepsilon \qquad (5.1.22)$$

where $f_\ell(k_i,r)$ is given by (5.1.4) and w is the long-range expression for $f_\ell(k_i,r)$ given by

$$w = k_i^2 - \frac{\ell(\ell+1)}{r^2} + \frac{2z}{r} + \frac{\alpha}{r^4}\,. \qquad (5.1.23)$$

ε is normally set to 10^{-6}. R coincides with the value of r defined earlier in the discussion immediately preceeding equation (5.1.19) on the asymptotic behaviour of $Y_\ell(k_i,r)$.

The JWKB solution to $u_\ell(k_i,r)$ is defined to be

$$u_\ell(k_i,r) = \zeta^{-\frac{1}{2}} \sin(\phi(r) + \delta_\ell) . \tag{5.1.24}$$

By substituting (5.1.24) into the asymptotic equation

$$\left[\frac{d^2}{dr^2} + w \right] u_\ell = 0 , \tag{5.1.25}$$

one finds that

$$\zeta^2 = w + \zeta^{\frac{1}{2}} \frac{d^2}{dr^2} \zeta^{-\frac{1}{2}} \tag{5.1.26}$$

with

$$\phi(r) = \int^r \zeta \, dr' . \tag{5.1.27}$$

The lower limit is left unspecified in (5.1.27); in practice it is chosen so that the above boundary condition (3.1.17) is satisfied. Equation (5.1.26) is a non-linear differential equation. However, provided

$$w \gg \zeta^{\frac{1}{2}} \frac{d^2}{dr^2} \zeta^{-\frac{1}{2}} ,$$

it may be solved iteratively and yields for the first-order solution, denoted by ζ_o,

$$\zeta_o = w^{\frac{1}{2}} . \tag{5.1.28}$$

It is noted that in the limit $r \to \infty$, $\zeta_o^{\frac{1}{2}} \to k_i^{\frac{1}{2}}$ so that (5.1.24) has the correct asymptotic behaviour according to (3.1.17). The next iteration yields ζ_1 where

$$\zeta_1 = w + w^{\frac{1}{4}} \frac{d^2}{dr^2} w^{-\frac{1}{4}} . \tag{5.1.29}$$

$\phi(r)$ is now determined by substituting ζ_1 for ζ in equation (5.1.27) and evaluating the integral by parts. Full details are given in the paper by Burgess (1963).

Having obtained expressions for $\zeta(r)$ and $\phi(r)$, one is now in a position to calculate the overall normalization constant of the $u_\ell(k_i,r)$. At the points $r = r_N$ and $r = r_{N-1}$ the respective numerical solution is equated with

$$A\,\zeta_l(r_i)\,\sin(\phi(r_i) + \delta_l), i = N, N-1 \qquad (5.1.30)$$

where A is the required normalization constant. Consequently (5.1.30) supplies two equations depending on A and δ_l. The phase shift δ_l is eliminated and a subsequent value obtained for A, say A_N. N is then increased by unity and the computation repeated to give another value for A, say A_{N+1}. This is continued until the following condition is satisfied for some value M

$$|A_M - A_{M-1}| < |A_M|\,\varepsilon. \qquad (5.1.31)$$

ε is usually taken to be 10^{-6}.

When a suitable value for A has been established, the $u_l(k_i,r)$ are normalized. The phase shift δ_l may subsequently be determined by considering (5.1.24) at the point $r = r_N$. Suppose δ_l has the value δ_N at this point. Then as in the above procedure for finding the normalization constant A, the phase shift is computed at $r = r_{N+1}$ to give the value δ_{N+1} say. This is continued until one has that

$$|\delta_D - \delta_{D-1}| < |\delta_D|\,\varepsilon \qquad (5.1.32)$$

for some point $r = r_D$. The above method of Burgess (1963) is only accurate for computing δ_l to the fourth decimal place; δ_l is chosen to lie in the range $-\pi < \delta_l \leq \pi$. Consequently ε is set to 10^{-5} in (5.1.32).

This essentially completes the method used to determine $u_l(k_i,r)$ over the range $0 < r \leq R$. For $r \geq R$, the JWKB approximation to $u_l(k_i,r)$ is constructed using equation (5.1.24) with ζ and $\phi(r)$ given as above by Burgess (1963).

§5.2 Numerical Procedure for the Scattering Equation

Under this heading the numerical techniques used to solve the differential equations arising in the DWPO models will be discussed. The method described earlier in §5.1 for solving the scattering equation avoids the need for an

iterative procedure and does not require the use of awkward outward and inward integration methods to normalize the solution. Numerically, equations (5.1.2) and (5.1.13) are solved simultaneously by the formula due originally to Numerov (1933). Numerov's method is particularly suited to equations of the type

$$y'' = b(r)y + c(r). \tag{5.2.1}$$

Here, $b(r)$ and $c(r)$ are independent of y and primes denote differentiation with respect to r. Following Fröberg (1966), the recurrence relation required to solve (5.2.1) by this method assumes the form

$$(1 - \frac{h^2}{12} b_{n+1})y_{n+1} = 2(1 - \frac{h^2}{12} b_n)y_n - (1 - \frac{h^2}{12} b_{n-1})y_{n-1} + h^2(b_n y_n + \frac{1}{12}$$

$$(c_{n+1} + 10c_n + c_{n-1})). \tag{5.2.2}$$

The notation should be clear; h is the mesh size, given by $r_{n+1} = r_n + h$. This relation was adopted by the program RADIAL to solve equation (5.1.2) and also in the initial version of the program to solve equation (5.1.13) in the adiabatic-exchange approximation. However, when considering the full polarized orbital treatment, formula (5.2.2) is no longer adequate, due essentially to the introduction of the first derivative term. Before drawing attention to the method used to cope with this further term, it is convenient to modify (5.2.2).

Hence using the formula given by Hartree (1958) that

$$y_{n+1} = 2y_n - y_{n-1} + \frac{h^2}{12} (y''_{n+1} + 10y''_n + y''_{n-1}) \tag{5.2.3}$$

and with the help of (5.2.1), the recurrence relation (5.2.2) is rewritten as

$$(y_{n+1} - \frac{h^2}{12} y''_{n+1}) = 2y_n - y_{n-1} + \frac{h^2}{12} (10y''_n + y''_{n-1}) , \tag{5.2.4a}$$

$$y''_{n+1} = b_{n+1} y_{n+1} + c_{n+1} . \tag{5.2.4b}$$

The latter relation (5.2.4b) is used to provide the second derivatives required by the former relation (5.2.4a).

Turning now to the full polarized orbital approximation of equation (5.1.13), one is essentially interested in an equation of the type

$$y'' = a(r)y' + b(r)y + c(r) . \qquad (5.2.5)$$

The first derivative may be expressed according to the result given by Sloan (1964) that

$$y'_{n+1} = \frac{1}{h}\left[\frac{9}{2}(y_{n+1} - y_n) - \frac{7}{2}(y_n - y_{n-1})\right] - \frac{h}{3}(8y''_n + y''_{n-1}) - O(h^4) . \qquad (5.2.6)$$

Then, substituting for y''_{n+1} in (5.2.4a) with the aid of (5.2.5) and employing (5.2.6) to eliminate the term in y'_{n+1}, one finds that the relation (5.2.4a) becomes

$$y_{n+1} = \left[2y_n - y_{n-1} + \frac{h^2}{12}(10y''_n + y''_{n-1}) + \frac{h^2}{12} c_{n+1} + \frac{h}{24} a_{n+1}\left\{ - 16y_n + 7y_{n-1} - \frac{h^2}{12}(64y''_n + 8y''_{n-1})\right\}\right] \Big/ \left[1 - \left(\frac{h^2}{12} b_{n+1} + \frac{9h}{24} a_{n+1}\right)\right]. \qquad (5.2.7a)$$

The next iteration (y_{n+2}) will require a knowledge of y''_{n+1}. This may be obtained from (5.2.5) and (5.2.6) in the form

$$\frac{h^2}{12} y''_{n+1} = \left(\frac{h^2}{12} b_{n+1} + \frac{9h}{24} a_{n+1}\right)y_{n+1} + \frac{h^2}{12} c_{n+1} + \frac{h}{24} a_{n+1}\left\{ - 16y_n + 7y_{n-1} - \frac{h^2}{12}(64y''_n + 8y''_{n-1})\right\}. \qquad (5.2.7b)$$

Note that when $a(r)$ is absent, the recurrence method (5.2.7) reduces to that in (5.2.4) as expected.

It will be observed that the linear operator D acting on $u_\ell(k_i,r)$ in equation (5.1.13) gives rise to integral terms of the type

$$g(r) = \int_\varepsilon^r w(t)\, y(t)\, dt. \qquad (5.2.8)$$

These terms are included implicitly in the function $c(r)$ of (5.2.5). Consequently, it would appear that a prior knowledge of y_{n+1} is required to determine such integrals as (5.2.8). This difficulty may be circumvented by the use of a Newton-Cotes formula of the open type. In practice, four such formulae were employed in turn (see equations (25.4.21 - 24) of

Abramowitz and Stegun, 1970) and the subsequent results checked against each other for stability by varying the mesh size. Generally, a reasonable degree of stability was achieved, particularly with the 4-point formula (25.4.23), the most trouble coming from the s-waves. However, rather than employ a method which depends on extrapolation, it was subsequently decided to abandon the Newton-Cotes formulae and to utilize the method outlined by Sloan (1964) which uses the well known Simpson formula for integration.

Using Simpson's rule (see, for example, Fröberg, 1966) it is easily seen that

$$g_{n+1} - g_{n-1} = \int_{r_{n-1}}^{r_{n+1}} w(t)\, y(t)\, dt$$

$$= \frac{h}{3}\left[w_{n+1}\, y_{n+1} + 4w_n\, y_n + w_{n-1}\, y_{n-1}\right],$$

so that one has immediately the result

$$g_{n+1} = \frac{h}{3} w_{n+1}\, y_{n+1} + g_{n-1} + \frac{h}{3}\left[4w_n\, y_n + w_{n-1}\, y_{n-1}\right]. \qquad (5.2.9)$$

It is then convenient to express the integrals from 0 to r explicitly, that is to let

$$c \to c + p\int_0^r \alpha y + q\int_0^r \beta y + t\int_0^r \gamma y\ , \qquad (5.2.10)$$

where p, q and t are the functions appearing in equation (5.1.17). The Greek notation should be clear from a comparison with (5.1.12) and also the definition of the W_ℓ integrals, equation (5.1.3). The integral terms are to be expressed according to (5.2.9). Hence putting

$$\pi = \int_0^r \alpha y, \qquad \rho = \int_0^r \beta y, \qquad \sigma = \int_0^r \gamma y,$$

a recurrence relation may be set up for each term as follows:

$$\pi_{n+1} = \frac{h}{3}\alpha_{n+1}y_{n+1} + \pi_{n-1} + \frac{h}{3}[4\alpha_n y_n + \alpha_{n-1}y_{n-1}],$$

$$\rho_{n+1} = \frac{h}{3}\beta_{n+1}y_{n+1} + \rho_{n-1} + \frac{h}{3}[4\beta_n y_n + \beta_{n-1}y_{n-1}], \qquad (5.2.11)$$

$$\sigma_{n+1} = \frac{h}{3}\gamma_{n+1}y_{n+1} + \sigma_{n-1} + \frac{h}{3}[4\gamma_n y_n + \gamma_{n-1}y_{n-1}].$$

Finally, (5.2.10) and (5.2.11) are incorporated into the two recurrence formulae of (5.2.7) to give

$$y_{n+1} = \Big[\Big\{2 + \frac{h^3}{9}(p_{n+1}\alpha_n + q_{n+1}\beta_n + t_{n+1}\gamma_n)\Big\}y_n - \Big\{1 - \frac{h^3}{36}(p_{n+1}\alpha_{n-1} + q_{n+1}\beta_{n-1} + t_{n+1}\gamma_{n-1})\Big\}y_{n-1} + \frac{h^2}{12}(10y''_n + y''_{n-1}) + \frac{h^2}{12}c_{n+1} + \frac{h^2}{12}(p_{n+1}\pi_{n-1} + q_{n+1}\rho_{n-1} + t_{n+1}\sigma_{n-1}) + \frac{h}{24}a_{n+1}\Big\{-16y_n + 7y_{n-1} - \frac{h^2}{12}(64y''_n + 8y''_{n-1})\Big\}\Big]\Big/\Big[1 - \Big(\frac{h^2}{12}b_{n+1} + \frac{9h}{24}a_{n+1}\Big) - \frac{h^3}{36}(p_{n+1}\alpha_{n+1} + q_{n+1}\beta_{n+1} + t_{n+1}\gamma_{n+1})\Big], \qquad (5.2.12a)$$

and

$$\frac{h^2}{12}y''_{n+1} = \Big(\frac{h^2}{12}b_{n+1} + \frac{9h}{24}a_{n+1}\Big)y_{n+1} + \frac{h^2}{12}c_{n+1} + \frac{h}{24}a_{n+1}\Big\{-16y_n + 7y_{n-1} - \frac{h^2}{12}(64y''_n + 8y''_{n-1})\Big\} + \frac{h^2}{12}(p_{n+1}\pi_{n+1} + q_{n+1}\rho_{n+1} + t_{n+1}\sigma_{n+1}). \qquad (5.2.12b)$$

The final version of RADIAL therefore adopted the recursion method (5.2.12). Results in the adiabatic-exchange approximation were then checked with those computed in the original version which employed the relation (5.2.2) and found to agree.

The method used above for treating the integrals of the type (5.2.8) generates two sequences for $g(r)$, since $g(r)$ is computed at alternate points rather than consecutive points. This is evident from the result (5.2.9) whereby $g_{n+1}, g_{n-1}, g_{n-3}, \ldots$ forms one sequence and $g_n, g_{n-2}, g_{n-4}, \ldots$ forms the other. Eventually, in order to determine values for the infinite integrals P_i, Q_i and T_i appearing in equation (5.1.17), the mean is taken of the

two limits belonging to the corresponding sequences of the finite integral $g(r)$. Concerning the integral Q_i, one sees that it has a singularity $1/r^2$ at the origin which has been avoided by commencing the integration at $\varepsilon > 0$ rather than the origin. In practice ε is set to the value 0.01; however, for the triplet s-wave in electron-hydrogen collisions, it is set to 0.04 in order to achieve a more stable result.

The Numerov methods outlined above provide a rapid means for integrating the differential equations encountered in §5.1. However, the methods are not self starting and consequently it is necessary to make power series expansions in r for the solutions about some regular point which in this case is taken to be the origin. The singularity possessed by $W_\ell(a,b;2)$ - see equation (5.1.13) - gives rise to the introduction of logarithmic terms in the series for $u_\ell(k_i,r)$ and $Y_\ell(k_i,r)$. One has that

$$u_\ell(k_i,r) = r^{\ell+1}[a_o + a_1 r + a_2 r^2 + a_3 r^3 + (a_4 + A_4 \log r)\, r^4 + (a_5 + A_5 \log r) r^5 + (a_6 + A_6 \log r) r^6 + \ldots], \qquad (5.2.13a)$$

$$Y_\ell(k_i,r) = r^{\ell+1}[b_o + b_1 r + b_2 r^2 + b_3 r^3 + b_4 r^4 + b_5 r^5 + (b_6 + B_6 \log r) r^6 + (b_7 + B_7 \log r) r^7 + \ldots], \qquad (5.2.13b)$$

Note that the logarithmic terms only arise in the full polarized orbital treatment, otherwise the A_i and B_i are set to zero. In practice 9 terms were retained in each of the series.

Homogeneous solutions are obtained by setting

$a_o = 1$ $\qquad$ $b_o = 0$

$a_o = 0$ $\qquad$ $b_o = 1.$

Inhomogeneous solutions are obtained by setting

$a_o = 0$ $\qquad$ $b_o = 0.$

Before discussing the practical details, a word is in order about the determination for non-hydrogenic systems of the parameter Z_o appearing in $u_{1s\to p}(r)$, equation (3.1.12). This parameter has been found to satisfy the equation (3.2.8) which for convenience will now be written as

$$f(x) = 0 \tag{5.2.14a}$$

where

$$f(x) = \sum_{n=0}^{25} \alpha_n x^n. \tag{5.2.14b}$$

Equation (5.2.14a) is solved iteratively by the Newton-Raphson method which may be summarized by the formula

$$x_{n+1} = x_n - \frac{f(x_n)}{f'(x_n)} . \tag{5.2.15}$$

Such a process involves a great deal of tedious algebra to rearrange (3.2.8) into the suitable polynomial expression (5.2.14b). In practice, the starting value x_o was taken to be the nuclear charge Z and the iteration terminated when

$$|x_{n+1} - x_n| < \varepsilon$$

where typically $\varepsilon = 10^{-10}$. The starting value was then altered slightly in order to test the sensitivity of the result. In each case, agreement to six decimal places was achieved after 7 or 8 iterations.

The differential equations were integrated on a grid which was divided into four intervals: $0 \leq r \leq r_{N1}$, $r_{N1} \leq r \leq r_{N2}$, $r_{N2} \leq r \leq r_{N3}$ and $r_{N3} \leq r \leq r_{N4}$. The step length was doubled at the end of each interval, and was normally set to an initial value $h = 0.004\ a_o$. Usually, the intervals were determined by setting N1 = 100, N2 = 200, N3 = 1000 for helium, N3 = 1500 for hydrogen and N4 = 2000 - 4500. Hence, this grid is consequently adopted to evaluate the basic radial integrals contributing to the cross sections. The point r_{N3} coincides with the point R defined in connection with equation (5.1.19). When starting the solutions, the series expansions were used for the first NSTART points where typically

$$NSTART = 2\ell + 14.$$

The numerical solution was also computed at the point r_{NSTART} and compared with the corresponding series solution; accuracy was required to within 5×10^{-4}%. This same condition was imposed at the step length doubling points N1 and N2 whereby the solutions were computed using both the new and old step length and compared.

The mixing coefficients were determined by solving the system of linear equations (5.1.18) by Cramer's rule. However, such a method may produce erroneous results if the system is ill-conditioned. To provide a check on the accuracy of the resultant values for the mixing coefficients, library routines employing double-precision and also tests for ill-conditioning were extensively used to solve (5.1.18). In every case, 6-figure agreement was obtained between the two methods.

As a further check on the numerical solutions and in particular the choice of N3, the mixing coefficients were calculated twice using the integrals P_i, Q_i, T_i $(i = 1,...5)$ computed up to the point N3-1 and then the point N3. The value for the mixing coefficient c_2 was required to satisfy the condition

$$|c_2^{(N3)} - c_2^{(N3-1)}| < |c_2^{(N3)}| \, \varepsilon$$

where $\varepsilon = 10^{-6}$.

Concerning the full polarized orbital treatment, a certain degree of sensitivity was noted in the choice of ε appearing in the integral $W_\ell(\varepsilon,b;2)$ and also in the choice of NSTART, particularly for the triplet s-wave in electron-hydrogen scattering. The values adopted here were found to produce the most stable results under change of the initial mesh size h.

When h was given a value such that $0.002 \leq h \leq 0.006$ atomic units, 3- to 4-figure agreement was found in both the $u_\ell(k_i,r)$ and the phase shift δ_ℓ. The latter are given in tables 1 and 2 and may be compared with published values whereby the agreement is seen to be very good, particularly in the adiabatic-exchange approximation.

§5.3 Numerical Methods for the Cross Sections

Having dealt with the scattering equation in the previous two sections (§5.1 and 5.2), the remaining parts of the chapter will be concerned with the numerical derivations of the differential and integral (total) cross sections for electron-helium collision processes in the DWPO models described in Chapters 3 and 4. In fact the programs to be described compute results not only for helium but for any two-electron atomic system .

Essentially two such programs have been written for this purpose. The first (POLORS) computes cross sections for $1^1S \rightarrow n^{1,3}S$ transitions. Initially, POLORS computed results in the DWPO I and DWPO II models (§3.3) but was later modified to also produce results in the DWPO III model (§4.4). The second (POLORP) computes cross sections for $1^1S \rightarrow n^{1,3}P$ transitions using the DWPO I and DWPO II models (§3.4) and also computes the (λ,χ) parameters (§3.5). The two programs employ basically the same numerical methods but incorporate different versions of RADIAL to compute the partial waves $u_\ell(k_i,r)$ and the phase shifts δ_ℓ. POLORS in its final form utilises the full polarized orbital version of RADIAL whereas POLORP utilises the simpler adiabatic-exchange version. In practice, RADIAL, POLORS and POLORP have been written so as to allow as much interchange as possible between routines which are common to at least two of the programs. Usually, such routines may be inserted into either program simply by adjusting their COMMON blocks. A typical example is given by the function routine which furnishes the function $f_\ell(k_i,r)$ defined by equation (5.1.4).

In both POLORS and POLORP, a grid is set up similar to that defined for RADIAL in §5.2. Simpson's rule could then be used to evaluate the integrals which did not allow a straightforward analytic evaluation. The $u_\ell(k_i,r)$ are computed in the DWPO approximation until the phase shift δ_ℓ becomes small enough to satisfy the inequality

$$\delta_\ell < \varepsilon$$

where usually $\varepsilon = 0.001$. At this point the RADIAL routines are switched off and subsequent $u_\ell(k_i,r)$ replaced by $r\sqrt{k_i}\, H_\ell(k_i r)$ where $H_\ell(k_i,r)$ is a regular Coulomb (Bessel) function with appropriate normalization. The $H_\ell(kr)$ are obtained in kr-multiplied form

$$kr\, H_\ell(kr) = G_\ell(kr) \qquad (3.1.25)$$

where $G_\ell(kr)$ is derived by solving the appropriate differential equation (3.1.26) using the Numerov formula given in (5.2.2). This was found to be a faster method for generating the $H_\ell(kr)$ rather than using the standard library routines available (McDowell et al., 1973). The $H_\ell(k_f r)$ are also generated by this method in order to evaluate the function $g_{ls,\ell}(r)$. This function, defined in equation (3.3.13) and subsequently modified in POLORS according to (4.4.18) is evaluated by integrating $g^{(1)}_{ls,\ell}(r)$ (and $g^{(p)}_{ls,\ell}(r)$) outwards and integrating $g^{(2)}_{ls,\ell}(r)$ inwards using Simpson's rule at half the basic step length. In the asymptotic region $g_{ls,\ell}(r)$ (as defined by (3.3.13) and in DWPO III subsequently modified according to (4.3.15)) may be replaced by its respective asymptotic form. However, comparison between results based on different grid parameters indicated such asymptotic contributions to be very small.

Both programs adopted the experimental atomic energy levels published by Martin (1960) unless specifically required to be otherwise (see §5.4 on the discussion of cross sections computed in the Born-Oppenheimer approximation where theoretically determined eigenenergies are also employed).

Attention will now be given to some individual aspects of POLORS and POLORP in turn.

Concerning POLORS, it was found that when $R_{ns}(r)$ was represented by a Cohen and McEachran function, it was quicker to evaluate $f_{ls,ns}(r)$ and $k_{ls,ns}(r)$, given by equations (3.3.3) and (3.3.8) respectively, by a numerical procedure similar to that adopted for $g_{ls,\ell}(r)$ rather than analytically. The integrals arising only for the p-wave in the DWPO III model were also evaluated by a similar such numerical procedure.

The computation of the partial wave elements in the sum (3.3.25) is terminated when the addition of another B_ℓ term (defined by expressions (3.3.26) or (3.3.27)) yields an overall change in the total cross section of less than 10^{-6}% at which point the differential cross section is computed. Percentage changes of 10^{-2} and 10^{-4} were also tried and found to be adequate at lower energies (k_i^2 < 40 eV) to reproduce 3-figure agreement in the differential cross sections. However, at higher energies, in the region of 200 eV, such a percentage change did not allow enough partial waves to contribute to the differential cross section. This lack of convergence in partial waves can be recognised by a characteristic oscillatory behaviour in the differential cross section at large scattering angles. By requiring a change of at least 10^{-6}%, this behaviour was eliminated for all impact energies considered in deriving differential cross section results.

Concerning POLORP, the long-range nature of the direct integrals, defined essentially by equation (3.4.7), makes a complete evaluation by Simpson's rule impractical. The difficulty arises from the oscillatory nature of the integrand in the asymptotic region, which provides a significant contribution to the integral. To overcome this problem, the integrals are divided into two parts

$$I(\ell,\lambda) = I_{N4} + I_\infty \tag{5.3.1}$$

where

$$I_{N4} = \int_0^{r_{N4}} H_\ell(k_f r) u_\lambda(k_i, r) f_{1s,np}(r)\,dr, \tag{5.3.2}$$

$$I_\infty = \beta \int_{r_{N4}}^{\infty} r^{-2} \sin\phi_f(r) \sin(\phi_i(r) + \delta_\lambda)\,dr. \tag{5.3.3}$$

The constant β is defined to be such that

$$r\, f_{1s,np}(r) \to \beta\, k_f \sqrt{k_i} \tag{5.3.4}$$

where account has been taken of the normalization of $H_\ell(k_f r)$ and $u_\lambda(k_i, r)$. The $\phi(r)$ are defined through equation (3.1.18).

The first integral I_{N4} is evaluated with the aid of Simpson's rule. The second integral I_∞ is evaluated using a method due to Belling (1968) and reviewed by Norcross (1974).

In this method, I_∞ is expressed as a difference of two integrals

$$I_\infty = \tfrac{1}{2}[g_1(r_{N4}) - g_2(r_{N4})]\beta \qquad (5.3.5)$$

where, writing $\chi_1(r) = \phi_i(r) + \delta_\lambda - \phi_f(r)$ and $\chi_2(r) = \phi_i(r) + \delta_\lambda + \phi_f(r)$, $g_i(R)$ is defined as

$$g_i(R) = \int_R^\infty r^{-2}\cos\chi_i \, dr, \quad (R = r_{N4};\ i = 1,2)$$

$$= P_i(R)\sin\chi_i(R) + Q_i(R)\cos\chi_i(R). \qquad (5.3.6)$$

Differentiating this result with respect to R and equating coefficients of $\sin\chi_i$ and $\cos\chi_i$, the functions P_i and Q_i are found to satisfy the first-order linear differential equations

$$\frac{dP_i}{dR} - \chi_i Q_i = 0 \qquad (5.3.7a)$$

$$\frac{dQ_i}{dR} + \chi_i P_i = -\frac{1}{R^2} \cdot \qquad (5.3.7b)$$

Following Belling (1968), P_i and Q_i are expressed in terms of asymptotic expansions and the coefficients obtained by a rapidly convergent iterative scheme. Consequently, $g_i(R)$ may be obtained to an accuracy of 5 to 6 figures, provided the lower limit of the integral in (5.3.3) is sufficiently large.

This long-range behaviour also effects the convergence of the partial wave sums. A method for computing these sums has already been discussed in §3.4. Typically ℓ_o occurring in equations (3.4.41) and (3.4.42) is set to 30. As a check on the numerical work, Born cross sections were computed for the $1^1S \to 2^1P$ transition at 29.6 eV and for the $1^1S \to 3^1P$ transition at 29.2 eV using firstly the partial wave treatment and secondly the analytic expressions for the T-matrix element (see Appendix C).

On comparing results, the integral cross sections were in at least 6-figure agreement and the differential cross sections were in agreement to 4 figures. Thus, this provided a useful check on the accuracy of the programming.

Finally, both programs were tested for sensitivity to changes in the initial step length h. POLORS was run for impact energies of 29.6 eV and 40.1 eV using an initial step length lying in the range $0.002 \leq h \leq 0.006$. The integrals were compared and found to be in 5-to 6-figure agreement except for $c_1(k_i)$ and $c_2^s(k_i)$ (see equations (3.3.15) and (3.3.18) respectively) which agreed to 2 usually 3 figures. Generally, the best agreement in the cross section (usually 3 figures) was achieved when h was chosen such that $0.003 \leq h \leq 0.005$. POLORP was similarly tested, it being found that cross sections generally agreed to a least 3 figures. Belling's method for evaluating I_∞ (see equation (5.3.3)) was found to give the most accurate results when $r_{N4} \sim 40\ a_o$; this was inferred from the good agreement obtained between the analytic and partial wave treatments for computing Born cross sections as referred to above.

When computing the scattering functions $u_\ell(k_i,r)$ in the DWPO approximation with a smaller value for h, for example h = 0.002, convergence difficulties arose in the RADIAL routines for higher order partial waves; typically for $\ell > 3$ at an impact energy of 29.6 eV. Coupled with this fact and with the most stable results being obtained for $0.003 \leq h \leq 0.005$, an initial step length of 0.004 was subsequently adopted for production runs.

§5.4 The Born and Born-Oppenheimer Approximations

Switches were incorporated into POLORS and POLORP so that the programs could produce results also in the Born and Born-Oppenheimer approximations. By comparing with published results, one has a valuable check on the consistency and accuracy of the respective program. Both approximations may be deduced from the DWPO I model with $u_\ell(k_i,r)$ replaced by $r\sqrt{k_i}H_\ell(k_ir)$ for all ℓ.

Born results for $1^1S \rightarrow n^1S$ transitions may then be derived from POLORS by omitting all exchange terms. In the case of $1^1S \rightarrow n^1P$ transitions, the 'Born-subtraction' procedure employed to perform the sum over partial waves is also neglected. Hence POLORP computes results in the Born approximation by means of a partial wave treatment and consequently allows the use of a slightly more sophisticated wave function for $R_{np}(r)$. Differential cross sections for the excitation of $1^1S \rightarrow 2^1S$ and $1^1S \rightarrow 2^1P$ transitions in helium have been computed using the Cohen and McEachran wave function for the excited state wave function $R_{n\ell}(r)$. The results at 29.6 and 40.1 eV are reproduced in graphical form in figures 1 and 2, and may be compared with similar Born results quoted in the paper by Thomas et al. (1974). The agreement is seen to be very good.

An extensive analysis of the Born-Oppenheimer approximation has been made for the excitation of $1^1S \rightarrow 2^3S$ and $1^1S \rightarrow 2^3P$ transitions in helium. Both programs were modified slightly so that results could be obtained either from using a 'prior' formulation or from using a 'post' formulation. Results for the total cross sections computed in the 'prior' formulation could then be compared directly with those published by Bell et al. (1966).

Adopting the notation of this thesis, Bell et al. (1966) take the T-matrix element to be

$$T_{if}^{-} = \sqrt{3}\langle \phi_f(12) e^{i\underline{k}_f \cdot \underline{r}_3} V_i \, \phi_i(23) \, e^{i\underline{k}_i \cdot \underline{r}_1} \rangle + \delta T_{if}^{(i)} \qquad (5.4.1)$$

where the interaction potential V_i is given by

$$V_i = -\frac{2}{r_1} + \frac{1}{r_{12}} + \frac{1}{r_{13}} . \qquad (5.4.2)$$

The additional increment $\delta T_{if}^{(i)}$ arises from the use of approximate target wave functions and is given by the expression

$$\delta T_{if}^{(i)} = \sqrt{3}\langle \phi_f(12) e^{i\underline{k}_f \cdot \underline{r}_3} [H_{23} - E_i] \, \phi_i(23) \, e^{i\underline{k}_i \cdot \underline{r}_1} \rangle . \qquad (5.4.3)$$

The atomic Hamiltonian H_{23} is given in an obvious notation as

$$H_{ij} = -\tfrac{1}{2}(\nabla_1^2 + \nabla_j^2) - \frac{2}{r_i} - \frac{2}{r_j} + \frac{1}{r_{ij}} . \qquad (5.4.4)$$

When the 'post' interaction potential is used, one derives, following a very similar procedure to Bell et al. (1966), the T-matrix element in the form

$$T_{if}^{-} = \sqrt{3}\langle \phi_f(12) e^{i\underline{k}_f \cdot \underline{r}_3} \; V_f \; \phi_i(23) e^{i\underline{k}_i \cdot \underline{r}_1} \rangle + \delta T_{if}^{(f)} . \qquad (5.4.5)$$

The interaction potential is given by

$$V_f = -\frac{2}{r_3} + \frac{1}{r_{13}} + \frac{1}{r_{23}} \qquad (2.3.1)$$

and the increment $\delta T_{if}^{(f)}$ is found to be

$$\delta T_{if}^{(f)} = \sqrt{3}\langle \phi_i(23) e^{i\underline{k}_i \cdot \underline{r}_1} [H_{12} - E_f] \; \phi_f(12) e^{i\underline{k}_f \cdot \underline{r}_3} \rangle . \qquad (5.4.6)$$

A partial wave reduction of the expressions for T_{if}^{-} appearing in equations (5.4.1) and (5.4.5) is straightforward and consequently will not be reproduced here. Apart from the term δT_{if}, the difference between the 'post' and 'prior' expressions occurs via the structure of certain orthogonality integrals, which arise only in consideration of the incoming s-wave in POLORS and also in consideration of the incoming p-wave in POLORP. The accuracy in the computation of the radial integrals was checked at various energies by using an initial mesh size of 0.002, 0.004 and 0.006. Between 5-and 6-figure agreement was obtained in each case. Results were also computed using variationally determined energy eigenvalues of Bell et al. (1966) rather than the experimental values tabulated by Martin (1960). Total cross sections for $1^1S \rightarrow 2^3S$ and $1^1S \rightarrow 2^3P$ excitation in helium computed from expression (5.4.1) and using either experimental or theoretical atomic energy levels are tabulated in tables 3 and 4 and compared with the results of Bell et al. (1966). The agreement between the present values obtained using theoretical energies and those of Bell et al. is seen to be most satisfactory.

The expression (5.4.5) was also employed to obtain cross sections using the post interaction potential. The excited state wave function was chosen to be either that of Morse et al. (1935) as in the above calculations or that of Cohen and McEachran (see Appendix A for details) and results compared with those of similar calculations based on the prior interaction formulation, (5.4.1). It was found that, for 2^3S excitation, the post-prior discrepancy vanished (cf. §1.2 for an earlier discussion of the post-prior discrepancy). Hence, provided the atomic wave functions are not assumed to be exact (which would result in the disappearance of the extra term δT_{if} in (5.4.1) and (5.4.5)), there is no difference between calculations using a formulation based on either the post (V_f) or prior (V_i) interaction potential terms. A comparison is given in table 5 between total cross sections for describing excitation of the 2^3S level when computed using (5.4.1) and (5.4.5) with δT_{if} set to zero. The results using the full expression are also tabulated to offer further comparison. Such a result was not found in the case of $1^1S \rightarrow 2^3P$ transitions.

Differential cross section results are given in figures 3 and 4 for excitation to the 2^3S and 2^3P levels respectively of helium at impact energies of 29.6, 40.1 and 55.5 eV using the prior expression (5.4.1) without the additional term $\delta T_{if}^{(i)}$. Here, the one parameter Hylleraas wave function (Hylleraas, 1929) was adopted to represent the ground (1^1S) state and for the excited levels, the wave functions of Veselov et al. (1961) for the 2^3S state and of Eckart (1930) for the 2^3P state. The results may then be compared with those published by Steelhammer and Lipsky (1970) and quoted by Thomas et al. (1974). Hence this provides an accurate check on the programs for excitation to these levels.

Moreover, differential cross section results for excitation of the $1^1S \rightarrow 2^3S$ transition at an impact energy of 29.6 eV were calculated from the full expression (5.4.1). In these calculations, two different wave functions were used for the excited state, namely the simple Hartree-Fock

function of Morse et al. (1935) and that of Cohen and McEachran described in Appendix A. The results are plotted in figure 5 and are observed to agree very closely.

CHAPTER 6

RESULTS

§6.1 Excitation of H(1s → 2s, 2p, 2s + 2p)

This section will essentially be concerned with a study of the results obtained from including exchange-polarization effects and also of the process of unitarization (to be outlined below) on the differential cross sections for the collision process

$$e + H(1s) \rightarrow e + H(2s,2p,2s + 2p).$$

Differential cross section data at pre-selected angles and impact energies are presented in tables 6 - 9 and compared graphically, where possible, with theory and absolute experimental measurement in figures 6 - 9.

Unitarization

For collisions which conserve the number of particles involved, such as considered here, the scattering or S-Matrix possesses the property of unitarity. However, theoretical models do not always yield a unitary S-matrix. The process of unitarization, introduced by Seaton (1961) and subsequently applied by Lawson et al. (1961) and Somerville (1963) to electron-hydrogen collisions, is designed to produce this property in the S-matrix. McDowell and coworkers have also developed the method and applied it to their results obtained in the DWPO I and DWPO II models where it produced a substantial improvement.

Briefly, one writes the T-matrix $\underline{T}$ in terms of the S-matrix $\underline{S}$ according to

$$\underline{T} = \underline{1} - \underline{S} \qquad (6.1.1)$$

with $\underline{1}$ the unit matrix. $\underline{S}$ can be defined in terms of a real symmetric matrix $\underline{R}$ (often referred to as the reactance matrix) such that

$$\underline{S} = \frac{\underline{1} + i\underline{R}}{\underline{1} - i\underline{R}} \tag{6.1.2}$$

which preserves the unitarity of $\underline{S}$. From (6.1.1), $\underline{T}$ is then written in terms of $\underline{R}$ as

$$\underline{T} = \frac{-2i\underline{R}}{\underline{1} - i\underline{R}} . \tag{6.1.3}$$

If, following Lawson et al. (1961), one now assumes that $|\underline{R}| \ll 1$, which is valid provided the interactions are weak, a first approximation to $\underline{T}$ is given by

$$\underline{T}^{(0)} = -2i\underline{R} . \tag{6.1.4}$$

Substituting (6.1.4) into (6.1.3), another approximation is obtained for $\underline{T}$:

$$\underline{T}^{(1)} = \frac{2\,\underline{T}^{(0)}}{2 + \underline{T}^{(0)}} . \tag{6.1.5}$$

By inserting (6.1.5) for $\underline{T}$ in (6.1.1) and using (6.1.4) one sees that $\underline{S}$ is unitary according to definition (6.1.2). The idea then is to substitute for $T^{(0)}$ into (6.1.5) and compute $T^{(1)}$ and to subsequently compute cross sections using $T^{(1)}$ rather than $T^{(0)}$. Results obtained from $T^{(1)}$ will be specifically referred to as unitarized, otherwise they may be assumed to be non-unitarized.

In computing $T^{(0)}$, the elements T_{1j} and T_{i1} (that is the elements of the first row and, from symmetry consideration, the elements of the first column) are obtained with appropriate phase in the DWPO approximation and the remaining elements in the Born approximation. The relevant Born integrals have been discussed by Kingston et al. (1976) who employ the unitarized Born approximation of Lawson et al. (1961) to compute the higher order partial waves in their treatment of electron impact excitation of the $n = 2$ states of atomic hydrogen.

H(1s → 2s) Transitions

Differential cross sections computed in the DWPO III model at impact energies of 50 and 100 eV are compared in figure 6 with the corresponding results in the DWPO I and DWPO II models published by McDowell et al. (1975b). The effect of allowing explicitly for target distortion enhances the forward peak in both cases compared to the DWPO I results. For scattering angles less than 50°, the DWPO II and DWPO III models yield similar results whereas for angles above 50°, the inclusion of exchange-polarization terms produces an increase in the cross section.

Table 6 presents unitarized and non-unitarized results for both these energies. On comparing columns (i) and (ii) in each case, the magnitude of the results is seen to vary considerably, by as much as a factor of 3. It is noted in each case that unitarization reduces the total (integral) cross section.

H(1s → 2p) Transitions

Differential cross section results for excitation of the 2p state are presented in table 7 and figure 7 at incident energies of 50 and 100 eV. On comparing with the DWPO I and DWPO II results of McDowell et al. (1975b), the explicit inclusion of target distortion in the T-matrix element is seen to slightly reduce the cross section in the forward direction. The predictions of DWPO II and DWPO III again coincide for smaller scattering angles (c.f. 1s → 2s transitions above) as expected since exchange-effects are relatively less important over this angular range. Contributions from exchange however begin to dominate for larger angles; one sees that the inclusion of exchange-polarization effects increases the cross section for angles above 100° as compared to the DWPO I and DWPO II results which do not allow for such effects. This was also the case for 1s → 2s transitions as shown in figure 6.

From table 7, a comparison may be made between the unitarized and non-unitarized results for each energy. Again, one sees that the magnitudes

differ by as much as a factor of 3 and that unitarization lowers the integral cross sections.

H(1s → (2s + 2p)) Transitions

Total differential cross sections for excitation to the n = 2 level have been computed in the DWPO III model at a number of incident energies. The results, unitarized and non-unitarized, are given in tables 8 and 9. In figure 8, a comparison of the non-unitarized results is made with the absolute experimental data of Williams (1976) for impact energies of 1.02, 1.21 and 1.44 Rydbergs. Similarly, results at higher impact energies of 54.4 eV (= 4 Ryd.), and 100 eV are illustrated in figure 9 with the absolute measurements of Williams and Willis (1975) and with the results of other theoretical methods.

Concerning the lower energies, essentially lying just above the ionization threshold, the agreement with experiment is considered highly satisfactory, particularly at 1.21 Ryd. Also in figure 8, the individual 2s and 2p contributions have been plotted. It is evident that in this model the dominant contribution to the n = 2 total differential cross section arises at all angles from excitation to the 2p state, especially in the forward direction. Moreover, Callaway et al. (1976) have considered excitation of the n = 2 level at these energies using a hybrid method and obtain even better agreement with experiment. Callaway et al. essentially combine the distorted wave polarized orbital approximation (without exchange-polarization) with a close-coupling pseudostate approach. The pseudostate expansion is employed for the lower order partial waves ($0 \leq L \leq 3$) and the DWPO approximation for the higher order partial waves. The method is further described in the earlier paper by Callaway et al. (1975). Their results have not been displayed in figure 8 but referring to the later paper, one sees that the individual contribution from the 2s and 2p states are basically similar to those obtained in the DWPO III model for angles less

than 90°. However, for angles above 90°, the hybrid method predicts a larger 2s and smaller 2p contribution than the DWPO III model. Overall the method is seen to yield a total result lying closer to the experimental points than that of the DWPO III model.

A comparison between the unitarized and non-unitarized data in table 8 shows that generally the process of unitarization produces results which detract from the already good agreement obtained with the DWPO III model and consequently are not illustrated in figure 8. However, unitarization improved the low energy results derived in the DWPO I and DWPO II models for excitation of alkali atoms (Kennedy, 1976).

Turning to the results at higher impact energies, these are compared in figure 9 with experiment and also with the theoretical treatments of Callaway et al. (1976) (figure 9(a) only) and of Kingston et al. (1976). The latter method is similar to the former but rather than employ distorted waves for the higher order partial waves, use is made of the unitarized Born approximation (c.f. the earlier discussion of this section on unitarization). At an incident energy of 54.4 eV, equivalently 4 Rydbergs, the theories agree reasonably well with each other and with experiment for scattering angles less than 30° except in the forward direction where the hybrid method of Callaway et al. produces a more enhanced peak. For angles above 30°, the DWPO III model tends to underestimate the experimental points though, in common with the approach of Callaway et al., yields a pronounced increase in the backward direction. Unitarization did not improve the situation. Generally, the models of Kingston et al. (1976) and of Callaway et al. (1976) give good agreement over the angular region for which there are experimental measurements at this energy.

Comparison with experiment at 100 eV between the DWPO III model and the calculation of Kingston et al. (1976) again shows good agreement for angles less than 30°. However, for larger angles the DWPO III results are too small whereas those of Kingston et al. remain satisfactory up to about 80°. The DWPO III cross section exhibits as at 54.4 eV, an increase in the backward direction.

Moreover, the unitarization procedure yields DWPO III results in better agreement with experiment than the corresponding non-unitarized results and consequently these have been plotted in figure 9(b). This improvement is hardly surprising since at higher energies the interaction potential becomes relatively weaker due to the shorter passage time of the scattered electron and hence the approximations made in connection with the process of unitarization (see in particular equation (6.1.4)) are more likely to be justified. Thus, the process of unitarization, while not producing improvement in DWPO III results at lower energies, does improve the results at higher energies.

Summary

As should be expected, the effects of exchange-polarization are found to be important at low electron impact energies in determining accurate differential cross sections. At higher energies, the DWPO III model provides accurate results for small scattering angles, due to the improved treatment of polarization, but tends to underestimate the differential cross sections for larger angles. The model does produce an increase in the backward cross section though not sufficient to give the accuracy of more sophisticated methods.

The process of unitarization outlined in this section begins to improve DWPO III results at impact energies above 100 eV, but has a contrary effect at the lower energies. This is not unexpected since at low energies where the non-unitarized results are already accurate, the assumption of weak coupling is invalid.

§6.2 Excitation of $He(1^1S \rightarrow n^1S)$

Total and differential cross sections have been computed for the inelastic processes

$$e + He(1^1S) \rightarrow e + He(n^1S)$$

in the DWPO I and DWPO II models for $n = 2,3,4,5$ and in the DWPO III model for $n = 2$. Total cross sections obtained in the DWPO I and DWPO II models are presented in tabular form in table 10 and compared graphically with absolute experiment and other theoretical models over the energy range from threshold to about 400 eV in figure 10. Differential cross sections at pre-selected impact energies are given in tables 11 - 15 and similarly compared with other results in figures 11 - 15.

Total Cross Sections

Concerning the DWPO approximation to the total cross sections illustrated in figure 10, the excited state is taken to be described in each case by the wave function due to Cohen and McEachran - see Appendix A for details.

2^1S Results for excitation of this state have been published by a number of experimental and theoretical groups and are compared in figure 10(a). At the higher energies there is generally good agreement between the different theoretical results and the absolute experimental measurements of Vriens et al. (1968); not shown are the measurements of Miller (1956) which agree closely with those of Vriens et al. Only the DWPO I results have been plotted in this figure; the DWPO II results have been omitted. For energies above 200 eV there is close agreement with the Coulomb-projected Born calculations of Hidalgo and Geltman (1972) which in fact neglect exchange and polarization effects. It follows therefore that this approximation is only expected to be valid at higher energies.

Moving to lower energies the DWPO I and particularly the DWPO II results (see table 10) remain lower than those of other models, with the exception of the results calculated in the eikonal distorted wave method (Joachain and Vanderpoorten, 1974a) which are consistent with the DWPO I results down to about 70 eV. It is noted that, apart from the lower energy data of Rice et al. (1972), the DWPO results are consistent with experimental measurements down to near threshold, and are the only results to agree with the measurements

of Brongersma et al. (1972) at very low energies. The other experimental points are due to Hall et al. (1973) and to Trajmar (1973) whose point at 40.1 eV coincides with that of Hall et al. at 39.2 eV. Theoretically, the second-order optical potential results of Winters (1974), computed in a partial wave treatment of the method, overestimate the experimental values whereas the many-body calculation of Thomas et al. (1974) and the multichannel eikonal treatment of Flannery and McCann (1975) are consistent with the experimental points of Rice et al. (1972) at 55.5 eV and Hall et al. (1973) at 48.2 and 39.2 e V: however, in the former case the method not unexpectedly fails for energies below 40 eV.

3^1S Total cross sections, computed in the DWPO I and DWPO II models, for excitation of this state, are displayed in figure 10(b) and compared with absolute experimental measurement and with the results from a ten-channel eikonal treatment (Flannery and McCann, 1975). A theoretical calculation has also been carried out by Bransden and Issa (1975) at energies above 200 eV. They use a nine-state impact parameter version of the second-order optical potential method and obtain results in very close agreement with the DWPO I model; consequently their results are omitted for clarity.

In the DWPO approximation, the overall profile including the shoulder between 60 and 100 eV, a feature which, while discernible in the previous case (c.f. figure 10(a)), is more prominent in the present work. It is observed that the effect of including target distortion explicitly in the T-matrix is to reduce the cross section by at most 10%. The best agreement with experiment is obtained with the measurements of Moustafa Moussa et al. (1969), those of St. John et al. (1964) tending to lie somewhat higher. At lower energies, reasonable agreement is obtained with the recent experimental point of Chutjian and Thomas (1975) at 39.7 eV but not at the lower energy of 29.2 eV.

The multichannel eikonal curve agrees closely with the DWPO II curve down to about 60 eV and then decreases, and exhibits quite a different behaviour relative to the DWPO approximation compared to that for $1^1S \rightarrow 2^1S$ transitions.

4^1S Calculations in the DWPO I and DWPO II models are illustrated, together with experimental results, in figure 10(c); a brief discussion of the experimental techniques, with particular emphasis on normalization procedures, is given by Scott and McDowell (1975b). Again it is observed that the main feature of the DWPO II model is to reduce the overall curve given by the DWPO I model, while at the same time preserving the shape, particularly the shoulder lying here between 60 an 150 eV.

Experimental evidence for such a shoulder is offered by the measurements of Moustafa Moussa et al. (1969) which, together with the measurement of Showalter and Kay (1975) at 200 eV, lie in closest accord with the theory. For energies above 50 eV, the results of van Raan et al. (1971) and of Pochat et al. (1973) lie some 20% higher than the DWPO results; at energies below this value both groups predict a maximum near 40 eV. However, the DWPO approximation predicts a peak value closer to 30 eV and of greater magnitude. The experimental data of St. John et al. (1964) indicates a peak value of comparable magnitude to the DWPO result but at 40 eV. Generally though, their measurements are in poor agreement and appear considerably too large compared to later measurements.

5^1S Total cross section results for the transition $1^1S \rightarrow 5^1S$ are given in figure 10(d) and compared with the absolute data provided by the groups referred to in the above discussion of 4^1S results. Once again, the behaviour of the DWPO I and DWPO II curves resembles that for the previous cases, the shoulder becoming more evident between 50 and 150 eV and the peak value attained once more at 30 eV.

The existence of a shoulder is again supported by the measurements of Moustafa Moussa et al. (1969); however, their results generally tend to lie below the DWPO curves. Reasonable agreement is obtained in the DWPO approximation with the data of St. John et al. (1964), van Raan et al. (1971) and Pochat et al. (1973) for energies above 150 eV. The recent measurement at 200 eV due to Showalter and Kay (1975) appears low. Below 150 eV, the results of van Raan et al. (1971) and of Pochat et al. (1973) agree well,

showing a similar variation with energy to that found in the 4^1S results. Their measurements lie above the DWPO results down to 40 eV at which point the former group seem to predict a maximum whereas the latter group seem to indicate the peak closer to 35 eV.

Coupled with the measurements of St. John et al. (1964), which seem high for energies below 150 eV, there remains some discrepancy between experimental results themselves, and with theory.

Summary

A comparison of total cross section results obtained in the DWPO I and DWPO II models for each state shows that the general shape of the curves remains unchanged. The effect of including target distortion explicitly in the T-matrix, or equivalently coupling the S and P states, does however make itself apparent over the energy range lying between the peak value and about 400 eV whereby the total cross section is lowered slight by some 5 - 10%. At 400 eV the curves essentially coincide for each case. The DWPO approximation introduces a shoulder into the cross section between roughly 50 and 150 eV which becomes progressively more evident the higher the state, being most evident for excitation of the 5^1S state.

Agreement with absolute experiment and, where available, with other theory varies, being least comparable at lower impact energies. Generally however, the overall agreement of the DWPO results with experiment is good.

Differential Cross Sections

Calculations in the DWPO I and DWPO II models utilized the excited state wave function of Cohen and McEachran (discussed in Appendix A); the results are given in tabular form (tables 11 and 13 - 15) and graphically in figures 11 and 13 - 15 where they are compared with absolute experiment and other theoretical data. Further calculations for excitation to the 2^1S state were performed in the DWPO I, II and III models using the simpler excited state

wave function of Byron and Joachain (see Appendix A). The results are tabulated in tables 11 and 12 and compared with absolute experimental measurements in figure 12.

2^1S Discussion for describing excitation of this state will first centre on the DWPO I and DWPO II results which are presented in table 11 at five incident energies. It is noted that use of either the wave function due to Cohen and McEachran or that due to Byron and Joachain makes no appreciable difference to the DWPO calculations, results differing by at most 10%. DWPO I results computed using the former wave function are plotted in figure 11.

At 29.6 eV, only the experimental points of Trajmar (1973) have been included in figure 11(a); those of Hall et al. (1973), obtained independently at 29.2 eV and by a different technique, lie in close agreement and are consequently omitted for clarity. The DWPO result agrees well in the forward direction with the many-body treatment of Thomas et al. (1974) and with the Glauber approximation (Yates and Tenney, 1972). Experimentally, however, the forward peak is considerably larger and is more accurately reproduced by the distorted wave calculation of Shelton et al. (1973). Each of the theoretical models reveals a minimum in the angular vicinity of that observed experimentally at 50° but differ over the magnitude, the many-body approach predicting a very deep structure. For large scattering angles, the many-body approach produces good agreement with experiment and coincides with the DWPO results in the backward direction. The Glauber model not unexpectedly fails at such angles due to a lack of exchange considerations. On the other hand, the distorted wave calculation of Shelton et al. (1973) continues to remain above the experimental results.

In figure 11(b), the situation illustrated for 40.1 eV is similar to that at 29.6 eV; again only the experimental measurements of Trajmar (1973) are plotted, those of Hall et al. (1973) at 39.7 eV being in very close agreement. The DWPO curve and that of Thomas et al. (1974) agree well over the whole angular range but fall below experiment in the forward and backward directions. The Glauber approximation, while producing similar agreement at small angles,

fails completely for angles greater than 70°. Each of these theories predicts a minimum of comparable depth; the calculation of Shelton et al. (1973) yields results lying above both experiment and other theory, especially in the magnitude of the dip. None, however, is able to reproduce the smaller magnitude observed by experiment.

Also shown are the ten-channel eikonal results of Flannery and McCann (1975). For angles less than 30° their results agree accurately with the experimentally observed forward peak. This is to be expected since their method takes into account the main effects contributing to small-angle scattering such as intermediate and long-range couplings between each channel, static distortion in each channel and polarization of each target state represented in the multichannel eikonal expansion. Exchange, however, is only included implicitly through the very nature of the expansion and is therefore probably one of the main reasons why the theory fails completely at large angles. Their results are not expected to be accurate for angles much above 30°.

For an energy of 81.63 eV, the DWPO I results and other theoretical results are compared in figure 11(c) with the experimental data published by Rice et al. (1972) and by Opal and Beaty (1972) (at 82 eV). In the forward direction the majority of theoretical treatments, including the DWPO I model, predict a similar peak which is smaller than that obtained in the ten-channel eikonal method (at 80 eV) of Flannery and McCann (1975) and in the second-order diagonalization method of Baye and Heenen (1974) (not shown). This latter method is essentially a high energy approximation. However, the results of Baye and Heenan compare well with experiment out to about 60° while those of Flannery and McCann rapidly fall away at larger angles. It is observed that the DWPO results, the calculations of Thomas et al. (1974), the second-order optical potential distorted wave results of Bransden and Winters (1975) and the Coulomb-projected Born results of Hidalgo and Geltman (1972) begin to diverge from each other for angles above 30°, the best overall agreement with experiment being maintained by the work of Thomas et al. followed by that of

Bransden and Winters; both these methods employ distorted waves calculated in the field of the final state. However, the measurements of Opal and Beaty (1972) afford evidence for a slight minimum and shoulder for angles greater than 30°. Similar structure is predicted by the DWPO approximation, though with a depth up to an order of magnitude smaller than that observed by Opal and Beaty, and to a much lesser extent by the many-body approach but with a comparable magnitude to the experimental points. The Coulomb-projected Born calculation, which omits exchange and distortion altogether, fails to predict any structure and falls off rapidly with increasing scattering angle.

Results at 100 eV are illustrated in figure 11(d). It is observed that the DWPO approximation exhibits a similar cross section to that at 81.63 eV, the dip structure being in the present case relatively less deep. The dip and shoulder structure is observed to have a higher magnitude in the experiment of Suzuki and Takayanagi (1973) and is also predicted by the Second Born calculations of Buckley and Walters (1975) which however are not shown. The second-order diagonalization method of Baye and Heenen (1974) again produces a more enhanced peak in the forward direction and remains in good agreement with experiment for smaller angles. The results of Bransden and Winters (1975) and of Hidalgo and Geltman (1972) are in close accord with the DWPO I results out to 40°, whereafter the second-order optical potential model seems to favour the experimental points of Crooks (1972) which do not predict the dip and shoulder structure mentioned earlier. For larger scattering angles, the Coulomb-projected Born results fall away rapidly as in figure 11(c) at 81.63 eV whereas the DWPO results lie about 50 - 70% below the measurements of Suzuki and Takayanagi (1973). It is noted again that the model of Bransden and Winters (1975), which allows for polarization effects in the initial channel and uses a distorted wave formalism to account for final channel scattering, produces results which lie above those of the other theoretical treatments for angles greater than 40°. These other methods do not incorporate final channel distortion effects.

The method of Bransden and Winters (1975), however, provides the best overall agreement with experiment, indicating that such effects probably become important for large-angle scattering.

Theoretical and experimental cross sections at 200 eV are compared in figure 11(e). The experimental measurements shown are due to: Opal and Beaty (1972), Suzuki and Takayanagi (1973) and Dillon and Lassettre (1975) and form a consistent description of the cross section for the angular range up to 150°. For angles between 5° and 30°, the different theoretical treatments are in close accord. Below 5°, the Coulomb-projected Born results (Hidalgo and Geltman, 1972) coincide with those of the DWPO I model whereas the Eikonal Born Series calculation of Byron and Joachain (1975), together with the second-order diagonalization procedure (Baye and Heenen, 1974) and the Second Born calculations of Buckley and Walters (1975)(not shown), predict a sharper peak. Comparable magnitude in the forward direction is, however, obtained by the DWPO II model (see table 11(e)). Above 30°, each of the theories, except the Eikonal Born Series, falls below experiment. The latter, which allows for long-range and exchange effects, remains in essentially complete agreement with the experimental data for all angles up to 150°.

Discussion will now centre on differential cross sections obtained in the DWPO III model employing the excited state wave function of Byron and Joachain (see Appendix A). The results are tabulated in table 12 and compared with the corresponding results from the DWPO I and DWPO II models (see table 11), together with the experimental measurements referred to above, in figure 12. Rather than make individual comments on each energy, the results will be taken together. It should be noted that the measurements of Hall et al. (1973) at 29.2 eV and 39.2 eV have been included in figure 12.

As in the case of hydrogen, when deriving the distorted waves $u_{\ell}(k_i,r)$ from equation (4.2.1), it is found that at most only those for $\ell = 0 - 4$ differ appreciably from the corresponding solutions obtained in the adiabatic-exchange approximation, equation (3.2.1). This is to be expected since exchange-polarization effects become less important for larger ℓ

(or in other words for larger impact parameters). For subsequent ℓ the appropriate adiabatic-exchange solutions are employed. The same remarks of course will apply to excitation of the 2^3S state, to be discussed in §6.3.

Turning to figure 12, it is noted that the forward peak produced by including distortion effects explicitly in the T-matrix (DWPO II and DWPO III) increases with increasing energy compared with the DWPO I result. For energies above 40.1 eV, the DWPO II and DWPO III results virtually coincide for angles less than 40^o, in accord with the expectation that for this process exchange becomes relatively less important at small angles the higher the impact energy. At 200 eV, the forward cross section compares well with that produced by the Eikonal Born Series illustrated in figure 11(e).

However, inclusion of exchange-polarization effects appears to generally make little improvement in the cross sections. Indeed the backward cross section is lowered in each case, contrary to the result noted in excitation of atomic hydrogen (§6.1). This failure of the DWPO III model indicates that other physical effects, even at the lower energies, are more important than exchange-polarization. Comparison with those calculations in figure 11 which allow for distortion effects in the final channel seems to suggest that final channel distortion is more important than exchange-polarization when computing large-angle differential cross sections for excitation of $He(2^1S)$.

3^1S Results computed in the DWPO I and DWPO II models for this state are tabulated in table 13 and DWPO I results displayed in figure 13 at four incident energies. The calculations used the excited state wave function of Cohen and McEachran (see Appendix A) in every case. The results of the two models yield curves of generally the same shape and exhibit a similar trend to that for $1^1S \rightarrow 2^1S$ transitions, namely that DWPO II produces an increasing forward enhancement over the DWPO I result with increasing energy whereas for large-angle scattering produces smaller results than DWPO I.

Experimental and theoretical results are not so numerous in this case as they are for excitation of the 2^1S state. The only absolute experimental

measurements known are those of Chutjian and Thomas (1975) at 29.2 and 39.7 eV; these authors also publish the results of a many-body calculation at these energies.

At 29.2 eV, one sees from figure 13(a) that the DWPO I and many-body theory results are in excellent agreement in the forward and backward directions and predict a similar angular position of the minimum, though somewhat shifted from that observed experimentally. Both theories, however, disagree considerably over the depth, DWPO producing a shallow dip and many-body theory a much deeper result. Neither theory reproduces the structure observed between 50° and 80°. Agreement with experiment at small angles is poor but improves at large angles. At such a close energy to threshold it may well be necessary to consider the effects of neighbouring states such as 3^1P and 3^1D.

The situation improves at 39.7 eV, illustrated in figure 13(b), particularly between the theoretical curves which now agree quite well over the full angular range. The overall agreement with experiment is also improved, the angular position of the minimum being correctly predicted at 60°, though not the full depth. There also appears to be some structure observed at 110° which neither theory reproduces. The forward cross section is again underestimated by both models.

Moving to higher energies, figure 13(c) compares at 100 eV the theoretical results of the DWPO I model with those of a ten-channel eikonal calculation (Flannery and McCann, 1975). No experimental measurements were available for this impact energy. Essentially, the behaviour of the two theories at this energy resembles that at 81.63 and 100 eV for excitation of the 2^1S state. The DWPO approximation produces the characteristic dip and shoulder structure whereas the multichannel calculation yields a larger peak value in the forward direction together with some structure at 7°, interpreted as arising from intermediate couplings with the $n^1P_{0,\pm1}$ states. Both theories differ widely in the backward direction, DWPO results being an order of magnitude higher than the multichannel eikonal results.

For 200 eV, a similar comparison to that at 100 eV is offered in figure 13(d). Good agreement is shown for small scattering angles (less than 30^{o}) apart from the characteristic forward enhancement produced by the ten-channel eikonal treatment. At larger angles, the two methods again diverge, DWPO I results being greater by a factor of 6. Presumably this is due to the distorted wave polarized orbital approximation taking account of exchange whereas the method of Flannery and McCann (1975) takes no explicit account of such effects.

$4^{1}S$ Tabular results, computed at four incident energies in the DWPO I and DWPO II models, are presented over the whole angular range in table 14. The small-angle (0^{o} - 20^{o}) results are plotted in figure 14 where they are compared with the absolute experimental measurements of Pochat (1973) and at higher energies with those of the First Born approximation, deduced from the accurate generalized oscillator strengths published by Bell et al. (1969).

At energies of 50 and 60 eV, the DWPO II results show a slight improvement over the DWPO I results, particularly in the latter case. Concerning an impact energy of 100 eV, the forward enhancement produced by the DWPO II model continues to increase relative to the DWPO I result and is in good agreement with Pochat's measurements for angles greater than 10^{o}. This enhancement is increased further at 200 eV where essentially the DWPO II model provides results in complete agreement with the experimental data at each of these angles. On the other hand, the DWPO I model and First Born approximation both fail in the forward direction at these energies. It is also noted from figure 14(b), that the DWPO I results approach those of the First Born approximation; this is to be expected since the latter approximation is the high energy limit of the DWPO I model (McDowell et al. 1975a).

$5^{1}S$ DWPO I and DWPO II results are tabulated for angles up to 180^{o} in table 15 and illustrated over the angular range 0^{o} - 20^{o} in figure 15. The experimental points are again the absolute data of Pochat (1973), and at the two higher impact energies a comparison is also provided with the First Born approximation, deduced, as in the $4^{1}S$ case, from the accurate generalized oscillator strengths tabulated by Bell et al. (1969).

The situation presented in figure 15 resembles closely that described previously in connection with the 4^1S state. For the lower energies of 50 and 60 eV, the DWPO II model provides a small improvement on the DWPO I result, producing reasonable agreement with experiment for angles above 15°. Turning to an impact energy of 100 eV, the DWPO II model gives good agreement with experiment over the latter half of the angular range, continuing to produce an increasing forward peak relative to the DWPO I model. By 200 eV, the agreement between experiment and the enhancement of the cross section due to the DWPO II model is basically complete. Again it is observed that the First Born approximation, plotted at 100 and 200 eV, fails to give a satisfactory account of small-angle scattering. As in figure 14(b), the DWPO I results are seen to approach the First Born results at higher energies.

Summary

From the differential cross section results obtained for excitation of the 2^1S and 3^1S states, one sees that at lower energies, the DWPO approximation reproduces the shape of the experimentally determined cross sections reasonably well, especially at energies close to 40 eV. The position of the minimum is correctly reproduced but, in common with other theoretical methods, the depth is not always accurately predicted. The magnitude of the forward cross section is relatively small compared with experiment at these energies.

At higher energies, the DWPO approximation produces results in better agreement with experiment for small angles (less than 30°), particularly when explicit account is taken of target distortion. For angles above 30°, the method predicts a shape comparable to that observed in experiment but with a smaller magnitude; this is particularly evident at 81.63 and 100 eV. Results in the DWPO II model for these angles are lower than those in the DWPO I model. Surprisingly, results in the DWPO III model are still lower, whereas for excitation of hydrogen, the inclusion of exchange-polarization effects increased the backward cross section. Generally DWPO III results for helium are not significantly different from those obtained in the

DWPO II model, particularly at lower energies. However, it should be noted that models which allow for distortion effects in the final channel yield results of a larger magnitude, similar to that measured experimentally.

Comparison of DWPO I and DWPO II results for excitation of the 4^1S and 5^1S states at angles up to 20^o shows that by allowing explicitly for target distortion, progressively better agreement is obtained with experiment as the impact energy increases. By 200 eV, the DWPO II model yields results which lie basically in complete agreement with experiment; models which neglect target distortion, such as the First Born approximation, fail to provide a satisfactory account of small-angle scattering at this energy. Consequently explicit allowance for coupling between S and P states (as in the DWPO II model) is seen to be essential for a good description of small-angle scattering.

§6.3 Excitation of $He(1^1S \rightarrow 2^3S)$

Results for the total and differential cross sections have been computed in the DWPO I and DWPO III models for the excitation process

$$e + He(1^1S) \rightarrow e + He(2^3S) \ .$$

Provided spin-dependent interactions are omitted (which is usually the case) this process can only occur via charge-exchange and consequently furnishes an exacting test of the theoretical treatment of exchange.

The total cross section, obtained in the DWPO I model, is tabulated in table 16 and is illustrated in figure 16 together with other theoretical predictions and absolute experimental data over the energy range from threshold to 200 eV. Differential cross sections at five impact energies are presented in the DWPO I model in table 17 and figure 17 and also in the DWPO III model in table 18 and figure 18.

Total Cross Section

This has been computed using the excited state wave function of Cohen and McEachran (see Appendix A for details) in the DWPO I model and is compared in figure 16 with the absolute experimental measurements supplied by four independent groups. Not shown in the figure are the measurements of Hall et al. (1973), obtained for energies less than 50 eV, and which agree closely with those of Trajmar (1973) at 29.6 and 40.1 eV and with that of Crooks et al. (1972) at 50 eV. Together with the low energy data of Brongersma et al. (1972) and the values at higher energies of Vriens et al.(1968), the experimental data are noted to yield a consistent result over the whole energy range. An interesting feature is the structure observed by Crooks et al. (1972) at 50 eV, due to a broad p-wave resonance which effects their differential cross section results by more than three orders of magnitude.

Figure 16 also shows the theoretical results obtained in the many-body approach (Thomas et al. 1974) and in the partial wave treatment of the second-order optical potential model (Winters, 1974). It is noted that the slopes of the theoretical curves are similar and that for energies above 80 eV, the DWPO I and second-order optical potential results agree very well. However, below this energy their remains some discrepancy over the magnitude of the total cross section, and in the case of the DWPO results, also over the shape. A close-coupling calculation by Smith et al. (1973) (not illustrated) gives results a factor of 2.5 smaller than those of Winters (1974) — see however the comment by Seaton (1974). Generally, the theoretical results tend to lie above the experimental points, particularly at higher energies. The sudden dip in the DWPO I curve at 30 eV appears,on comparison of integral results in table 17, to be connected with the choice of excited state wave function.

Summary

For energies less than 50 eV, the DWPO approximation predicts a total cross section which is considerably inconsistent with other results, both

experimental and theoretical. At energies above 80 eV, the DWPO I and second-order optical potential results agree very closely but increasingly overestimate the size of the experimental measurements with increasing impact energy.

Differential Cross Sections

These have been computed at five impact energies ranging from 29.6 to 200 eV and are illustrated in figures 17 and 18. In the case of the DWPO I model, results have been obtained using the wave function of either Cohen and McEachran or Morse et al. for the excited state (see Appendix A) and are tabulated in table 17; figure 17 displays at each energy the results derived by using the Cohen and McEachran function. In table 18, results computed in the DWPO III model, employing the wave function of Morse et al., are presented and compared with the corresponding DWPO I results and with absolute experimental data in figure 18. Consideration will first be given to the DWPO I results (c.f. table 17 and figure 17).

At an impact energy of 29.6 eV, figure 17(a) shows DWPO I results obtained using either wave function for the excited state. Absolute experimental results have been published by Trajmar (1973) and by Hall et al. (1973) (at 29.2 eV); the latter, obtained independently and using a completely different normalization procedure, agree significantly well with the former and have subsequently been omitted. Comparison is also made with the many-body method of Thomas et al. (1974) and the distorted wave calculation of Shelton et al. (1973). Comparing the cross sections computed in the DWPO I model, it is immediately obvious that for this transition, the model is sensitive to the choice of wave function for the 2^3S state; results differ by as much as a factor of five. This sensitivity has been investigated and found to arise principally from the integral defined by equation (3.3.18), that is the overlap between $R_{2s}(r)$ and the s-wave $u_o(k_i,r)$, and to a lesser extent from the integral $J^{(A)}(0,k_i,k_f)$, equation (3.3.12). It becomes most apparent in the magnitude of the first term of the partial wave

sum (3.3.25); when computed using the Cohen and McEachran function, B_o^- (c.f. equation (3.3.26b)) has a magnitude half that obtained using the wave function of Morse et al. However, when this same process is considered in the Born-Oppenheimer approximation (using the full expression (5.4.5)), that is, neglecting distortion, the sensitivity vanishes as illustrated by figure 5.

In figure 17(a), the DWPO method predicts minima at similar positions to the experimental values at 45° and 115°, though underestimating the magnitudes by a substantial amount. In fact, renormalizing the DWPO I results by a factor of 10 produces very good agreement with experiment (Scott and McDowell, 1975a). The calculations of Shelton et al. (1973) and Thomas et al. (1974) on the other hand predict the correct magnitude but disagree over the shape. These models, including the DWPO I model, are essentially first-order calculations; a recent matrix-variational calculation (not shown) by Thomas and Nesbet (1974), designed to model a second-order many-body approach, yields far more encouraging results.

Figure 17(b) illustrates theoretical results at 40.1 eV and compares them with the corresponding absolute experimental measurements of Trajmar (1973). Similar experimental results, obtained independently using different techniques, have been published by Hall et al. (1973) (referred to above) at 39.7 eV and by Crooks et al. (1972) at 40 eV; both sets of results are in very close agreement with Trajmar's measurements and have been omitted for clarity. Using the Cohen and McEachran wave function, the DWPO I model again predicts two minima, at 25° and 105°, which are also obtained using the simpler function of Morse et al. (c.f. table 17(a)). Experiment, however, predicts only a single minimum at 95° and while agreement is better than at 29.6 eV, the DWPO I results again considerably underestimate the forward and backward cross sections. Many-body theory gives good agreement at angles between 15° and 35° and, in common with the other distorted wave calculation (Shelton et al. 1973), produces a single minimum at 65°. Both calculations yield results of comparable magnitude with experiment in the forward and backward directions.

By 81.63 eV, the forward peak produced in the DWPO I model at lower energies is seen to vanish and that the cross section suffers a sharp decrease at small angles, contrary to the absolute experimental data of Yagishita et al. (1976) given for 80 eV. This forward dip, referred to as an Ochkur dip, may be removed by a more sophisticated account of exchange; see for example Huo (1974), Ochkur and Burkova (1975) and the summary at the end of this section. The second-order optical potential results of Bransden and Winters (1975) show much better agreement with the observed data at these angles, though at larger angles, in common with those of the DWPO I model, bear little resemblance to the experimental measurements of either Opal and Beaty (1972) (at 82 eV) or Yagishita et al. (1976). It is noted from table 17(b) that the sensitivity to the choice of atomic wave function observed in the DWPO I results for lower energies is beginning to diminish; this is because the s-wave no longer provides the dominant contribution to the scattering cross section, more terms contributing to the partial wave sum (3.3.25).

Moving to 100 eV (figure 17(d)), the DWPO I model exhibits a similar shape to that at 81.63 eV. The experimental data provided by Crooks (1972), Suzuki and Takayanagi (1973) and by Yagishita et al. (1976) reveal a very large increase again in the forward cross section. For larger angles, essentially above 30°, where the results of the two Japanese experiments virtually coincide (hence only the earlier points of Suzuki and Takayanagi are plotted), there is some confusion between the experimental values. Theoretically, the many-body calculation of Thomas et al. (1974) and the partial wave treatment of the second-order optical potential method (Bransden and Winters, 1975) predict comparable shapes to each other, including the structure between 30° and 40°, but differ in magnitude with increasing angle, the former producing results lying above the latter.

Finally, at 200 eV, the DWPO I model is compared in figure 17(e) with the absolute experimental measurements of a number of groups: Opal and Beaty (1972), Suzuki and Takayanagi (1973), Dillon (1975) and Yagishita

et al. (1976). Again the DWPO approximation produces a sharp dip in the forward direction as in the previous cases at 81.63 and 100 eV. A more involved theoretical treatment (Ochkur and Burkova, 1975) using the Second Born approximation is however able to predict results in good agreement with experiment for small angles. Experimentally there is evidence for a certain degree of structure between 20° and 40°. For angles between 50° and 75°, the DWPO approximation is in good agreement with the experimental measurements while for larger angles underestimates the observed cross section. Inspection of table 17(e) shows that the sensitivity exhibited by the excited state to the choice of wave function has virtually disappeared.

Similar calculations in the DWPO III model are presented in table 18; in order to ease the computation, the excited state is described by the simpler wave function of Morse et al. (1935). The results are compared in figure 18 with corresponding DWPO I results from table 17 and also with the absolute experimental data referred to in connection with figure 17. As discussed in §6.2 concerning DWPO III results for excitation of the 2^1S state, only the first five distorted wave functions (viz. $u_\ell(k_i,r)$, $\ell = 0 - 4$) are computed allowing for exchange-polarization effects—for higher ℓ, the corresponding adiabatic-exchange solutions are employed.

At the lower energies (29.6 and 40.1 eV), the inclusion of exchange-polarization terms is noted to further reduce the peak in the forward direction, but otherwise increases the overall magnitude (particularly at 29.6 eV) of the DWPO I results while at the same time preserving the general shape of the curve for angles above 20°. The agreement on an absolute scale with the data given by Trajmar (1973) and Hall et al. (1973) remains however poor.

Considering the differential cross section at higher energies (81.63, 100 and 200 eV), the Ochkur dip is still prominent in the forward direction. For angles less than 90°, there is little difference between the two models in predicting the cross section. A significant feature, however, for larger angles is the enhancement produced by DWPO III, especially at 200 eV.

One concludes therefore that such an increase in the backward direction is due to exchange-polarization effects alone. Despite this improvement, discrepancy with experiment continues to exist.

Summary

The results presented in this section indicate that theoretical predictions of differential cross sections for production of the $1^1S \rightarrow 2^3S$ transition in helium by electron impact are less successful than for the $1^1S \rightarrow n^1S$ transitions studied in §6.2. Probably the best agreement with experiment is obtained by the distorted wave treatment of the second-order optical potential method.

At lower energies, the DWPO approximation yields a result too small compared with experiment while at higher energies, the overall magnitude is improved but fails to agree in shape with the experimental data. A degree of sensitivity to the excited state wave function is apparent, especially at lower impact energies.

The inclusion of exchange-polarization terms increases the overall magnitude at low energies by as much as a factor of 2 but is still unable to provide reasonable agreement with experiment. At higher energies, the DWPO approximation fails completely to predict the large increase in the differential cross section at small angles, whereas in the backward direction, allowance for exchange-polarization effects does produce a substantial increase, particularly at 200 eV. A similar increase has been observed in §6.1 concerning 1s → 2s transitions in atomic hydrogen.

The DWPO approximation is essentially a theory which provides a first-order treatment for dealing with those transitions which can only occur via exchange processes whereas it provides a second-order treatment for those transitions which can also occur via direct means (as in §6.2). Huo (1974) has shown by using a limiting selection rule for exchange scattering at relatively high energies that where the orbital term symbols of the initial and final atomic states remain unchanged, the second-order term in the

exchange T-matrix element becomes more important in the small and large-angle regions compared with the first-order term. In fact Huo shows that the second-order term dominates in the forward direction at high energies (above 300 eV) while the first-order term is important at low energies. Such a result could help to explain the sudden decrease in the forward direction of the differential cross section computed in the DWPO approximation at higher energies. Moreover, according to Ochkur and Burkova (1975), spin-exchange transitions in helium, such as to the 2^3S state, occur in two steps: 1) an elastic exchange process between the incoming electron and the ground state electron of opposite spin and 2) the subsequent interaction with the other ground state electron which produces a transition to some excited state. This argument may be generalized to atoms possessing more than two electrons.

Such a two-particle process can only be described by second-order formalism. Their theory is supported by the excellent agreement with experiment which they obtain, at 200 eV for angles less than 90°, using the Second Born approximation.

§6.4 Excitation of $He(1^1S \rightarrow n^1P)$

Results computed in the DWPO I and DWPO II models have been obtained for the inelastic processes

$$e + He(1^1S) \rightarrow e + He(n^1P),\ n = 2,3,4,5.$$

Total (integral) cross sections are tabulated in table 19 for $n = 2,3,4,5$ and displayed graphically in figure 19. Differential cross sections have been obtained for $n = 2,3$ and are given in tables 20-23. They are compared with other results, both theoretical and experimental, in figures 20-23. Finally, the orientation and alignment parameters (λ,χ) have been determined for $n = 2,3$ and are presented for the whole angular range in tables 24-27 and illustrated in figures 24-27 for angles up to 50°.

Total Cross Sections

2^1P An abundance of theoretical and absolute experimental data has accumulated over recent years for electron impact excitation of $1^1S \rightarrow 2^1P$ transitions in helium. Table 19(a) lists the integral and total integral cross section results when computed in the DWPO I and DWPO II models for energies from just above threshold to 300 eV. The excited state is taken to be described by the simple Hartree-Fock wave function of Marse et al. (discussed in Appendix A). The total integral results are plotted in figure 19(a) and compared with absolute experimental measurements. It will be observed that the DWPO I results extend over the region up to 1000 eV. In fact, as seen from table 19(a), by 300 eV the approximation agrees with the Born or'Born plus Polarized-Born'to 3 figures so that consequently only the corresponding Born cross section is plotted for energies above 300 eV. Born results alone increase far too rapidly for energies below 300 eV and peak much higher and closer to threshold than DWPO results (Scott and McDowell, 1976).

From an experimental point of view, there is good consistency throughout the energy regions considered between the various sets of data, though the results of Moustafa Moussa et al. (1969) for $E > 80$ eV and of Chutjian and Srivastava (1975) at 60 and 80 eV would appear rather low. At lower energies both DWPO models are in close agreement with the values provided by Donaldson et al. (1972) and Hall et al. (1973). Proceeding to the peak value, correctly positioned with respect to energy by both models, the DWPO I model begins to overestimate the experimental results while the DWPO II model gives a lower cross section which is in good accord with the measurements of de Jongh and van Eck (1971). However, the theoretical results are still of greater magnitude than those of Donaldson et al. (1972) until $E > 200$ eV where the agreement with DWPO II is very good. DWPO I continues to remain in good agreement with the points of de Jongh and van Eck (1971) for increasing energy and for $200 < E < 1000$ eV is also in close accord with the recent data published by Dillon and Lassettre (1975). Overall, when compared with

experiment, the effect of including target distortion via the ground state wave function appearing in the T-matrix element is to lower the total (integral) cross section and hence produce better peak values than the simpler (DWPO I) model which contains no such explicit account of target distortion.

Theoretical results from other models have been omitted from figure 19(a); to do justice to each would only obscure the results of others. However, the essential features of their results will be briefly described below.

For high energies, as one would expect, most of the theories agree reasonably well. As the impact energy decreases below 300 eV, the results of the Coulomb-projected Born approximation of Hidalgo and Geltman (1972) begin to rise too sharply, followed for $E < 150$ eV by those of the second-order optical potential method, calculated in an impact parameter treatment by Berrington et al. (1973). A partial wave treatment of the latter method (Winters, 1974) does, however, provide results above 100 eV in good agreement with those of DWPO I. The second-order diagonalization procedure of Baye and Heenen (1974), in common with other high energy approximations, also overestimates grossly the peak value.

The results of the ten-channel eikonal treatment of Flannery and McCann (1975) agree closely with the DWPO I results down to 80 eV; for $E < 80$ eV, they continue to overestimate, hardly surprising since the method is essentially a high energy approximation. Good agreement is obtained between DWPO II results and those in the distorted wave calculation of Madison and Shelton (1973) for $E > 125$ eV. However, for $E < 125$ eV, their results increase too quickly and shift the position of the peak from the experimental point at 90 eV down to 70 eV. This lack of agreement is probably due to omission of exchange in the former theory and to a neglect of polarization in the latter. Judging from the better agreement of the DWPO II model with experiment at the peak value, it appears that exchange (in fact, this is neglected in the actual calculation of the distorted waves by Madison and Shelton) and polarization become important in calculating total cross sections

for energies less than 150 eV.

The eikonal distorted wave method of Joachain and Vanderpoorten (1974a) gives results consistent with DWPO II down to 60 eV; below 60 eV, their results are more in line with those of DWPO I. The best agreement with experiment over the size and position of the maximum is provided by the Glauber calculation of Chan and Chen (1974a); such a calculation is expected to give a very good description of small-angle scattering which, since the major contribution to the total cross section comes from small angles, accounts for the close agreement. For energies from 90 eV down to 30 eV, the many-body theory approach of Thomas et al. (1974) yields results lying between those of DWPO I and DWPO II; their calculations allow for distortion in both the entry and exit channels.

3^1P Theoretical results for excitation to this state are not quite so numerous as in the previous case but nevertheless form a substantial volume of material for comparison with experimental measurements. DWPO I and DWPO II results are tabulated in table 19(b) and, together with other theoretical results and absolute experimental data, are displayed in figure 19(b).

For energies above 300 eV, theory and experiment agree quite well; the experimental measurements are due to Moustafa Moussa et al. (1969), de Jongh and van Eck (1971) and Donaldson et al. (1972). As in the previous case, DWPO I and II total cross sections agree to 3 figures with the corresponding Born results; consequently Born values are plotted for energies in this region.

For energies below 300 eV, the DWPO I results tend to favour the data of Donaldson et al. (1972) while the DWPO II results are smaller by at most 10%, preserving the profile, and in good agreement with the measurements of Moustafa Moussa et al. (1969) except at 80 eV. At energies away from 90 eV (the position of the maximum), the DWPO I and DWPO II results come into closer agreement with each other and also with the points of de Jongh and van Eck (1971) which otherwise are comparatively smaller. The experimental point of Showalter and Kay (1975) at 200 eV appears rather low and at 80 eV

the measurement of Chutjian (1976) also seems low, though that at 100 eV is compatible with other experimental values.

Concerning other theoretical methods, the results of a nine-state impact parameter version of the second-order optical potential model (Bransden and Issa, 1975) begin to increase too steeply for energies below 300 eV, followed by those in the second-order diagonalization procedure (Baye and Heenen, 1974). The only other remaining curve is that of Flannery and McCann (1975), obtained in their ten-channel eikonal treatment. The results are reasonably good down to 100 eV, where they agree with the experimental point of Chutjian (1976), falling between those of Moustafa Moussa et al. (1969) and Donaldson et al. (1972). Below this energy, the peak value of the cross section is obtained at 70 eV, shifted from the 90 eV predicted by Donaldson et al. (1972). Not shown are the Glauber results of Chan and Chen (1974b) which lie generally below experiment.

4^1P Here the DWPO approximation to the integral cross sections in both models is computed without the Born-subtraction artifice described in §3.4 to perform the sums over partial wave cross sections. Instead the first 30 terms are retained for $E < 150$ eV and the first 40 for $E \geq 150$ eV, this being found adequate to produce a smooth total differential cross section at small angles which is where the main contribution to the cross section arises. With less terms or at an energy above 300 - 400 eV, the total differential cross section exhibits a more extensive oscillatory nature, characteristic of a lack of convergence in partial waves, which extends into this small-angle region (less than 40° - 50°).

Since there is now no need to obtain an expression for the Born T-matrix (which it will be recalled would be required in closed form), a more complicated wave function may be taken for the excited state; that of Cohen and McEachran (see Appendix A) is adopted. Further, the p-wave $u_1(k_i,r)$ is made orthogonal to $R_{np}(r)$; hence the integral $c_2^p(k_i)$, given by (3.4.36), vanishes. The subsequent DWPO I and DWPO II results are given in table 19(c) and are displayed in figure 19(c) with absolute experimental measurements.

One sees that the measurements of de Jongh and van Eck (1971) and of Donaldson et al. (1972) agree closely with each other at all energies except 80 eV; the point due to Showalter and Kay (1975) at 200 eV coincides with that of the former group. The results of Moustafa Moussa et al. (1969) are comparatively low.

The maximum is observed to occur in the vicinity of 90 eV and is very well predicted in shape and magnitude by the DWPO II model when compared with the data of Donaldson et al. (1972). DWPO I results lie approximately 10% higher at this energy, being in closer agreement with those of DWPO II for energies away from this value. The second-order diagonalization procedure of Baye and Heenen (1974) yields results which agree well with the data of de Jongh and van Eck (1971) for energies above 300 eV; however for energy values below this, the method improves little on the First Born Approximation (Bell et al. 1969, not shown), the results increasing far too rapidly for energies below 200 eV. Also not displayed are the Glauber results of Chan and Chen (1974b), which lie above those of the DWPO models.

Overall, the DWPO II model produces the most satisfactory agreement with experiment, being in best accord with the measurements of Donaldson et al. (1972).

5^1P Total (integral) cross sections have been obtained in the DWPO I and DWPO II models. The comments on the computation of 4^1P cross sections, given in the first two paragraphs of the previous section, all apply to this case also. However, using the coefficients published by McEachran and Cohen (1969) gave very large integral cross section results. Consequently the coefficients were modified according to the procedure outlined in Appendix A. Results obtained from using both the modified and unmodified coefficients are presented in table 19(d); the modified results are illustrated in figure 19(d).

The only experimental points available are those of Moustafa Moussa et al. (1969) and, at 200 eV, that of Showalter and Kay (1975). The DWPO I result agrees well with this latter measurement, the DWPO II result being some 10% lower. However, both models predict results of similar shape, but lying considerably higher than the data of Moustafa Moussa et al. (1969). Further, the DWPO results attain a maximum value at about 90eV, whereas that of Moustafa Moussa et al. seems to be nearer 80 eV. The second-order diagonalization method of Baye and Heenen (1974) once more increases too rapidly for energies below 200 eV and subsequently predicts a much larger peak value of the cross section.

Summary

The DWPO I and DWPO II models produce total integral cross sections of similar profile which generally speaking are in good agreement with absolute experimental measurements, particularly in the latter model; the DWPO II results tend to lie at most 10% below those of the DWPO I model. Compared with other theoretical predictions, where results are available for comparison, the DWPO models provide total integral cross sections which, taken over the full range of impact energies illustrated, are the most consistent with experiment.

It is noted that for energies above 300 eV, the DWPO I and DWPO II models yield total integral cross sections which agree to at least 3 figures with those obtained in their high energy limits, namely the Born and 'Born plus polarized-Born' approximations respectively. Hence one concludes not surprisingly, that exchange effects become negligible in computing total integral cross sections for energies above this value.

Differential Cross Sections

Differential cross section results, computed in the DWPO I and DWPO II models for excitation of the n^1P_o, $n^1P_{\pm 1}$, n^1P (n = 2,3 only) states, are

tabulated over the whole angular range in tables 20 - 23 and the total differential cross section displayed graphically in figures 20 - 23, together with other theoretical results and absolute experimental data.

2^1P DWPO I results are plotted for five incident energies in figure 20 where they are compared with experimental and other theoretical results. Figure 21 illustrates for small-angle scattering the results of the DWPO II model at four incident energies and includes also those of the DWPO I model and of experiment for comparison. Throughout the calculations, the simple Hartree-Fock function of Morse et al. (1935) has been utilized to describe the excited state (see Appendix A). Consideration is first given to the DWPO I results, figure 20.

For electron impact energies of 29.6 and 40.1 eV, only the absolute experimental data of Truhlar et al. (1973) have been plotted, those of Hall et al. (1973) (at 29.2 and 39.7 eV) lying in close agreement and consequently omitted. At 29.6 eV, DWPO I results are in reasonable accord with the experimental points for smaller angles, except in the forward direction itself where they tend to fall slightly below experiment but nevertheless provide the closest theoretical agreement. The close-coupling results (at 29 eV) obtained by Truhlar et al. (1973) appear generally too high, in common with the results of the distorted wave calculation of Madison and Shelton (1973) which, while too small in the forward direction, are too high for angles greater than 30°.

The many-body method (Thomas et al. 1974) yields results which follow closely those of the DWPO I model out to 60°, both sets lying close to experiment. However, for angles greater than 60°, the many-body results follow more closely the experimental trend than the DWPO I values; the latter fall at their lowest point (about 125°) to an order of magnitude below experiment.

The situation at 40.1 eV displays theoretical curves in better agreement with each other and with experiment at smaller angles, DWPO I providing once more the closest agreement. The close-coupling calculation

shows some oscillation for angles above 120° which could well be due to a lack of convergence in the partial wave sums. Also shown are the ten-channel eikonal results of Flannery and McCann (1975). However, for angles above 60°, both the DWPO I and multichannel eikonal results continue to decrease too rapidly and fall considerably below experiment while the many-body treatment produces excellent agreement over the whole angular range.

Moving to figure 20(c), where the DWPO I results have been plotted for an incident energy of 81.63 eV, there exist more numerous theoretical calculations. Experimentally, the measurements given by Opal and Beaty (1972) at 82 eV and by Chutjian and Srivastava (1975) at 80 eV are in good agreement out to about 105° whereafter the former measurements lie below the latter. Experimental data have also been given by Truhlar et al. (1970) but are omitted for clarity. On the theoretical side, it was decided to also omit the results of the eikonal distorted wave method (Joachain and Vanderpoorten, 1974a) and of the second-order diagonalization procedure (Baye and Heenen, 1974) in order to maintain a reasonably distinct figure. Both sets of results range over the angular region from 0° to 80° and are consistent with those of other theoretical treatments.

Good agreement is obtained between each of the represented models and with experiment for angles less than 30°, with perhaps the exception of the Coulomb-projected Born calculation of Hidalgo and Geltman (1972) at 82 eV which produces results lying consistently high. DWPO I results provide the best overall agreement with experiment out to 40°; above this point, they tend to underestimate both sets of data. The results of the ten-channel eikonal treatment at 80 eV follow a similar pattern, though falling further below experiment than those of DWPO I in the backward direction, due most probably to an explicit omission of exchange effects. Generally,the best agreement with experiment is obtained by the distorted wave calculation of Madison and Shelton (1973) at 80 eV and by the application of many-body theory (Thomas et al. 1974). Both these methods allow for final channel distortion but omit the long-range polarization effects; this would account for the superior performance of the DWPO approximation in the forward direction.

At 100 eV, the DWPO I results are again in best accord with the experimental data shown, which is due at 5° to Chamberlain et al. (1970) and over the rest of the angular range to Suzuki and Takayanagi (1973). In figure 20(d), the theoretical results of the eikonal distorted wave method (Joachain and Vanderpoorten, 1974a) and of the second-order diagonalization procedure (Baye and Heenen, 1974) have been included, and agree quite well with experiment over the range given for each method. The results of Madison and Shelton (1973) and of the Glauber treatment (Chan and Chen, 1974a) have, however, been omitted for reasons of clarity. The former results are found to be quite reasonable on comparison with the absolute experimental values of Crooks and Rudd (1972). The Glauber model, with results given only for angles less than 20°, shows comparable agreement with DWPO I.

The partial wave treatment of the second-order optical potential method (Winters, 1974) provides results in close agreement with experiment for angles less than 50°; for angles above 50°, following closely the DWPO I values, the results fall below experiment. Results in the ten-channel eikonal treatment, provided by Flannery (1975), show a familiar behaviour to that of previous cases, that is good agreement in the forward direction and for angles less than 30° with experiment (as expected), but underestimating for large angles. Figure 20(d) also shows an improvement in the Coulomb-projected Born approximation, which is expected to be better at higher energies.

The final energy considered is 200 eV, figure 20(e), where again a large volume of data is available. The experimental results of the four groups represented, absolute in each case, form a consistent shape, those of Suzuki and Takayanagi (1973) coinciding well with the small-angle data of Chamberlain et al. (1970) and of Dillon and Lassettre (1975) and at larger angles with those of Opal and Beaty (1972). Theoretical predictions are in good agreement with these measurements for angles less than 30°; for angles above 30°, they begin to diverge from each other. DWPO I and the ten-channel eikonal results (Flannery 1975) exhibit a similar behaviour to

that at previous energies, falling below other theory and experiment for angles above 40°, particularly in the latter model. The eikonal distorted wave method and the second-order diagonalization procedure show predictions not unlike those illustrated at 100 eV in figure 20(d), being in reasonable agreement with other models and experiment over their respective angular regions. The Glauber treatment of Chan and Chen (1974(a)) has again been omitted; values are given only for angles up to 20° and agree closely with other theoretical results.

For large-angle scattering, the profile of the Coulomb-projected Born calculation decreases too rapidly and lies below experiment and just above that of DWPO I, whereas the distorted wave calculation (Madison and Shelton, 1973) provides a good cross section out to 120°. Since this latter method treats the initial and final channel on an equivalent footing, this good agreement with experiment lends further support to the necessity to allow for final channel distortion.

Corresponding DWPO II results for excitation to this state are presented in table 21. A general comparison between tables 20 and 21 shows that for each of the five incident energies, the DWPO II total differential cross section results are some 10 - 20% smaller than those computed in the DWPO I model for all angles. Results obtained in both models for impact energies of 29.6, 40.1, 80 and 100 eV are displayed at small angles with absolute experimental data in figure 21.

For the lower two energies, the DWPO II model yields very good agreement with the measurements obtained by Truhlar et al. (1973) and at 29.2 and 39.7 eV by Hall et al. (1973), improving over the DWPO I results. A certain degree of discrepancy does however remain in the forward direction itself.

Considering 80 eV, the two DWPO models produce results lying closer together and in good accord with the data of Chutjian and Srivastava (1975) though neither predicting the slight lowering of the cross section observed at 15°. Finally the DWPO models are compared at 100 eV with the measurement of Chamberlain et al. (1970) at 5° and with the measurements of Suzuki and

Takayanagi (1973) over the remainder of the angular range up to 36°. Again, there appears to be some structure observed at 15° which is not found theoretically. The DWPO II model agrees well with experiment, however, for angles above 20°. The First Born approximation, deduced from the accurate generalized oscillator strengths tabulated by Bell et al. (1969), yields results of larger magnitude than those of either DWPO model; this approximation fails to allow for polarization effects.

Overall the consequence of explicitly including target distortion in the T-matrix element is to lower the total differential cross section and to subsequently provide better agreement with published experimental data at small angles. Both the DWPO I and DWPO II models, however, underestimate experiment at large angles, particularly the DWPO II model.

3^1P Differential cross sections describing excitation to this state and computed in the DWPO I model are tabulated at four incident energies in table 22. Corresponding results in the DWPO II model are given in table 23. Both calculations employed the simple Hartree-Fock function of Goldberg and Clogston (1939 , see also Appendix A) for the excited state. Graphical comparisons of the DWPO I results for the total differential cross sections with theory and experiment are presented in figure 22. Figure 23 offers a closer examination of small-angle scattering, allowing for the improved treatment of polarization in the DWPO II model, at lower impact energies. Attention will first be given to figure 22.

Comparison is made at the lower energies of 29.2 and 39.7 eV with the absolute experimental data of Chutjian and Thomas (1975). It must be emphasised that their apparatus was unable to resolve between excitation to the $3^{1,3}D$ and 3^1P states so that in fact the points plotted represent the combined result for excitation to the $3^{1,3}D$ and 3^1P states. The 3^1P state lies only 0.014 and 0.013 eV from the 3^3D and 3^1D states respectively. However, comparing with the many-body calculations, also given in the paper by Chutjian and Thomas (1975), one sees that the main contribution to the cross section for angles less than 60° arises from the $1^1S \rightarrow 3^1P$ transition;

consequently the experimental points plotted in figure 22 (and 23) over this angular region allow one to make a useful comparison with observation for excitation of the 3^1P state alone. At larger angles it appears from the many-body calculations that, while the 3^1P cross section drops smoothly, the 3^3D cross section increases, providing a substantial contribution (about 80% at 136°) for an energy of 29.2 eV and a lesser contribution (about 30% at 136°) at 39.7 eV to the joint differential cross section. At both energies, the 3^1D contribution is at most 12%; the overall effect of the $3^{1,3}D$ states is to flatten the cross section for large angles. All theoretical calculations represented in figure 22 apply to the 3^1P state alone.

Comparing the DWPO I results in figures 22(a) and 22(b) with those of the many-body calculation and with the experimental measurements, shows excellent agreement out to 60°, except at 29.2 eV in the forward direction itself where both calculations fall below the experimental points. At large angles (essentially above 60°) the DWPO I results decrease rapidly below the many-body results which at 29.2 eV lie themselves below the experimental measurements. In figure 22(b), many-body theory is in very good accord with experiment over the whole angular range at 39.7 eV. Also shown in this figure are the ten-channel eikonal results (at 40 eV) of Flannery and McCann (1975) which predict a more enhanced forward peak but, similar to the DWPO I results, drop to at least an order of magnitude below experiment at 136°.

In figure 22(c), at 100 eV, the experimental points (Chutjian, 1976) have been corrected for contributions due to the $3^{1,3}D$ states, following a procedure outlined in Chutjian's paper. The DWPO I results are seen to be in very good agreement for angles less than 40°, tending to underestimate at larger angles. The ten-channel eikonal results are also in good agreement at small angles, in common with the Glauber method (Chan and Chen, 1974b). Concerning also figure 22(d), which illustrates only theoretical results, the Glauber approximation results are shown for angles less than

10^{o}, the results merging into the ten-channel eikonal points of Flannery and McCann (1975) for angles between 10^{o} and 20^{o}. The results of Flannery and McCann extend over the whole angular range and comparison with the results of the DWPO I model shows that both models exhibit a similar trend, the eikonal method dropping below the DWPO I model for angles above 50^{o}, due presumably to explicit neglect of exchange effects, whereas the DWPO models allow explicitly for such effects.

DWPO II results are plotted for small angles in figure 23 at 29.2 and 39.7 eV and compared with the DWPO I results and also with the experimental measurements referred to above in connection with figure 22. At 29.2 eV, DWPO II results appear somewhat low in the forward direction but otherwise are in good agreement with experiment, especially for angles above 20^{o}. An overall comparison for the complete angular region between DWPO I and DWPO II is obtainable from tables 22 and 23. Essentially, the DWPO II model yields differential cross section results (total and magnetic sublevel) some 10%, or 20% in some cases, smaller than the DWPO I model, thus producing less comparable results with experiment, where available, for large angles.

Summary

Differential scattering for excitation of the $2^{1}P$ and $3^{1}P$ levels of helium has been studied in the DWPO I and DWPO II models for impact energies varying from approximately 30 eV to 200 eV. On comparison with absolute experimental data and with other theoretical methods, the DWPO approximation reproduces the best overall agreement with small-angle measurements, especially in the DWPO II model. For larger angles, the approximation consistently underestimates experimental data for each impact energy whereas models which allow for distortion in the final channel as well as in the initial channel (e.g. the many-body approach) yield more compatible results.

The DWPO models incorporate an account of the effects due to the long-range adiabatic polarization interaction and, particularly in the DWPO II model, this is undoubtedly the reason for such accurate small-angle differential cross sections. This in turn accounts for the accurate total (integral) cross section values, since the most significant contribution to the total integrated cross section comes from the small-angle region of the differential cross section

The (λ,χ) Parameters

These parameters, referred to as the orientiation and alignment parameters, have been defined in equations (3.5.4) and discussed in §3.5. They have been computed in the DWPO I and DWPO II models for the 2^1P and 3^1P states, and are presented over the whole range of angles in tables 24 - 27 and, in the DWPO I model, up to 50° in figures 24 - 27. The same excited state wave functions used in deriving differential cross sections, discussed in the last section, are of course, employed here also. The results of this section are compared with the experimental data of Eminyan and coworkers and with other theoretical predictions.

2^1P Results for λ and χ are tabulated in tables 24 and 25 respectively, for incident energies of 40, 60, 80, 100 and 200 eV. The DWPO I results are displayed in figures 24 and 25 and compared with the experimental data of Eminyan et al. (1974) in each case and with available theoretical results. Comparison between DWPO I and DWPO II results for λ in table 24 and for χ in table 25 shows that there is at most 10% difference between them so that consequently, discussion will be confined to the DWPO I results. Consideration is first given to λ.

The first energy considered is 40 eV where for angles less than 15° there is good agreement between each of the four theories represented and with experiment. For angles out to 50°, best agreement with experiment is maintained by the distorted wave calculation of Madison and Shelton (1973),

followed by the ten-channel eikonal results of Flannery and McCann (1975). The DWPO I results fail to predict a minimum over this angular range and underestimate the experimental measurements; a similar comment applies to the many-body approach (Thomas et al., 1974), represented at 40.1 eV.

Proceeding to a higher impact energy of 60 eV, the situation alters in that the DWPO I is in best accord with experiment (there is no distorted wave calculation by Madison and Shelton at this energy), the agreement extending out to 25° where experiment finds a sharper rise in the results. The multichannel eikonal results and many-body theory results show a similar trend to those of the DWPO I model, but of smaller magnitude.

At 80 eV, best agreement with experiment is obtained by the distorted wave calculation of Madison and Shelton (1973) at 78 eV; DWPO I results agree well out to 20° with experiment whereafter they fail to produce the more rapid increase measured by experiment and predicted accurately by the former calculation. The multichannel eikonal and many-body treatments are both in disagreement with experiment at each angle.

Moving to 100 and 200 eV, excellent agreement is once more obtained with experiment by Madison and Shelton's distorted wave model. The DWPO I results lie in reasonable agreement with experiment for angles less than 20° whereas at 200 eV the DWPO I results are in slightly better agreement with the two experimental points than those of Madison and Shelton. At this latter energy, these two theoretical methods remain in good agreement with each other up to 40° where the DWPO approximation predicts a peak value. The results of Flannery and McCann (1975) in their multichannel eikonal method and those in the eikonal distorted wave Born approximation (Joachain and Vanderpoorten, 1974b) produce a lower minimum than that observed experimentally and by the former two (distorted wave) methods.

Generally, however, λ is best reproduced in figure 24 by the distorted wave calculation of Madison and Shelton (1973).

Considering χ, the situation with respect to this parameter is quite different from that for λ when comparing theoretical models. At 40 eV,

the distorted wave results of Madison and Shelton (1973) are in best accord with experiment while those of the ten-channel eikonal treatment (Flannery and McCann, 1975) show a clear improvement over the DWPO I results, particularly at lower angles (less than 40°). Figure 25(b) illustrates only the DWPO I results and experiment, the agreement here at 60 eV being better than that at 40 eV.

For impact energies of 80 and 100 eV, the ten-channel eikonal results provide the best agreement with experiment, those of Madison and Shelton (at 78 eV) being too large and producing a shape of opposite curvature whereas the DWPO I results reveal a similar but somewhat lower shape to the ten-channel eikonal results. At 100 eV, the calculations of Flannery and McCann show a certain degree of structure at 20°, not resolved experimentally nor predicted by other theoretical calculations. The results of the eikonal distorted wave Born approximation (Joachain and Vanderpoorten, 1974b) have been plotted for 100 eV and exhibit a similar but lower profile to those of Madison and Shelton (1973).

A similar behaviour of the theoretical results amongst themselves is repeated to a certain extent for angles less than 25° at an impact energy of 200 eV. However, as shown in figure 25(e), only two experimental points are available which in this case support best the eikonal distorted wave calculation of Joachain and Vanderpoorten (1974b). The DWPO I results give quite a different shape at all angles, whereas the ten-channel eikonal results begin to increase away from other theoretical results for angles greater than 20°.

For the most part, however, the best overall agreement of χ with experiment is obtained by the ten-channel eikonal model of Flannery and McCann (1975).

3^1P Results for λ and χ are presented for the whole range of angles in tables 26 and 27 respectively for impact energies of 50, 80, 100 and 200 eV. Experimental measurements have been published by Eminyan et al. (1975) for angles only up to 30°. In figures 26 and 27, results for λ and χ

respectively, obtained in the DWPO I model, are compared with these measurements and with those of a four-channel eikonal treatment as appears in the paper by Flannery and McCann (1975). As for the 2^1P state, a comparison of tables 26 and 27 shows that the DWPO I and DWPO II results differ by at most 10% so that discussion may be subsequently confined to the DWPO I results. To begin with, λ is first discussed.

Figure 26(a) illustrates results for 50 eV impact energy. Generally there is little resemblance to the experimental points in either theory. Neither predicts agreement for angles above 20°; a ten-channel calculation (Flannery 1975) reduces the multichannel eikonal result between 10° and 30° so that it coincides to a larger extent with the DWPO I result, while at angles above 30° it returns to a profile similar to that produced by the less sophisticated four-channel treatment.

At energies of 80 and 100 eV, both theories agree reasonably well with experiment out to about 15°, the agreement with DWPO I at 80 eV continuing out to 25°. However, neither theoretical curve increases rapidly enough at larger angles to follow the experimental points. For these energies, and indeed at 200 eV also, the multichannel eikonal results show considerable structure about the minimum predicted between 15° and 30° in each case, whereas the DWPO results exhibit a very smooth behaviour.

Figure 26(d) offers only a comparison between the two theories, which without experimental data, is difficult to assess. In common with the 2^1P result for this energy, one observes that the DWPO approximation predicts a peak at an angle of 40°.

Generally speaking, where measurements have been made, the DWPO models yield values of λ in better agreement with experiment.

Turning to χ, the DWPO I and four-channel eikonal results are compared with experiment, where available, in figure 27. For the lowest energy (40 eV) both models exhibit different curves, neither agreeing with experiment at any angle though there is some experimental evidence at 20° for the maximum predicted by the four-channel eikonal method (Flannery and McCann, 1975) at an angle of 30°. Figure 27(b) shows that at 80 eV, the eikonal

results are to be preferred to the DWPO I results; neither theory, however, produces the correct magnitude but the overall shapes are in better accord than at 50 eV.

Results at 100 eV show the four-channel treatment at its best for the 3^1P state; agreement with the experimental points is good whereas the DWPO I results continue to underestimate the measurements. A certain degree of structure is revealed in the four-channel eikonal results, not found in the DWPO calculations. This is most evident in figure 27(d) where at 200 eV, there are no experimental values and little resemblance between the results of either theory.

However, overall in figure 26, the better agreement for χ with experiment where available is obtained with the four-channel eikonal treatment.

Summary

Theoretically χ is more difficult to determine accurately than λ. λ is most accurately computed for the 2^1P state in the distorted wave calculation of Madison and Shelton with the results of the DWPO approximation being in good agreement with experiment over the first half of the angular range illustrated. For the 3^1P state, the DWPO approximation produces results for λ closer to experiment than the multichannel eikonal method.

χ on the other hand is generally best predicted for both states by the multichannel eikonal approach of Flannery and McCann. DWPO results consistently underestimate this parameter, while at the same time exhibiting the general shape of the experimental measurements.

Moreover, it is difficult to draw any conclusions from these results except to say that there is so far no one theory which consistently agrees with the available measurements of both λ and χ.

§6.5 Excitation of $He(1^1S \rightarrow 2^3P)$

Total (integral) cross sections and differential cross sections have been computed in the DWPO I model for the excitation process

$$e + He(1^1S) \rightarrow e + He(2^3P).$$

Integral cross sections are tabulated in table 28 and illustrated in figure 28. Differential cross sections for excitation of the 2^3P_0, $2^3P_{\pm1}$ and 2^3P states are presented in table 29 and the total 2^3P differential cross section displayed at five impact energies in figure 29.

Total Cross Sections

These have been obtained in the DWPO I model incorporating the excited state wave function of McEachran and Cohen (1969, see also Appendix A). The total integrated cross section for excitation to the 2^3P state is illustrated in figure 28 for energies from just above threshold to 200 eV and compared with the many-body theory results (Thomas et al., 1974). The experimental points are absolute measurements in each case, obtained by Jobe and St. John . (1967) and at lower energies by Trajmar (1973) and Hall et al. (1973).

The results of the latter two mentioned experimental groups are a little higher than those of Jobe and St.John but overall the measurements form a consistent curve. DWPO I predicts accurately the position of the maximum at 35 eV but overestimates by a factor of at least 2 the magnitude of the observed peak. For the rest of the energy range considered, the DWPO I results agree well in shape with the experimental data but continue to remain at a higher magnitude. Total integrated cross section results in the many-body theory of Thomas et al. (1974) are published for energies only up to 81.63 eV and lie higher still than the DWPO I results.

Summary

Generally, the agreement between the results of the DWPO I model and with the shape of the experimental measurements is good; the theoretical results, however, lie as much as a factor of 2 above the measured values. Moreover, compared with the other spin-exchange transition, considered in §6.3, the situation is considerably more satisfactory.

Differential Cross Sections

These have been computed using either the excited state wave function of Cohen and McEachran or that of Morse et al. (see Appendix A for details) and the results given in table 29. Those obtained from using the Cohen and McEachran function are illustrated for five incident energies in figure 29 and compared with other theoretical results and with absolute experimental measurements.

At 29.6 eV, the cross section calculated using the simpler wave function is also shown in figure 29(a). Both may be compared with the absolute experimental results of Trajmar (1973) which agree closely with those of Hall et al. (1973) obtained at 29.2 eV (not shown); both experiments utilized different normalization procedures. Theoretically, the many-body theory results of Thomas et al. (1974) are also shown and the distorted wave results of Shelton et al. (1973). The theories agree fairly well in the forward direction but none is able to reproduce the experimental values at small angles nor indeed at any other angle. It is noted that the latter two models exhibit a similar result to each other.

Use of the simpler Hartree-Fock function in the DWPO I model reduces the cross section for large angles below that obtained using the Cohen and McEachran function; the cross section in the backward direction is decreased by 80%. This sensitivity to the excited state wave function is found to mainly arise, here and at higher energies, from the overlap integral

(3.4.36) of the radial function $R_{2p}(r)$ and the p-wave $u_1(k_i,r)$. The corresponding integral (3.3.18) was also found to be chiefly responsible for similar discrepancies observed in excitation of the 2^3S state discussed in §6.3. A lesser degree of sensitivity arises in the integrals defined by (3.4.31), decreasing with increasing ℓ, and also in that defined by (3.4.34).

For an energy of 40.1 eV, the theoretical models again agree quite well in the forward direction but overestimate the experimental results, in this case by a factor of almost 10. The measurements are those of Trajmar (1973) and Gelebart et al. (1975). Corresponding measurements were made by Hall et al. (1973) at 39.2 eV (not shown) and are in close agreement with those displayed. Once more, none of the available theoretical models represented in figure 29(b) is able to reproduce the curve indicated by the experimental points. It is, however, noted that the distorted wave calculation of Shelton et al. (1973) and similarly that of the many-body theory (Thomas et al. 1974) produce comparable results to each other. Both calculations omit polarization effects but allow for distortion in the initial and final channels. The primary difference between the two methods lies in the computation of these distorted waves: Shelton et al. allow for distortion only by the static-field of the target whereas Thomas et al. allow for distortion by the Hartree-Fock field of the target.

Comparison of the DWPO I results in table 29(b) reveals again a comparatively severe drop in the cross section at large angles when the simpler wave function is used for the excited state.

Moving to a higher energy, one sees at 81.63 eV that the DWPO I results and those of the many-body theory agree very closely out to an angle of 60° after which the many-body results overestimate the experimental data of both Opal and Beaty (1972) at 82 eV and Chutjian and Srivastava (1975) at 80 eV. The DWPO I results on the other hand follow closely the measurements of Opal and Beaty for angles above 50°. For angles less than 40°, both theories overestimate the experimental points of Chutjian and Srivastava (1975)

and Yagishita et al. (1976) at 80 eV, which together with those of Opal and Beaty (1972) exhibit a certain degree of scatter amongst themselves.

The sensitivity to the choice of atomic wave function for the excited state in the DWPO I model has decreased and from table 29(c) one sees that both sets of results now agree to within 20% due to the increased number of partial waves contributing to the differential cross section. For increasing ℓ the integrals are again noted to be less sensitive to $R_{2p}(r)$.

In figure 29(d) results are shown at 100 eV; the DWPO I model reproduces reasonably well the experimental profile obtained by Suzuki and Takayanagi (1973) and Yagishita et al. (1976). For angles above 60°, the measurements of these two experiments agree with each other. Finally, at 200 eV, the DWPO I results are again compared with the recent data of Yagishita et al. (1976) and reproduce very well their measured cross section, including the peak observed at 10°.

The DWPO results do, however, continue to be sensitive to the choice of excited state wave function; results computed at 100 and 200 eV using the simpler representation of the Hartree-Fock solution lie higher for large scattering angles than those obtained using the Cohen and McEachran function. Overall however, this sensitivity has diminished with increasing impact energy.

Summary

The agreement of the DWPO I results with experiment is at its best for the higher energies (above 81.63 eV), especially for angles less than 40° at 200 eV. Below 81.63 eV, agreement is poor; there is also no other theoretical treatment capable of adequately reproducing the experimental results. Where available, the distorted wave calculations of Shelton et al. (1973) and the many-body calculations of Thomas et al. (1974) agree well with each other; both these models employ distorted waves in the final as well as in the initial channel.

A certain amount of sensitivity arises in the DWPO I model, particularly at low energies, concerning the choice of wave function for the excited state.

§6.6 Conclusions

Integral and differential cross sections together with, where appropriate, orientation and alignment parameters, have been computed over the intermediate energy region (§1.1) in a distorted wave polarized orbital approximation for the inelastic collision processes:

$$e + H(1s) \rightarrow e + H(2s,\ 2p,\ 2s + 2p), \tag{1}$$

$$e + He(1^1S) \rightarrow e + He(n^1L), \tag{2}$$

$$e + He(1^1S) \rightarrow e + He(2^3L), \tag{3}$$

$$n = 2,3,4,5;\quad L = S,P\,.$$

Results for each process represented in (1) - (3) have been summarized in the appropriate sections of this chapter. The aims of the present section (§6.6) are to formulate general conclusions from this work and to discuss directions for future study into these collision processes.

Concerning the work on excitation of atomic hydrogen (process (1) above), the inclusion of exchange-polarization effects in the DWPO approximation greatly improved the total differential cross sections for the lower impact energies (less than 1.44 Rydbergs), particularly for large-angle scattering. The unitarization technique failed to improve the accuracy of the differential cross sections until the impact energy reached 100 eV. One concludes immediately that in the case of low energy inelastic electron scattering by atomic hydrogen, exchange-polarization effects are important.

Turning to helium and in particular to the transition where spin is conserved, i.e. process (2), the DWPO approximation produces total (integral)

excitation cross sections in close agreement with experiment over the whole energy range, whereas comparable models (other distorted wave methods, including lowest-order many-body theory) fail at lower energies. As far as the differential cross sections are concerned, the DWPO approximation gives accurate results in the forward direction for energies above 100 eV, failing to an increasing extent as the energy decreases below this value. Such accuracy with experiment at small angles would account for the good total cross section values. Agreement with experiment is improved in the DWPO II model though not so dramatically as in case of atomic hydrogen or the alkali atoms; this is probably because helium has such a relatively small polarizability.

Nevertheless, for $L = S$ in process (2), it has been shown that allowing explicitly for polarization effects in the T-matrix element, as well as in calculating the distorted wave, yields excellent agreement with experiment at 200 eV for small scattering angles; whereas models which omit polarization effects, such as the First Born approximation, do not provide such a satisfactory description.

Generally, the DWPO approximation yields a reasonable profile for the cross section at lower energies, improving with increasing energy at small angles while at the same time becoming less comparable with experiment at larger angles. The explicit inclusion of polarization effects in the direct and exchange terms of the T-matrix element reduces further the cross section for large-angle scattering. It is this large-angle region where theoretical models which also allow for distortion in the final channel produce substantially better results. Hence, it is concluded that such final channel effects are important for accurately describing large-angle scattering.

The predictions of λ and χ allow no firm conclusions to be drawn, except that distorted wave treatments predict λ more accurately than χ; the latter is most accurately calculated in a multichannel eikonal treatment.

Finally, in connection with the spin-exchange processes (3), the DWPO approximation is considerably less successful, especially for the process where the total orbital angular momentum symbol remains unchanged. A discussion of differential scattering for this case, $L = S$, has already been given in §6.3; surprisingly, allowance for exchange-polarization effects did little to improve the situation. One concludes that much work remains to be done in order to achieve a complete understanding of such simple rearrangement collisions.

Concerning the DWPO approximation in general, recent work using a hybrid method to study process (1) and discussed in §6.1, shows that the DWPO approximation to the lower order partial waves is less accurate than for the higher order waves. A 12% difference between total integrated cross sections for excitation of $H(2p)$ at an impact energy of 0.86 Rydbergs is obtained when the close-coupling pseudostate expansion includes partial waves for $0 \leq L \leq 2$ rather than $0 \leq L \leq 3$. In the forward direction, the corresponding total differential cross section is reduced by almost 50%. However, DWPO calculations of total cross sections for inelastic electron scattering off positive ions, where the $\ell = 0$ contribution is relatively less than for the neutral atom, show that the DWPO approximation treats the higher partial waves (classically, the larger impact parameters) very well.

Further extensions of the DWPO approximation would be to treat the exchange term of the T-matrix element to second-order and to allow for distortion in the final channel. Work in this direction has already commenced in connection with excitation of $H(1s \rightarrow 2s)$.

APPENDIX A

Atomic Wave Functions

When dealing with atoms which possess more than one bound electron, exact analytic wave functions are no longer available so that consequently it is necessary to choose suitable approximate functions. For helium, however, such functions have been determined to a high degree of accuracy. This appendix will be concerned with the forms employed to represent the wave functions for (i) the initial (ground) state and (ii) the final (excited) state.

(i) Ground (1^1S) State

$$\phi_i(12) = \phi_{1s}(1)\,\phi_{1s}(2)$$

where

$$\phi_{1s}(\underline{r}) = R_{1s}(r)\,Y_{oo}(\hat{r})\ .$$

$R_{1s}(r)$ is chosen to be the simple Hartree-Fock wave function of Green et al. (1954) which is expressed as

$$R_{1s}(r) = N_1(e^{-ar} + c_1 e^{-br})\ . \qquad \text{(A.1a)}$$

The parameters a, b, c_1 and the normalization constant N_1 have the values

$$a = 1.4558, \quad b = 2a, \quad c_1 = 0.6 \quad \text{and} \quad N_1 = 2.968468. \qquad \text{(A.1b)}$$

Polarization Term:

For convenience, $\phi_{pol}(\underline{r},\underline{t})$, the first-order perturbation correction to $\phi_{1s}(\underline{r})$ due to dipole polarization, will also be summarized under this heading:

$$\phi_{pol}(\underline{r},\underline{t}) = -\frac{\varepsilon(r,t)}{t^2}\cdot\frac{u_{1s\to p}(r)}{r}\cdot\frac{P_1(\cos\theta_{rt})}{\sqrt{\pi}}$$

with

$$u_{1s\to p}(r) = Z_o^{-3/2}\, re^{-Z_o r}\,(Z_o r + \tfrac{1}{2} Z_o^2 r^2)\ . \qquad \text{(A.2a)}$$

If the radial component of $\phi_{1s}(r)$ is given by (A.1) it is found that, to ensure the direct polarization potential has the correct asymptotic behaviour, Z_o has for helium the value

$$Z_o = 1.598960 \qquad \text{(A.2b)}$$

and for hydrogen the value

$$Z_o = 1 \ . \qquad \text{(A.2c)}$$

(ii) Excited ($n^{1,3}L$) State

$$\phi_f^{\pm}(12) = \frac{1}{\sqrt{2}} \left[u_{1s}(1)\ v_{n\ell}^{\pm}(2) \pm v_{n\ell}^{\pm}(1)\ u_{1s}(2) \right]$$

where

$$u_{1s}(\underline{r}) = w(r)\ Y_{oo}(\hat{r}); \quad v_{n\ell}^{\pm}(\underline{r}) = R_{n\ \ell}^{\pm}(r)\ Y_{\ell m}(\hat{r}) .$$

The plus sign refers to singlet states and the minus sign to triplet states. The function $w(r)$ is taken throughout to have the hydrogenic form

$$w(r) = 2Z^{3/2}\ e^{-Zr} \qquad \text{(A.3)}$$

where Z denotes the nuclear charge. $R_{n\ell}^{\pm}(r)$ is given below depending on the value of L(L = S or P) and the spin (singlet or triplet) of the excited state. Essentially $R_{n\ell}^{\pm}(r)$ is represented by two different types of function, namely (a) the simple Hartree-Fock wave function and (b) the "frozen-core" Hartree-Fock wave function of Cohen and McEachran (1967a,b). Details of the appropriate functions are presented under the headings (a) and (b) respectively and further references quoted accordingly.

The latter wave function has the basic form of an expansion in a series of associated Laguerre functions:

$$R_{n\ell}^{\pm}(r) = \sum_{j=2\ell+1}^{N} a_j\ e^{-\alpha r}\ r^{\ell}\ L_j^{2\ell+1}(2\alpha r) \qquad \text{(A.4)}$$

where $\alpha = Z/n$ and the coefficients a_j are appropriately tabulated up to some value $j = N$. The Laguerre polynomials $L_j^{k}(x)$ are defined by the formula

$$L_j^{k}(x) = \frac{d^k}{dx^k} \left[e^x \frac{d^j}{dx^j} \left(e^{-x} x^j \right) \right] .$$

S-States:

(a) $n = 2$

$$R_{2s}^{\pm}(r) = N_2 (e^{-pr} - c_2 r\ e^{-qr}) \qquad \text{(A.5a)}$$

The values assigned to the parameters of $R^{+}_{2s}(r)$ are taken to be those given by Byron and Joachain (1975);

$$p = 0.865, \quad q = 0.522, \quad c_2 = 0.432784 \quad \text{and} \quad N_2 = 0.61928. \qquad (A.5b)$$

For $R^{-}_{2s}(r)$, the parameters are obtained from the paper by Morse et al. (1935);

$$p = 1.57, \quad q = 0.61, \quad c_2 = 0.34081 \quad \text{and} \quad N_2 = 1.05. \qquad (A.5c)$$

(b) $n = 2 - 5$

The appropriate Cohen and McEachran function is determined by putting $\ell = 0$ in (A.4). The coefficients a_j, which were used, are those tabulated by Crothers and McEachran (1970).

In connection with all the above functions for the S-states, it is emphasised that the $R^{\pm}_{ns}(r)$ are forced to be orthonormal to $R_{1s}(r)$ using the following transformation on the former function:

$$R^{\pm}_{ns}(r) \rightarrow \{R^{\pm}_{ns}(r) - A\, R_{1s}(r)\}/\sqrt{(1-A^2)} \qquad (A.6)$$

where

$$A = \int_0^{\infty} R_{1s}(r)\, R^{\pm}_{ns}(r)\, r^2\, dr.$$

$R_{1s}(r)$ and $R^{\pm}_{ns}(r)$ are assumed to be individually normalized before applying the transformation (A.6).

P-States:

(a) $n = 2$

$$R^{\pm}_{2p}(r) = N_2\, r\, e^{-pr} \qquad (A.7a)$$

The normalization constant is trivially given by $N_2 = 2p^{5/2}/\sqrt{3}$. The parameter p is taken for both singlet and triplet functions from Morse et al. (1935).

For $R^{+}_{2p}(r)$:

$$p = 0.485. \qquad (A.7b)$$

For $R^{-}_{2p}(r)$:

$$p = 0.55. \qquad (A.7c)$$

(a) $n = 3$

$$R^{+}_{3p}(r) = N_3\, r\, (e^{-pr} - c_3\, r\, e^{-qr}) \qquad \text{(A.8a)}$$

The parameters are obtained from the paper by Goldberg and Clogston (1939);

$$p = 0.325,\quad q = 0.325,\quad c_3 = 0.162939 \quad \text{and} \quad N_3 = 0.113034. \qquad \text{(A.8b)}$$

(b) $n = 2 - 5$

The appropriate Cohen and McEachran function is obtained by putting $\ell = 1$ in (A.4). The coefficients a_j are tabulated by McEachran and Cohen (1969). However, for the case $n = 5$, the a_j are modified as follows.

Let f_k denote the generalized oscillator strength (see equation (1.2.13)) at some 20 momentum-transfer values K and computed using the wave functions $R_{1s}(r)$ and $R_{5p}(r)$ as given above. Let g_k denote the corresponding generalized oscillator strength tabulated by Bell et al. (1968) at the 20 values of K in their table 1. These authors employ a more sophisticated wave function for $\phi_i(12)$ than that given above. The quantity

$$\sum_{k=1}^{20} |f_k - g_k|^2$$

is then formulated and minimized with respect to the a_j. The modified a_j are found to be

$$\begin{aligned} a_3 &= 1.0 & a_7 &= 1.4438,-4 \\ a_4 &= 4.5694,-1 & a_8 &= -8.3183,-5 \\ a_5 &= 1.1351,-2 & a_9 &= 7.9979,-6 \\ a_6 &= -1.7240,-4 & a_{10} &= -2.5054,-7 \end{aligned} \qquad \text{(A.9)}$$

where ,n denotes multiplication by 10^n, whereas the original Cohen and McEachran coefficents were,

$$\begin{aligned} a_3 &= 1.0 & a_7 &= -\ 1.0793,-4 \\ a_4 &= 3.8579,-1 & a_8 &= \ \ 5.0251,-5 \\ a_5 &= 3.8271,-2 & a_9 &= -\ 5.4226,-6 \\ a_6 &= -4.5652,-3 & a_{10} &= \ \ 3.7851,-7. \end{aligned}$$

APPENDIX B

Power Series Expansions for the Direct Potentials

$V_{ls,ls}(r)$:

$$2V_{ls,ls}(r) = -2Z/r - (a_o - a_2r^2 + a_3r^3 - a_4r^4 + a_5r^5 - a_6r^6 + a_7r^7 - \ldots) \tag{B.1a}$$

where the coefficients a_n are given by the general formula

$$a_n = 4N_1^2\left[(2a)^{n-2} + 2c_1(a+b)^{n-2} + c_1^2(2b)^{n-2}\right]|n-1|/(n+1)! \tag{B.1b}$$

The parameters on the right hand side are given in (A.1b).

$V_{pol}(r)$:

$$2V_{pol}(r) = -4(b_1r + b_2r^2 + b_3r^3 + b_4r^4 + b_5r^5 + b_6r^6 + b_7r^7 + \ldots)/3 \tag{B.2a}$$

where the coefficients b_n are given by the general formula

$$b_n = \frac{N_1}{\sqrt{Z_o}}\left[\left(\frac{p_1}{n+4} - \frac{Z_o}{Z_1}\right)\frac{Z_1^{n-1}}{(n-1)!} + c_1\left(\frac{p_2}{n+4} - \frac{Z_o}{Z_2}\right)\frac{Z_2^{n-1}}{(n-1)!}\right]. \tag{B.2b}$$

The notation of equation (3.2.5) has been adopted. The parameters a, b, c_1 and N_1 are given in (A1.b) and Z_o in (A.2).

APPENDIX C

Analytic Expressions for Various Integrals

The integrals appearing below are all evaluated by elementary methods so that only the final result will be presented. Notation follows exactly that in Appendix A.

B:

$$B = \int_0^\infty w(r)\, R_{1s}(r)\, r^2\, dr$$

$$= 4\, N_1\, Z^{3/2}\left[\, 1/(Z+a)^3 + c_1/(Z+b)^3 \,\right]. \qquad (C.1)$$

$f_{1s,w}(r)$:

$$f_{1s,w}(r) = r\int_0^\infty w(t)\, R_{1s}(t)\, \gamma_o(r,t)\, t^2\, dt$$

$$= B - 2Z^{3/2}\, N_1\left[\left\{r + \frac{2}{Z+a}\right\}\frac{e^{-(Z+a)r}}{(Z+a)^2} + c_1\left\{r + \frac{2}{Z+b}\right\}\frac{e^{-(Z+b)r}}{(Z+b)^2}\right] \qquad (C.2)$$

with B as in (C.1).

$f_{1s,ns}(r)$:

$$f_{1s,ns}(r) = r\int_0^\infty R_{1s}(t)\, R_{ns}(t)\, t^2\, dt$$

This is evaluated for the case $n = 2$ only. Further, $R_{ns}(r)$ will be taken to be defined by (A.5) and will, of course, be subjected to the modification (A.6) to ensure orthogonality to $R_{1s}(r)$.

$$f_{1s,2s}(r) = -\frac{N_1}{\sqrt{(1-A^2)}}\left[N_2\left\{\left[r + \frac{2}{u}\right]\frac{e^{-ur}}{u^2} + c_1\left[r + \frac{2}{v}\right]\frac{e^{-vr}}{v^2} - c_2\left[r^2 + \frac{4r}{w} + \frac{6}{w^2}\right]\frac{e^{-wr}}{w^2}\right.\right.$$

$$\left. - c_1c_2\left[r^2 + \frac{4r}{x} + \frac{6}{x^2}\right]\frac{e^{-xr}}{x^2}\right\} - AN_1\left\{\left[r + \frac{2}{2a}\right]\frac{e^{-2ar}}{(2a)^2} + 2c_1\left[r + \frac{2}{a+b}\right]\frac{e^{-(a+b)r}}{(a+b)^2} +\right.$$

$$\left.\left. c_1^2\left[r + \frac{2}{2b}\right]\frac{e^{-2br}}{(2b)^2}\right\}\right] \qquad (C.3)$$

where

$$A = \int_0^\infty R_{1s}(r)\, R_{2s}(r)\, r^2\, dr$$

$$= N_1 N_2 \left[\frac{2}{u^3} + \frac{2c_1}{v^3} - \frac{6c_2}{w^3} - \frac{6c_1c_2}{x^3} \right] \qquad (C.4)$$

and $u = a + p$, $v = b + p$, $w = a + q$, $x = b + q$.

$\underline{g^{(1)}_{ls,\ell}(r)}$:

$$g^{(1)}_{ls,\ell}(r) = \frac{1}{r^\ell} \int_0^r R_{ls}(t)\, H_\ell(k_f t)\, t^{\ell+2}\, dt$$

This is evaluated only for small r. The function $R_{ls}(r)$ assumes the form indicated in (A.1). $H_\ell(k_f r)$ is a regular Coulomb function and by writing $x = k_f r$ may be expressed using results from Abramowitz and Stegun (1970) as

$$H_\ell(x) = c_\ell(\eta)\, x^\ell \sum_{k=0}^{\infty} A_k(\eta)\, x^k. \qquad (C.5)$$

Here, $\eta = -\frac{z}{k_f}$ with z the residual charge given by $z = Z - N$; Z denotes the nuclear charge and N the number of bound electrons. The normalization factor $c_\ell(\eta)$ is defined by

$$c_\ell(\eta) = 2^\ell\, e^{-\pi\eta/2}\, \frac{|\Gamma(\ell+1+i\eta)|}{(2\ell+1)!}$$

and the coefficients A_k by:

$$A_o(\eta) = 1; \quad A_1(\eta) = \frac{\eta}{\ell+1}; \quad A_k(\eta) = \frac{2\eta A_{k-1}(\eta) - A_{k-2}(\eta)}{k(k + 2\ell + 1)}, \; k \geq 2.$$

Then the required series expansion of $g^{(1)}_{ls,\ell}(r)$ is derived to be

$$g^{(1)}_{ls,\ell}(r) = N_1\, c_\ell(\eta)\, k_f^\ell\, r^{\ell+3} \sum_{n=0}^{n_{max}} \frac{[a_n(a) + c_1 a_n(b)]\, r^n}{2\ell + 3 + n} \qquad (C.6)$$

where:

$$a_n(\alpha) = \sum_{m=0}^{n} A_m \frac{(-\alpha)^{n-m}}{(n-m)!}\, k_f^m .$$

In practice, n_{max} is typically set to $n_{max} = 5$.

$\underline{k_{ls,ns}(r)}$:

$$k_{ls,ns}(r) = -\frac{1}{r^3} \int_0^r u_{ls\to p}(t)\, R_{ns}(t)\, t^2\, dt$$

The comments made in connection with $R_{ns}(t)$ in the above evaluation of

$f_{1s,ns}(r)$ also apply to the evaluation of $k_{1s,ns}(r)$. The case $n = 2$ only is considered.

$$k_{1s,2s}(r) = -\frac{1}{r^3} \cdot \frac{Z_o^{-\frac{1}{2}}}{\sqrt{(1-A^2)}} \left[N_2 \left\{ F_1(u,r) + \frac{Z_o}{2} F_2(u,r) - c_2 F_2(v,r) - c_2 \frac{Z_o}{2} F_3(v,r) \right\} \right.$$

$$\left. - AN_1 \left\{ F_1(w,r) + \frac{Z_o}{2} F_2(w,r) + c_1 F_1(x,r) + c_1 \frac{Z_o}{2} F_2(x,r) \right\} \right] \qquad (C.7)$$

where, writing $\beta = \alpha r$,

$$F_1(\alpha,r) = [24 - (\beta^4 + 4\beta^3 + 12\beta^2 + 24\beta + 24)e^{-\beta}]/\alpha^5,$$

$$F_2(\alpha,r) = [120 - (\beta^5 + 5\beta^4 + 20\beta^3 + 60\beta^2 + 120\beta + 120)e^{-\beta}]/\alpha^6, \qquad (C8a)$$

$$F_3(\alpha,r) = [720 - (\beta^6 + 6\beta^5 + 30\beta^4 + 120\beta^3 + 360\beta^2 + 720\beta + 720)e^{-\beta}]/\alpha^7.$$

Here, one has that $u = Z_o + p$, $v = Z_o + q$, $w = Z_o + a$, $x = Z_o + b$. A, however, is as above in (C.4).

For small r, the $F_i(\alpha,r)$ $(i = 1,2,3)$ may be written

$$F_1(\alpha,r) = \left[\frac{\beta^5}{5} - \frac{\beta^6}{6} + \frac{\beta^7}{14} - \frac{\beta^8}{48} + \frac{\beta^9}{216} \cdots\right]\frac{1}{\alpha^5},$$

$$F_2(\alpha,r) = \left[\frac{\beta^6}{6} - \frac{\beta^7}{7} + \frac{\beta^8}{16} - \frac{2\beta^9}{3} + \cdots\right]\frac{1}{\alpha^6}, \qquad (C.8b)$$

$$F_3(\alpha,r) = \left[\frac{\beta^7}{7} - \frac{\beta^8}{8} + \frac{\beta^9}{18} \cdots\right]\frac{1}{\alpha^7}.$$

Apart from a factor of r^{-1}, the definition adopted here for $k_{1s,ns}(r)$ agrees with that of McDowell et al. (1974). Further, as a check, if the expressions in (C.8b) are inserted into (C.7) and the appropriate hydrogenic substitutions made for a, b, c_1, N_1 and Z_o together with of course $A = 0$, the result is found to correspond exactly with equation (10') of McDowell et al. (1974).

$f_{1s,np}(r)$:

$$f_{1s,np}(r) = r \int_0^\infty R_{1s}(t)\, R_{np}(t)\, \gamma_1(r,t)\, t^2\, dt$$

This integral is expressed for the cases $n = 2,3$ with $R_{np}(r)$ given by equations (A.7) and (A.8). The expression for $n = 3$ only is presented;

that for $n = 2$ may easily be deduced by setting $c_3 = 0$ and replacing N_3 by N_2 together with the appropriate choice for the parameter p.

$$f_{1s,np}(r) = \frac{N_1 N_3}{r}\left[G_1(u,r) + c_1\, G_1(v,r) - c_3 G_2(w,r) - c_1 c_3 G_2(x,r)\right] \qquad (C.9)$$

where, putting $\beta = \alpha r$,

$$G_1(\alpha,r) = [24 - (3\beta^3 + 12\beta^2 + 24\beta + 24)e^{-\beta}]/\alpha^5 ,$$
$$G_2(\alpha,r) = [120 - (3\beta^4 + 18\beta^3 + 60\beta^2 + 120\beta + 120)e^{-\beta}]/\alpha^6 . \qquad (C.10a)$$

Here, one has that $u = a + p$, $v = b + p$, $w = a + q$, $x = b + q$. For small r, $G_1(\alpha,r)$ and $G_2(\alpha,r)$ may be written

$$G_1(\alpha,r) = \left[\beta^3 - \frac{3\beta^5}{10} + \frac{\beta^6}{6} - \frac{3\beta^7}{56} + \ldots\right]\frac{1}{\alpha^5} ,$$
$$G_2(\alpha,r) = \left[2\beta^3 - \frac{\beta^6}{6} + \frac{9\beta^7}{84} - \ldots\right]\frac{1}{\alpha^6} . \qquad (C.10b)$$

$t_{1s,np}(r)$:

$$t_{1s,np}(r) = -\frac{4}{5r^4}\int_o^r u_{1s\to p}(t)\, R_{np}(t)\, t^3\, dt$$

This is presented for $n = 2,3$ only. The comments made above concerning the evaluation of $f_{1s,np}(r)$ also apply directly to the evaluation of $t_{1s,np}(r)$.

$$t_{1s,np}(r) = \frac{-4}{5r^4}\cdot\frac{N_3}{\sqrt{Z_o}}\left[\frac{1}{u^7}\left\{\left[1 + \frac{7Z_o}{2u}\right][720 - (x^6 + 6x^5 + 30x^4 + 120x^3 + 360x^2 + \right.\right.$$
$$+720x + 720)\, e^{-x}] - \frac{Z_o}{2u}\, x^7 e^{-x}\Big\} - \frac{c_3}{v^8}\Big\{\Big[1 + \frac{8Z_o}{2v}\Big][5040 - (y^7 + 7y^6 + 42y^5 \qquad (C.11a)$$
$$\left.\left. + 210y^4 + 840y^3 + 2520y^2 + 5040y + 5040)e^{-y}] - \frac{Z_o}{2v}\, y^8\, e^{-y}\Big\}\right]$$

where $u = Z_o + p$, $v = Z_o + q$; $x = ur$, $y = vr$.

For small r, $t_{1s,np}(r)$ is written as

$$t_{1s,np}(r) = -\frac{4}{5}\frac{N_3}{\sqrt{Z_o}}\left[r^3(1 + \frac{7Z_o}{2u})(a_o + a_1 x + a_2 x^2 + a_3 x^3 + a_4 x^4 + a_5 x^5 + \ldots)\right.$$

$$- c_3 r^4 \left(1 + \frac{8Z_o}{2v}\right)(b_o + b_1 y + b_2 y^2 + b_3 y^3 + b_4 y^4 + \ldots) \Big] \qquad \text{(C.11b)}$$

where

$$a_m = \frac{(-1)^m}{m!} \cdot \frac{2u - mZ_o}{(m+7)(2u+7Z_o)} ,$$

$$b_m = \frac{(-1)^m}{m!} \cdot \frac{2v - mZ_o}{(m+8)(2v+8Z_o)} .$$

Equations (C.11) may be checked against equations (29) and (30) of McDowell et al. (1975a) by making the appropriate substitutions mentioned after equation (C.8b). To within a misprint of $\sqrt{Z}$, exact agreement is obtained in each case.

$t^{\ell,\lambda}_{ls\to p}(r)$:

$$t^{\ell,\lambda}_{ls\to p}(r) = \int_0^r u_{ls\to p}(t)\, H_\ell(k_f t)\, t^{\lambda+1}\, dt$$

This is evaluated only for small r. The function $u_{ls\to p}(r)$ assumes the form given in (A.2a) with $Z_o = 1.598960$ for helium as in (A.2b) and with $Z_o = 1$ for hydrogen as in (A.2c). $H_\ell(k_f r)$ is a regular Coulomb function and expressed according to the series in (C.5). Hence one finds that, writing $x = k_f r$,

$$t^{\ell,\lambda}_{ls\to p}(r) = \frac{c_\ell(\eta)}{\sqrt{Z_o}}\; x^\ell\, r^{\lambda+4} \left[\sum_{n=0}^{\infty} \frac{a_n x^n}{\ell+\lambda+n+4} + \frac{Z_o}{2k_f} \sum_{n=1}^{\infty} \frac{a_{n-1} x^n}{\ell+\lambda+n+4} \right]$$

where:

$$a_n = \sum_{m=0}^{n} A_m \frac{(-\alpha)^{n-m}}{(n-m)!} , \quad \alpha = \frac{Z_o}{k_f} .$$

By defining

$$b_n = \frac{k_f^n}{2(\ell+\lambda+n+4)} \sum_{m=0}^{n} (m+2-n) \frac{(-\alpha)^{n-m}}{(n-m)!} A_m$$

the final result may be written as

$$t^{\ell,\lambda}_{ls\to p}(r) = \frac{c_\ell(\eta)}{\sqrt{Z_o}}\; (k_f r)^\ell\, r^{\lambda+4} \sum_{n=0}^{n_{max}} b_n r^n . \qquad \text{(C.12)}$$

Typically $n_{max} = 5$ in practice.

$d_2(k_f)$:

$$d_2(k_f) = \int_o^\infty R_{ls}(r)\, H_o(k_f r)\, f_{ls,w}(r)\, r\, dr$$

For helium, $H_o(k_f r) = j_o(k_f r)$ where $j_o(x)$ is a spherical Bessel function of the first kind:

$$j_o(x) = \frac{\sin x}{x} .$$

Using (A.1) for $R_{ls}(r)$ and (C.2) for $f_{ls,w}(r)$ one has that

$$d_2(k_f) = 4Z^{3/2} N_1^2 \left[\left[\frac{1}{s^3} + \frac{c_1}{t^3} \right] \left[\frac{1}{a^2+k_f^2} + \frac{c_1}{b^2+k_f^2} \right] \right.$$

$$- \frac{1}{s^3(u^2+k_f^2)} \left[1 + \frac{us}{u^2+k_f^2} \right] - \frac{c_1}{s^3(v^2+k_f^2)} \left[1 + \frac{vs}{v^2+k_f^2} \right]$$

$$\left. - \frac{c_1}{t^3(w^2+k_f^2)} \left[1 + \frac{wt}{w^2+k_f^2} \right] - \frac{c_1^2}{t^3(x^2+k_f^2)} \left[1 + \frac{xt}{x^2+k_f^2} \right] \right] \qquad (C.13)$$

where $s = Z + a$, $t = Z + b$; $u = s + a$, $v = s + b$, $w = t + a$, $x = t + b$.

<u>$d_3(k_f)$:</u>

$$d_3(k_f) = \int_o^\infty R_{ls}(r)\, H_o(k_f r)\, r\, dr$$

As in the evaluation of $d_2(k_f)$ in equation (C.13) above, $H_o(k_f r)$ is replaced by a zero-order spherical Bessel function. Hence, with (A.1) for $R_{ls}(r)$, one easily finds that

$$d_3(k_f) = N_1 \left[\frac{1}{a^2+k_f^2} + \frac{c_1}{b^2+k_f^2} \right] . \qquad (C.14)$$

APPENDIX D

The Born T-Matrix Elements and Total Cross Sections

Only the cases for $n = 3$ are considered in detail; corresponding expressions for $n = 2$ may subsequently be easily deduced. The atomic wave functions are collected together for convenience:

$$\phi_{1s}(r) = R_{1s}(r)\, Y_{oo}(\hat{r})$$

$$\phi_{pol}(\underline{r},\underline{t}) = -\frac{\varepsilon(r,t)}{t^2} \cdot \frac{u_{1s\to p}(r)}{r} \cdot \frac{P_1(\cos\theta_{rt})}{\sqrt{\pi}}$$

$$\phi_f(\underline{r},\underline{t}) = \frac{1}{\sqrt{2}}\left[w(r)\, Y_{oo}(\hat{r})\, R_{np}(t)\, Y_{1m}(\hat{t}) + R_{np}(r)\, Y_{1m}(\hat{r})\, w(t)\, Y_{oo}(\hat{t})\right]$$

The radial functions are given by: (A.1) for $R_{1s}(r)$, (A.2) for $u_{1s\to p}(r)$, (A.3) for $w(r)$ and (A.8) for $R_{3p}(r)$. $n = 2$ results are obtained by setting $c_3 = 0$, together with replacing N_3 by N_2 and inserting the appropriate value for p as indicated in (A.7) for $R_{2p}(r)$.

The interaction term is defined as

$$V_f = -\frac{2}{r_3} + \frac{1}{r_{13}} + \frac{1}{r_{23}} \quad .$$

Let $\underline{K}$ denote the momentum transfer vector

$$\underline{K} = \underline{k}_i - \underline{k}_f \quad .$$

The above expressions are defined in a frame of reference where the z-axis is along $\underline{k}_i$ and the xz plane defined as the plane containing $\underline{K}$ and $\underline{k}_i$. The axis of quantization for the atomic states is hence taken along $\underline{k}_i$. The angle between $\underline{K}$ and $\underline{k}_i$ will be denoted by β and is given by

$$\cos\beta = \frac{K^2 + k_i^2 - k_f^2}{2k_iK} \quad . \tag{D.1}$$

The plane wave $e^{i\underline{K}\cdot\underline{r}}$ can then be expressed as

$$e^{i\underline{K}\cdot\underline{r}} = 4\pi \sum_{\lambda=0}^{\infty} \sum_{\mu=-\lambda}^{\lambda} i^{\lambda}\, j_{\lambda}(Kr)\, Y_{\lambda\mu}(\hat{r})\, Y_{\lambda\mu}(\beta,0) \tag{D.2}$$

where $\hat{r}$ is the direction of $\underline{r}$ with respect to $\underline{k}_i$ and $j_\ell(x)$ is a spherical Bessel function of the first kind (see, for example, Abramowitz and Stegun (1970) §10)

$T_{if}^{B}(m)$:

$$T_{if}^{B}(m) = \langle \phi_f(12) e^{i\underline{k}_f \cdot \underline{r}_3} V_f \phi_{1s}(1) \phi_{1s}(2) e^{i\underline{k}_i \cdot \underline{r}_2} \rangle$$

Making use of the orthogonality relationship between atomic wave functions and also the symmetry exhibited by electrons 1 and 2, $T_{if}^{B}(m)$ reduces to

$$T_{if}^{B}(m) = \frac{2}{\sqrt{2}} \int \phi_f(12) \frac{e^{i\underline{K} \cdot \underline{r}_3}}{r_{13}} \phi_{1s}(1) \phi_{1s}(2) \, d\underline{r}_{123} \, . \qquad (D.3)$$

This is further simplified with the aid of the well known result

$$\int \frac{e^{i\underline{K} \cdot \underline{r}}}{|\underline{r}-\underline{t}|} d\underline{r} = \frac{4\pi}{K^2} e^{i\underline{K} \cdot \underline{t}} \qquad (D.4)$$

which is often referred to as Bethe's Integral. Hence effecting the integration over $\underline{r}_3$ with the help of (D.4), and inserting the appropriate substitutions,

$$T_{if}^{B}(m) = B\sqrt{2} \frac{4\pi}{K^2} \int R_{1s}(r) R_{np}(r) Y_{oo}(\hat{r}) Y_{1m}^{*}(\hat{r}) e^{i\underline{K} \cdot \underline{r}} d\underline{r} \, . \qquad (D.5)$$

B is defined by (C.1). The plane wave expansion (D.2) is now made and the angular integration carried out to yield

$$T_{if}^{B}(m) = i \, B\sqrt{2} \frac{(4\pi)^{3/2}}{K^2} \int_o^\infty R_{1s}(r) R_{np}(r) j_1(Kr) r^2 dr \, Y_{1m}(\beta,0) \qquad (D.6)$$

The analytic expressions for the radial functions are then inserted, noting that,

$$j_1(x) = (\sin x - x \cos x)/x^2 \qquad (D.7)$$

and the resulting elementary integral evaluated. Hence the required expression for $T_{if}^{B}(m)$ is

$$T_{if}^{B}(m) = i \, 2^{7/2} \, B \frac{(4\pi)^{3/2}}{K} N_1 N_3 \left[\left\{ \frac{u}{(u^2+K^2)^3} + \frac{c_1 v}{(v^2+K^2)^3} \right\} - c_3 \left\{ \frac{5w^2-K^2}{(w^2+K^2)^4} + \frac{c_1(5x^2-K^2)}{(x^2+K^2)^4} \right\} \right] Y_{1m}(\beta,0) \qquad (D.8)$$

with $u = a + p$, $v = b + p$, $w = a + q$, $x = b + q$.

$T_{if}^{PB}(m)$:

$$T_{if}^{PB}(m) = 2\langle\phi_f(12)e^{i\underline{k}_f\cdot\underline{r}_3}\, V_f\, \phi_{1s}(1)\, \phi_{pol}(23)\, e^{i\underline{k}_i\cdot\underline{r}_3}\rangle$$

Substituting for the atomic wave functions in terms of their radial and angular components and employing orthogonality of the spherical harmonics, one finds

$$T_{if}^{PB}(m) = -\frac{2}{(2\pi)^{\frac{1}{2}}}\left[P + Q\right] \qquad (D.9)$$

where:

$$P = \frac{1}{4\pi}\int w(r_1)\, R_{np}(r_2)\, Y_{1m}^{*}(r_2)\, e^{i\underline{K}\cdot\underline{r}_3}\left(\frac{1}{r_{23}} - \frac{1}{r_3}\right) R_{1s}(1)\frac{\varepsilon(23)}{r_3^2}\frac{u_{1s\to p}(r_2)}{r_2} P_1(\cos\theta_{23})\,d\underline{r}_{123}$$

$$Q = \frac{1}{4\pi}\int w(r_1)\, R_{np}(r_2)\, Y_{1m}^{*}(\hat{r}_2)\, e^{i\underline{K}\cdot\underline{r}_3}\left(\frac{1}{r_{13}} - \frac{1}{r_3}\right) R_{1s}(1)\,\frac{\varepsilon(23)}{r_3^2}\frac{u_{1s\to p}(r_2)}{r_2} P_1(\cos\theta_{23})\,d\underline{r}_{123}$$

The integrals P and Q are considered in turn. Concerning P, the integration over $\underline{r}_1$ is separable and gives the result defined as B (viz. equation (C.1)). Using the spherical harmonic addition theorem to express $P_1(\cos\theta_{23})$ in terms of spherical harmonics and using also the well known multipole expansion on $\frac{1}{r_{23}}$, integration over $\underline{r}_2$ gives the result that

$$P = \frac{4\pi B}{3}\sum_{\nu=-1}^{1}\int \frac{e^{i\underline{K}\cdot\underline{r}}}{r^2} F_{npm}(r)\, Y_{1\nu}(\hat{r})\, d\underline{r}$$

with:

$$F_{npm}(r) = 3\sum_{\lambda\neq 0}^{\infty}\sum_{\mu=-\lambda}^{\lambda}\sqrt{\frac{4\pi}{2\lambda+1}}\, Y_{\lambda\mu}(\hat{r})\int_0^r R_{np}(t)\, u_{1s\to p}(t)\left(\frac{t}{r}\right)^{\lambda+1} dt$$

$$\begin{pmatrix}1 & \lambda & 1\\ 0 & 0 & 0\end{pmatrix}\begin{pmatrix}1 & \lambda & 1\\ m & \mu & \nu\end{pmatrix}.$$

The Wigner 3-j symbols arise from the integration over three spherical haromonics. The expansion (D.2) is now employed for $e^{i\underline{K}\cdot\underline{r}}$ and the angular integration over $\hat{r}$ performed:

$$P = \frac{(4\pi)^2}{3}\, B\sum_{\lambda\neq 0}^{\infty}\sum_{\lambda'=0}^{\infty}\sum_{\mu'=-\lambda'}^{\lambda} i^{\lambda'} Y_{\lambda'\mu'}(\beta,0)\,\sqrt{3(2\lambda'+1)}\int_0^{\infty} j_{\lambda'}(Kr)\left(\int_0^r R_{np}(t)u_{1s\to p}(t)\left(\frac{t}{r}\right)^{\lambda+1} dt\right) dr$$

$$\begin{pmatrix} 1 & \lambda & 1 \\ 0 & 0 & 0 \end{pmatrix} \begin{pmatrix} \lambda' & \lambda & 1 \\ 0 & 0 & 0 \end{pmatrix} \sum_{\nu=-1}^{1} \sum_{\mu=-\lambda}^{\lambda} 3 \begin{pmatrix} 1 & \lambda & 1 \\ m & \mu & \nu \end{pmatrix} \begin{pmatrix} \lambda' & \lambda & 1 \\ \mu' & \mu & \nu \end{pmatrix}.$$

At this point the orthogonality property satisfied by the Wigner 3-j symbols, given for example by Edmonds (1974, equation (3.7.7)), is introduced and consequently the sum over the latter two symbols reduced to $\delta_{\lambda' 1} \delta_{\mu' m}$. P then becomes a single infinite sum over λ. However, by applying the triangle inequality satisfied by the arguments appearing in the upper row of a 3-j symbol, one sees that $\lambda = 0$ or 2. Hence P reduces to a single term which on evaluating the remaining 3-j symbols gives the result

$$P = i(4\pi)^2 B \, Y_{1m}(\beta,0) \cdot \frac{2}{15} I_{np} \qquad (D.10)$$

where I_{np} is defined to be the radial integral

$$I_{np} = \int_0^\infty j_1(Kr) \frac{1}{r^3} \left(\int_0^r R_{np}(t) \, u_{ls \to p}(t) \, t^3 \, dt \right) dr . \qquad (D.11)$$

Attention is now focussed on the expression Q which will similarly be evaluated. This is relatively straightforward compared to the integral P above. Inserting the plane wave expansion (D.2), the appropriate multipole expansion for $\frac{1}{r_{13}}$ and expressing $P_1(\cos \theta_{23})$ in terms of spherical harmonics, it is seen that the angular integration can easily be performed using only orthogonality of the spherical harmonics. Consequently Q may be summarized as

$$Q = \frac{i(4\pi)^2}{3} Y_{1m}(\beta,0) \int_0^\infty j_1(Kr)[f_{ls,w}(r)-B] \left(\int_0^r R_{np}(t) \, u_{ls \to p}(t) t dt \right) dr \qquad (D.12)$$

following previous notation. See (C.1) and (C.2) for B and $f_{ls,w}(r)$ respectively. When analytic expressions are appropriately inserted for the radial functions appearing in (D.12), the subsequent integral is found to be virtually impossible to evaluate in closed form. Since $T_{if}^{PB}(m)$ is required to be available in closed form, it is consequently necessary to make some approximation in (D.12). For large r it is easily seen from (C.2) that

$$f_{ls,w}(r) \underset{r \to \infty}{\to} B . \qquad (D.13)$$

The approximation is hence made to replace $f_{ls,w}(r)$ by its asymptotic form for all r. Physically this amounts to neglecting the interaction of the core electron with the valence and scattering electrons, which in the present situation is considered to be a reasonable approximation. Hence one sees in fact that Q vanishes!

The evaluation of $T_{if}^{PB}(m)$ subsequently centres on the determination of I_{np} in (D.11). $T_{if}^{PB}(m)$ is written as

$$T_{if}^{PB}(m) = - i\ 4\ B\ \frac{\sqrt{2}}{15}\ (4\pi)^{3/2}\ Y_{1m}(\beta,0)\ I_{np}\ . \qquad (D.14)$$

Inserting the analytic expressions (A.2a) and (A.8a) for $u_{ls\to p}(r)$ and $R_{np}(r)$ respectively into the integral I_{np}, equation (D.14) becomes:

$$T_{if}^{PB}(m) = -i\ 4\ B\ \frac{\sqrt{2}}{15}\ (4\pi)^{3/2}\ Y_{1m}(\beta,0)\ .\sqrt{\frac{N_3}{Z_o}}\ \left[A_1(p)\ -c_3\ A_2(q)\right] \qquad (D.15)$$

where, writing $\gamma = \alpha + Z_o$,

$$A_1(\alpha) = \int_0^\infty \frac{j_1(Kr)}{r^3}\left(\int_0^r t^6 e^{-\gamma t}\ (1 + \frac{Z_o}{2}\ t)\ dt\right)\ dr\ , \qquad (D.16a)$$

$$A_2(\alpha) = \int_0^\infty \frac{j_1(Kr)}{r^3}\left(\int_0^r t^7\ e^{-\gamma t}\ (1 + \frac{Z_o}{2}\ t)\ dt\right)\ dr\ . \qquad (D.16b)$$

By observing the very close resemblance between (D.16a) and (D.16b) it is noted that the latter may be obtained from the former using the techniques of parametric differentiation under the integral sign, that is

$$A_2(\alpha) = - \frac{\partial}{\partial\gamma}\ A_1(\alpha)\ . \qquad (D.17)$$

Hence one seeks to evaluate $A_1(\alpha)$. Making the appropriate substitution for the spherical Bessel function given by (D.7), and putting $y = t/r$, (D.16a) can be written in the form,

$$A_1(\alpha) = \frac{1}{K^2}\int_0^1 y^6\left(\int_0^\infty (\sin Kr - Kr\cos Kr)(r^2 + \frac{Z_o}{2}\ yr^3)\ e^{-\gamma ry}dr\right)dy. \qquad (D.18)$$

The integral over r is performed with the help of integral results from the book by Gradshteyn and Ryzhik (1965, page 490 formulae 5 and 6). Thus

$$A_1(\alpha) = \frac{1}{K^2}\int_0^1 \frac{y^6}{[(\gamma y)^2+K^2]^{3/2}}\left[2\sin 3\theta - 6\sin\theta\cos 4\theta + \frac{3Z_o}{2\gamma}(2\cos\theta\sin 4\theta - 8\sin\theta\cos\theta\cos 5\theta)\right] dy \qquad (D.19)$$

where $\tan\theta = K/\gamma y$. At this point, one redefines the variable of integration to be ϕ where $\phi = 1/\theta$. After a certain amount of manipulation (D.19) takes the form

$$A_1(\alpha) = \frac{8K^2}{\gamma^7}\int_0^{\tan^{-1}\gamma/K} \frac{\sin^6\phi}{\cos^2\phi}\left[(6\sin^2\phi - 1) + \frac{3Z_o}{2\gamma}(16\sin^4\phi - 6\sin^2\phi)\right]d\phi. \qquad (D.20)$$

(D.20) can now be evaluated by using standard integral results for powers of trignometric functions and is consequently straightforward. The contribution arising from the lower limit of integration is then seen to vanish. For the contribution arising from the upper limit it is convenient to let

$$x = K/\gamma$$

so that the upper limit of ϕ is given by $\tan\phi = 1/x$. The resulting expression is then summarized as

$$A_1(\alpha) = \frac{8}{\gamma^5}\left[\left\{5x + \frac{x^3}{(1+x^2)^3} + \frac{5x^3}{2(1+x^2)^2} + \frac{25x^3}{4(1+x^2)} - \frac{45x^2}{4}\tan^{-1}\frac{1}{x}\right\}\right.$$

$$\left. + \frac{3Z_o}{2\gamma}\left\{10x + \frac{2x^3}{(1+x^2)^4} + \frac{4x^3}{(1+x^2)^3} + \frac{15x^3}{2(1+x^2)^2} + \frac{65x^3}{4(1+x^2)} - \frac{105x^2}{4}\tan^{-1}\frac{1}{x}\right\}\right] \qquad (D.21a)$$

The corresponding result for $A_2(\alpha)$ is obtained from (D.17). The differentiation is straightforward but laborious so that only the final result is presented.

$$A_2(\alpha) = \frac{24}{\gamma^6}\left[\left\{10x + \frac{2x^3}{(1+x^2)^4} + \frac{4x^3}{(1+x^2)^3} + \frac{15x^3}{2(1+x^2)^2} + \frac{65x^3}{4(1+x^2)} - \frac{105x^2}{4}\tan^{-1}\frac{1}{x}\right\}\right. \qquad (D.21b)$$

$$\left. + \frac{Z_o}{2\gamma}\left\{70x + \frac{16x^3}{(1+x^2)^5} + \frac{26x^3}{(1+x^2)^4} + \frac{42x^3}{(1+x^2)^3} + \frac{70x^3}{(1+x^2)^2} + \frac{140x^3}{(1+x^2)} - 210x^2\tan^{-1}\frac{1}{x}\right\}\right].$$

The required result for $T_{if}^{PB}(m)$ is then obtained by substituting from (D.21) the appropriate expressions into (D.15).

Due to the approximation based on line (D.13), the above evaluation of $T_{if}^{PB}(m)$ may be compared directly with the evaluation of the corresponding term, $T_D(PB)$, for excitation of the 2p state of atomic hydrogen, given by

McDowell et al. (1975b). Allowing for the appropriate external factor and atomic wave function parameters, the above expression derived for $T_{if}^{PB}(m)$ is seen to be in exact agreement with equation (19) of McDowell et al. for $T_D(PB)$.

The Total Cross Sections:

So far, analytic expressions in terms of K have been derived for $T_{if}^{B}(m)$ and $T_{if}^{PB}(m)$ as required by equations (3.4.43) and (3.4.44). The corresponding integral cross sections in the Born and Born plus Polarized-Born Approximation must now be considered in connection with equations (3.4.57-58). The following treatment is designed to be applicable to both approximations: hence, for generality, the T-matrix element will be denoted by T_m and the corresponding integral cross section by Q_m. Q will denote the total integrated cross section. $\delta Q_m(B)$ and $\delta Q_m(B+PB)$ are then obtained from the respective expressions for Q_m by replacing T_m by $T_{if}^{B}(m)$ and by $T_{if}^{B}(m) + T_{if}^{PB}(m)$ respectively.

The general expression for Q_m is given by

$$Q_m = \frac{1}{2\pi^2} \cdot \frac{k_f}{k_i} \int_{-1}^{1} |T_m|^2 \, d(\cos\theta) \qquad \pi a_o^2 \, . \tag{D.22}$$

Since T_m depends explicitly on K rather than the scattering angle θ, it is desirable to express Q_m as an integral over K instead of θ. This is easily achieved since

$$K^2 = k_i^2 + k_f^2 - 2k_i k_f \cos\theta \, . \tag{D.23}$$

Consequently equation (D.22) becomes

$$Q_m = \frac{1}{2\pi^2} \cdot \frac{1}{k_i^2} \int_{K_{min}}^{K_{max}} |T_m|^2 \, K \, dK \qquad \pi a_o^2 \tag{D.24}$$

where $K_{min} = k_i - k_f$ and $K_{max} = k_i + k_f$.

The total integrated cross section is expressed as

$$Q = Q_o + 2Q_1 \tag{D.25}$$

where use has been made of the fact that $Q_1 = Q_{-1}$ due to mirror symmetry in the plane of scattering. Q is independent of the angle β. This may readily be seen by expressing Q in the form

$$Q = \frac{1}{2\pi^2} \cdot \frac{1}{k_i^2} \int_{K_{min}}^{K_{max}} \left[|T_o|^2 + 2|T_1|^2 \right] K \, dK \quad \pi a_o^2. \tag{D.26a}$$

T_m depends on β only through the term $Y_{lm}(\beta,0)$ (viz. equations (D.8) for $T_{if}^{B}(m)$ and (D.14) for $T_{if}^{PB}(m)$); inserting the well known analytic expressions for the $Y_{lm}(\beta,0)$ into (D.26a) one observes that the β-dependence of the integrand is expressed as $(\cos^2\beta + \sin^2\beta)$ which can, of course, be replaced by unity. Hence, in (D.26a), by choosing $\beta = 0$, or equivalently choosing the axis of quantization along $\underline{K}$, one sees that T_1 vanishes and that only T_o remains in the integrand, a result which greatly facilitates computation:

$$Q = \frac{1}{2\pi^2} \cdot \frac{1}{k_i^2} \int_{K_{min}}^{K_{max}} |T_o(\beta=0)|^2 \, K \, dK \quad \pi a_o^2 \, . \tag{D.26b}$$

In practice then, Q_o is computed from (D.24) and Q from (D.26b). Q_1 is then obtained directly from (D.25).

For $n = 2$, exact analytic expressions for Q_o and Q were derived in the Born approximation. For the 'Born plus Polarized-Born' approximation and also each of the $n = 3$ results, the integrals were evaluated numerically by Simpson's rule.

REFERENCES

Abramowitz, M. and Stegun, I.A., 1970, "Handbook of Mathematical Functions" (New York:Dover Publications Inc.).

Baluja, K.L. and Taylor, H.S., 1976, J. Phys. B:Atom. Molec.Phys., 9, 829-35.

Bates, D.R. and Massey, H.S.W., 1943, Phil. Trans. Roy. Soc., 239A, 269-304.

Baye, D. and Heenen, P.H., 1974, J. Phys. B:Atom. Molec. Phys., 7, 938-49.

Bell, K.L., Eissa, H. and Moiseiwitsch, B.L., 1966, Proc. Phys. Soc., 88, 57-63.

Belling, J.A., 1968, J. Phys. B (Proc. Phys. Soc.), 1, 136-8.

Bell, K.L., Kennedy, D.J. and Kingston, A.E., 1968, J. Phys. B (Proc. Phys. Soc.), 1, 204-17.

———— 1969, J. Phys. B:Atom. Molec. Phys., 2, 26-43.

Bell, K.L. and Kingston, A.E., 1967a, Proc. Phys. Soc., 90, 31-7.

———— 1967b, Proc. Phys. Soc., 90, 337-42.

———— 1967c, Proc. Phys. Soc., 90, 895-9.

Berrington, K.A., Bransden, B.H. and Coleman, J.P., 1973, J. Phys. B:Atom. Molec. Phys., 6, 436-49.

Berrington, K.A., Burke, P.G. and Sinfailam, A.L., 1975, J. Phys. B:Atom. Molec. Phys., 8, 1459-73.

Bransden, B.H., 1970, "Atomic Collision Theory" (New York:Benjamin).

Bransden, B.H. and Coleman, J.P., 1972, J. Phys. B:Atom. Molec. Phys., 5, 537-45.

Bransden, B.H., Coleman, J.P. and Sullivan, J., 1972, J. Phys. B:Atom. Molec. Phys., 5, 546-58.

Bransden, B.H. and Issa, M.R., 1975, J. Phys. B:Atom. Molec. Phys., 8, 1088-94.

Bransden, B.H. and McDowell, M.R.C., 1976, in preparation for "Physics Reports".

Bransden, B.H. and Winters, K.H., 1975, J. Phys. B:Atom. Molec. Phys., 8, 1236-44.

Brongersma, H.H., Knoop, F.W.E. and Backx, C., 1972, Chem. Phys. Lett., 13, 16-9.

Buckley, B.D. and Walters, H.R.J., 1974, J. Phys. B:Atom. Molec. Phys., 7, 1380-400.

———— 1975, J. Phys. B:Atom. Molec. Phys., 8, 1693-715.

Burgess, A., 1963, Proc. Phys. Soc., 81, 442-52.

Burke, P.G., Hibbert, A. and Robb, W.D., 1971, J. Phys. B:Atom. Molec. Phys., 4, 153-61.

Burke, P.G. and Robb, W.D., 1972, J. Phys. B:Atom. Molec. Phys., 5, 44-54.

Burke, P.G. and Taylor, A.J., 1966, Proc. Phys. Soc., 88, 549-62.

Burke, P.G. and Webb, T.G., 1970, J. Phys. B:Atom. Molec. Phys., 3, L131-4.

Byron, F.W. Jr. and Joachain, C.J., 1973a, Phys. Rev. A., 8, 1267-82.

———— 1973b, Phys. Rev. A, 8, 3266-9.

———— 1974a, Phys. Rev. A, 9, 2559-68.

———— 1974b, J. Phys. B:Atom. Molec. Phys., 7, L212-5.

———— 1975, J. Phys. B:Atom. Molec. Phys., 8, L284-8.

Byron, F.W. Jr. and Latour, L.J. Jr., 1976, Phys. Rev. A, 13, 649-64.

Callaway, J., LaBahn, R.W., Pu, R.T. and Duxler, W.M., 1968, Phys. Rev., 168, 12-21.

Callaway, J., McDowell, M.R.C. and Morgan, L.A., 1975, J. Phys. B:Atom. Molec. Phys. 8, 2181-90.

———— 1976, J. Phys. B:Atom. Molec. Phys., in press.

Callaway, J. and Wooten, J.W., 1974, Phys. Rev. A, 9, 1924-31.

———— 1975, Phys. Rev. A, 11, 1118-20.

Chamberlain, G.E., Mielczarek, S.R. and Kuyatt, C.E., 1970, Phys. Rev. A, 2, 1905-22.

Chan, F.T. and Chen S.T., 1974a, Phys. Rev. A, 9, 2393-7.

———— 1974b, Phys. Rev. A, 10, 1151-6.

Chutjian, A. and Srivastava, S.K., 1975, J. Phys. B:Atom. Molec. Phys., 8, 2360-8.

Chutjian, A. and Thomas, L.D., 1975, Phys. Rev. A, 11, 1583-95.

Cohen, M. and McEachran, R.P., 1967a, Proc. Phys. Soc., 92, 37-41.

———— 1967b, Proc. Phys. Soc., 92, 539-42.

Crooks, G.B., 1972, Ph.D. Thesis, University of Nebraska.

Crooks, G.B., DuBois, R.D., Golden, D.E. and Rudd, M.E., 1972, Phys. Rev. Lett., 29, 327-9.

Crooks, G.B. and Rudd, M.E., 1972, Bull. Amer. Phys. Soc., 17, 131.

Crothers, D.S.F. and McEachran, R.P., 1970,J. Phys. B:Atom. Molec. Phys. 3, 976-90.

Csanak, G. and Taylor, H.S., 1973, J. Phys. B:Atom. Molec. Phys., 6, 2055-71.

Csanak, G., Taylor, H.S. and Tripathy, D.N., 1973, J. Phys. B:Atom. Molec. Phys., 6, 2040-54.

Csanak, G., Taylor, H.S. and Yaris, R., 1971, "Advances in Atomic and Molecular Physics", ed. Bates, D.R. and Estermann, I. (New York:Academic Press), 7, 287-361.

Dillon, M.A., 1975, J. Chem. Phys., 63, 2035-45.

Dillon, M.A. and Lassettre, E.N., 1975, J. Chem. Phys., 62, 2373-90.

Donaldson, F.G., Hender, M.A. and McConkey, J.W., 1972, J. Phys. B:Atom. Molec. Phys., 5, 1192-210.

Drachman, R.J. and Temkin, A., 1972, "Case Studies in Atomic Collision Physics II", ed. McDowell, M.R.C. and McDaniel, E.W. (Amsterdam:North Holland), 399-481.

Duxler, W.M., Poe R.T. and LaBahn, R.W., 1971, Phys. Rev. A, 4, 1935-44.

Eckart, C., 1930, Phys. Rev., 36, 878-92.

Edmonds, A.R., 1974, "Angular Momentum in Quantum Mechanics" (Princeton University Press).

Eminyan, M., Kleinpoppen, H., Slevin, J. and Standage, M.C., 1976, "Electron and Photon Interactions with Atoms", ed. Kleinpoppen, H. and McDowell, M.R.C. (New York:Plenum Press), 455-83.

Eminyan, M., MacAdam, K.B., Slevin, J. and Kleinpoppen, H., 1973, Phys. Rev. Letts., 31, 576-9.

———— 1974, J. Phys. B:Atom. Molec. Phys., 7, 1519-42.

Eminyan, M., MacAdam, K.B., Slevin, J., Standage, M.C. and Kleinpoppen, H., 1975, J. Phys. B:Atom. Molec. Phys., 8, 2058-66.

Fano, U. and Macek, J.H., 1973, Rev. Mod. Phys., 45, 553-72.

Flannery, M.R., 1975, Private communication to M.R.C. McDowell.

Flannery, M.R. and McCann,K.J., 1974, Phys. Rev. A, 9, 1947-53.

———— 1975, J. Phys. B:Atom. Molec. Phys., 8, 1716-33.

Fröberg, C.E., 1966, "Introduction to Numerical Analysis" (Addison-Wesley).

Gelebart, F., Pochat, A. and Peresse, J., 1975, Private Communication to M.R.C. McDowell.

Geltman, S. and Burke, P.G., 1970, J. Phys. B:Atom. Molec. Phys., 3, 1062-72.

Gerjuoy, E. and Thomas, B.K., 1974, Rep. Prog. Phys., 37, 1345-431.

Goldberg, L. and Clogston, A.M., 1939, Phys. Rev., 56, 696-9.

Goldberger, M.L. and Watson, K.M., 1964, "Collision Theory" (New York:John Wiley).

Gradshteyn, I.S. and Ryzhik, I.M., 1965, "Tables of Integrals, Series and Products" (New York: Academic Press).

Green, L.C., Mulder, M.M., Lewis, M.N. and Woll, J.W. Jr., 1954, Phys. Rev., 93, 757-61.

Hall, R.I., Joyez, G., Mazeau, J., Reinhardt, J. and Schermann, C., 1973, J. Physique, 34, 827-43.

Hartree, D.R., 1957, "The Calculation of Atomic Structures" (New York:John Wiley).

———— 1958, "Numerical Analysis", 2nd Ed. (Oxford University Press).

Hidalgo, M.B. and Geltman, S., 1972, J. Phys. B:Atom. Molec. Phys., 5, 617-26.

Huo, W.M., 1974, J. Chem. Phys., 60, 3544-57.

Hylleraas, E.A., 1929, Z. Physik, 54, 347-66.

Joachain, C.J., 1974, Comp. Phys. Commun., 6, 358-71.

Joachain, C.J. and Vanderpoorten, R., 1973, J. Phys. B:Atom. Molec. Phys., 6, 622-41.

———— 1974a, J. Phys. B:Atom. Molec. Phys., 7, 817-30.

———— 1974b, J. Phys. B:Atom. Molec. Phys., 7, L528-30.

Jobe, J.D. and St.John, R.M., 1967, Phys. Rev., 164, 117-21.

Johnston, D.R., Oudemans, G.J. and Cole, R.H., 1960, J. Chem. Phys., 33, 1310-7.

de Jongh, J.P. and van Eck, J., 1971, Abstr. 7th Int. Conf. on Physics of Electronic and Atomic Collisions (Amsterdam:North Holland), 701-3.

Kennedy, J.V., 1976, Ph.D. Thesis, University of London.

Kingston, A.E., Fon, W.C., and Burke, P.G., 1976, J. Phys. B:Atom. Molec. Phys., 9, 605-18.

Kleinpoppen, H., 1976, Comments Atom. Mol. Phys., in press.

LaBahn, R.W. and Callaway, J., 1964, Phys. Rev., 135, A1539-46.

Lawson, J., Lawson, W. and Seaton, M.J., 1961, Proc. Phys. Soc., 77, 192-8.

Lloyd, M.D. and McDowell, M.R.C., 1969, J. Phys. B:Atom. Molec. Phys., 2, 1313-22.

Macek, J. and Jaecks, D.H., 1971, Phys. Rev. A, 4, 2288-300.

Madison, D.H. and Shelton, W.N., 1973, Phys. Rev. A, 7, 499-513.

Marriott, R., 1958, Phys. Soc. Proc., 72, 121-9.

Martin, W.C., 1960, J. Res. Natn. Bur. Std., 64A, 19-28.

Martin, P.C. and Schwinger, J., 1959, Phys. Rev., 115, 1342-73.

McDowell, M.R.C. and Coleman, J.P., 1970, "Introduction to the Theory of Ion-Atom Collisions" (Amsterdam:North Holland).

McDowell, M.R.C., Morgan, L.A. and Myerscough, V.P., 1973, J. Phys. B:Atom. Molec. Phys., 6, 1435-51.

———— 1974, Comp. Phys. Commun., 7, 38-49.

———— 1975a, J. Phys. B:Atom. Molec. Phys., 8, 1053-72.

———— 1975b, J. Phys. B:Atom. Molec. Phys., 8, 1838-50.

McDowell, M.R.C., Myerscough, V.P. and Narain, U., 1974, J. Phys. B:Atom. Molec. Phys., 7 L195-7.

McEachran, R.P. and Cohen, M., 1969, J. Phys. B:Atom. Molec. Phys., 2, 1271-3.

Messiah, A., 1970, "Quantum Mechanics" (Amsterdam:North Holland).

Miller, W.F., 1956, Ph.D. Thesis, Purdue University.

Morgan, L.A. and McDowell, M.R.C., 1975, J. Phys. B:Atom. Molec. Phys., 8, 1073-81.

Morse, P.M. and Allis, W.P., 1933, Phys. Rev., 44, 269-76.

Morse, P.M., Young, L.A. and Haurwitz, E.S., 1935, Phys. Rev., 48, 948-54.

Mott, N.F. and Massey, H.S.W., 1965, "The Theory of Atomic Collisions", 3rd Ed. (Oxford University Press).

Moustafa Moussa, H.R., de Heer, F.J. and Schutten, J., 1969, Physica, 40, 517-49.

Norcross, D.W., 1974, Comp. Phys. Commun., 6, 257-64.

Numerov, B., 1933, Publ. Observ. Astrophys. Centr., Russia, 2, 188.

Oberoi, R.S. and Nesbet, R.K., 1973, Phys. Rev. A, 8, 2969-79.

Ochkur, V.I. and Burkova, L.A., 1975, Abstr. 9th Int. Conf. on Physics of Electronic and Atomic Collisions (Seattle: University of Washington Press), 839-40.

Opal, C.B. and Beaty, E.C., 1972, J. Phys. B:Atom. Molec. Phys., 5, 627-35.

Ormonde, S. and Golden, D.E., 1973, Phys. Rev. Lett., 31, 1161-4.

Pochat, A., 1973, Thesis, L'Université de Bretagne Occidentale.

Pochat, A., Rozuel, D. and Peresse, J., 1973, J. Physique, 34, 701-9.

van Raan, A.F.J., de Jongh, J.P., van Eck, J. and Heideman, H.G.M., 1971, Physica, 53, 45-59.

Rescigno, T.N., McCurdy, C.W. Jr. and McKoy, V., 1974, J. Phys. B:Atom. Molec. Phys., 7, 2396-402.

Rice, J.K., Truhlar, D.G., Cartwright, D.C. and Trajmar, S., 1972, Phys. Rev. A, 5, 762-82.

St.John, R.M., Miller, F.L. and Lin, C.C., 1964, Phys. Rev., 134, A888-97.

Schneider, B., Taylor, H.S. and Yaris, R., 1970, Phys. Rev. A, 1, 855-67.

Scott, T. and McDowell, M.R.C., 1975a, J. Phys. B:Atom. Molec. Phys., 8, 1851-65.

———— 1975b, J. Phys. B:Atom. Molec. Phys., 8, 2369-76.

———— 1976, J. Phys. B:Atom. Molec. Phys., in press.

Seaton, M.J., 1961, Proc. Phys. Soc., 77, 174-83.

———— 1974, Quart. J.R. Astron. Soc., 15, 370-91.

Shelton, W.N., Baluja, K.L. and Madison, D.H., 1973, Abstr. 8th Int. Conf. on Physics of Electronic and Atomic Collisions (Beograd:Institute of Physics), 296-7.

Showalter, J.G. and Kay, R.B., 1975, Phys. Rev. A, 11, 1899-910.

Sloan, I.H., 1964, Proc. Roy. Soc. (London) A, 281, 151-63.

Smith, K., Golden, D.E., Ormonde, S., Torres, B.W. and Davies, A.R., 1973, Phys. Rev. A, 8, 3001-11.

Somerville, W.B., 1963, Proc. Phys. Soc., 82, 446-55.

Steelhammer, J.C. and Lipsky, S., 1970, J. Chem. Phys., 53, 4112-4.

Sullivan, J., Coleman, J.P. and Bransden, B.H., 1972, J. Phys. B:Atom. Molec. Phys., 5, 2061-5.

Suzuki, H. and Takayanagi, T., 1973, Abstr. 8th Int. Conf. on Physics of Electronic and Atomic Collisions (Beograd:Institute of Physics), 286-7.

Syms R.F., McDowell, M.R.C., Morgan, L.A. and Myerscough, V.P., 1975, J. Phys. B: Atom. Molec. Phys., 8, 2817-34.

Taylor, J.R., 1972, "Scattering Theory" (New York:John Wiley).

Temkin, A., 1957, Phys. Rev., 107, 1004-12.

———— 1959, Phys. Rev., 116, 358-63.

Temkin A., and Lamkin, J.C. 1961, Phys. Rev., 121, 788-94.

Thomas, L.D., Csanak, G., Taylor, H.S. and Yarlagadda, B.S., 1974, J. Phys. B: Atom. Molec. Phys., 7, 1719-33.

Thomas, L.D. and Nesbet, R.K., 1974, Abstr. 4th Int. Conf. Atom. Phys. (Heidelberg), 468-70.

Trajmar, S., 1973, Phys. Rev. A, 8, 191-203.

Truhlar, D.G., Rice, J.K., Kuppermann, A., Trajmar, S. and Cartwright, D.C., 1970, Phys. Rev. A, 1, 778-802.

Truhlar, D.G., Trajmar, S., Williams, W., Ormonde, S. and Torres, B., 1973, Phys. Rev. A, 8, 2475-82.

Veselov, M.G., Antonova, I.M., Brattsev, V.F. and Kirillova, I.V., 1961, Opt. Spectrosc., 10, 367-8.

Vriens, L., Simpson, J.A. and Mielczarek, S.R., 1968, Phys. Rev., 165, 7-15.

Williams, J.F., 1976, J. Phys. B:Atom. Molec. Phys., 9, 1519-27.

Williams, J.F. and Willis, B.A., 1975, J. Phys. B:Atom. Molec. Phys., 8, 1641-69.

Winters, K.H., 1974, Ph.D. Thesis, University of Durham.

Winters, K.H., Clark, C.D., Bransden, B.H. and Coleman, J.P., 1974, J. Phys. B:Atom. Molec. Phys., 7, 788-98.

Woollings, M.J. and McDowell, M.R.C., 1973, J. Phys. B:Atom. Molec. Phys., 6, 450-61.

Wykes, J., 1972, J. Phys. B:Atom. Molec. Phys., 5, 1126-37.

Yagishita, A., Takayanagi, T. and Suzuki, H., 1976, J. Phys. B:Atom. Molec. Phys., 9, L53-7.

Yarlagadda, B.S., Csanak, G., Taylor, H.S., Schneider, B. and Yaris, R., 1973, Phys. Rev. A, 7, 146-54.

Yarlagadda, B.S. and Taylor, H.S., 1975, J. Phys. B:Atom. Molec. Phys., 8, 2041-9.

Yates, A.C. and Tenney, A., 1972, Phys. Rev. A, 6, 1451,-6.

TABLES

Notation:

,n denotes that entry is to be multiplied by 10^n.

ELECTRON-HYDROGEN PARTIAL WAVE PHASE SHIFTS IN RADIANS

(FULL POLARIZED ORBITAL APPROXIMATION)

	s-wave		p-wave		d-wave	
k_i (a.u.)	singlet	triplet	singlet	triplet	singlet	triplet
0.1	2.5883	2.9435				
	2.583	2.945				
0.3	1.7534	2.5204	0.0181	0.1120		
	1.750	2.519	0.0210	0.1151		
0.5	1.2524	2.1337	0.0040	0.2870	0.0246	0.0329
	1.251	2.133	0.0064	0.2867	0.0266	0.0350
0.7	0.9588	1.8123	-0.0098	0.4066	0.0425	0.0669
	0.947	1.815	-0.010	0.4063		
0.75	0.9087	1.7479	-0.0103	0.4232	0.0461	0.0751
					0.0456	0.0746
0.8	0.8647	1.6836	-0.0093	0.4353	0.0496	0.0833
	0.854	1.682	-0.0095	0.4351		
1.0	0.7588	1.4649	0.0137	0.4522	0.0630	0.1129
	0.758	1.460	0.0135	0.4520	0.0627	0.112

For each value of the momentum k_i, the first line of the results comes from the present work and the second line, where available, from the article by Drachman and Temkin (1972).

TABLE 1

ELECTRON-HELIUM PARTIAL WAVE PHASE SHIFTS (RADIANS) COMPUTED IN THE ADIABATIC-EXCHANGE (A.E.) AND POLARIZED ORBITAL (P.O.) APPROXIMATION

	s-wave		p-wave		d-wave	
k_i (a.u.)	AE	PO	AE	PO	AE	PO
0.30	2.7518	2.7467				
	2.7520	2.7546				
0.40	2.6243	2.6179	0.0578		0.0044	
	2.6196	2.6223	0.0617		0.0073	
0.50	2.4970	2.4894	0.0932	0.0905	0.0088	
	2.4918	2.4942	0.0971	0.0926	0.0116	
0.60	2.3754	2.3666	0.1339	0.1298	0.0141	0.0139
	2.3701	2.3719	0.1375	0.1302	0.0170	0.0167
0.70	2.2604	2.2506	0.1771	0.1715	0.0205	0.0201
	2.2556	2.2564	0.1803	0.1696	0.0234	0.0228
0.75	2.2057	2.1953	0.1988	0.1924	0.0242	0.0235
	2.2011	2.2012	0.2015	0.1891	0.0270	0.0262
0.80	2.1527	2.1418	0.2223	0.2152	0.0280	0.0272
	2.1485	2.1479	0.2223	0.2081	0.0307	0.0298
1.0	0.9579	1.9453	0.2976	0.2878	0.0452	0.0434
	1.9571	1.9530	0.2959	0.2749	0.0477	0.0458
1.1	1.8719	1.8583	0.3278	0.3169	0.0546	0.0522
	1.8722	1.8662	0.3254	0.3016	0.0570	0.0544
1.25	1.7589	1.7440	0.3627	0.3504	0.0709	0.0675
	1.7572	1.7483	0.3600	0.3332	0.0712	0.0676

continued.....

TABLE 2

TABLE 2 continued...

	s-wave		p-wave		d-wave	
k_i (a.u.)	AE	PO	AE	PO	AE	PO
1.5	1.5960	1.5792	0.3999	0.3855	0.0947	0.0895
	1.5943	1.5811	0.3967	0.3671	0.0943	0.0890
1.75	1.4634	1.4451	0.4185	0.4025	0.1158	0.1092
	1.4610	1.4445	0.4152	0.3852	0.1152	0.1086
2.0	1.3541	1.3348	0.4259	0.4088	0.1343	0.1265
	1.3507	1.3321	0.4232	0.3941	0.1333	0.1256

For each value of the momentum k_i, the first line of the results comes from the present work and the second line from the paper by Duxler et al. (1971).

TABLE 3

TOTAL CROSS SECTION IN UNITS OF πa_o^2 FOR EXCITATION OF $He(2^3S)$ IN THE BORN-OPPENHEIMER APPROXIMATION COMPUTED FROM EXPRESSION (5.4.1).

k_i (a.u.)	This work		Bell et al. (1966)
	Experimental Energy Levels	Theoretical Energy Levels	
1.2	-	1.01	9.52,-1
1.359	1.18	1.28	1.21
1.5	8.57,-1	8.91,-1	8.48,-1
1.6	6.34,-1	6.51,-1	6.23,-1
1.65	5.40,-1	5.52,-1	5.23,-1
1.8	3.27,-1	3.32,-1	3.17,-1
1.922	2.16,-1	2.18,-1	2.08,-1
2.0	1.66,-1	1.67,-1	1.59,-1
3.0	6.71,-3	6.70,-3	6.45,-3
4.0	5.03,-4	5.01,-4	3.63,-4

TABLE 4

TOTAL INTEGRATED CROSS SECTION IN UNITS OF πa_o^2 FOR EXCITATION OF $He(2^3P)$ IN THE BORN-OPPENHEIMER APPROXIMATION COMPUTED FROM EXPRESSION (5.4.1).

k_i (a.u.)	This work		Bell et al. (1966)
	Experimental Energy Levels	Theoretical Energy Levels	
1.25	1.25,-1	2.89,-1	2.89,-1
1.359	2.05,-1	2.41,-1	2.41,-1
1.5	1.28,-1	1.38,-1	1.41,-1
1.6	8.91,-2	9.36,-2	9.61,-2
1.65	7.49,-2	7.78,-2	8.01,-2
1.8	4.55,-2	4.63,-2	4.78,-2
1.922	3.10,-2	3.13,-2	3.22,-2
2.0	2.45,-2	2.46,-2	2.53,-2
3.0	1.77,-3	1.75,-3	1.77,-3
4.0	2.48,-4	2.46,-4	2.49,-4

TABLE 5

TOTAL CROSS SECTION IN UNITS OF πa_o^2 FOR EXCITATION OF $He(2^3S)$ COMPUTED IN THE BORN-OPPENHEIMER APPROXIMATION USING THE PRIOR AND POST FORMULATION WITH AND WITHOUT δT_{if} OF EXPRESSION (5.4.1) AND (5.4.5).

E(eV)	Prior	Post	with δT_{if}
29.6	1.22	9.33,-1	8.78,-1
	1.27	9.82,-1	9.17,-1
40.1	4.89,-1	4.28,-1	4.14,-1
	5.11,-1	4.63,-1	4.32,-1
81.63	3.02,-2	3.43,-2	3.55,-2
	3.15,-2	3.77,-2	3.70,-2
100	1.24,-2	1.47,-2	1.54,-2
	1.29,-2	1.60,-2	1.61,-2
200	5.64,-4	6.60,-4	6.98,-4
	5.91,-4	6.86,-4	7.31,-4

For each value of the energy E, the first line of the results is obtained using the excited state wave function of Cohen and McEachran and the second line using that of Morse et al. - see Appendix A for details.

TABLE 6

DIFFERENTIAL CROSS SECTION IN UNITS OF $a_o^2 sr^{-1}$ FOR ELECTRON IMPACT EXCITATION OF H(2s) COMPUTED IN THE DWPO III MODEL AT INCIDENT ENERGIES OF 50 AND 100 eV. COLUMN (i) GIVES THE NON-UNITARIZED RESULT AND COLUMN (ii) THE CORRESPONDING UNITARIZED RESULT.

θ^o	50 eV		100 eV	
	(i)	(ii)	(i)	(ii)
0	1.61	3.32	2.54	4.69
5	1.21	1.86	1.31	1.44
10	6.34,-1	5.43,-1	4.34,-1	2.65,-1
15	2.93,-1	1.31,-1	1.42,-1	6.08,-2
20	1.33,-1	3.25,-1	5.03,-2	1.96,-2
25	6.20,-2	1.06,-2	1.94,-2	8.51,-3
30	3.13,-2	5.37,-3	8.00,-3	5.09,-3
35	1.75,-2	3.97,-3	3.62,-3	3.69,-3
40	1.10,-2	3.52,-3	1.89,-3	2.77,-3
45	7.68,-3	3.30,-3	1.19,-3	2.23,-3
50	5.81,-3	3.13,-3	8.71,-4	1.87,-3
55	4.64,-3	2.94,-3	7.03,-4	1.57,-3
60	3.80,-3	2.71,-3	5.99,-4	1.33,-3
70	2.57,-3	2.23,-3	4.53,-4	8.99,-4
80	1.72,-3	1.79,-3	3.37,-4	6.61,-4
90	1.19,-3	1.44,-3	2.47,-4	4.57,-4
100	8.84,-4	1.23,-3	1.80,-4	3.55,-4
110	7.78,-4	1.16,-3	1.36,-4	2.71,-4
120	8.31,-4	1.19,-3	1.11,-4	2.23,-4
130	9.89,-4	1.31,-3	1.05,-4	2.05,-4
140	1.22,-3	1.49,-3	1.07,-4	1.88,-4
150	1.45,-3	1.68,-3	1.20,-4	2.03,-4
160	1.64,-3	1.83,-3	1.31,-4	1.95,-4
170	1.80,-3	1.94,-3	1.40,-4	2.15,-4
180	1.87,-3	1.99,-3	1.50,-4	1.90,-4
Integral (πa_o^2)	7.82,-2	6.54,-2	4.99,-2	4.48,-2

TABLE 7

DIFFERENTIAL CROSS SECTION IN UNITS OF $a_o^2 sr^{-1}$ FOR ELECTRON IMPACT EXCITATION OF H(2p) COMPUTED IN THE DWPO III MODEL AT INCIDENT ENERGIES OF 50 AND 100 eV. COLUMN (i) GIVES THE NON-UNITARIZED RESULT AND COLUMN (ii) THE CORRESPONDING UNITARIZED RESULT.

θ°	50 eV		100 eV	
	(i)	(ii)	(i)	(ii)
0	3.88,+1	3.57,+1	9.68,+1	9.35,+1
5	2.22,+1	1.96,+1	2.16,+1	2.00,+1
10	8.02	6.56	4.08	3.60
15	2.88	2.24	9.50,-1	8.60,-1
20	1.07	8.51,-1	2.45,-1	2.44,-1
25	4.14,-1	3.62,-1	6.76,-2	8.11,-2
30	1.65,-1	1.71,-1	2.04,-2	3.32,-2
35	6.90,-2	8.93,-2	6.89,-3	1.61,-2
40	3.08,-2	5.16,-2	2.74,-3	8.95,-3
45	1.53,-2	3.31,-2	1.33,-3	5.58,-3
50	8.82,-3	2.30,-2	8.14,-4	3.75,-3
55	5.90,-3	1.68,-2	6.16,-4	2.72,-3
60	4.39,-3	1.27,-2	5.07,-4	2.06,-3
70	2.72,-3	7.36,-3	3.21,-4	1.14,-3
80	1.58,-3	4.18,-3	1.85,-4	6.21,-4
90	7.69,-4	2.29,-3	9.40,-5	3.43,-4
100	4.19,-4	1.34,-3	7.44,-5	2.16,-4
110	5.17,-4	9.49,-4	1.02,-4	1.75,-4
120	8.88,-4	9.28,-4	1.31,-4	1.56,-4
130	1.43,-3	1.18,-3	1.62,-4	1.52,-4
140	2.14,-3	1.58,-3	2.18,-4	1.88,-4
150	3.03,-3	2.09,-3	3.26,-4	2.45,-4
160	3.96,-3	2.62,-3	4.78,-4	3.47,-4
170	4.68,-3	2.98,-3	6.25,-4	4.29,-4
180	4.96,-3	3.11,-3	6.94,-4	4.56,-4
Integral (πa_o^2)	8.93,-1	7.75,-1	6.63,-1	6.20,-1

TABLE 8(a)

DIFFERENTIAL CROSS SECTIONS IN UNITS OF $a_o^2 sr^{-1}$ FOR ELECTRON IMPACT EXCITATION OF THE N = 2 LEVEL OF ATOMIC HYDROGEN COMPUTED IN THE DWPO III MODEL AT INCIDENT ENERGIES OF (a) 1.02, (b) 1.21 and (c) 1.44 Rydbergs. COLUMN (i) GIVES THE NON-UNITARIZED RESULT AND COLUMN (ii) THE CORRESPONDING UNITARIZED RESULT.

E = 1.02 Rydbergs

θ^o	2s		2p		Total	
	(i)	(ii)	(i)	(ii)	(i)	(ii)
0	6.38,-2	2.48,-1	1.08	8.77,-1	1.15	1.13
5	6.15,-2	2.32,-1	1.05	8.30,-1	1.11	1.06
10	5.50,-2	1.89,-1	9.52,-1	7.06,-1	1.01	8.95,-1
15	4.59,-2	1.35,-1	8.11,-1	5.46,-1	8.57,-1	6.80,-1
20	3.60,-2	8.37,-2	6.56,-1	3.89,-1	6.92,-1	4.73,-1
25	2.69,-2	4.54,-2	5.09,-1	2.63,-1	5.36,-1	3.08,-1
30	1.97,-2	2.18,-2	3.83,-1	1.75,-1	4.03,-1	1.96,-1
35	1.48,-2	1.02,-2	2.80,-1	1.19,-1	2.95,-1	1.29,-1
40	1.20,-2	6.49,-3	2.01,-1	8.66,-2	2.13,-1	9.31,-2
45	1.11,-2	6.82,-3	1.43,-1	6.90,-2	1.54,-1	7.58,-2
50	1.16,-2	8.71,-3	1.01,-1	5.91,-2	1.13,-1	6.78,-2
55	1.29,-2	1.08,-2	7.09,-2	5.31,-2	8.38,-2	6.39,-2
60	1.48,-2	1.25,-2	5.01,-2	4.88,-2	5.16,-2	6.13,-2
70	1.89,-2	1.44,-2	2.79,-2	4.17,-2	4.68,-2	5.62,-2
80	2.26,-2	1.44,-2	2.31,-2	3.52,-2	4.57,-2	4.96,-2
90	2.57,-2	1.25,-2	3.13,-2	2.89,-2	5.70,-2	4.14,-2
100	2.85,-2	8.92,-3	5.00,-2	2.40,-2	7.85,-2	3.29,-2
110	3.11,-2	4.71,-3	7.74,-2	2.31,-2	1.09,-1	2.78,-2
120	3.38,-2	1.36,-3	1.11,-1	2.95,-2	1.45,-1	3.08,-2
130	3.66,-2	1.94,-4	1.48,-1	4.50,-2	1.84,-1	4.52,-2
140	3.93,-2	1.78,-3	1.84,-1	6.93,-2	2.24,-1	7.11,-2
150	4.17,-2	5.62,-3	2.17,-1	9.86,-2	2.59,-1	1.04,-1
160	4.37,-2	1.03,-2	2.43,-1	1.27,-1	2.87,-1	1.37,-1
170	4.50,-2	1.41,-2	2.60,-1	1.47,-1	3.05,-1	1.61,-1
180	4.54,-2	1.55,-2	2.66,-1	1.55,-1	3.11,-1	1.70,-1
Integral (πa_o^2)	1.09,-1	5.68,-2	5.65,-1	3.05,-1	6.74,-1	3.61,-1

TABLE 8(b)

E = 1.21 Rydbergs

θ°	2s		2p		Total	
	(i)	(ii)	(i)	(ii)	(i)	(ii)
0	1.59,-1	5.41,-1	2.70	2.24	2.86	2.78
5	1.51,-1	4.89,-1	2.55	2.07	2.70	2.56
10	1.28,-1	3.63,-1	2.18	1.65	2.30	2.01
15	9.72,-2	2.23,-1	1.71	1.16	1.81	1.38
20	6.70,-2	1.14,-1	1.26	7.44,-1	1.32	8.58,-1
25	4.20,-2	4.77,-2	8.83,-1	4.62,-1	9.25,-1	5.10,-1
30	2.39,-2	1.68,-2	6.08,-1	2.91.-1	6.32,-1	3.08,-1
35	1.25,-2	6.64,-3	4.13,-1	1.96,-1	4.26,-1	2.03,-1
40	6.46,-3	5.68,-3	2.81,-1	1.44,-1	2.88,-1	1.49,-1
45	4.12,-3	7.42,-3	1.94,-1	1.13,-1	1.98,-1	1.21,-1
50	4.06,-3	9.07,-3	1.36,-1	9.30,-2	1.40,-1	1.02,-1
55	5.19,-3	9.90,-3	9.66,-2	7.77,-2	1.02,-1	8.76,-2
60	6.80,-3	1.00,-2	6.98,-2	6.52,-2	7.67,-2	7.52,-2
70	9.91,-3	9.30,-3	3.79,-2	4.58,-2	4.78,-2	5.51,-2
80	1.22,-2	8.00,-3	2.28,-2	3.26,-2	3.50,-2	4.06,-2
90	1.38,-2	6.15,-3	1.98,-2	2.45,-2	3.36,-2	3.06,-2
100	1.55,-2	3.88,-3	2.68,-2	2.09,-2	4.24,-2	2.48,-2
110	1.76,-2	1.83,-3	4.25,-2	2.23,-2	6.01,-2	2.41,-2
120	2.02,-2	8.65,-4	6.50,-2	2.94,-2	8.53,-2	3.03,-2
130	2.32,-2	1.65,-3	9.15,-2	4.24,-2	1.15,-1	4.41,-2
140	2.64,-2	4.29,-3	1.19,-1	6.00,-2	1.45,-1	6.43,-2
150	2.93,-2	8.23,-3	1.44,-1	7.96,-2	1.74,-1	8.79,-2
160	3.16,-2	1.24,-2	1.65,-1	9.76,-2	1.97,-1	1.10,-1
170	3.31,-2	1.55,-2	1.78,-1	1.10,-1	2.11,-1	1.26,-1
180	3.37,-2	1.67,-2	1.83,-1	1.15,-1	2.17,-1	1.32,-1
Integral (πa_o^2)	7.80,-2	6.36,-2	7.00,-1	4.44,-1	7.78,-1	5.07,-1

TABLE 8(c)

E = 1.44 Rydbergs

θ^{o}	2s		2p		Total	
	(i)	(ii)	(i)	(ii)	(i)	(ii)
0	3.22,-1	9.16,-1	5.22	4.42	5.54	5.34
5	3.00,-1	7.95,-1	4.80	3.96	5.10	4.75
10	2.43,-1	5.29,-1	3.78	2.88	4.03	3.41
15	1.74,-1	2.75,-1	2.67	1.81	2.84	2.09
20	1.13,-1	1.14,-1	1.76	1.06	1.87	1.17
25	6.76,-2	3.72,-2	1.11	6.04,-1	1.18	6.41,-1
30	3.78,-2	1.03,-2	6.96,-1	3.65,-1	7.33,-1	3.75,-1
35	2.06,-2	4.95,-3	4.35,-1	2.38,-1	4.55,-1	2.43,-1
40	1.18,-2	5.88,-3	2.80,-1	1.71,-1	2.92,-1	1.77,-1
45	8.06,-3	7.27,-3	1.85,-1	1.30,-1	1.93,-1	1.37,-1
50	7.02,-3	7.66,-3	1.27,-1	1.02,-1	1.34,-1	1.10,-1
55	7.16,-3	7.28,-3	9.08,-2	8.16,-2	9.79,-2	8.89,-2
60	7.63,-3	6.52,-3	6.62,-2	6.57,-2	7.38,-2	7.22,-2
70	8.26,-3	4.86,-3	3.67,-2	4.29,-2	4.50,-2	4.77,-2
80	8.23,-3	3.42,-3	2.06,-2	2.85,-2	2.88,-2	3.19,-2
90	8.12,-3	2.19,-3	1.34,-2	2.01,-2	2.15,-2	2.23,-2
100	8.57,-3	1.26,-3	1.40,-2	1.63,-2	2.26,-2	1.76,-2
110	9.87,-3	9.88,-4	2.14,-2	1.68,-2	3.12,-2	1.77,-2
120	1.20,-2	1.71,-3	3.41,-2	2.12,-2	4.60,-2	2.30,-2
130	1.46,-2	3.57,-3	5.03,-2	2.91,-2	6.49,-2	3.27,-2
140	1.74,-2	6.41,-3	6.80,-2	3.91,-2	8.54,-2	4.55,-2
150	2.01,-2	9.74,-3	8.47,-2	4.95,-2	1.05,-1	5.92,-2
160	2.22,-2	1.28,-2	9.86,-2	5.86,-2	1.21,-1	7.14,-2
170	2.36,-2	1.50,-2	1.08,-1	6.49,-2	1.31,-1	7.99,-2
180	2.41,-2	1.57,-2	1.11,-1	6.76,-2	1.35,-1	8.33,-2
Integral (πa_o^2)	7.70,-2	6.92,-2	8.13,-1	5.58,-1	8.90,-1	6.27,-1

TABLE 9(a)

DIFFERENTIAL CROSS SECTIONS IN UNITS OF $a_o^2 sr^{-1}$ FOR ELECTRON IMPACT EXCITATION OF THE N = 2 LEVEL OF ATOMIC HYDROGEN COMPUTED IN THE DWPO III MODEL AT INCIDENT ENERGIES OF (a) 54.4 eV (= 4 Ryd) AND (b) 100 eV. THE FOURTH COLUMN GIVES THE TOTAL UNITARIZED RESULT.

E = 54.4 eV

θ^o	2s	2p	Total	
0	1.73	4.39,+1	4.56,+1	4.42,+1
5	1.25	2.31,+1	2.43,+1	2.24,+1
10	6.24,-1	7.66	8.28	6.82
15	2.76,-1	2.60	2.88	2.18
20	1.21,-1	9.29,-1	1.05	7.88,-1
25	5.52,-2	3.45,-1	4.00,-1	3.24,-1
30	2.73,-2	1.33,-1	1.60,-1	1.50,-1
35	1.50,-2	5.36,-2	6.86,-2	7.87,-2
40	9.22,-3	2.32,-2	3.25,-2	4.66,-2
45	6.35,-3	1.13,-2	1.77,-2	3.08,-2
50	4.77,-3	6.43,-3	1.12,-2	2.19,-2
55	3.78,-3	4.31,-3	8.09,-3	1.65,-2
60	3.07,-3	3.26,-3	6.33,-3	1.28,-2
70	2.09,-3	2.09,-3	4.19,-3	8.03,-3
80	1.44,-3	1.20,-3	2.64,-3	4.98,-3
90	9.91,-4	5.84,-4	1.58,-3	3.13,-3
100	7.33,-4	3.39,-4	1.07,-3	2.14,-3
110	6.29,-4	4.08,-4	1.04,-3	1.75,-3
120	6.49,-4	6.79,-4	1.33,-3	1.72,-3
130	7.56,-4	1.07,-3	1.83,-3	1.95,-3
140	9.12,-4	1.59,-3	2.50,-3	2.38,-3
150	1.09,-3	2.26,-3	3.35,-3	2.91,-3
160	1.23,-3	3.00,-3	4.23,-3	3.44,-3
170	1.34,-3	3.59,-3	4.92,-3	3.83,-3
180	1.38,-3	3.81,-3	5.19,-3	3.97,-3
Integral (πa_o^2)	7.46,-2	8.70,-1	9.44,-1	8.27,-1

TABLE 9(b)

E = 100 eV

θ^{o}	2s	2p	Total	
0	2.54	9.68,+1	9.94,+1	9.82,+1
5	1.31	2.16,+1	2.30,+1	2.14,+1
10	4.34,-1	4.08	4.51	3.87
15	1.42,-1	9.50,-1	1.09	9.20,-1
20	5.03,-2	2.45,-1	2.95,-1	2.63,-1
25	1.94,-2	6.76,-2	8.69,-2	8.96,-2
30	8.00,-3	2.04,-2	2.84,-2	3.83,-2
35	3.62,-3	6.89,-3	1.05,-2	1.98,-2
40	1.89,-3	2.74,-3	4.63,-3	1.17,-2
45	1.19,-3	1.33,-3	2.52,-3	7.80,-3
50	8.71,-4	8.16,-4	1.68,-3	5.63,-3
55	7.03,-4	6.16,-4	1.32,-3	4.30,-3
60	5.99,-4	5.07,-4	1.11,-3	3.39,-3
70	4.53,-4	3.21,-4	7.74,-4	2.04,-3
80	3.37,-4	1.85,-4	5.23,-4	1.28,-3
90	2.47,-4	9.40,-5	3.42,-4	8.00,-4
100	1.80,-4	7.44,-5	2.55,-4	5.71,-4
110	1.36,-4	1.02,-4	2.37,-4	4.46,-4
120	1.11,-4	1.31,-4	2.42,-4	3.79,-4
130	1.05,-4	1.62,-4	2.67,-4	3.57,-4
140	1.07,-4	2.18,-4	3.25,-4	3.76,-4
150	1.20,-4	3.26,-4	4.47,-4	4.48,-4
160	1.31,-4	4.78,-4	6.08,-4	5.42,-4
170	1.40,-4	6.25,-4	7.65,-4	6.44,-4
180	1.50,-4	6.94,-4	8.44,-4	6.46,-4
Integral (πa_o^2)	4.99,-2	6.63,-1	7.13,-1	6.65,-1

TOTAL CROSS SECTION IN UNITS OF πa_o^2 FOR ELECTRON IMPACT EXCITATION OF $He(n^1S)$ n = 2, 3, 4, 5 COMPUTED IN THE DWPO I (FIRST COLUMN) AND DWPO II (SECOND COLUMN) MODELS.

E (eV)	2^1S		3^1S		4^1S		5^1S	
	(I)	(II)	(I)	(II)	(I)	(II)	(I)	(II)
25	2.82,-2	2.75,-2	5.03,-3	5.02,-3	1.81,-3	1.83,-3	7.98,-4	8.09,-4
30	2.68,-2	2.53,-2	6.22,-3	5.97,-3	2.70,-3	2.63,-3	1.33,-3	1.30,-3
40	2.05,-2	1.88,-2	4.83,-3	4.45,-3	1.97,-3	1.83,-3	9.70,-4	9.03,-4
50	1.73,-2	1.58,-2	3.93,-3	3.56,-3	1.49,-3	1.34,-3	7.22,-4	6.50,-4
60	1.58,-2	1.45,-2	3.43,-3	3.09,-3	1.30,-3	1.16,-3	6.31,-4	5.64,-4
70	1.49,-2	1.37,-2	3.23,-3	2.93,-3	1.22,-3	1.10,-3	5.93,-4	5.32,-4
80	1.42,-2	1.32,-2	3.10,-3	2.84,-3	1.18,-3	1.07,-3	5.72,-4	5.17,-4
90	1.36,-2	1.27,-2	2.99,-3	2.76,-3	1.14,-3	1.04,-3	5.55,-4	5.06,-4
100	1.30,-2	1.23,-2	2.89,-3	2.68,-3	1.10,-3	1.02,-3	5.37,-4	4.93,-4
125	1.17,-2	1.12,-2	2.63,-3	2.47,-3	1.01,-3	9.43,-4	4.92,-4	4.59,-4
150	1.05,-2	1.01,-2	2.39,-3	2.27,-3	9.20,-4	8.68,-4	4.49,-4	4.23,-4
200	8.65,-3	8.43,-3	1.99,-3	1.91,-3	7.67,-4	7.35,-4	3.75,-4	3.59,-4
300	6.29,-3	6.21,-3	1.46,-3	1.43,-3	5.64,-4	5.50,-4	2.76,-4	2.69,-4

TABLE 10

TABLE 11(a)

DIFFERENTIAL CROSS SECTION IN UNITS OF $a_o^2 sr^{-1}$ FOR ELECTRON IMPACT EXCITATION OF $He(2^1S)$ COMPUTED IN THE DWPO I AND DWPO II MODELS AT INCIDENT ENERGIES OF (a) 29.6 eV, (b) 40.1 eV, (c) 81.63 eV, (d) 100 eV AND (e) 200 eV. COLUMN (A) IS OBTAINED USING THE EXCITED STATE WAVE FUNCTION OF COHEN AND McEACHRAN AND (B) USING THAT OF BYRON AND JOACHAIN - SEE APPENDIX A FOR DETAILS.

E = 29.6 eV

θ^o	(I)		(II)	
	(A)	(B)	(A)	(B)
0	2.34,-1	2.34,-2	2.52,-2	2.52,-2
5	2.29,-2	2.29,-2	2.44,-2	2.45,-2
10	2.15,-2	2.15,-2	2.24,-2	2.24,-2
15	1.93,-2	1.93,-2	1.95,-2	1.94,-2
20	1.66,-2	1.66,-2	1.61,-2	1.60,-2
25	1.38,-2	1.37,-2	1.28,-2	1.26,-2
30	1.11,-2	1.10,-2	9.80,-3	9.62,-3
35	8.64,-3	8.47,-3	7.40,-3	7.17,-3
40	6.64,-3	6.43,-3	5.63,-3	5.35,-3
45	5.14,-3	4.88,-3	4.43,-3	4.12,-3
50	4.12,-3	3.82,-3	3.74,-3	3.40,-3
55	3.53,-3	3.20,-3	3.44,-3	3.08,-3
60	3.29,-3	2.96,-3	3.42,-3	3.04,-3
70	3.57,-3	3.18,-3	3.90,-3	3.49,-3
80	4.36,-3	3.95,-3	4.63,-3	4.21,-3
90	5.28,-3	4.85,-3	5.35,-3	4.91,-3
100	6.13,-3	5.69,-3	5.95,-3	5.50,-3
110	6.84,-3	6.39,-3	6.42,-3	5.96,-3
120	7.40,-3	6.95,-3	6.77,-3	6.31,-3
130	7.84,-3	7.38,-3	7.04,-3	6.57,-3
140	8.17,-3	7.70,-3	7.25,-3	6.76,-3
150	8.41,-3	7.94,-3	7.40,-3	6.91,-3
160	8.58,-3	8.11,-3	7.50,-3	7.01,-3
170	8.68,-3	8.20,-3	7.56,-3	7.07,-3
180	8.71,-3	8.23,-3	7.58,-3	7.09,-3
Integral (πa_o^2)	2.70,-2	2.55,-2	2.55,-2	2.40,-2

TABLE 11(b)

E = 40.1 eV

θ°	(I)		(II)	
	(A)	(B)	(A)	(B)
0	4.66,-2	4.71,-2	5.78,-2	5.85,-2
5	4.50,-2	4.55,-2	5.46,-2	5.53,-2
10	4.05,-2	4.09,-2	4.64,-2	4.69,-2
15	3.40,-2	3.44,-2	3.57,-2	3.61,-2
20	2.65,-2	2.69,-2	2.52,-2	2.55,-2
25	1.93,-2	1.95,-2	1.64,-2	1.66,-2
30	1.30,-2	1.32,-2	9.85,-3	9.96,-3
35	8.02,-3	8.15,-3	5.44,-3	5.48,-3
40	4.54,-3	4.59,-3	2.78,-3	2.76,-3
45	2.35,-3	2.35,-3	1.40,-3	1.34,-3
50	1.19,-3	1.14,-3	8.70,-4	7.83,-4
55	7.66,-4	6.87,-4	8.63,-4	7.57,-4
60	8.20,-4	7.17,-4	1.14,-3	1.02,-3
70	1.60,-3	1.47,-3	1.96,-3	1.82,-3
80	2.56,-3	2.42,-3	2.70,-3	2.56,-3
90	3.34,-3	3.19,-3	3.22,-3	3.07,-3
100	3.89,-3	3.74,-3	3.55,-3	3.38,-3
110	4.26,-3	4.10,-3	3.74,-3	3.56,-3
120	4.49,-3	4.33,-3	3.85,-3	3.67,-3
130	4.65,-3	4.48,-3	3.92,-3	3.73,-3
140	4.76,-3	4.58,-3	3.97,-3	3.76,-3
150	4.83,-3	4.65,-3	4.00,-3	3.79,-3
160	4.88,-3	4.69,-3	4.02,-3	3.81,-3
170	4.90,-3	4.71,-3	4.03,-3	3.82,-3
180	4.91,-3	4.72,-3	4.03,-3	3.82,-3
Integral (πa_o^2)	2.04,-2	2.01,-2	1.87,-2	1.83,-2

TABLE 11(c)

E = 81.63 eV

θ^{o}	(I)		(II)	
	(A)	(B)	(A)	(B)
0	1.07,-1	1.08,-1	1.67,-1	1.67,-1
5	1.00,-1	1.00,-1	1.42,-1	1.43,-1
10	8.16,-2	8.17,-2	9.52,-2	9.57,-2
15	5.81,-2	5.83,-2	5.56,-2	5.59,-2
20	3.67,-2	3.69,-2	2.94,-2	2.95,-2
25	2.06,-2	2.07,-2	1.42,-2	1.42,-2
30	1.03,-2	1.04,-2	6.20,-3	6.19,-3
35	4.54,-3	4.56,-3	2.38,-3	2.35,-3
40	1.71,-3	1.70,-3	7.60,-4	7.35,-4
45	5.36,-4	5.19,-4	2.15,-4	1.98,-4
50	1.87,-4	1.74,-4	1.30,-4	1.25,-4
55	1.92,-4	1.88,-4	2.11,-4	2.16,-4
60	3.16,-4	3.23,-4	3.29,-4	3.42,-4
70	5.68,-4	5.91,-4	5.17,-4	5.38,-4
80	6.97,-4	7.28,-4	5.93,-4	6.17,-4
90	7.30,-4	7.62,-4	5.97,-4	6.20,-4
100	7.20,-4	7.50,-4	5.85,-4	6.05,-4
110	6.92,-4	7.20,-4	5.60,-4	5.78,-4
120	6.58,-4	6.83,-4	5.20,-4	5.36,-4
130	6.30,-4	6.53,-4	4.97,-4	5.10,-4
140	6.09,-4	6.30,-4	4.89,-4	5.02,-4
150	5.90,-4	6.09,-4	4.65,-4	4.77,-4
160	5.75,-4	5.94,-4	4.44,-4	4.55,-4
170	5.72,-4	5.91,-4	4.58,-4	4.69,-4
180	5.74,-4	5.92,-4	4.77,-4	4.87,-4
Integral (πa_o^2)	1.41,-2	1.42,-2	1.31,-2	1.32,-2

TABLE 11(d)

E = 100 eV

θ°	(I)		(II)	
	(A)	(B)	(A)	(B)
0	1.22,-1	1.22,-1	1.98,-1	2.00,-1
5	1.12,-1	1.12,-1	1.62,-1	1.62,-1
10	8.75,-2	8.77,-2	9.92,-2	9.97,-2
15	5.87,-2	5.88,-2	5.33,-2	5.34,-2
20	3.43,-2	3.44,-2	2.60,-2	2.60,-2
25	1.77,-2	1.78,-2	1.17,-2	1.17,-2
30	8.18,-3	8.19,-3	4.86,-3	4.80,-3
35	3.38,-3	3.35,-3	1.85,-3	1.79,-3
40	1.26,-3	1.22,-3	6.55,-4	6.11,-4
45	4.70,-4	4.38,-4	2.70,-4	2.43,-4
50	2.60,-4	2.40,-4	2.03,-4	1.90,-4
55	2.66,-4	2.59,-4	2.38,-4	2.38,-4
60	3.29,-4	3.34,-4	2.94,-4	3.01,-4
70	4.31,-4	4.51,-4	3.64,-4	3.81,-4
80	4.58,-4	4.85,-4	3.75,-4	3.97,-4
90	4.42,-4	4.70,-4	3.57,-4	3.80,-4
100	4.10,-4	4.38,-4	3.30,-4	3.52,-4
110	3.77,-4	4.03,-4	3.02,-4	3.23,-4
120	3.48,-4	3.73,-4	2.78,-4	2.99,-4
130	3.25,-4	3.48,-4	2.59,-4	2.79,-4
140	3.07,-4	3.29,-4	2.44,-4	2.64,-4
150	2.93,-4	3.15,-4	2.33,-4	2.53,-4
160	2.84,-4	3.06,-4	2.26,-4	2.45,-4
170	2.78,-4	3.00,-4	2.22,-4	2.40,-4
180	2.77,-4	2.98,-4	2.21,-4	2.39,-4
Integral (πa_o^2)	1.30,-2	1.31,-2	1.23,-2	1.23,-2

TABLE 11(e)

E = 200 eV

θ^{o}	(I)		(II)	
	(A)	(B)	(A)	(B)
0	1.57,-1	1.57,-1	2.94,-1	2.96,-1
5	1.33,-1	1.34,-1	1.84,-1	1.85,-1
10	8.37,-2	8.41,-2	8.01,-2	8.04,-2
15	4.11,-2	4.13,-2	3.11,-2	3.12,-2
20	1.69,-2	1.70,-2	1.13,-2	1.13,-2
25	6.16,-3	6.19,-3	3.99,-3	3.96,-3
30	2.14,-3	2.12,-3	1.41,-3	1.38,-3
35	7.77,-4	7.55,-4	5.48,-4	5.26,-4
40	3.49,-4	3.31,-4	2.67,-4	2.53,-4
45	2.20,-4	2.10,-4	1.76,-4	1.68,-4
50	1.78,-4	1.74,-4	1.44,-4	1.40,-4
55	1.58,-4	1.58,-4	1.27,-4	1.26,-4
60	1.43,-4	1.45,-4	1.15,-4	1.16,-4
70	1.14,-4	1.19,-4	9.18,-5	9.47,-5
80	8.91,-5	9.42,-5	7.20,-5	7.58,-5
90	6.98,-5	7.48,-5	5.70,-5	6.11,-5
100	5.58,-5	6.07,-5	4.59,-5	5.02,-5
110	4.56,-5	5.04,-5	3.78,-5	4.21,-5
120	3.83,-5	4.30,-5	3.19,-5	3.62,-5
130	3.31,-5	3.77,-5	2.77,-5	3.20,-5
140	2.95,-5	3.40,-5	2.47,-5	2.90,-5
150	2.69,-5	3.14,-5	2.26,-5	2.68,-5
160	2.52,-5	2.97,-5	2.13,-5	2.55,-5
170	2.43,-5	2.87,-5	2.05,-5	2.47,-5
180	2.41,-5	2.85,-5	2.05,-5	2.47,-5
Integral (πa_o^2)	8.65,-3	8.70,-3	8.43,-3	8.47,-3

TABLE 12(a)

DIFFERENTIAL CROSS SECTION IN UNITS OF $a_o^2 sr^{-1}$ FOR ELECTRON IMPACT EXCITATION OF $He(2^1S)$ COMPUTED IN THE DWPO III MODEL AT INCIDENT ENERGIES OF (a) 29.6, 40.1, 81.63 eV and (b) 100 AND 200 eV.

θ^o	29.6 eV	40.1 eV	81.63 eV
0	2.28,-2	5.48,-2	1.64,-1
5	2.21,-2	5.18,-2	1.40,-1
10	2.02,-2	4.38,-2	9.36,-2
15	1.74,-2	3.36,-2	5.46,-2
20	1.43,-2	2.36,-2	2.88,-2
25	1.12,-2	1.53,-2	1.39,-2
30	8.49,-3	9.11,-3	6.03,-3
35	6.28,-3	4.96,-3	2.27,-3
40	4.65,-3	2.46,-3	6.95,-4
45	3.56,-3	1.17,-3	1.79,-4
50	2.93,-3	6.81,-4	1.20,-4
55	2.65,-3	6.80,-4	2.25,-4
60	2.63,-3	9.38,-4	3.63,-4
70	3.05,-3	1.70,-3	5.71,-4
80	3.70,-3	2.36,-3	6.44,-4
90	4.31,-3	2.80,-3	6.26,-4
100	4.81,-3	3.04,-3	5.82,-4
110	5.19,-3	3.16,-3	5.24,-4
120	5.46,-3	3.21,-3	4.55,-4
130	5.66,-3	3.22,-3	4.06,-4
140	5.81,-3	3.22,-3	3.78,-4
150	5.92,-3	3.22,-3	3.42,-4
160	6.00,-3	3.23,-3	3.14,-4
170	6.04,-3	3.23,-3	3.21,-4
180	6.06,-3	3.23,-3	3.35,-4
Integral (πa_o^2)	2.09,-2	1.65,-2	1.28,-2

TABLE 12(b)

θ^{o}	100 eV	200 eV
0	1.97,-1	2.96,-1
5	1.60,-1	1.84,-1
10	9.82,-2	8.03,-2
15	5.26,-2	3.12,-2
20	2.57,-2	1.14,-2
25	1.15,-2	3.98,-3
30	4.72,-3	1.37,-3
35	1.74,-3	5.03,-4
40	5.78,-4	2.33,-4
45	2.22,-4	1.57,-4
50	1.84,-4	1.37,-4
55	2.46,-4	1.31,-4
60	3.22,-4	1.25,-4
70	4.14,-4	1.07,-4
80	4.24,-4	8.55,-5
90	3.91,-4	6.58,-5
100	3.41,-4	4.92,-5
110	2.90,-4	3.59,-5
120	2.45,-4	2.59,-5
130	2.08,-4	1.86,-5
140	1.81,-4	1.34,-5
150	1.61,-4	9.93,-6
160	1.48,-4	7.75,-6
170	1.40,-4	6.58,-6
180	1.38,-4	6.31,-6
Integral (πa_o^2)	1.21,-2	8.44,-3

TABLE 13(a)

DIFFERENTIAL CROSS SECTION IN UNITS OF $a_o^2 sr^{-1}$ FOR ELECTRON IMPACT EXCITATION OF $He(3^1S)$ COMPUTED IN THE DWPO I AND DWPO II MODELS AT INCIDENT ENERGIES OF (a) 29.2 AND 39.7 eV AND (b) 100 AND 200 eV.

θ^o	29.2 eV		39.7 eV	
	DWPO I	DWPO II	DWPO I	DWPO II
0	3.15,-3	3.21,-3	7.35,-3	8.78,-3
5	3.11,-3	3.15,-3	7.14,-3	8.38,-3
10	2.97,-3	2.98,-3	6.54,-3	7.32,-3
15	2.77,-3	2.73,-3	5.66,-3	5.88,-3
20	2.51,-3	2.42,-3	4.61,-3	4.38,-3
25	2.23,-3	2.10,-3	3.53,-3	3.04,-3
30	1.94,-3	1.80,-3	2.53,-3	1.98,-3
35	1.67,-3	1.54,-3	1.70,-3	1.22,-3
40	1.44,-3	1.33,-3	1.08,-3	7.32,-4
45	1.25,-3	1.18,-3	6.59,-4	4.66,-4
50	1.12,-3	1.09,-3	4.22,-4	3.58,-4
55	1.03,-3	1.04,-3	3.26,-4	3.56,-4
60	9.99,-4	1.04,-3	3.31,-4	4.15,-4
70	1.04,-3	1.11,-3	5.01,-4	6.04,-4
80	1.17,-3	1.24,-3	7.30,-4	7.84,-4
90	1.34,-3	1.37,-3	9.30,-4	9.17,-4
100	1.51,-3	1.49,-3	1.08,-3	1.00,-3
110	1.66,-3	1.59,-3	1.18,-3	1.05,-3
120	1.78,-3	1.67,-3	1.24,-3	1.08,-3
130	1.88,-3	1.73,-3	1.29,-3	1.10,-3
140	1.96,-3	1.78,-3	1.32,-3	1.11,-3
150	2.01,-3	1.81,-3	1.34,-3	1.12,-3
160	2.05,-3	1.84,-3	1.35,-3	1.13,-3
170	2.08,-3	1.85,-3	1.36,-3	1.13,-3
180	2.08,-3	1.85,-3	1.36,-3	1.13,-3
Integral (πa_o^2)	6.24,-3	6.03,-3	4.88,-3	4.50,-3

TABLE 13(b)

θ^{o}	100 eV		200 eV	
	DWPO I	DWPO II	DWPO I	DWPO II
0	2.30,-2	3.79,-2	3.03,-2	5.71,-2
5	2.15,-2	2.17,-2	2.67,-2	3.88,-2
10	1.76,-2	2.06,-2	1.83,-2	1.80,-2
15	1.26,-2	1.17,-2	9.89,-3	7.50,-3
20	7.90,-3	6.02,-3	4.39,-3	2.92,-3
25	4.36,-3	2.85,-3	1.70,-3	1.07,-3
30	2.13,-3	1.24,-3	6.05,-4	3.91,-4
35	9.20,-4	4.83,-4	2.18,-4	1.48,-4
40	3.52,-4	1.71,-4	9.31,-5	6.92,-5
45	1.26,-4	6.40,-5	5.51,-5	4.33,-5
50	5.94,-5	4.23,-5	4.34,-5	3.47,-5
55	5.64,-5	5.06,-5	3.87,-5	3.06,-5
60	7.26,-5	6.54,-5	3.52,-5	2.82,-5
70	1.02,-4	8.64,-5	2.87,-5	2.29,-5
80	1.13,-4	9.17,-5	2.27,-5	1.81,-5
90	1.11,-4	8.84,-5	1.79,-5	1.42,-5
100	1.04,-4	8.20,-5	1.43,-5	1.14,-5
110	9.56,-5	7.52,-5	1.17,-5	9.44,-6
120	8.84,-5	6.92,-5	9.85,-6	8.05,-6
130	8.24,-5	6.43,-5	8.51,-6	7.04,-6
140	7.77,-5	6.06,-5	7.55,-6	6.29,-6
150	7.42,-5	5.78,-5	6.90,-6	5.69,-6
160	7.18,-5	5.59,-5	6.47,-6	5.26,-6
170	7.05,-5	5.48,-5	6.22,-6	4.98,-6
180	7.00,-5	5.46,-5	6.11,-6	4.58,-6
Integral (πa_o^2)	2.89,-3	2.68,-3	1.99,-3	1.91.-3

TABLE 14(a)

DIFFERENTIAL CROSS SECTION IN UNITS OF $a_o^2 sr^{-1}$ FOR ELECTRON IMPACT EXCITATION OF $He(4^1S)$ COMPUTED IN THE DWPO I AND DWPO II MODELS AT INCIDENT ENERGIES OF (a) 50 AND 60 eV AND (b) 100 AND 200 eV.

θ^o	50 eV		60 eV	
	DWPO I	DWPO II	DWPO I	DWPO II
0	3.98,-3	5.23,-3	5.20,-3	7.37,-3
5	3.84,-3	4.91,-3	5.00,-3	6.77,-3
10	3.45,-3	4.07,-3	4.42,-3	5.34,-3
15	2.88,-3	3.03,-3	3.59,-3	3.73,-3
20	2.23,-3	2.06,-3	2.67,-3	2.35,-3
25	1.59,-3	1.27,-3	1.80,-3	1.35,-3
30	1.04,-3	7.13,-4	1.09,-3	6.91,-4
35	6.09,-4	3.55,-4	5.84,-4	3.06,-4
40	3.12,-4	1.53,-4	2.63,-4	1.06,-4
45	1.35,-4	5.91,-5	8.90,-5	2.15,-5
50	4.95,-5	3.28,-5	1.52,-5	1.72,-6
55	2.68,-5	4.42,-5	9.97,-6	1.36,-5
60	4.13,-5	7.33,-5	1.71,-5	3.76,-5
70	1.14,-4	1.41,-4	7.49,-5	8.62,-5
80	1.87,-4	1.92,-4	1.23,-4	1.18,-4
90	2.38,-4	2.23,-4	1.51,-4	1.33,-4
100	2.69,-4	2.38,-4	1.65,-4	1.39,-4
110	2.86,-4	2.44,-4	1.70,-4	1.39,-4
120	2.95,-4	2.46,-4	1.71,-4	1.37,-4
130	3.00,-4	2.46,-4	1.70,-4	1.34,-4
140	3.02,-4	2.45,-4	1.68,-4	1.32,-4
150	3.02,-4	2.44,-4	1.67,-4	1.30,-4
160	3.03,-4	2.43,-4	1.66,-4	1.29,-4
170	3.03,-4	2.42,-4	1.65,-4	1.28,-4
180	3.03,-4	2.42,-4	1.65,-4	1.28,-4
Integral (πa_o^2)	1.49,-3	1.34,-3	1.30,-3	1.16,-3

TABLE 14(b)

θ^{o}	100 eV		200 eV	
	DWPO I	DWPOII	DWPO I	DWPO II
0	8.36,-2	1.38,-2	1.12,-2	2.11,-2
5	7.86,-3	1.16,-2	9.90,-3	1.45,-2
10	6.52,-3	7.67,-3	6.92,-3	6.87,-3
15	4.76,-3	4.42,-3	3.86,-3	2.93,-3
20	3.04,-3	2.32,-3	1.76,-3	1.16,-3
25	1.72,-3	1.12,-3	6.89,-4	4.30,-4
30	8.55,-4	4.93,-4	2.48,-4	1.59,-4
35	3.77,-4	1.96,-4	8.98,-5	6.00,-5
40	1.46,-4	7.04,-5	3.78,-5	2.76,-5
45	5.26,-5	2.60,-5	2.18,-5	1.70,-5
50	2.38,-5	1.63,-5	1.71,-5	1.35,-5
55	2.15,-5	1.92,-5	1.52,-5	1.19,-5
60	2.76,-5	2.49,-5	1.38,-5	1.10,-5
70	3.96,-5	3.33,-5	1.15,-5	9.05,-6
80	4.40,-5	3.55,-5	9.04,-6	7.20,-6
90	4.33,-5	3.43,-5	7.21,-6	5.68,-6
100	4.05,-5	3.17,-5	5.74,-6	4.58,-6
110	3.73,-5	2.90,-5	4.73,-6	3.78,-6
120	3.44,-5	2.66,-5	3.96,-6	3.22,-6
130	3.19,-5	2.46,-5	3.43,-6	2.82,-6
140	3.00,-5	2.31,-5	3.05,-6	2.52,-6
150	2.86,-5	2.20,-5	2.78,-6	2.28,-6
160	2.77,-5	2.12,-5	2.61,-6	2.11,-6
170	2.71,-5	2.08,-5	2.50,-6	2.00,-6
180	2.69,-5	2.06,-5	2.53,-6	1.86,-6
Integral (πa_o^2)	1.10,-3	1.02,-3	7.67,-4	7.35,-4

TABLE 15(a)

DIFFERENTIAL CROSS SECTION IN UNITS OF $a_o^2 sr^{-1}$ FOR ELECTRON IMPACT EXCITATION OF $He(5^1S)$ COMPUTED IN THE DWPO I AND DWPO II MODELS AT INCIDENT ENERGIES OF (a) 50 AND 60 eV AND (b) 100 AND 200 eV.

θ^o	50 eV		60 eV	
	DWPO I	DWPO II	DWPO I	DWPO II
0	1.86,-3	2.45,-3	2.45,-3	3.47,-3
5	1.80,-3	2.30,-3	2.36,-3	3.20,-3
10	1.62,-3	1.92,-3	2.09,-3	2.53,-3
15	1.36,-3	1.44,-3	1.71,-3	1.78,-3
20	1.06,-3	9.79,-4	1.28,-3	1.13,-3
25	7.64,-4	6.10,-4	8.68,-4	6.51,-4
30	5.01,-4	3.44,-4	5.31,-4	3.36,-4
35	2.96,-4	1.73,-4	2.86,-4	1.49,-4
40	1.53,-4	7.56,-5	1.30,-4	5.22,-5
45	6.72,-5	2.98,-5	4.45,-5	1.09,-5
50	2.53,-5	1.68,-5	7.92,-6	1.08,-6
55	1.37,-5	2.22,-5	5.93,-7	6.88,-6
60	2.04,-5	3.62,-5	8.38,-6	1.87,-5
70	5.55,-5	6.92,-5	3.70,-5	4.29,-5
80	9.13,-5	9.45,-5	6.10,-5	5.87,-5
90	1.17,-4	1.10,-4	7.52,-5	6.65,-5
100	1.32,-4	1.17,-4	8.21,-5	6.92,-5
110	1.41,-4	1.20,-4	8.47,-5	6.93,-5
120	1.45,-4	1.21,-4	8.51,-5	6.84,-5
130	1.47,-4	1.21,-4	8.47,-5	6.71,-5
140	1.48,-4	1.20,-4	8.40,-5	6.60,-5
150	1.49,-4	1.20,-4	8.33,-5	6.50,-5
160	1.49,-4	1.19,-4	8.27,-5	6.43,-5
170	1.49,-4	1.19,-4	8.24,-5	6.39,-5
180	1.49,-4	1.19,-4	8.23,-5	6.38,-5
Integral (πa_o^2)	7.22,-4	6.50,-4	6.31,-4	5.64,-4

TABLE 15(b)

θ°	100 eV		200 eV	
	DWPO I	DWPO II	DWPO I	DWPO II
0	3.98,-3	6.59,-3	5.29,-3	1.01,-2
5	3.75,-3	5.57,-3	4.73,-3	7.01,-3
10	3.13,-3	3.70,-3	3.37,-3	3.35,-3
15	2.30,-3	2.15,-3	1.90,-3	1.44,-3
20	1.48,-3	1.13,-3	8.72,-4	5.75,-4
25	8.44,-4	5.50,-4	3.45,-4	2.15,-4
30	4.24,-4	2.44,-4	1.25,-4	7.94,-5
35	1.88,-4	9.73,-5	4.51,-5	3.00,-5
40	7.34,-5	3.49,-5	1.88,-5	1.37,-5
45	2.63,-5	1.27,-5	1.08,-5	8.36,-6
50	1.16,-5	7.83,-6	8.37,-6	6.63,-6
55	1.04,-5	9.24,-6	7.47,-6	5.87,-6
60	1.34,-5	1.21,-5	6.86,-6	5.44,-6
70	1.95,-5	1.64,-5	5.66,-6	4.48,-6
80	2.18,-5	1.76,-5	4.51,-6	3.57,-6
90	2.15,-5	1.70,-5	3.57,-6	2.83,-6
100	2.01,-5	1.57,-5	2.87,-6	2.28,-6
110	1.86,-5	1.44,-5	2.35,-6	1.88,-6
120	1.71,-5	1.32,-5	1.98,-6	1.61,-6
130	1.59,-5	1.22,-5	1.71,-6	1.40,-6
140	1.49,-5	1.15,-5	1.52,-6	1.26,-6
150	1.42,-5	1.09,-5	1.39,-6	1.14,-6
160	1.38,-5	1.05,-5	1.30,-6	1.06,-6
170	1.35,-5	1.03,-5	1.25,-6	1.00,-6
180	1.34,-5	1.02,-5	1.23,-6	9.33,-7
Integral (πa_o^2)	5.37,-4	4.93,-4	3.75,-4	3.59,-4

TABLE 16

TOTAL CROSS SECTION IN UNITS OF πa_o^2 FOR ELECTRON IMPACT EXCITATION OF $He(2^3S)$ COMPUTED IN THE DWPO I MODEL.

E(eV)	T.C.S.
25	7.80,-3
30	2.18,-3
40	3.80,-3
50	4.83,-3
60	4.58,-3
70	3.93,-3
80	3.26,-3
90	2.66,-3
100	2.16,-3
125	1.32,-3
150	8.41,-4
200	3.98,-4
300	1.27,-4

TABLE 17(a)

DIFFERENTIAL CROSS SECTION IN UNITS OF $a_o^2 sr^{-1}$ FOR ELECTRON IMPACT EXCITATION OF He(2^3S) COMPUTED IN THE DWPO I MODEL AT INCIDENT ENERGIES OF (a) 29.6 AND 40.1 eV, (b) 81.63 AND 100 eV AND (c) 200 eV. COLUMN (A) IS OBTAINED USING THE EXCITED STATE WAVE FUNCTION OF COHEN AND McEACHRAN AND (B) USING THAT OF MORSE ET AL. - SEE APPENDIX A FOR DETAILS.

θ^o	29.6 eV		40.1 eV	
	(A)	(B)	(A)	(B)
0	1.84,-3	2.64,-3	1.69,-3	1.59,-3
5	1.76,-3	2.55,-3	1.59,-3	1.47,-3
10	1.53,-3	2.30,-3	1.31,-3	1.16,-3
15	1.20,-3	1.94,-3	9.70,-4	7.76,-4
20	8.46,-4	1.54,-3	7.00,-4	4.51,-4
25	5.22,-4	1.17,-3	5.86,-4	2.88,-4
30	2.82,-4	8.86,-4	6.57,-4	3.20,-4
35	1.49,-4	7.17,-4	8.75,-4	5.14,-4
40	1.24,-4	6.64,-4	1.16,-3	7.97,-4
45	1.83,-4	7.06,-4	1.44,-3	1.08,-3
50	2.93,-4	8.09,-4	1.64,-3	1.30,-3
55	4.20,-4	9.37,-4	1.73,-3	1.41,-3
60	5.32,-4	1.06,-3	1.69,-3	1.40,-3
70	6.41,-4	1.19,-3	1.33,-3	1.09,-3
80	5.78,-4	1.16,-3	8.01,-4	6.07,-4
90	4.21,-4	1.03,-3	3.50,-4	1.97,-4
100	2.84,-4	9.10,-4	1.23,-4	1.57,-5
110	2.54,-4	8.96,-4	1.60,-4	1.05,-4
120	3.72,-4	1.03,-3	4.23,-4	4.29,-4
130	6.23,-4	1.29,-3	8.39,-4	9.10,-4
140	9.60,-4	1.65,-3	1.32,-3	1.45,-3
150	1.32,-3	2.02,-3	1.79,-3	1.98,-3
160	1.63,-3	2.35,-3	2.17,-3	2.40,-3
170	1.85,-3	2.57,-3	2.42,-3	2.68,-3
180	1.92,-3	2.65,-3	2.51,-3	2.78,-3
Integral (πa_o^2)	2.30,-3	4.76,-3	3.81,-3	3.32,-3

TABLE 17(b)

θ°	81.63 eV		100 eV	
	(A)	(B)	(A)	(B)
0	9.25,-4	9.73,-4	6.19,-4	6.70,-4
5	8.92,-4	9.37,-4	6.04,-4	6.55,-4
10	8.72,-4	9.12,-4	6.41,-4	6.94,-4
15	1.01,-3	1.05,-3	8.52,-4	9.14,-4
20	1.35,-3	1.40,-3	1.23,-3	1.31,-3
25	1.80,-3	1.86,-3	1.63,-3	1.73,-3
30	2.20,-3	2.29,-3	1.90,-3	2.02,-3
35	2.44,-3	2.54,-3	1.98,-3	2.12,-3
40	2.47,-3	2.59,-3	1.89,-3	2.02,-3
45	2.32,-3	2.44,-3	1.67,-3	1.80,-3
50	2.05,-3	2.17,-3	1.41,-3	1.52,-3
55	1.73,-3	1.84,-3	1.13,-3	1.24,-3
60	1.41,-3	1.49,-3	8.85,-4	9.69,-4
70	8.44,-4	8.98,-4	5.02,-4	5.55,-4
80	4.66,-4	4.95,-4	2.72,-4	3.04,-4
90	2.60,-4	2.75,-4	1.55,-4	1.75,-4
100	1.81,-4	1.89,-4	1.10,-4	1.23,-4
110	1.79,-4	1.88,-4	1.05,-4	1.15,-4
120	2.20,-4	2.34,-4	1.21,-4	1.30,-4
130	2.80,-4	2.99,-4	1.44,-4	1.54,-4
140	3.42,-4	3.67,-4	1.69,-4	1.80,-4
150	3.98,-4	4.28,-4	1.90,-4	2.02,-4
160	4.41,-4	4.75,-4	2.07,-4	2.19,-4
170	4.68,-4	5.04,-4	2.17,-4	2.30,-4
180	4.76,-4	5.14,-4	2.20,-4	2.33,-4
Integral (πa_o^2)	3.15,-3	3.32,-3	2.16,-3	2.33,-3

TABLE 17(c)

θ^{o}	200 eV	
	(A)	(B)
0	1.09,-4	1.21,-4
5	1.20,-4	1.34,-4
10	2.19,-4	2.40,-4
15	4.22,-4	4.53,-4
20	5.97,-4	6.40,-4
25	6.50,-4	7.01,-4
30	5.95,-4	6.45,-4
35	4.87,-4	5.31,-4
40	3.72,-4	4.08,-4
45	2.72,-4	3.00,-4
50	1.93,-4	2.15,-4
55	1.36,-4	1.52,-4
60	9.46,-5	1.07,-4
70	4.63,-5	5.36,-5
80	2.40,-5	2.85,-5
90	1.42,-5	1.71,-5
100	1.03,-5	1.21,-5
110	8.93,-6	1.01,-5
120	8.69,-6	9.43,-6
130	8.89,-6	9.30,-6
140	9.21,-6	9.38,-6
150	9.52,-6	9.52,-6
160	9.75,-6	9.65,-6
170	9.89,-6	9.72,-6
180	9.96,-6	9.76,-6
Integral (πa_o^2)	3.98,-4	4.38,-4

TABLE 18(a)

DIFFERENTIAL CROSS SECTION IN UNITS OF $a_o^2 sr^{-1}$ FOR ELECTRON IMPACT EXCITATION OF $He(2^3S)$ COMPUTED IN THE DWPO III MODELS AT INCIDENT ENERGIES OF (a) 29.6, 40.1 AND 81.63 eV AND (b) 100 AND 200 eV.

θ^o	29.6 eV	40.1 eV	81.63 eV
0	2.02,-3	2.46,-4	1.25,-3
5	1.98,-3	2.21,-4	1.31,-3
10	1.88,-3	1.69,-4	1.52,-3
15	1.75,-3	1.45,-4	1.91,-3
20	1.62,-3	2.05,-4	2.43,-3
25	1.53,-3	3.77,-4	2.94,-3
30	1.50,-3	6.47,-4	3.30,-3
35	1.54,-3	9.65,-4	3.43,-3
40	1.63,-3	1.27,-3	3.33,-3
45	1.77,-3	1.49,-3	3.04,-3
50	1.91,-3	1.60,-3	2.64,-3
55	2.04,-3	1.58,-3	2.19,-3
60	2.15,-3	1.45,-3	1.74,-3
70	2.24,-3	9.59,-4	9.67,-4
80	2.20,-3	4.23,-4	4.45,-4
90	2.14,-3	8.85,-5	1.77,-4
100	2.15,-3	8.37,-5	1.18,-4
110	2.31,-3	4.24,-4	2.14,-4
120	2.64,-3	1.05,-3	4.12,-4
130	3.10,-3	1.85,-3	6.66,-4
140	3.63,-3	2.71,-3	9.34,-4
150	4.15,-3	3.51,-3	1.18,-3
160	4.59,-3	4.16,-3	1.38,-3
170	4.88,-3	4.58,-3	1.51,-3
180	4.98,-3	4.72,-3	1.55,-3
Integral (πa_o^2)	9.88,-3	4.78,-3	4.57,-3

TABLE 18(b)

θ^{o}	100 eV	200 eV
0	1.00,-3	2.41,-4
5	1.08,-3	2.94,-4
10	1.31,-3	4.67,-4
15	1.72,-3	7.04,-4
20	2.21,-3	8.74,-4
25	2.62,-3	9.09,-6
30	2.83,-3	8.36,-4
35	2.82,-3	7.10,-4
40	2.62,-3	5.74,-4
45	2.30,-3	4.49,-4
50	1.93,-3	3.43,-4
55	1.55,-3	2.57,-4
60	1.20,-3	1.88,-4
70	6.50,-4	9.34,-5
80	2.98,-4	3.90,-5
90	1.21,-4	1.31,-5
100	8.02,-5	8.29,-6
110	1.37,-4	1.92,-5
120	2.59,-4	4.14,-5
130	4.15,-4	7.04,-5
140	5.82,-4	1.02,-4
150	7.37,-4	1.32,-4
160	8.61,-4	1.56,-4
170	9.41,-4	1.72,-4
180	9.69,-4	1.78,-4
Integral (πa_o^2)	3.35,-3	7.22,-4

TOTAL (INTEGRAL) CROSS SECTIONS IN UNITS OF πa_o^2 FOR ELECTRON IMPACT EXCITATION OF $He(n^1P)$, WITH (a) n = 2, (b) n = 3, (c) n = 4 AND (d) n = 5, COMPUTED IN THE DWPO I AND DWPO II MODELS.

	DWPO I			DWPO II		
E (eV)	2^1P_o	$2^1P_{\pm1}$	2^1P	2^1P_o	$2^1P_{\pm1}$	2^1P
25	1.88,-2	2.37,-3	2.35,-2	1.47,-2	1.93,-3	1.86,-2
	8.41,-2	4.50,-3	9.31,-2	7.35,-2	3.92,-3	8.14,-2
30	3.18,-2	6.62,-3	4.50,-2	2.60,-2	5.45,-3	3.69,-2
	1.07,-1	1.19,-2	1.31,-1	9.46,-2	1.04,-2	1.15,-1
40	5.84,-2	1.57,-2	8.99,-2	5.04,-2	1.35,-2	7.74,-2
	1.14,-1	2.30,-2	1.59,-1	1.02,-1	2.03,-2	1.42,-1
50	7.21,-2	2.23,-2	1.17,-1	6.38,-2	1.95,-2	1.03,-1
	1.07,-1	2.95,-2	1.66,-1	9.68,-2	2.62,-2	1.49,-1
60	7.69,-2	2.65,-2	1.30,-1	6.90,-2	2.34,-2	1.16,-1
	9.84,-2	3.31,-2	1.65,-1	8.97,-2	2.96,-2	1.49,-1
70	7.71,-2	2.92,-2	1.35,-1	7.00,-2	2.60,-2	1.22,-1
	9.00,-2	3.51,-2	1.60,-1	8.27,-2	3.15,-2	1.46,-1
80	7.51,-2	3.08,-2	1.37,-1	6.87,-2	2.77,-2	1.24,-1
	8.26,-2	3.61,-2	1.55,-1	7.63,-2	3.26,-2	1.41,-1
90	7.21,-2	3.18,-2	1.36,-1	6.63,-2	2.87,-2	1.24,-1
	7.61,-2	3.65,-2	1.49,-1	7.06,-2	3.30,-2	1.37,-1
100	6.86,-2	3.23,-2	1.33,-1	6.35,-2	2.92,-2	1.22,-1
	7.05,-2	3.65,-2	1.43,-1	6.57,-2	3.31,-2	1.32,-1
125	6.03,-2	3.25,-2	1.25,-1	5.63,-2	2.96,-2	1.15,-1
	5.92,-2	3.57,-2	1.31,-1	5.57,-2	3.25,-2	1.21,-1

continued.....

TABLE 19(a) continued.....

E (eV)	2^1P_o	$2^1P_{\pm1}$	2^1P	2^1P_o	$2^1P_{\pm1}$	2^1P
150	5.30,-2	3.18,-2	1.17,-1	4.98,-2	2.91,-2	1.08,-1
	5.10,-2	3.43,-2	1.20,-1	4.82,-2	3.14,-2	1.11,-1
200	4.21,-2	2.97,-2	1.02,-1	4.00,-2	2.74,-2	9.47,-2
	3.98,-2	3.13,-2	1.03,-1	3.80,-2	2.89,-2	9.58,-2
300	2.94,-2	2.55,-2	8.05,-2	2.82,-2	2.38,-2	7.57,-2
	2.76,-2	2.64,-2	8.04,-2	2.66,-2	2.45,-2	7.57,-2

For each value of the energy the first line gives the DWPO result and the second line the corresponding Born or 'Born plus Polarized-Born' result.

	DWPO I			DWPO II		
E (eV)	3^1P_o	$3^1P_{\pm1}$	3^1P	3^1P_o	$3^1P_{\pm1}$	3^1P
25	3.08,-3	1.38,-4	3.36,-3	2.32,-3	9.89,-5	2.52,-3
	1.58,-2	4.18,-4	1.67,-2	1.37,-2	3.61,-4	1.44,-2
30	5.57,-3	1.01,-3	7.59,-3	4.36,-3	8.03,-4	5.96,-3
	2.52,-2	2.14,-3	2.95,-2	2.20,-2	1.86,-3	2.57,-2
40	1.24,-2	3.19,-3	1.88,-2	1.05,-2	2.70,-3	1.59,-2
	2.85,-2	5.05,-3	3.86,-2	2.53,-2	4.43,-3	3.41,-2
50	1.66,-2	4.90,-3	2.64,-2	1.45,-2	4.25,-3	2.30,-2
	2.72,-2	6.84,-3	4.09,-2	2.44,-2	6.05,-3	3.65,-2
60	1.84,-2	6.05,-3	3.05,-2	1.63,-2	5.32,-3	2.70,-2
	2.52,-2	7.89,-3	4.09,-2	2.28,-2	7.01,-3	3.68,-2
70	1.88,-2	6.82,-3	3.25,-2	1.69,-2	6.05,-3	2.90,-2
	2.31,-2	8.48,-3	4.00,-2	2.11,-2	7.57,-3	3.62,-2
80	1.86,-2	7.31,-3	3.32,-2	1.68,-2	6.52,-3	2.99,-2
	2.12,-2	8.80,-3	3.88,-2	1.94,-2	7.89,-3	3.52,-2
90	1.80,-2	7.62,-3	3.33,-2	1.64,-2	6.83,-3	3.01,-2
	1.95,-2	8.96,-3	3.74,-2	1.80,-2	8.05,-3	3.41,-2
100	1.73,-2	7.81,-3	3.29,-2	1.58,-2	7.02,-3	2.99,-2
	1.81,-2	9.00,-3	3.61,-2	1.67,-2	8.12,-3	3.30,-2
125	1.53,-2	7.94,-3	3.12,-2	1.42,-2	7.20,-3	2.86,-2
	1.52,-2	8.85,-3	3.29,-2	1.42,-2	8.03,-3	3.03,-2
150	1.35,-2	7.83,-3	2.92,-2	1.26,-2	7.14,-3	2.69,-2
	1.30,-2	8.55,-3	3.01,-2	1.23,-2	7.79,-3	2.79,-2

TABLE 19(b)

continued.....

TABLE 19(b) continued...

	DWPO I			DWPO II		
E (eV)	3^1P_o	$3^1P_{\pm 1}$	3^1P	3^1P_o	$3^1P_{\pm 1}$	3^1P
200	1.08,-2	7.37,-3	2.55,-2	1.02,-2	6.77,-3	2.37,-2
	1.02,-2	7.85,-3	2.59,-2	9.65,-3	7.20,-3	2.41,-2
300	7.50,-3	6.39,-3	2.03,-2	7.16,-3	5.92,-3	1.90,-2
	7.03,-3	6.63,-3	2.03,-2	6.75,-3	6.14,-3	1.90,-2

For each value of the energy, the first line gives the DWPO result and the second line the corresponding Born or 'Born plus Polarized-Born' result.

	DWPO I			DWPO II		
E (eV)	4^1P_o	$4^1P_{\pm1}$	4^1P	4^1P_o	$4^1P_{\pm1}$	4^1P
30	3.86,-3	3.28,-4	4.52,-3	4.01,-3	2.56,-4	4.52,-3
40	4.46,-3	1.18,-3	6.82,-3	3.84,-3	9.91,-4	5.82,-3
50	6.41,-3	1.89,-3	1.02,-2	5.56,-3	1.63,-3	8.82,-3
60	7.43,-3	2.39,-3	1.22,-2	6.56,-3	2.09,-3	1.07,-2
70	7.77,-3	2.72,-3	1.32,-2	6.95,-3	2.40,-3	1.17,-2
80	7.72,-3	2.93,-3	1.36,-2	6.98,-3	2.61,-3	1.22,-2
90	7.50,-3	3.07,-3	1.36,-2	6.82,-3	2.74,-3	1.23,-2
100	7.19,-3	3.15,-3	1.35,-2	6.58,-3	2.83,-3	1.22,-2
125	6.36,-3	3.23,-3	1.28,-2	5.89,-3	2.92,-3	1.17,-2
150	5.61,-3	3.19,-3	1.20,-2	5.23,-3	2.90,-3	1.10,-2
200	4.43,-3	2.99,-3	1.04,-2	4.17,-3	2.74,-3	9.65,-3
300	2.96,-3	2.51,-3	7.97,-3	2.82,-3	2.31,-3	7.43,-3

TABLE 19(c)

	DWPO I			DWPO II		
E (eV)	5^1P_o	$5^1P_{\pm1}$	5^1P	5^1P_o	$5^1P_{\pm1}$	5^1P
30	1.43,-3	1.41,-4	1.71,-3	1.48,-3	1.09,-4	1.70,-3
	1.46,-3	2.28,-4	1.92,-3	1.49,-3	1.83,-4	1.85,-3
40	2.08,-3	5.52,-4	3.18,-3	1.77,-3	4.62,-4	2.69,-3
	2.98,-3	7.90,-4	4.56,-3	2.62,-3	6.70,-4	3.96,-3
50	3.06,-3	8.98,-4	4.86,-3	2.65,-3	7.74,-4	4.20,-3
	4.12,-3	1.23,-3	6.57,-3	3.61,-3	1.07,-3	5.74,-3
60	3.56,-3	1.14,-3	5.84,-3	3.14,-3	9.94,-4	5.13,-3
	4.66,-3	1.53,-3	7.72,-3	4.14,-3	1.35,-3	6.83,-3
70	3.74,-3	1.30,-3	6.34,-3	3.35,-3	1.15,-3	5.64,-3
	4.83,-3	1.74,-3	8.30,-3	4.33,-3	1.54,-3	7.41,-3
80	3.72,-3	1.40,-3	6.53,-3	3.36,-3	1.25,-3	5.85,-3
	4.81,-3	1.87,-3	8.56,-3	4.35,-3	1.67,-3	7.69,-3
90	3.61,-3	1.47,-3	6.56,-3	3.28,-3	1.31,-3	5.91,-3
	4.70,-3	1.96,-3	8.62,-3	4.28,-3	1.76,-3	7.79,-3
100	3.46,-3	1.51,-3	6.49,-3	3.17,-3	1.36,-3	5.88,-3
	4.53,-3	2.01,-3	8.55,-3	4.14,-3	1.81,-3	7.76,-3
125	3.07,-3	1.55,-3	6.17,-3	2.84,-3	1.40,-3	5.64,-3
	4.05,-3	2.06,-3	8.17,-3	3.74,-3	1.87,-3	7.48,-3
150	2.71,-3	1.53,-3	5.78,-3	2.52,-3	1.39,-3	5.31,-3
	3.58,-3	2.04,-3	7.66,-3	3.34,-3	1.86,-3	7.05,-3
200	2.14,-3	1.44,-3	5.02,-3	2.02,-3	1.32,-3	4.65,-3
	2.84,-3	1.91,-3	6.67,-3	2.68,-3	1.75,-3	6.19,-3

continued.....

TABLE 19(d)

TABLE J9(d) continued...

	DWPO I			DWPO II		
E (eV)	5^1P_o	$5^1P_{\pm1}$	5^1P	5^1P_o	$5^1P_{\pm1}$	5^1P
300	1.43,-3	1.21,-3	3.85,-3	1.36,-3	1.11,-3	3.59,-3
	1.91,-3	1.61,-3	5.12,-3	1.82,-3	1.48,-3	4.78,-3

For each value of the energy E, the first line of the results is computed using the modified Cohen and McEachran coefficients for the excited state wave function and the second line using the unmodified coefficients - see Appendix A for details.

TABLE 20(a)

DIFFERENTIAL CROSS SECTIONS IN UNITS OF $a_o^2 sr^{-1}$ FOR ELECTRON IMPACT EXCITATION OF $He(2^1P)$ COMPUTED IN THE DWPO I MODEL AT INCIDENT ENERGIES OF (a) 29.6 eV, (b) 40.1 eV, (c) 81.63 eV, (d) 100 eV AND (e) 200 eV.

E = 29.6 eV

θ^o	m = 0	m = 1	Total
0	1.85,-1	0	1.85,-1
5	1.75,-1	1.31,-3	1.78,-1
10	1.49,-1	4.43,-3	1.58,-1
15	1.16,-1	7.67,-3	1.31,-1
20	8.30,-2	9.65,-3	1.02,-1
25	5.55,-2	1.00,-2	7.55,-2
30	3.51,-2	9.10,-3	5.33,-2
35	2.11,-2	7.54,-3	3.62,-2
40	1.22,-2	5.83,-3	2.38,-2
45	6.73,-3	4.30,-3	1.53,-2
50	3.59,-3	3.06,-3	9.71,-3
55	1.87,-3	2.14,-3	6.14,-3
60	9.83,-4	1.48,-3	3.94,-3
70	3.67,-4	7.28,-4	1.82,-3
80	2.42,-4	3.97,-4	1.04,-3
90	1.70,-4	2.49,-4	6.69,-4
100	8.87,-5	1.76,-4	4.40,-4
110	2.70,-5	1.33,-4	2.93,-4
120	1.62,-5	1.03,-4	2.22,-4
130	6.53,-5	7.73,-5	2.20,-4
140	1.62,-4	5.39,-5	2.70,-4
150	2.80,-4	3.29,-5	3.46,-4
160	3.91,-4	1.57,-5	4.23,-4
170	4.71,-4	4.12,-6	4.79,-4
180	4.99,-4	0	4.99,-4
Integral (πa_o^2)	3.05,-2	6.22,-3	4.30,-2

TABLE 20(b)

E = 40.1 eV

θ^{o}	m = 0	m = 1	Total
0	7.36,-1	0	7.36,-1
5	6.48,-1	1.42,-2	6.77,-1
10	4.56,-1	3.91,-2	5.34,-1
15	2.72,-1	5.07,-2	3.74,-1
20	1.47,-1	4.66,-2	2.40,-1
25	7.43,-2	3.54,-2	1.45,-1
30	3.58,-2	2.39,-2	8.37,-2
35	1.65,-2	1.50,-2	4.65,-2
40	7.33,-3	8.94,-3	2.52,-2
45	3.18,-3	5.18,-3	1.35,-2
50	1.47,-3	2.97,-3	7.42,-3
55	8.68,-4	1.74,-3	4.34,-3
60	7.26,-4	1.06,-3	2.85,-3
70	7.64,-4	5.09,-4	1.78,-3
80	7.23,-4	3.42,-4	1.41,-3
90	5.58,-4	2.76,-4	1.11,-3
100	3.58,-4	2.34,-4	8.26,-4
110	1.90,-4	1.99,-4	5.89,-4
120	8.77,-5	1.65,-4	4.17,-4
130	5.34,-5	1.28,-4	3.10,-4
140	7.33,-5	9.10,-5	2.55,-4
150	1.25,-4	5.57,-5	2.36,-4
160	1.84,-4	2.64,-5	2.37,-4
170	2.29,-4	6.83,-6	2.42,-4
180	2.45,-4	0	2.45,-4
Integral (πa_o^2)	5.87,-2	1.58,-2	9.03,-2

TABLE 20(c)

E = 81.63 eV

θ^{o}	m = 0	m = 1	Total
0	3.93	0	3.93
5	2.15	2.99,-1	2.74
10	6.48,-1	3.15,-1	1.28
15	1.94,-1	1.72,-1	5.38,-1
20	6.50,-2	7.75,-2	2.20,-1
25	2.40,-2	3.21,-2	8.83,-2
30	9.76,-3	1.26,-2	3.49,-2
35	4.39,-3	4.72,-3	1.38,-2
40	2.26,-3	1.73,-3	5.71,-3
45	1.35,-3	6.59,-4	2.66,-3
50	9.23,-4	3.08,-4	1.54,-3
55	6.98,-4	2.08,-4	1.11,-3
60	5.54,-4	1.86,-4	9.26,-4
70	3.53,-4	1.85,-4	7.22,-4
80	2.18,-4	1.78,-4	5.73,-4
90	1.29,-4	1.60,-4	4.49,-4
100	7.51,-5	1.39,-4	3.53,-4
110	5.06,-5	1.16,-4	2.82,-4
120	4.61,-5	9.06,-5	2.27,-4
130	5.58,-5	6.69,-5	1.89,-4
140	7.20,-5	4.59,-5	1.64,-4
150	8.76,-5	2.76,-5	1.43,-4
160	1.02,-4	1.20,-5	1.26,-4
170	1.18,-4	2.52,-6	1.23,-4
180	1.28,-4	0	1.28,-4
Integral (πa_o^2)	7.46,-2	3.10,-2	1.37,-1

TABLE 20(d)

E = 100 eV

θ^{o}	m = 0	m = 1	Total
0	5.43	0	5.43
5	2.25	4.98,-1	3.25
10	5.03,-1	3.68,-1	1.24
15	1.31,-1	1.60,-1	4.52,-1
20	4.12,-2	6.13,-2	1.64,-1
25	1.51,-2	2.19,-2	5.90,-2
30	6.30,-3	7.45,-3	2.12,-2
35	3.01,-3	2.40,-3	7.82,-3
40	1.66,-3	7.54,-4	3.17,-3
45	1.04,-3	2.64,-4	1.57,-3
50	7.15,-4	1.43,-4	1.00,-3
55	5.22,-4	1.26,-4	7.75,-4
60	3.93,-4	1.31,-4	6.55,-4
70	2.21,-4	1.38,-4	4.97,-4
80	1.21,-4	1.31,-4	3.83,-4
90	6.42,-5	1.16,-4	2.95,-4
100	3.58,-5	9.81,-5	2.32,-4
110	2.68,-5	8.00,-5	1.87,-4
120	2.96,-5	6.15,-5	1.53,-4
130	3.89,-5	4.49,-5	1.29,-4
140	5.07,-5	2.95,-5	1.10,-4
150	6.38,-5	1.69,-5	9.77,-5
160	7.34,-5	7.78,-6	8.89,-5
170	8.05,-5	1.84,-6	8.42,-5
180	8.43,-5	0	8.43,-5
Integral (πa_o^2)	6.86,-2	3.23,-2	1.33,-1

TABLE 20 (e)

E = 200 eV

θ^o	m = 0	m = 1	Total
0	1.36,+1	0	1.36,+1
5	1.16	1.10	3.35
10	1.16,-1	2.73,-1	6.62,-1
15	2.40 ,-2	6.30,-2	1.50,-1
20	7.29,-3	1.40,-2	3.53,-2
25	2.86,-3	2.94,-3	8.74,-3
30	1.38,-3	5.48,-4	2.47,-3
35	7.66,-4	8.23,-5	9.31,-4
40	4.63,-4	1.82,-5	4.99,-4
45	2.93,-4	2.46,-5	3.42,-4
50	1.93,-4	3.56,-5	2.64,-4
55	1.30,-4	4.11,-5	2.12,-4
60	8.61,-5	4.20,-5	1.70,-4
70	3.49,-5	3.92,-5	1.13,-4
80	1.38,-5	3.32,-5	8.02,-5
90	4.41,-6	2.67,-5	5.77,-5
100	2.38,-6	2.13,-5	4.50,-5
110	3.36,-6	1.58,-5	3.50,-5
120	5.94,-6	1.16,-5	2.91,-5
130	8.49,-6	7.88,-6	2.42,-5
140	1.17,-5	4.94,-6	2.15,-5
150	1.33,-5	2.91,-6	1.91,-5
160	1.54,-5	1.13,-6	1.77,-5
170	1.65,-5	3.59,-7	1.72,-5
180	1.59,-5	0	1.59,-5
Integral (πa_o^2)	4.21,-2	2.97,-2	1.02,-1

TABLE 21 (a)

DIFFERENTIAL CROSS SECTIONS IN UNITS OF $a_o^2 sr^{-1}$ FOR ELECTRON IMPACT EXCITATION OF $He(2^1P)$ COMPUTED IN THE DWPO II MODEL AT INCIDENT ENERGIES OF (a) 29.6 eV, (b) 40.1 eV, (c) 81.63 eV, (d) 100 eV AND (e) 200 eV.

E = 29.6 eV

θ^o	m = 0	m = 1	Total
0	1.59,-1	0	1.59,-1
5	1.50,-1	1.15,-3	1.53,-1
10	1.28,-1	3.89,-3	1.35,-1
15	9.80,-2	6.69,-3	1.11,-1
20	6.91,-2	8.35,-3	8.58,-2
25	4.53,-2	8.58,-3	6.25,-2
30	2.80,-2	7.71,-3	4.34,-2
35	1.63,-2	6.30,-3	2.89,-2
40	9.02,-3	4.81,-3	1.86,-2
45	4.75,-3	3.49,-3	1.17,-2
50	2.38,-3	2.44,-3	7.27,-3
55	1.16,-3	1.67,-3	4.51,-3
60	5.85,-4	1.13,-3	2.85,-3
70	2.60,-4	5.31,-4	1.32,-3
80	2.21,-4	2.75,-4	7.71,-4
90	1.70,-4	1.65,-4	5.00,-4
100	9.04,-5	1.13,-4	3.16,-4
110	2.68,-5	8.36,-5	1.94,-4
120	1.08,-5	6.41,-5	1.39,-4
130	5.03,-5	4.83,-5	1.47,-4
140	1.33,-4	3.39,-5	2.01,-4
150	2.36,-4	2.09,-5	2.78,-4
160	3.33,-4	1.00,-5	3.54,-4
170	4.02,-4	2.65,-6	4.08,-4
180	4.27,-4	0	4.27,-4
Integral (πa_o^2)	2.46,-2	5.07,-3	3.47,-2

TABLE 21(b)

E = 40.1 eV

θ^{o}	m = 0	m = 1	Total
0	6.65,-1	0	6.65,-1
5	5.84,-1	1.30,-2	6.10,-1
10	4.06,-1	3.53,-2	4.76,-1
15	2.38,-1	4.53,-2	3.29,-1
20	1.26,-1	4.11,-2	2.08,-1
25	6.17,-2	3.07,-2	1.23,-1
30	2.87,-2	2.05,-2	6.96,-2
35	1.27,-2	1.26,-2	3.79,-2
40	5.31,-3	7.42,-3	2.01,-2
45	2.18,-3	4.23,-3	1.07,-2
50	1.01,-3	2.40,-3	5.80,-3
55	6.71,-4	1.38,-3	3.43,-3
60	6.49,-4	8.30,-4	2.31,-3
70	7.50,-4	3.88,-4	1.53,-3
80	7.08,-4	2.57,-4	1.22,-3
90	5.43,-4	2.05,-4	9.52,-4
100	3.48,-4	1.72,-4	6.93,-4
110	1.86,-4	1.46,-4	4.79,-4
120	8.46,-5	1.21,-4	3.26,-4
130	4.48,-5	9.42,-5	2.33,-4
140	5.36,-5	6.69,-5	1.87,-4
150	9.12,-5	4.11,-5	1.73,-4
160	1.37,-4	1.95,-5	1.76,-4
170	1.72,-4	5.06,-6	1.82,-4
180	1.85,-4	0	1.85,-4
Integral (πa_o^2)	5.06,-2	1.36,-2	7.77,-2

TABLE 21(c)

E = 81.63 eV

θ^{o}	m = 0	m = 1	Total
0	3.73	0	3.73
5	2.02	2.81,-1	2.58
10	5.91,-1	2.89,-1	1.17
15	1.71,-1	1.53,-1	4.78,-1
20	5.55,-2	6.76,-2	1.91,-1
25	2.01,-2	2.75,-2	7.51,-2
30	8.01,-3	1.07,-2	2.93,-2
35	3.60,-3	3.98,-3	1.16,-2
40	1.87,-3	1.46,-3	4.78,-3
45	1.14,-3	5.59,-4	2.26,-3
50	7.98,-4	2.65,-4	1.33,-3
55	6.12,-4	1.79,-4	9.71,-4
60	4.90,-4	1.60,-4	8.11,-4
70	3.16,-4	1.58,-4	6.31,-4
80	1.97,-4	1.51,-4	4.99,-4
90	1.17,-4	1.36,-4	3.90,-4
100	6.92,-5	1.18,-4	3.05,-4
110	4.64,-5	9.83,-5	2.43,-4
120	4.08,-5	7.67,-5	1.94,-4
130	4.77,-5	5.66,-5	1.61,-4
140	6.05,-5	3.88,-5	1.38,-4
150	7.29,-5	2.34,-5	1.20,-4
160	8.41,-5	1.01,-5	1.04,-4
170	9.79,-5	2.10,-6	1.02,-4
180	1.06,-4	0	1.06,-4
Integral (πa_o^2)	6.83,-2	2.79,-2	1.24,-1

TABLE 21(d)

E = 100 eV

θ^{o}	m = 0	m = 1	Total
0	5.20	0	5.20
5	2.12	4.72,-1	3.07
10	4.58,-1	3.38,-1	1.13
15	1.15,-1	1.42,-1	4.00,-1
20	3.52,-2	5.31,-2	1.41,-1
25	1.27,-2	1.87,-2	5.01,-2
30	5.27,-3	6.32,-3	1.79,-2
35	2.54,-3	2.04,-3	6.63,-3
40	1.42,-3	6.47,-4	2.72,-3
45	9.03,-4	2.30,-4	1.36,-3
50	6.28,-4	1.26,-4	8.79,-4
55	4.62,-4	1.10,-4	6.82,-4
60	3.49,-4	1.14,-4	5.77,-4
70	1.98,-4	1.19,-4	4.37,-4
80	1.09,-4	1.13,-4	3.36,-4
90	5.86,-5	9.99,-5	2.58,-4
100	3.29,-5	8.48,-5	2.03,-4
110	2.43,-5	6.91,-5	1.63,-4
120	2.60,-5	5.31,-5	1.32,-4
130	3.36,-5	3.88,-5	1.11,-4
140	4.34,-5	2.55,-5	9.43,-5
150	5.44,-5	1.46,-5	8.36,-5
160	6.24,-5	6.73,-6	7.58,-5
170	6.84,-5	1.59,-6	7.16,-5
180	7.18,-5	0	7.18,-5
Integral (πa_o^2)	6.35,-2	2.92,-2	1.22,-1

TABLE 21(e)

E = 200 eV

θ^{o}	m = 0	m = 1	Total
0	1.33,+1	0	1.33,+1
5	1.09	1.04	3.16
10	1.04,-1	2.45,-1	5.93,-1
15	2.09,-2	5.46,-2	1.30,-1
20	6.31,-3	1.20,-2	3.04,-2
25	2.51,-3	2.54,-3	7.60,-3
30	1.23,-3	4.86,-4	2.20,-3
35	6.91,-4	7.64,-5	8.44,-4
40	4.20,-4	1.70,-5	4.54,-4
45	2.67,-4	2.14,-5	3.10,-4
50	1.76,-4	3.10,-5	2.38,-4
55	1.18,-4	3.60,-5	1.90,-4
60	7.88,-5	3.70,-5	1.53,-4
70	3.21,-5	3.49,-5	1.02,-4
80	1.28,-5	2.97,-5	7.21,-5
90	4.13,-6	2.39,-5	5.19,-5
100	2.19,-6	1.92,-5	4.05,-5
110	3.01,-6	1.42,-5	3.15,-5
120	5.30,-6	1.05,-5	2.62,-5
130	7.58,-6	7.12,-6	2.18,-5
140	1.05,-5	4.47,-6	1.94,-5
150	1.19,-5	2.63,-6	1.72,-5
160	1.39,-5	1.02,-6	1.59,-5
170	1.48,-5	3.27,-7	1.55,-5
180	1.43,-5	0	1.43,-5
Integral (πa_o^2)	4.00,-2	2.74,-2	9.47,-2

TABLE 22(a)

DIFFERENTIAL CROSS SECTIONS IN UNITS OF $a_o^2 sr^{-1}$ FOR ELECTRON IMPACT EXCITATION OF $He(3^1P)$ COMPUTED IN THE DWPO. I MODEL AT INCIDENT ENERGIES OF (a) 29.2 eV, (b) 39.7 eV, (c) 100 eV AND (d) 200 eV.

E = 29.2 eV

θ^o	m = 0	m = 1	Total
0	2.20,-2	0	2.20,-2
5	2.12,-2	9.96,-5	2.14,-2
10	1.89,-2	3.54,-4	1.96,-2
15	1.57,-2	6.59,-4	1.71,-2
20	1.23,-2	9.08,-4	1.41,-2
25	9.06,-3	1.04,-3	1.11,-2
30	6.36,-3	1.05,-3	8.45,-3
35	4.26,-3	9.62,-4	6.19,-3
40	2.75,-3	8.21,-4	4.39,-3
45	1.71,-3	6.64,-4	3.04,-3
50	1.03,-3	5.14,-4	2.06,-3
55	6.05,-4	3.87,-4	1.38,-3
60	3.51,-4	2.85,-4	9.20,-4
70	1.25,-4	1.50,-4	4.26,-4
80	5.79,-5	8.17,-5	2.21,-4
90	3.43,-5	4.79,-5	1.30,-4
100	2.16,-5	3.07,-5	8.30,-5
110	1.70,-5	2.12,-5	5.93,-5
120	2.36,-5	1.51,-5	5.38,-5
130	4.25,-5	1.07,-5	6.39,-5
140	7.06,-5	7.20,-6	8.50,-5
150	1.02,-5	4.29,-6	1.11,-4
160	1.31,-4	2.00,-6	1.35,-4
170	1.51,-4	5.09,-7	1.52,-4
180	1.59,-4	0	1.59,-4
Integral (πa_o^2)	5.00,-3	8.42,-4	6.68,-3

TABLE 22(b)

E = 39.7 eV

θ^{o}	m = 0	m = 1	Total
0	1.24,-1	0	1.24,-1
5	1.12,-1	1.85,-3	1.16,-1
10	8.50,-2	5.51,-3	9.60,-2
15	5.57,-2	7.93,-3	7.15,-2
20	3.29,-2	8.12,-3	4.91,-2
25	1.80,-2	6.82,-3	3.17,-2
30	9.31,-3	5.04,-3	1.94,-2
35	4.54,-3	3.42,-3	1.14,-2
40	2.09,-3	2.19,-3	6.47,-3
45	9.08,-4	1.35,-3	3.60,-3
50	3.91,-4	8.12,-4	2.01,-3
55	2.00,-4	4.88,-4	1.18,-3
60	1.54,-4	3.01,-4	7.55,-4
70	1.79,-4	1.35,-4	4.49,-4
80	1.89,-4	8.21,-5	3.53,-4
90	1.55,-4	6.16,-5	2.78,-4
100	1.04,-4	5.01,-5	2.04,-4
110	5.65,-5	4.15,-5	1.40,-4
120	2.56,-5	3.39,-5	9.33,-5
130	1.32,-5	2.64,-5	6.60,-5
140	1.60,-5	1.89,-5	5.37,-5
150	2.76,-5	1.17,-5	5.10,-5
160	4.16,-5	5.58,-6	5.28,-5
170	5.26,-5	1.46,-6	5.55,-5
180	5.67,-5	0	5.67,-5
Integral (πa_o^2)	1.22,-2	3.13,-3	1.85,-2

TABLE 22(c)

E = 100 eV

θ^{o}	m = 0	m = 1	Total
0	1.12	0	1.12
5	5.33,-1	9.71,-2	7.27,-1
10	1.38,-1	8.49,-2	3.08,-1
15	3.89,-2	4.14,-2	1.22,-1
20	1.28,-2	1.73,-2	4.73,-2
25	4.75,-3	6.63,-3	1.80,-2
30	1.96,-3	2.39,-3	6.74,-3
35	9.04,-4	8.11,-4	2.53,-3
40	4.77,-4	2.65,-4	1.01,-3
45	2.90,-4	9.15,-5	4.73,-4
50	1.98,-4	4.36,-5	2.85,-4
55	1.45,-4	3.43,-5	2.13,-4
60	1.10,-4	3.48,-5	1.79,-4
70	6.52,-5	3.70,-5	1.39,-4
80	3.76,-5	3.52,-5	1.08,-4
90	2.13,-5	3.13,-5	8.40,-5
100	1.27,-5	2.66,-5	6.58,-5
110	9.38,-6	2.17,-5	5.28,-5
120	9.44,-6	1.68,-5	4.30,-5
130	1.15,-5	1.22,-5	3.59,-5
140	1.44,-5	8.04,-6	3.05,-5
150	1.75,-5	4.66,-6	2.69,-5
160	2.01,-5	2.08,-6	2.43,-5
170	2.20,-5	5.36,-7	2.30,-5
180	2.24,-5	0	2.24,-5
Integral (πa_o^2)	1.73,-2	7.81,-3	3.29,-2

TABLE 22(d)

E = 200 eV

θ^{o}	m = 0	m = 1	Total
0	2.87	0	2.87
5	3.18,-1	2.54,-1	8.25,-1
10	3.55,-2	7.34,-2	1.82,-1
15	7.67,-3	1.88,-2	4.52,-2
20	2.33,-3	4.52,-3	1.14,-2
25	8.96,-4	1.01,-3	2.92,-3
30	4.17,-4	2.02,-4	8.21,-4
35	2.26,-4	3.29,-5	2.92,-4
40	1.35,-4	5.95,-6	1.47,-4
45	8.48,-5	6.14,-6	9.71,-5
50	5.57,-5	9.23,-6	7.42,-5
55	3.75,-5	1.10,-5	5.95,-5
60	2.50,-5	1.15,-5	4.80,-5
70	1.03,-5	1.09,-5	3.21,-5
80	4.16,-6	9.28,-6	2.27,-5
90	1.40,-6	7.48,-6	1.64,-5
100	7.45,-7	5.98,-6	1.27,-5
110	9.78,-7	4.45,-6	9.89,-6
120	1.68,-6	3.27,-6	8.21,-6
130	2.39,-6	2.23,-6	6.84,-6
140	3.27,-6	1.40,-6	6.07,-6
150	3.75,-6	8.20,-7	5.39,-6
160	4.34,-6	3.21,-7	4.98,-6
170	4.64,-6	1.00,-7	4.84,-6
180	4.50,-6	0	4.50,-6
Integral (πa_o^2)	1.08,-2	7.37,-3	2.55,-2

TABLE 23(a)

DIFFERENTIAL CROSS SECTIONS IN UNITS OF $a_o^2 sr^{-1}$ FOR ELECTRON IMPACT EXCITATION OF $He(3^1P)$ COMPUTED IN THE DWPO II MODEL AT INCIDENT ENERGIES OF (a) 29.2 eV, (b) 39.7 eV, (c) 100 eV AND (d) 200 eV.

E = 29.2 eV

θ^o	m = 0	m = 1	Total
0	1.82,-2	0	1.82,-2
5	1.75,-2	8.57,-5	1.77,-2
10	1.55,-2	3.04,-4	1.61,-2
15	1.28,-2	5.62,-4	1.39,-2
20	9.85,-3	7.69,-4	1.14,-2
25	7.13,-3	8.73,-4	8.88,-3
30	4.88,-3	8.71,-4	6.62,-3
35	3.18,-3	7.89,-4	4.76,-3
40	1.97,-3	6.64,-4	3.30,-3
45	1.17,-3	5.29,-4	2.23,-3
50	6.67,-4	4.03,-4	1.47,-3
55	3.67,-4	2.97,-4	9.60,-4
60	1.98,-4	2.13,-4	6.25,-4
70	6.49,-5	1.07,-4	2.79,-4
80	3.44,-5	5.44,-5	1.43,-4
90	2.33,-5	2.98,-5	8.29,-5
100	1.43,-5	1.80,-5	5.02,-5
110	1.03,-5	1.18,-5	3.39,-5
120	1.62,-5	8.21,-6	3.26,-5
130	3.34,-5	5.78,-6	4.50,-5
140	5.92,-5	3.91,-6	6.71,-5
150	8.83,-5	2.36,-6	9.30,-5
160	1.15,-4	1.11,-6	1.17,-4
170	1.33,-4	2.84,-7	1.34,-4
180	1.40,-4	0	1.40,-4
Integral (πa_o^2)	3.86,-3	6.63,-4	5.19,-3

TABLE 23(b)

E = 39.7 eV

θ^{o}	m = 0	m = 1	Total
0	1.10,-1	0	1.10,-1
5	9.95,-2	1.67,-3	1.03,-1
10	7.44,-2	4.93,-3	8.43,-2
15	4.79,-2	7.03,-3	6.20,-2
20	2.76,-2	7.11,-3	4.19,-2
25	1.47,-2	5.88,-3	2.65,-2
30	7.30,-3	4.28,-3	1.59,-2
35	3.38,-3	2.87,-3	9.11,-3
40	1.45,-3	1.81,-3	5.07,-3
45	5.80,-4	1.09,-3	2.77,-3
50	2.35,-4	6.48,-4	1.53,-3
55	1.35,-4	3.83,-4	9.01,-4
60	1.33,-4	2.32,-4	5.96,-4
70	1.83,-4	1.00,-4	3.84,-4
80	1.91,-4	5.93,-5	3.10,-4
90	1.55,-4	4.36,-5	2.42,-4
100	1.03,-4	3.50,-5	1.73,-4
110	5.62,-5	2.88,-5	1.14,-4
120	2.53,-5	2.35,-5	7.24,-5
130	1.18,-5	1.84,-5	4.86,-5
140	1.21,-5	1.33,-5	3.86,-5
150	2.06,-5	8.26,-6	3.71,-5
160	3.16,-5	3.97,-6	3.95,-5
170	4.03,-5	1.04,-6	4.24,-5
180	4.37,-5	0	4.37,-5
Integral (πa_o^2)	1.04,-2	2.65,-3	1.57,-2

TABLE 23(c)

E = 100 eV

θ^{o}	m = 0	m = 1	Total
0	1.07	0	1.07
5	5.01,-1	9.17,-2	6.84,-1
10	1.25,-1	7.77,-2	2.81,-1
15	3.40,-2	3.67,-2	1.07,-1
20	1.08,-2	1.49,-2	4.07,-2
25	3.93,-3	5.64,-3	1.52,-2
30	1.60,-3	2.02,-3	5.63,-3
35	7.41,-4	6.86,-4	2.11,-3
40	3.96,-4	2.27,-4	8.50,-4
45	2.44,-4	8.02,-5	4.05,-4
50	1.69,-4	3.88,-5	2.46,-4
55	1.25,-4	3.02,-5	1.85,-4
60	9.53,-5	3.03,-5	1.56,-4
70	5.71,-5	3.18,-5	1.21,-4
80	3.33,-5	3.01,-5	9.36,-5
90	1.91,-5	2.68,-5	7.28,-5
100	1.15,-5	2.27,-5	5.70,-5
110	8.51,-6	1.86,-5	4.56,-5
120	8.38,-6	1.43,-5	3.70,-5
130	9.95,-6	1.04,-5	3.08,-5
140	1.23,-5	6.87,-6	2.61,-5
150	1.49,-5	3.99,-6	2.29,-5
160	1.71,-5	1.78,-6	2.06,-5
170	1.86,-5	4.58,-7	1.95,-5
180	1.89,-5	0	1.89,-5
Integral (πa_o^2)	1.58,-2	7.02,-3	2.99,-2

TABLE 23(d)

E = 200 eV

θ^{o}	m = 0	m = 1	Total
0	2.79	0	2.79
5	2.99,-1	2.40,-1	7.78,-1
10	3.17,-2	6.58,-2	1.63,-1
15	6.61,-3	1.62,-2	3.90,-2
20	2.00,-3	3.86,-3	9.72,-3
25	7.74,-4	8.72,-4	2.52,-3
30	3.66,-4	1.78,-4	7.22,-4
35	2.00,-4	3.07,-5	2.62,-4
40	1.20,-4	5.89,-6	1.32,-4
45	7.56,-5	5.48,-6	8.65,-5
50	4.96,-5	8.03,-6	6.57,-5
55	3.34,-5	9.59,-6	5.26,-5
60	2.23,-5	1.01,-5	4.24,-5
70	9.19,-6	9.60,-6	2.84,-5
80	3.71,-6	8.21,-6	2.01,-5
90	1.25,-6	6.64,-6	1.45,-5
100	6.67,-7	5.32,-6	1.13,-5
110	8.72,-7	3.96,-6	8.79,-6
120	1.49,-6	2.91,-6	7.31,-6
130	2.12,-6	1.98,-6	6.08,-6
140	2.91,-6	1.24,-6	5.40,-6
150	3.33,-6	7.30,-7	4.79,-6
160	3.85,-6	2.85,-7	4.42,-6
170	4.12,-6	8.96,-8	4.30,-6
180	3.98,-6	0	3.98,-6
Integral (πa_o^2)	1.02,-2	6.77,-3	2.37,-2

TABLE 24(a)

VALUES OF λ FOR ELECTRON IMPACT EXCITATION OF $He(2^1P)$ COMPUTED IN THE DWPO I AND DWPO II MODELS AT INCIDENT ENERGIES OF (a) 40 AND 60 eV, (b) 80 AND 100 eV AND (c) 200 eV.

θ^o	40 eV		60 eV	
	DWPO I	DWPO II	DWPO I	DWPO II
0	1.000	1.000	1.000	1.000
5	0.958	0.958	0.884	0.883
10	0.855	0.853	0.671	0.669
15	0.730	0.726	0.505	0.501
20	0.614	0.606	0.399	0.393
25	0.514	0.503	0.335	0.326
30	0.430	0.414	0.296	0.285
35	0.357	0.335	0.277	0.263
40	0.292	0.265	0.277	0.263
45	0.235	0.205	0.305	0.296
50	0.198	0.173	0.371	0.372
55	0.199	0.195	0.455	0.467
60	0.254	0.280	0.516	0.535
70	0.428	0.491	0.535	0.560
80	0.513	0.580	0.484	0.511
90	0.502	0.570	0.407	0.436
100	0.432	0.501	0.325	0.355
110	0.323	0.389	0.256	0.283
120	0.210	0.259	0.227	0.247
130	0.171	0.191	0.269	0.279
140	0.290	0.288	0.392	0.392
150	0.530	0.528	0.576	0.571
160	0.774	0.775	0.786	0.782
170	0.941	0.942	0.946	0.945
180	1.000	1.000	1.000	1.000

TABLE 24(b)

θ°	80 eV		100 eV	
	DWPO I	DWPO II	DWPO I	DWPO II
0	1.000	1.000	1.000	1.000
5	0.790	0.790	0.693	0.693
10	0.518	0.516	0.406	0.404
15	0.369	0.366	0.290	0.287
20	0.301	0.296	0.252	0.249
25	0.275	0.269	0.256	0.253
30	0.279	0.272	0.297	0.294
35	0.312	0.306	0.386	0.384
40	0.384	0.379	0.524	0.524
45	0.491	0.490	0.663	0.662
50	0.589	0.590	0.714	0.714
55	0.621	0.626	0.674	0.677
60	0.595	0.603	0.599	0.604
70	0.492	0.503	0.445	0.453
80	0.387	0.401	0.315	0.324
90	0.294	0.310	0.217	0.227
100	0.221	0.236	0.154	0.162
110	0.185	0.197	0.143	0.149
120	0.202	0.210	0.194	0.197
130	0.289	0.291	0.303	0.303
140	0.441	0.439	0.462	0.460
150	0.616	0.612	0.653	0.650
160	0.805	0.802	0.825	0.823
170	0.954	0.953	0.956	0.956
180	1.000	1.000	1.000	1.000

TABLE 24(c)

θ°	200 eV	
	DWPO I	DWPO II
0	1.000	1.000
5	0.345	0.345
10	0.175	0.175
15	0.160	0.161
20	0.206	0.208
25	0.327	0.331
30	0.557	0.558
35	0.823	0.819
40	0.927	0.925
45	0.857	0.862
50	0.731	0.740
55	0.612	0.622
60	0.506	0.515
70	0.308	0.315
80	0.172	0.177
90	0.076	0.079
100	0.053	0.054
110	0.096	0.096
120	0.204	0.202
130	0.350	0.348
140	0.541	0.539
150	0.696	0.694
160	0.873	0.872
170	0.958	0.958
180	1.000	1.000

TABLE 25(a)

VALUES OF χ IN RADIANS ($-\pi < \chi \leq \pi$) FOR ELECTRON IMPACT EXCITATION OF $He(2^1P)$ COMPUTED IN THE DWPO I AND DWPO II MODELS AT INCIDENT ENERGIES OF (a) 40 AND 60 eV, (b) 80 AND 100 eV AND (c) 200 eV.

θ°	40 eV		60 eV	
	DWPO I	DWPO II	DWPO I	DWPO II
5	-8.78,-2	-8.32,-2	-5.93,-2	-5.72,-2
10	-1.03,-1	-9.82,-2	-8.52,-2	-8.29,-2
15	-1.30,-1	-1.25,-1	-1.31,-1	-1.29,-1
20	-1.71,-1	-1.66,-1	-2.01,-1	-2.01,-1
25	-2.31,-1	-2.26,-1	-3.04,-1	-3.08,-1
30	-3.15,-1	-3.13,-1	-4.55,-1	-4.67,-1
35	-4.38,-1	-4.42,-1	-6.75,-1	-7.02,-1
40	-6.18,-1	-6.39,-1	-9.89,-1	-1.04
45	-8.89,-1	-9.47,-1	-1.41	-1.49
50	-1.29	-1.42	-1.92	-2.01
55	-1.81	-2.00	-2.45	-2.53
60	-2.35	-2.52	-2.93	-3.00
70	-3.12	3.05	2.71	2.66
80	2.71	2.64	2.38	2.35
90	2.47	2.42	2.20	2.18
100	2.31	2.29	2.03	2.03
110	2.16	2.17	1.79	1.82
120	1.85	1.92	1.45	1.50
130	1.25	1.37	1.06	1.12
140	6.83,-1	7.58,-1	7.70,-1	8.23,-1
150	4.05,-1	4.38,-1	5.89,-1	6.31,-1
160	2.79,-1	2.97,-1	4.90,-1	5.25,-1
170	2.21,-1	2.32,-1	4.55,-1	4.87,-1

TABLE 25(b)

θ°	80 eV		100 eV	
	DWPO I	DWPO II	DWPO I	DWPO II
5	-4.85,-2	-4.72,-2	-4.33,-2	-4.24,-2
10	-8.44,-2	-8.32,-2	-8.82,-2	-8.76,-2
15	-1.47,-1	-1.47,-1	-1.64,-1	-1.66,-1
20	-2.41 ,-1	-2.44,-1	-2.76,-1	-2.83,-1
25	-3.77,-1	-3.87,-1	-4.36,-1	-4.49,-1
30	-5.71,-1	-5.90,-1	-6.56,-1	-6.78,-1
35	-8.41,-1	-8.73,-1	-9.52,-1	-9.81,-1
40	-1.20	-1.25	-1.35	-1.38
45	-1.67	-1.72	-1.88	-1.91
50	-2.23	-2.27	-2.52	-2.54
55	-2.78	-2.81	-3.04	-3.05
60	3.07	3.05	2.91	2.91
70	2.58	2.57	2.55	2.55
80	2.33	2.32	2.34	2.34
90	2.13	2.13	2.11	2.12
100	1.89	1.90	1.78	1.79
110	1.54	1.57	1.35	1.38
120	1.16	1.20	9.53,-1	9.87,-1
130	8.48,-1	8.90,-1	6.89,-1	7.19,-1
140	6.37,-1	6.72,-1	5.33,-1	5.59,-1
150	5.12,-1	5.41,-1	4.41,-1	4.62,-1
160	4.45,-1	4.71,-1	3.84,-1	4.03,-1
170	4.22,-1	4.46,-1	3.71,-1	3.89,-1

TABLE 25(c)

θ°	200 eV	
	DWPO I	DWPO II
5	-4.09,-2	-4.05,-2
10	-1.19,-1	-1.21,-1
15	-2.37,-1	-2.44,-1
20	-3.92,-1	-4.04,-1
25	-5.91,-1	-6.04,-1
30	-8.49,-1	-8.61,-1
35	-1.28	-1.28
40	-2.26	-2.21
45	-3.07	-3.03
50	2.92	2.95
55	2.78	2.80
60	2.71	2.72
70	2.60	2.61
80	2.44	2.45
90	2.07	2.09
100	1.39	1.41
110	7.76,-1	7.99,-1
120	4.81,-1	4.96,-1
130	3.54,-1	3.65,-1
140	2.79,-1	2.88,-1
150	2.40,-1	2.48,-1
160	2.28,-1	2.36,-1
170	1.91,-1	1.98,-1

TABLE 26(a)

VALUES OF λ FOR ELECTRON IMPACT EXCITATION OF $He(3^1P)$ COMPUTED IN THE DWPO I AND DWPO II MODELS AT INCIDENT ENERGIES OF (a) 50 AND 80 eV AND (b) 100 AND 200 eV.

θ°	50 eV		80 eV	
	DWPO I	DWPO II	DWPO I	DWPO II
0	1.000	1.000	1.000	1.000
5	0.939	0.938	0.822	0.821
10	0.800	0.797	0.564	0.562
15	0.653	0.648	0.408	0.404
20	0.532	0.523	0.328	0.322
25	0.439	0.426	0.291	0.283
30	0.368	0.350	0.283	0.273
35	0.310	0.287	0.300	0.287
40	0.263	0.235	0.349	0.336
45	0.230	0.202	0.438	0.428
50	0.229	0.211	0.542	0.535
55	0.280	0.286	0.601	0.599
60	0.378	0.407	0.599	0.602
70	0.532	0.579	0.520	0.531
80	0.563	0.611	0.430	0.445
90	0.528	0.579	0.347	0.365
100	0.458	0.511	0.278	0.297
110	0.370	0.421	0.239	0.256
120	0.296	0.338	0.248	0.261
130	0.284	0.311	0.320	0.328
140	0.381	0.392	0.457	0.460
150	0.573	0.577	0.624	0.623
160	0.784	0.784	0.807	0.805
170	0.941	0.941	0.953	0.952
180	1.000	1.000	1.000	1.000

TABLE 26(b)

θ^{o}	100 eV		200 eV	
	DWPO I	DWPO II	DWPO I	DWPO II
0	1.000	1.000	1.000	1.000
5	0.733	0.732	0.385	0.384
10	0.448	0.446	0.195	0.194
15	0.319	0.316	0.170	0.169
20	0.271	0.266	0.205	0.205
25	0.264	0.259	0.307	0.307
30	0.291	0.284	0.508	0.506
35	0.358	0.351	0.775	0.765
40	0.474	0.466	0.919	0.911
45	0.613	0.604	0.874	0.873
50	0.694	0.685	0.751	0.756
55	0.679	0.674	0.630	0.635
60	0.612	0.611	0.521	0.525
70	0.468	0.473	0.322	0.324
80	0.348	0.356	0.183	0.184
90	0.254	0.263	0.085	0.086
100	0.193	0.202	0.059	0.059
110	0.178	0.186	0.099	0.099
120	0.220	0.226	0.204	0.204
130	0.319	0.323	0.350	0.349
140	0.473	0.473	0.539	0.539
150	0.653	0.652	0.696	0.695
160	0.829	0.828	0.871	0.871
170	0.954	0.953	0.959	0.958
180	1.000	1.000	1.000	1.000

TABLE 27(a)

VALUES OF χ IN RADIANS ($-\pi < \chi \leq \pi$) FOR ELECTRON IMPACT EXCITATION OF $He(3^1P)$ COMPUTED IN THE DWPO I AND DWPO II MODELS AT INCIDENT ENERGIES OF (a) 50 AND 80 eV AND (b) 100 AND 200 eV .

θ°	50 eV		80 eV	
	DWPO I	DWPO II	DWPO I	DWPO II
5	-7.71,-2	-7.32,-2	-5.22,-2	-5.05,-2
10	-9.57,-2	-9.13,-2	-8.50,-2	-8.33,-2
15	-1.28,-1	-1.24,-1	-1.41,-1	-1.40,-1
20	-1.78,-1	-1.74,-1	-2.26,-1	-2.28,-1
25	-2.51,-1	-2.48,-1	-3.48,-1	-3.56,-1
30	-3.56,-1	-3.58,-1	-5.24,-1	-5.42,-1
35	-5.11,-1	-5.24,-1	-7.75,-1	-8.07,-1
40	-7.44,-1	-7.81,-1	-1.12	-1.17
45	-1.09	-1.18	-1.58	-1.64
50	-1.58	-1.73	-2.13	-2.19
55	-2.14	-2.31	-2.70	-2.75
60	-2.66	-2.80	3.10	3.07
70	2.88	2.79	2.54	2.52
80	2.46	2.40	2.27	2.56
90	2.25	2.21	2.08	2.07
100	2.10	2.09	1.87	1.87
110	1.94	1.95	1.58	1.60
120	1.67	1.72	1.26	1.30
130	1.29	1.36	9.64,-1	1.01
140	8.98,-1	9.71,-1	7.46,-1	7.85,-1
150	6.42,-1	6.97,-1	6.09,-1	6.44,-1
160	5.02,-1	5.44,-1	5.31,-1	5.62,-1
170	4.32,-1	4.66,-1	4.98,-1	5.29,-1

TABLE 27(b)

θ°	100 eV		200 eV	
	DWPO I	DWPO II	DWPO I	DWPO II
5	-4.59,-2	-4.46,-2	-4.10,-2	-4.05,-2
10	-8.69,-2	-8.59,-2	-1.14,-1	-1.15,-1
15	-1.56,-1	-1.57,-1	-2.21,-1	-2.28,-1
20	-2.58,-1	-2.63,-1	-3.66,-1	-3.78,-1
25	-4.03,-1	-4.16,-1	-5.56,-1	-5.71,-1
30	-6.06,-1	-6.28,-1	-8.02,-1	-8.18,-1
35	-8.84,-1	-9.16,-1	-1.18	-1.19
40	-1.26	-1.30	-2.03	-1.99
45	-1.77	-1.81	-2.97	-2.91
50	-2.40	-2.43	2.95	2.99
55	-2.97	-2.98	2.78	2.82
60	2.92	2.92	2.69	2.72
70	2.52	2.51	2.58	2.59
80	2.28	2.28	2.42	2.43
90	2.06	2.06	2.06	2.07
100	1.77	1.78	1.42	1.43
110	1.40	1.42	8.15,-1	8.24,-1
120	1.04	1.07	5.07,-1	5.16,-1
130	7.79,-1	8.09,-1	3.72,-1	3.80,-1
140	6.11,-1	6.38,-1	2.93,-1	2.99,-1
150	5.07,-1	5.31,-1	2.52,-1	2.58,-1
160	4.49,-1	4.71,-1	2.36,-1	2.43,-1
170	4.14,-1	4.35,-1	2.02,-1	2.08,-1

TABLE 28

TOTAL (INTEGRAL) CROSS SECTION IN UNITS OF πa_o^2 FOR ELECTRON IMPACT EXCITATION OF $He(2^3P)$ COMPUTED IN THE DWPO I MODEL.

E (eV)	m = 0	m = 1	Total
25	2.18,-2	7.00,-3	3.58,-2
30	3.82,-2	9.31,-3	5.68,-2
40	3.65,-2	6.50,-3	4.95,-2
50	2.42,-2	3.89,-3	3.20,-2
60	1.52,-2	2.41,-3	2.00,-2
70	9.70,-3	1.58,-3	1.29,-2
80	6.37,-3	1.09,-3	8.54,-3
90	4.32,-3	7.83,-4	5.88,-3
100	3.02,-3	5.83,-4	4.19,-3
125	1.38,-3	3.13,-4	2.01,-3
150	7.14,-4	1.88,-4	1.09,-3
200	2.45,-4	8.64,-5	4.14,-4
300	5.21,-5	2.69,-5	1.06,-4

TABLE 29(a)

DIFFERENTIAL CROSS SECTIONS IN UNITS OF $a_o^2 sr^{-1}$ FOR ELECTRON IMPACT EXCITATION OF $He(2^3P)$ COMPUTED IN THE DWPO I MODEL AT INCIDENT ENERGIES OF (a) 29.6, (b) 40.1 (c) 81.63 (d) 100 AND (e) 200 eV. COLUMNS (A) ARE OBTAINED USING THE EXCITED STATE WAVE FUNCTION OF COHEN AND McEACHRAN AND COLUMNS (B) USING THAT OF MORSE ET AL. - SEE APPENDIX A FOR DETAILS.

E = 29.6 eV

	(A)			(B)		
θ^o	m = 0	m = 1	Total	m = 0	m = 1	Total
0	5.58,-2	0	5.58,-2	8.04,-2	0	8.04,-2
5	5.52,-2	1.18,-4	5.54,-2	7.97,-2	1.21,-4	7.99,-2
10	5.35,-2	4.54,-4	5.44,-2	7.76,-2	4.66,-4	7.85,-2
15	5.07,-2	9.60,-4	5.27,-2	7.42,-2	9.86,-4	7.62,-2
20	4.71,-2	1.57,-3	5.03,-2	6.97,-2	1.61,-3	7.29,-2
25	4.28,-2	2.20,-3	4.72,-2	6.43,-2	2.26,-3	6.88,-2
30	3.81,-2	2.79,-3	4.37,-2	5.83,-2	2.86,-3	6.40,-2
35	3.31,-2	3.29,-3	3.97,-2	5.20,-2	3.37,-3	5.87,-2
40	2.81,-2	3.67,-3	3.54,-2	4.55,-2	3.75,-3	5.30,-2
45	2.33,-2	3.92,-3	3.11,-2	3.92,-2	4.00,-3	4.72,-2
50	1.88,-2	4.03,-3	2.68,-2	3.31,-2	4.11,-3	4.13,-2
55	1.47,-2	4.04,-3	2.28,-2	2.75,-2	4.11,-3	3.57,-2
60	1.11,-2	3.96,-3	1.90,-2	2.24,-2	4.03,-3	3.05,-2
70	5.60,-3	3.62,-3	1.28,-2	1.40,-2	3.67,-3	2.14,-2
80	2.16,-3	3.17,-3	8.50,-3	8.01,-3	3.21,-3	1.44,-2
90	4.59,-4	2.69,-3	5.85,-3	4.03,-3	2.72,-3	9.47,-3
100	6.54,-5	2.23,-3	4.53,-3	1.66,-3	2.26,-3	6.17,-3
110	5.42,-4	1.80,-3	4.14,-3	4.61,-4	1.82,-3	4.10,-3
120	1.52,-3	1.39,-3	4.30,-3	3.56,-5	1.41,-3	2.85,-3
130	2.70,-3	1.02,-3	4.74,-3	7.35,-5	1.03,-3	2.13,-3
140	3.88,-3	6.83,-4	5.25,-3	3.46,-4	6.92,-4	1.73,-3
150	4.92,-3	4.00,-4	5.72,-3	6.92,-4	4.05,-4	1.50,-3
160	5.71,-3	1.83,-4	6.08,-3	1.00,-3	1.86,-4	1.38,-3
170	6.21,-3	4.67,-5	6.31,-3	1.22,-3	4.73,-5	1.31,-3
180	6.38,-3	0	6.38,-3	1.29,-3	0	1.29,-3
Integral (πa_o^2)	3.74,-2	9.32,-3	5.61,-2	5.94,-2	9.46,-3	7.83,-2

TABLE 29(b)

E = 40.1 eV

	(A)			(B)		
θ^{o}	m = 0	m = 1	Total	m = 0	m = 1	Total
0	6.43,-2	0	6.43,-2	8.21,-2	0	8.21,-2
5	6.35,-2	2.01,-4	6.39,-2	8.11,-2	2.04,-4	8.15,-2
10	6.11,-2	7.53,-4	6.26,-2	7.83,-2	7.64,-4	7.99,-2
15	5.73,-2	1.52,-3	6.03,-2	7.39,-2	1.54,-3	7.70,-2
20	5.24,-2	2.33,-3	5.70,-2	6.83,-2	2.36,-3	7.30,-2
25	4.68,-2	3.03,-3	5.28,-2	6.17,-2	3.06,-3	6.78,-2
30	4.07,-2	3.53,-3	4.78,-2	5.46,-2	3.55,-3	6.17,-2
35	3.47,-2	3.78,-3	4.23,-2	4.74,-2	3.80,-3	5.50,-2
40	2.89,-2	3.82,-3	3.65,-2	4.04,-2	3.81,-3	4.81,-2
45	2.35,-2	3.68,-3	3.09,-2	3.39,-2	3.66,-3	4.12,-2
50	1.87,-2	3.43,-3	2.56,-2	2.80,-2	3.39,-3	3.48,-2
55	1.46,-2	3.12,-3	2.08,-2	2.28,-2	3.07,-3	2.89,-2
60	1.11,-2	2.79,-3	1.67,-2	1.83,-2	2.74,-3	2.38,-2
70	5.90,-3	2.19,-3	1.03,-2	1.13,-2	2.13,-3	1.56,-2
80	2.72,-3	1.71,-3	6.14,-3	6.67,-3	1.66,-3	1.00,-2
90	9.95,-4	1.36,-3	3.72,-3	3.71,-3	1.32,-3	6.35,-3
100	2.28,-4	1.09,-3	2.42,-3	1.92,-3	1.06,-3	4.05,-3
110	4.37,-5	8.76,-4	1.80,-3	9.02,-4	8.53,-4	2.61,-3
120	1.81,-4	6.82,-4	1.55,-3	3.64,-4	6.66,-4	1.70,-3
130	4.66,-4	5.05,-4	1.48,-3	1.16,-4	4.93,-4	1.10,-3
140	7.93,-4	3.42,-4	1.48,-3	3.12,-5	3.35,-4	7.01,-4
150	1.09,-3	2.02,-4	1.50,-3	2.90,-5	1.98,-4	4.25,-4
160	1.33,-3	9.33,-5	1.52,-3	5.81,-5	9.14,-5	2.41,-4
170	1.48,-3	2.39,-5	1.53,-3	8.70,-5	2.34,-5	1.34,-4
180	1.53,-3	0	1.53,-3	9.84,-5	0	9.84,-5
Integral (πa_o^2)	3.63,-2	6.46,-3	4.93,-2	5.34,-2	6.37,-3	6.61,-2

TABLE 29(c)

E = 81.63 eV

	(A)			(B)		
θ^{o}	m = 0	m = 1	Total	m = 0	m = 1	Total
0	1.70,-2	0	1.70,-2	1.91,-2	0	1.91,-2
5	1.66,-2	2.16,-4	1.70,-2	1.87,-2	2.16,-4	1.91,-2
10	1.54,-2	7.31,-4	1.68,-2	1.74,-2	7.29,-4	1.88,-2
15	1.36,-2	1.26,-3	1.61,-2	1.54,-2	1.24,-3	1.79,-2
20	1.15,-2	1.56,-3	1.47,-2	1.32,-2	1.54,-3	1.63,-2
25	9.40,-3	1.59,-3	1.26,-2	1.09,-2	1.55,-3	1.40,-2
30	7.42,-3	1.42,-3	1.03,-2	8.69,-3	1.36,-3	1.14,-2
35	5.71,-3	1.16,-3	8.02,-3	6.80,-3	1.09,-3	8.97,-3
40	4.29,-3	8.83,-4	6.06,-3	5.24,-3	8.12,-4	6.86,-3
45	3.17,-3	6.47,-4	4.47,-3	3.99,-3	5.82,-4	5.15,-3
50	2.31,-3	4.63,-4	3.23,-3	3.02,-3	4.07,-4	3.83,-3
55	1.66,-3	3.30,-4	2.31,-3	2.27,-3	2.84,-4	2.84,-3
60	1.17,-3	2.36,-4	1.64,-3	1.71,-3	2.00,-4	2.11,-3
70	5.61,-4	1.32,-4	8.25,-4	9.72,-4	1.11,-4	1.19,-3
80	2.47,-4	8.69,-5	4.21,-4	5.56,-4	7.39,-5	7.03,-4
90	9.43,-5	6.66,-5	2.27,-4	3.21,-4	5.79,-5	4.36,-4
100	2.76,-5	5.50,-5	1.38,-4	1.88,-4	4.85,-5	2.85,-4
110	5.00,-6	4.59,-5	9.68,-5	1.13,-4	4.07,-5	1.95,-4
120	4.12,-6	3.70,-5	7.80,-5	7.35,-5	3.28,-5	1.39,-4
130	1.29,-5	2.79,-5	6.87,-5	5.38,-5	2.47,-5	1.03,-4
140	2.48,-5	1.91,-5	6.31,-5	4.57,-5	1.69,-5	7.96,-5
150	3.62,-5	1.14,-5	5.90,-5	4.39,-5	1.00,-5	6.40,-5
160	4.54,-5	5.25,-6	5.59,-5	4.48,-5	4.63,-6	5.41,-5
170	5.12,-5	1.34,-6	5.39,-5	4.63,-5	1.18,-6	4.86,-5
180	5.32,-5	0	5.32,-5	4.69,-5	0	4.69,-5
Integral (πa_o^2)	5.96,-3	1.03,-3	8.02,-3	7.53,-3	9.51,-4	9.43,-3

TABLE 29(d)

E = 100 eV

	(A)			(B)		
θ^{o}	m = 0	m = 1	Total	m = 0	m = 1	Total
0	1.01,-2	0	1.01,-2	1.10,-2	0	1.10,-2
5	9.81,-3	1.97,-4	1.02,-2	1.07,-2	1.97,-4	1.11,-2
10	8.95,-3	6.38,-4	1.02,-2	9.78,-3	6.34,-4	1.10,-2
15	7.71,-3	1.03,-3	9.77,-3	8.46,-3	1.01,-3	1.05,-2
20	6.32,13	1.18,-3	8.68,-3	6.97,-3	1.15,-3	9.27,-3
25	4.97,-3	1.10,-3	7.17,-3	5.52,-3	1.06,-3	7.63,-3
30	3.77,-3	8.99,-4	5.57,-3	4.24,-3	8.43,-4	5.93,-3
35	2.79,-3	6.69,-4	4.13,-3	3.19,-3	6.11,-4	4.41,-3
40	2.03,-3	4.69,-4	2.96,-3	2.36,-3	4.16,-4	3.20,-3
45	1.45,-3	3.17,-4	2.08,-3	1.74,-3	2.72,-4	2.29,-3
50	1.02,-3	2.10,-4	1.44,-3	1.28,-3	1.75,-4	1.63,-3
55	7.16,-4	1.39,-4	9.95,-4	9.42,-4	1.13,-4	1.17,-3
60	4.96,-4	9.38,-5	6.83,-4	6.95,-4	7.44,-5	8.44,-4
70	2.28,-4	4.80,-5	3.24,-4	3.84,-4	3.79,-5	4.60,-4
80	9.74,-5	3.09,-5	1.59,-4	2.16,-4	2.53,-5	2.67,-4
90	3.62,-5	2.41,-5	8.45,-5	1.24,-4	2.05,-5	1.65,-4
100	1.03,-5	2.04,-5	5.12,-5	7.34,-5	1.76,-5	1.09,-4
110	1.92,-6	1.73,-5	3.64,-5	4.57,-5	1.49,-5	7.56,-5
120	1.84,-6	1.40,-5	2.98,-5	3.13,-5	1.21,-5	5.54,-5
130	5.31,-6	1.05,-5	2.64,-5	2.46,-5	9.06,-6	4.27,-5
140	9.85,-6	7.19,-6	2.42,-5	2.22,-5	6.17,-6	3.46,-5
150	1.42,-5	4.25,-6	2.27,-5	2.21,-5	3.63,-6	2.94,-5
160	1.76,-5	1.96,-6	2.15,-5	2.29,-5	1.67,-6	2.62,-5
170	1.98,-5	4.99,-7	2.08,-5	2.37,-5	4.25,-7	2.45,-5
180	2.05,-5	0	2.05,-5	2.40,-5	0	2.40,-5
Integral (πa_o^2)	3.02,-3	5.83,-4	4.19,-3	3.62,-3	5.33,-4	4.68,-3

TABLE 29(e)

E = 200 eV

	(A)			(B)		
θ°	m = 0	m = 1	Total	m = 0	m = 1	Total
0	1.48,-3	0	1.48,-3	1.47,-3	0	1.47,-3
5	1.39,-3	1.19,-4	1.63,-3	1.38,-3	1.18,-4	1.62,-3
10	1.16,-3	3.09,-4	1.78,-3	1.15,-3	3.03,-4	1.75,-3
15	8.76,-4	3.64,-4	1.60,-3	8.57,-4	3.50,-4	1.56,-3
20	6.13,-4	2.94,-4	1.20,-3	5.93,-4	2.73,-4	1.14,-3
25	4.09,-4	1.92,-4	7.93,-4	3.91,-4	1.71,-4	7.33,-4
30	2.66,-4	1.11,-4	4.89,-4	2.52,-4	9.42,-5	4.40,-4
35	1.72,-4	6.07,-5	2.93,-4	1.62,-4	4.82,-5	2.58,-4
40	1.10,-4	3.19,-5	1.74,-4	1.05,-4	2.36,-5	1.52,-4
45	7.13,-5	1.65,-5	1.04,-4	6.87,-5	1.13,-5	9.14,-5
50	4.61,-5	8.49,-6	6.31,-5	4.59,-5	5.41,-6	5.67,-5
55	2.99,-5	4.43,-6	3.88,-5	3.11,-5	2.65,-6	3.64,-5
60	1.94,-5	2.41,-6	2.42,-5	2.15,-5	1.41,-6	2.43,-5
70	8.04,-6	9.88,-7	1.00,-5	1.07,-5	6.64,-7	1.20,-5
80	3.16,-6	7.06,-7	4.57,-6	5.59,-6	5.67,-7	6.72,-6
90	1.09,-6	6.47,-7	2.39,-6	3.06,-6	5.44,-7	4.15,-6
100	2.88,-7	5.93,-7	1.47,-6	1.79,-6	4.95,-7	2.78,-6
110	4.70,-8	5.10,-7	1.07,-6	1.18,-6	4.18,-7	2.02,-6
120	5.24,-8	4.08,-7	8.68,-7	9.14,-7	3.28,-7	1.57,-6
130	1.55,-7	3.01,-7	7.56,-7	8.36,-7	2.39,-7	1.31,-6
140	2.83,-7	2.01,-7	6.84,-7	8.52,-7	1.58,-7	1.17,-6
150	4.00,-7	1.16,-7	6.33,-7	9.04,-7	9.07,-8	1.09,-6
160	4.92,-7	5.25,-8	5.97,-7	9.62,-7	4.08,-8	1.04,-6
170	5.50,-7	1.33,-8	5.76,-7	1.00,-6	1.03,-8	1.02,-6
180	5.69,-7	0	5.69,-7	1.02,-6	0	1.02,-6
Integral (πa_o^2)	2.45,-4	8.44,-5	4.14,-4	2.43,-4	7.53,-5	3.93,-4

FIGURES

FIGURE CAPTIONS

Figure 1

Differential cross section for electron impact excitation of $He(2^1S)$ computed in the First Born approximation at incident energies of 29.6 and 40.1 eV.

Figure 2

Differential cross section for electron impact excitation of $He(2^1P)$ computed in the First Born approximation at incident energies of 29.6 and 40.1 eV.

Figure 3

Differential cross section for electron impact excitation of $He(2^3S)$ computed in the Born-Oppenheimer approximation at incident energies of 29.6, 40.1 and 55.5 eV.

Figure 4

Differential cross section for electron impact excitation of $He(2^3P)$ computed in the Born-Oppenheimer approximation at incident energies of 29.6, 40.1 and 55.5 eV.

Figure 5

Differential cross section for electron impact excitation of $He(2^3S)$ computed in the Born-Oppenheimer approximation at an incident energy of 29.6 eV using expression (5.4.1).

———— Obtained using the excited state wave function of Cohen and McEachran.

---------- Obtained using the excited state wave function of Morse et al.

Figure 6

Differential cross section for electron impact excitation of H(2s) computed in the DWPO approximation at incident energies of (a) 50 eV and (b) 100 eV.

—·—·— DWPO I (McDowell et al., 1975b)

— — — DWPO II (McDowell et al., 1975b)

———— DWPO III (present work)

Figure 7

Differential cross section for electron impact excitation of H(2p) computed in the DWPO approximation at incident energies of (a) 50 eV and (b) 100 eV.

Theory as for figure 6.

Figure 8

Differential cross section for electron impact excitation of H(n = 2) computed in the DWPO III model at incident energies of (a) 1.02, (b) 1.21 and (c) 1.44 Rydbergs.

---------- Excitation of the 2s state.

—— —— —— Excitation of the 2p state.

———————— Excitation of the n = 2 level.

Experiment: ⊕ , Williams (1976).

Figure 9

Differential cross section for electron impact excitation of H(n = 2) at incident energies of (a) 5.4.4 eV (= 4 Ryd.) and (b) 100 eV.

———————— DWPO III

—·——·—— Hybrid close-coupling unitarized Born approximation: Kingston et al. (1976).

——··——··—— Hybrid pseudo-state close-coupling distorted wave model: Callaway et al. (1976), (a) only.

——-——-—— Unitarized DWPO III model, (b) only.

Experiment: ⊕ , Williams and Willis (1975).

Figure 10

Total cross section for electron impact excitation of $He(n^1S)$.

(a) n = 2:

———————— DWPO I

——··——··—— Multichannel eikonal method: Flannery and McCann (1975).

——+——+—— Eikonal distorted wave method: Joachain and Vanderpoorten (1974a).

——·——·—— Many-body theory: Thomas et al. (1974).

Figure 10 continued

—— —— —— Second-order optical potential distorted wave model: Winters (1974).

---------- Coulomb-projected Born approximation: Hidalgo and Geltman (1972).

Experiment: ⊖, Hall et al. (1973); ⏃, Trajmar (1973); ⊕, Brongersma et al. (1972) ⊞, Rice et al. (1972); ▲, Vriens et al. (1968).

(b) n = 3:

———————— DWPO I

—·——·—— DWPO II

——··——··—— Multichannel eikonal method: Flannery and McCann (1975).

Experiment: ⊕, Chutjian and Thomas (1975); ⊖, Moustafa Moussa et al. (1969); ⏃, St.John et al. (1964).

(c) n = 4:

———————— DWPO I

——·——·—— DWPO II

Experiment: ▽, Showalter and Kay (1975); ⊕, Pochat et al. (1973); ▲, van Raan et al. (1971); ⊖, Moustafa Moussa et al. (1969); ⏃, St. John et al. (1964).

(d) n = 5:

Same as in figure 10(c).

Figure 11

Differential cross section for electron impact excitation of $He(2^1S)$ at incident energies of (a) 29.6 eV, (b) 40.1 eV, (c) 81.63 eV, (d) 100 eV and (e) 200 eV.

———————— DWPO I

——·——·—— Many-body theory: Thomas et al. (1974).

——··——··—— Multichannel eikonal method: Flannery and McCann (1975).

——···——···—— Second-order diagonalization method: Baye and Heenen (1974).

——+——+—— Eikonal Born Series: Byron and Joachain (1975).

—— —— —— (a) and (b), distorted wave calculation: Shelton et al. (1973); (c) and (d), second-order optical potential distorted wave model: Bransden and Winters (1975).

Figure 11 continued

- - - - - - - - (a) and (b), Glauber approximation: Yates and Tenney (1972); (c) to (e), Coulomb-projected Born approximation: Hidalgo and Geltman (1972).

Experiment: ⊞ , Dillon and Lassettre (1975); ⧋ , Suzuki and Takayanagi (1973); ▲ , Trajmar (1973); ▼ , Crooks (1972); ● , Opal and Beaty (1972); ⧈ , Rice et al. (1972).

Figure 12

Differential cross section for electron impact excitation of $He(2^1S)$ computed in the DWPO approximation at incident energies of (a) 29.6 eV, (b) 40.1 eV, (c) 81.63 eV, (d) 100 eV and (e) 200 eV.

- - - - - - - - DWPO I

—— —— —— DWPO II

———————— DWPO III

Experiment: ⊞ , Dillon and Lassettre (1975); ○ , Hall et al. (1973); ⧋ , Suzuki and Takayanagi (1973); ▲ , Trajmar (1973); ▼ , Crooks (1972); ● , Opal and Beaty (1972); ▽ , Rice et al. (1972).

Figure 13

Differential cross section for electron impact excitation of $He(3^1S)$ at incident energies of (a) 29.2 eV, (b) 39.7 eV, (c) 100 eV and (d) 200 eV.

———————— DWPO I

——·——·—— Many-body theory: Thomas et al. (1974).

——··——··—— Multichannel eikonal method: Flannery and McCann (1975).

Experiment: ○ , Chutjian and Thomas (1975).

Figure 14

Small-angle differential cross section for electron impact excitation of $He(4^1S)$ at incident energies of (a) 50 eV, (b) 60 eV, (c) 100 eV and (d) 200 eV.

———————— DWPO I

——·——·—— DWPO II

Figure 14 continued

—— —— —— First Born approximation: Bell et al. (1969).

Experiment: ⧳ , Pochat (1973).

Figure 15

As for figure 14, but for excitation of $He(5^1S)$.

Figure 16

Total cross section for electron impact excitation of $He(2^3S)$.

———————— DWPO I

——·——·—— Many-body theory: Thomas et al. (1974).

—— —— —— Second-order optical potential distorted wave model: Winters (1974).

Experiment: ⧋ , Trajmar (1973); ⧲ , Brongersma et al. (1972); ⧳ , Crooks et al. (1972); ⧍ , Vriens et al. (1968).

Figure 17

Differential cross section for electron impact excitation of $He(2^3S)$ at incident energies of (a) 29.6 eV, (b) 40.1 eV, (c) 81.63 eV, (d) 100 eV and 200 eV.

———————— DWPO I (with excited state wave function of Cohen and McEachran).

-------- DWPO I (with excited state wave function of Morse et al.).

——·——·—— Many-body theory: Thomas et al. (1974).

—— —— —— (a) and (b), distorted wave calculation: Shelton et al. (1973); (c) and (d), second-order optical potential distorted wave model: Bransden and Winters (1975).

Experiment: ⧲ , Yagishita et al. (1976); ⧳ , Dillon (1975); ⧍ , Suzuki and Takayanagi (1973); ⧋ , Trajmar (1973); ⧩ , Crooks (1972); ⧳ , Opal and Beaty (1972).

Figure 18

Differential cross section for electron impact excitation of $He(2^3S)$ computed in the DWPO approximation at incident energies of (a) 29.6 eV, (b) 40.1 eV, (c) 81.63 eV, (d) 100 eV and (d) 200 eV.

Figure 18 continued

– – – – – – – – – DWPO I

———————— DWPO III

Experiment: ⊞ , Yagishita et al. (1976), ⊟ , Dillon (1975); ⊖ , Hall et al. (1973); ⊼ , Suzuki and Takayanagi (1973); ▲ , Trajmar (1973); ▼ , Crooks (1972); ◆ , Opal and Beaty (1972).

Figure 19

Total integrated cross section for electron impact excitation of $He(n^1P)$.

(a) n = 2:

———————— DWPO I

——·——·—— DWPO II

Experiment: ⊞ , Chutjian and Srivastava (1975); ▲ , Dillon and Lassettre (1975); ⊖ , Hall et al. (1973); ◆ , Donaldson et al. (1972); ⊼ , de Jongh and van Eck (1971) ■ , Moustafa Moussa et al. (1969).

(b) n = 3:

———————— DWPO I

——·——·—— DWPO II

——··——··—— Multichannel eikonal method: Flannery and McCann (1975).

——···——···—— Second-order diagonalization method: Baye and Heenen (1974).

——–——–—— Second-order optical potential method: Bransden and Issa (1975).

Experiment: ⊖ , Chutjian (1976); ⊻ , Showalter and Kay (1975); other symbols as in figure 19(a).

(c) n = 4:

Same as in figure 19(b).

(d) n = 5:

Same as in figure 19(b).

Figure 20

Total differential cross section for electron impact excitation of $He(2^1P)$ at incident energies of (a) 29.6 eV, (b) 40.1 eV, (c) 81.63 eV, (d) 100 eV and (e) 200 eV.

———————— DWPO I

——·——·—— Many-body theory: Thomas et al. (1974).

——··——··—— Multichannel eikonal method: Flannery and McCann (1975).

——···——···—— Second-order diagonalization method: Baye and Heenen (1974).

—— + ——+—— Eikonal distorted wave method: Joachain and Vanderpoorten (1974a).

—— —— —— (a) to (c) and (e), distorted wave calculation: Madison and Shelton (1973); (d), second-order optical potential distorted wave model: Winters (1974).

- - - - - - - - (a) and (b), 2-state close-coupling calculation: Truhlar et al. (1973); (c) to (d), Coulomb-projected Born approximation: Hidalgo and Geltman (1972).

Experiment: ⊕ , Chutjian and Srivastava (1975); ▲ , Dillon and Lassettre (1975); △ , Suzuki and Takayanagi (1973); ⊖ , Truhlar et al. (1973); ● , Opal and Beaty (1972); ■ , Chamberlain et al. (1970).

Figure 21

Small-angle total differential cross section for electron impact excitation of $He(2^1P)$ at incident energies of (a) 29.6 and 40.1 eV and (b) 80 and 100 eV.

———————— DWPO I

——·——·—— DWPO II

—— —— —— First Born approximation: Bell et al. (1969).

Experiment: – ▼ , Hall et al. (1973); other symbols as for figure 20.

Figure 22

Total differential cross section for electron impact excitation of $He(3^1P)$ at incident energies of (a) 29.2 eV, (b) 39.7 eV, (c) 100 eV and (d) 200 eV.

———————— DWPO I

——·——·—— Many-body theory: Chutjian and Thomas (1975).

——··——··—— Multichannel eikonal method: Flannery and McCann (1975).

--------- Glauber approximation: Chan and Chen (1974b).

Experiment: ⊥ , Chutjian (1976); ⊖ , Chutjian and Thomas (1975).

Figure 23

Small-angle total differential cross section for electron impact excitation of $He(3^1P)$ computed in the DWPO approximation at incident energies of 29.2 and 39.7 eV.

———————— DWPO I

——·——·—— DWPO II

Experiment: ⊖ , Chutjian and Thomas (1975).

Figure 24

λ for electron impact excitation of $He(2^1P)$ at incident energies of (a) 40 eV, (b) 60 eV, (c) 80 eV, (d) 100 eV and (e) 200 eV.

———————— DWPO I

——·——·—— Many-body theory: Thomas et al. (1974).

——··——··—— Multichannel eikonal method: Flannery and McCann (1975).

——+——+—— Eikonal distorted wave method: Joachain and Vanderpoorten (1974b).

—— —— —— Distorted wave calculation: Madison and Shelton (1973).

Experiment: ⊥ , Eminyan et al. (1974).

Figure 25

$|\chi|$ for electron impact excitation of $He(2^1P)$ at incident energies of (a) 40 eV, (b) 60 eV, (c) 80 eV, (d) 100 eV and (e) 200 eV.

Theory and experiment as for figure 24.

Figure 26

λ for electron impact excitation of $He(3^1P)$ at incident energies of (a) 50 eV, (b) 80 eV, (c) 100 eV and (d) 200 eV.

———————— DWPO I

—··—··— Multichannel eikonal method: Flannery and McCann (1975).

Experiment: ⊥ , Eminyan et al. (1975).

Figure 27

$|\chi|$ for electron impact excitation of $He(3^1P)$ at incident energies of (a) 50 eV, (b) 80 eV, (c) 100 eV and (d) 200 eV.

Theory and experiment as for figure 26.

Figure 28

Total integrated cross section for electron impact excitation of $He(2^3P)$.

———————— DWPO I

—·—·— Many-body theory: Thomas et al. (1974).

Experiment: ⊥ , Hall et al. (1973); ▲ , Trajmar (1973); ⊔ , Jobe and St. John (1967).

Figure 29

Total differential cross section for electron impact excitation of $He(2^3P)$ at incident energies of (a) 29.6 eV, (b) 40.1 eV, (c) 81.63 eV, (d) 100 eV and (e) 200 eV.

———————— DWPO I (with excited state wave function of Cohen and McEachran).

- - - - - - - - - DWPO I (with excited state wave function of Morse et al.).

—·—·— Many-body theory: Thomas et al. (1974).

—— —— —— Distorted wave calculation: Shelton et al. (1973).

Experiment: ⊔ , Yagishita et al. (1976); ○ , Chutjian and Srivastava (1975); △ , Suzuki and Takayanagi (1973); ▲ , Trajmar (1973); ⊥ , Gelebart et al. (1975) on (b), Opal and Beaty (1972) on (c).

Figure 1

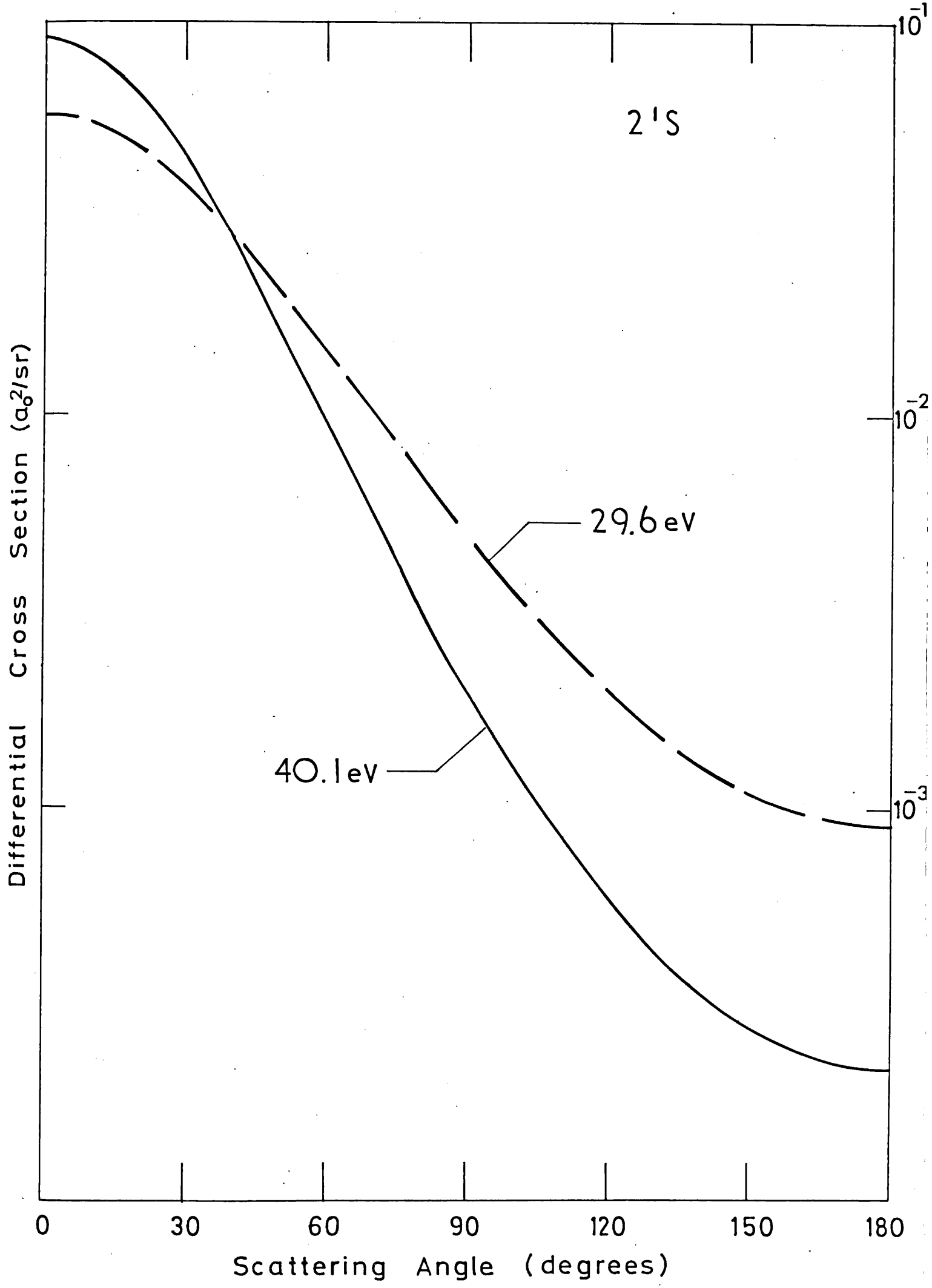
2 ¹S
29.6 eV
40.1 eV
Differential Cross Section (a_0^2/sr)
10^{-1}
10^{-2}
10^{-3}
0
30
60
90
120
150
180
Scattering Angle (degrees)

Figure 2

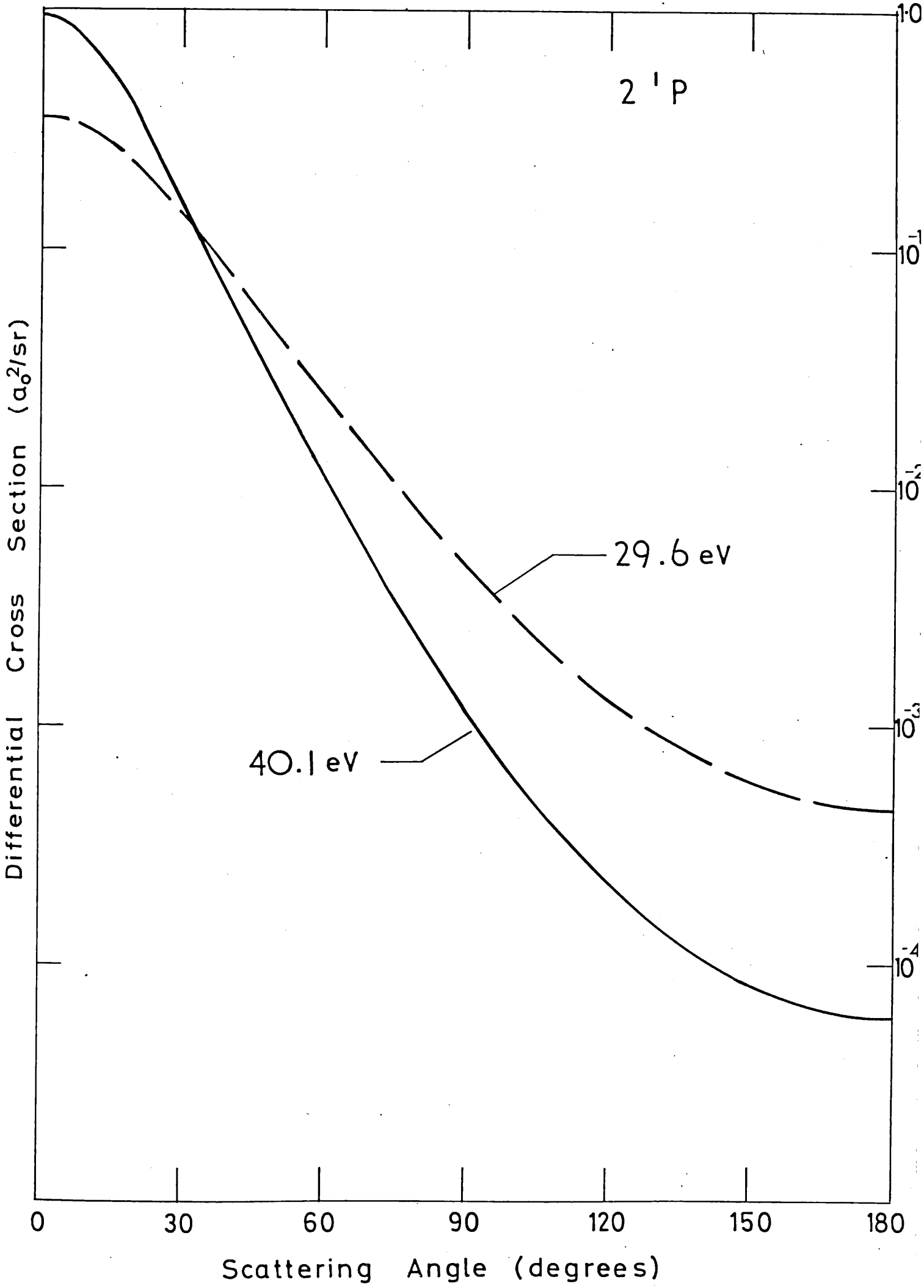
2 ¹P
29.6 eV
40.1 eV
Differential Cross Section (a_0^2/sr)
1·0
10^{-1}
10^{-2}
10^{-3}
10^{-4}
0
30
60
90
120
150
180
Scattering Angle (degrees)

Figure 3

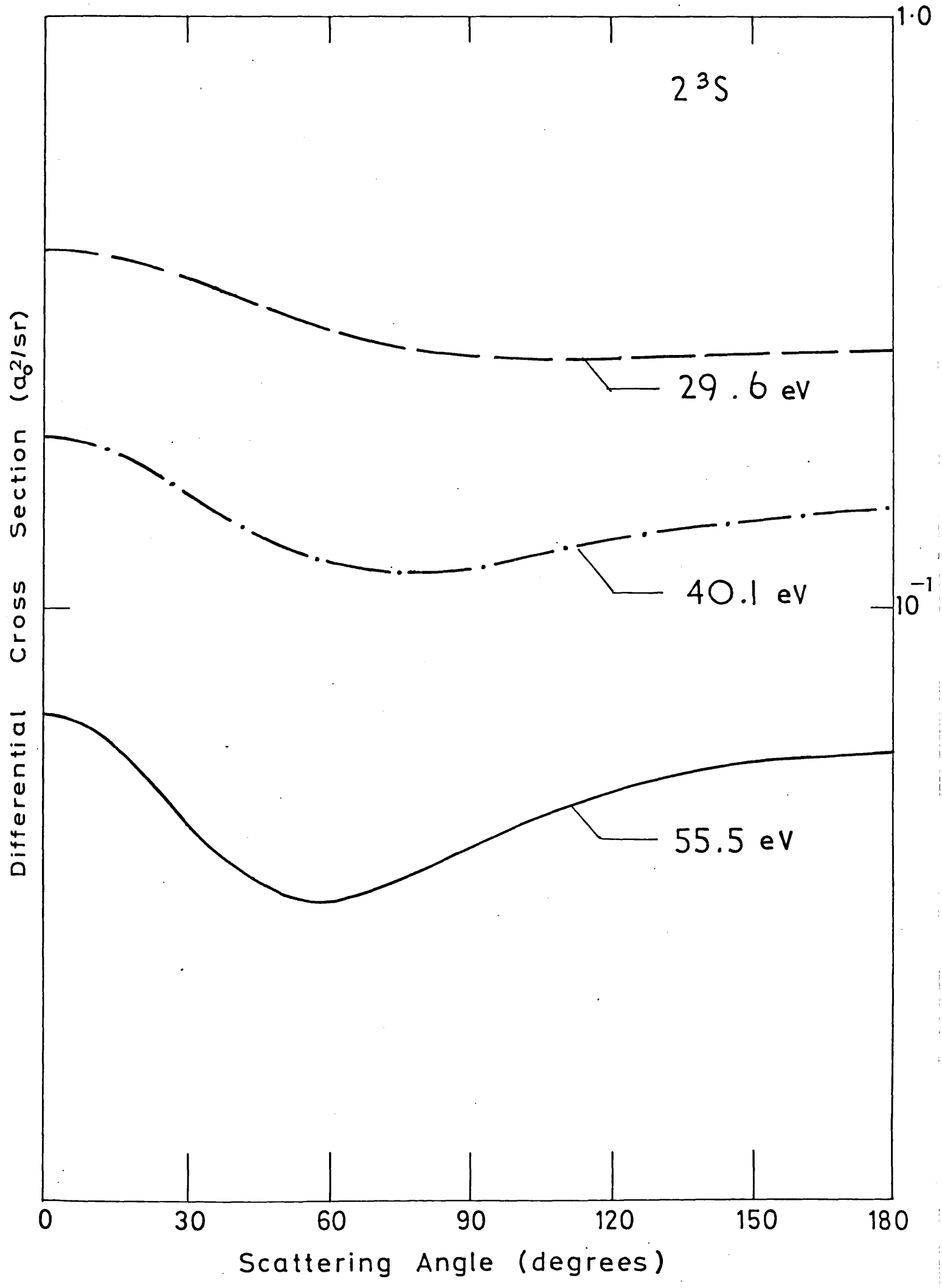
1·0
2^3S
29.6 eV
40.1 eV
10^{-1}
55.5 eV
Differential Cross Section (a_0^2/sr)
0
30
60
90
120
150
180
Scattering Angle (degrees)

Figure 4

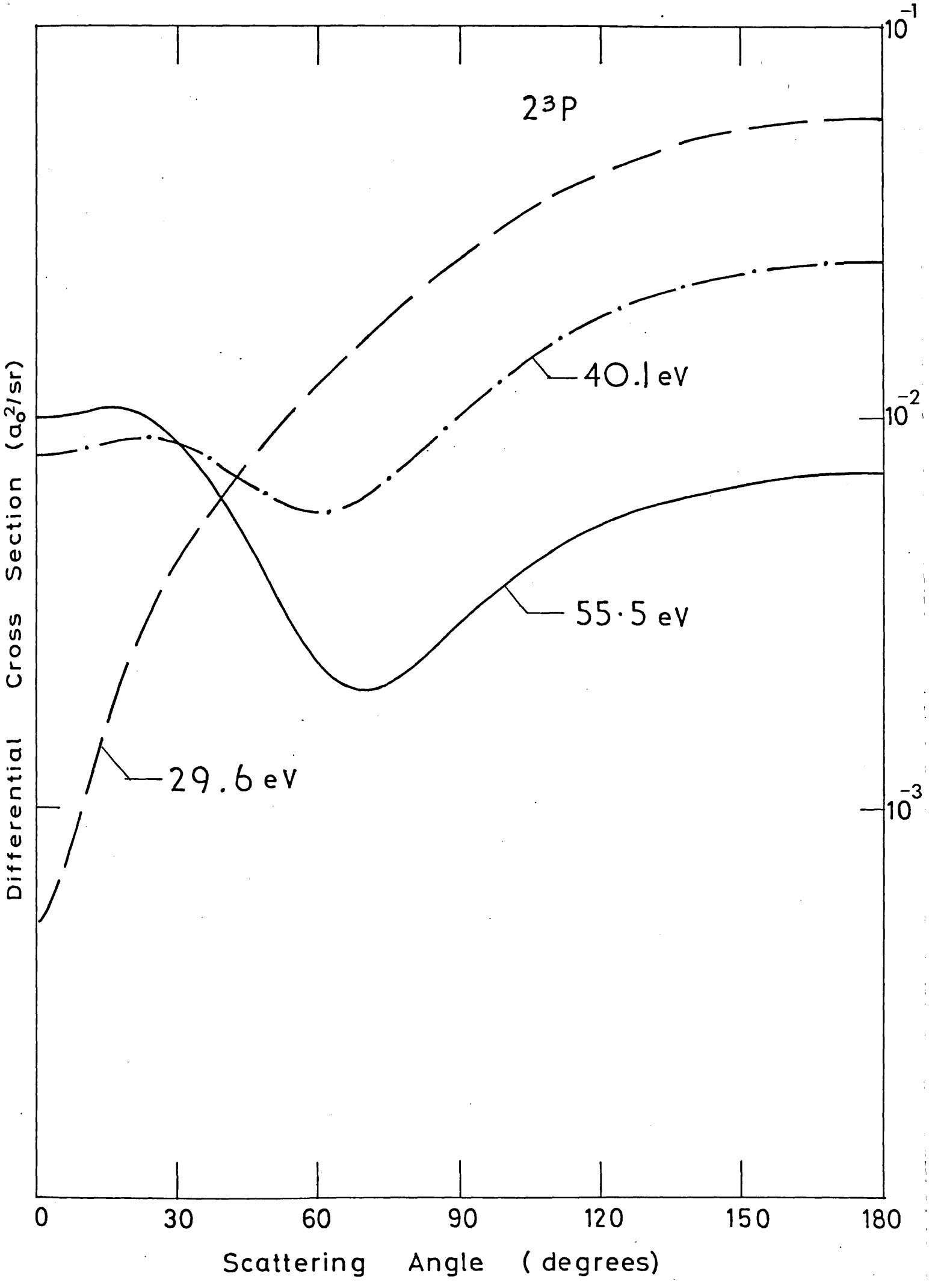
2^3P
40.1 eV
55·5 eV
29.6 eV
10^{-1}
10^{-2}
10^{-3}
Differential Cross Section (a_o^2/sr)
0
30
60
90
120
150
180
Scattering Angle (degrees)

Figure 5

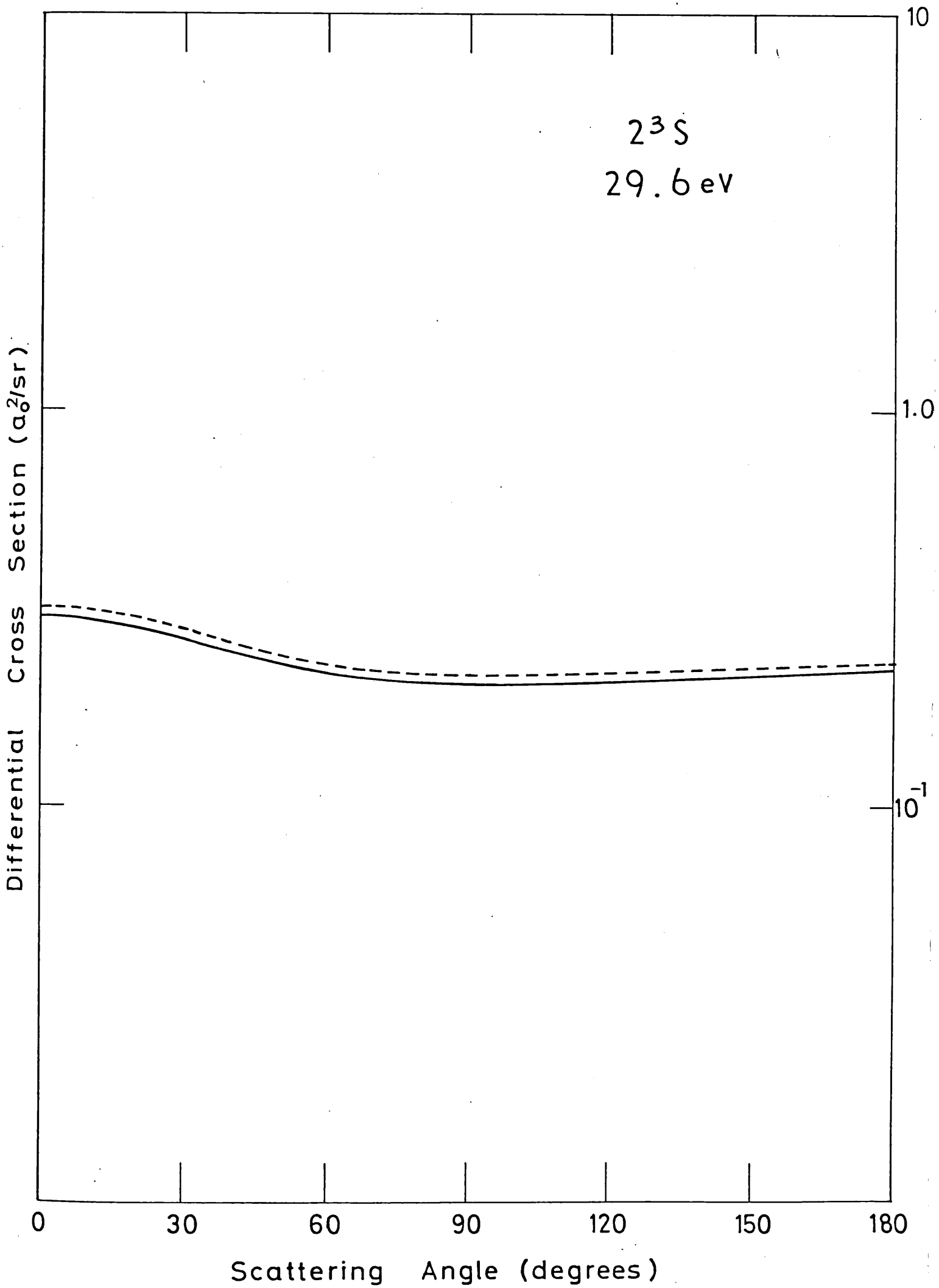
2^3S
29.6 eV
10
1.0
10^{-1}
Differential Cross Section (a_0^2/sr)
0
30
60
90
120
150
180
Scattering Angle (degrees)

Figure 6(a)

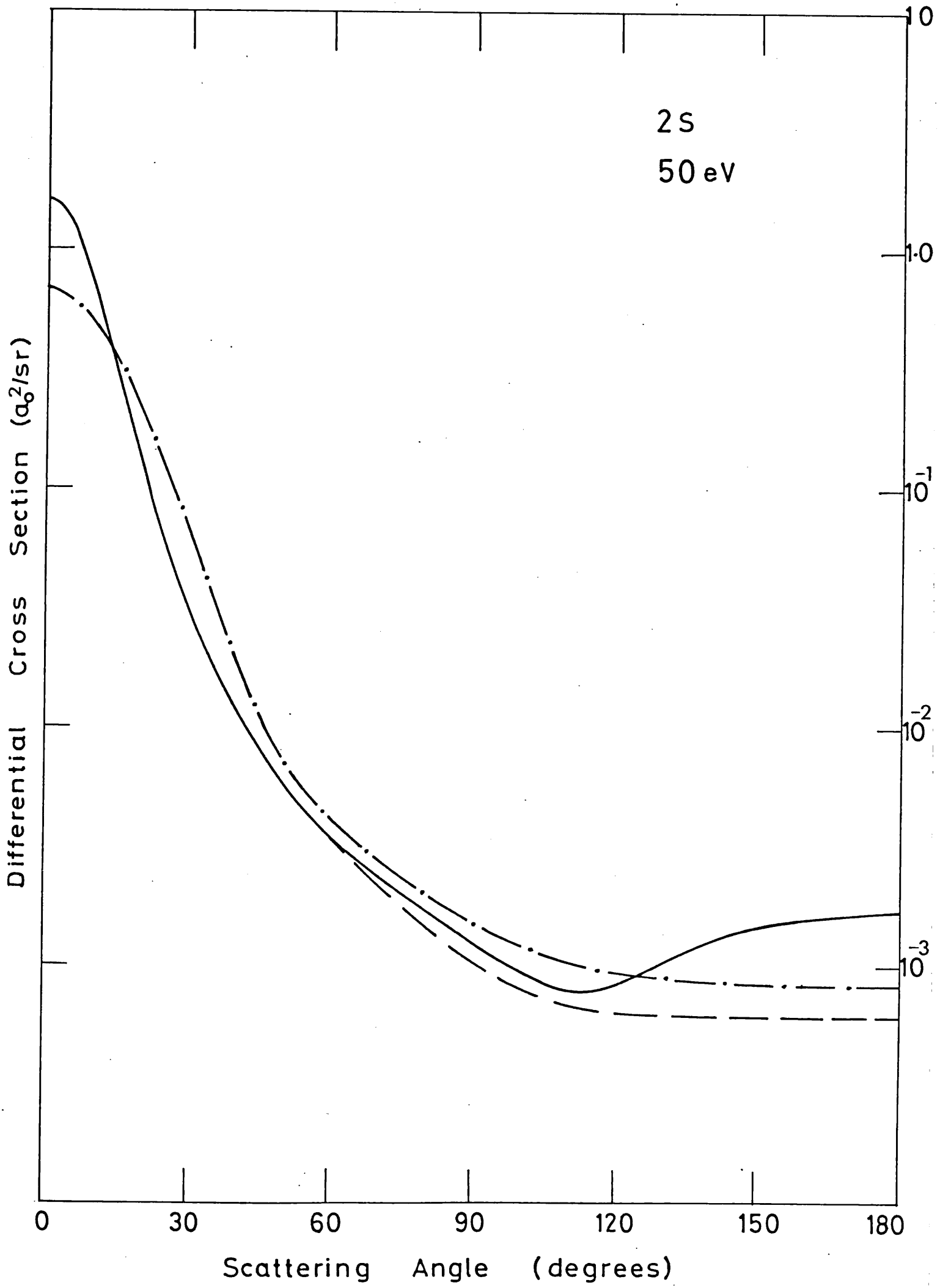
2S
50 eV
1·0
10^-1
10^-2
10^-3
Differential Cross Section (a0^2/sr)
0
30
60
90
120
150
180
Scattering Angle (degrees)

Figure 6 (b)

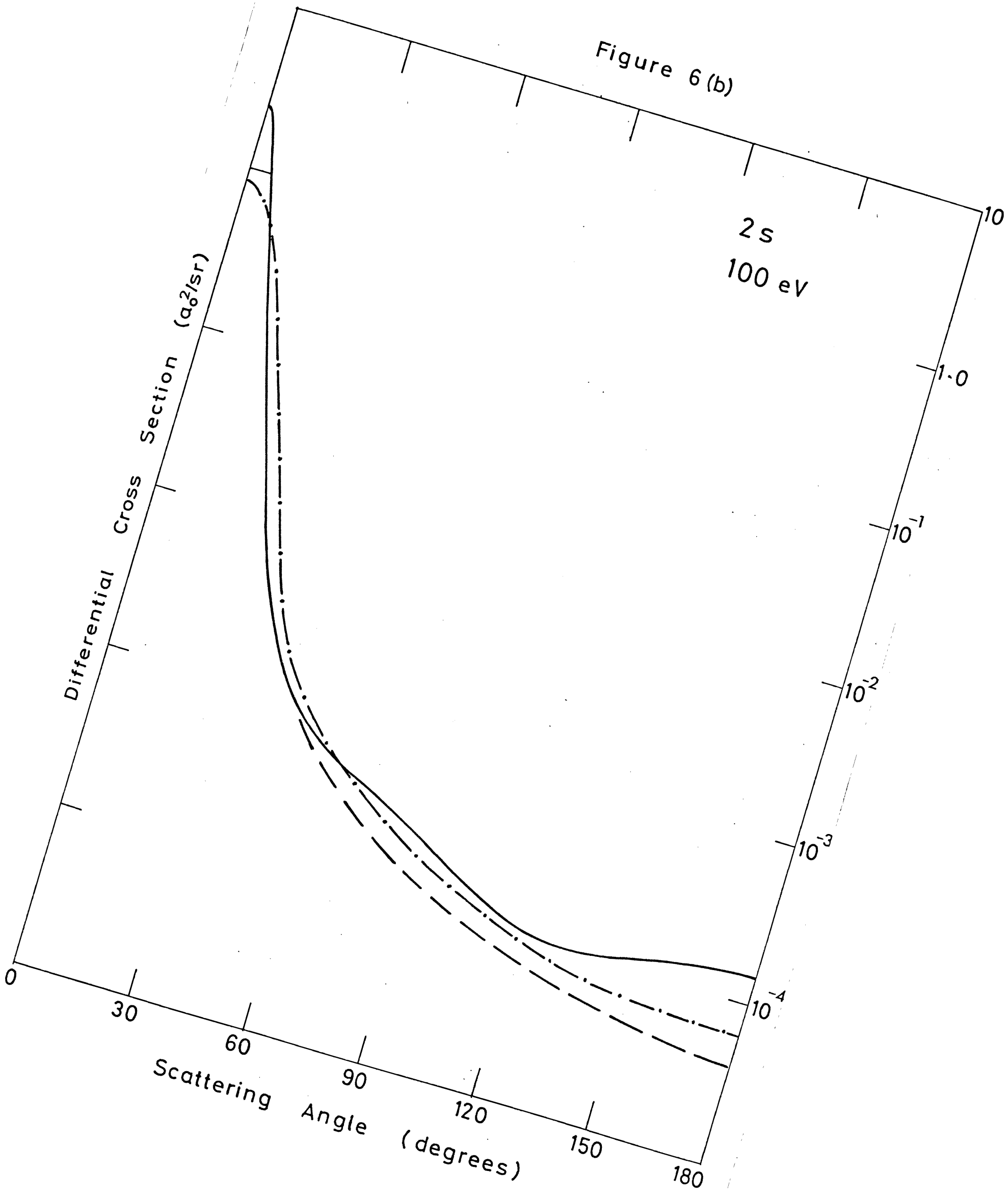
2s
100 eV
Differential Cross Section (a_0^2/sr)
10
1·0
10^{-1}
10^{-2}
10^{-3}
10^{-4}
0
30
60
90
120
150
180
Scattering Angle (degrees)

Figure 7 (a)

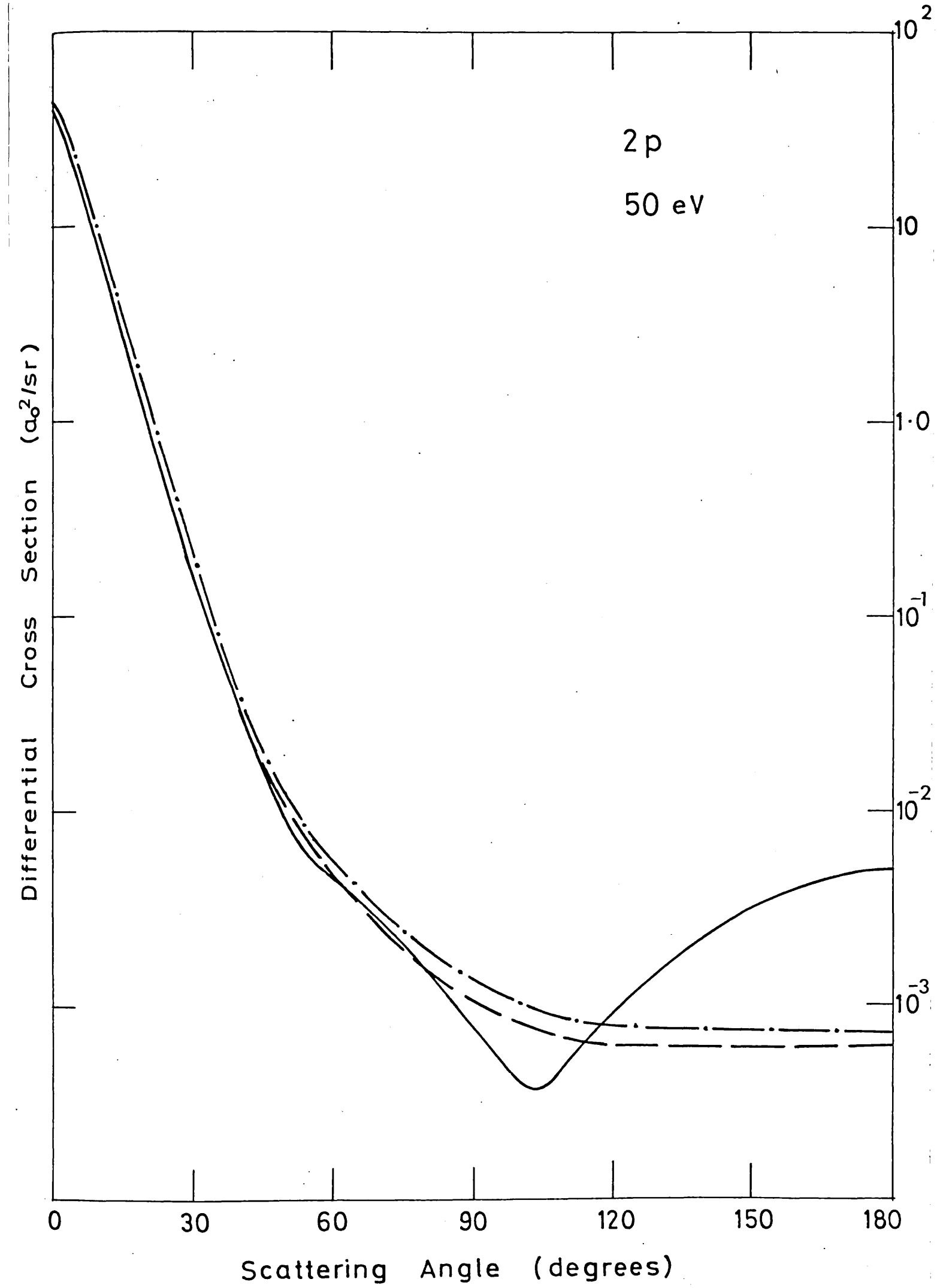
2p
50 eV
10^2
10
1·0
10^{-1}
10^{-2}
10^{-3}
Differential Cross Section (a_0^2/sr)
0
30
60
90
120
150
180
Scattering Angle (degrees)

Figure 7 (b)

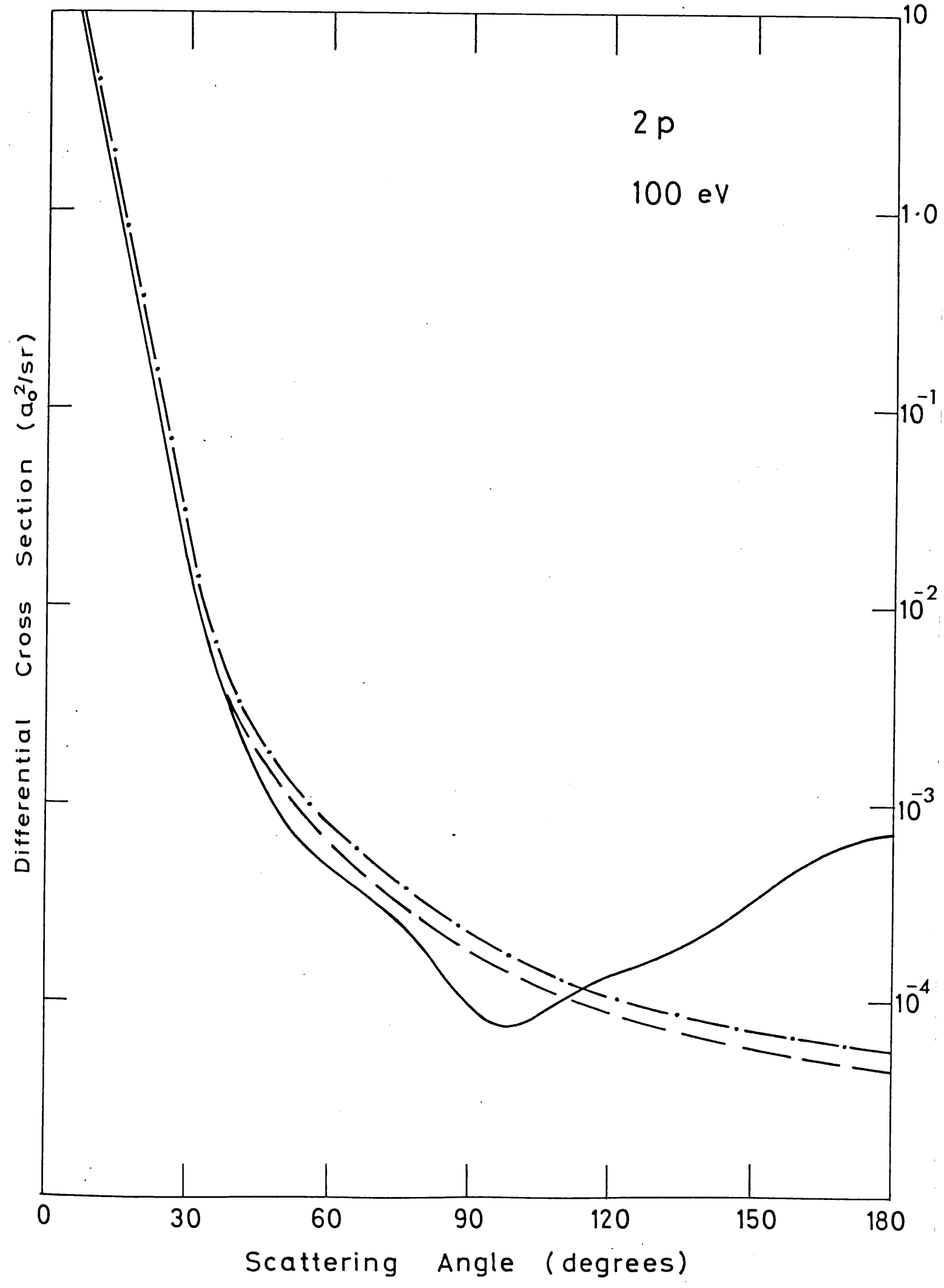
2p
100 eV
10
1·0
10^{-1}
10^{-2}
10^{-3}
10^{-4}
Differential Cross Section (a_0^2/sr)
0
30
60
90
120
150
180
Scattering Angle (degrees)

Figure 8 (a)

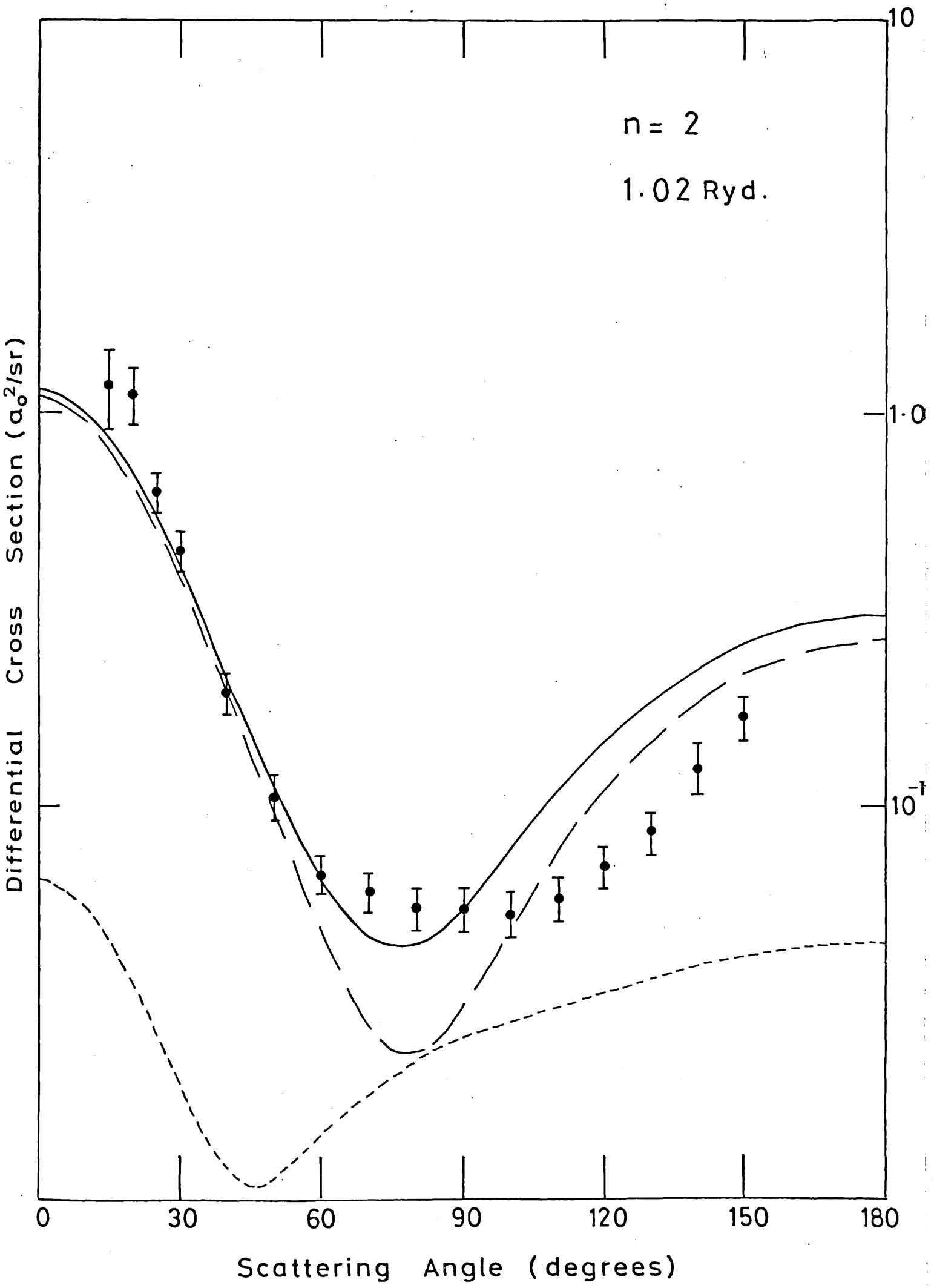
n = 2
1·02 Ryd.
10
1·0
10^{-1}
Differential Cross Section (a_o^2/sr)
0
30
60
90
120
150
180
Scattering Angle (degrees)

Figure 8 (b)

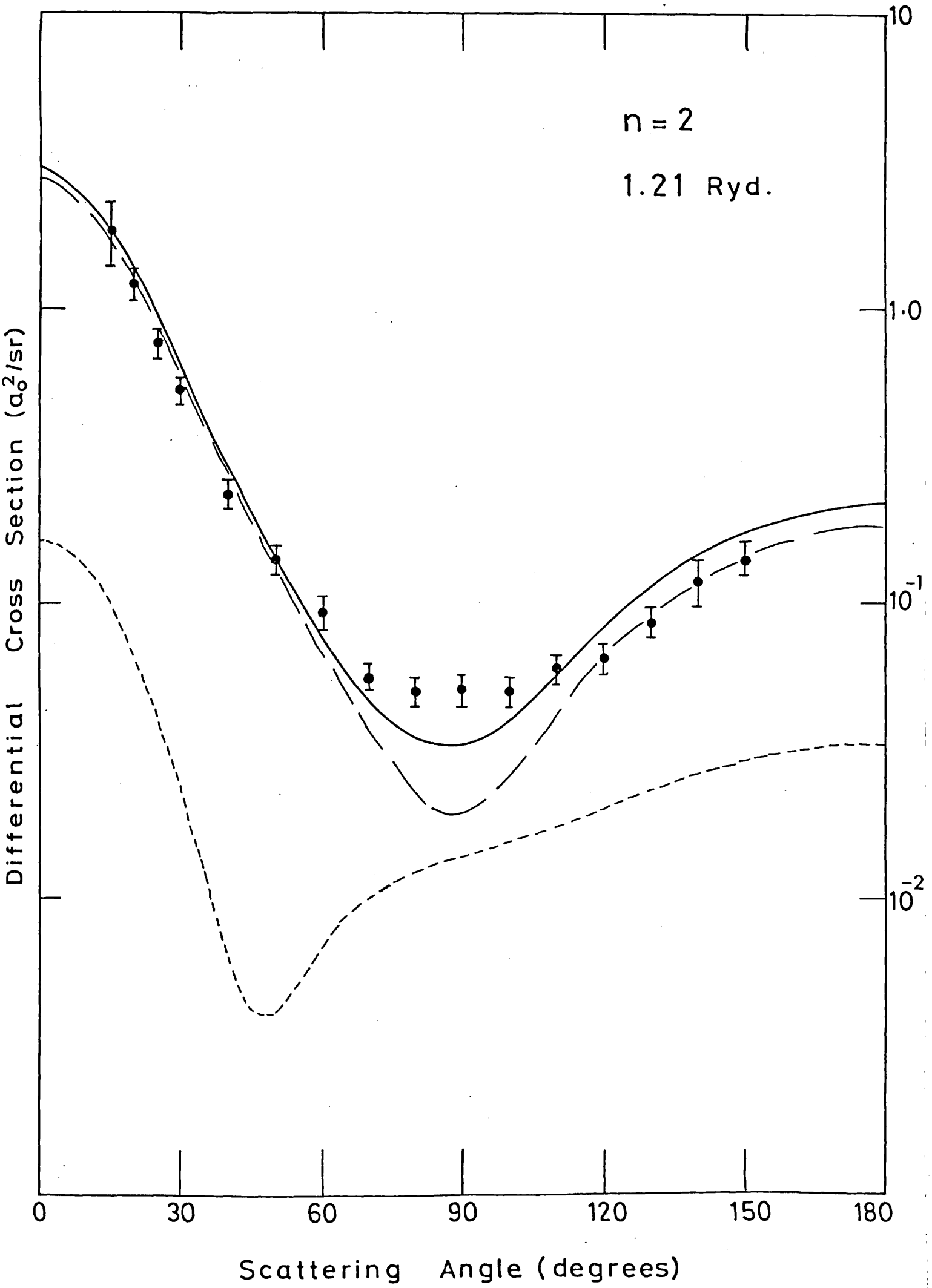
n = 2
1.21 Ryd.
10
1·0
10^{-1}
10^{-2}
Differential Cross Section (a_0^2/sr)
0
30
60
90
120
150
180
Scattering Angle (degrees)

Figure 8 (c)

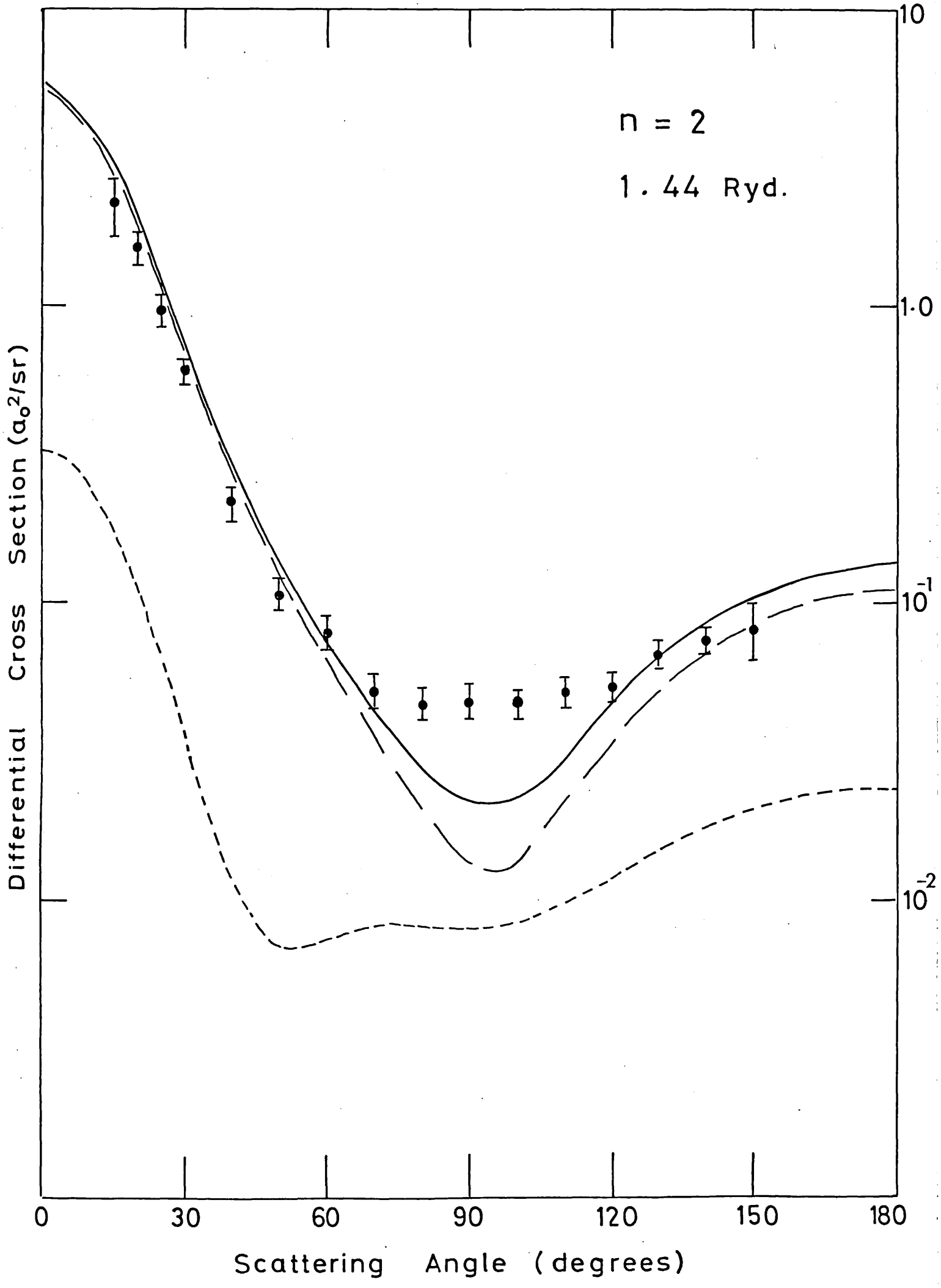
n = 2
1.44 Ryd.
10
1·0
10^{-1}
10^{-2}
Differential Cross Section (a_o^2/sr)
0
30
60
90
120
150
180
Scattering Angle (degrees)

Figure 9(a)

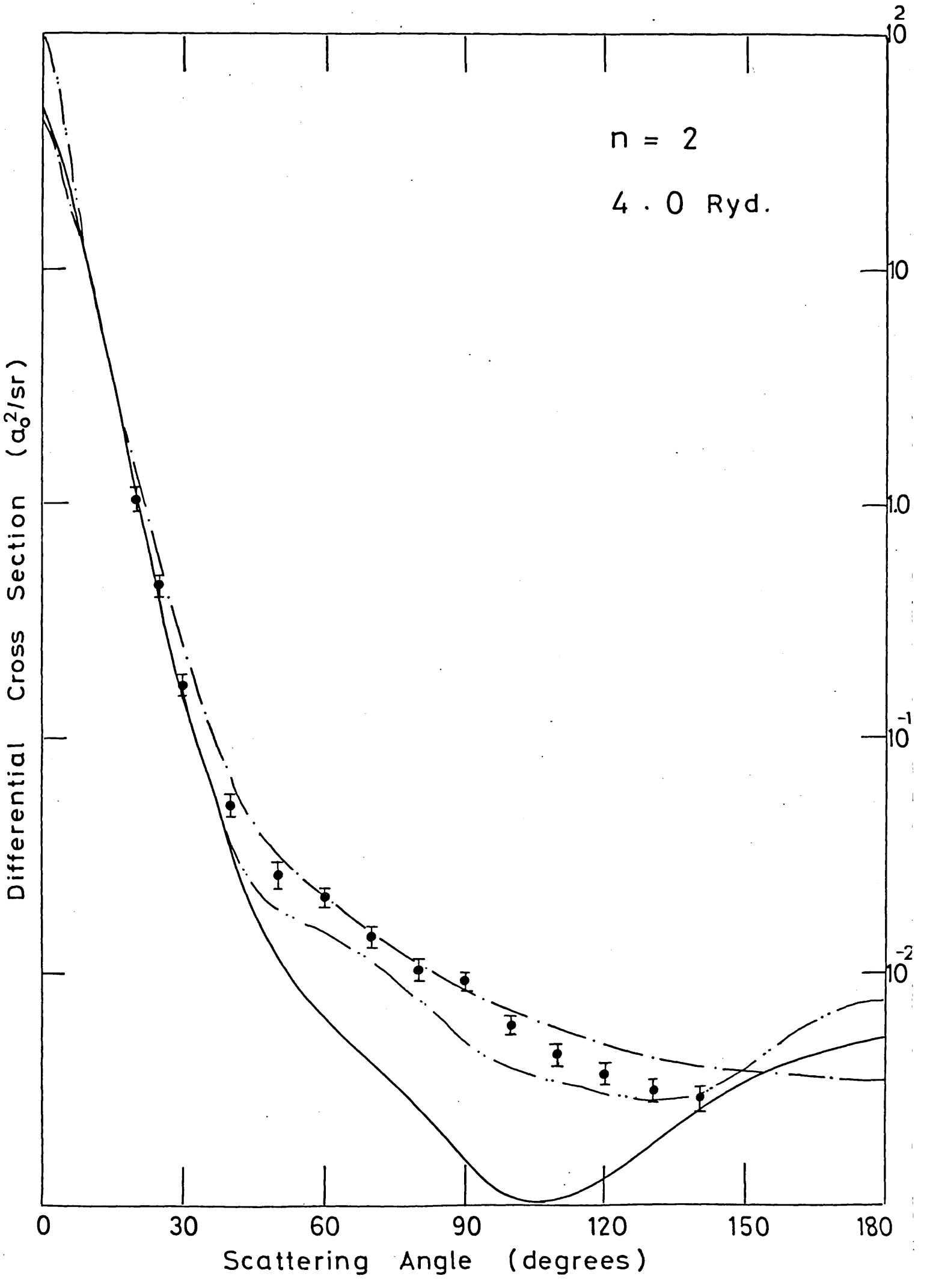
n = 2
4.0 Ryd.
Differential Cross Section (a_0^2/sr)
10^2
10
1.0
10^{-1}
10^{-2}
0
30
60
90
120
150
180
Scattering Angle (degrees)

Figure 9 (b)

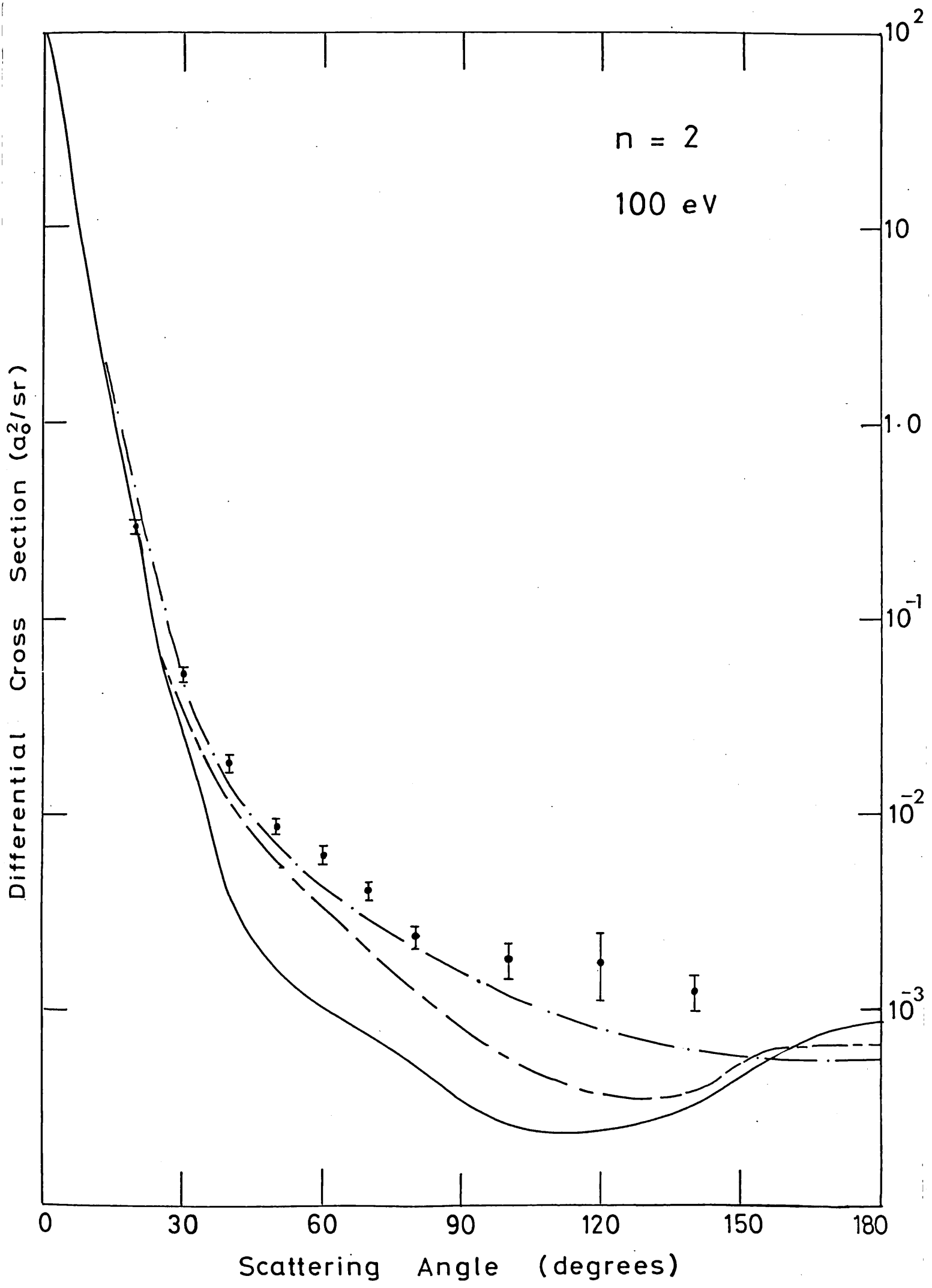
n = 2
100 eV
Differential Cross Section (a_0^2/sr)
10^2
10
1·0
10^{-1}
10^{-2}
10^{-3}
0
30
60
90
120
150
180
Scattering Angle (degrees)

Figure 10 (a)

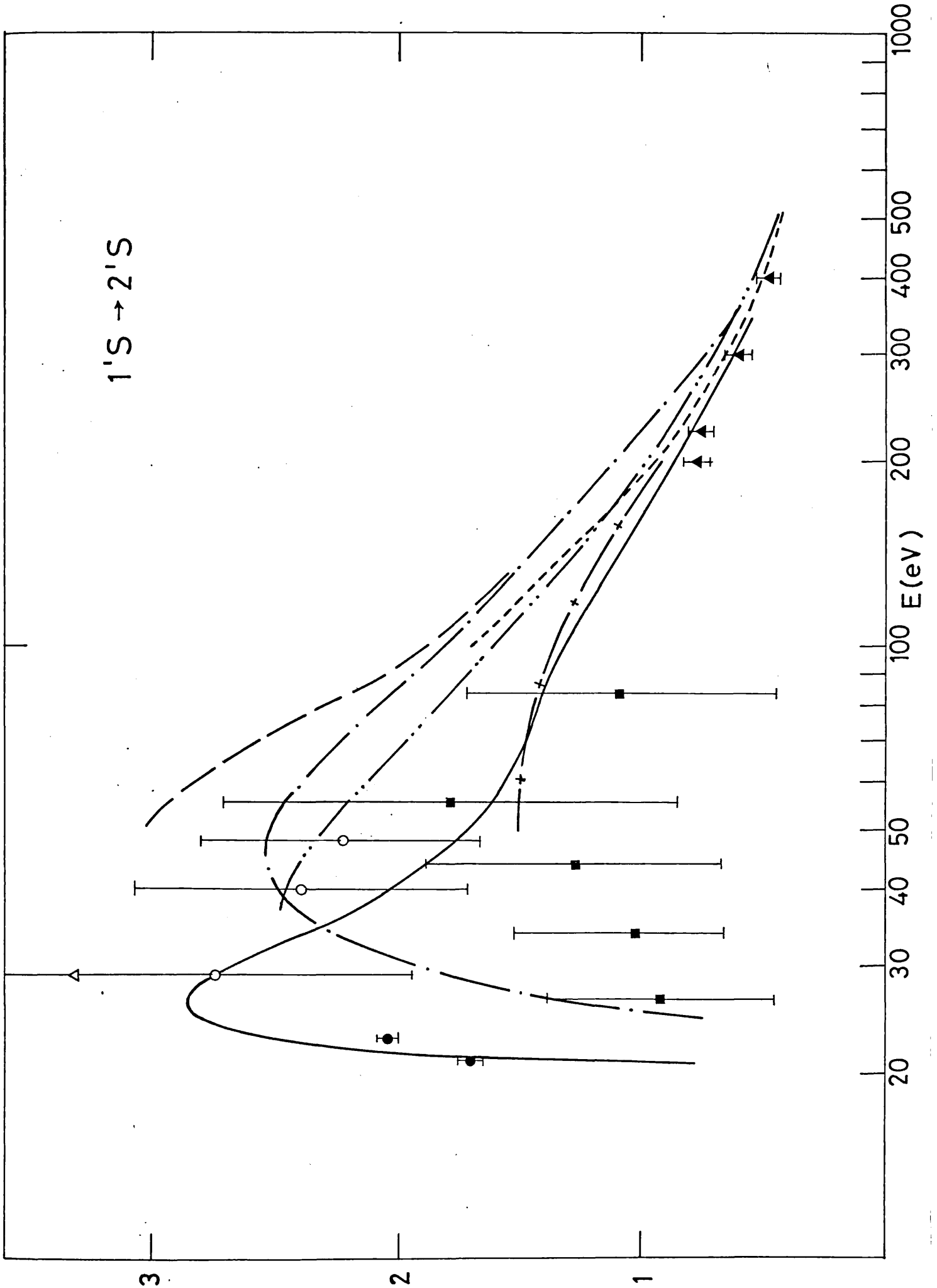
1'S → 2'S
Total Cross Section ($10^{-2} \times \pi a_o^2$)
E(eV)
1
2
3
20
30
40
50
100
200
300
400
500
1000

Figure 10 (b)

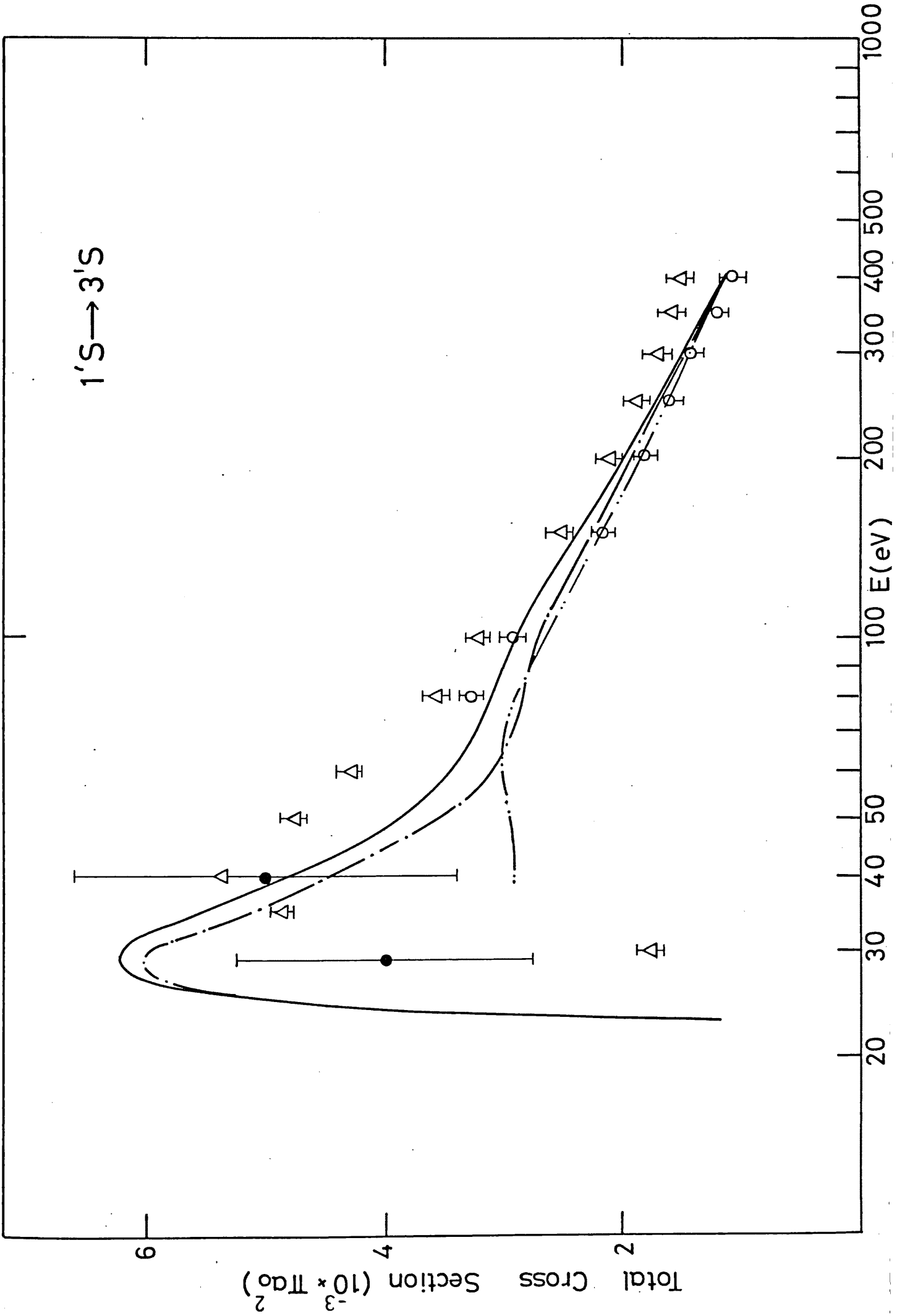
1'S⟶3'S
Total Cross Section ($10^{-3} \times \pi a_0^2$)
2
4
6
20
30
40
50
100 E(eV)
200
300
400
500
1000

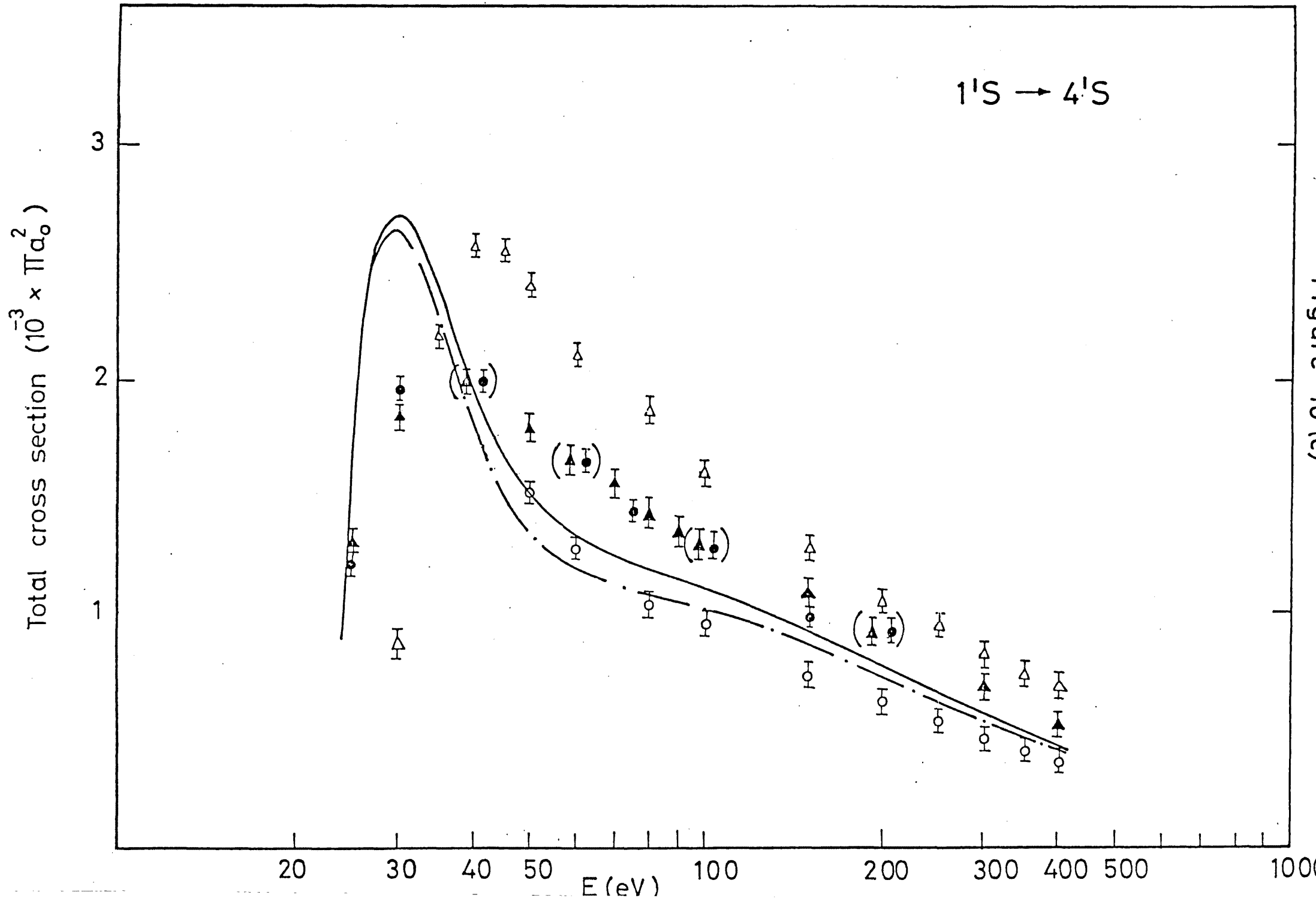
1¹S → 4¹S
Total cross section ($10^{-3} \times \pi a_o^2$)
3
2
1
20
30
40
50
100
200
300
400
500
1000
E (eV)

Figure 10 (c)

Figure 10(d)

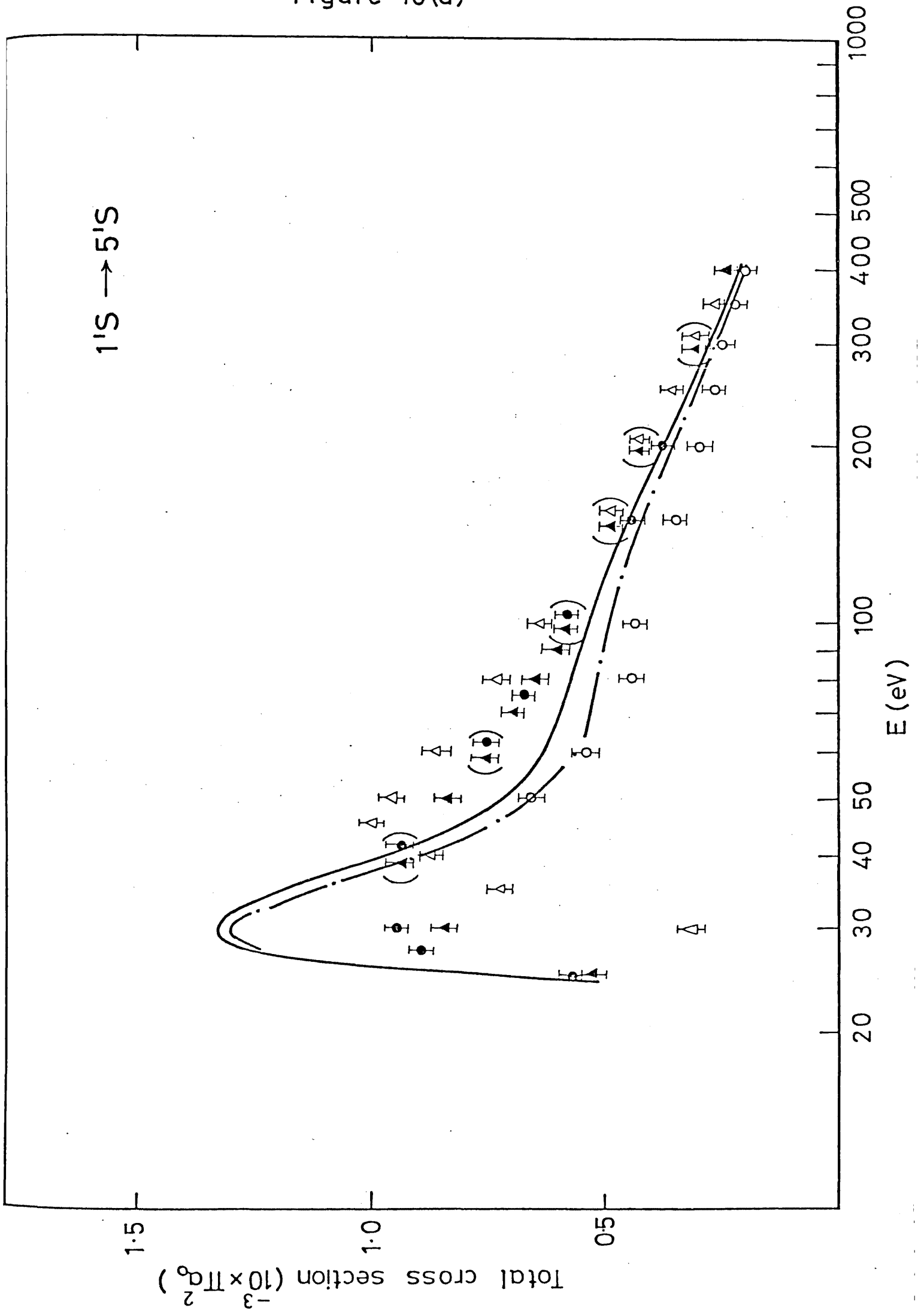
1'S → 5'S
Total cross section ($10^{-3} \times \pi a_0^2$)
1·5
1·0
0·5
E (eV)
20
30
40
50
100
200
300
400
500
1000

Figure 11(a)

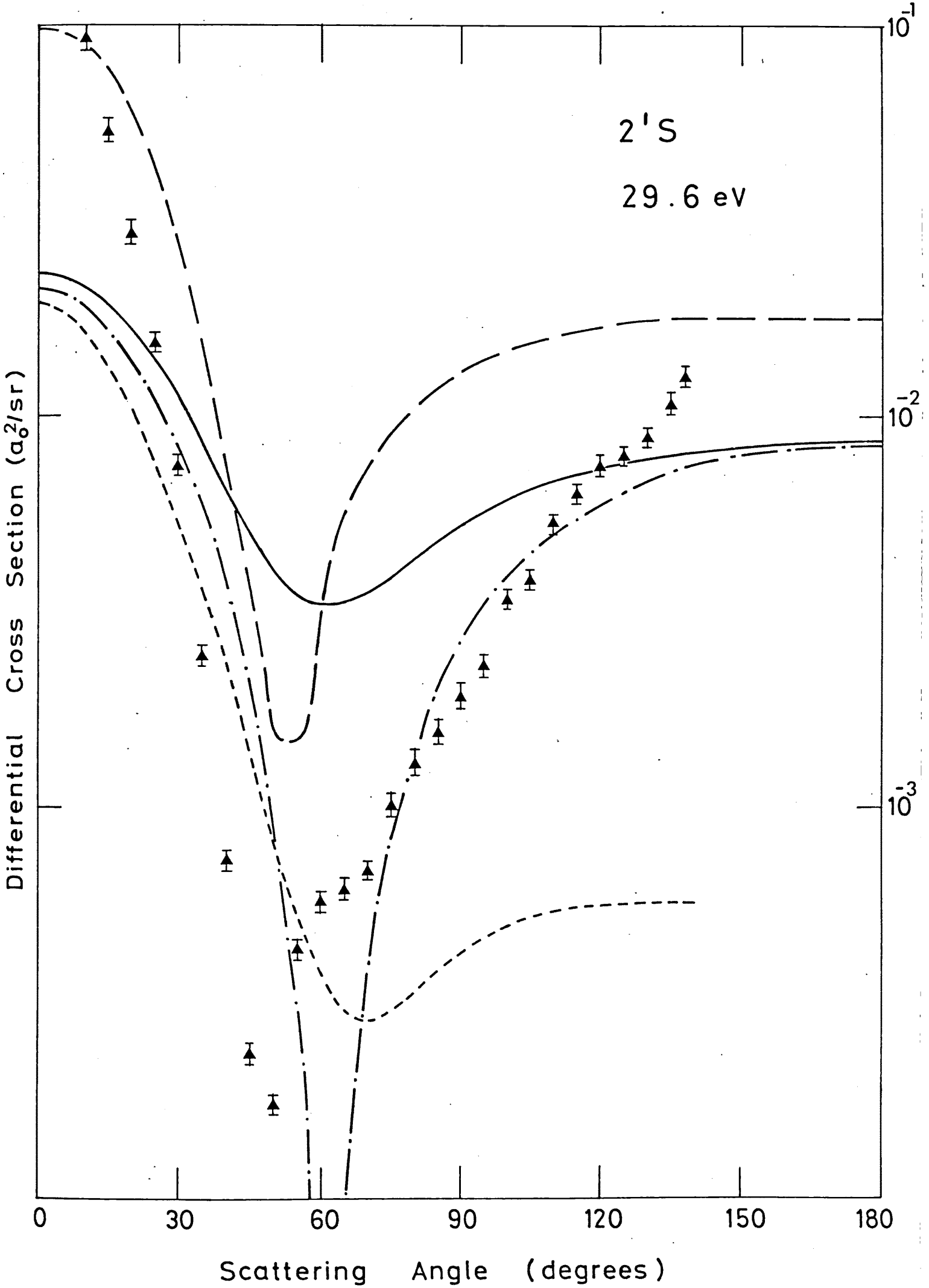
2¹S
29.6 eV
Differential Cross Section (a_0^2/sr)
10^{-1}
10^{-2}
10^{-3}
0
30
60
90
120
150
180
Scattering Angle (degrees)

Figure 11 (b)

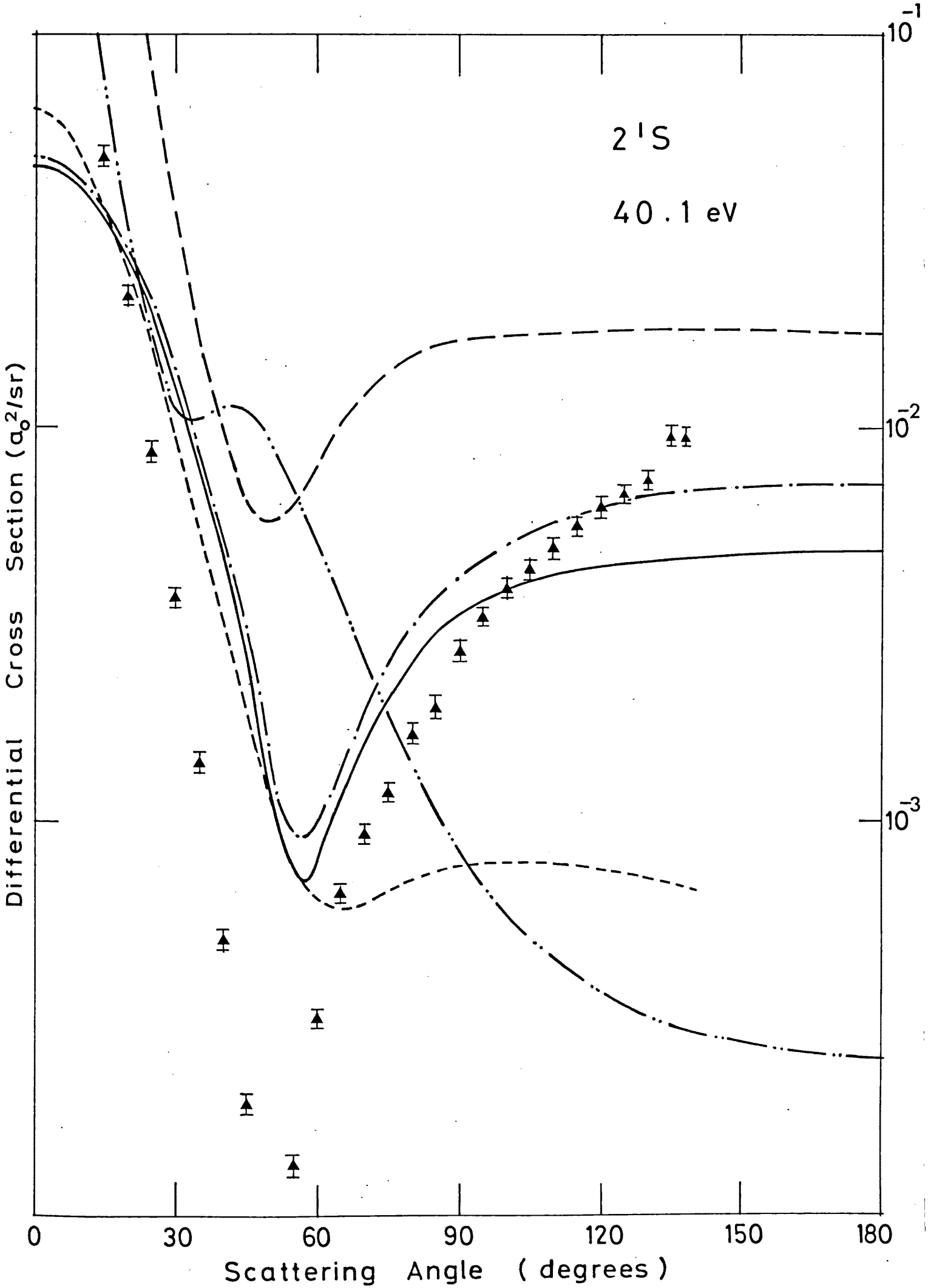
2 ¹S
40.1 eV
Differential Cross Section (a_0^2/sr)
10^{-1}
10^{-2}
10^{-3}
0
30
60
90
120
150
180
Scattering Angle (degrees)

Figure 11 (c)

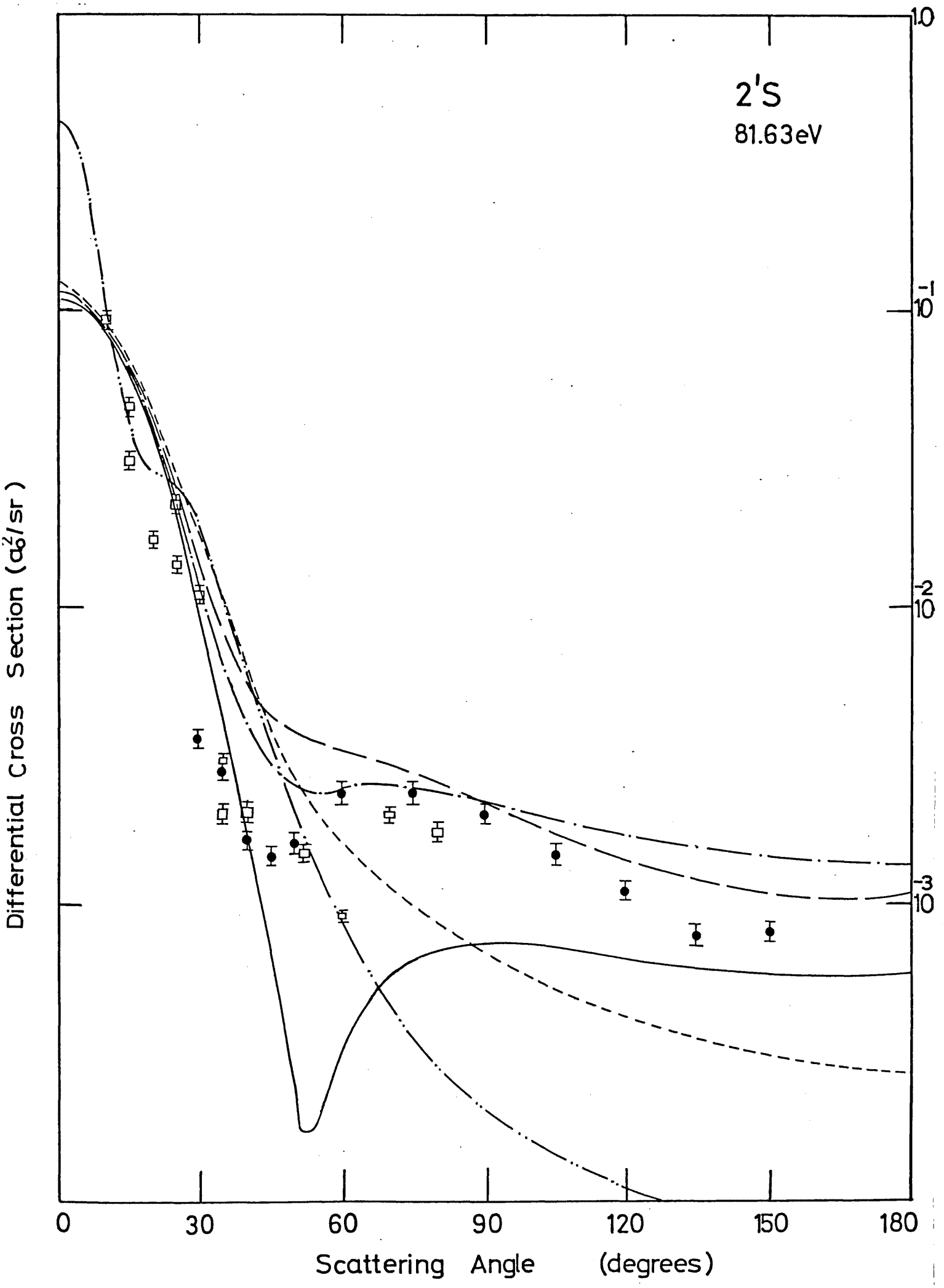
2'S
81.63eV
1.0
10^-1
10^-2
10^-3
Differential Cross Section (a0^2/sr)
0
30
60
90
120
150
180
Scattering Angle (degrees)

Figure 11 (d)

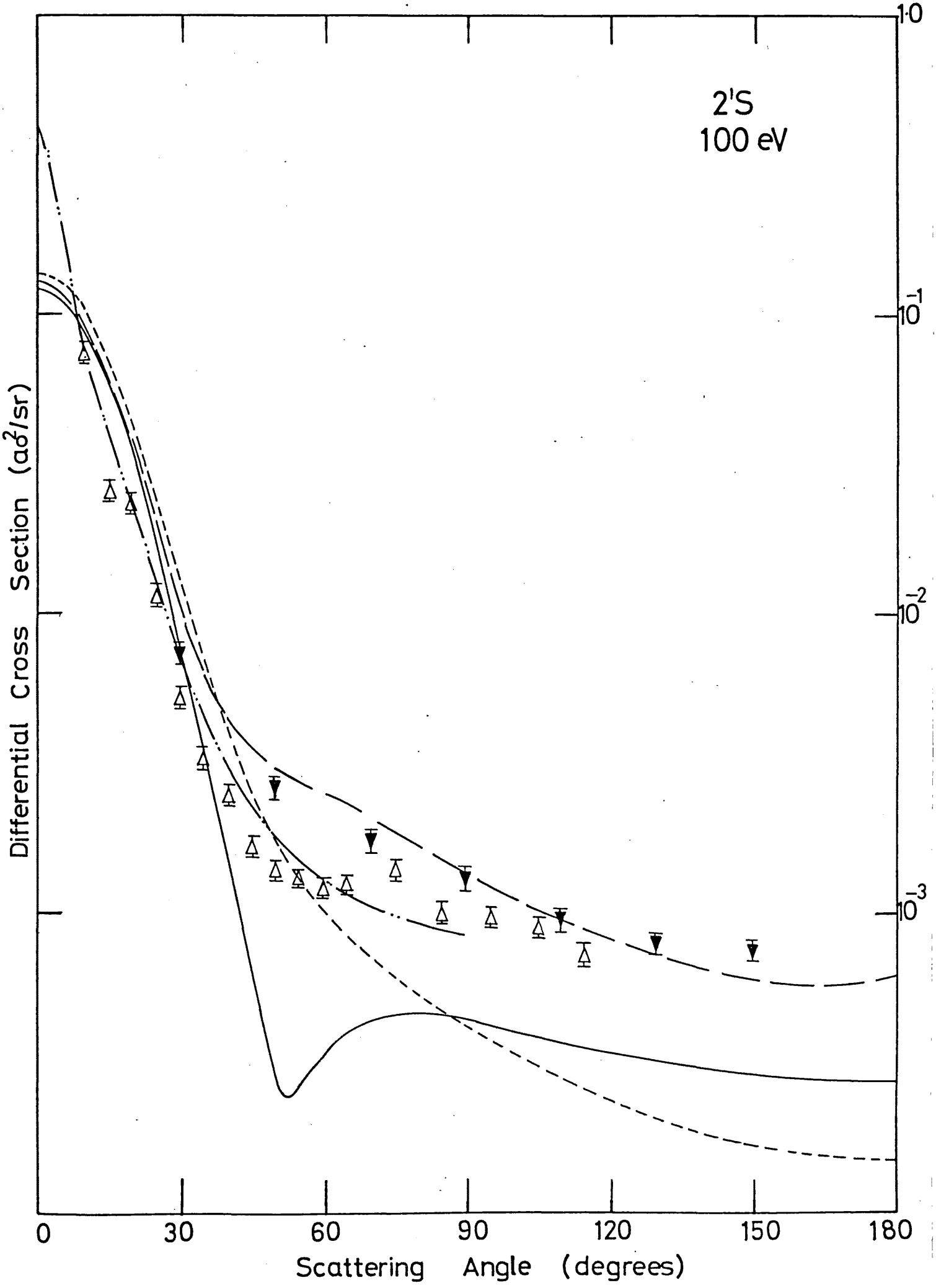
2¹S
100 eV
1·0
10⁻¹
10⁻²
10⁻³
Differential Cross Section (aσ²/sr)
0
30
60
90
120
150
180
Scattering Angle (degrees)

Figure 11 (e)

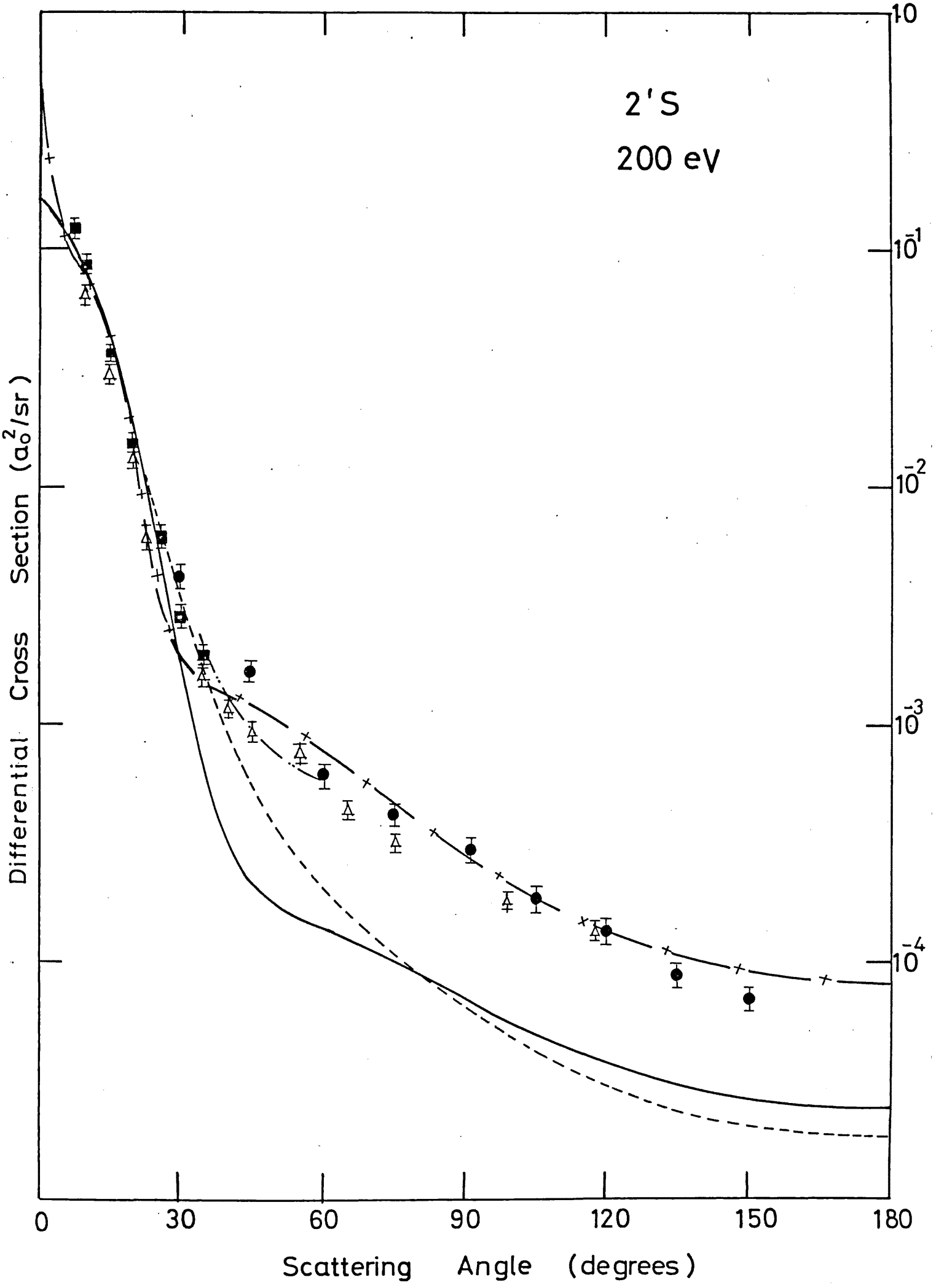
2'S
200 eV
10
10^{-1}
10^{-2}
10^{-3}
10^{-4}
Differential Cross Section (a_o^2/sr)
0
30
60
90
120
150
180
Scattering Angle (degrees)

Figure 12 (a)

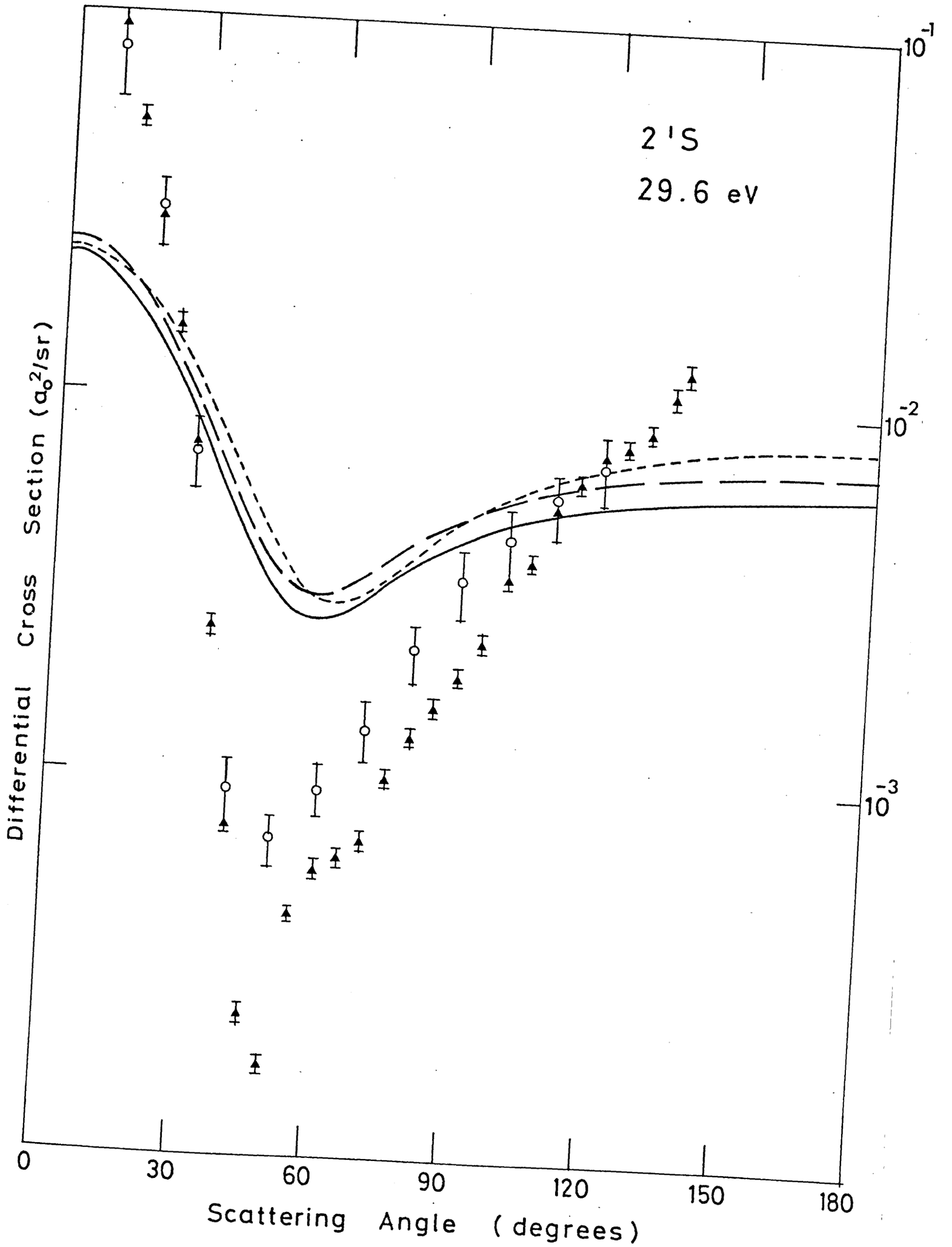
2 ¹S
29.6 eV
Differential Cross Section (a_0^2/sr)
10^{-1}
10^{-2}
10^{-3}
0
30
60
90
120
150
180
Scattering Angle (degrees)

Figure 12 (b)

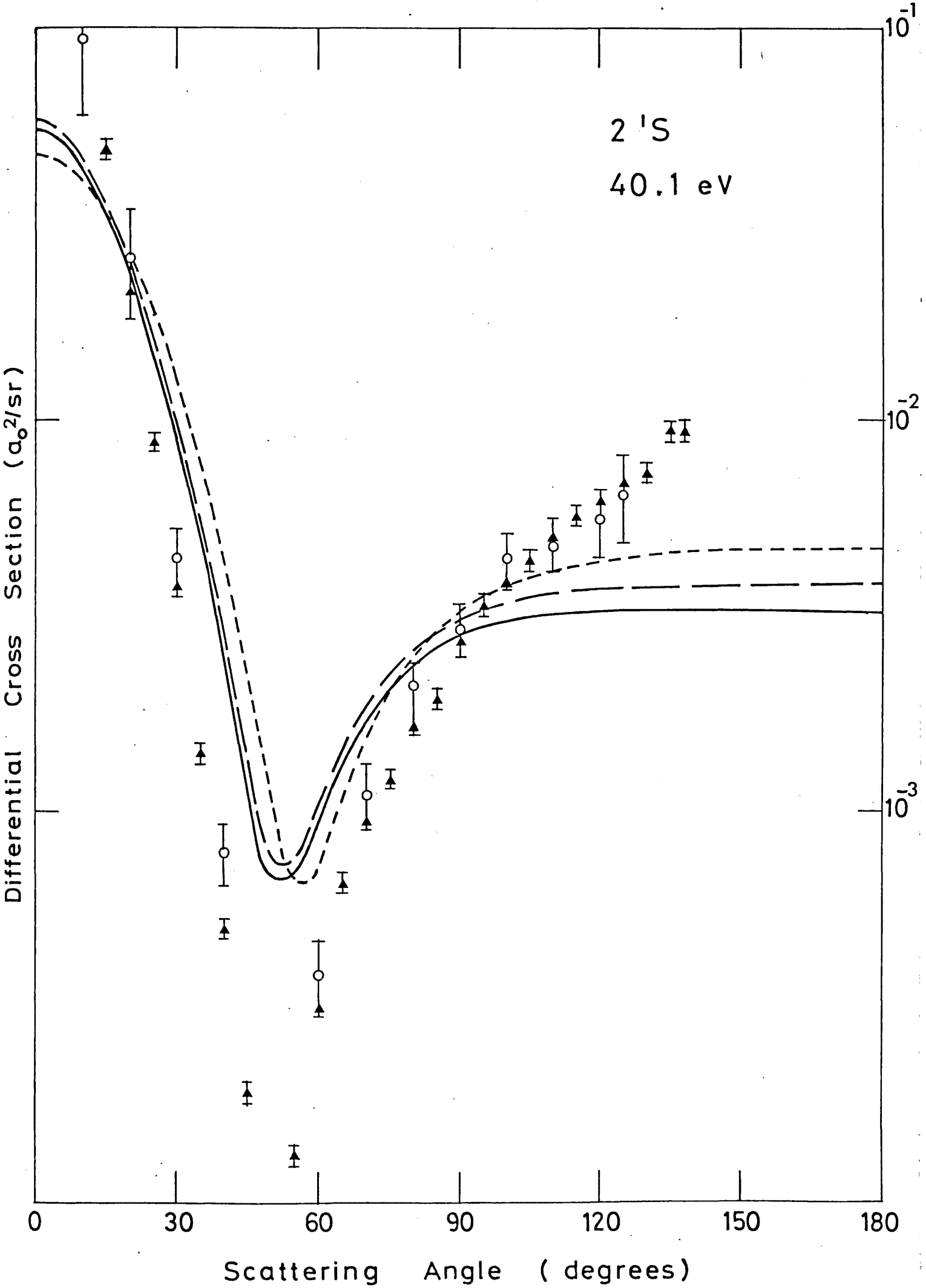
2 ¹S
40.1 eV
10⁻¹
10⁻²
10⁻³
Differential Cross Section (a₀²/sr)
0
30
60
90
120
150
180
Scattering Angle (degrees)

Figure 12 (c)

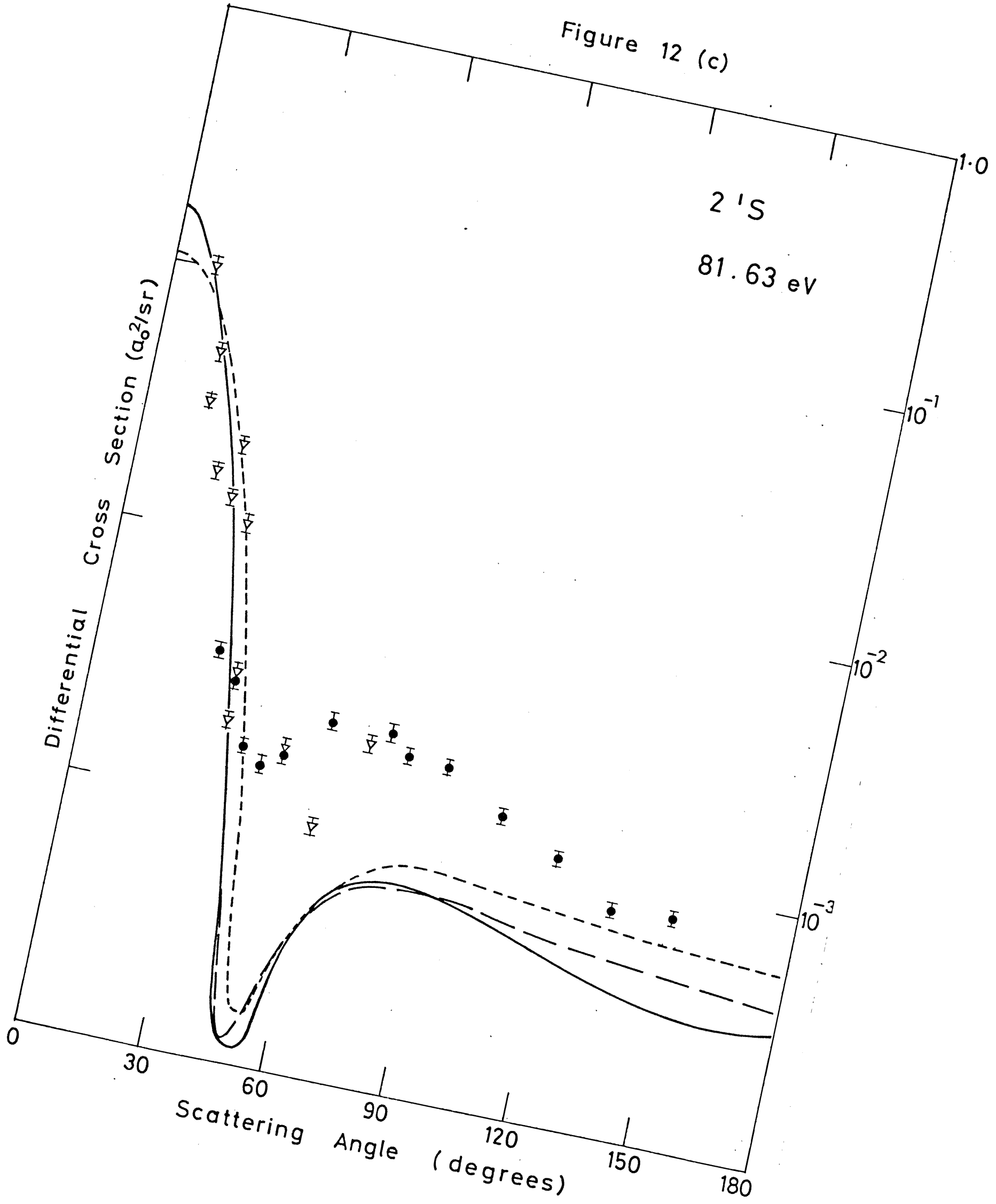
2 ¹S
81.63 eV
Differential Cross Section (a_0^2/sr)
1·0
10^{-1}
10^{-2}
10^{-3}
0
30
60
90
120
150
180
Scattering Angle (degrees)

Figure 12 (d)

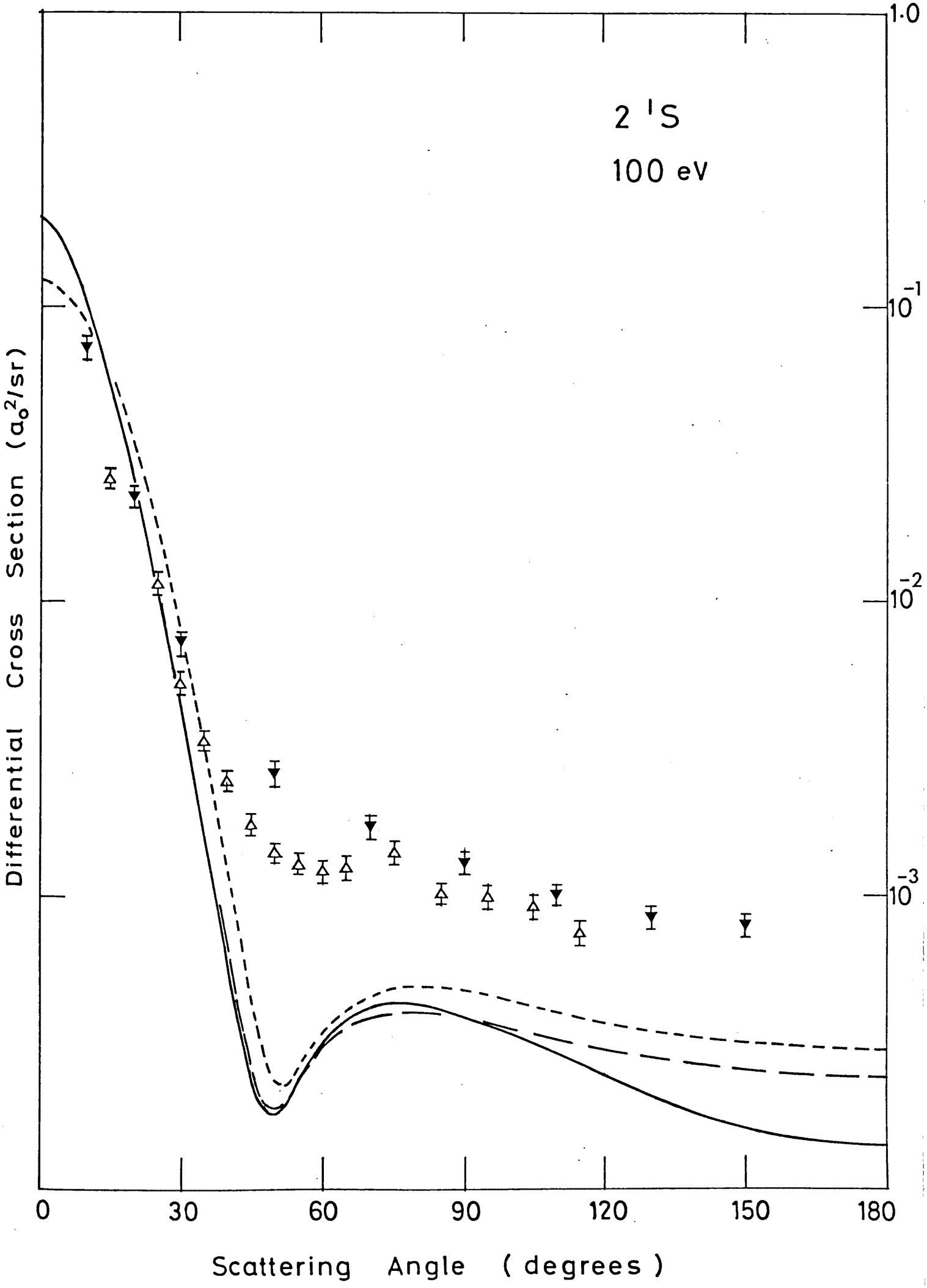
2 ¹S
100 eV
1·0
10⁻¹
10⁻²
10⁻³
Differential Cross Section (a₀²/sr)
0
30
60
90
120
150
180
Scattering Angle (degrees)

Figure 12 (e)

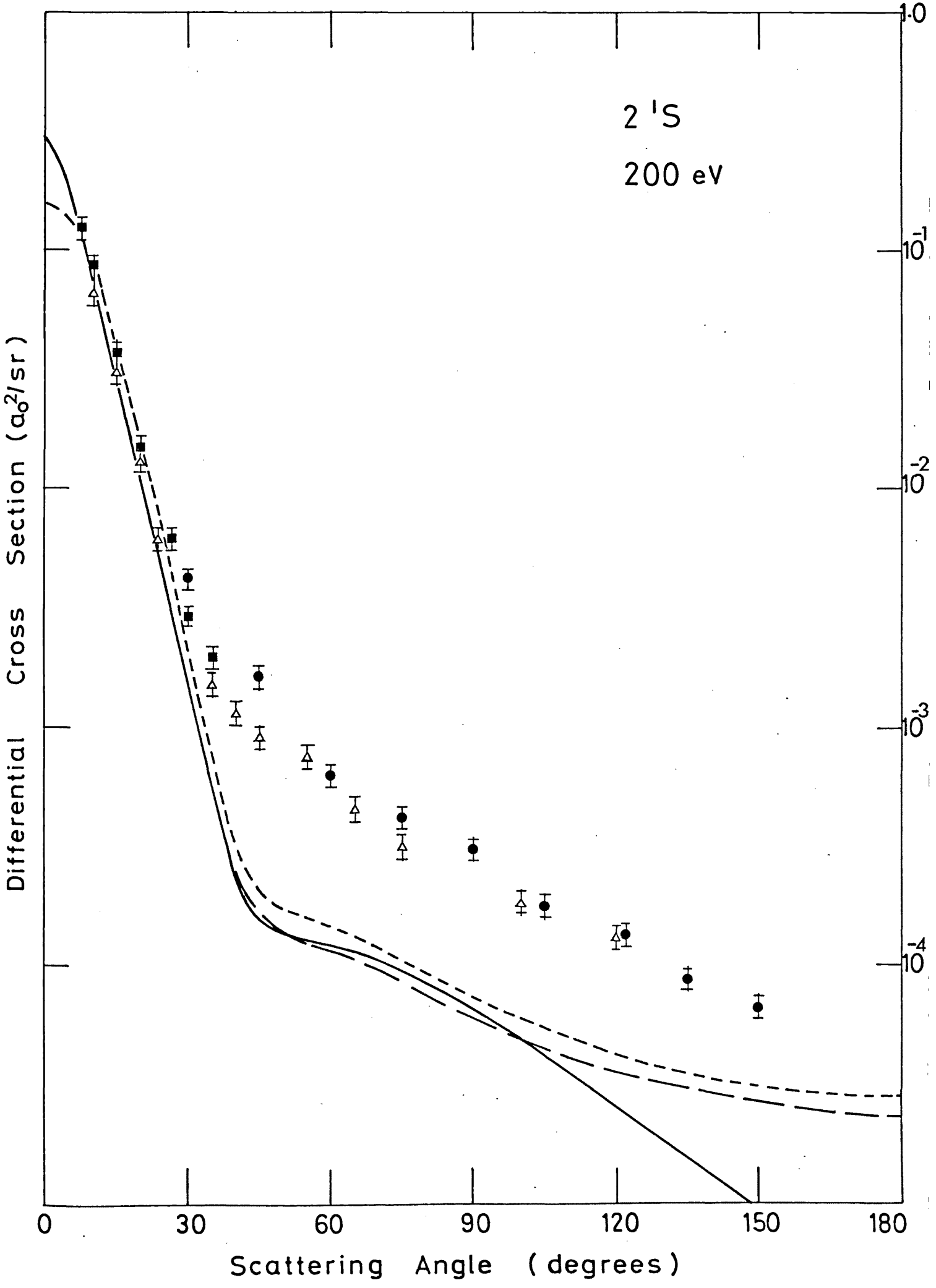
2 ¹S
200 eV
Differential Cross Section (a_0^2/sr)
1·0
10⁻¹
10⁻²
10⁻³
10⁻⁴
0
30
60
90
120
150
180
Scattering Angle (degrees)

Figure 13 (a)

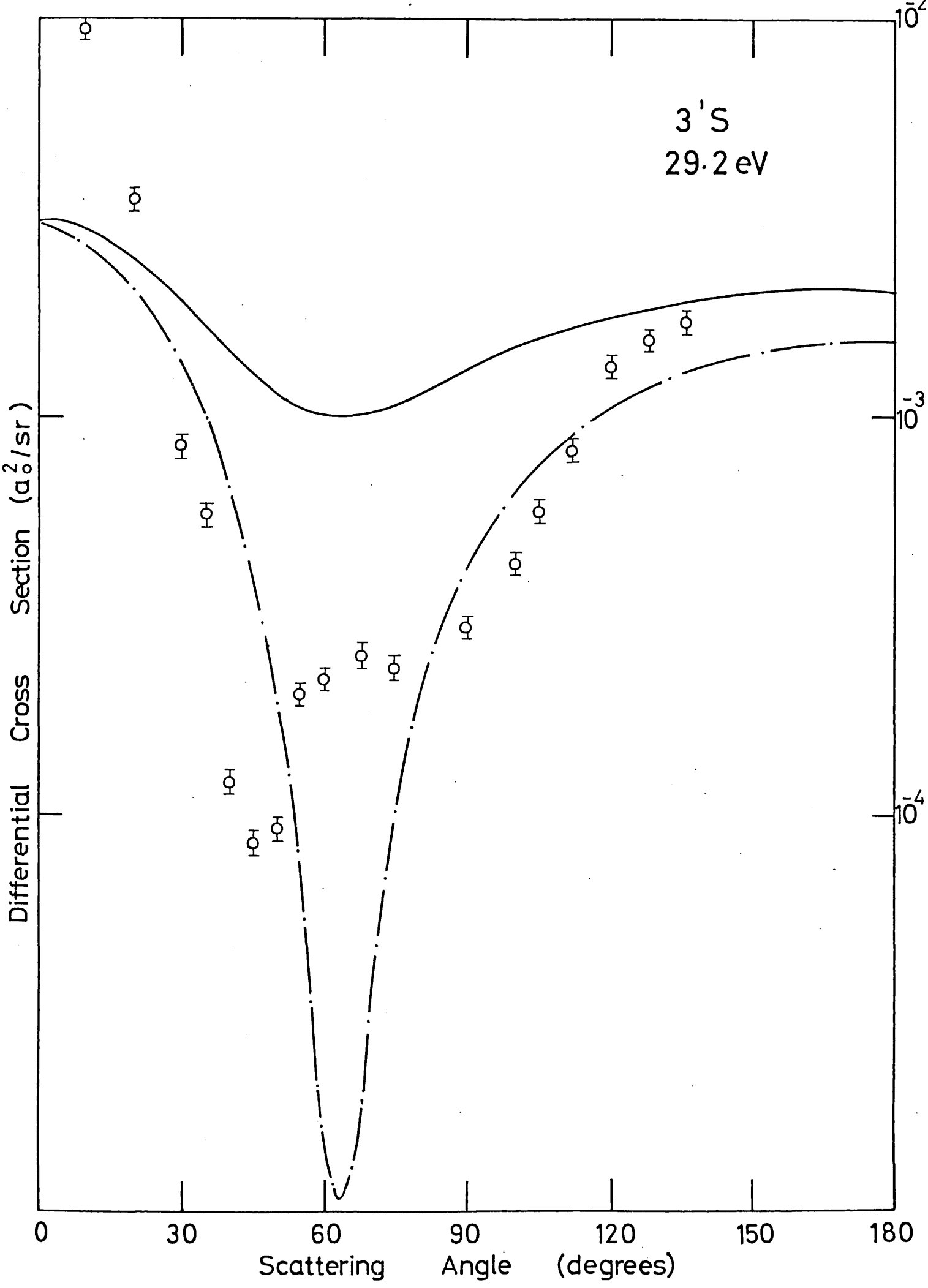
3 ¹S
29·2 eV
10⁻²
10⁻³
10⁻⁴
Differential Cross Section (a₀²/sr)
0
30
60
90
120
150
180
Scattering Angle (degrees)

Figure 13 (b)

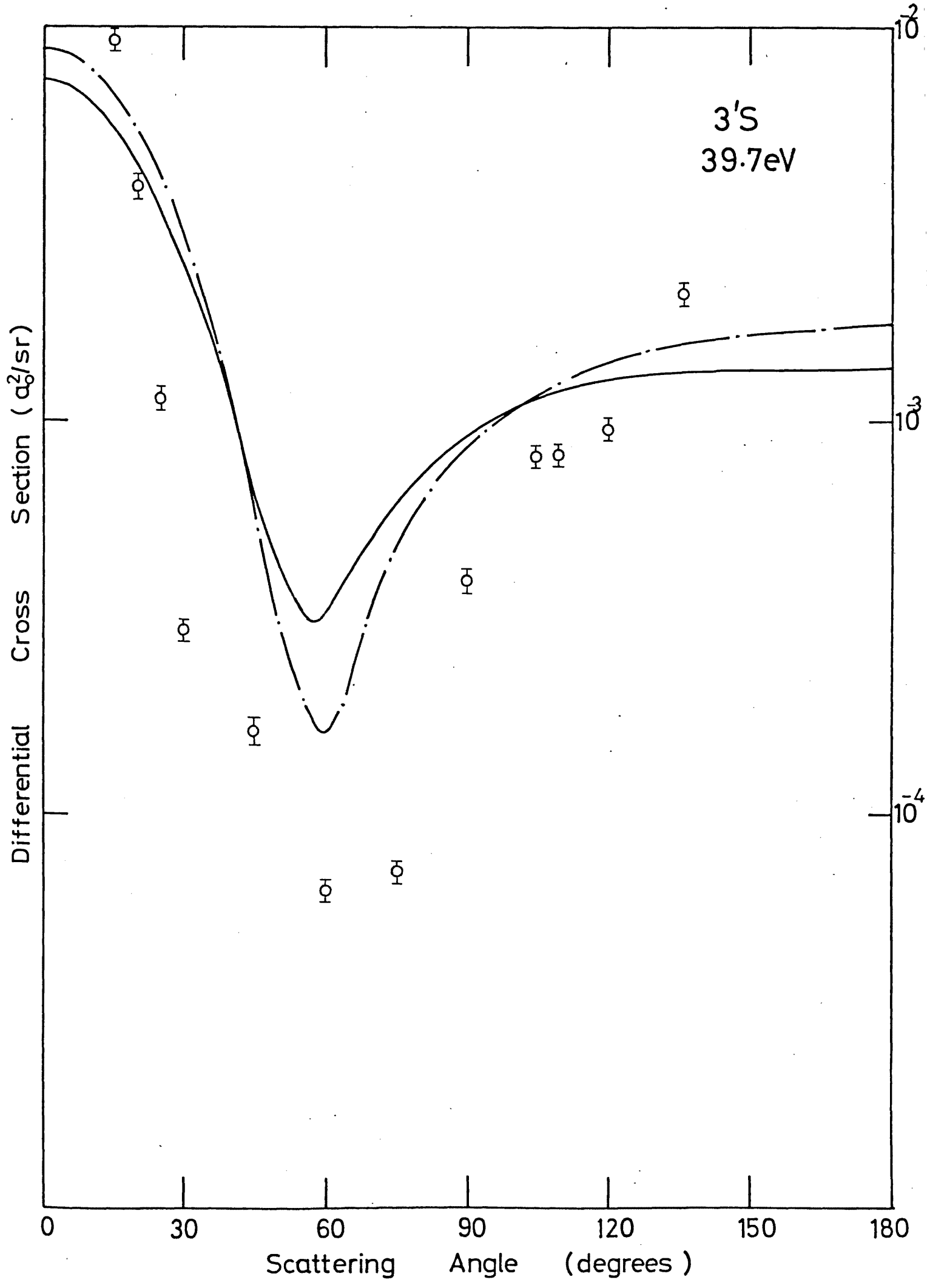
3'S
39·7eV
Differential Cross Section (a_0^2/sr)
10^{-2}
10^{-3}
10^{-4}
0
30
60
90
120
150
180
Scattering Angle (degrees)

Figure 13 (c)

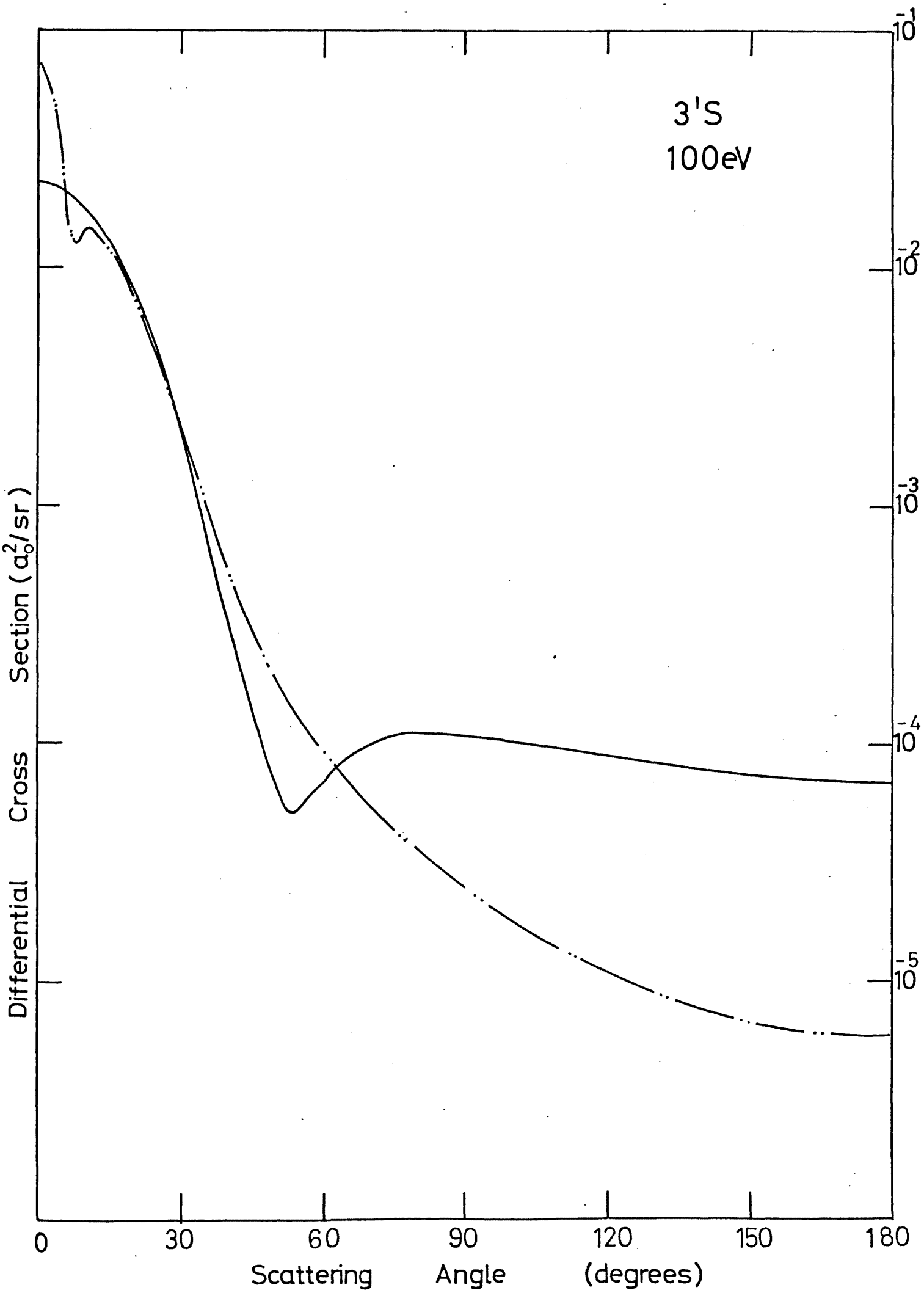
3¹S
100eV
Differential Cross Section (a_o^2/sr)
10^{-1}
10^{-2}
10^{-3}
10^{-4}
10^{-5}
0
30
60
90
120
150
180
Scattering Angle (degrees)

Figure 13(d)

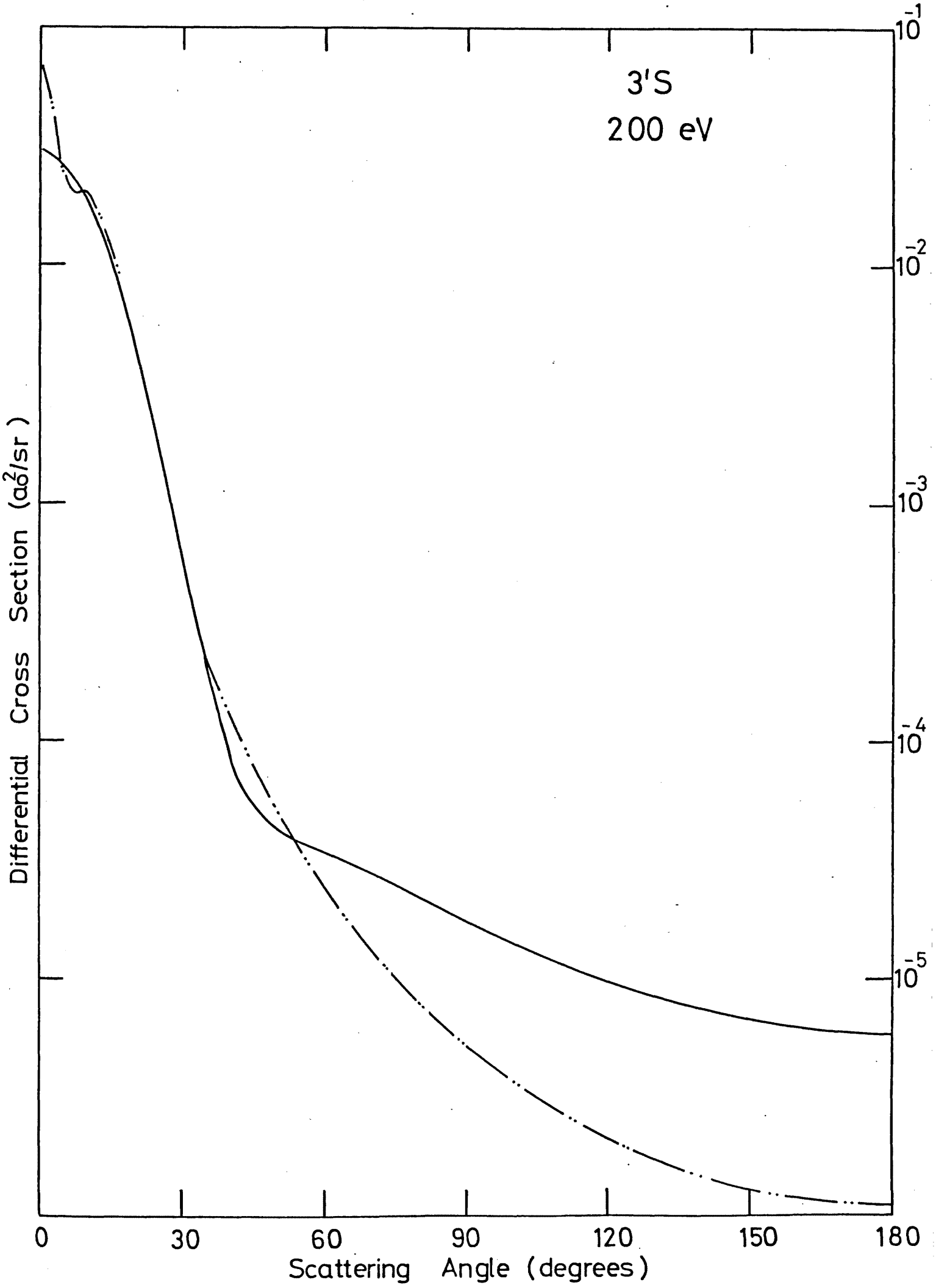
3'S
200 eV
Differential Cross Section (a_0^2/sr)
10^{-1}
10^{-2}
10^{-3}
10^{-4}
10^{-5}
0
30
60
90
120
150
180
Scattering Angle (degrees)

Figure 14

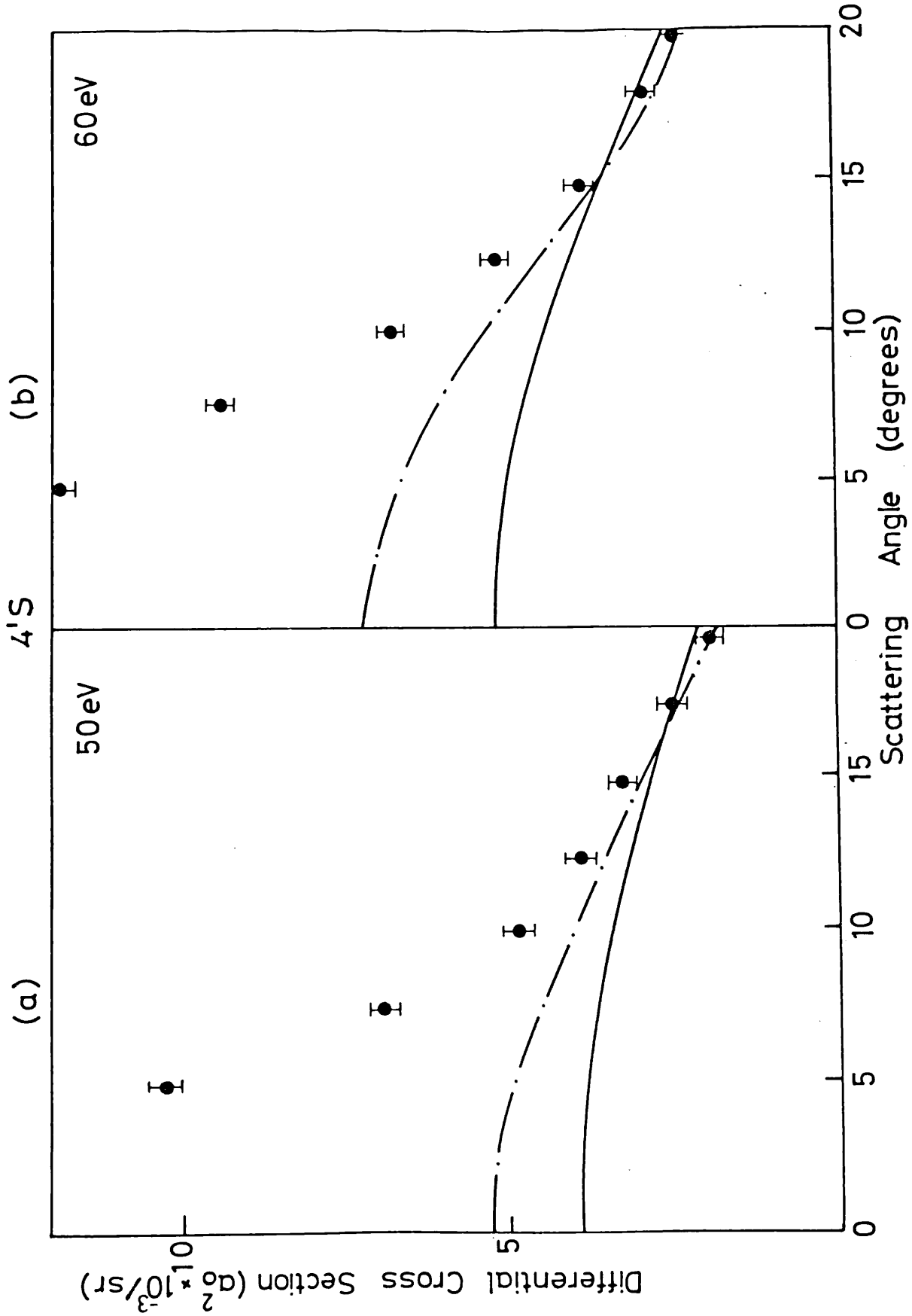
4'S
(a)
50eV
(b)
60eV
Differential Cross Section ($a_0^2 \times 10^{-3}$/sr)
Scattering Angle (degrees)
0
5
10
15
20

Figure 14

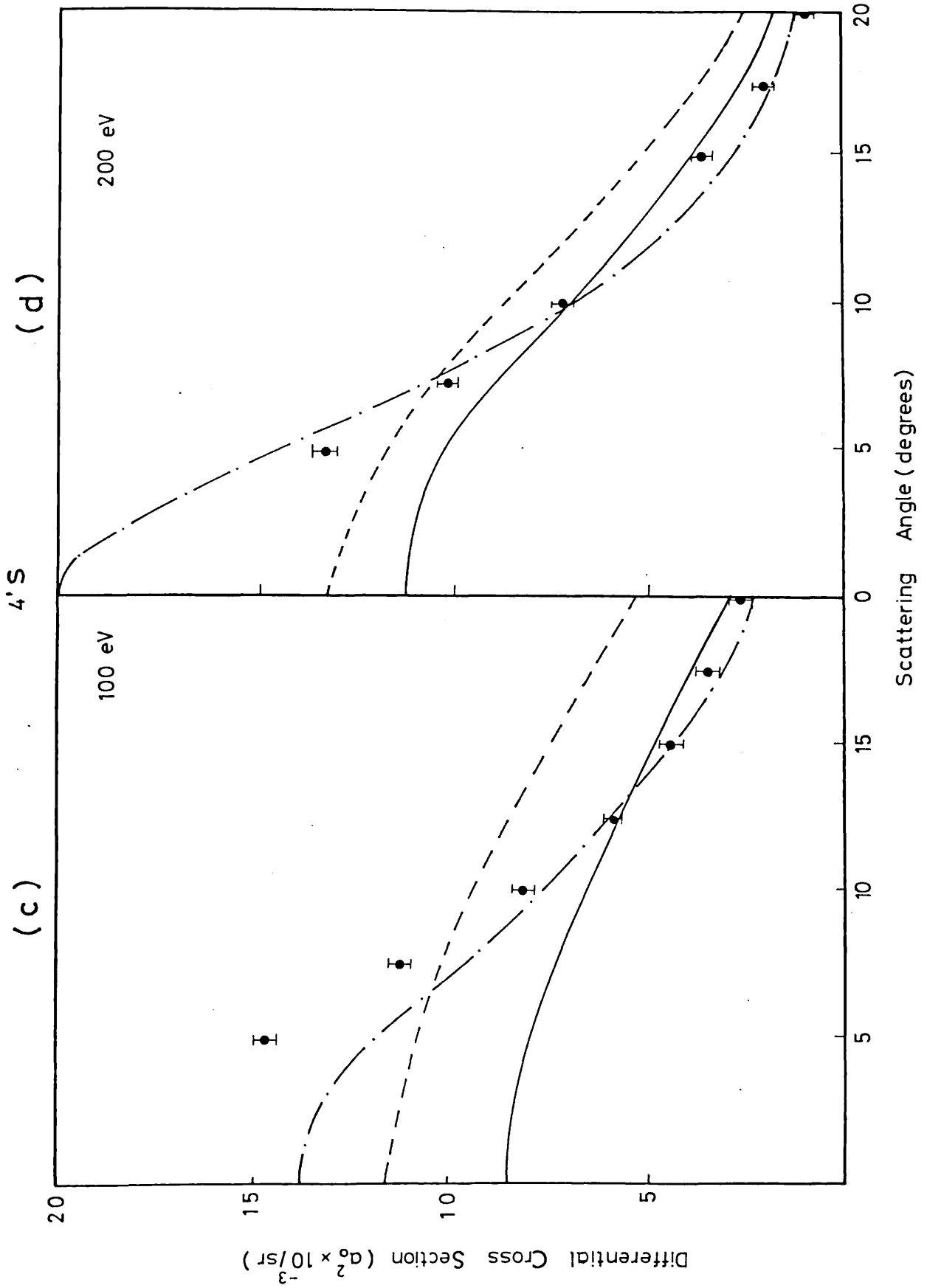
4'S
(c)
100 eV
(d)
200 eV
Differential Cross Section ($a_o^2 \times 10^{-3}$/sr)
Scattering Angle (degrees)
0
5
10
15
20

Figure 15

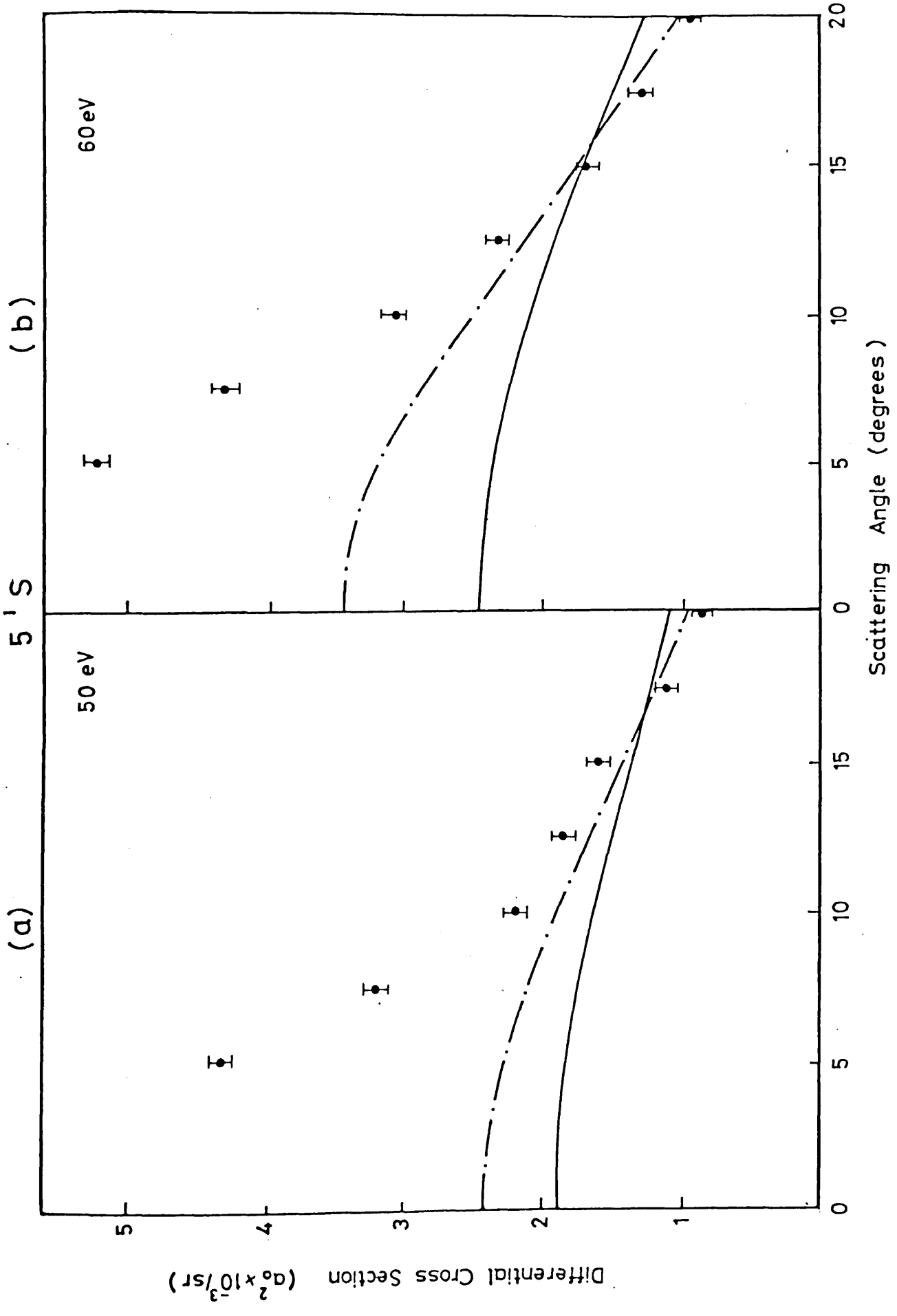
5 ¹S
(a)
50 eV
(b)
60eV
Differential Cross Section (a₀² x 10⁻³/sr)
Scattering Angle (degrees)
0
5
10
15
20
1
2
3
4
5

Figure 15

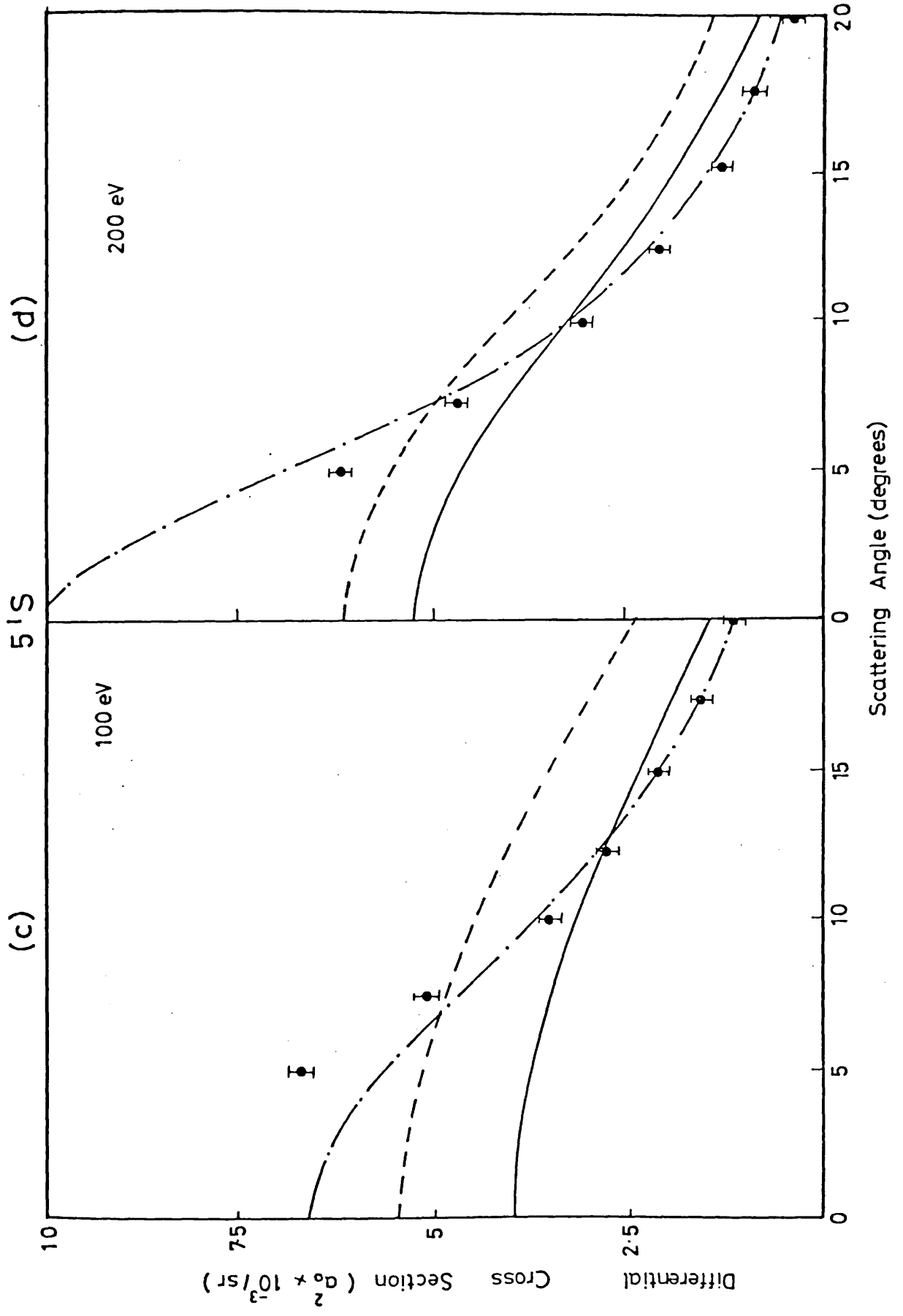
5¹S
(d)
200 eV
(c)
100 eV
Differential Cross Section ($a_o^2 \times 10^{-3}$/sr)
10
7·5
5
2·5
0
5
10
15
20
Scattering Angle (degrees)

Figure 16

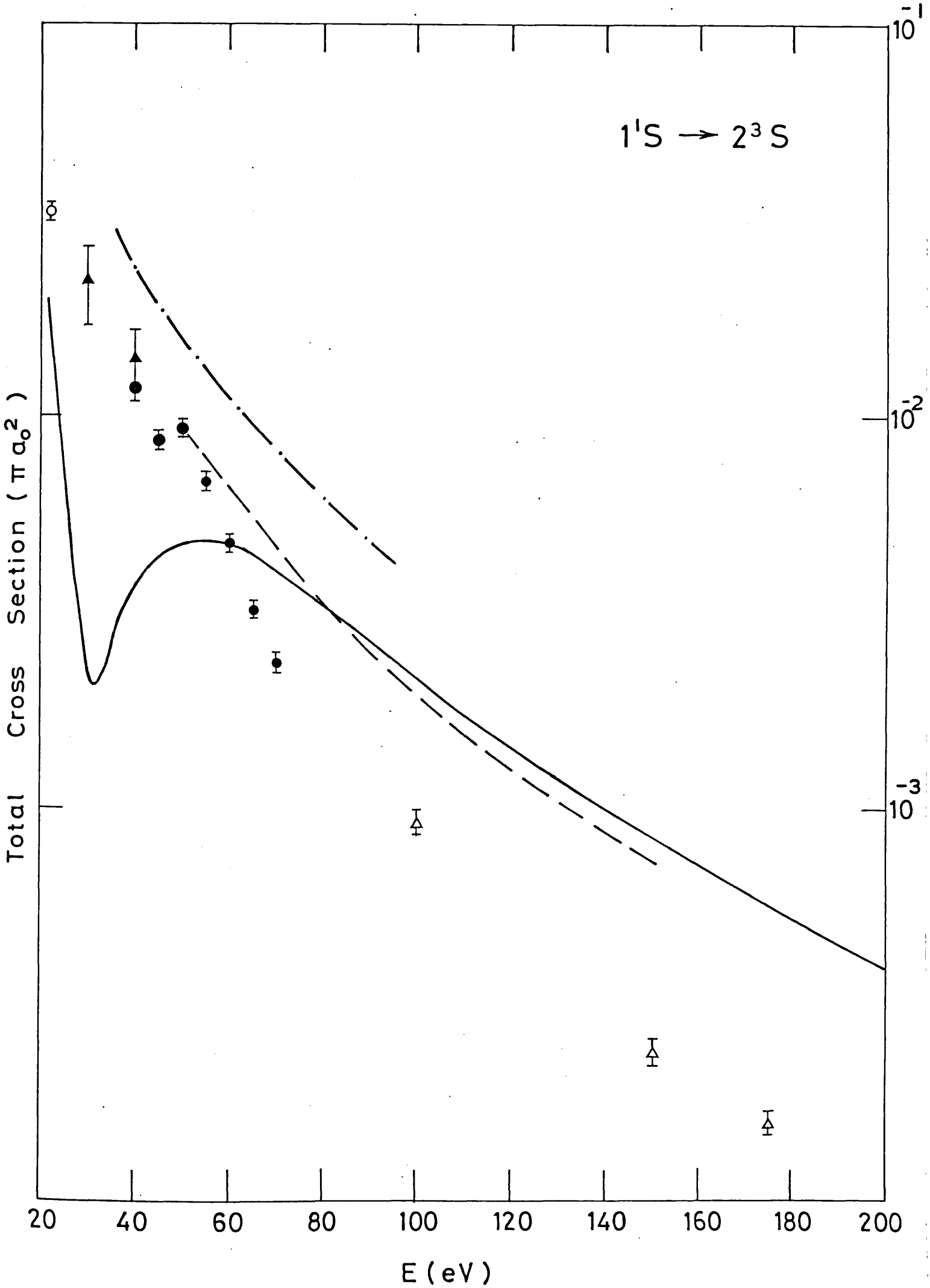
$1^1S \rightarrow 2^3S$
Total Cross Section (πa_0^2)
10^{-1}
10^{-2}
10^{-3}
20
40
60
80
100
120
140
160
180
200
E (eV)

Figure 17 (a)

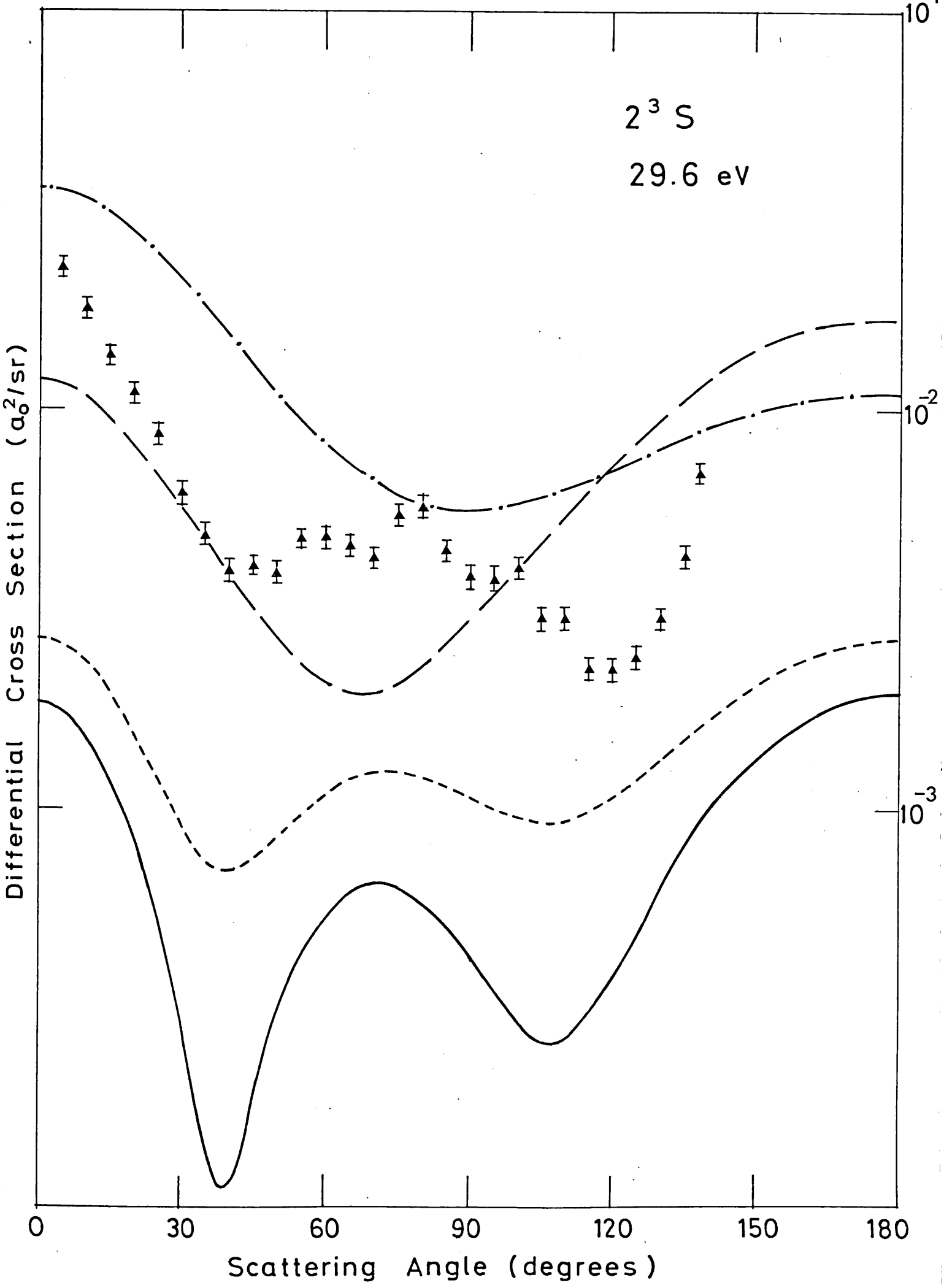
2^3S
29.6 eV
10^{-1}
10^{-2}
10^{-3}
Differential Cross Section (a_o^2/sr)
0
30
60
90
120
150
180
Scattering Angle (degrees)

Figure 17 (b)

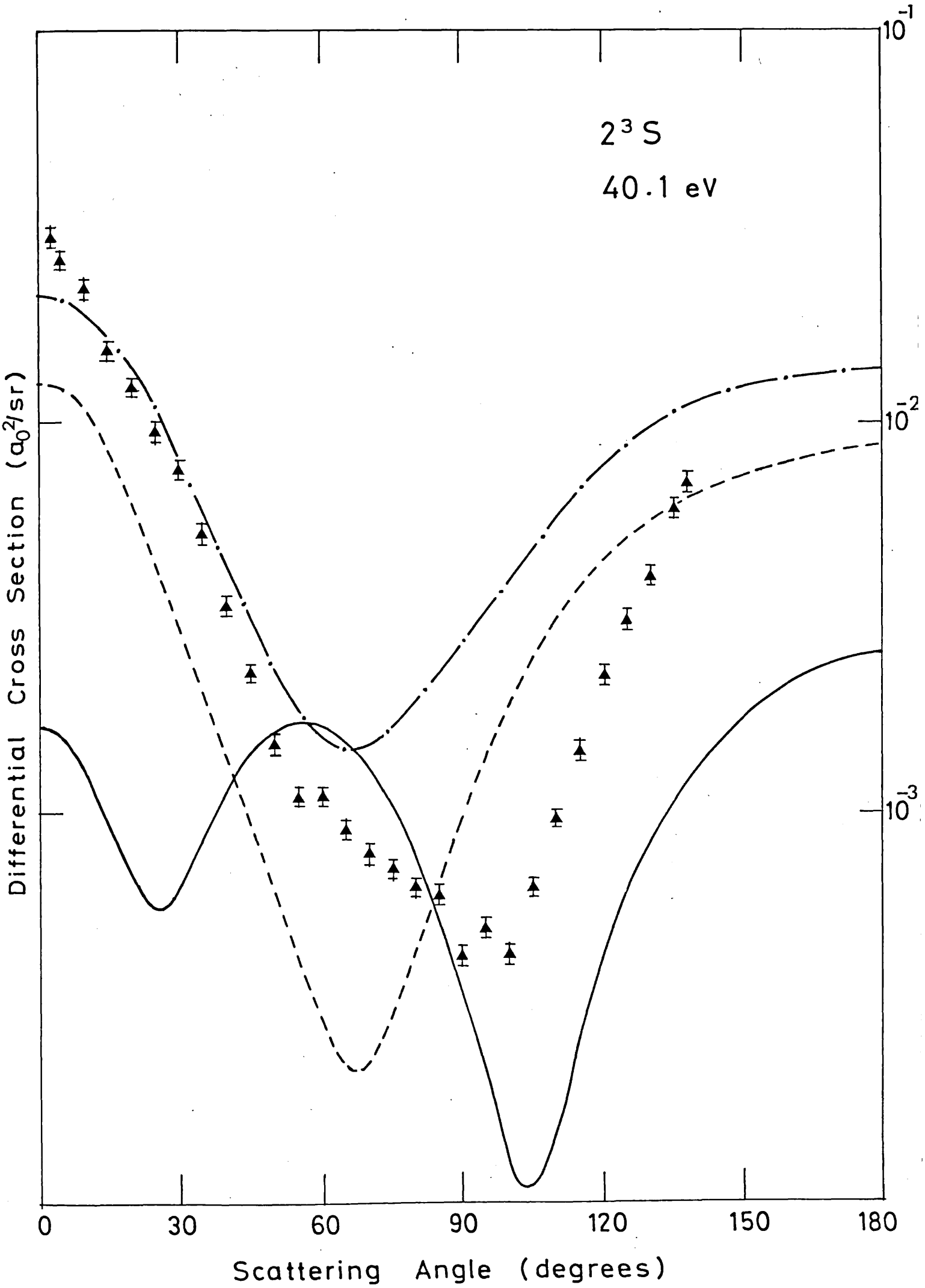
2^3S
40.1 eV
10^{-1}
10^{-2}
10^{-3}
Differential Cross Section (a_0^2/sr)
0
30
60
90
120
150
180
Scattering Angle (degrees)

Figure 17 (c)

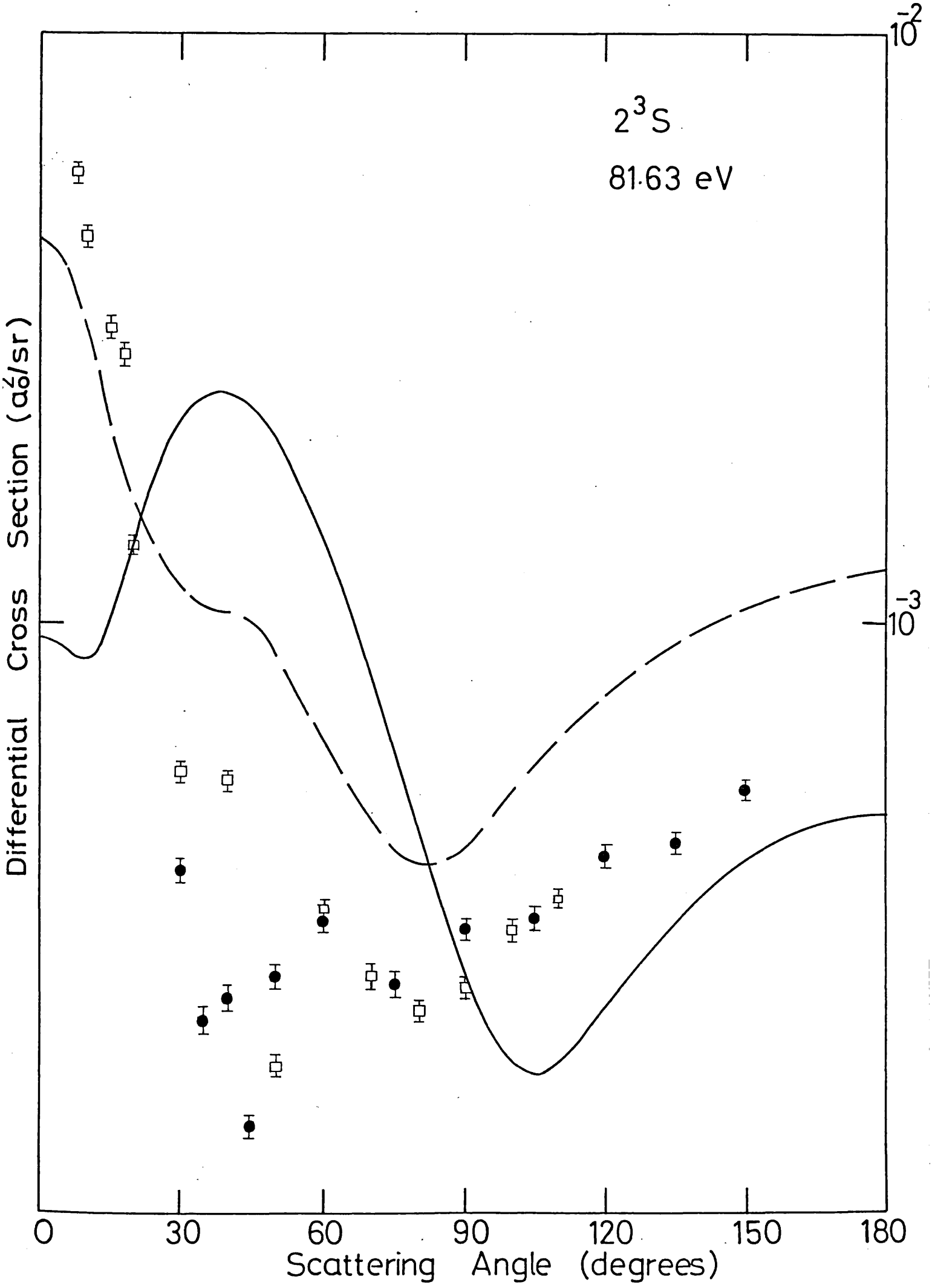
10^{-2}
2^3S
81·63 eV
10^{-3}
Differential Cross Section (a_0^2/sr)
0
30
60
90
120
150
180
Scattering Angle (degrees)

Figure 17 (d)

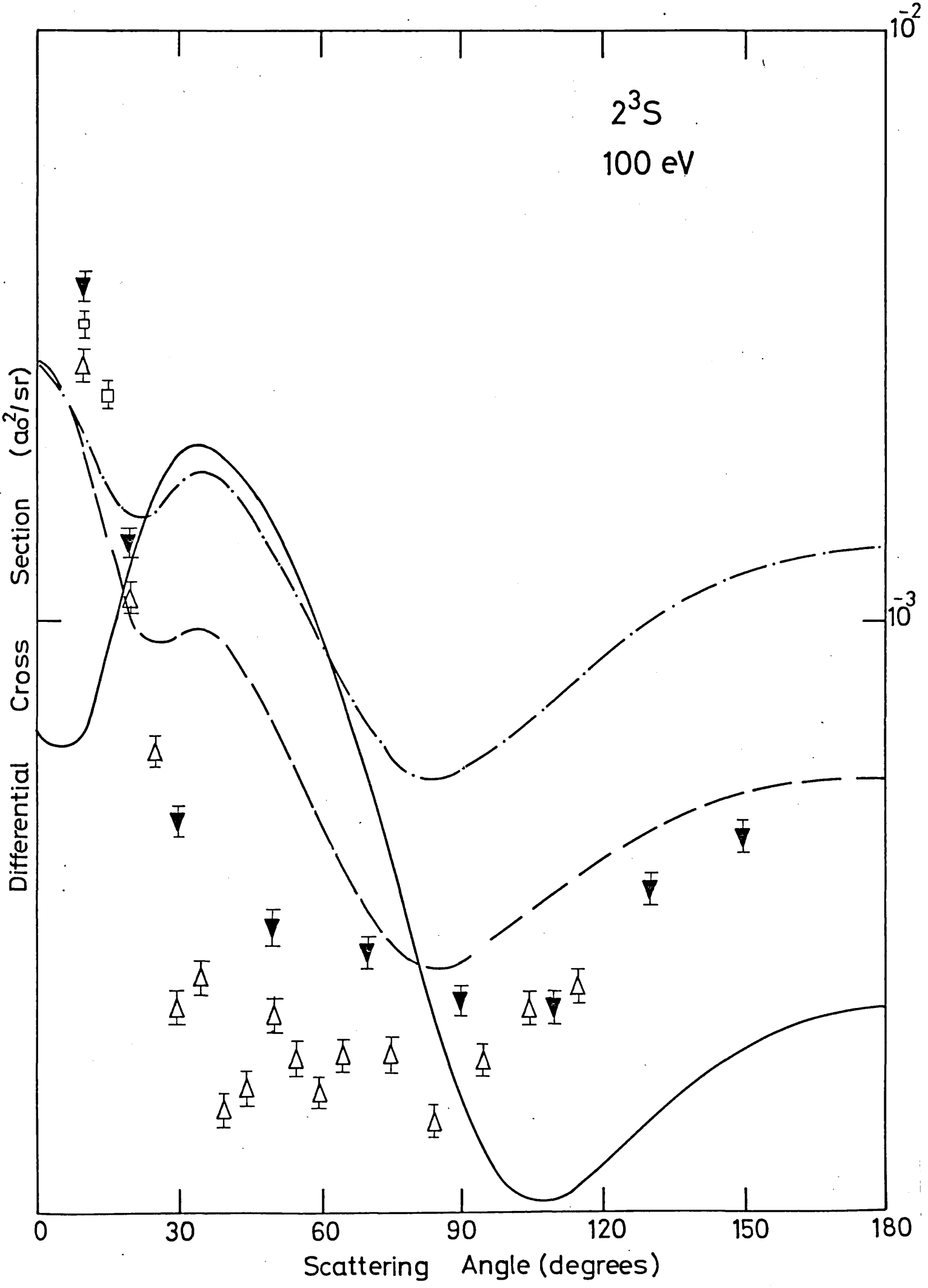
10^{-2}
2^3S
100 eV
Differential Cross Section (a_0^2/sr)
10^{-3}
0
30
60
90
120
150
180
Scattering Angle (degrees)

Figure 17 (e)

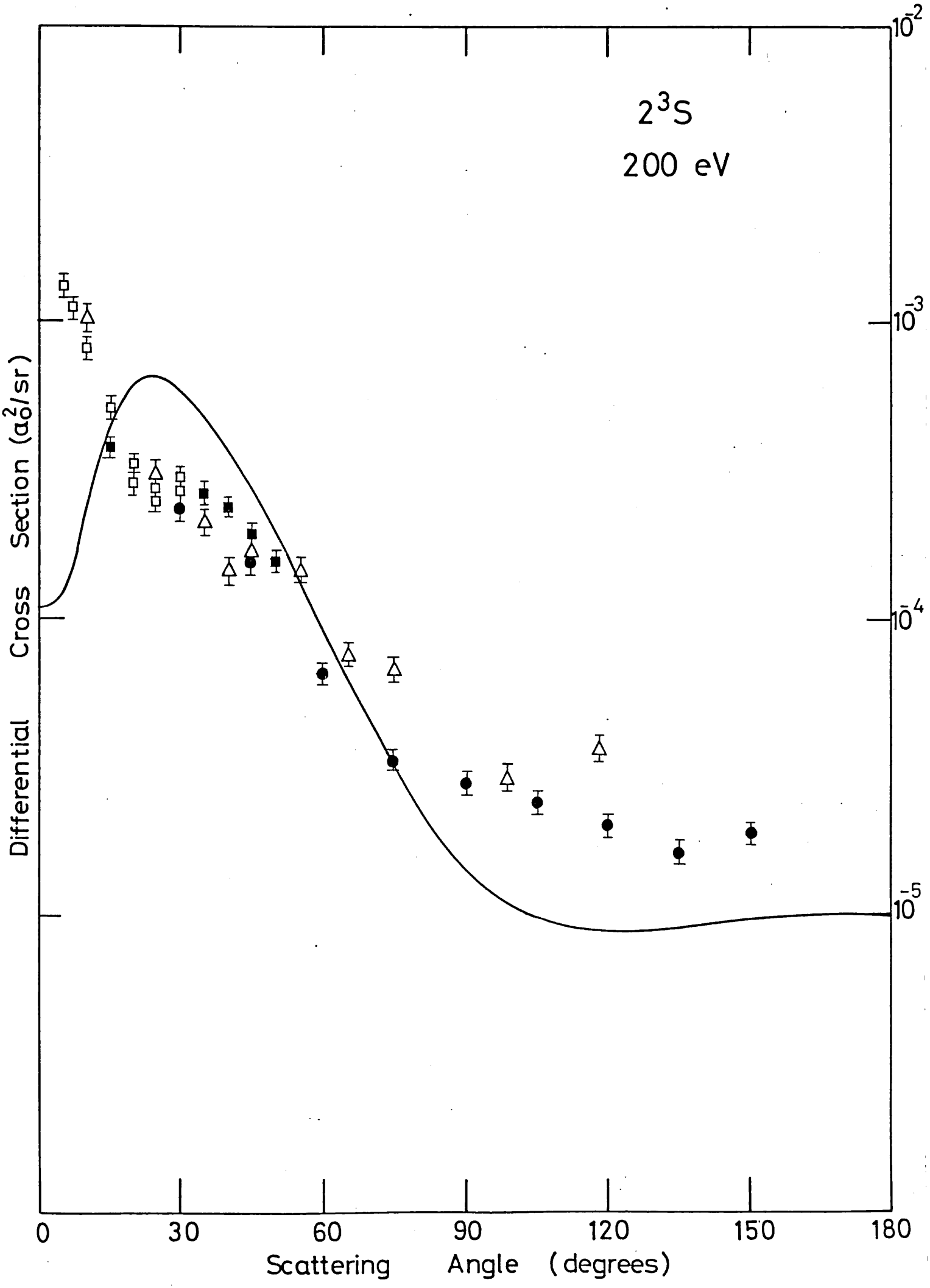
2^3S
200 eV
Differential Cross Section (a_0^2/sr)
10^{-2}
10^{-3}
10^{-4}
10^{-5}
0
30
60
90
120
150
180
Scattering Angle (degrees)

Figure 18 (a)

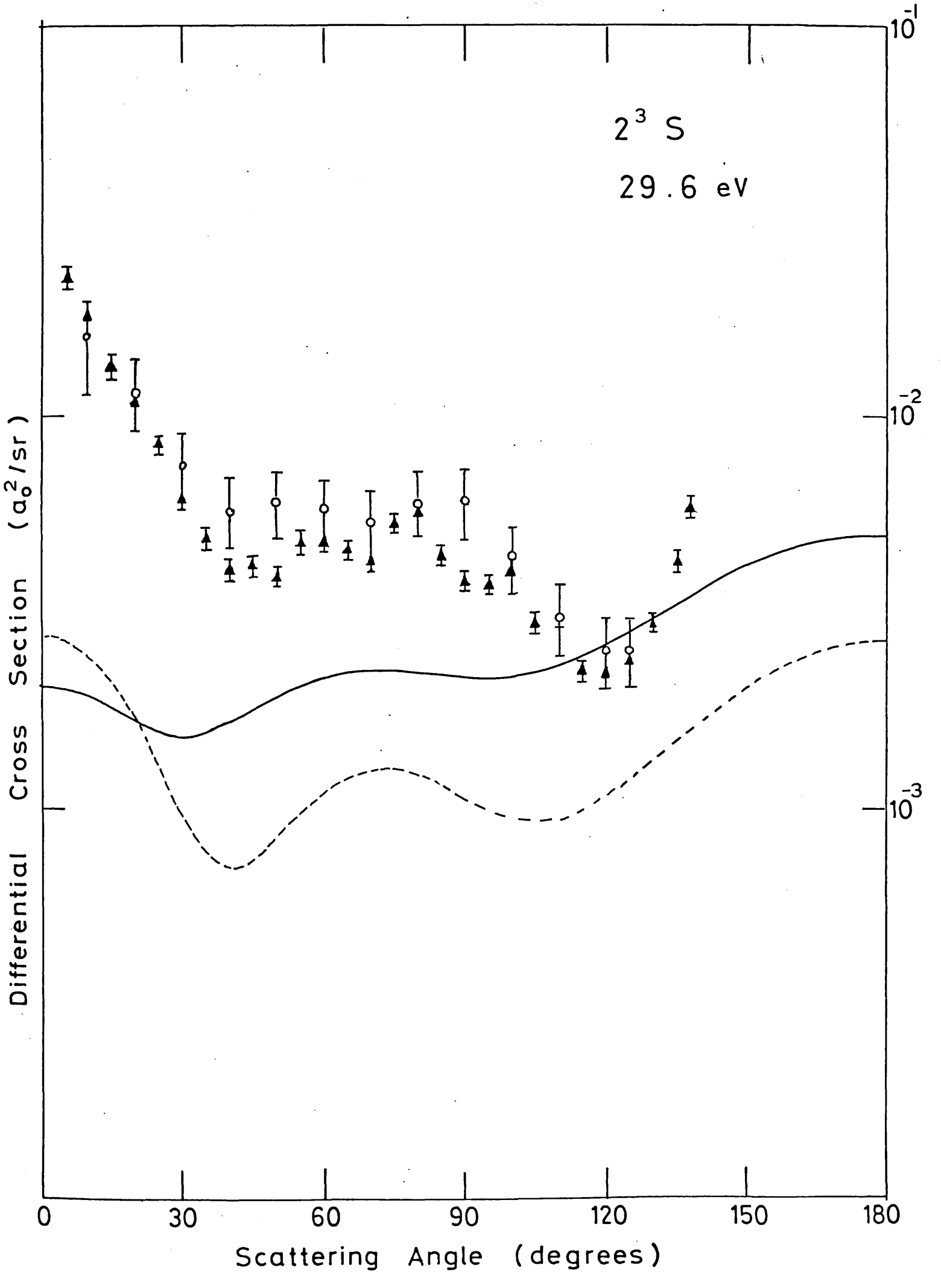
2^3 S
29.6 eV
10^{-1}
10^{-2}
10^{-3}
Differential Cross Section (a_o^2/sr)
0
30
60
90
120
150
180
Scattering Angle (degrees)

Figure 18(b)

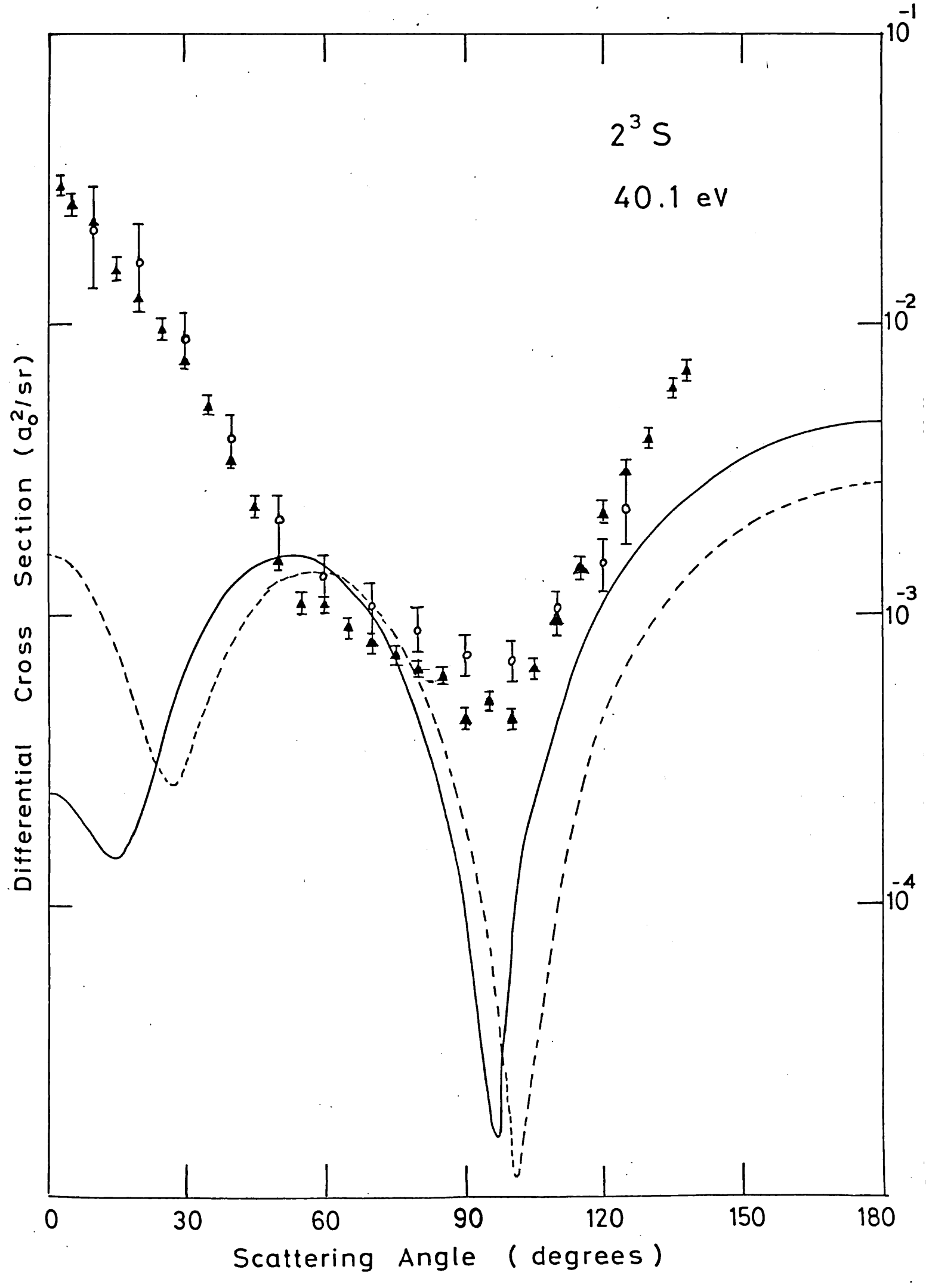
2^3S
40.1 eV
Differential Cross Section (a_o^2/sr)
10^{-1}
10^{-2}
10^{-3}
10^{-4}
0
30
60
90
120
150
180
Scattering Angle (degrees)

Figure 18 (c)

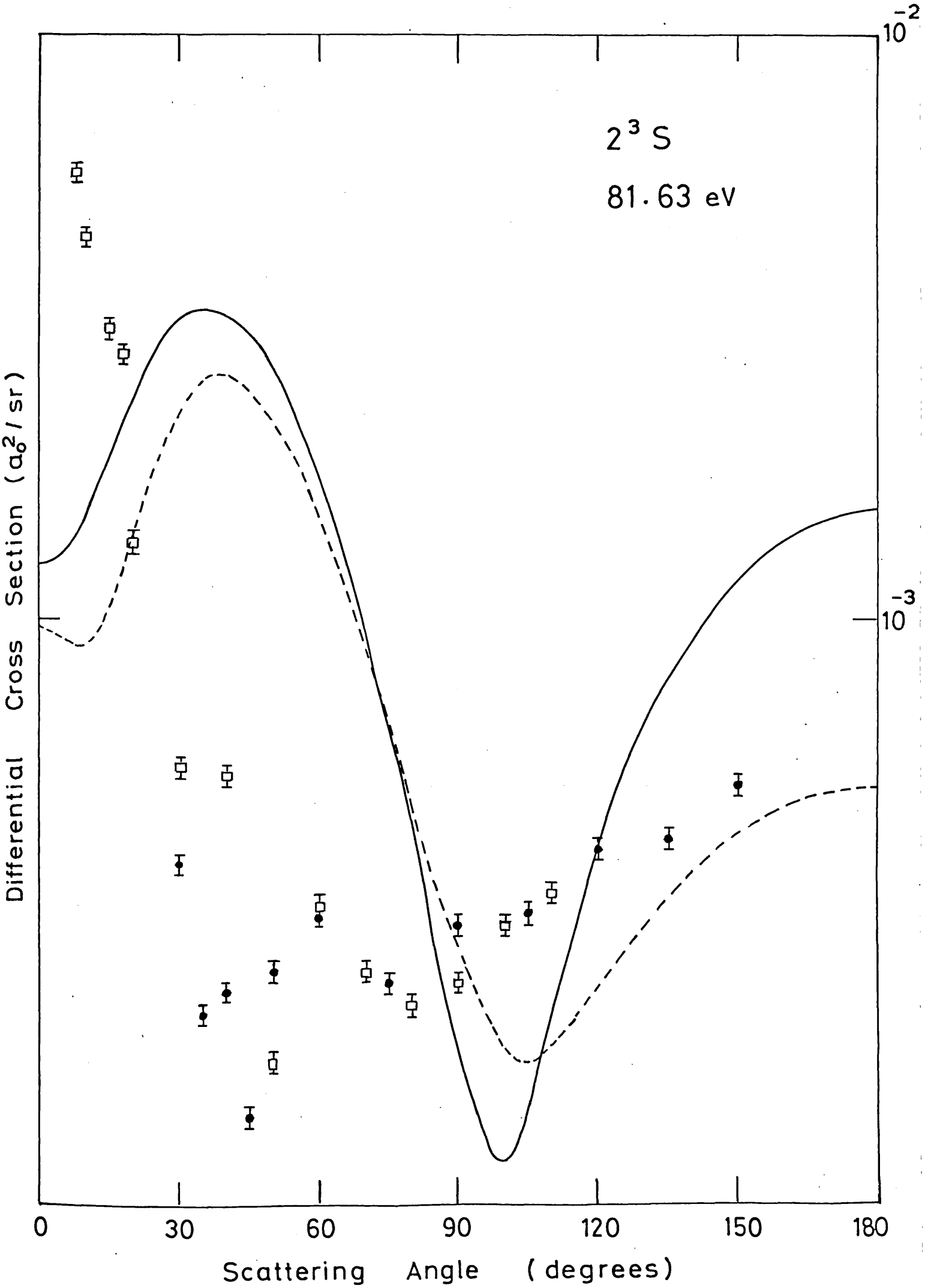
2^3S
81.63 eV
10^{-2}
10^{-3}
Differential Cross Section (a_0^2/sr)
0
30
60
90
120
150
180
Scattering Angle (degrees)

Figure 18 (d)

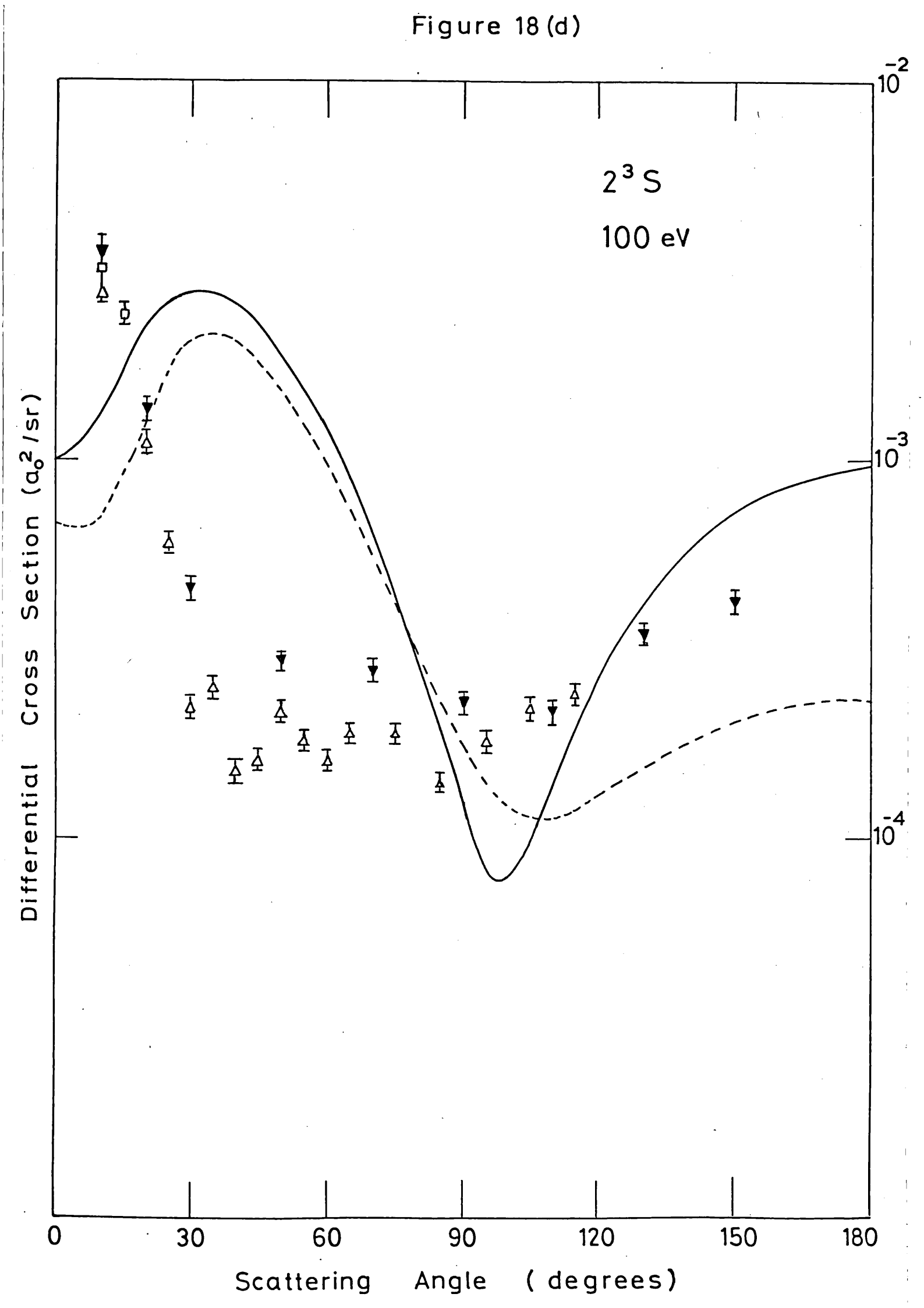
2^3S
100 eV
10^{-2}
10^{-3}
10^{-4}
Differential Cross Section (a_0^2/sr)
0
30
60
90
120
150
180
Scattering Angle (degrees)

Figure 18 (e)

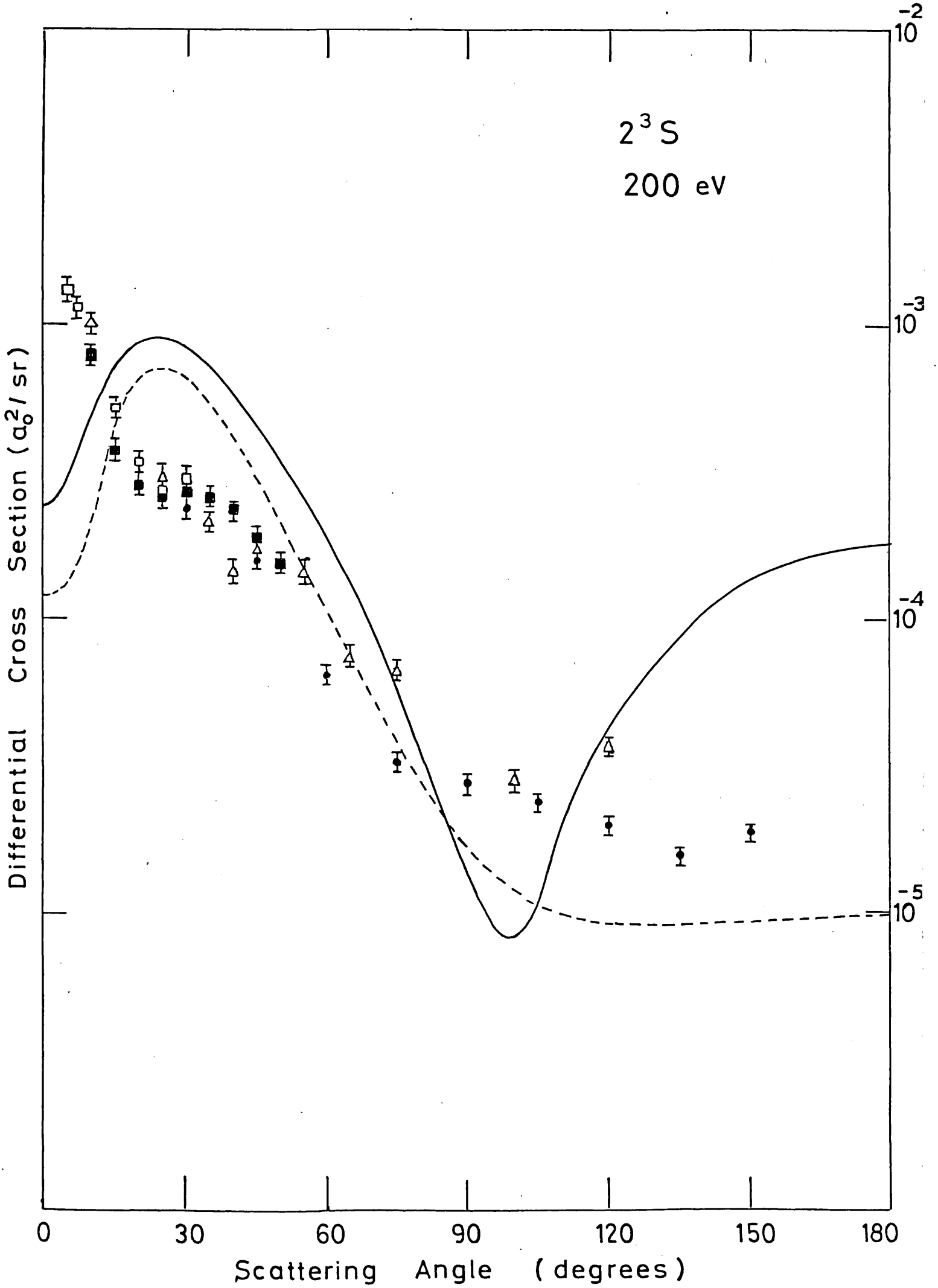
2^3S
200 eV
Differential Cross Section (a_o^2/ sr)
10^{-2}
10^{-3}
10^{-4}
10^{-5}
0
30
60
90
120
150
180
Scattering Angle (degrees)

Figure 19 (a)

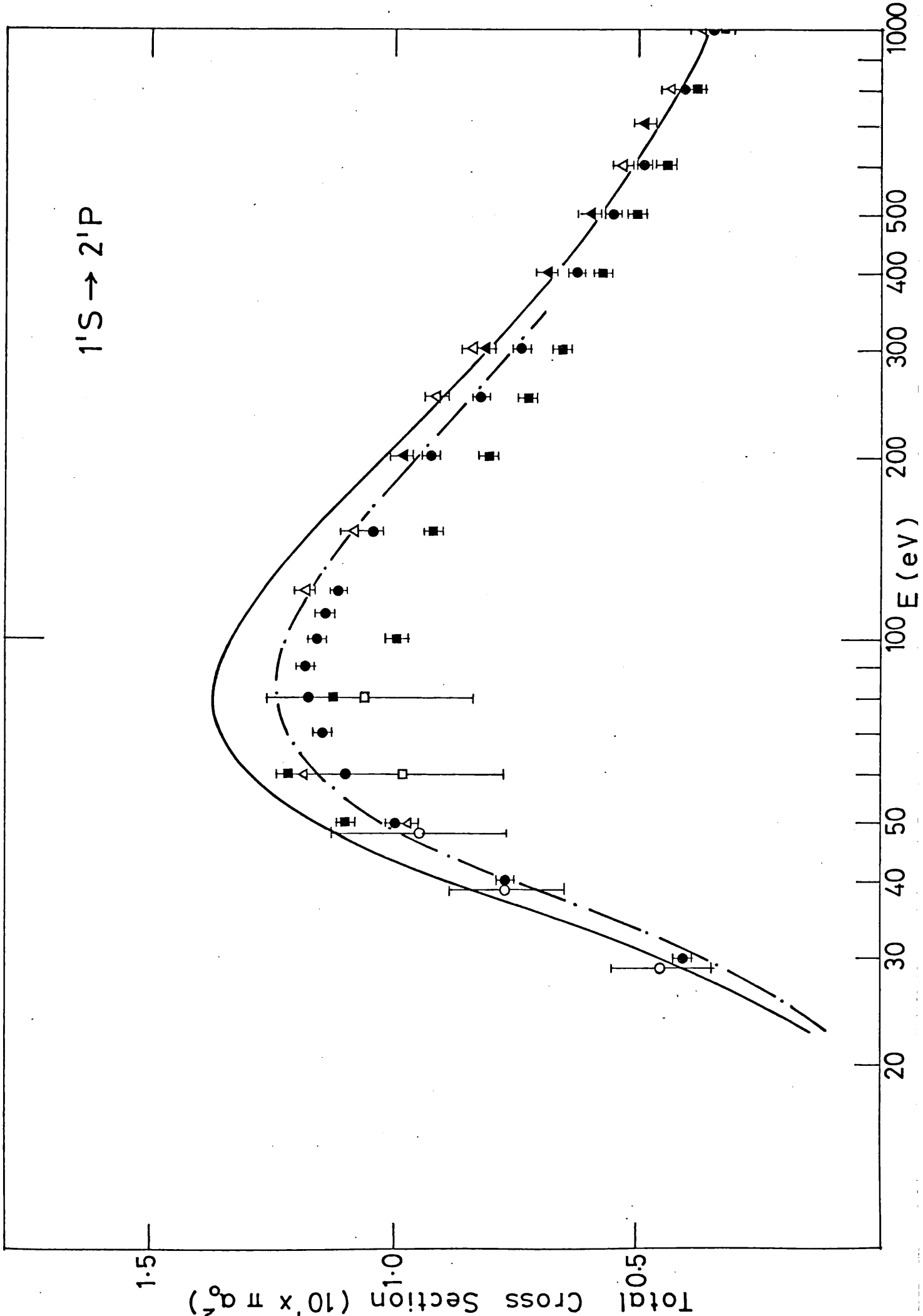
1¹S → 2¹P
Total Cross Section ($10^{-1} \times \pi a_o^2$)
1·5
1·0
0·5
20
30
40
50
100
200
300
400
500
1000
E (eV)

Figure 19 (b)

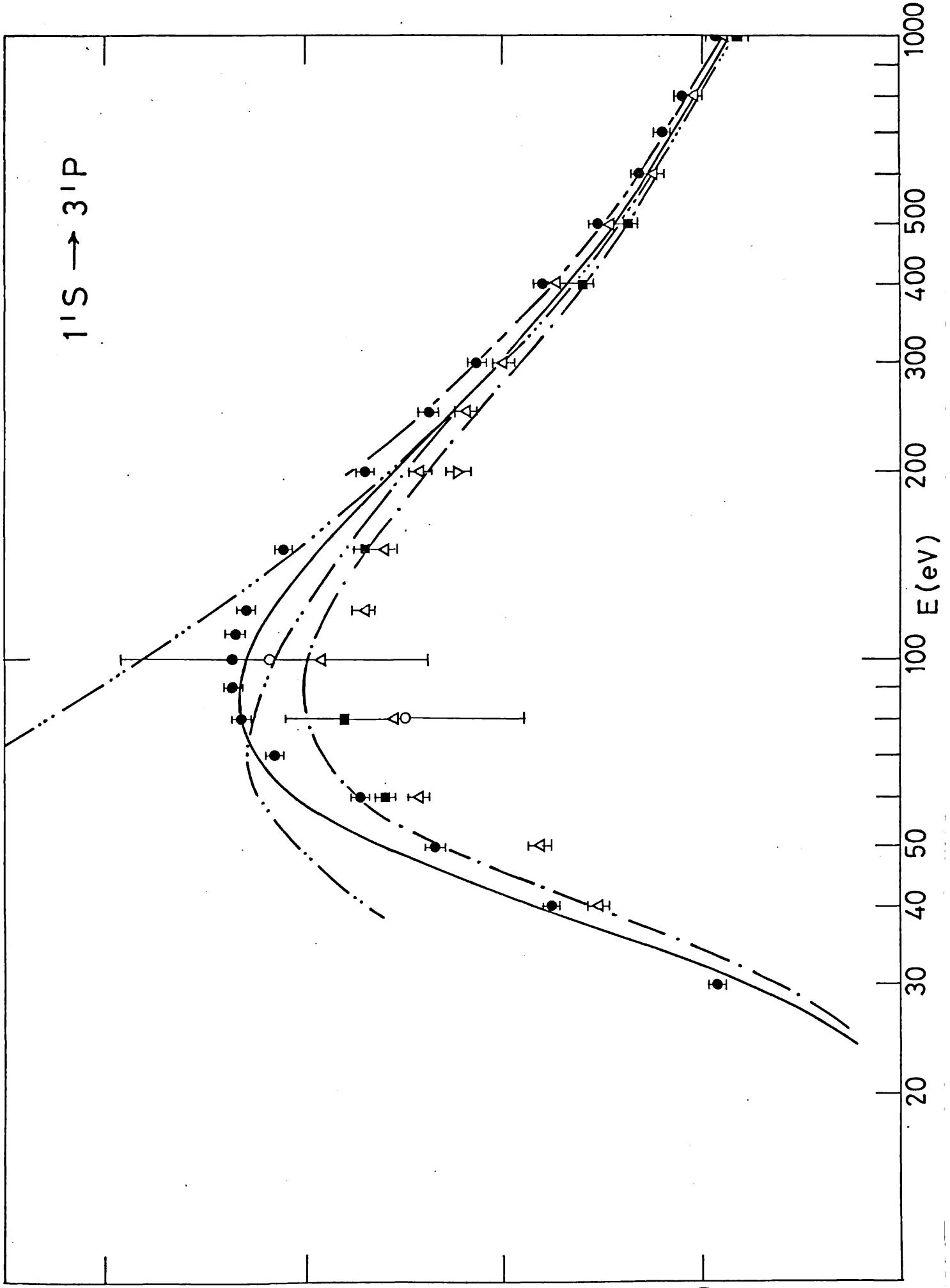
1¹S → 3¹P
Total Cross Section ($10^{-2} \times \pi a_o^2$)
4·0
3·0
2·0
1·0
E (eV)
20
30
40
50
100
200
300
400
500
1000

Figure 19 (b)

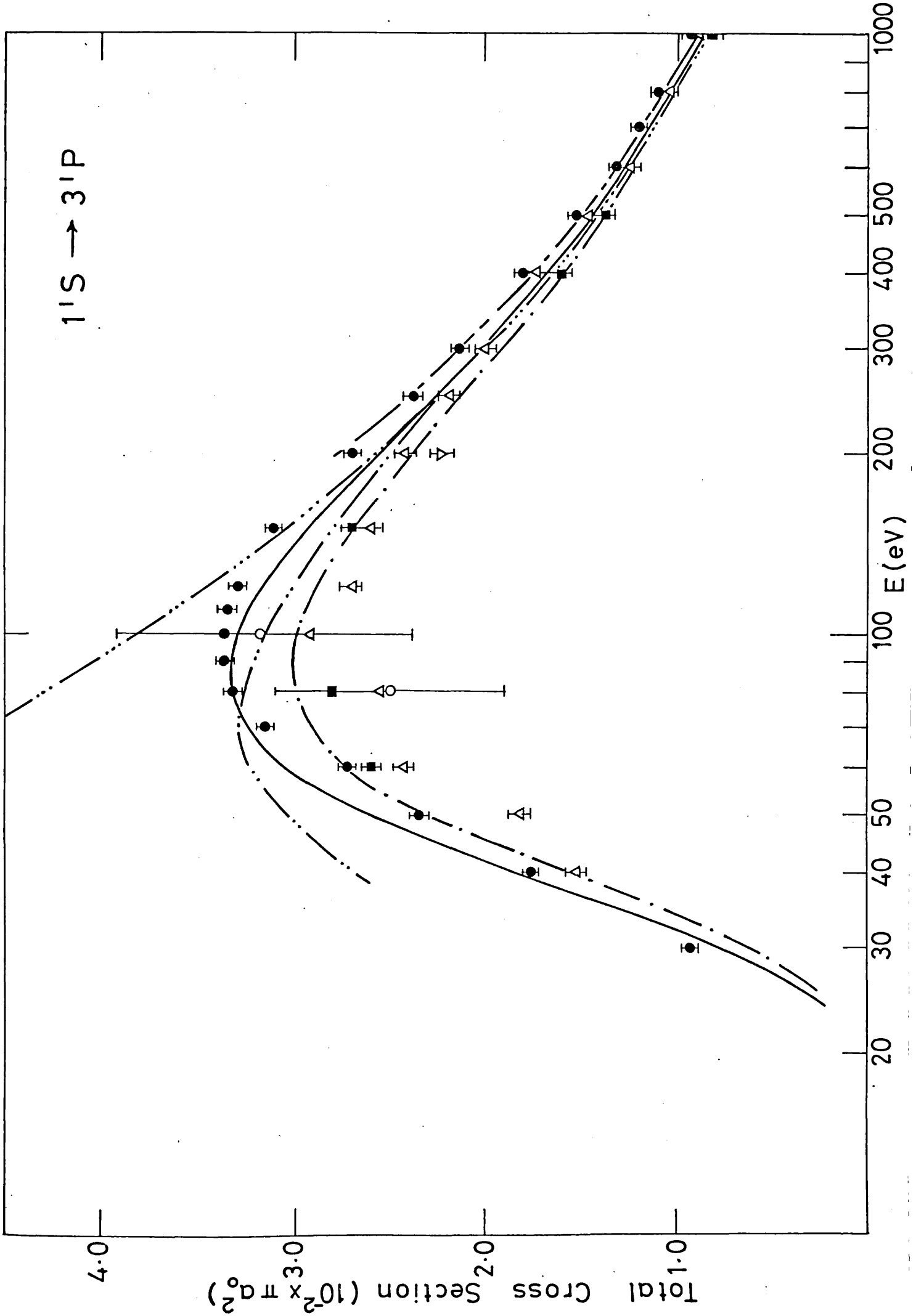
$1^1S \rightarrow 3^1P$
Total Cross Section ($10^{-2} \times \pi a_o^2$)
4·0
3·0
2·0
1·0
E (eV)
1000
500
400
300
200
100
50
40
30
20

Figure 19 (c)

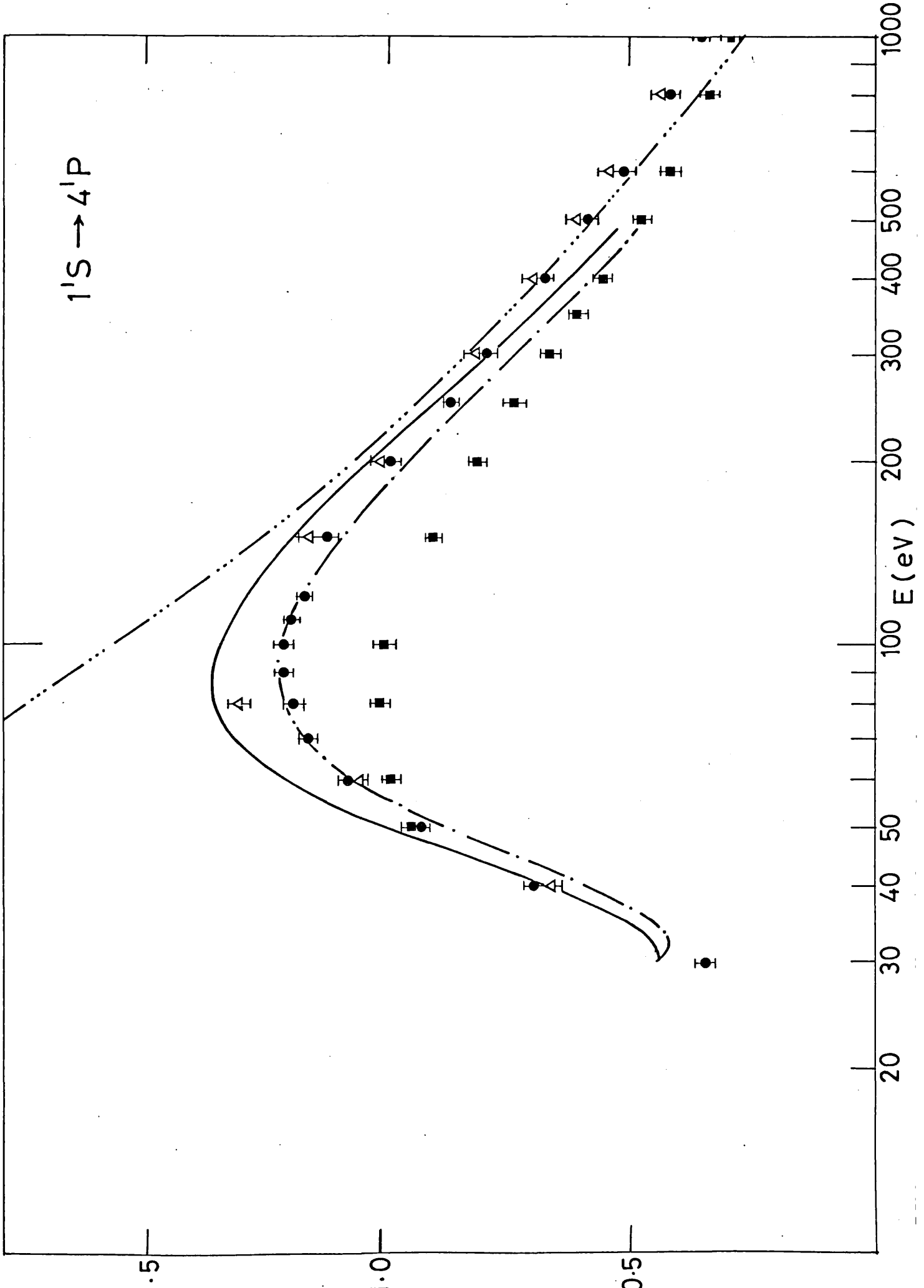
$1^1S \rightarrow 4^1P$
Total Cross Section ($10^{-2} \times \pi a_o^2$)
1·5
1·0
0·5
E (eV)
20
30
40
50
100
200
300
400
500
1000

Figure 19 (d)

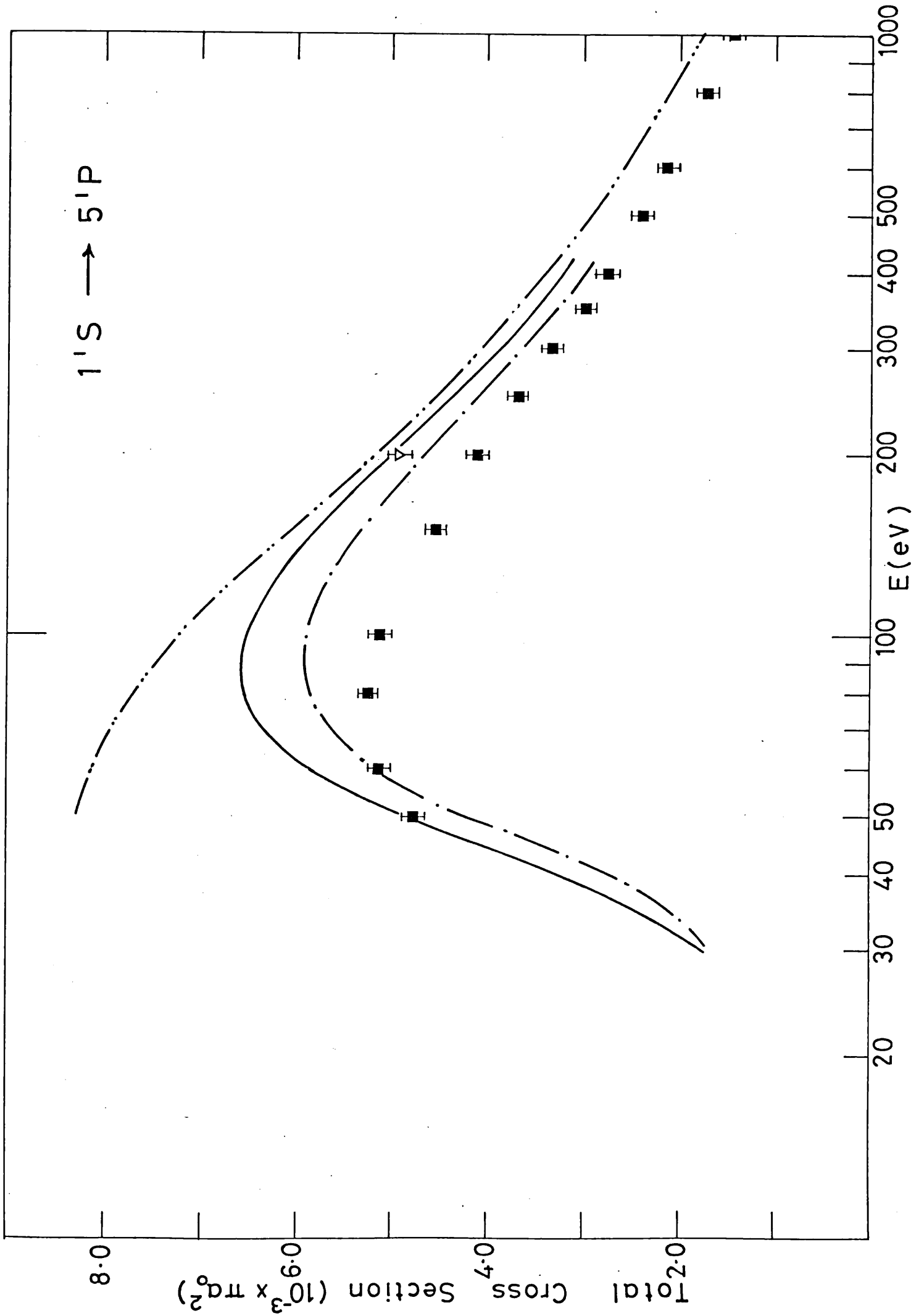
1¹S → 5¹P
Total Cross Section (10^{-3} x πa_0^2)
2·0
4·0
6·0
8·0
E(eV)
20
30
40
50
100
200
300
400
500
1000

Figure 20 (a)

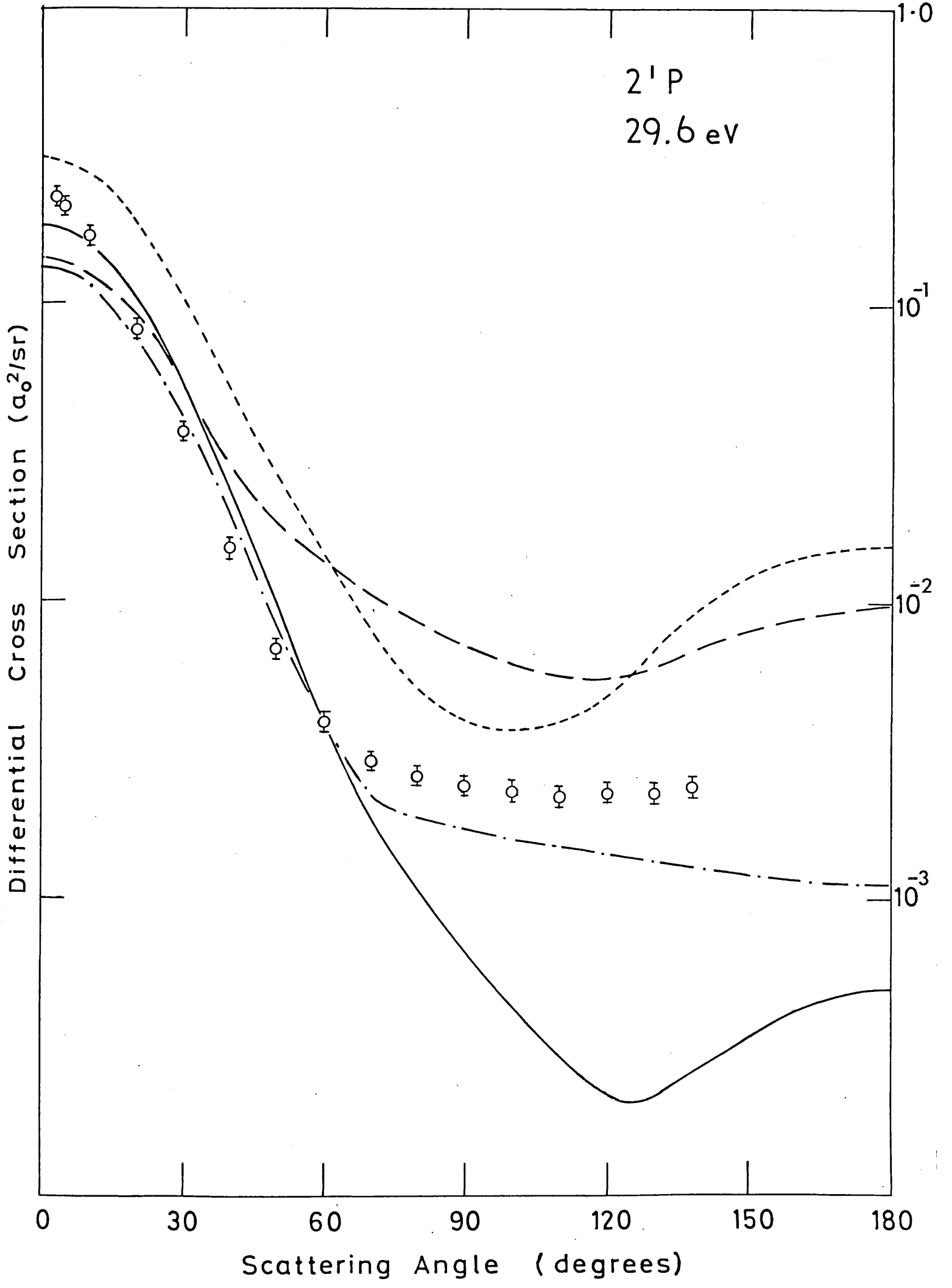
2¹P
29.6 eV
1·0
10⁻¹
10⁻²
10⁻³
Differential Cross Section (a_0^2/sr)
0
30
60
90
120
150
180
Scattering Angle (degrees)

Figure 20 (b)

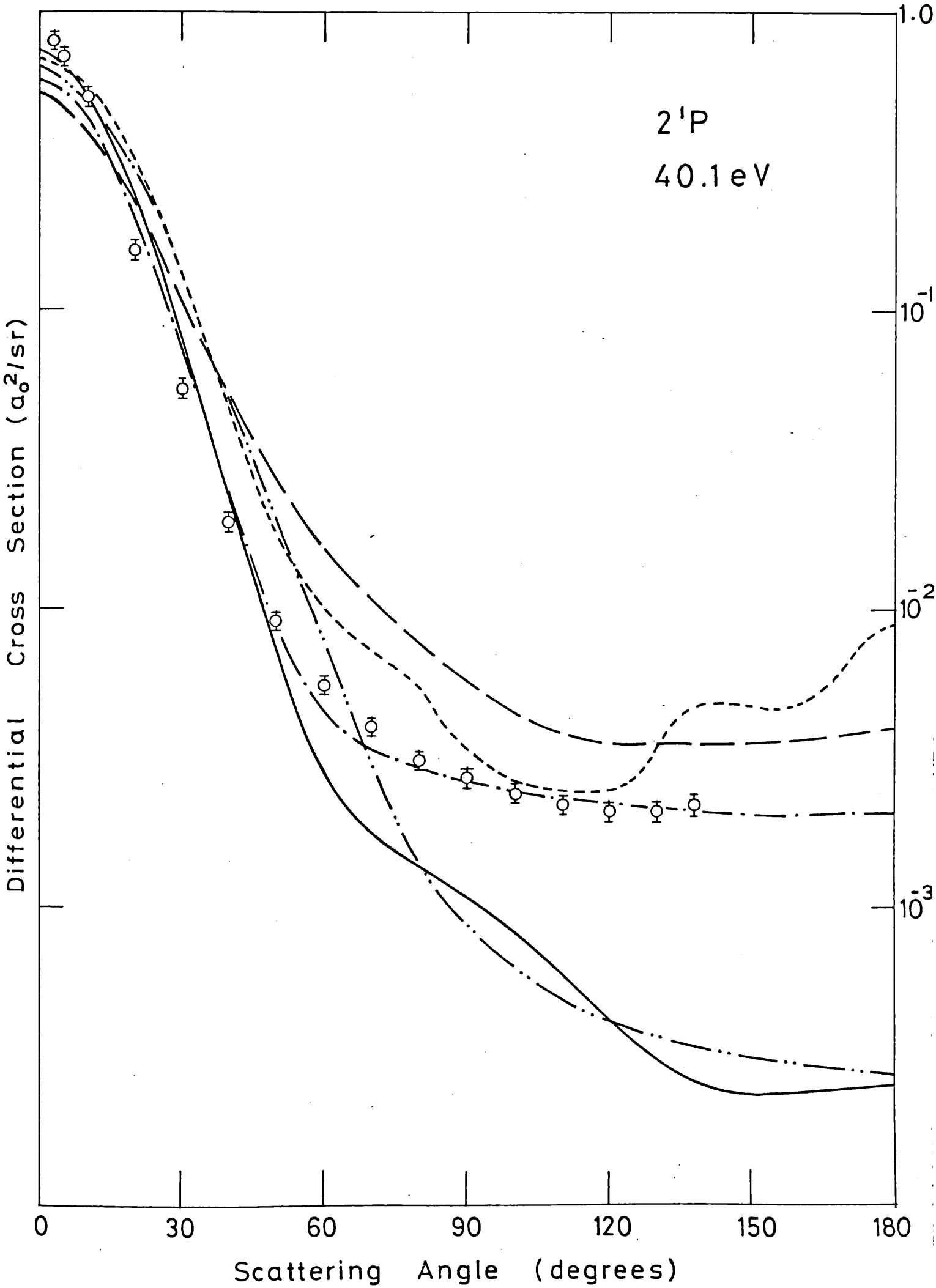
2¹P
40.1 eV
1·0
10⁻¹
10⁻²
10⁻³
Differential Cross Section (a₀²/sr)
0
30
60
90
120
150
180
Scattering Angle (degrees)

Figure 20 (c)

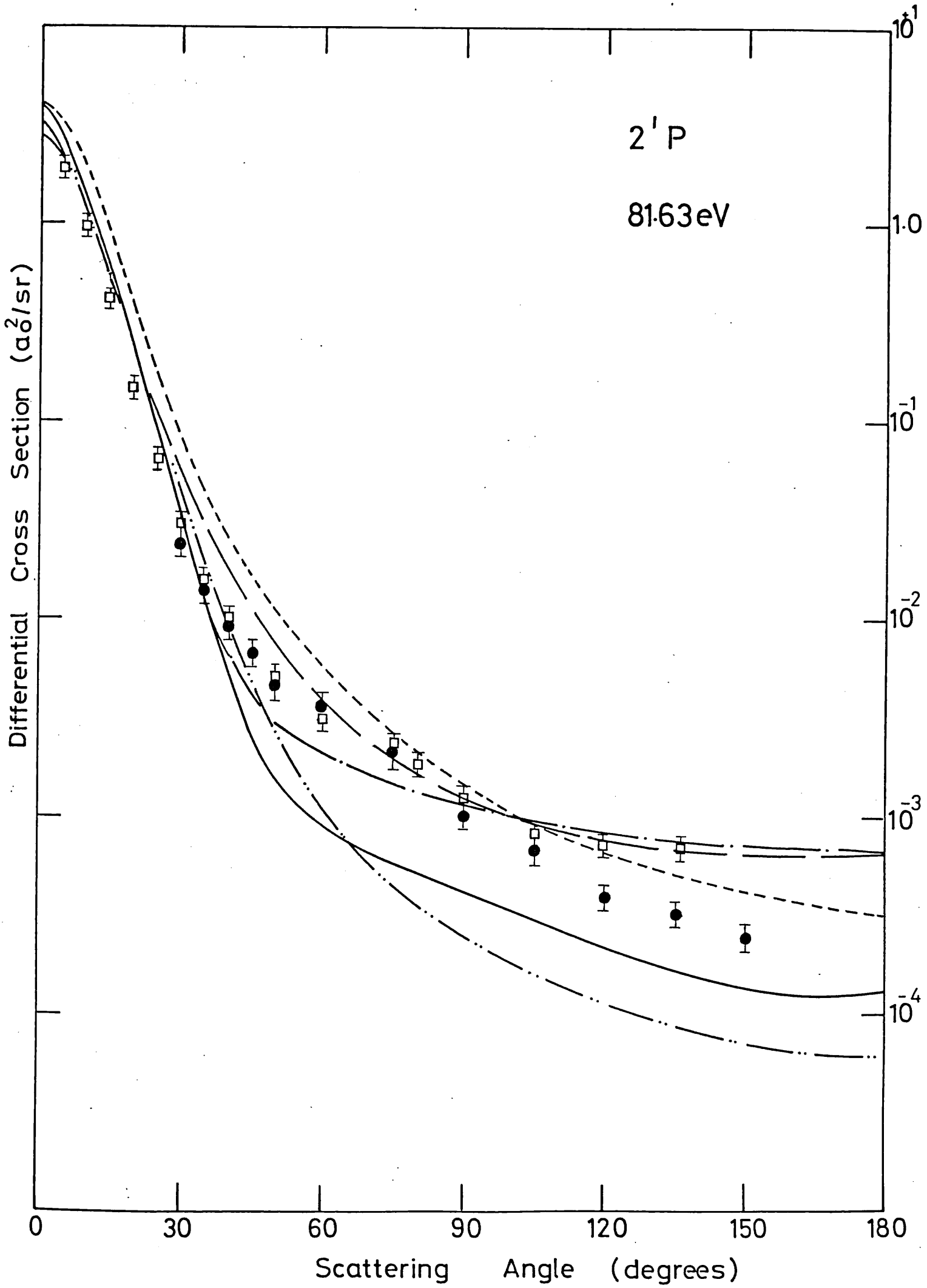
2 ' P
81·63eV
Differential Cross Section (a_0^2/sr)
10^{1}
1·0
10^{-1}
10^{-2}
10^{-3}
10^{-4}
0
30
60
90
120
150
180
Scattering Angle (degrees)

Figure 20 (d)

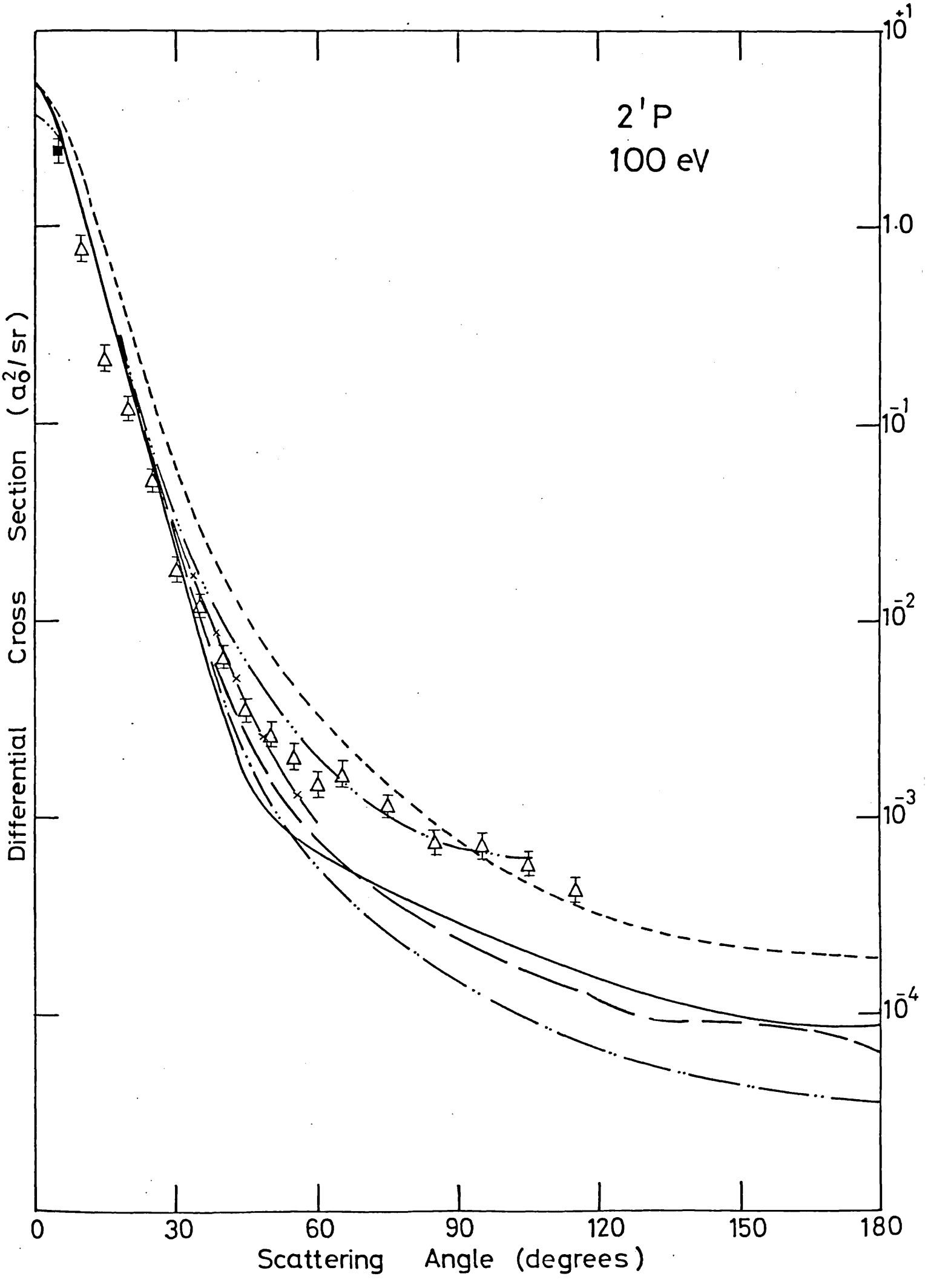
2 ¹P
100 eV
Differential Cross Section (a_0^2/sr)
10^{+1}
1·0
10^{-1}
10^{-2}
10^{-3}
10^{-4}
0
30
60
90
120
150
180
Scattering Angle (degrees)

Figure 20 (e)

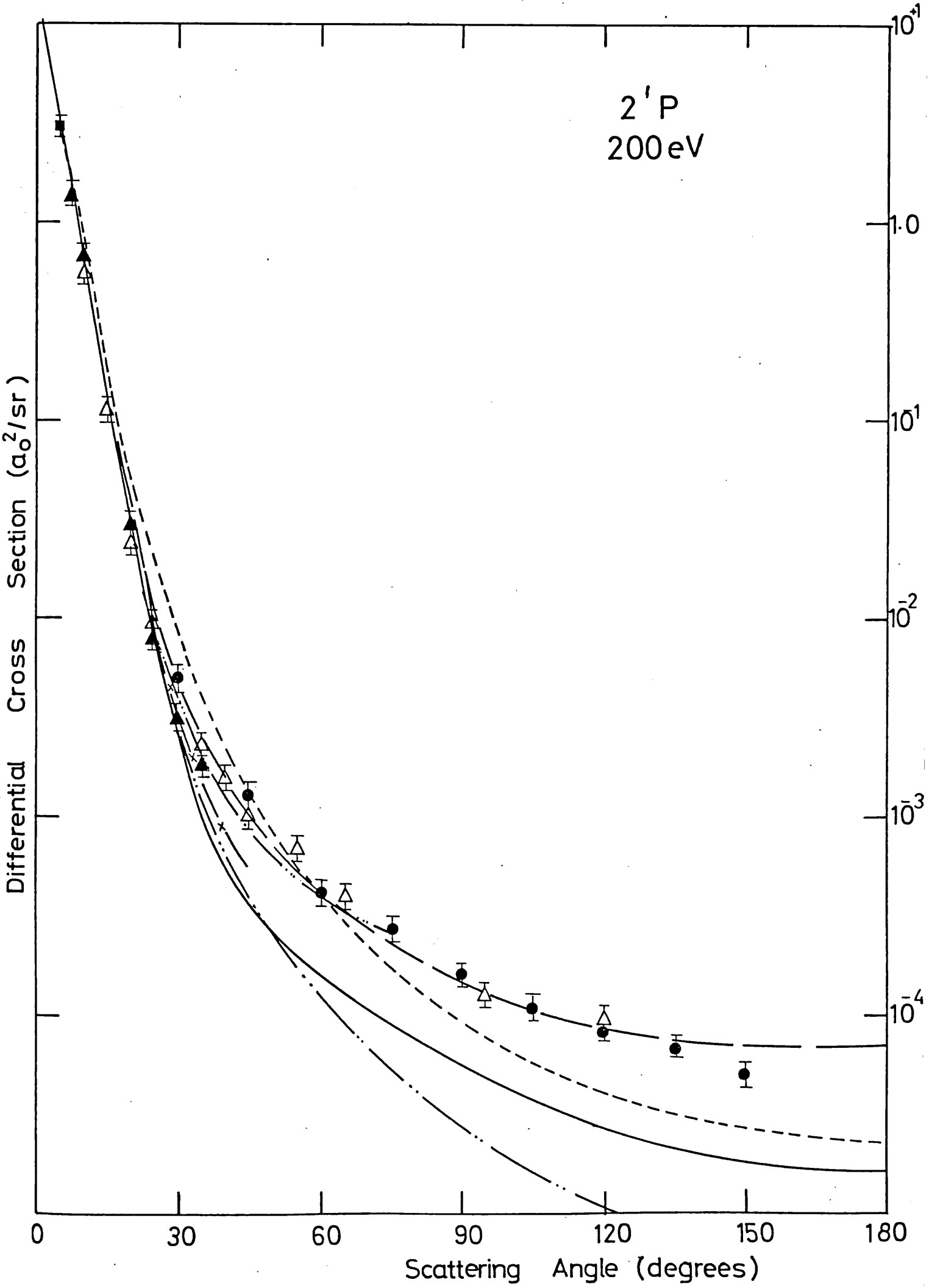
2 ' P
200 eV
Differential Cross Section (a_o^2/sr)
10^{+1}
1.0
10^{-1}
10^{-2}
10^{-3}
10^{-4}
0
30
60
90
120
150
180
Scattering Angle (degrees)

Figure 21 (a)

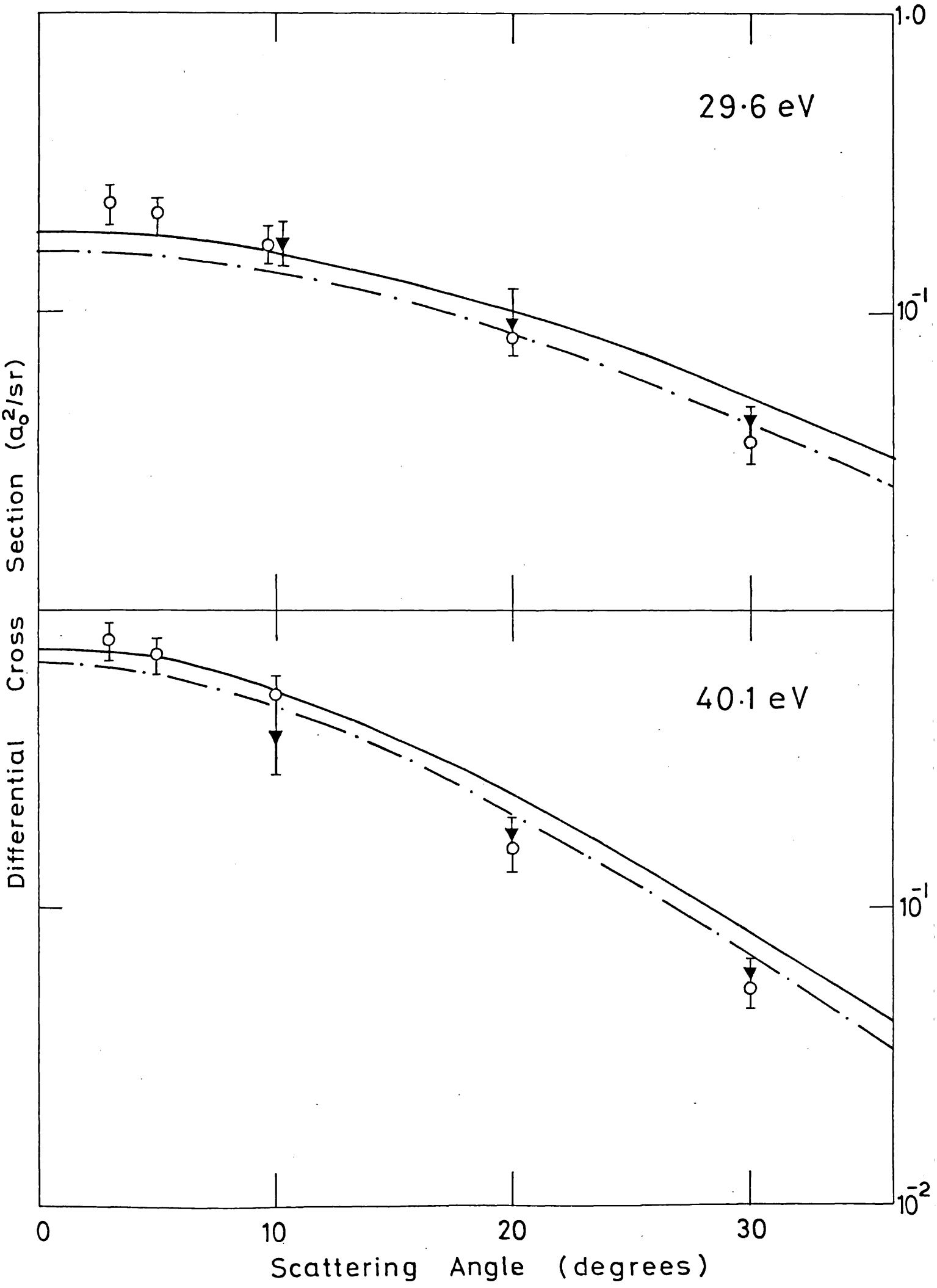
29·6 eV
40·1 eV
1·0
10^{-1}
10^{-1}
10^{-2}
Differential Cross Section (a_0^2/sr)
0
10
20
30
Scattering Angle (degrees)

Figure 21 (b)

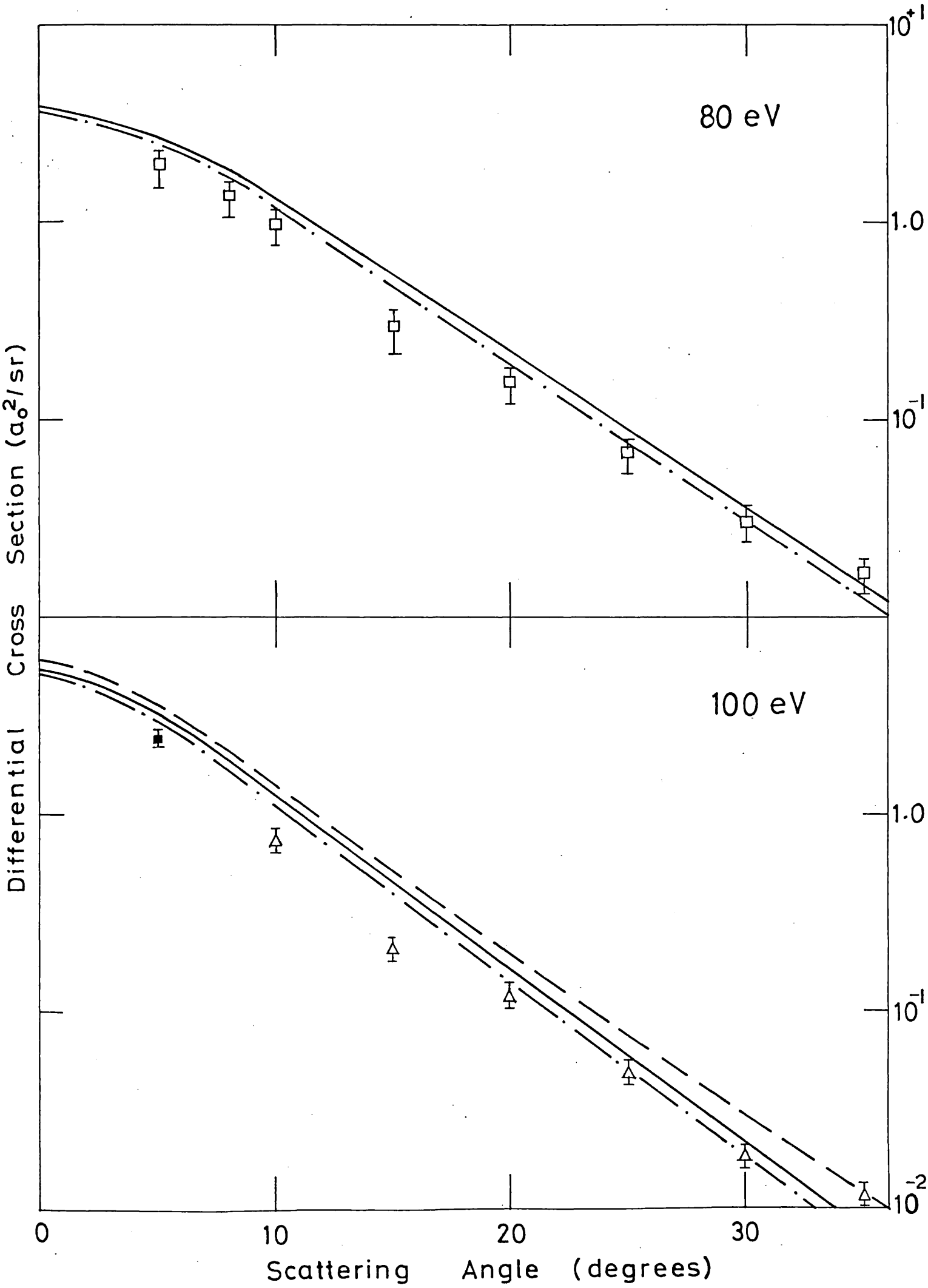
80 eV
100 eV
Differential Cross Section (a_o^2/sr)
10^{+1}
1.0
10^{-1}
1.0
10^{-1}
10^{-2}
0
10
20
30
Scattering Angle (degrees)

Figure 22 (a)

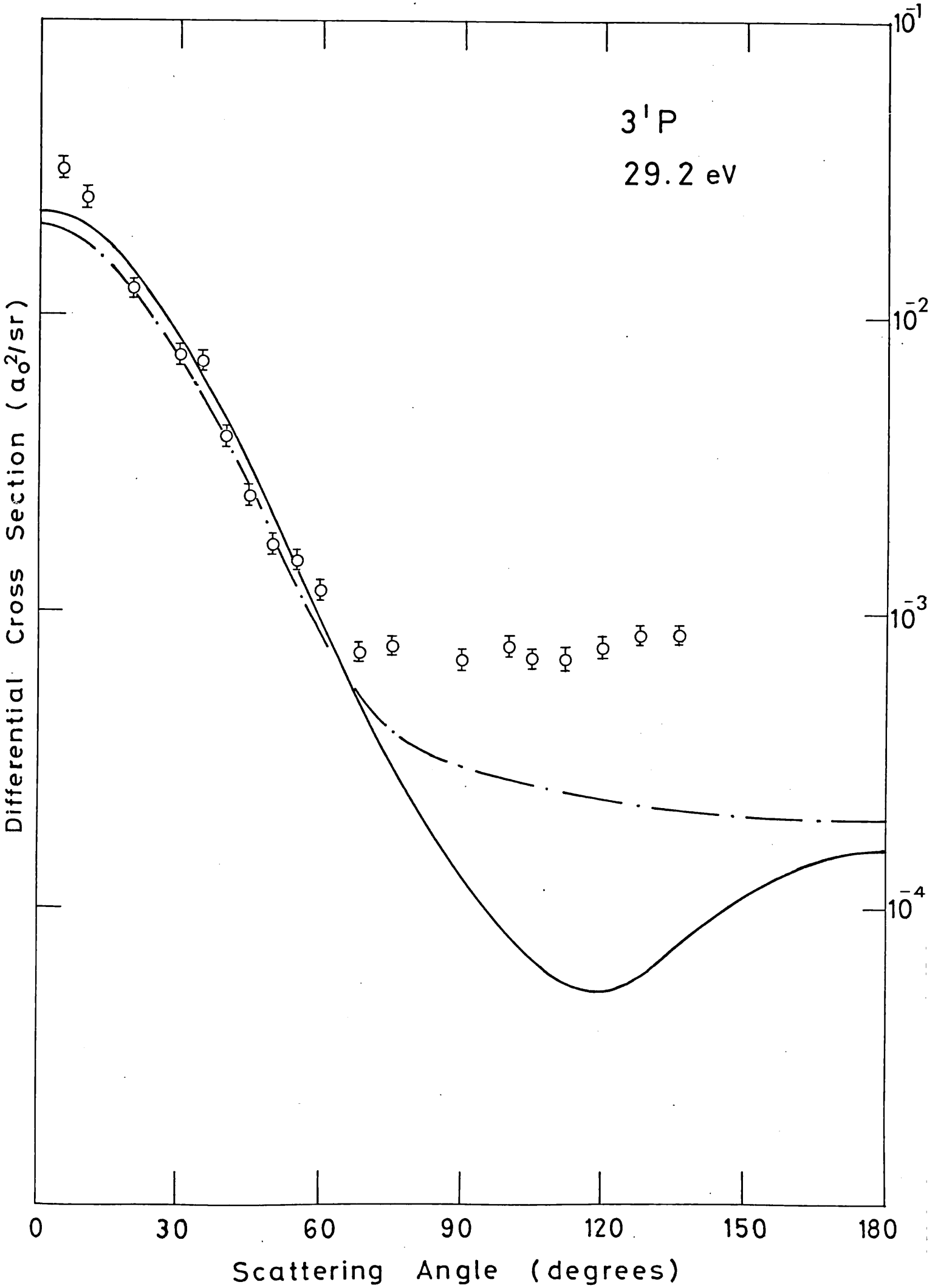
3¹P
29.2 eV
Differential Cross Section (a_o^2/sr)
10^{-1}
10^{-2}
10^{-3}
10^{-4}
0
30
60
90
120
150
180
Scattering Angle (degrees)

Figure 22 (b)

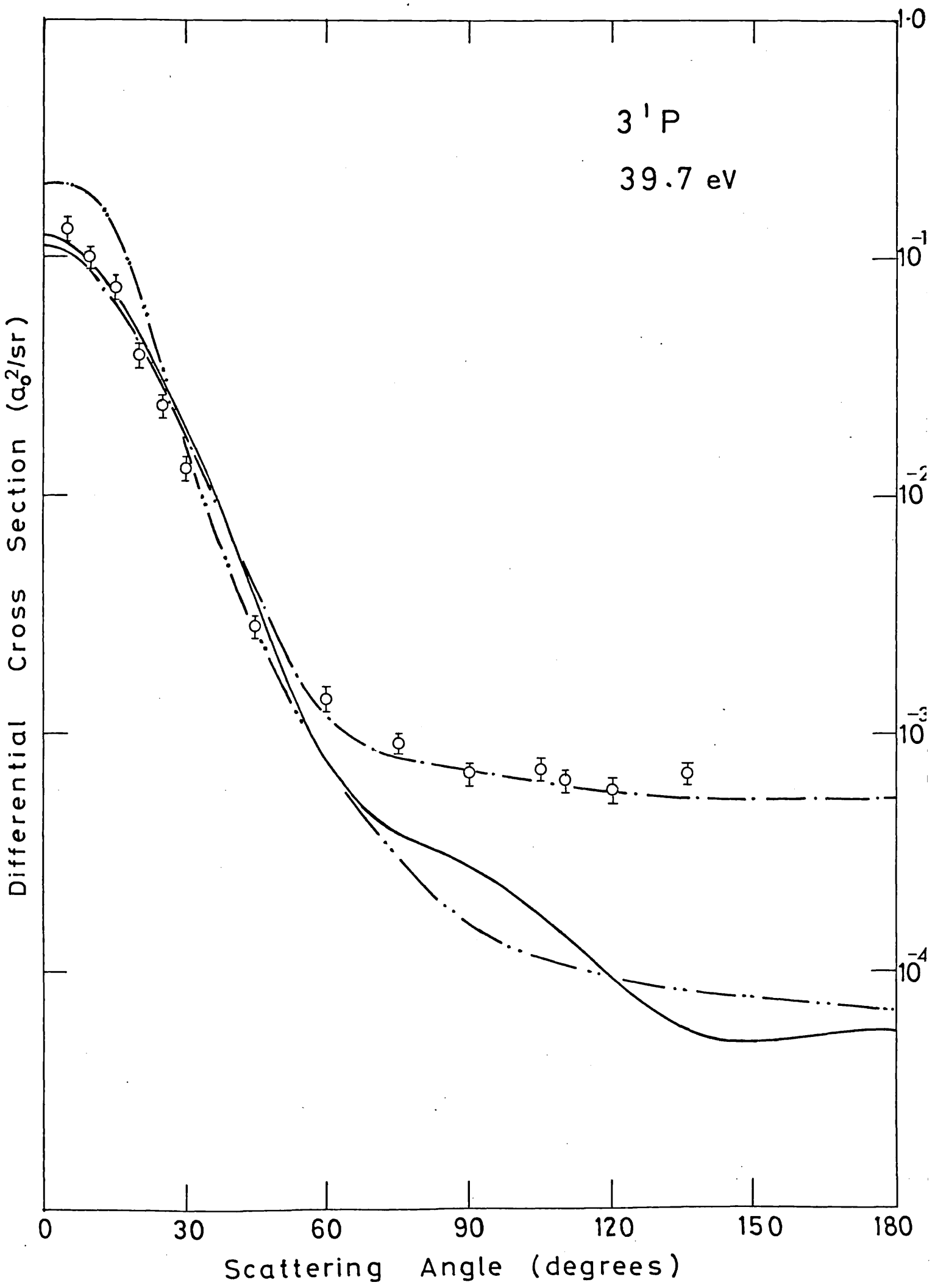
3 ¹P
39.7 eV
1·0
10⁻¹
10⁻²
10⁻³
10⁻⁴
Differential Cross Section (a₀²/sr)
0
30
60
90
120
150
180
Scattering Angle (degrees)

Figure 22 (c)

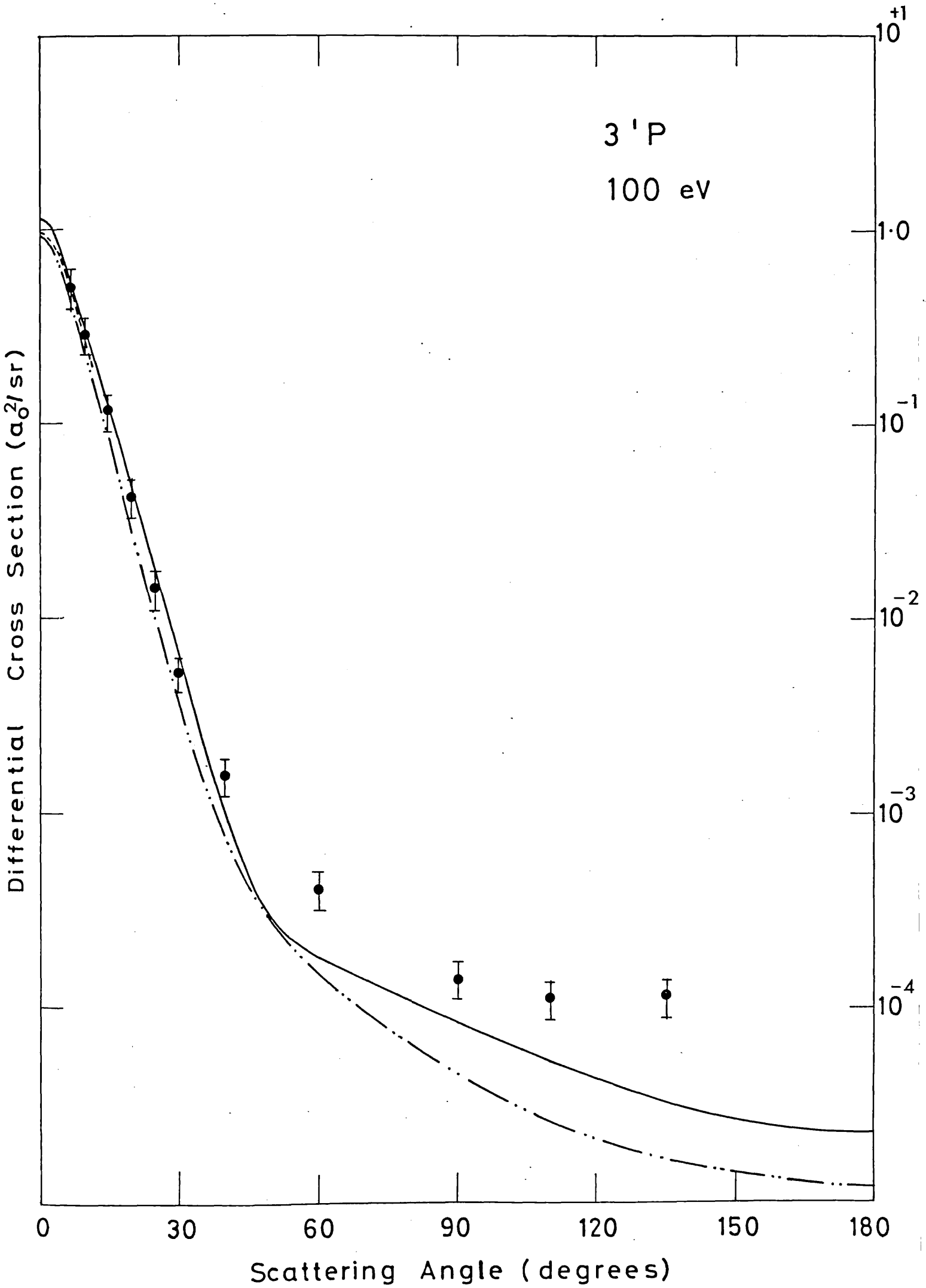
3 ¹P
100 eV
Differential Cross Section (a_0^2/sr)
10^{+1}
1·0
10^{-1}
10^{-2}
10^{-3}
10^{-4}
0
30
60
90
120
150
180
Scattering Angle (degrees)

Figure 22 (d)

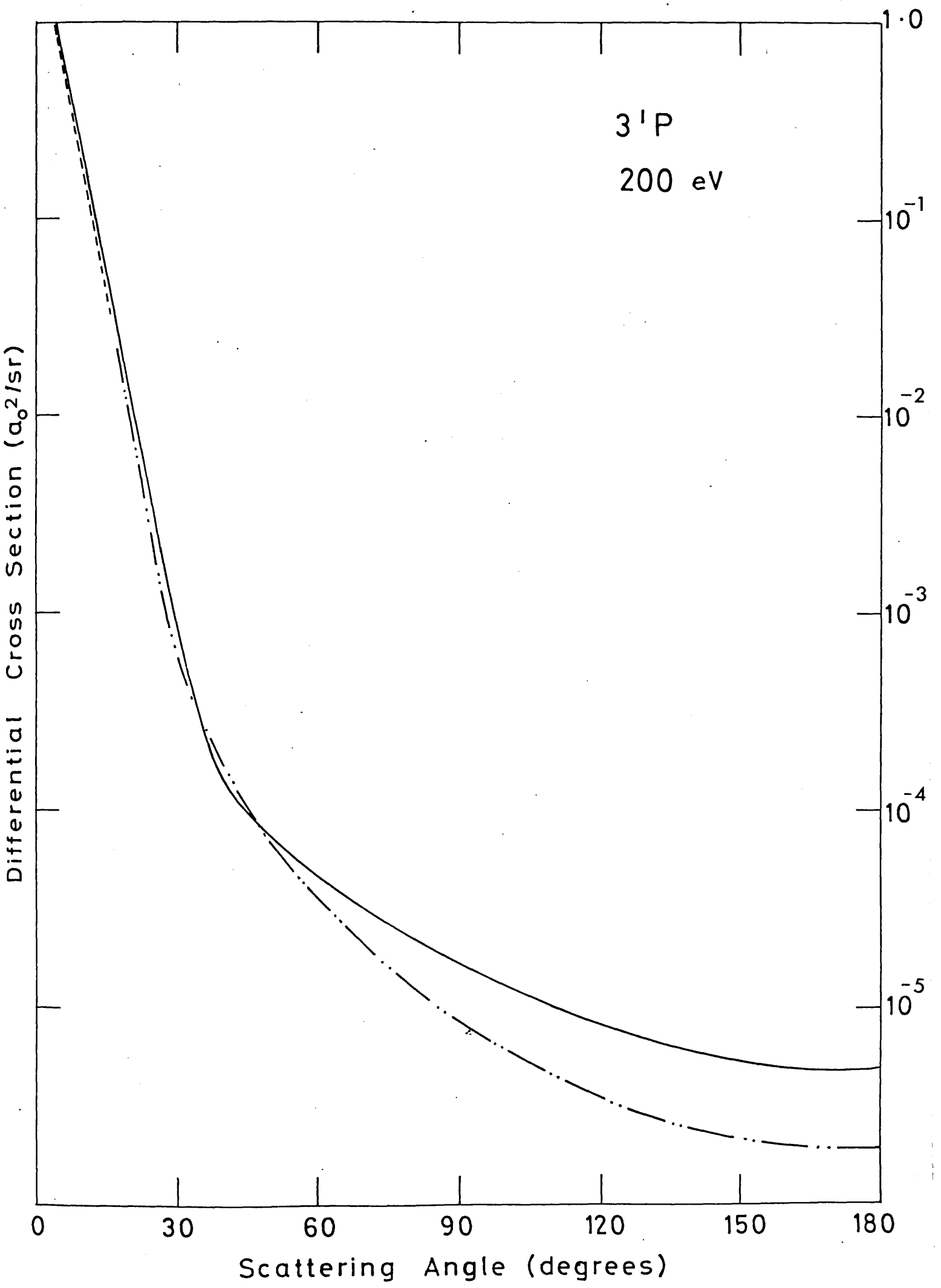
3 ¹P
200 eV
1·0
10⁻¹
10⁻²
10⁻³
10⁻⁴
10⁻⁵
Differential Cross Section (a₀²/sr)
0
30
60
90
120
150
180
Scattering Angle (degrees)

Figure 23

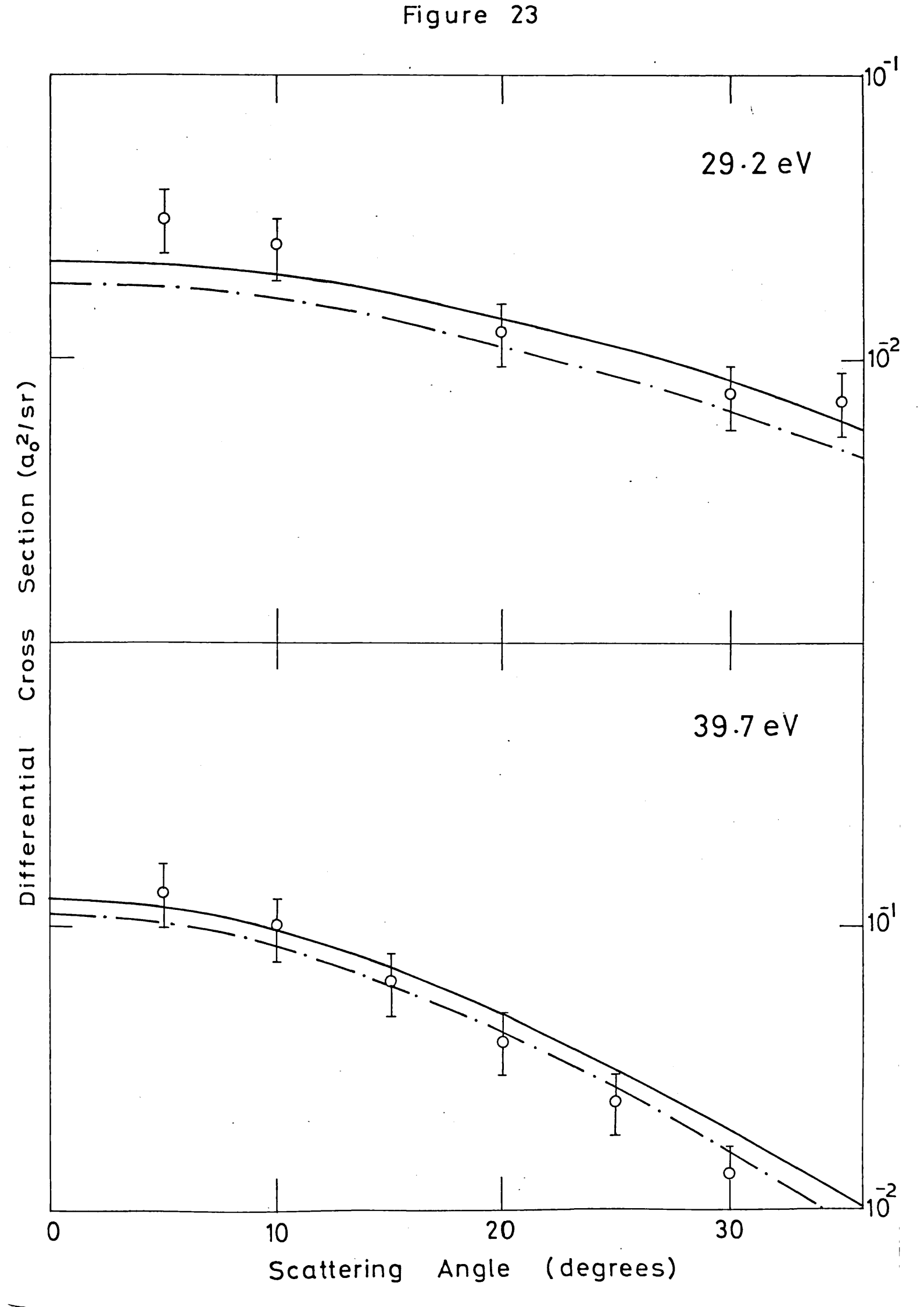
29·2 eV
39·7 eV
Differential Cross Section (a_o^2/sr)
10^{-1}
10^{-2}
10^{-1}
10^{-2}
0
10
20
30
Scattering Angle (degrees)

Figure 24

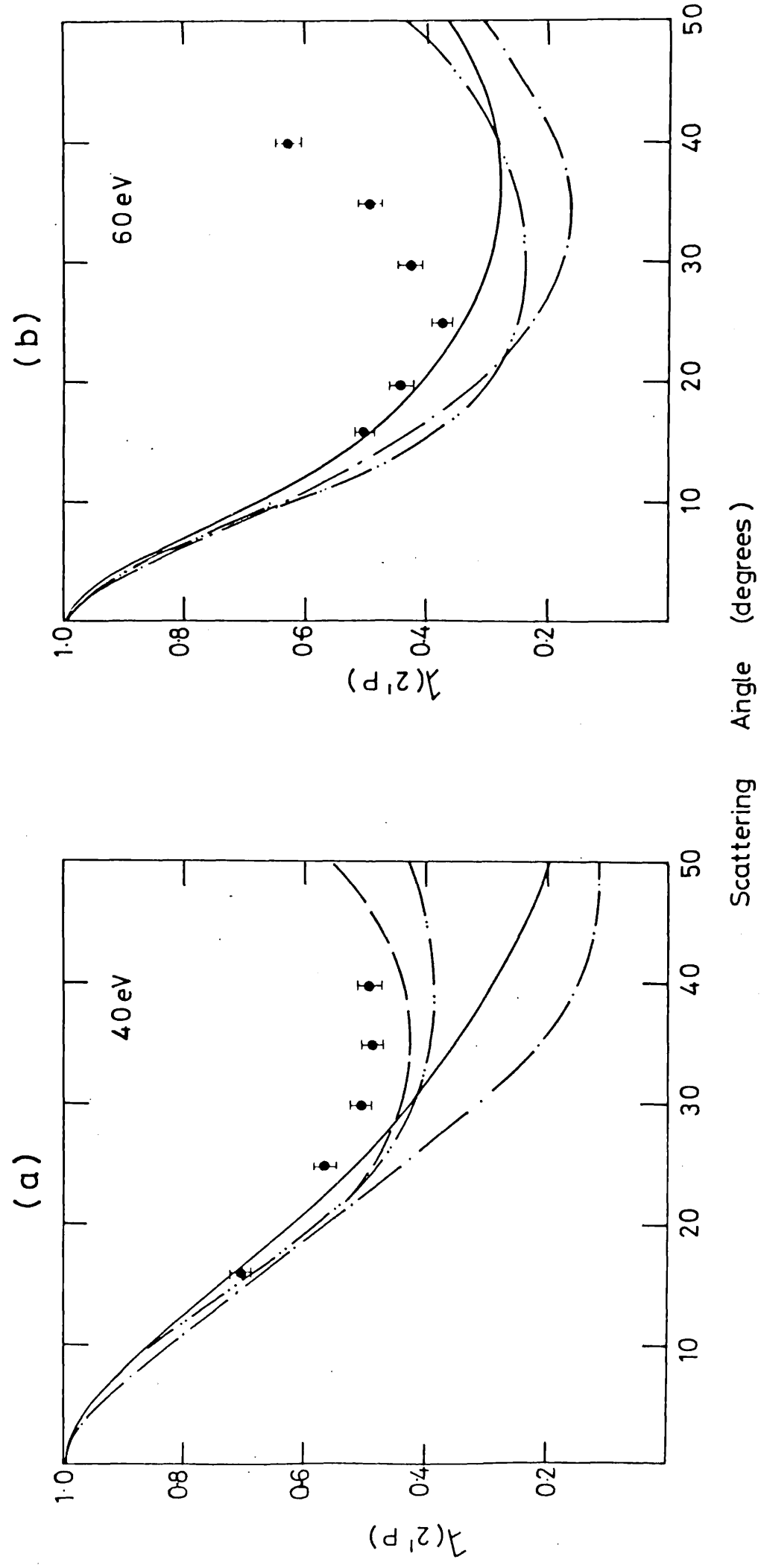
(a)
40eV
(b)
60eV
λ(2,p)
1·0
0·8
0·6
0·4
0·2
10
20
30
40
50
Scattering Angle (degrees)

Figure 24

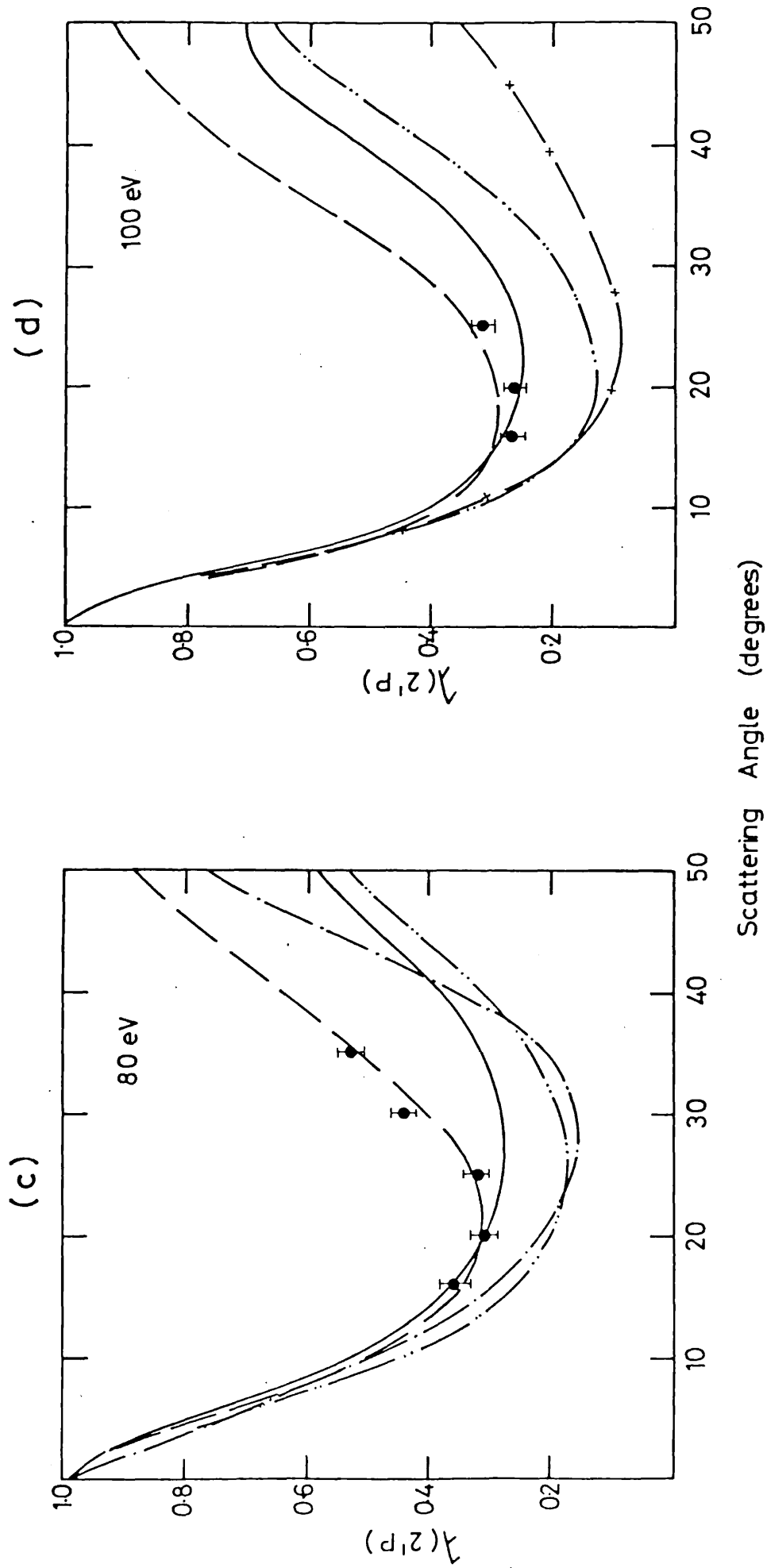
(c)
80 eV
(d)
100 eV
λ(2¹P)
1·0
0·8
0·6
0·4
0·2
10
20
30
40
50
Scattering Angle (degrees)

Figure 24

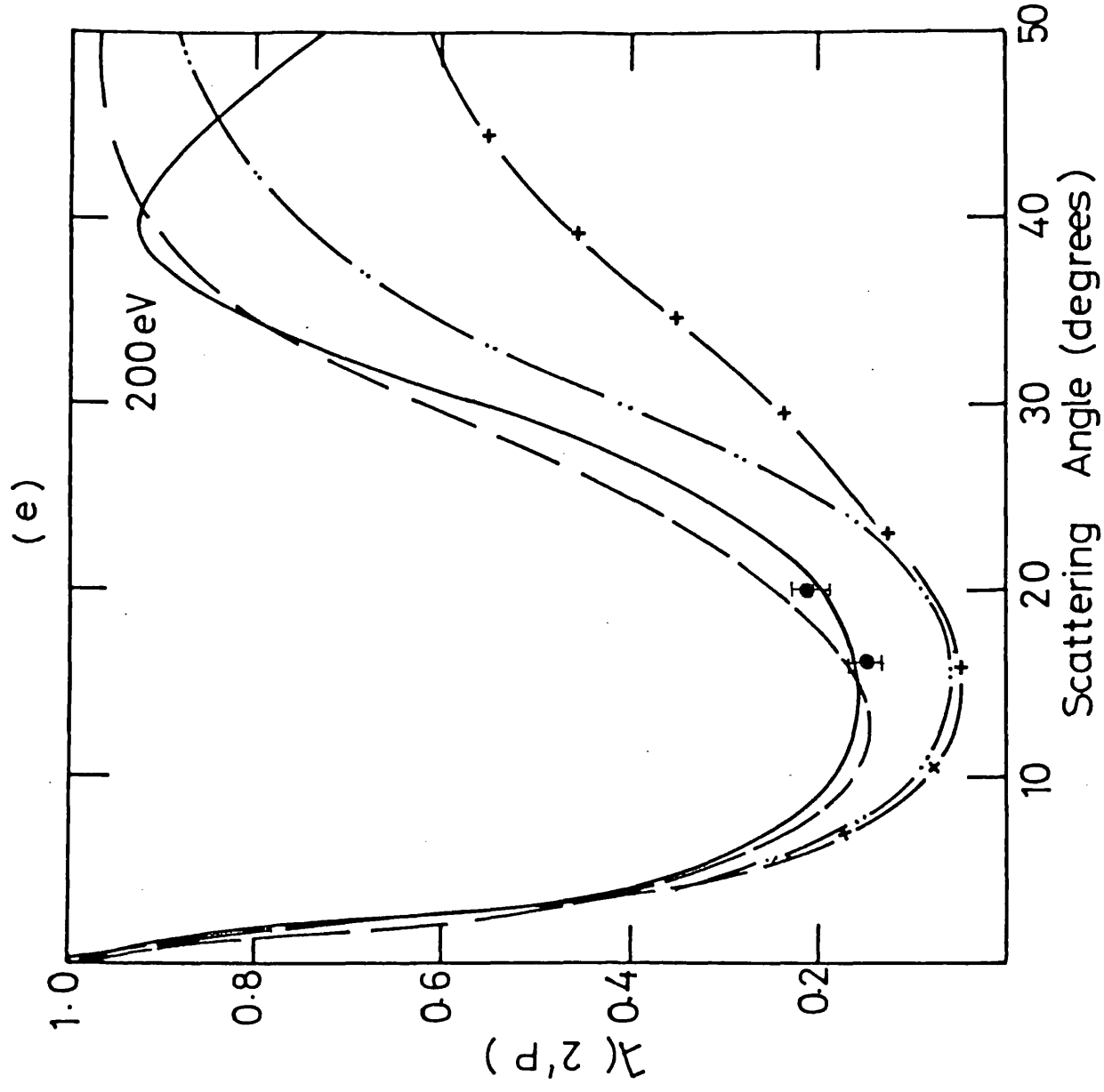
(e)
200eV
1·0
0·8
0·6
0·4
0·2
λ(2,P)
10
20
30
40
50
Scattering Angle (degrees)

Figure 25

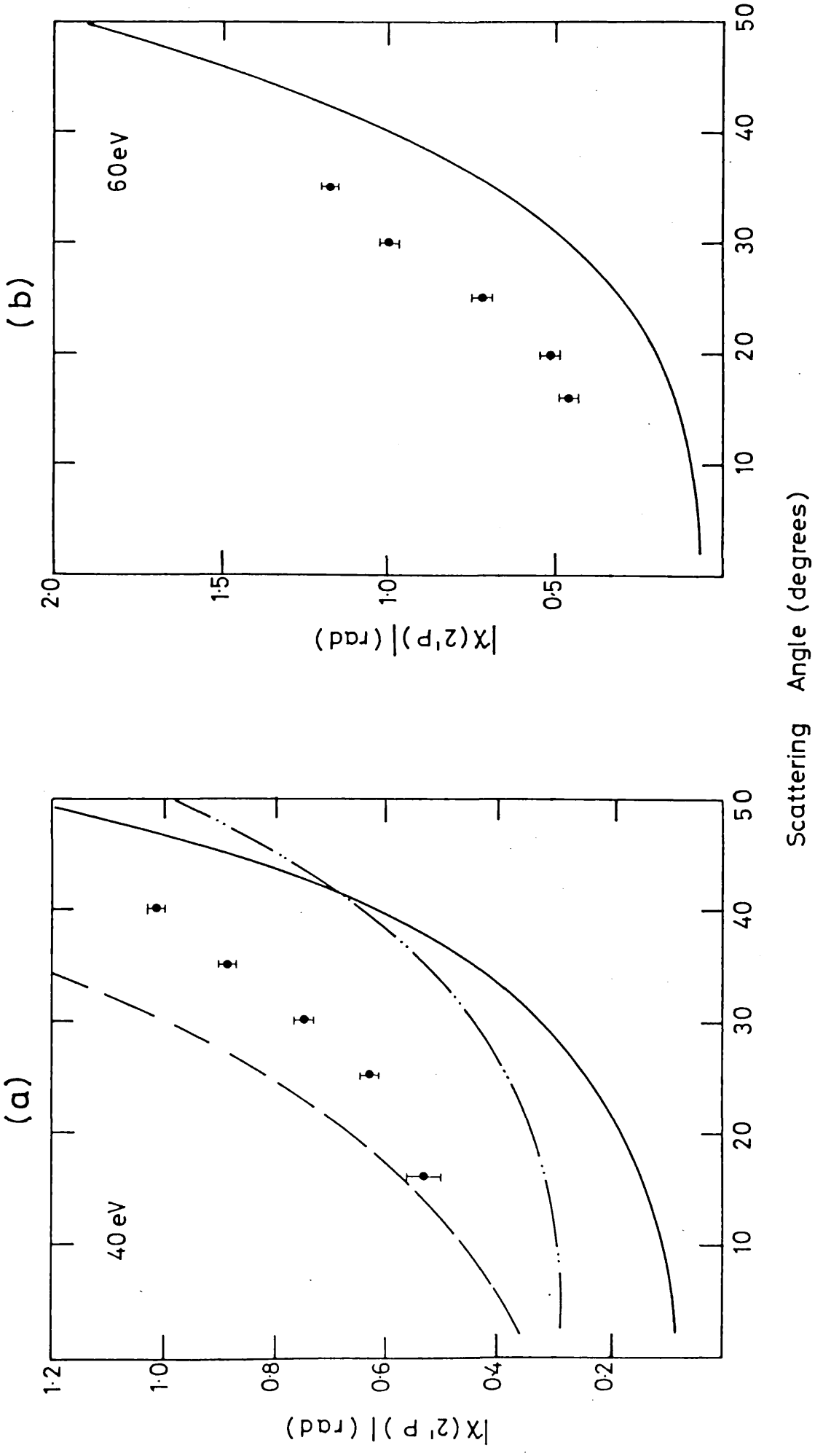

Figure 25

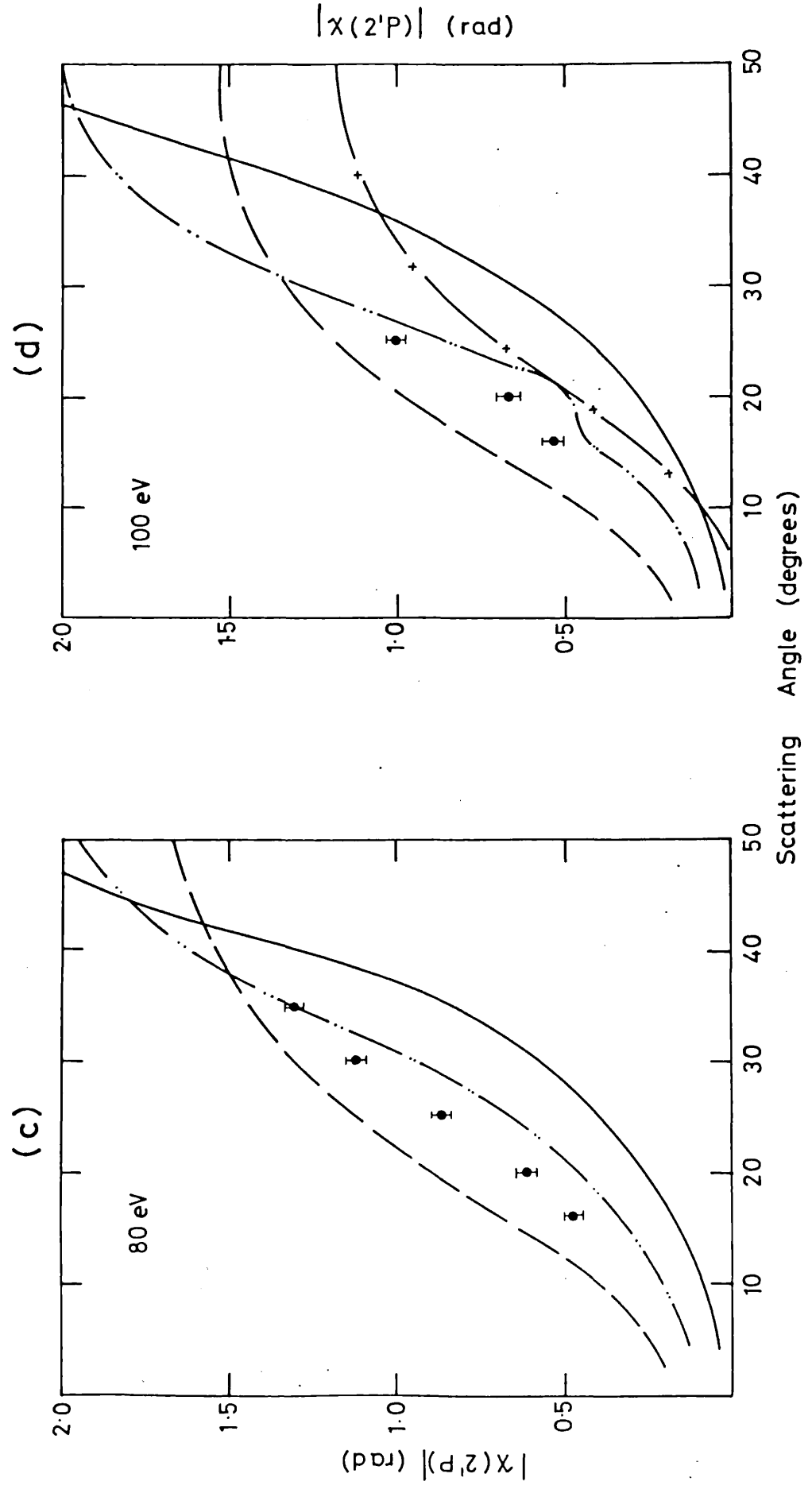
(c)
80 eV
(d)
100 eV
|χ(2'P)| (rad)
2·0
1·5
1·0
0·5
10
20
30
40
50
Scattering Angle (degrees)

Figure 25

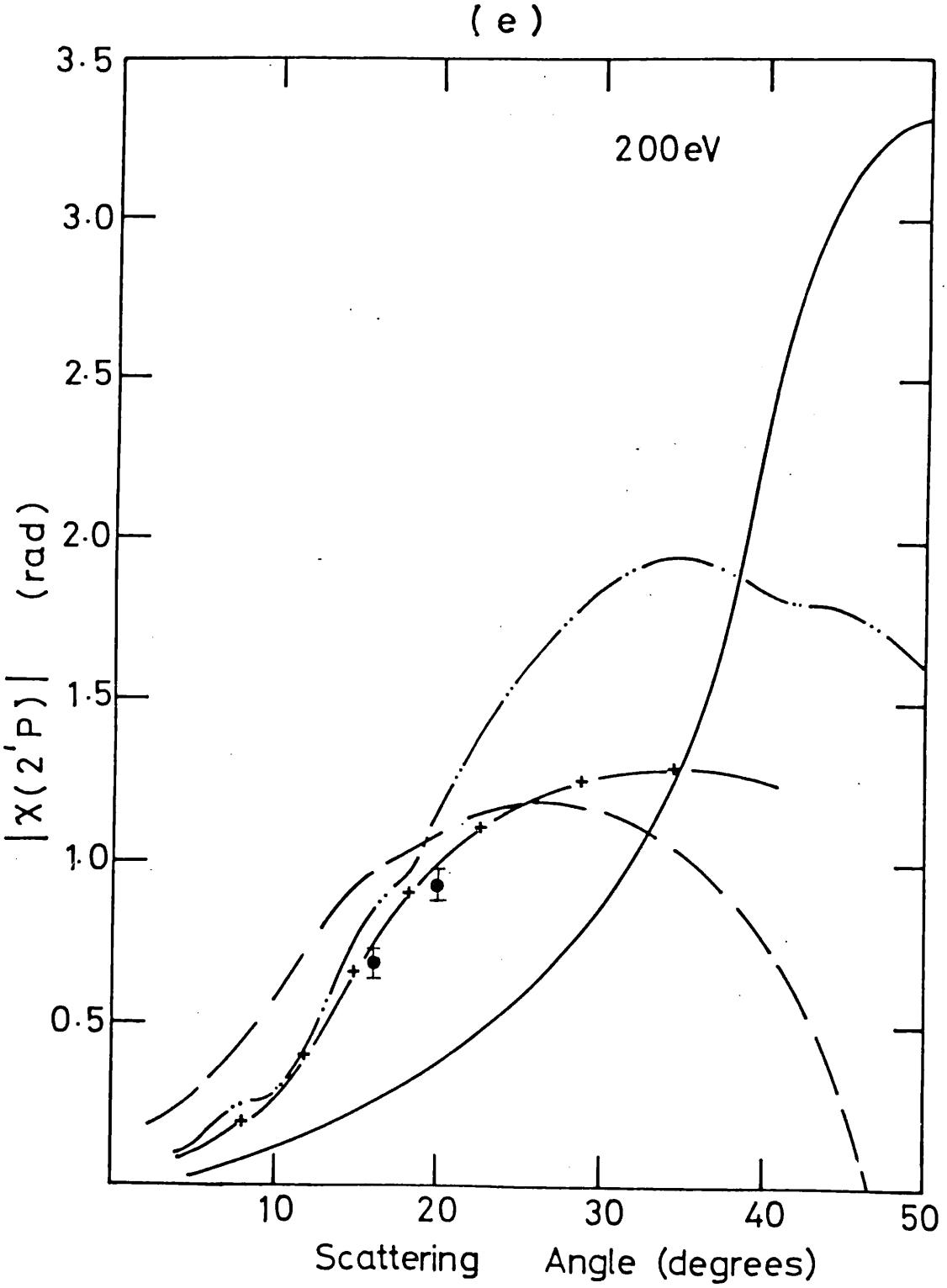
(e)
200eV
3·5
3·0
2·5
2·0
1·5
1·0
0·5
|χ(2¹P)| (rad)
10
20
30
40
50
Scattering Angle (degrees)

Figure 26

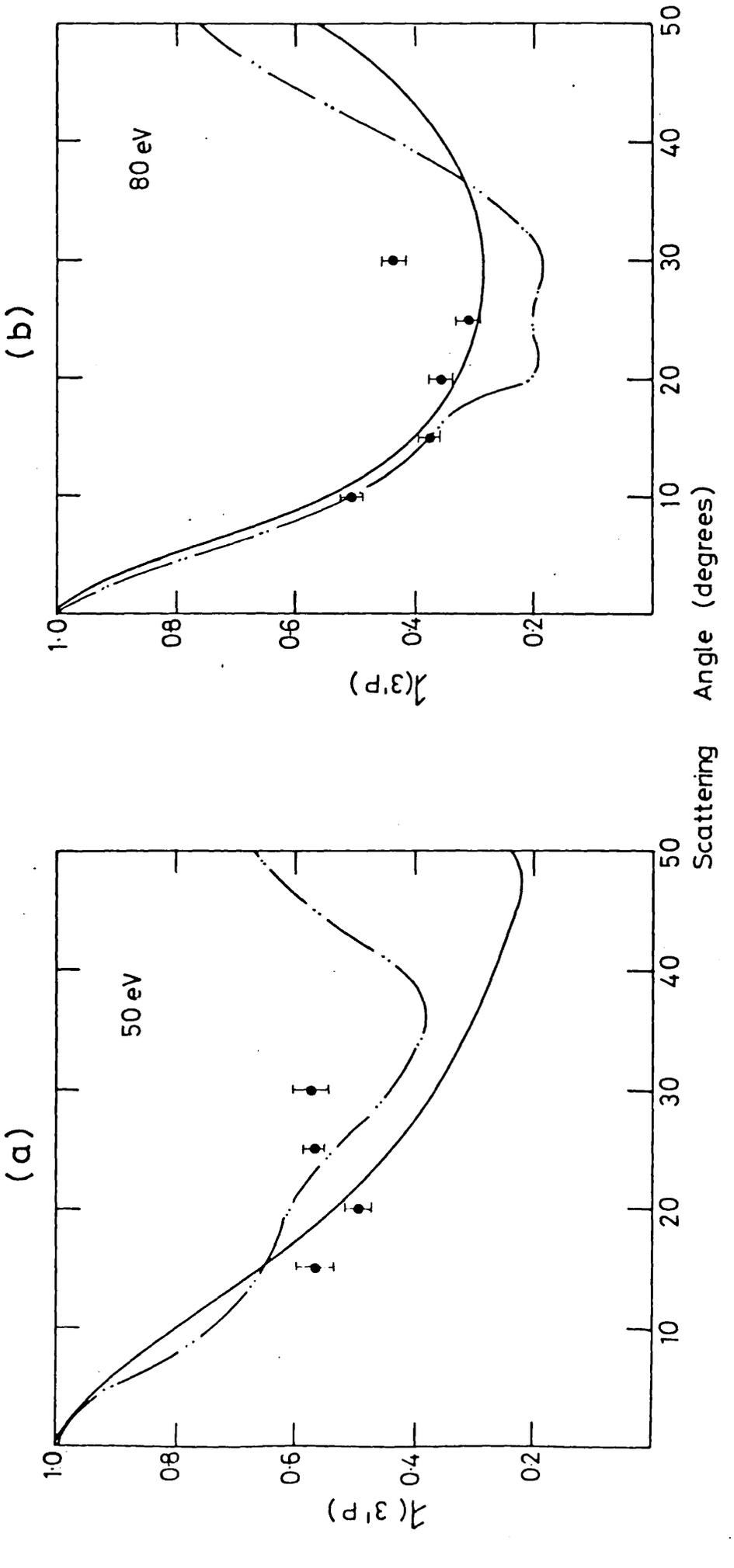
(a)
50 eV
(b)
80 eV
$A(3^1P)$
1·0
0·8
0·6
0·4
0·2
10
20
30
40
50
Scattering Angle (degrees)

Figure 26

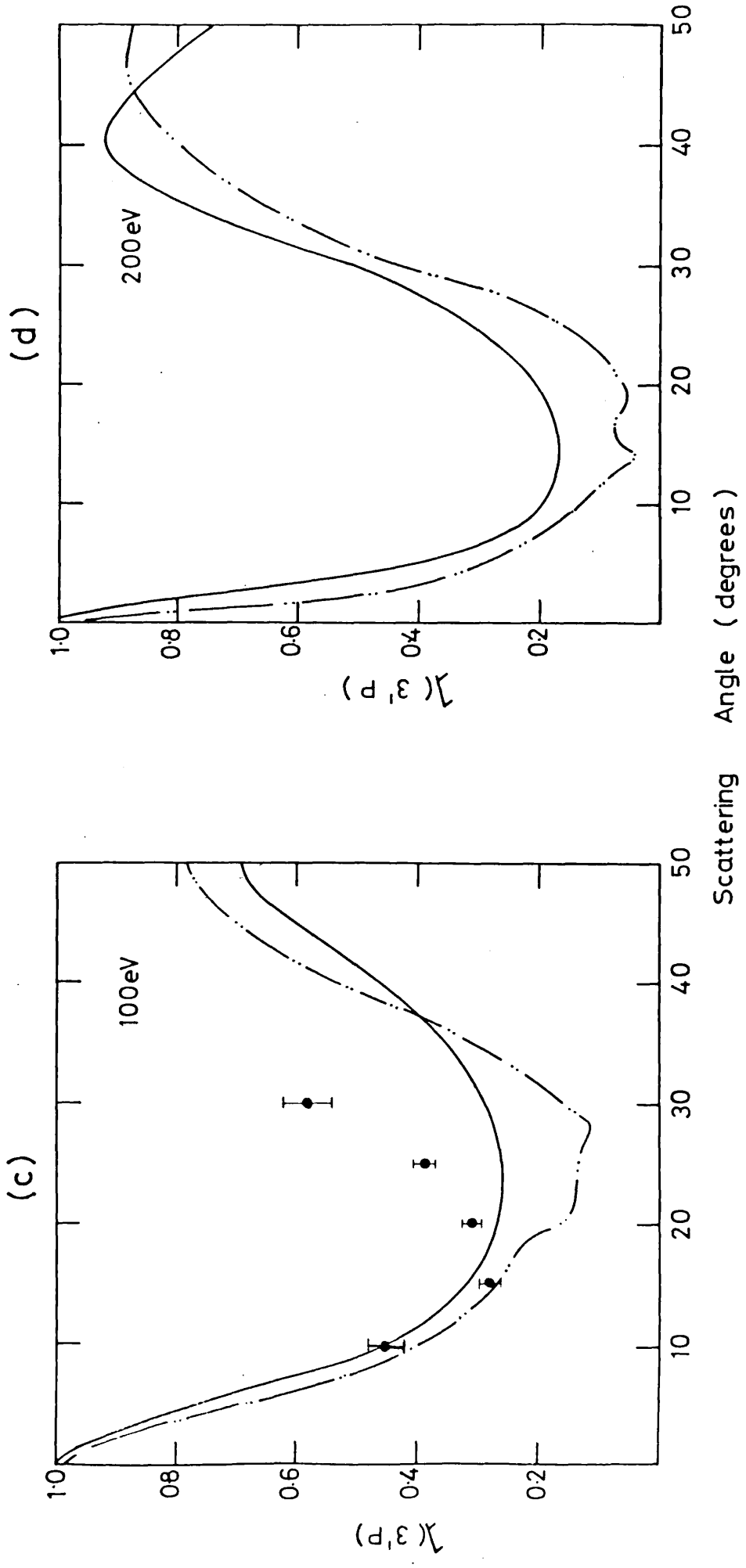
(d)
200eV
(c)
100eV
λ(3¹P)
1·0
0·8
0·6
0·4
0·2
10
20
30
40
50
Scattering Angle (degrees)

Figure 27

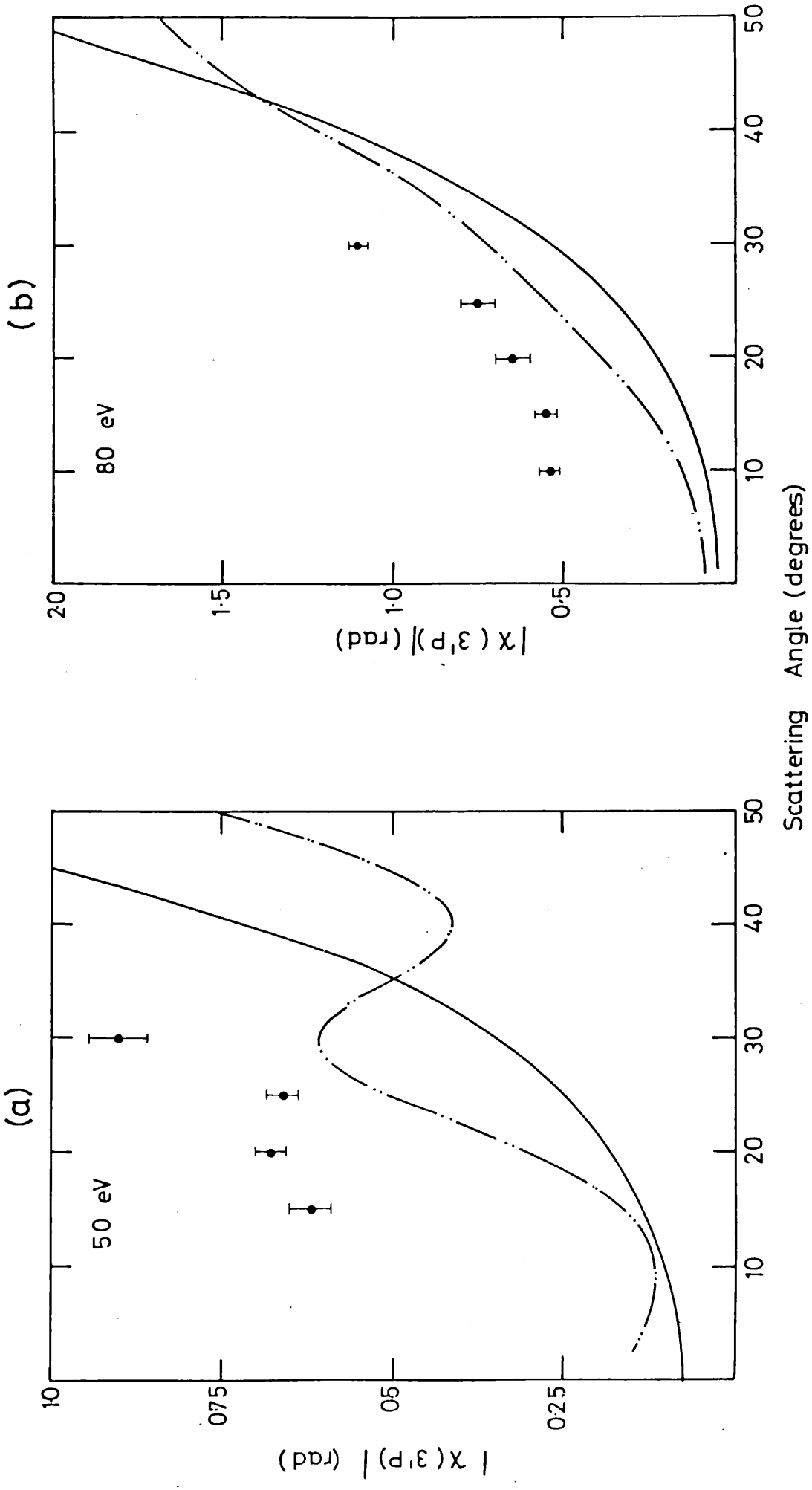

Figure 27

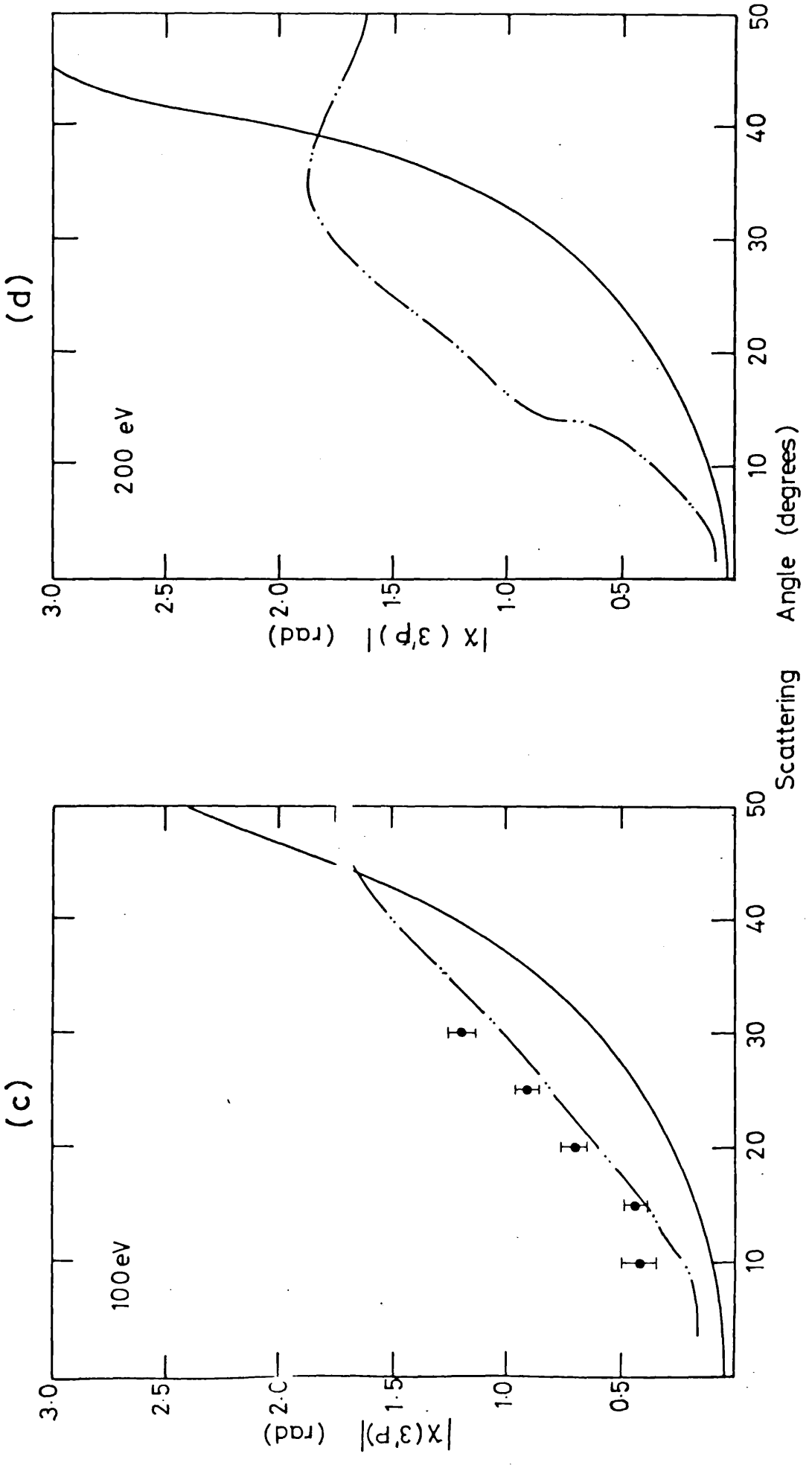
(d)
200 eV
|χ (3'P)| (rad)
3·0
2·5
2·0
1·5
1·0
0·5
10
20
30
40
50
Scattering Angle (degrees)
(c)
100eV
|χ(3'P)| (rad)

Figure 28

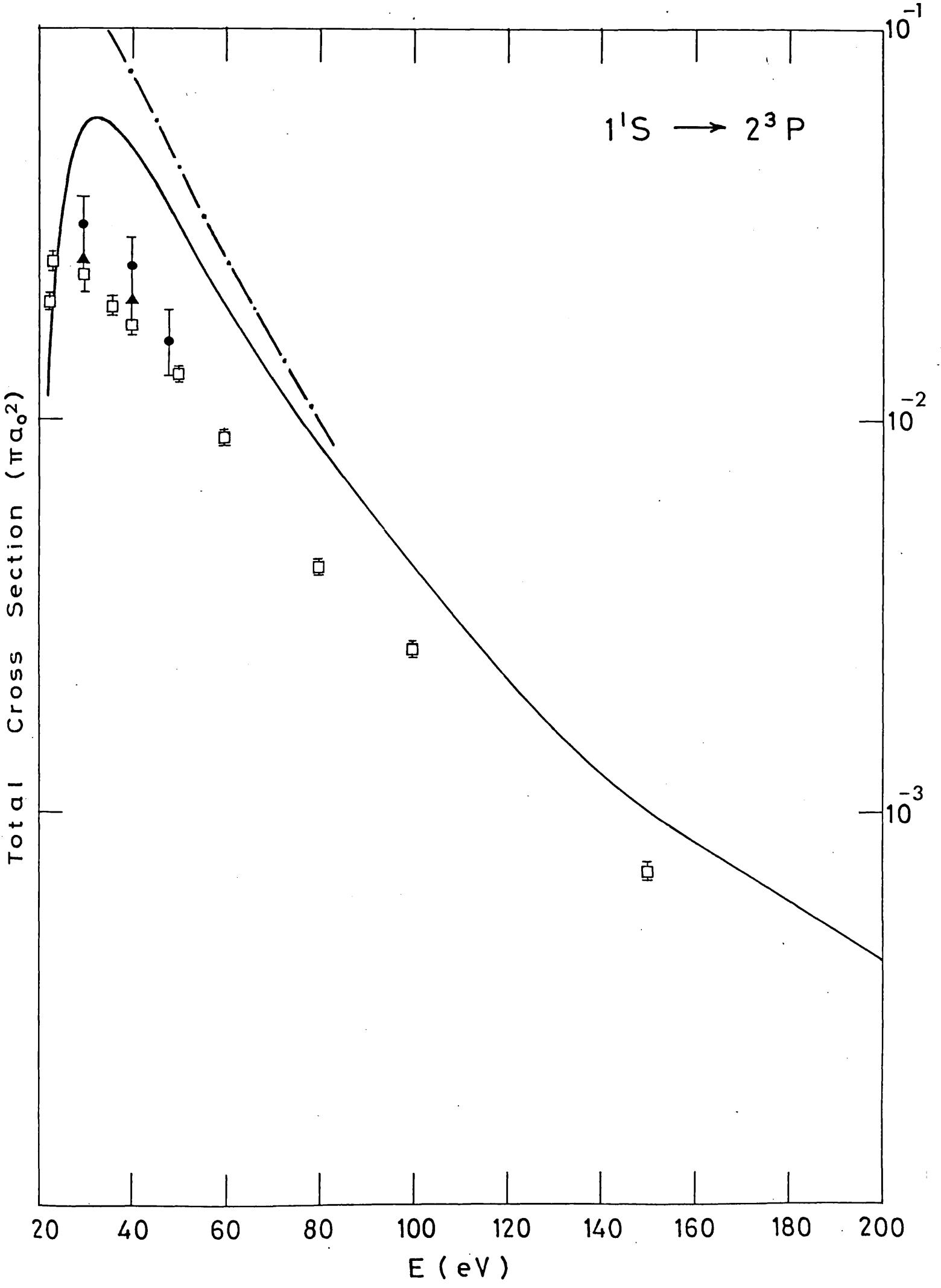
$1^1S \longrightarrow 2^3P$
Total Cross Section (πa_0^2)
10^{-1}
10^{-2}
10^{-3}
20
40
60
80
100
120
140
160
180
200
E (eV)

Figure 29 (a)

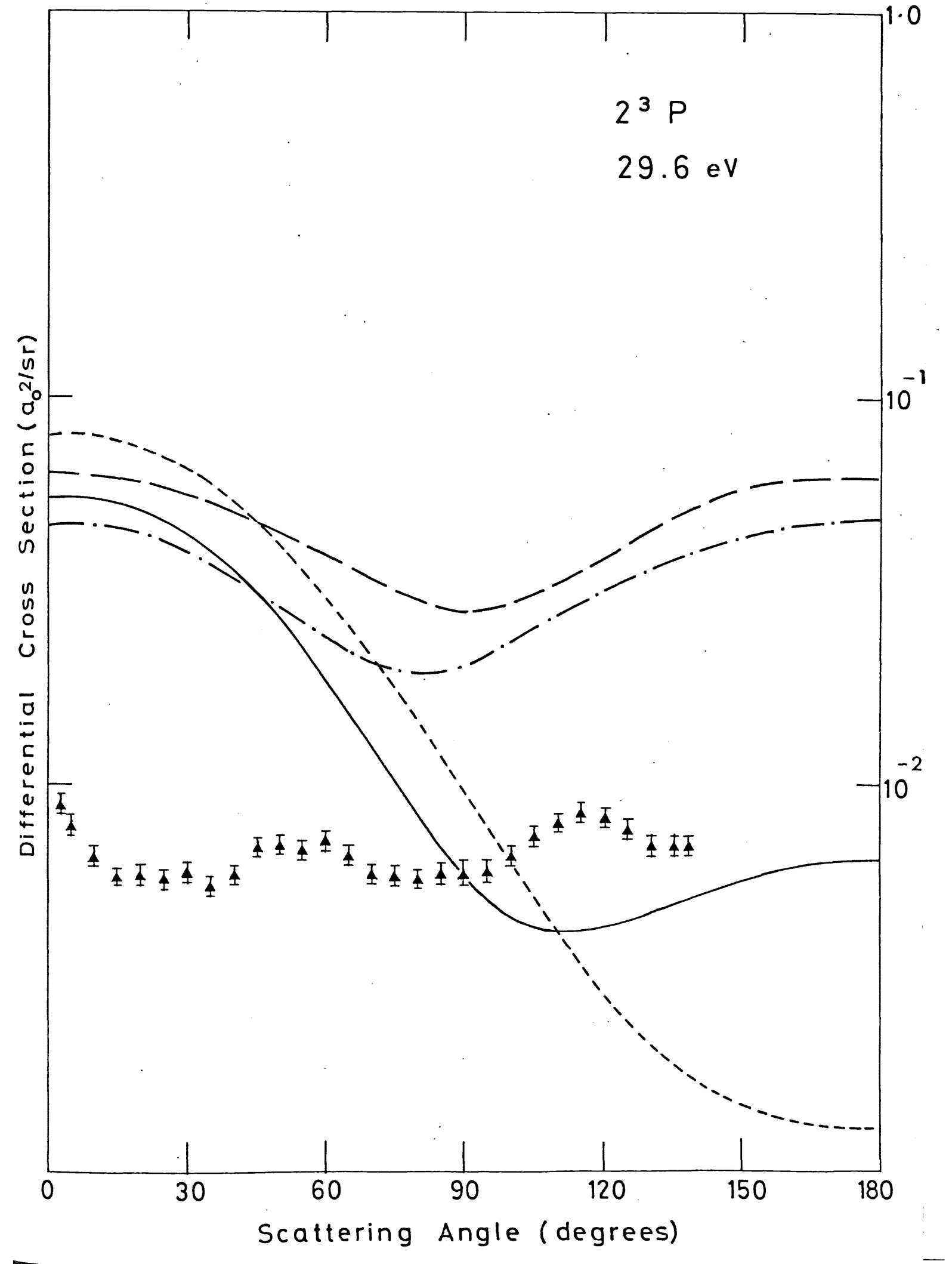
2³ P
29.6 eV
1·0
10⁻¹
10⁻²
Differential Cross Section (a₀²/sr)
0
30
60
90
120
150
180
Scattering Angle (degrees)

Figure 29 (b)

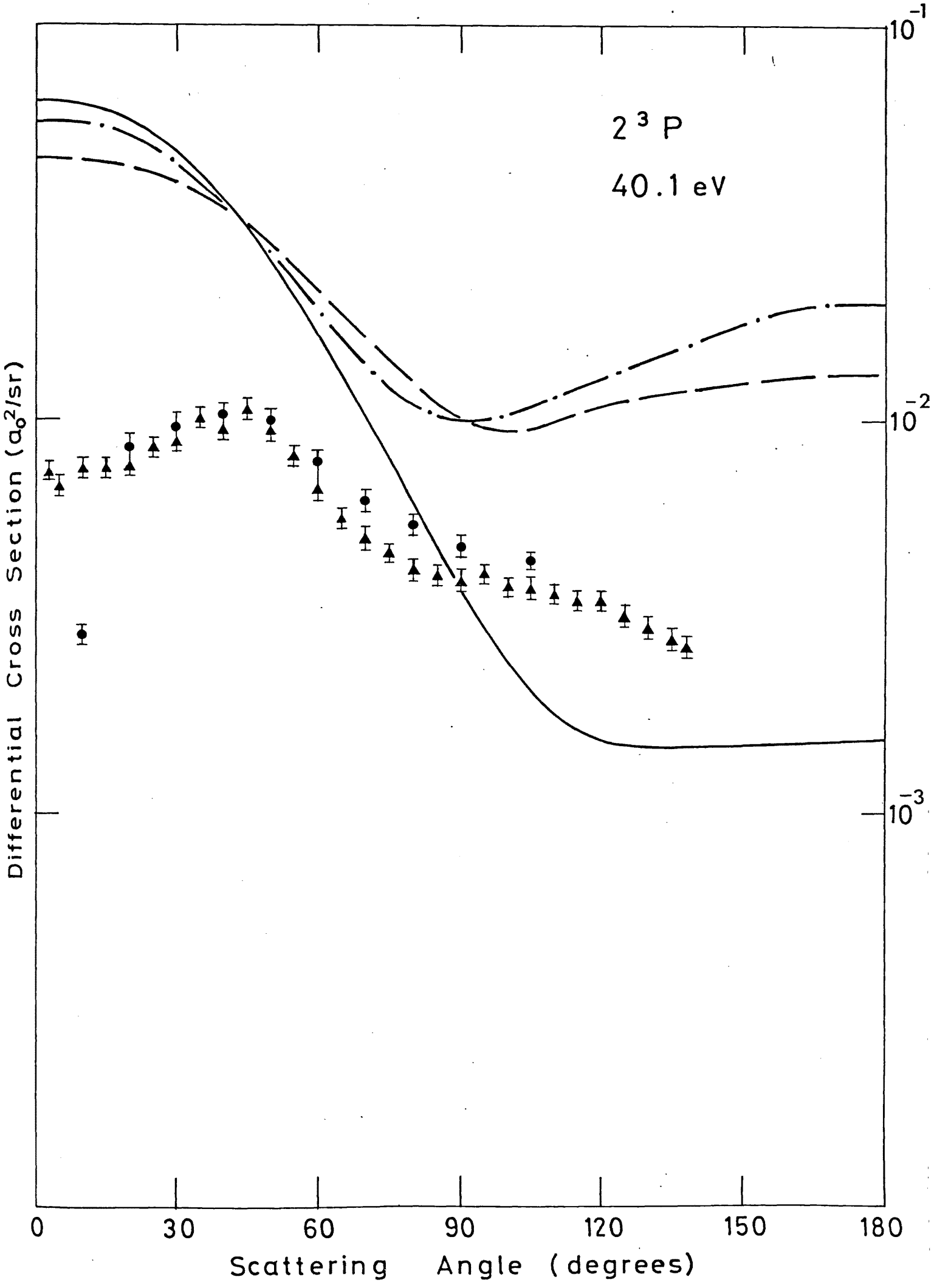
2^3P
40.1 eV
10^{-1}
10^{-2}
10^{-3}
Differential Cross Section (a_0^2/sr)
0
30
60
90
120
150
180
Scattering Angle (degrees)

Figure 29 (c)

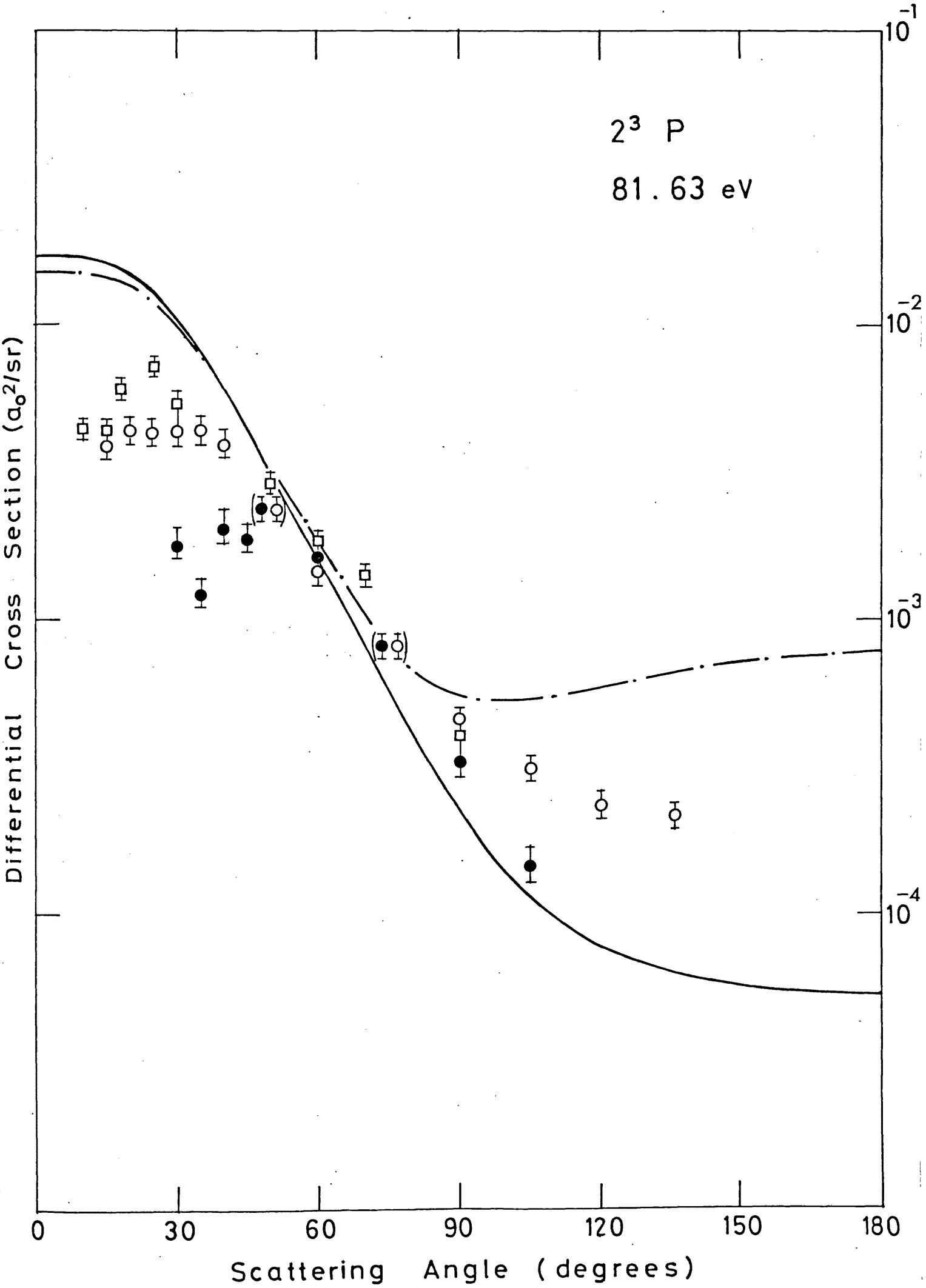
2^3 P
81.63 eV
Differential Cross Section (a_0^2/sr)
10^{-1}
10^{-2}
10^{-3}
10^{-4}
0
30
60
90
120
150
180
Scattering Angle (degrees)

Figure 29 (d)

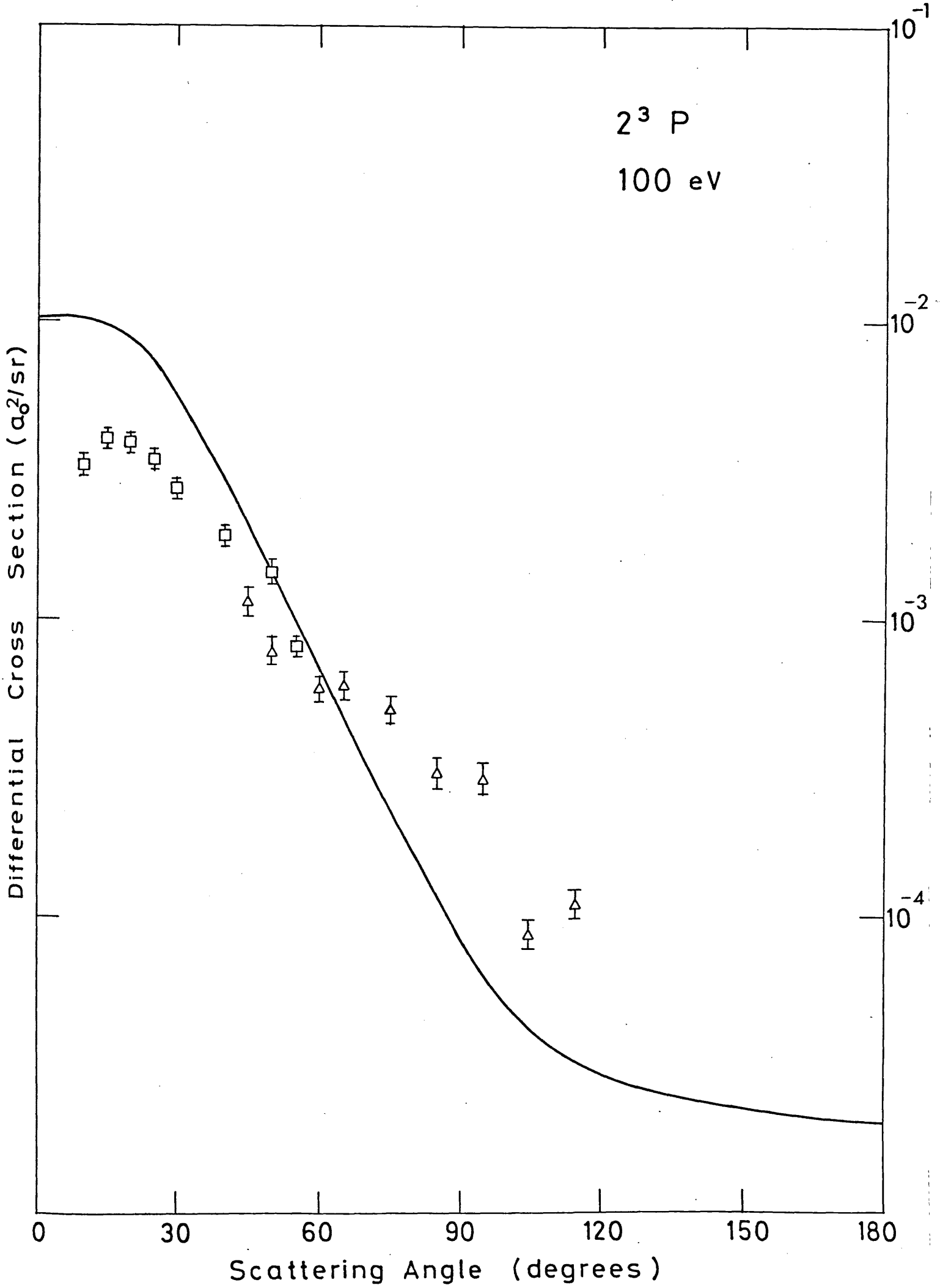
2^3 P
100 eV
10^{-1}
10^{-2}
10^{-3}
10^{-4}
Differential Cross Section (a_0^2/sr)
0
30
60
90
120
150
180
Scattering Angle (degrees)

Figure 29 (e)

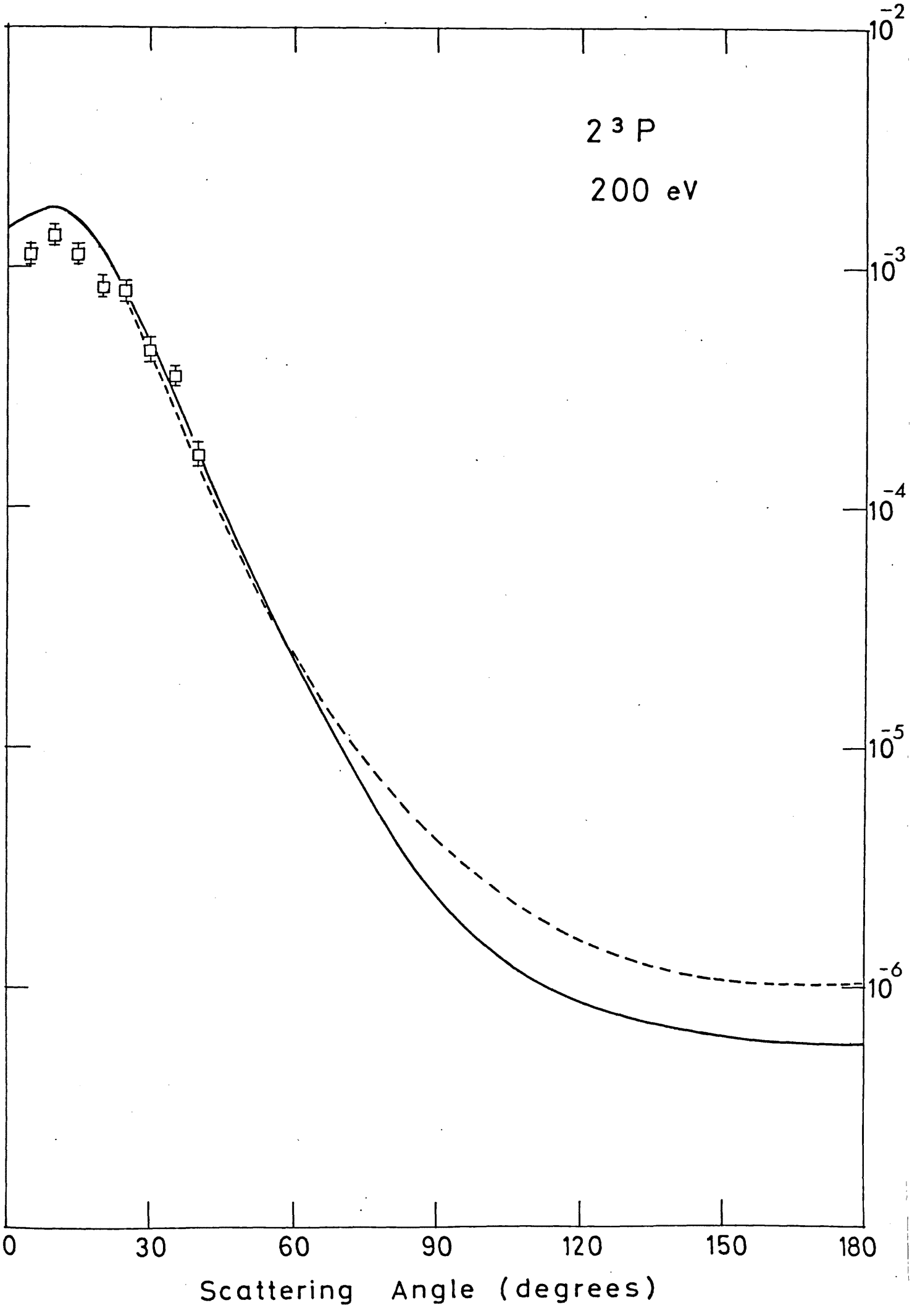
2^3P
200 eV
10^{-2}
10^{-3}
10^{-4}
10^{-5}
10^{-6}
Differential Cross Section (a_0^2/sr)
0
30
60
90
120
150
180
Scattering Angle (degrees)

J. Phys. B: Atom. Molec. Phys., Vol. 8, No. 11, 1975. Printed in Great Britain.

Electron impact excitation of n^1S and n^3S states of He at intermediate energies

T Scott and M R C McDowell

Department of Mathematics, Royal Holloway College, Englefield Green, Surrey TW20 0EX, England

Received 19 February 1975

Abstract. Total and differential cross sections are calculated for electron impact excitation of the 2^1S, 2^3S and 3^1S states of helium in a distorted wave model at impact energies between 30 and 300 eV. The results are compared with other theoretical models and with recent absolute experimental measurements.

1. Introduction

The study of electron impact excitation of helium atoms has received considerable attention during the last few years. Close-coupling methods have been used to study the low-energy resonances (Smith *et al* 1973, Ormonde and Golden 1973, Oberoi and Nesbet 1973) whereas the Born and related methods have provided reasonably accurate total cross sections at high energies. However, it is the intermediate energy region, from the first ionization threshold to the Born region and where an infinite number of channels may be open, which provides much current interest.

There have been a number of important recent studies. The second-order optical potential method of Bransden and Coleman (1972) has been applied, initially in an impact parameter treatment, to 2^1S excitation of helium by Berrington *et al* (1973) and by Nicholls and Winters (1973). More recently Bransden and Winters (1975) have used a partial wave formalism which has produced both singlet and triplet differential cross sections in close agreement with the experimental measurements at higher energies by Crooks and Rudd (1972).

The many-body theory of Martin and Schwinger (1959) has been developed and applied by Thomas *et al* (1974) to electron impact excitation of the $n = 2$ levels of helium using a first-order form of the theory. The method predicts the position of the deep minimum at about 50°, characteristic of 2^1S differential cross sections at low energies, with reasonable accuracy. Preliminary results for the $n = 3$ states at two energies are given by Taylor *et al* (1975).

Both these calculations employ distorted waves in the initial and in the final channel, but whereas the model of Thomas *et al* requires both to be calculated in the field of the ground state, Bransden and Winters allow for polarization effects in the initial channel, and calculate the distorted wave in the final channel in the field of the final state. A similar, but simpler, model was employed earlier by Shelton *et al* (1973). The eikonal distorted wave method has been utilized by Joachain and Vanderpoorten (1974) who have calculated cross sections for 2^1S excitation at intermediate and higher energies.

At higher energies, attempts have also been made to improve on the first Born predictions in a number of ways, among the most interesting recent calculations being the Glauber treatment by Yates and Tenney (1972) and the Coulomb projected Born calculations of Hidalgo and Geltman (1972).

In this paper we apply the distorted wave polarized orbital (DWPO) model of McDowell *et al* (1973, 1974), which allows for the effects of distortion in the initial channel, including polarization, and also for distortion of the target by the dipole polarization. We restrict ourselves in this paper to total and differential cross sections for 2^1S, 2^3S and 3^1S excitation at energies from 29·2 to 300 eV. There are many recent absolute experimental measurements on these cross sections (Trajmar 1973, Rice *et al* 1972, Crooks and Rudd 1972, Opal and Beaty 1972, Brongersma *et al* 1972, Suzuki and Takayanagi 1973, Dillon and Lassettre 1975, Moustafa Moussa *et al* 1969, Hall *et al* 1973), so that they provide a stringent test of any theoretical model.

We outline our theoretical model in the next section (§ 2). Details of the calculations and the approximate wavefunctions employed are described in § 3, our results being presented and compared with those of other theoretical models, and with experiment in § 4. Finally we summarize our results and present our conclusions in § 5.

2. Theory

The theory developed below is for a general two-electron atom or ion carrying a nuclear charge Z. We adopt atomic units throughout.

The transition matrix is defined by

$$T_{if} = \langle \Phi_f V_f \Psi_i^+ \rangle \tag{1}$$

where Φ_f is the unperturbed wavefunction in the final channel, V_f the interaction potential in this channel and Ψ_i^+ the exact wavefunction describing the total system in the initial channel. The differential cross section $I(\Omega)$ for a transition from an initial state i to a final state f is then expressed in terms of the T-matrix by

$$I(\Omega) = \frac{1}{4\pi^2}\frac{k_f}{k_i}|T_{if}|^2 \quad a_0^2 \text{ sr}^{-1} \tag{2}$$

with $\boldsymbol{k}_i$ and $\boldsymbol{k}_f$ the initial and final momentum of the incoming and outgoing electron respectively. By integrating (2) over all solid angles we obtain the total cross section Q_{if} given by

$$Q_{if}(k_i^2) = \frac{1}{2\pi^2}\frac{k_f}{k_i}\int_{-1}^{+1}|T_{if}|^2 \, d(\cos\theta) \quad \pi a_0^2 \tag{3}$$

with $\hat{\boldsymbol{k}}_i \cdot \hat{\boldsymbol{k}}_f = \cos\theta$.

We assume the centre of mass to be fixed at the nucleus and let $\boldsymbol{r}_3$ be the position vector of the incident electron with respect to this point. The initially bound electrons have position vectors $\boldsymbol{r}_1$ and $\boldsymbol{r}_2$.

The Schrödinger equation describing the complete process is

$$(H-E)\Psi_i^+ = 0 \tag{4}$$

with

$$E = \tfrac{1}{2}k_i^2 + E_0 = \tfrac{1}{2}k_f^2 + E_n. \tag{5}$$

E_0 and E_n refer to the ground and excited state energies of the target atom respectively.

H is divided into two parts

$$H = H_f + V_f \tag{6}$$

where it is convenient to choose

$$H_f = -\tfrac{1}{2}(\nabla_1^2+\nabla_2^2+\nabla_3^2)-\frac{Z}{r_1}-\frac{Z}{r_2}-\frac{z}{r_3}+\frac{1}{r_{12}}, \tag{7}$$

$$V_f = -\left(\frac{2}{r_3}-\frac{1}{r_{13}}-\frac{1}{r_{23}}\right) \tag{8}$$

in the notation of McDowell *et al* (1973) where now $z = Z-2$.

The system considered has total spin $S = \frac{1}{2}$ and hence is a doublet. Denoting the doublet spin functions by S^+ and S^- (plus and minus signs referring to singlet and triplet states of the target respectively), the final unperturbed state of the total system can be represented by

$$\Phi_f(12,3) = \psi_f^{\pm}(12,3)S^{\pm}(12,3) \tag{9}$$

where $\psi_f^{\pm}(12,3)$ represents the spatial part of Φ_f and is the product of a bound state function $\phi_f(12)$ and an outgoing Coulomb wavefunction $\chi_{k_f}(z,3)$.

$$\psi_f^{\pm}(12,3) = \phi_f(12)\chi_{k_f}(z,3), \tag{10}$$

$$S^+(12,3) = \frac{1}{\sqrt{2}}(\alpha_1\beta_2-\alpha_2\beta_1)\alpha_3, \tag{11}$$

$$S^-(12,3) = \frac{1}{\sqrt{6}}[2\beta_3\alpha_1\alpha_2-\alpha_3(\alpha_1\beta_2+\beta_1\alpha_2)]. \tag{12}$$

The total antisymmetrized wavefunction Ψ_i^+ is written as

$$\Psi_i^+ = \mathscr{A}\phi_i(12)F(3)S^+(12,3) \tag{13}$$

with $\phi_i(12)$ the unperturbed spatial part of the ground state wavefunction and $F(3)$ the distorted wave. We now obtain the following expressions for the T-matrix, on integrating over spin functions,

$$T_{if}^+ = \langle\psi_f(12,3)V_f\phi_i(12)F(3)\rangle-\langle\psi_f(12,3)V_f\phi_i(23)F(1)\rangle \tag{14}$$

$$T_{if}^- = \sqrt{3}\langle\psi_f(12,3)V_f\phi_i(23)F(1)\rangle. \tag{15}$$

The distorted wave is derived by the procedure adopted by McDowell *et al* (1973). Thus, $F(3)$ is expanded in partial waves

$$F(3) = \frac{1}{\sqrt{k_i}}\sum_{l=0}^{\infty} A_l\frac{u_l(k_ir_3)}{r_3}P_l(\cos\theta_3) \tag{16}$$

where $u_l(k_ir)$ satisfies

$$\left(\frac{d^2}{dr^2}+k_i^2-\frac{l(l+1)}{r^2}-2V_{1s,1s}(r)-2V_{pol}(r)\right)u_l(k_ir) = X_l(r)rR_{1s}(r) \tag{17}$$

with

$$X_l(r) = -(\epsilon_{1s} - k_i^2)\,\delta_{l0}\int_0^\infty tR_{1s}(t)u_l(k_i t)\,\mathrm{d}t - \frac{2}{2l+1}\int_0^\infty tR_{1s}(t)u_l(k_i t)\gamma_l(t,r)\,\mathrm{d}t \tag{18}$$

and

$$\gamma_l(r,r') = \frac{r_<^l}{r_>^{l+1}}. \tag{19}$$

Equation (17) is to be solved subject to the usual boundary conditions,

$$u_l(k_i,0) = 0, \qquad u_l(k_i,r) \underset{r\to\infty}{\sim} k_i^{-1/2}\sin(k_i r - \tfrac{1}{2}l\pi + \delta_l).$$

The polarization induced by the incoming electron is only taken into account by means of the direct polarization potential $V_{pol}(r)$ so that (17) produces elastic scattering solutions in the adiabatic exchange approximation, the effect of exchange polarization terms having been neglected.

The direct static potential $V_{1s,1s}(r)$ is given by

$$V_{1s,1s}(r) = -\frac{Z}{r} + \left\langle \phi_{1s}(t)\frac{2}{|r-t|}\phi_{1s}(t)\right\rangle \tag{20}$$

and $V_{pol}(r)$ by

$$V_{pol}(r) = \left\langle \phi_{1s}(t)\frac{2}{|r-t|}\phi_{pol}(r,t)\right\rangle \tag{21}$$

with $\phi_{pol}(r,t)$ the dipole component of the perturbed atomic wavefunction.

It is consistent with our neglect of exchange polarization terms in (17) to include the dipole distortion of the atom, through the ground state wavefunction $\phi_i(12)$, in the direct transition amplitude alone. This results in a modified T-matrix describing singlet–singlet transitions of the form

$$T_{if}^{mod} = T_{if}^{+} + T_{if}^{pol} \tag{22}$$

where T_{if}^{+} is given by (14) and

$$T_{if}^{pol} = 2\langle\psi_f(12,3)V_f\phi_{1s}(1)\phi_{pol}(2,3)F(3)\rangle. \tag{23}$$

We discuss results obtained with both T_{if}^{+} and T_{if}^{mod} and refer to these as the DWPO I and DWPO II approximations respectively.

3. Numerical methods and choice of atomic wavefunctions

The elastic scattering phaseshifts were obtained from solutions of (17) by the method of Burgess (1963) and on comparison with those of Duxler *et al* (1971), were found to be in good agreement. A further check on the numerical work was provided by incorporating in the code switches to output the Born and Born–Oppenheimer approximation results for total and differential cross sections. Born results were in reasonable agreement with those of Bell *et al* (1969) considering the more complex wavefunctions employed by the latter. The Born–Oppenheimer 2^3S total cross sections were compared with those of Bell *et al* (1966) and were in good agreement. These latter results will be discussed further below.

3.1. Choice of atomic wavefunctions

(i) The wavefunction describing the ground state was taken to be the separable Hartree–Fock wavefunction of Green *et al* (1954)

$$\phi_i(12) = \phi_{1s}(1)\phi_{1s}(2) \tag{24}$$

with

$$\phi_{1s}(r) = R_{1s}(r)Y_{00}(\hat{r}), \tag{25}$$

$$R_{1s}(r) = N_1(e^{-ar} + c_1 e^{-2ar}), \tag{26}$$

$$a = 1{\cdot}4558, \qquad c_1 = 0{\cdot}6, \qquad N_1 = 2{\cdot}968468.$$

The dipole part of the distortion induced in the ground state is given by

$$\phi_{pol}(\boldsymbol{r}, t) = -\frac{\epsilon(r, t)}{t^2}\frac{U_{1s\to p}(r)}{r}\frac{P_1(\cos\theta_{rt})}{\sqrt{\pi}} \tag{27}$$

where $\epsilon(r, t)$ is a unit step function which causes the perturbation to vanish when the incoming electron is 'inside' the atom. The radial function $U_{1s\to p}(r)$ is the usual Sternheimer function

$$U_{1s\to p}(r) = Z_0^{-3/2} r e^{-Z_0 r}(Z_0 r + \tfrac{1}{2}Z_0^2 r^2). \tag{28}$$

The parameter $Z_0 (= 1{\cdot}598)$ is evaluated by matching the asymptotic behaviour of $V_{pol}(r)$ to $-\alpha/2r^4$ with α the dipole polarizability of helium, taken to be $1{\cdot}395\, a_0^3$. In the DWPO II model $\phi_{1s}(\boldsymbol{r}_i)$ is replaced by

$$\phi_{1s}(\boldsymbol{r}_i) + \phi_{pol}(\boldsymbol{r}_i, \boldsymbol{r}_3), \qquad i = 1, 2. \tag{29}$$

This results in the expression (22) instead of (14).

(ii) The wavefunction describing the excited state is taken to have the form

$$\phi_f^{\pm}(12) = \frac{1}{\sqrt{2}}[W_{1s}(1)V_{ns}(2) \pm V_{ns}(1)W_{1s}(2)]. \tag{30}$$

The core orbital $W_{1s}(r)$ is taken to be a 1s hydrogenic eigenfunction while the valence orbital $V_{ns}(\boldsymbol{r})$ is

$$V_{ns}(\boldsymbol{r}) = R_{ns}(r)Y_{00}(\hat{r}). \tag{31}$$

$R_{ns}(r)$ is taken to be the analytic Hartree–Fock frozen core wavefunction due to Cohen and McEachran (1967a, b)

$$R_{ns}(r) = e^{-\beta r}\sum_{j=1}^{N} a_j^{(N)} L_j^1(2\beta r) \tag{32}$$

with $\beta = Z/n$. The $a_j^{(N)}$ coefficients are tabulated by Crothers and McEachran (1970). The $L_j^1(x)$ are Laguerre polynomials and n denotes the principal quantum number of the state concerned.

In order to test the sensitivity of the cross sections to this choice of $R_{ns}(r)$ we also computed results for $n = 2$ by taking $R_{ns}(r)$ to have the form

$$R_{2s}(r) = N_2(e^{-pr} - c_2 r e^{-qr}). \tag{33}$$

The values of the parameters are, for the 2^1S state (Byron and Joachain 1974)

$$p = 0{\cdot}865, \qquad q = 0{\cdot}522, \qquad c_2 = 0{\cdot}432784, \qquad N_2 = 0{\cdot}61928$$

and for the 2^3S state (Morse *et al* 1935).

$$p = 1{\cdot}57, \qquad q = 0{\cdot}61, \qquad c_2 = 0{\cdot}34081, \qquad N_2 = 1{\cdot}05.$$

These functions were also used by Bransden and Winters (1975) and allow us to make a direct comparison with their work.

4. Results and discussion

We have calculated total and differential cross sections for excitation of 2^1S and 2^3S at energies of 29·6, 40·1, 81·63, 200 eV in both DWPO I and DWPO II models. In addition we have evaluated the total and differential cross sections for 3^1S in the DWPO I model at a number of energies.

Our code was checked by comparing our Born–Oppenheimer results (obtained by replacing $u_l(k_i r)$ in DWPO I by $k_i^{-1/2} r j_l(k_i r)$, where $j_l(x)$ is the lth regular spherical Bessel function) with the 'prior' calculations of Bell *et al* (1966). Provided it is not assumed when deriving an expression for the exchange amplitude that the approximate helium wavefunctions adopted are exact, there is no post–prior discrepancy. The total cross section results are found to be insensitive to the representation of the Hartee–Fock ground state, and to that of the excited state.

4.1. 2^1S excitation of helium

Our total cross section results for the $1^1S \rightarrow 2^1S$ transition are shown in figure 1 and compared with those of other theoretical models and with experiment. At energies above 200 eV they are in close agreement with the Coulomb-projected Born calculation of Hidalgo and Geltman (1972) and with the experimental measurements of Vriens *et al* (1968). Our results are consistent with the measurements of Rice *et al* (1972) above 50 eV but at lower energies they agree with the results of Trajmar (1973) at 30 and 40 eV and with those of Brongersma *et al* (1972) at 21 and 23 eV. As in the case of hydrogen our model does not give the low-energy resonances.

If we ignore the measurements of Rice *et al* (1972) at energies below 50 eV, we are then consistent with all other available experiments over the energy range from 20 to 400 eV.

The many-body theory calculation by Thomas *et al* (1974), while also consistent with experiment at energies above 40 eV, not unexpectedly fails at lower energies. However the eikonal distorted wave calculation of Joachain and Vanderpoorten (1974) appears to give good results down to 80 eV whereas the Coulomb-projected Born results of Hidalgo and Geltman (1972) and the second-order optical potential result of Winters (1974) increase rather too rapidly with decreasing energy below 200 eV.

Differential cross sections for $1^1S \rightarrow 2^1S$ are shown in figure 2 (*a*), (*b*), (*c*), (*d*) at four energies. The results were insensitive (within 10%) when the Cohen–McEachran excited state function was replaced by that of Byron and Joachain. Our results, using Cohen–McEachran wavefunctions (in the DWPO I approximation) agree well in shape with the experimental results of Trajmar (1973) at 29·6 eV. However, they fail to show the forward and backward peaks and underestimate the depth of the observed minimum

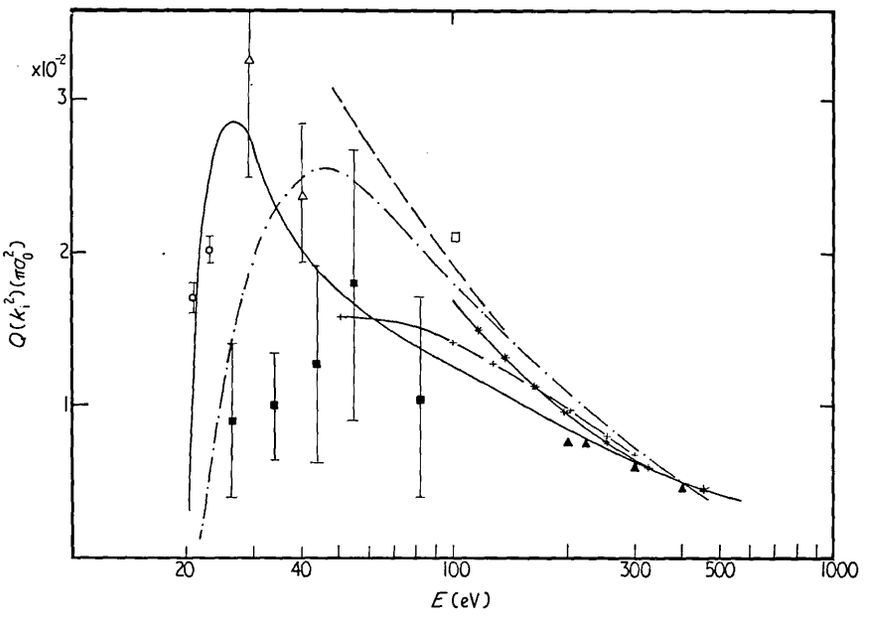

Figure 1. Theoretical and experimental total cross section results for the excitation of the 2^1S state of helium by electron impact. —— present results (DWPO I), –·–·– many-body theory (Thomas *et al* 1974), — — — second-order optical potential distorted wave results (Winters 1974), ——+——+——+ eikonal distorted wave method (Joachain and Vanderpoorten 1974), ——*——*—— Coulomb-projected Born approximation (Hildalgo and Geltman 1972). Experimental results: △ Trajmar (1973), ◇ Brongersma *et al* (1972), ▮ Rice *et al* (1972), ▲ Vriens *et al* (1968), □ Lassettre (1965).

near 60°. Independent measurements, using different techniques, by Hall *et al* (1973) and Crooks and Rudd (1972) are in excellent agreement with Trajmar's work, and will not be discussed separately. In the forward direction our results agree well with the many-body calculation of Thomas *et al* (1974) and with the Glauber approximation (Yates and Tenney 1972), though the many-body method gives a much deeper minimum. A distorted wave Born approximation calculation (Shelton *et al* 1973) succeeds in predicting the forward peak but fails at larger angles. We are again in agreement with Thomas *et al* at large angles, where the Glauber approach fails completely, tending at 29·6 eV to a value close to $9 \times 10^{-3}\ a_0^2\,\mathrm{sr}^{-1}$ for $\theta > 140°$, where the experiment of Trajmar (1973) (but not that of Hall *et al* 1973) indicates a much larger backward cross section. The addition of target distortion to our model (DWPO II) has little effect in this case, unlike that of $1s \rightarrow ns$ excitation in atomic hydrogen, but it produces some forward enhancement. Presumably this is because $He(1^1S)$ has a comparatively low polarizability. The results at 40·1 eV (figure 2(*b*)) show a similar picture, except that all the calculations but that of Shelton *et al* (1973) now agree in the forward direction and at the minimum, and correctly account for the experimental behaviour at small angles. They again underestimate both the depth of the minimum and backward cross section. The Glauber result remains an order of magnitude too small for large angles, while the DWBA gives results much larger than experiment at all angles.

Opal and Beaty (1972) have extended the measurements to higher energies and we make comparisons with their results at 81·63 eV (figure 2(*c*)) and 200 eV (figure 2(*d*)). At the first of these energies we also show the many-body result (Thomas *et al* 1974) and

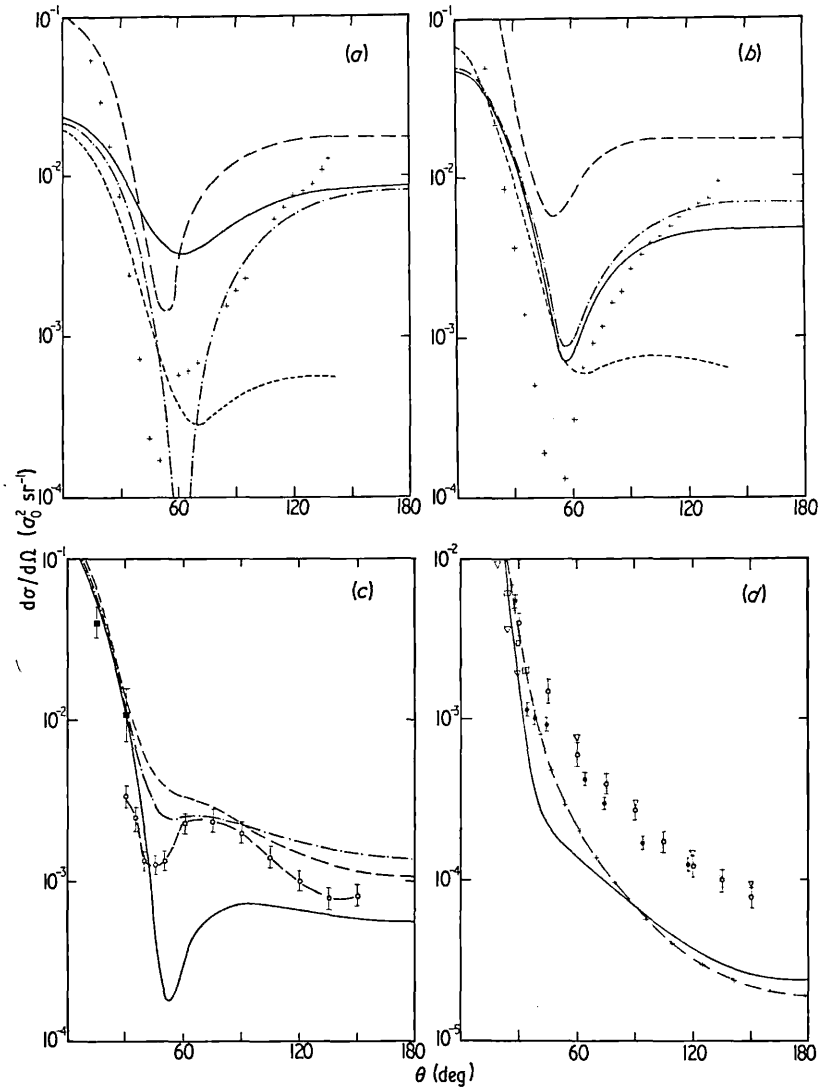

Figure 2. Differential cross section results for the excitation of the 2^1S state of helium by electron impact at (*a*) 29·6, (*b*) 40·1, (*c*) 81·63 and (*d*) 200 eV. (*a*) ——— present results (DWPO I), – · – · – many-body theory (Thomas *et al* 1974), — — — distorted wave calculation of Shelton *et al* (1973), - - - - - Glauber approximation (Yates and Tenney 1972), + experiment (Trajmar 1973). (*b*) as for (*a*). (*c*) ——— present results (DWPO I), – · – · – many-body theory (Thomas *et al* 1974), — — — second-order optical potential distorted wave results (Bransden and Winters 1975), ⊖ experiment (Opal and Beaty 1972), ▮ experiment (Rice *et al* 1972). (*d*) – × – × – Coulomb-projected Born approximation (Hidalgo and Geltman 1972), ▽ preliminary eikonal Born series results (Byron and Joachain 1975), ⧫ experiment (Suzuki and Takayanagi 1973), □ experiment (Dillon and Lassettre 1975). Other symbols as for (*c*).

a second-order potential distorted wave result of Bransden and Winters (1975). All the theories agree at small angles and are in excellent agreement with the measurements of Rice *et al* (1972) for $\theta < 45°$. The many-body theory shows a shallow minimum at 52°, where our model predicts a very deep minimum. Both experiments (Rice *et al* 1972, Opal and Beaty 1972) show minima (at 60° and 45° respectively), deeper than predicted in the many-body theory, but much shallower than we obtain. The distorted wave

calculations of Bransden and Winters (1975) fail to predict a minimum but agree well with the many-body result at large angles, the experimental results lying between these theoretical predictions and ours.

At 200 eV the experimental results of Opal and Beaty (1972), Suzuki and Takayanagi (1973) and of Dillon and Lassettre (1975) are in good agreement over a wide angular range. Our calculation and that of Hidalgo and Geltman (1972) agree well with each other, but fall below experiment for angles greater than 40°. Preliminary eikonal Born series calculations by Byron and Joachain (1975) are, however, in essentially complete agreement with experiment at this energy for all angles from 20° to 150°. Comparison with the results of Bransden and Winters (1975) at 150 eV (their figure 1(*d*)) suggests that inclusion of final-channel distortion is necessary to account for the large observed backward cross sections at moderate and higher energies. A similar conclusion was reached by McDowell *et al* (1975) in the case of $n = 2$ excitation of atomic hydrogen.

4.2. 2^3S excitation of helium

The observed differential cross section at 29·6 eV (Trajmar 1973, Hall *et al* 1973, Crooks *et al* 1972) show two minima, at 45° and at 115°. Our model reproduces the shape of the experimental curve accurately (figure 3). When we employ the Cohen–McEachran excited state function, we must renormalize our calculation by a factor of 10 to produce the agreement shown in figure 3. Changing to the Hartree–Fock representation of the excited state due to Morse *et al* (1935) shifts these results by as much as a factor of five at some angles but preserves the two minima. The transition matrix element is very sensitive to the approximate wavefunctions employed at low impact energies (though this sensitivity is absent if distortion is neglected), whereas the experimental measurements of different groups, all claiming absolute values, agree well for this transition†.

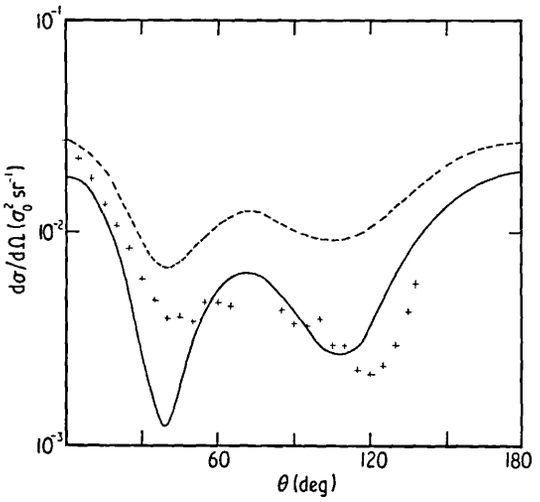

Figure 3. Differential cross section results for the excitation of the 2^3S state of helium by electron impact at 29·6 eV. ——— present model employing the Cohen and McEachran excited state wavefunction and renormalized by a factor of 10, - - - - - present model employing the Hartree–Fock representation for the excited state wavefunction due to Morse *et al* (1935) and renormalized by a factor of 10, + experiment (Trajmar 1973).

† *Note added in proof.* This sensitivity arises from the overlap of the $l = 0$ component of the distorted wave with the radial part of the 2^3S function.

We suggest that it is therefore a valid procedure to normalize the theoretical calculations to experiment, say at 20°. The other theoretical models, ie the many-body theory of Thomas *et al* (1974) and the distorted wave calculation of Shelton *et al* (1973) show only a single shallow minimum near 90° and 70° respectively (figure 4(a)).

At 40·1 eV our model again predicts two minima but only one (at 95°) is observed experimentally, and our results are much too small at both small and large angles. The

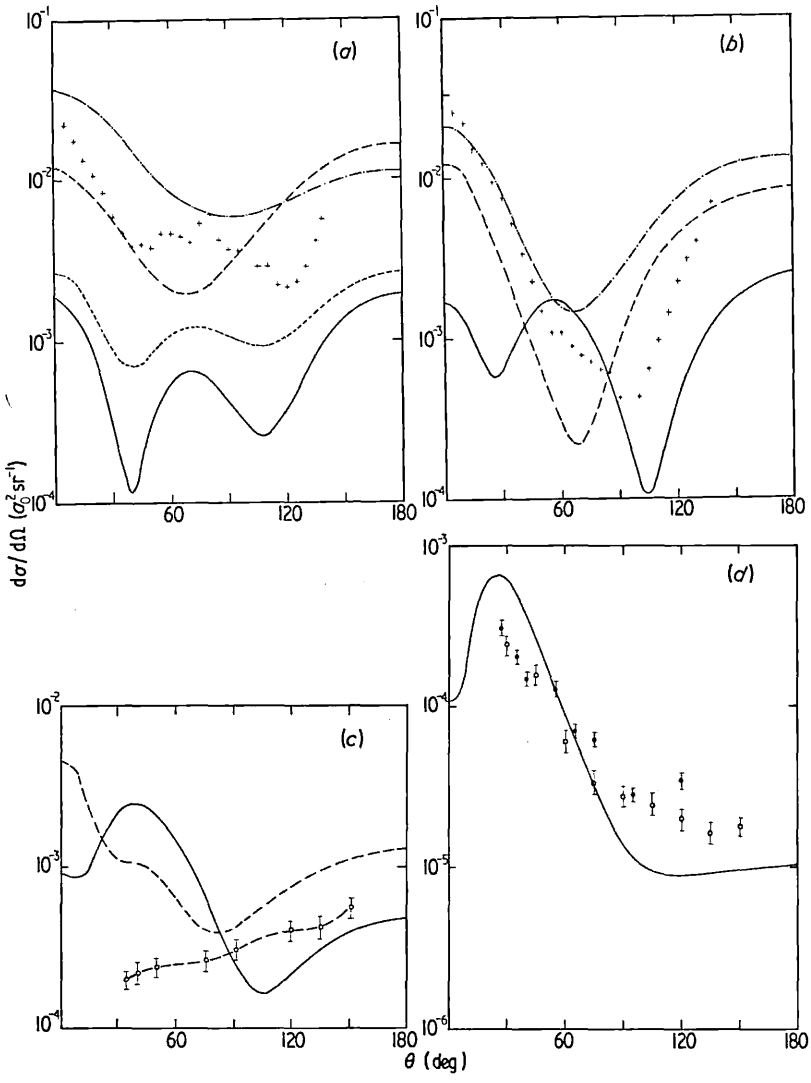

Figure 4. Differential cross section results for the excitation of the 2^3S state of helium by electron impact at (*a*) 29·6, (*b*) 40·1, (*c*) 81·63 and (*d*) 200 eV. (*a*) ——— present results employing the Cohen and McEachran excited state wavefunction, - - - - - present results employing the Hartree–Fock representation for the excited state wavefunction due to Morse *et al* (1935), – · – · – many-body theory (Thomas *et al* 1974), — — — distorted wave calculation of Shelton *et al* (1973), + experiment (Trajmar 1973). (*b*) as for (*a*). (*c*) ——— present results, — — — second-order optical potential distorted wave results (Bransden and Winters 1975), ○ experiment (Opal and Beaty 1972). (*d*) ◆ experiment (Suzuki and Takayanagi 1973). Other symbols as for (*c*).

other theoretical models shown in figure 4(*b*) (Thomas *et al* 1974, Shelton *et al* 1973) predict a single minimum, but at a much smaller angle (65°). At 81·6 eV neither our results nor those of Bransden and Winters (1975), shown in figure 4(*c*), bear much resemblance to each other or to the experimental data of Opal and Beaty (1972) except at large angles. At 200 eV (figure 4(*d*)), allowing for our underestimate at large angles through failure of our model to include final-channel distortion, the agreement with experiments of Opal and Beaty (1972) and of Suzuki and Takayanagi (1973) is reasonable. However, we find a sharp decrease in the differential cross section at small angles ($\theta < 25°$), which is known as an Ochkur dip. In treating excitation to triplet states our model is essentially first order apart from local distortions in the incident wave, whereas it is second order for transitions in which the direct amplitude enters. A more sophisticated treatment of exchange removes this forward dip (Byron and Joachain 1975).

Our calculated total cross sections for 2^3S are shown in figure 5. They are compared with the experimental measurements of Brongersma *et al* (1972), Trajmar (1973), Crooks *et al* (1972) and Vriens *et al* (1968) over the complete energy range. In addition we show the theoretical results of Thomas *et al* (1974) using lowest-order many-body theory and those of Winters (1974) using the second-order optical potential model. A close-coupling calculation by Smith *et al* (1973) (see however Seaton 1974) gives results a factor of 2·5 smaller than those of Winters (1974). The slopes of the theoretical results are in good agreement, though there is some disagreement as to the magnitude of the cross section below 80 eV. At higher energies our results and those of Winters are in essentially complete agreement.

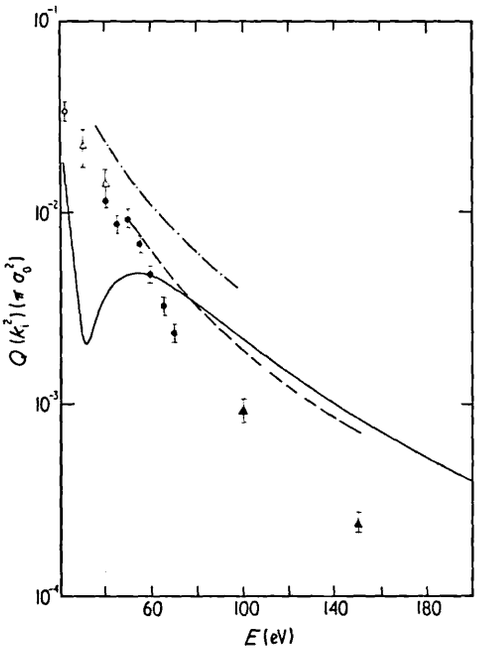

Figure 5. Theoretical and experimental total cross section results for the excitation of the 2^3S state of helium by electron impact. ——— present results, –·–·– many-body theory (Thomas *et al* 1974), — — — second-order optical potential distorted wave results (Winters 1974). Experimental results: △ Trajmar (1973), ○ Brongersma *et al* (1972), ◆ Crooks *et al* (1972), ▲ Vriens *et al* (1968).

However, the experimental results from 22 eV to 200 eV reported in four independent experiments, each in a separate energy range, form a consistent whole, and give an energy dependence which is much more rapidly decreasing at high energies than is the theory.

A confirmation of the results of Vriens *et al* (1968) (which involve an extrapolation from 5° to the forward direction) would be especially helpful in advancing our understanding of $^1S \rightarrow {}^3S$ transitions.

4.3. 3^1S excitation of helium

In view of the success of our model for 2^1S excitation we thought it worthwhile to extend the work to the 3^1S case. Our total cross sections are compared with experiment (Moustafa Moussa *et al* 1969) in figure 6. The second-order optical potential results (calculated in a nine-state impact parameter version) of Bransden and Issa (1975) are shown for comparison. Their results are available for $E \geqslant 200$ eV only, and lie slightly above ours at these energies, ours being within 10% of experiment in this range. At intermediate energies ($100 \leqslant E \leqslant 300$ eV) our results lie as much as 20% above the experimental data, but we are again in close agreement at lower energies. The overall agreement is highly satisfactory.

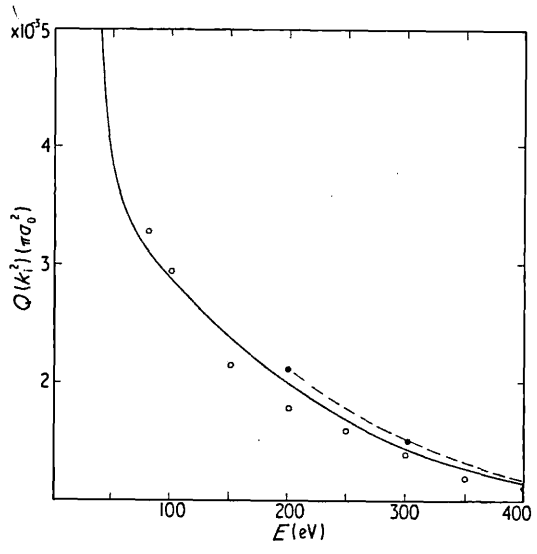

Figure 6. Theoretical and experimental total cross section results for the excitation of the 3^1S state of helium by electron impact. ——— present results (DWPO 1), — • — second-order optical potential model (Bransden and Issa 1975), o experiment (Moustafa Moussa *et al* 1969).

Neither of the available theoretical models (Taylor *et al* 1975, and this paper) give results in agreement with the experimental measurements of Chutjian and Thomas (1974) for the 3^1S differential cross section at 29·2 eV except at large angles (figure 7(*a*)), both theories predicting unstructured minima near 60° and failing to predict the forward peak. It may well be necessary to include explicitly coupling with 3^1P and 3^1D at least, to obtain agreement with experiment this close to threshold. However, similar calculations at 39·7 eV are in much better agreement with each other (figure 7(*b*)) and with

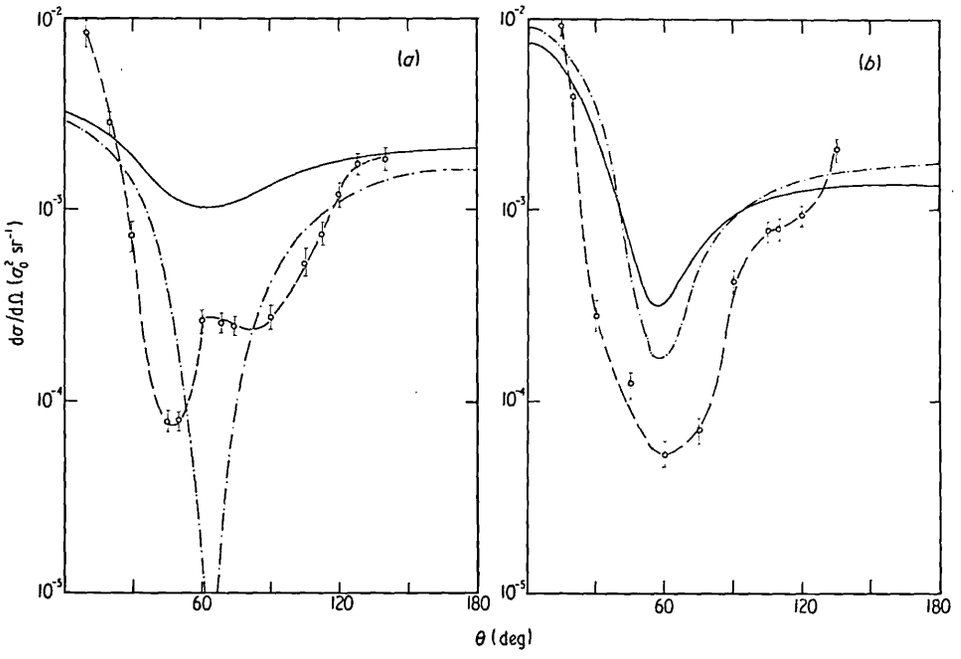

Figure 7. Differential cross section results for the excitation of the 3^1S state of helium by electron impact at (*a*) 29·2 and (*b*) 39·7 eV. (*a*) ——— present results (DWPO I), – · – · – many-body theory (Taylor *et al* 1974), – Q – experiment (Chutjian and Thomas 1974). (*b*) as for (*a*).

experiment, the minimum being in the correct position, but neither theory showing the structure observed near 110°.

5. Conclusion

We have presented the results of our distorted wave calculations of total and differential cross sections for electron impact excitation of the 2^1S, 2^3S, and 3^1S states of helium at energies between 30 and 300 eV. Detailed tables of our results will be published elsewhere (Scott 1976).

At low energies ($E < 100$ eV) we reproduce the shape of the ^1S absolute experimental measurements well, including the positions of the minima, but in common with other similar theoretical models we do not always predict accurately the depth of the minimum. At higher energies our model underestimates the backward scattering, and we believe this to be due to its failure to allow for distortion effects in the final channel.

Our model is less successful for 2^3S excitation, though it gives a better account of the detailed structure in the differential cross section at the lowest energy considered than the other available models, and yields total cross sections for 2^3S in good agreement with the work of Winters (1974) at energies above 80 eV. We believe that further experimental measurements of the total cross section for $1^1S \rightarrow 2^3S$ at energies above 100 eV would help to resolve the discrepancy between the two sets of theoretical results and the experimental data of Vriens *et al* (1968). A further measurement of the differential cross section at 80 eV would also be helpful†.

† Such measurements have been carried out by Pochat, Gelebert and Peresse (1975 private communication) and confirm Opal and Beaty's work.

The total cross sections for both the 2^1S and 3^1S transitions agree well with experiment at all energies. We intend to extend this work to higher members of the helium isoelectronic sequence which are of interest in plasma and astrophysical applications and to the 4^1S and 5^1S states (Scott and McDowell 1975).

Since the model yields results for the S–S transitions of comparable accuracy to the many-body theory model of Taylor and his colleagues it will be interesting to examine its predictions for S–P transitions, and in particular for the coincidence experiments of Eminyan *et al* (1974). This work is now under way.

Acknowledgments

One of us (TS) is indebted to the Science Research Council for a Postgraduate Studentship. We wish to thank Dr F J de Heer for a useful discussion of the experimental results, and Professor C Joachain and Dr E Lassettre for permission to quote unpublished results.

References

Bell K L, Eissa H and Moiseiwitsch B L 1966 *Proc. Phys. Soc.* **88** 57–63
Bell K L, Kennedy D J and Kingston A E 1969 *J. Phys.* B: *Atom. Molec. Phys.* **2** 26–43
Berrington K A, Bransden B H and Coleman J P 1973 *J. Phys.* B: *Atom. Molec. Phys.* **6** 436–49
Bransden B H and Coleman J P 1972 *J. Phys.* B: *Atom. Molec. Phys.* **5** 537–45
Bransden B H and Issa M R 1975 *J. Phys.* B: *Atom. Molec. Phys.* **8** 1088–94
Bransden B H and Winters K H 1975 *J. Phys.* B: *Atom. Molec. Phys.* **8** 1236–44
Brongersma H H, Knoop F W E and Backx C 1972 *Chem. Phys. Lett.* **13** 16–9
Burgess A 1963 *Proc. Phys. Soc.* **81** 442–52
Byron F W Jr and Joachain C J 1974 private communication to B H Bransden
—— 1975 *Phys. Rev.* to be published
Chutjian A and Thomas L D 1974 unpublished, but see Taylor *et al* (1975)
Cohen M and McEachran R P 1967a *Proc. Phys. Soc.* **92** 37–41
—— 1967b *Proc. Phys. Soc.* **92** 539–42
Crooks G B, DuBois R D, Golden D E and Rudd M E 1972 *Phys. Rev. Lett.* **29** 327–9
Crooks G B and Rudd M E 1972 *PhD Thesis* University of Nebraska
Crothers D S F and McEachran R P 1970 *J. Phys.* B: *Atom Molec. Phys.* **3** 976–90
Dillon M A and Lassettre E N 1975 *J. Chem. Phys.* to be published
Duxler W M, Poe R T and LaBahn R W 1971 *Phys. Rev.* A **4** 1935–44
Eminyan M, MacAdam K B, Slevin J and Kleinpoppen H 1974 *J. Phys.* B: *Atom. Molec. Phys.* **7** 1519–42
Green L C, Mulder M M, Lewis M N and Woll J W Jr 1954 *Phys. Rev.* **93** 757–61
Hall R I, Joyez G, Mazeau J, Reinhardt J and Scherman C 1973 *J. Physique* **34** 827–43
Hidalgo M B and Geltman S 1972 *J. Phys.* B: *Atom. Molec. Phys.* **5** 617–26
Joachain C J and Vanderpoorten R 1974 *J. Phys.* B: *Atom. Molec. Phys.* **7** 817–30
Lassettre E N 1965 *J. Chem. Phys.* **43** 4474–86
Martin P C and Schwinger J 1959 *Phys. Rev.* **115** 1342–73
McDowell M R C, Morgan L A and Myserscough V P 1973 *J. Phys.* B: *Atom. Molec. Phys.* **6** 1435–51
—— 1975 *J. Phys.* B: *Atom. Molec. Phys.* **8** 1053–72
McDowell M R C, Myerscough V P and Narain U 1974 *J. Phys.* B: *Atom. Molec. Phys.* **7** L195–7
Morse P M, Young L A and Haurwitz E S 1935 *Phys. Rev.* **48** 948–54
Moustafa Moussa H R, de Heer F J and Schutter J 1969 *Physica* **40** 517–49
Nicholls P S and Winters K H 1973 *J. Phys.* B: *Atom. Molec. Phys.* **6** L250–1
Oberoi R S and Nesbet R K 1973 *Phys. Rev.* A **8** 2469–79
Opal C B and Beaty E C 1972 *J. Phys.* B: *Atom. Molec. Phys.* **5** 627–35
Ormonde S and Golden D E 1973 *Phys. Rev. Lett.* **31** 1161–4

Rice J K, Truhlar D G, Cartwright D C and Trajmar S 1972 *Phys. Rev.* A **5** 762–82
Scott T 1976 *Thesis* University of London
Scott T and McDowell M R C 1975 *J. Phys.* B: *Atom. Molec. Phys.* **8** in press
Seaton M J 1974 *Quart. J. R. Astron. Soc* **15** 370–91
Shelton W N, Baluja K L and Madison D H 1973 *Proc. 8th Int. Conf. on Physics of Electronic and Atomic Collisions* (Beograd: Institute of Physics) Abstracts pp 296–7
Smith K, Golden D E, Ormonde S, Torres B W and Davies A R 1973 *Phys. Rev.* A **8** 3001–11
Suzuki H and Takayanagi T 1973 *Proc. 8th Int. Conf. on Physics of Electronic and Atomic Collisions* (Beograd: Institute of Physics) Abstracts pp 286–7
Taylor H S, Chutjian A and Thomas L D 1975 *Electron and Photon Interactions with Atoms* ed H Kleinpoppen and M R C McDowell (New York: Plenum)
Thomas L D, Csanak Gy, Taylor H S and Yarlagadda B S 1974 *J. Phys.* B: *Atom. Molec. Phys.* **7** 1719–33
Trajmar S 1973 *Phys. Rev.* A **8** 191–203
Vriens L, Simpson J A and Mielczarek S R 1968 *Phys. Rev.* **165** 7–15
Winters K H 1974 *PhD Thesis* University of Durham
Yates A C and Tenney A 1972 *Phys. Rev.* A **6** 1451–6

J. Phys. B: Atom. Molec. Phys., Vol. 8, No. 14, 1975. Printed in Great Britain.

Electron impact excitation of He(n^1S), ($n = 4, 5$) at intermediate energies

T Scott and M R C McDowell

Mathematics Department, Royal Holloway College, Englefield Green, Surrey TW20 0EX, England

Received 5 May 1975

Abstract. The distorted wave polarized orbital approximation is applied to the excitation of 4^1S and 5^1S levels of helium. Results are presented for total cross sections over an electron impact energy range of 25 to 400 eV and also for small-angle differential cross sections at impact energies of 50, 60, 100 and 200 eV. These are compared with experiment and the accurate Born results of Bell *et al.* The introduction of explicit s–p coupling into the T matrix has a marked influence on the small-angle differential cross sections, producing a strong enhancement, and bringing them into close agreement with experiment at the highest energy considered.

1. Introduction

We extend the work of a previous paper (Scott and McDowell 1975 to be referred to as I) which discussed $n \leqslant 3$ only, by applying the distorted wave polarized orbital model (DWPO) outlined in I to calculate both total and small-angle differential cross sections for electron impact excitation of the 4^1S and 5^1S states of helium from its ground state. In particular, we shall examine in more detail the effect of explicit inclusion of coupling between S and P states in the direct term of the T matrix.

We outline briefly the theoretical model described in I. The T matrix may be written

$$T_{if} = \langle \Phi_f V_f \Psi_i^+ \rangle \tag{1}$$

where the notation follows that adopted in I. Consequently the differential cross section, $I(\Omega)$, is given by

$$I(\Omega) = \frac{1}{4\pi^2} \frac{k_f}{k_i} |T_{if}|^2 \qquad a_0^2 \text{ sr}^{-1} \tag{2}$$

and by integrating over all solid angles the total cross section, Q_{if}, is obtained in the form

$$Q_{if}(k_i^2) = \frac{1}{2\pi^2} \frac{k_f}{k_i} \int_{-1}^{1} |T_{if}|^2 \, \mathrm{d}(\cos\theta) \quad \pi a_0^2. \tag{3}$$

Recalling I(14) we express the T matrix of our DWPO I model as

$$T_{if}^{+} = \langle \psi_f(12, 3) V_f \phi_i(12) F(3) \rangle - \langle \psi_f(12, 3) V_f \phi_i(23) F(1) \rangle \tag{4}$$

where polarization effects are included only implicitly through the distorted wave $F(r)$.

In the DWPO II model we restate I(22) and I(23) whereby the transition matrix becomes

$$T_{if}^{mod} = T_{if}^{+} + T_{if}^{pol} \tag{5}$$

with T_{if}^{+} as above and T_{if}^{pol} given by

$$T_{if}^{pol} = 2\langle \psi_f(12, 3) V_f \phi_{1s}(1) \phi_{pol}(23) F(3) \rangle. \tag{6}$$

We note that $\phi_{pol}(r, t)$ is the dipole component of the perturbed atomic wavefunction and provides a coupling between the S and P states of the atom. Hence DWPO II allows explicitly for polarization distortion of the ground state of the target atom.

Following exactly the procedure indicated in I, the distorted wave $F(r)$ is decomposed into partial waves which satisfy the radial scattering equation I(17). We emphasize that the effect of polarization is taken into account via the direct potential term $V_{pol}(r)$ (equation (21) of I) but that the terms arising from exchange polarization effects and all other non-adiabatic effects are neglected.

We have obtained results in both DWPO I and DWPO II approximations and compare our total cross sections with the experimental work of St John *et al* (1964), Moustafa Moussa *et al* (1969), van Raan *et al* (1971) and Pochat *et al* (1973). In addition the differential cross sections calculated at four intermediate impact energies, over the angular range from 0° to 20°, are compared with the recent experimental data of Pochat (1973). At 100 eV and 200 eV we also make a comparison with the Born approximation deduced from the accurate generalized oscillator strengths tabulated by Bell *et al* (1969).

Each experimental group claims their results to be absolute and for convenience we briefly summarize their methods of normalization.

The highest values are obtained by St John *et al* (1964), and may be influenced by the relatively high current electron beam ($\simeq 1$ mA) used. They used published values to correct for the polarization of the emitted radiation, and apparently did not correct for instrumental polarization effects.

Moustafa Moussa *et al* (1969) normalized via their $2^1S \rightarrow 2^1P$ value, which in turn depends on the theoretical optical oscillator strength for that transition. However, different monochromators are required for 2^1P (where the radiation is in the vacuum UV) and for 4^1S where the radiation is in the visible. The transfer between instruments may introduce error. In addition these authors used published polarization data.

Pochat *et al* (1973) normalize via the measurement of the 2^1P differential cross section which is scaled to the 5° value of Chamberlain *et al* (1970).

In the experiment of van Raan *et al* the measurements were carried out at low gas pressures and low electron current to avoid certain problems discussed by Heideman (1968). Their quoted results, which we use, are based on their own absolute calibration with a tungsten lamp and an independent measurement of the polarization. However these results imply a high value for the $1^1S \rightarrow 3^1P$ optical oscillator strength, and if we renormalize their data to the theoretical value (Schiff and Pekeris 1964) this reduces it by 10% and brings it into close agreement with our DWPO II values.

The best values, in our view, would lie between those of van Raan *et al* (1971) (which are close to those of Pochat *et al* 1973) and the lower results of Moustafa Moussa *et al* (1969).

2. Results

2.1. 4^1S excitation of helium

The total cross sections obtained from both approximations for the transition $1^1S \rightarrow 4^1S$ are plotted in figure 1, where they are compared with experiment. We have denoted the coincidence of experimental points of two groups (to within plotting accuracy) by parenthesis. The presence of the shoulder lying between 60 and 150 eV has been noted in $1^1S \rightarrow 2^1S$ and $1^1S \rightarrow 3^1S$ transitions (I) but is more pronounced for the 4^1S excitation.

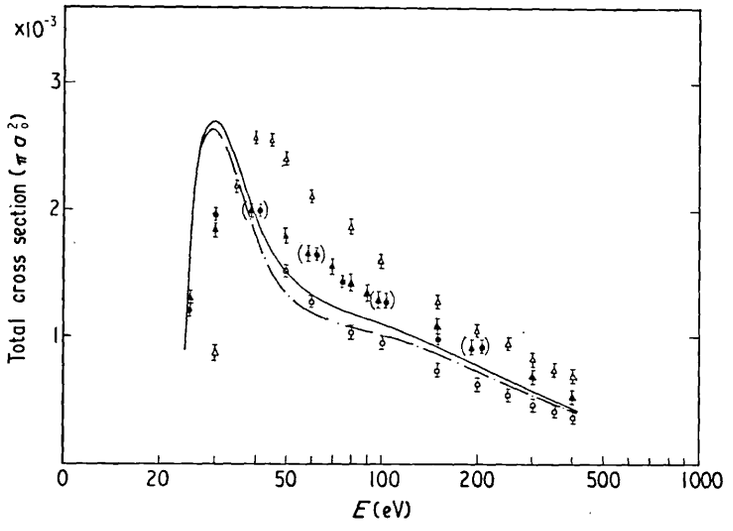

Figure 1. Theoretical and experimental total cross section results for the excitation of the 4^1S state of helium by electron impact. —— present results (DWPO I), —·— present results (DWPO II), ♦ experiment (Pochat *et al* 1973), ▲ experiment (van Raan *et al* 1971), ○ experiment (Moustafa Moussa *et al* 1969), △ experiment (St John *et al* 1964).

Our results, particularly in DWPO II, are in very close accord with the tabulated data of Moustafa Moussa *et al* (1969) and we see that there is evidence from their results for the existence of such a shoulder. The results of Pochat *et al* (1973) and of van Raan *et al* (1971) are seen to exhibit similar shapes but with a slight rise at the position where we predict a shoulder. However, the results of our models are too large compared with these experiments at energies below 40 eV and at higher energies tend to lie approximately 20% below the experimental points of these two groups.

The peak obtained by St John *et al* (1964) is of comparable magnitude to ours but generally the agreement is poor. We observe that our peak, occurring at 30 eV, does not coincide with that of any of the experiments. Both Pochat *et al* (1973) and van Raan *et al* (1971) find a maximum lying closer to 40 eV.

The differential cross sections for small-angle scattering (0°–20°) are illustrated in figure 2 and are presented at four impact energies. The experimental data are due to Pochat (1973). For the lower energies of 50 and 60 eV, DWPO I is poor but DWPO II results show an improvement for scattering angles above 15°. At 100 eV, DWPO II predicts a close correspondence for angles above 10° and the forward enhancement compared with the DWPO I result becomes increasingly important. The first Born approximation result

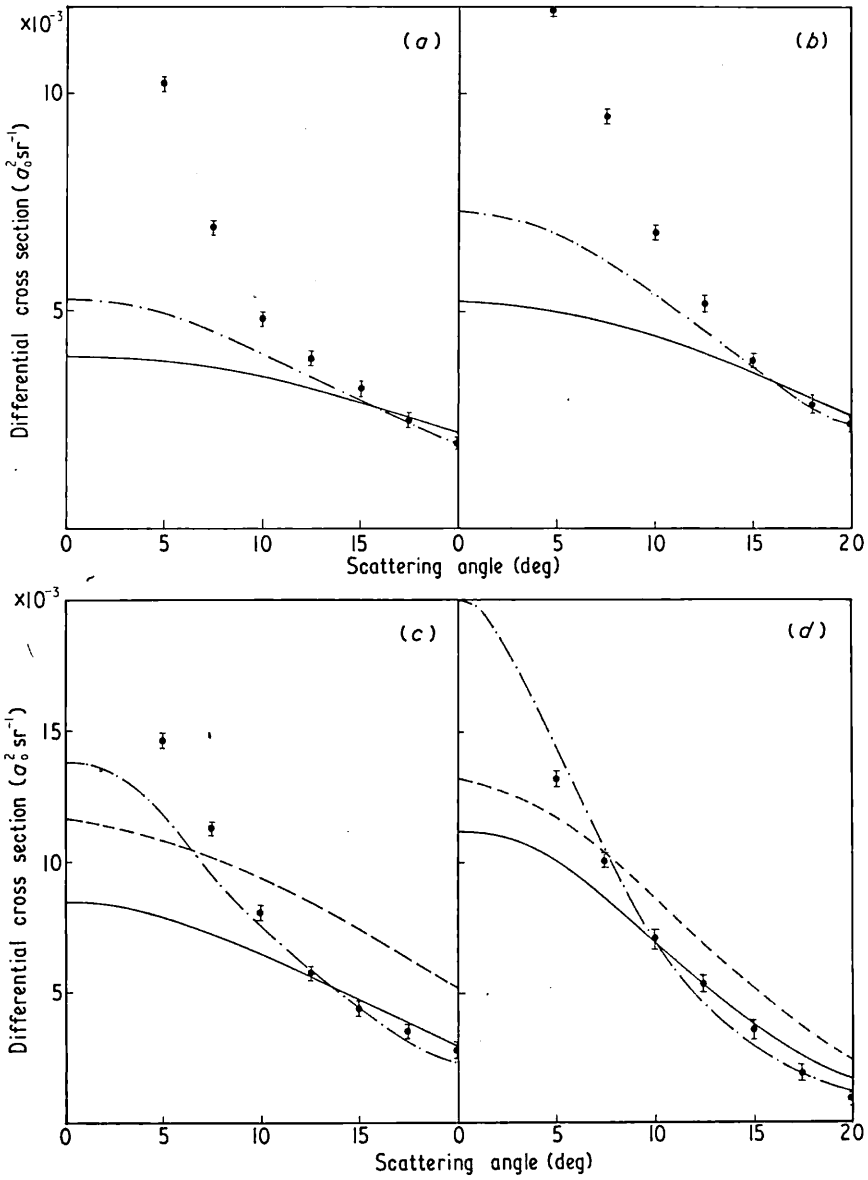

Figure 2. Theoretical and experimental differential cross section results for the excitation of the 4^1S state of helium by electron impact at (*a*) 50 eV, (*b*) 60 eV, (*c*) 100 eV and (*d*) 200 eV. ---- first Born approximation due to Bell *et al* (1969). Other symbols as for figure 1.

deduced from the accurate generalized oscillator strengths given by Bell *et al* (1969) is shown for the higher energies, and is seen to lie between DWPO I and DWPO II and to correspond closely in shape to our DWPO I results.

By 200 eV, the forward enhancement produced by the DWPO II model (including s–p coupling) gives results essentially in complete agreement with Pochat's measurements over this angular range. We also see that our DWPO I curve approaches the Born for higher energies, as we should expect since the Born approximation is the high-energy limit of DWPO I (McDowell *et al* 1975).

2.2. 5^1S excitation of helium

Figure 3 illustrates the total cross section in both approximations and also shows the experimental work of the groups listed for 4^1S excitation. The shoulder predicted by our theory has become comparatively more prominent but extends over the same energy range as for previous singlet–singlet cross sections. Our peak value occurs approximately at 30 eV which is similar to that for 4^1S excitation.

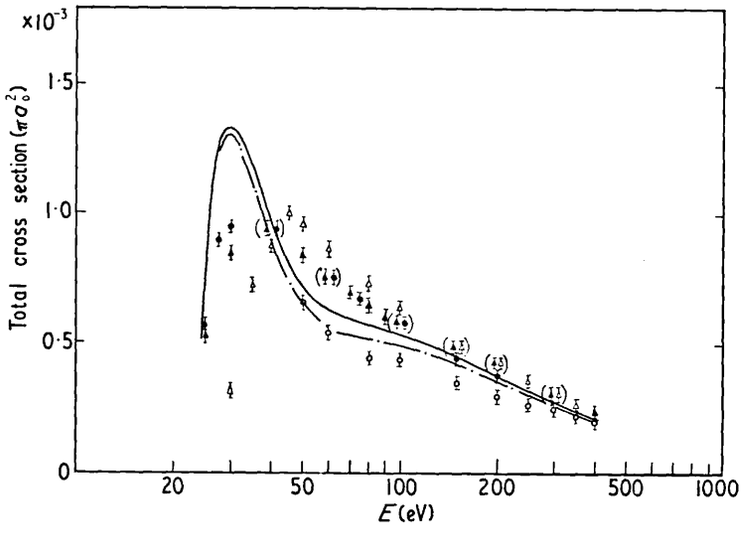

Figure 3. Theoretical and experimental total cross section results for the excitation of the 5^1S state of helium by electron impact. Symbols as for figure 1.

The points due to Moustafa Moussa *et al* (1969) again afford evidence for such a shape but we note that both our curves lie higher than their data for energies above 60 eV whereas for the 3^1S (I) and 4^1S cases, agreement is very close. At impact energies above 150 eV our results are in best accord with the two measurements of Pochat *et al* (1973), but in general there is close agreement between theory and all the experiments above this energy. Below 150 eV the work of Pochat *et al* (1973) and the tabulated points of van Raan *et al* (1971) agree well and give a similar variation with energy to that found for 4^1S. Their data lie above our results for energies greater than 40 eV, but the former group indicate a maximum at about 35 eV whereas the latter seem to predict the peak close to 40 eV.

The data of St John *et al* (1964) exhibit a generally shifted curve and tend to have an overall magnitude higher than that found by the other experimental groups. Their peak value does not reach the same magnitude as given by our theory whereas for the $1^1S \rightarrow 4^1S$ cross section, the absolute magnitudes are comparable. In summary, the agreement at impact energies above 150 eV is satisfactory but below this figure there remains a discrepancy between both theory and experiment, and among the different experiments. It is perhaps worth observing that for both 4^1S and 5^1S excitation the effect of coupling the S and P states only begins to become apparent after the peak value of the total cross section has been reached, and has little effect on the total cross sections at energies above 200 eV.

Turning now to the differential cross section for scattering angles between 0° and 20°, we compare our theory with the absolute experimental results of Pochat (1973) at energies of 50, 60, 100 and 200 eV. The comparison is shown in figure 4. For 100 and 200 eV impact energies we have also plotted the Born approximation results which we deduced from the generalized oscillator strengths of Bell *et al* (1969), as for the 4^1S case. The situation resembles closely that for the previous case. The DWPO II model produces an increasing forward enhancement relative to DWPO I as the impact energy is increased,

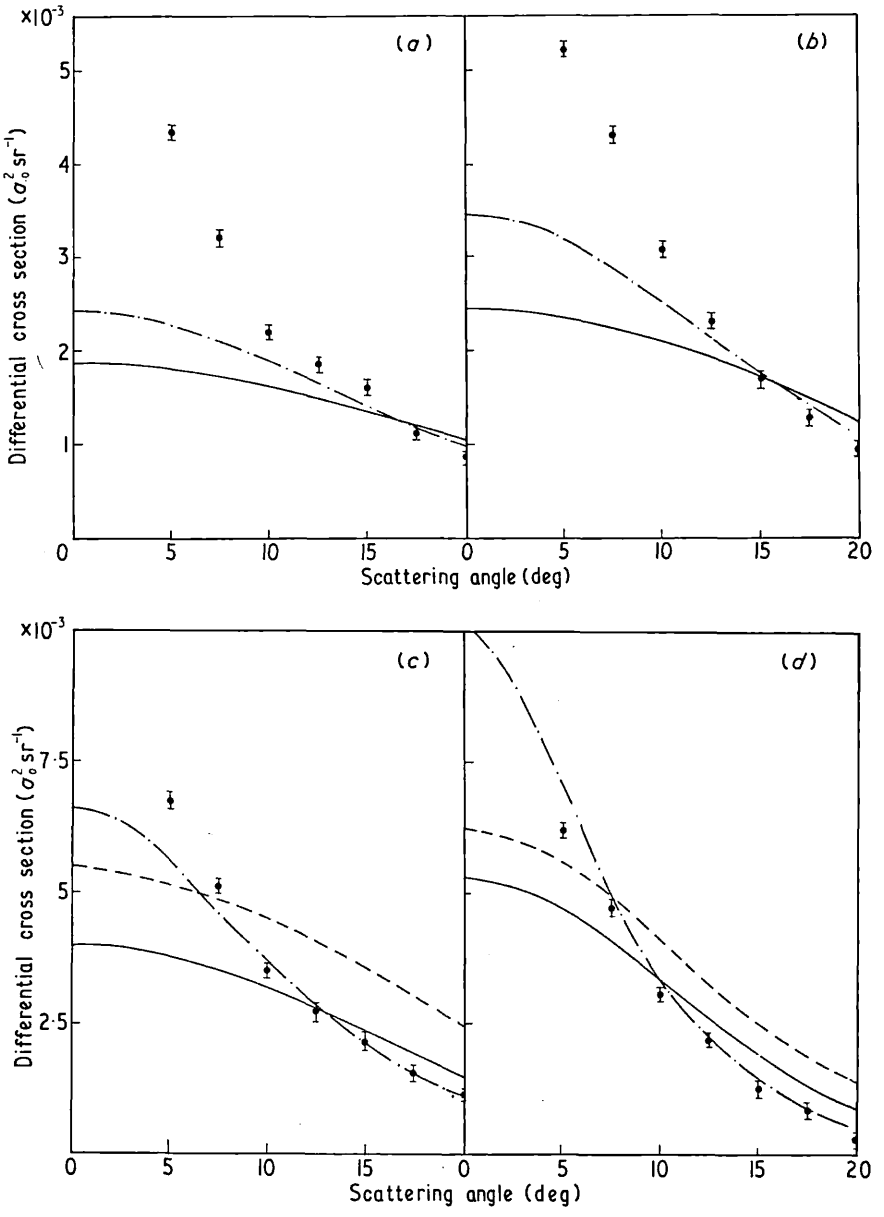

Figure 4. Theoretical and experimental differential cross section results for the excitation of the 5^1S state of helium by electron impact at (*a*) 50 eV, (*b*) 60 eV, (*c*) 100 eV and (*d*) 200 eV. Symbols as for figure 2.

becoming more and more in line with the experimental data of Pochat (1973). At 100 eV we see that DWPO II predicts the cross section well over the latter half of the angular range concerned, and at 200 eV DWPO II produces sufficient forward enhancement to agree most satisfactorily with the experimental data over the whole of this angular range. The results obtained in the first Born approximation again exhibit a similar behaviour to those of the DWPO I model, which approach the FBA at high energies. Contrary to what might have been expected we see that even at 200 eV the first Born approximation fails to give a satisfactory account of small-angle scattering.

3. Conclusions

We have calculated total and differential cross sections for

$$e + He(1^1S) \rightarrow e + He(n^1S), \qquad n = 4, 5$$

at low and intermediate energies, in a distorted wave model, both with and without target distortion.

The shape of the experimental total cross section is well reproduced by both models, at energies above 40 eV, though the theoretical models give the maximum cross section at a lower energy than is found experimentally. At energies between 40 and 100 eV the results of different experimental groups differ by a factor of two whereas the difference between our two theoretical models is at most 5%. We cannot, therefore, distinguish between these on the basis of total excitation cross section data.

The recent small-angle differential cross section measurements of Peresse and his colleagues (Pochat 1973, Pochat *et al* 1973) do, however, allow such a distinction to be drawn. We find that models without target distortion ('s–p coupling') such as the first Born approximation and DWPO I do not account for the observed strong enhancement of these inelastic differential cross sections in the forward direction. Inclusion of target distortion (in the ground state) as in our DWPO II model gives a completely satisfactory account of the measurements at 200 eV, though failing to an increasing extent with decreasing impact energy.

We can describe this forward enhancement as due to elastic scattering off intermediate P states by a polarization-type interaction. The increasing inadequacy of this model at energies below 100 eV suggests that our failure to include exchange polarization terms may be significant at such low energies.

Acknowledgments

We are indebted to Professor J Peresse and Dr A Pochat for drawing our attention to their work, and for helpful discussions. One of us (TS) is the holder of an SRC Research Training Support Grant.

References

Bell K L, Kennedy D J and Kingston A E 1969 *J. Phys.* B: *Atom. Molec. Phys.* **2** 26–43
Chamberlain G E, Mielczarek S R and Kuyatt C E 1970 *Phys. Rev.* A **2** 1905–22
Heideman H G M 1968 *Thesis* University of Utrecht

McDowell M R C, Morgan L A and Myerscough V P 1975 *J. Phys.* B: *Atom. Molec. Phys.* **8** 1053–72
Moustafa Moussa H R, de Heer F J and Schutten J 1969 *Physica* **40** 517–49
Pochat A 1973 *Thesis* L'Universite de Bretagne Occidentale
Pochat A, Rozuel D and Peresse J 1973 *J. Physique* **34** 701–9
van Raan A F J, De Jongh J P, Van Eck J and Heideman H G M 1971 *Physica* **53** 45–59
St John R M, Miller F L and Lin C C 1964 *Phys. Rev.* **134** A888–97
Schiff B and Pekeris C L 1964 *Phys. Rev.* **134** A638–40
Scott T and McDowell M R C 1975 *J. Phys.* B: *Atom. Molec. Phys.* **8** 1851–65

J. Phys. B: Atom. Molec. Phys., Vol. 9, No. 8, 1976. Printed in Great Britain. © 1976

Equivalent exchange potentials in electron scattering

B H Bransden†§, M R C McDowell‡, C J Noble† and T Scott‡

† School of Physical Sciences, The Flinders University of South Australia, Bedford Park, South Australia 5042, Australia

‡ Mathematics Department, Royal Holloway College, University of London, Egham, Surrey, England

Received 24 December 1975

Abstract. A number of local potentials have been suggested to represent the non-local exchange kernel in electron–atom scattering. A comparative numerical study has been made in which phase shifts for the elastic scattering of electrons by H, He^+ and He using these potentials are tested against those calculated from the exchange integro–differential equations. The influence of additional long range polarization potentials is also investigated. It is shown that, except at the lowest energies, exchange effects can be represented accurately by the Furness–McCarthy and related potentials.

1. Introduction

In developing equations to determine the wavefunction for the elastic scattering of electrons by atoms, many authors have replaced the integral kernel describing the exchange interaction by an equivalent local potential. This has the advantage of making the scattering equations easier to solve numerically and the procedure might be expected to be accurate at high energies for which exchange effects are comparatively small.

Although a fairly large number of variants of the equivalent local potential have been suggested, no systematic study of the accuracy of the resulting phase shifts or of the range of energies over which these potentials may be employed has yet appeared‖. In this paper, after reviewing briefly the derivation of the selected equivalent potentials, we use these to calculate phase shifts within a simple model for which the exact phase shifts can be calculated.

The model we have chosen is the static exchange approximation for electron scattering by the ground states of H, He^+ or He. We have also investigated whether the presence of an additional polarization potential modifies the accuracy with which the exchange potentials represent the effect of the exchange kernel.

2. The exchange equations

The static exchange equation¶ describing the elastic scattering of electrons by an

§ Permanent address: The University of Durham, South Road, Durham, England.

‖ See however, Riley and Truhlar (1976).

¶ The derivation of the static exchange equation has been discussed by Bransden (1970) and by Mott and Massey (1965).

atomic target has the form, in atomic units

$$[\nabla^2 + (2Z/r) + k^2]\, F(r) = 2V_s(r)\, F(r) + 2\tau \int K(r, r')\, F(r')\, \mathrm{d}r'. \tag{1}$$

In this equation, Z is the net charge on the target atom or ion, $\frac{1}{2}k^2$ is the energy of the incident electron, $V_s(r)$ is the static interaction between the atom and the incident electron, and $K(r,r')$ is the exchange kernel. The parameter τ is -1 for the scattering of electrons by H or He^+ when the overall spin is $S = 1$, the triplet state, and is $+1$ when the overall spin is $S = 0$, the singlet state. When the target is neutral helium $\tau = -1$. The model represented by equation (1) makes no allowance for inelastic channels. With the addition of a polarization potential, it does however represent elastic scattering rather well, even at high energies, although strictly the effective potential develops an imaginary component above the lowest inelastic threshold.

The static interaction $V_s(r)$ is the matrix element of the instantaneous interaction between the electron and the target with respect to the ground state target wavefunction. The ground state wavefunction is denoted by $\phi(x)$ for H and He^+, where

$$\phi(x) = (\alpha^3/\pi)^{1/2}\, \mathrm{e}^{-\alpha x} \tag{2}$$

with $\alpha = 1$ for H and $\alpha = 2$ for He^+. For helium we employ the approximate wavefunction of Byron and Joachain (1966)

$$\Phi(x_1, x_2) = \phi(x_1)\, \phi(x_2), \tag{3}$$

with

$$\phi(x) = (N/\sqrt{4\pi})\, (\mathrm{e}^{-\alpha x} + \beta \mathrm{e}^{-\gamma x}),$$

$N = 2{\cdot}6051$, $\alpha = 1{\cdot}41$, $\beta = 0{\cdot}799$ and $\gamma = 2{\cdot}61$.

In each case $V_s(r)$ has the form

$$V_s(r) = \mu \int \mathrm{d}x |\phi(x)|^2 \left(\frac{1}{|x - r|} - \frac{1}{x}\right), \tag{4}$$

with $\mu = 1$ for H and He^+ and $\mu = 2$ for He, and the corresponding exchange kernel is

$$K(r, r') = \phi(r)\, \phi(r')\, [-(\tfrac{1}{2}k^2 - \epsilon) + (1/|r - r'|)] \tag{5}$$

where ϵ is the ground state energy of the target.

By expanding the wavefunction $F(r)$ in partial waves, and solving the resulting radial equations numerically, the exact phase shifts in the static exchange model have been obtained in the momentum interval $0{\cdot}5 \leqslant k \leqslant 10{\cdot}0$ for $0 \leqslant l \leqslant 8$. To examine the exchange potentials in the presence of polarization we have also obtained the exact phase shifts when a polarization potential $V_p(r)$ is added to the static potential V_s. We shall refer to this case as the adiabatic-exchange model. For this purpose, we chose the form (Bransden 1970) for electron scattering by H and He^+

$$V_p^A(r) = -\frac{9}{4y^4}\left[1 - \frac{4}{27}\mathrm{e}^{-2y}\left(y^5 + \frac{9}{2}y^4 + 9y^3 + \frac{27}{2}y^2 + \frac{27}{2}y + \frac{27}{4}\right)\right], \tag{6}$$

where $y = r$ for H, $y = 2r$ for He^+.

At the lower energies, for $k \leqslant 1$ for H, and $k \leqslant 2{\cdot}0$ for He^+, our phase shifts can be compared with those published in the literature and collected together by Mott and Massey (1965) and Drachman and Temkin (1972). The agreement is excellent.

For scattering by neutral helium, the method of Duxler *et al* (1971) (see Drachman and Temkin 1972) allows an approximation consistent with the wavefunction (3) to be obtained. Calculations were carried out with this potential, denoted by $V_p^B(r)$, which has the explicit form

$$V_p^B(r) = -\frac{2}{3r^4}\frac{N}{\sqrt{Z_0}}\sum_{i=1}^{2} C_i\left\{\frac{24p_i}{Z_i^5} - \left[\left(\frac{24}{Z_i^5} + \frac{24r}{Z_i^4} + \frac{12r^2}{Z_i^3} + \frac{4r^3}{Z_i^2} + \frac{r^4}{Z_i}\right)p_i + \frac{Z_0 r^5}{Z_i}\right]e^{-Z_i r}\right\}, \tag{7}$$

where

$$C_1 = 1, C_2 = \beta, Z_1 = \alpha + Z_0, Z_2 = \gamma + Z_0, p_i = 2 + (5Z_0/Z_i), \qquad i = 1,2. \tag{8}$$

The parameters α, β, γ are defined below equation (3), and the scaling parameter Z_0 is $Z_0 = 1{\cdot}60315$.

For comparative purposes, we also made calculations with the simple Buckingham polarization potential

$$V_p^C(r) = -\frac{9}{4[(Zr)^2 + d^2]^2}, \tag{9}$$

where the parameter d was chosen to be 1·0 and the effective charge Z is 1 for H, 2 for He^+ and 1·341 for He. Electron–helium calculations were also performed using potential (6) with $y = 1{\cdot}341r$, consistent with a polarizability of 1·39.

3. The exchange potentials

The term proportional to $(\frac{1}{2}k^2 - \epsilon)$ in the exchange kernel only contributes to scattering in the $l = 0$ partial wave. Such behaviour cannot be represented by a non-singular potential, and it has been usual either to drop the term completely, or to remove it by requiring the function $F(r)$ to be orthogonal to $\phi(r)$. In the case of the $S = 1$, triplet state for the electron–hydrogen system, this does not involve modification of equation (1), because it is easily shown that if $F(r)$ is a particular solution of the equation then $F(r) + \lambda\phi(r)$ is also a solution. It is then possible to pick λ so that the orthogonality condition is satisfied. For the $S = 0$, singlet state, $F(r)$ can also be made orthogonal to $\phi(r)$ but at the expense of including an inhomogeneous term proportional to $\phi(r)$ in equation (1). In the published applications of the potentials to be described (with some exceptions), no attempt has been made to ensure that the computed wavefunction is in fact orthogonal to $\phi(r)$, and for this reason we have followed the same course. The orthogonality condition is only important at low energies† ($k \leqslant 1$), because the oscillatory nature of $F(r)$ ensures that the overlap

† This statement is not necessarily true in other contexts, for example, when the wavefunction $F(r)$ is required in the calculation of ionization cross sections.

between $F(\boldsymbol{r})$ and $\phi(r)$ is in any case small, and decreasing for increasing k. Thus in this approximation,

$$\int K(r, r')\, F(r')\, \mathrm{d}r' \approx \phi(r) \int (1/|r - r'|)\, \phi(r')\, F(r')\, \mathrm{d}r', \tag{10}$$

and the problem is then to determine a potential $V_{\mathrm{E}}(r)$ such that

$$V_{\mathrm{E}}(r)\, F(r) = \int K(r, r')\, F(r')\, \mathrm{d}r'. \tag{11}$$

It should be noted that strictly it is not necessary to satisfy this strong condition, because all that is required is that the functions $F(\boldsymbol{r})$ and $F(\boldsymbol{r}')$ on the left and right hand sides of (11) should have the same phase shifts to a good approximation. However in what follows, the functions will be chosen to be identical.

3.1. Expansion methods

The first group of potentials which we shall consider involve the Taylor expansion of the function $F(\boldsymbol{r}')$ about the point $\boldsymbol{r}' = \boldsymbol{r}$. In general, this will lead to a series of velocity dependent potentials as discussed in chapter 8 of the monograph by Mott and Massey (1965). The very simplest approximation of this type is to retain just the first term of such an expansion. In which case, we have from (11)

$$V_{\mathrm{E}}^{(1)}(r) = \phi(r) \int \frac{\phi(r')}{|\boldsymbol{r}' - \boldsymbol{r}|}\, \mathrm{d}r'. \tag{12}$$

This potential has been employed by Yu (1975) to calculate orbitals for bound states from which generalized oscillator strengths are calculated. Because the momentum dependence of $V_{\mathrm{E}}^{(1)}$ is ignored, this approximation would not be expected to be satisfactory except at low energies. Calculation shows that this potential is much too strong for small k which suggests that in the bound state problem, for highly excited states near the continuum, it will not be a satisfactory approximation either.

To retain the momentum dependence of the potential, Furness and McCarthy (1973) follow Perey and Buck (1962) in expanding the product $\phi(r')F(r')$

$$V_{\mathrm{E}}(r)\, F(r) = \phi(r) \int (1/|r - r'|) \exp[(r' - r).\nabla]\, [\phi(r)\, F(r)]\, \mathrm{d}r'.$$

Because $[\phi(r)F(r)]$ is square integrable, the integration can be carried out to give

$$V_{\mathrm{E}}(r)F(r) = 4\pi\phi(r)|\nabla|^{-2}[\phi(r)F(r)], \tag{13}$$

where the inverse operator $|\nabla|^{-2}$ acts to the right on $[\phi(r)F(r)]$. Since $\boldsymbol{p} = -\mathrm{i}\nabla$ is the momentum operator, further approximations, valid at high energies, can be made; first, the action of $\boldsymbol{p}$ on $\phi(r)$ can be ignored and secondly, $\boldsymbol{p}$ can be replaced by the local classical momentum, i.e.

$$p^2 \rightarrow p_{\mathrm{c}}^2 = (k^2 - 2V(r)), \tag{14}$$

where $V(r) = V_{\mathrm{D}}(r) + \tau V_{\mathrm{E}}(r)$, and V_{D} is the direct potential, $V_{\mathrm{D}}(r) = V_{\mathrm{s}}(r) + (Z/r) + V_{\mathrm{p}}(r)$.

The accuracy of the first of these approximations depends on the variation of $\phi(r')$ with r' being much smoother than the variation of $F(r')$, so that $\phi(r')$ can be replaced by $\phi(r)$ in (10).

Combining (13) and (14) provides a quadratic equation for V_E, from which τV_E is found to be

$$\tau V_E^{(2)} = \tfrac{1}{4}\{k^2 - 2V_D(r) - [(k^2 - 2V_D(r))^2 - 32\pi\tau|\phi(r)|^2]^{1/2}\}, \tag{15}$$

where the solution is chosen so that $V_E(r) \to 0$ as $k \to \infty$.

In their original paper, Furness and McCarthy gave a slightly different expression for $V_E^{(2)}$, but the correct result was first given by Vanderpoorten (1975).

In circumstances for which the exchange potential is less important than the direct potential it is permissible to write

$$V_E^{(3)}(r) = \frac{4\pi|\phi(r)|^2}{k^2 - 2V_D(r)}. \tag{16}$$

This is a particularly useful expression because it can be easily generalized for use in the coupled channel approach to inelastic scattering. For example, Bransden and Noble (1976) have discussed electron scattering by hydrogen and helium ions in a coupled channel approximation, employing a matrix exchange potential, which preserves time reversal invariance,

$$V_{ij} = 2\pi\phi_i^*(r)\phi_j(r)[(k_i^2 + |2\epsilon_i| - 2V_{ii})^{-1} + (k_j^2 + |2\epsilon_j| - 2V_{jj})^{-1}]$$

where i and j label the different channels and the corresponding orbitals and other quantities. A similar potential has been proposed by Riley and Truhlar (1976).

In the high energy limit, the Furness–McCarthy potential becomes

$$V_E^{(4)}(r) = \frac{4\pi|\phi(r)|^2}{k^2}. \tag{17}$$

In the first Born approximation, Vanderpoorten has pointed out that this potential gives the Ochkur approximation to the exchange amplitude. In this connection it should be noted that the comparative study of approximations to the exchange amplitude by Abiodun and Seaton (1966) has already shown that the Ochkur exchange amplitude in the static-exchange model is, for $l = 0$, accurate to a few per cent for $k > 2$.

It is not necessary to ignore completely the operation of $\boldsymbol{p}$ on the target wavefunction $\phi(r)$. To the first approximation, it can be taken into account (Bransden and Noble 1975) in the expression for the local momentum, which becomes

$$p_c^2 = k^2 + |2\epsilon| - 2V(r), \tag{18}$$

where ϵ is the ground state energy of the target atom. Each of the expressions (15) to (17) will be modified appropriately. We have chosen just two of these for numerical study:

$$V_E^{(5)}(r) = \frac{4\pi|\phi(r)|^2}{k^2 + |2\epsilon| - 2V_D(r)}, \tag{19}$$

and

$$V_E^{(6)}(r) = \frac{4\pi|\phi(r)|^2}{k^2 + |2\epsilon|}. \tag{20}$$

In the first Born approximation $V_E^{(6)}(r)$ yields the exchange amplitude suggested by Bely (1967) as an improvement on the Ochkur approximation.

3.2. Slater potentials

We now consider a group of potentials which resemble the well known Slater potential (Slater 1951) employed in bound state problems, which has the form

$$V_E^{(7)}(r) = A\left|\frac{3}{4\pi}\rho(r)\right|^{1/3}, \tag{21}$$

where $\rho(r)$ is the electron density, and A is a constant. It is easy to verify that if A has the magnitude required by bound state problems (Herman and Skillman 1963), the resulting potential is quite unsuitable for representing exchange effects in scattering problems, being considerably too large. Bauer and Browne (1964) adjusted the constant A so that for $l = 0$, the best possible agreement was obtained with the exact low energy electron–hydrogen phase shifts, in the energy interval $k < 0{\cdot}8$. In the singlet state, the additional constraint was imposed that $F(r)$ was orthogonal to the bound state solution of the equations representing H^-. The orthogonality condition $\langle\phi|F\rangle = 0$, discussed above, was also imposed. Bauer and Browne showed how to apply their potential to electron scattering by complex atoms and achieved considerable success at low energies. In the present work, we have tested this potential at higher energies and in angular momentum states with $l \neq 0$. For $l = 0$, we have not imposed the orthogonality conditions, so that we obtain slightly different and poorer results at very low energies.

3.3. The Mittleman–Watson potential

A different approach to the problem is to return to equation (10) and to recognize that since $F(r)$ behaves similarly to a plane wave, we can write approximately

$$V_E(r)\,F(r) = \int \frac{\phi(r)\phi(r')}{|r - r'|}\exp[ik.(r' - r)]\,dr'\,F(r). \tag{22}$$

This idea is due to Massey and Mohr (1934) who employed it to localize the optical potential, rather than the exchange kernel.

Starting from equation (22), Mittleman and Watson (1960) complete the evaluation of $V_E(r)$ by using the Thomas–Fermi approximation to represent the bound state orbitals $\phi(r)$. They find

$$V_E^{(8)}(r) = -\frac{1}{\pi k}\left(kP(r) - \tfrac{1}{2}(k^2 - P^2(r))\ln\left|\frac{k + P(r)}{k - P(r)}\right|\right), \tag{23}$$

where $P(r)$ is the Fermi momentum

$$P(r) = (3\pi^2 N|\phi(r)|^2)^{1/3}, \tag{24}$$

where $N = 1$ for He^+ and H and $N = 2$ for He.

Although the derivation of $V_E^{(8)}$ suggests that it should be most accurate for atomic targets composed of many electrons, Byron and Joachain (1975) have used

this potential, apparently successfully, for a helium target. For large k, it is clear from (22) that $V_E^{(8)}$ again reduces to the Ochkur form (17), while for smaller k it resembles the potential of Slater. However the assumptions on which (23) is based break down in this region.

Recently we received a preprint (Riley and Truhlar 1976) in which a potential of the Mittleman–Watson form is rederived. However in place of the incident momentum k, various forms of local momentum $p_c(r)$ are employed. On the basis of numerical calculations for scattering by helium and argon (without allowance for polarization), Riley and Truhlar conclude that out of those considered the most satisfactory choice for $p_c(r)$ is

$$p_c(r) = (k^2 + P^2(r))^{1/2}. \tag{25}$$

Replacing k in (23) by $p_c(r)$, we obtain $V_E^{(9)}$, termed by Riley and Truhlar, 'the asymtotically adjusted free-electron gas approximation'. Unfortunately, Riley and Truhlar have employed a slightly different helium wavefunction from the one used here, so to obtain an accurate comparison, we have recomputed their results for helium and extended them to include the effect of polarization and also to scattering by H and He^+.

An alternative technique based on equation (22) is to compute the integral using an accurate orbital ϕ (or the exact wavefunction in the case of H or He^+). The resulting potential might be expected to be superior to the Mittleman–Watson potential for light atoms, but no calculations based on this idea have been reported to our knowledge. From (22) this potential can be written as

$$V_L(r) = \phi(r) \int \mathrm{d}\boldsymbol{R}\, \phi(|\boldsymbol{R} - \boldsymbol{r}|)\, \mathrm{e}^{\mathrm{i}\boldsymbol{k}\cdot\boldsymbol{R}}.$$

We have investigated the spherically symmetrical approximation in which $\phi(|\boldsymbol{R} - \boldsymbol{r}|)$ in the integral is replaced by the first term in a Legendre polynomial expansion in terms of the angle between $\boldsymbol{R}$ and $\boldsymbol{r}$. This defines the potential $V_E^{(10)}(r)$.

4. Numerical results

Phase shifts have been calculated for $l \leqslant 8$ and $k = 0{\cdot}5$, 1·0, 2·0, 3·0, 5·0, 7·0 and 10·0, from the static exchange equations for electron scattering by H, He^+ and He, and also from the adiabatic exchange equations. Further sets of phase shifts were obtained by replacing the exchange kernels by each of the potentials $V_E^{(i)}$. Two separate numerical programs based on the Fox–Goodwin algorithm and the Runge–Kutta method respectively were available and both were used to confirm the accuracy of the phase shifts, which are determined to an accuracy of 10^{-4} radians. For e^-–H scattering, Vanderpoorten (1975) compared the results of using potentials $V_E^{(2)}$ and $V_E^{(4)}$ with the static exchange phase shifts at 50 and 100 eV, for $l = 0, 1, 2$, and his results agree with ours for this case. The complete tables of phase shifts are too lengthy to reproduce here but tables 1–7 illustrate the results obtained with the most successful potentials. The polarization potentials employed in calculating the phase shifts displayed in tables 1–7 were V_p^A

for H and He^+ (see equation (6)) and V_p^B for He (see equation (7)). The results calculated with the Buckingham potential V_p^C, and those employing V_p^A for He are discussed briefly below. The complete tables of phase shifts can be obtained on request.

4.1. Electron scattering by atomic hydrogen

In tables 1–3, the exact phase shifts for $l = 0$, 1 and 2 obtained by solving the integro–differential equation (1) for electron scattering by hydrogen are compared with results obtained from the Furness and McCarthy potential $V_E^{(2)}$, the Ochkur potential $V_E^{(4)}$, the modified potential of Bransden and Noble $V_E^{(5)}$, the Bauer and Browne potential $V_E^{(7)}$, the potential of Mittleman and Watson $V_E^{(8)}$, and the Riley and Truhlar potential $V_E^{(9)}$. The results are given both for the static-exchange model and for the adiabatic-exchange model.

Of the potentials shown in the tables, the Furness and McCarthy potential provides the most accurate phase shifts for $k \geqslant 1{\cdot}0$. Below $k = 0{\cdot}5$ for certain ranges of r the argument of the square root in (15) becomes negative for the case $\tau = +1$ and it becomes impossible to define the Furness–McCarthy potential. The agreement with the exact phase shifts for $k \geqslant 2$ is remarkable, the difference rarely exceeding 1%. The extension of the Furness–McCarthy potential to coupled channel situations is somewhat complicated, so it is important to assess the simplified versions $V_E^{(4)}$ and $V_E^{(5)}$ which are easily generalized. Both potentials provide phase shifts which agree quite closely with exact phases down to $k = 3{\cdot}0$. Below $k = 3$, the potential $V_E^{(5)}$ remains adequate down to $k = 1{\cdot}0$ while the Ochkur potential ceases to produce sensible results at such low energies. The other potentials of this group, $V_E^{(3)}$ and $V_E^{(6)}$, are distinctly less good for $k \leqslant 3$, although adequate at the higher energies.

No reasonable results were obtained using the Yu potential $V_E^{(1)}$, nor could reasonable results be obtained with a Slater potential of the magnitude used in bound state calculations. By adjusting the constant A to produce a reasonable fit to the $l = 0$ phase shifts at $k = 1{\cdot}0$ (giving $A = 0{\cdot}141$), the Slater potential $V_E^{(7)}$ produces phase shifts for $l = 0$ that are in fair agreement with the exact phases over the whole energy region, but for $l \neq 0$, the agreement with the exact phase shifts becomes very poor.

The potential of Mittleman and Watson, $V_E^{(8)}$, produces accurate phase shifts for $k \geqslant 3$. For $2 \leqslant k \leqslant 5$ the phase shifts are in reasonable agreement with the exact ones, but are distinctly less accurate than those provided by the Furness–McCarthy potential and by its simplified versions. Below $k = 2$, the potential $V_E^{(8)}$ fails to produce reasonable results.

The variation of the Mittleman and Watson potential, introduced by Riley and Truhlar, $V_E^{(9)}$, is much more successful than $V_E^{(8)}$, and is comparable in accuracy with the Furness and McCarthy potential $V_E^{(2)}$ for $k \geqslant 2$. At $k = 1{\cdot}0$, the Furness and McCarthy potential is superior but at $k = 0{\cdot}5$ neither potential is successful, being particularly poor in the singlet state ($S = 0$).

The potential $V_E^{(10)}$, also based on (22), represents the exact phase shifts slightly less accurately than $V_E^{(8)}$. For example, at $k = 2$ the triplet and singlet s-wave phase shifts given by this potential in the adiabatic-exchange model are 0·9359 and 0·6046 radians, respectively. This is probably due to the crude approximation in which only the zero order term in the angular expansion of the integrand was employed. However taking higher order terms produces an over-complicated result and is hardly likely

Table 1. s-wave phase shifts (radians) for e^-–H scattering.

	(*a*) Static-exchange model							(*b*) Adiabatic-exchange model						
k (au)	Exact	2	4	5	7	8	9	Exact	2	4	5	7	8	9
0·5	2·070	2·0159	1·7111	1·9151	1·6126	3·063	2·255	2·1462	2·1307	1·8154	2·0396	1·8413	0·135	2·3864
	1·031	1·6807	2·4023	0·0214	0·2298	2·367	2·6907	1·1577	1·7483	2·5072	0·4156	0·7314	2·468	2·8933
1·0	1·3912	1·3385	2·0042	1·2834	1·1997	2·0441	1·4552	1·480	1·4510	2·1146	1·4004	1·3426	2·1526	1·5768
	0·5431	0·5051	2·7724	0·4234	0·5730	2·6046	1·7638	0·666	0·5523	2·9476	0·6422	0·7572	2·7628	0·3841
2·0	0·8270	0·8139	0·8971	0·8027	0·8515	0·9326	0·8377	0·7270	0·8323	0·8997	0·8239	0·8783	0·9287	0·9154
	0·5415	0·5521	0·4801	0·5817	0·5342	0·4429	0·5450	0·6286	0·6610	0·5962	0·6777	0·6231	0·5638	0·6278
3·0	0·6245	0·6190	0·6374	0·6162	0·6804	0·6415	0·6263	0·6763	0·6601	0·6770	0·6577	0·7187	0·6805	0·6802
	0·5184	0·5239	0·5069	0·5286	0·4637	0·5027	0·5183	0·5747	0·5843	0·5681	0·5879	0·5264	0·5645	0·5729
5·0	0·4478	0·4462	0·4487	0·4459	0·5002	0·4490	0·4476	0·4797	0·4783	0·4807	0·4780	0·5301	0·4810	0·4804
	0·4206	0·4212	0·4189	0·4217	0·3671	0·4186	0·4200	0·4538	0·4557	0·4534	0·4561	0·4038	0·4531	0·4530
7·0	0·3622	0·3595	0·3601	0·3594	0·4025	0·3602	0·3599	0·3835	0·3827	0·3833	0·3826	0·4246	0·3834	0·3835
	0·3495	0·3496	0·3490	0·3497	0·3065	0·3489	0·3492	0·3733	0·3734	0·3728	0·3734	0·3314	0·3727	0·3728
10·0	0·2848	0·2837	0·2838	0·2937	0·3157	0·2838	0·2837	0·3009	0·2993	0·2993	0·2992	0·3307	0·2993	0·3003
	0·2806	0·2801	0·2799	0·2801	0·2480	0·2799	0·2799	0·2973	0·2957	0·2956	0·2957	0·2641	0·2955	0·2965

Exact: Phase shift computed from the integro-differential equation retaining the exchange kernel. The number at the head of each column refers to the equivalent exchange potentials defined in the text. For each value of the momentum the first line of results refers to the scattering in the $S = 1$ state and the second line to scattering in the $S = 0$ state. The polarization potential is defined by equation (6).

Table 2. p-wave phase shifts (radians) for e^-–H scattering.

	(*a*) Static-exchange model							(*b*) Adiabatic-exchange model						
k (au)	Exact	2	4	5	7	8	9	Exact	2	4	5	7	8	9
0·5	0·169	0·2237	−0·0715	0·0896	0·2355	−0·8199	0·2691	0·3115	0·3597	0·0146	0·2088	0·3686	2·4958	0·4583
	−0·0713	0·0297	−0·1307	−0·0192	−0·1455	−0·1448	−0·0887	0·0133	0·1050	−0·0647	0·0736	−0·0638	−0·0813	−0·0126
1·0	0·3579	0·3416	0·5273	0·2563	0·3369	0·7157	0·3443	0·503	0·4823	0·7067	0·4002	0·4799	0·9135	0·5021
	−0·1057	−0·0766	−0·1174	−0·0051	−0·1042	−0·1462	−0·0624	0·0192	0·0328	−0·0055	0·1249	0·0250	−0·0387	0·0577
2·0	0·3298	0·3185	0·3423	0·3053	0·3711	0·3524	0·3182	0·4152	0·4642	0·5006	0·4529	0·5062	0·5148	0·4065
	0·1096	0·1225	0·1117	0·1445	0·0753	0·1035	0·1324	0·2015	0·2650	0·2420	0·2874	0·2325	0·2294	0·2206
3·0	0·2926	0·2891	0·2957	0·2861	0·3528	0·2976	0·2896	0·3509	0·3736	0·3821	0·3708	0·4332	0·3843	0·3485
	0·2027	0·2068	0·2017	0·2111	0·1436	0·1998	0·2076	0·2628	0·2936	0·2866	0·2977	0·2347	0·2844	0·2667
5·0	0·2482	0·2476	0·2487	0·2472	0·3013	0·2489	0·2479	0·2829	0·2909	0·2921	0·2905	0·3431	0·2923	0·2825
	0·2238	0·2244	0·2233	0·2248	0·1705	0·2231	0·2241	0·2587	0·2683	0·2671	0·2687	0·2159	0·2669	0·2588
7·0	0·2175	0·2173	0·2176	0·2172	0·2600	0·2176	0·2174	0·2421	0·2457	0·2460	0·2456	0·2877	0·2461	0·2418
	0·2078	0·2078	0·2075	0·2079	0·1650	0·2075	0·2077	0·2324	0·2364	0·2361	0·2365	0·1943	0·2361	0·2321
10·0	0·1847	0·1840	0·1840	0·1839	0·2158	0·1840	0·1839	0·1999	0·2025	0·2026	0·2025	0·2341	0·2026	0·2008
	0·1811	0·1805	0·1804	0·1805	0·1486	0·1804	0·1803	0·1999	0·1990	0·1990	0·1991	0·1674	0·1989	0·1972

Notation: see footnote of table 1.

Table 3. d-wave phase shifts (radians) for e^-–H scattering.

	(*a*) Static-exchange model							(*b*) Adiabatic-exchange model						
k (au)	Exact	2	4	5	7	8	9	Exact	2	4	5	7	8	9
0·5	0·0070	0·0142	0·0235	0·0047	0·0649	0·0272	0·0148	0·0355	0·0435	0·0563	0·0338	0·0980	0·0608	0·0453
	−0·00397	−0·0060	−0·0127	−0·0017	−0·0555	−0·0140	−0·0097	0·0233	0·0209	0·0142	0·0267	−0·0307	0·0127	0·0176
1·0	0·0559	0·0641	0·0734	0·0431	0·1460	0·0800	0·0623	0·1280	0·1354	0·1489	0·1140	0·2206	0·1568	0·1361
	−0·0172	−0·0283	−0·0281	−0·0054	−0·1035	−0·0313	−0·0214	0·0495	0·0375	0·0360	0·0619	−0·0396	0·0325	0·0437
2·0	0·1275	0·1262	0·1307	0·1184	0·1993	0·1328	0·1245	0·2016	0·2442	0·2540	0·2353	0·3076	0·2577	0·1993
	0·0336	0·0342	0·0327	0·0439	−0·0376	0·0309	0·0382	0·1077	0·1283	0·1234	0·1406	0·0668	0·1202	0·1111
3·0	0·1490	0·1478	0·1498	0·1455	0·2145	0·1505	0·1473	0·2056	0·2242	0·2273	0·2219	0·2878	0·2282	0·2040
	0·0934	0·0946	0·0933	0·0974	0·0280	0·0926	0·0957	0·1506	0·1672	0·1649	0·1702	0·1037	0·1640	0·1523
5·0	0·1558	0·1554	0·1559	0·1551	0·2082	0·1561	0·1554	0·1911	0·1976	0·1982	0·1973	0·2494	0·1984	0·1906
	0·1364	0·1367	0·1363	0·1371	0·0839	0·1361	0·1368	0·1719	0·1788	0·1782	0·1792	0·1268	0·1781	0·1720
7·0	0·1494	0·1492	0·1494	0·1491	0·1911	0·1494	0·1492	0·1703	0·1775	0·1777	0·1774	0·2190	0·1777	0·1742
	0·1410	0·1409	0·1408	0·1410	0·0990	0·1407	0·1409	0·1703	0·1693	0·1691	0·1694	0·1277	0·1691	0·1659
10·0	0·1360	0·1353	0·1353	0·1352	0·1667	0·1353	0·1351	0·1517	0·1539	0·1539	0·1539	0·1851	0·1539	0·1524
	0·1327	0·1320	0·1320	0·1320	0·1006	0·1320	0·1319	0·1517	0·1507	0·1506	0·1507	0·1194	0·1506	0·1492

Notation: see footnote of table 1.

Table 4. Phase shifts (radians) for e^-–He^+ scattering.

	(*a*) Static-exchange model						(*b*) Adiabatic-exchange model					
l	Exact	2	4	5	8	9	Exact	2	4	5	8	9
$k = 1{\cdot}0$ (au)												
0	0·8145	0·7841	2·2883	0·7843	1·4142	0·9677	0·0382	0·8176	2·3256	0·8172	1·4495	1·0023
	0·3219	−0·0021	1·7391	0·2302	1·9108	−0·0860	0·3557	0·0904	1·7792	0·2867	1·9661	−0·0250
1	0·2125	0·2138	1·5541	0·1922	1·0787	0·3542	0·2588	0·2586	1·6094	0·2372	1·1353	0·4059
	−0·0779	−0·1066	2·8477	−0·0508	2·8187	−0·1508	−0·0388	−0·0641	−0·2654	−0·0105	−0·2953	−0·1155
2	0·0157	0·0211	0·0606	0·0168	0·0712	0·0366	0·0294	0·0363	0·0780	0·0321	0·0892	0·0527
	−0·0067	−0·0138	−0·0353	−0·0079	−0·0405	−0·0241	0·0064	0·0009	−0·0218	0·0068	−0·0271	−0·0100
3	0·0014	0·0017	0·0036	0·0013	0·0040	0·0030	0·0050	0·0070	0·0089	0·0065	0·0093	0·0083
	−0·0001	−0·0012	−0·0029	−0·0007	−0·0031	−0·0023	0·0034	0·0040	0·0023	0·0045	0·0021	0·0028
$k = 3{\cdot}0$ (au)												
0	0·4913	0·4796	0·5954	0·4785	0·6725	0·5138	0·5113	0·5022	0·6180	0·5011	0·6948	0·5368
	0·2941	0·3014	0·1835	0·3106	0·1005	0·2732	0·3184	0·3264	0·2084	0·3354	0·1258	0·2975
1	0·1887	0·1802	0·2223	0·1777	0·2416	0·1918	0·2147	0·2063	0·2493	0·2039	0·2687	0·2186
	0·0355	0·0443	0·0121	0·0513	−0·0023	0·0382	0·0629	0·0716	0·0385	0·0784	0·0239	0·0647
2	0·0605	0·0604	0·0702	0·0587	0·0727	0·0641	0·0812	0·0811	0·0912	0·0794	0·0938	0·0850
	0·0055	0·0052	−0·0027	0·0078	−0·0048	0·0027	0·0260	0·0257	0·0175	0·0283	0·0154	0·0230
3	0·0188	0·0195	0·0218	0·0187	0·0221	0·0207	0·0329	0·0335	0·0359	0·0327	0·0362	0·0347
	0·0009	0·0000	−0·0019	0·0009	−0·0023	−0·0010	0·0148	0·0139	0·0118	0·0148	0·0115	0·0128

Notation: see footnote of table 1.

to improve on the excellent results obtained with the simple forms of the other potentials. This potential will not be considered further.

The higher order phase shifts (not shown in the tables) are given accurately by each of the potentials investigated, with the exceptions of $V_E^{(1)}$ and $V_E^{(7)}$. For example, at $k = 1.0$, $l = 8$, the exact $S = 0$ and $S = 1$ phase shifts for the static exchange model are 0·0337 and 0·0352 respectively. Both the Mittleman–Watson and the Furness–McCarthy potentials give the results 0·0333 and 0·0347 for $S = 0$ and $S = 1$ respectively, while the Slater potential $V_E^{(7)}$ gives 0·0067 and 0·0614.

4.2. Electron scattering by He^+

It cannot be accepted without test that the degree of success achieved by the various exchange potentials for the e^-–H system will be repeated for other systems. For this reason calculations have been carried out for the e^-–He^+ system, in which the target is more compact and where the long range Coulomb interaction might modify considerably potentials of the Furness–McCarthy type. The calculated phase shifts show, in fact, that the relative success of the various potentials is about the same as for the e^-–H system. The most successful potential for $k \geqslant 3.0$ is again the Furness–McCarthy potential, but for $k < 2.0$ the results rapidly deteriorate. In contrast the modified potential $V_E^{(5)}$, which allows to some extent for the variation of $\phi(r')$ with r' in the exchange kernel, is only slightly less accurate for $k \geqslant 3$ and remains useful at low energies down to $k = 0.5$. The Slater potential $V_E^{(7)}$ is less accurate at all energies than $V_E^{(5)}$, but is comparatively more successful than for the e^-–H system. The Mittleman–Watson potential on the other hand completely fails below $k = 3$, although providing accurate phase shifts at the highest energies. In table 4, the situation is illustrated at the momenta $k = 1.0$ and 3·0, with and without the polarization potential.

4.3. Electron scattering by He

The phase shifts obtained using the five most successful potentials are compared in the case of electron–helium scattering, with those obtained from the solution of the exchange integro–differential equations, in tables 5, 6 and 7 for $l = 0$, 1 and 2. The Furness–McCarthy potential $V_E^{(2)}$, the modified potential of Bransden and Noble $V_E^{(5)}$ and the potential of Riley and Truhlar $V_E^{(9)}$ reproduce the exact phase shifts to a remarkable degree, in both the static-exchange and the adiabatic-exchange models. Useful results are obtained over a wider energy range than for H or He^+. For s-waves, all three potentials $V_E^{(2)}$, $V_E^{(5)}$ and $V_E^{(9)}$ remain good down to the lowest momentum considered, $k = 0.5$, but for $l \geqslant 1$, the Bransden and Noble potential $V_E^{(5)}$ gives the best phase shifts at low energies although being slightly less successful at the highest energies considered.

4.4. Polarization potentials

Examination of the tables shows that the general conclusions about the successes or failures of the various exchange potentials examined are the same for both the static-exchange and the adiabatic-exchange models. This is an important result because in applications the exchange potential is often used in conjunction with effective polarization and absorptive potentials which are approximations to the exact

Table 5. s-wave phase shifts (radians) for e^-–He scattering.

	(*a*) Static-exchange model						(*b*) Adiabatic-exchange model					
k (au)	Exact	2	4	5	8	9	Exact	2	4	5	8	9
0·5	2·4357	2·4059	3·0427	2·4154	2·7500	2·4433	2·4972	2·5097	0·1937	2·4965	2·9443	2·5466
1·0	1·8902	1·8388	2·9150	1·8433	2·2068	1·8683	1·9631	1·9567	3·1122	1·9511	2·3345	1·9823
2·0	1·2791	1·2401	1·5225	1·2362	1·5241	1·2661	1·3575	1·3400	1·6283	1·3358	1·6202	1·3532
3·0	0·9934	0·9696	1·0483	0·9674	1·1128	0·9906	1·0557	1·0467	1·1290	1·0447	1·1914	1·0549
5·0	0·7258	0·7159	0·7283	0·7154	0·7329	0·7282	0·7680	0·7659	0·7792	0·7654	0·7843	0·7689
7·0	0·5908	0·5859	0·5893	0·5857	0·5901	0·5939	0·6210	0·6223	0·6259	0·6221	0·6268	0·6235
10·0	0·4734	0·4706	0·4714	0·4705	0·4715	0·4756	0·4967	0·4963	0·4971	0·4961	0·4973	0·4965

Exact: Phase shift computed from the integro–differential equation retaining the exchange kernel. The number at the head of each column refers to the equivalent exchange potential defined in the text. The polarization potential is defined by equation (7).

Table 6. p-wave phase shifts (radians) for e^-–He scattering.

	(*a*) Static-exchange model						(*b*) Adiabatic-exchange model					
k (au)	Exact	2	4	5	8	9	Exact	2	4	5	8	9
0·5	0·0409	0·0626	0·3670	0·0327	0·2039	0·0687	0·0938	0·1300	0·8267	0·0882	0·4130	0·1289
1·0	0·1840	0·1833	0·5394	0·1425	0·4024	0·1788	0·2980	0·3153	0·7910	0·2675	0·6180	0·2964
2·0	0·3265	0·2971	0·3537	0·2844	0·4126	0·2977	0·4259	0·4141	0·4788	0·4022	0·5368	0·4008
3·0	0·3470	0·3244	0·3448	0·3207	0·3649	0·3325	0·4194	0·4117	0·4340	0·4083	0·4535	0·4066
5·0	0·3343	0·3223	0·3269	0·3217	0·3290	0·3314	0·3787	0·3766	0·3814	0·3760	0·3836	0·3760
7·0	0·3109	0·3030	0·3045	0·3028	0·3050	0·3101	0·3424	0·3416	0·3432	0·3414	0·3437	0·3416
10·0	0·2773	0·2717	0·2721	0·2717	0·2722	0·2766	0·2991	0·2984	0·2989	0·2983	0·2990	0·2984

Notation: see table 5.

Table 7. d-wave phase shifts (radians) for e^-–He scattering.

	(*a*) Static-exchange model						(*b*) Adiabatic-exchange model					
k (au)	Exact	2	4	5	8	9	Exact	2	4	5	8	9
0·5	0·00092	0·0018	0·0068	0·0007	0·0033	0·0025	—	0·0124	0·0184	0·0108	0·0149	0·0124
1·0	0·0124	0·0152	0·0190	0·0102	0·0214	0·0181	0·0453	0·0527	0·0584	0·0463	0·0616	0·0516
2·0	0·0737	0·0654	0·0696	0·0604	0·0747	0·0725	0·1344	0·1365	0·1423	0·1314	0·1475	0·1336
3·0	0·1229	0·1107	0·1137	0·1084	0·1166	0·1197	0·1818	0·1813	0·1852	0·1792	0·1880	0·1791
5·0	0·1700	0·1598	0·1611	0·1593	0·1619	0·1685	0·2124	0·2122	0·2137	0·2118	0·2145	0·2115
7·0	0·1840	0·1764	0·1770	0·1763	0·1772	0·1834	0·2157	0·2153	0·2160	0·2152	0·2162	0·2151
10·0	0·1838	0·1781	0·1783	0·1781	0·1784	0·1830	0·2060	0·2054	0·2057	0·2053	0·2057	0·2053

Notation: see table 5.

'optical' potential. As indicated earlier, to help assess this point we repeated the calculations with other forms of polarization potential. The Buckingham polarization potential (9) behaves quite differently from the forms (6) or (7) at small r, so we checked the success of the exchange potentials in the presence of the Buckingham potential in detail. One case is illustrated in table 8, where the phase shifts using the Furness–McCarthy potential are shown for e^-–H scattering at $k = 2{\cdot}0$ and $k = 5{\cdot}0$.

Table 8. Phase shifts (radians) for electron scattering by hydrogen, using the Buckingham polarization potential.

		$k = 2{\cdot}0$		$k = 5{\cdot}0$	
l		A	B	A	B
0	$S = 1$	1·4795	1·4705	0·7721	0·7739
	0	1·3270	1·3211	0·7519	0·7521
1	$S = 1$	0·8508	0·8420	0·5573	0·5568
	0	0·6596	0·6706	0·5356	0·5359
2	$S = 1$	0·3803	0·3777	0·4139	0·4134
	0	0·2784	0·2801	0·3957	0·3958

A From solution of the exchange integro–differential equation.
B Computed from the Furness and McCarthy exchange potential $V_E^{(2)}$.

It is interesting to see how different the phase shifts given by the Buckingham potential are from those shown in tables 1–3 obtained using (7). but the exchange potential is equally successful in either case. Comparing the detailed tables of phase shifts produced with the Buckingham potential with those produced from potentials (6) and (7), shows that the success of the exchange potentials does not depend to a significant extent on the other potentials present.

5. Conclusions

In the derivations of the exchange potentials outlined earlier, the approximations made, with one or two exceptions, become more accurate as the energy increases. This accounts for the excellent agreement between the results obtained with the Furness–McCarthy potential and its simplifications, and the results of the Mittleman–Watson and Riley–Truhlar potentials at the highest energies considered. What is somewhat surprising is that this agreement and the agreement with the phase shifts obtained from the exact exchange kernels remains good to very low momenta—about $k = 0{\cdot}5$ for helium, $k = 1{\cdot}0$ for H and $k = 2{\cdot}0$ for He^+.

The potential with the widest range of application appears to be that of Furness and McCarthy ($V_E^{(2)}$), but it is important to notice that the modified potential $V_E^{(5)}$ is nearly as effective, since this potential can easily be generalized to represent the off-diagonal exchange kernels encountered in coupled channel situations. Riley and Truhlar have also explored this point and have proposed the use of an off-diagonal potential rather similar to that employed in the coupled channel calculations of Bransden and Noble.

Acknowledgments

One of us (BHB) would like to acknowledge the kind hospitality of the School of Physical Sciences, Flinders University, during the period over which this work was carried out. We should like to thank Mr R F Syms for supplying us with his accurate phase shifts for H and He^+, Dr M E Riley and Dr D G Truhlar for sending us a copy of their results before publication and Professor I E McCarthy for illuminating discussions. This work was supported in part by the Science Research Council.

References

Abiodun R A and Seaton M J 1966 *Proc. Phys. Soc.* **87** 145–51
Bauer E and Browne H N 1964 *Atomic Collision Processes* ed M R C McDowell (Amsterdam: North-Holland) pp 16–27
Bely O 1967 *Nuovo Cim.* B **49** 66–86
Bransden B H 1970 *Atomic Collision Theory* (New York: Benjamin)
Bransden B H and Noble C J 1976 *J. Phys. B: Atom. Molec. Phys.* **9** 1507–17 in press
Byron F W Jr and Joachain C J 1966 *Phys. Rev.* **146** 1–8
——1975 *Preprint*
Drachman R J and Temkin A 1972 *Case Studies in Atomic Collision Physics* vol 2, eds M R C McDowell and E W McDaniel (Amsterdam: North-Holland) pp 398–481
Duxler W M, Poe R T and LaBahn R W 1971 *Phys. Rev.* A **4** 1935–44
Furness J B and McCarthy I E 1973 *J. Phys. B: Atom. Molec. Phys.* **6** 2280–91
Herman F and Skillman S 1963 *Atomic Structure Calculations* (Englewood Cliffs, New Jersey: Prentice-Hall)
Massey H S W and Mohr C B O 1934 *Proc. R. Soc.* A **146** 880–900
Mittleman M H and Watson K M 1960 *Ann. Phys., NY* **10** 268–79
Mott N F and Massey H S W 1965 *Theory of Atomic Collisions* 3rd edn (London and New York: Oxford University Press)
Perey F G and Buck B 1962 *Nucl. Phys.* **32** 353–80
Riley M E and Truhlar D G 1976 *Phys. Rev.* to be published
Slater J C 1951 *Phys. Rev.* **81** 385–90
Vanderpoorten R 1975 *J. Phys. B: Atom. Molec. Phys.* **8** 926–39
Yu S 1975 *J. Phys. B: Atom. Molec. Phys.* **8** 1752–5